Author responses in blue. Planned additions to the manuscript are underlined (or shown via screen shot).

Anonymous Referee #1

This is an excellent and thorough review of the current state-of-science on the acidity of atmospheric aerosols and droplets. Below are some comments intended to improve the manuscript:

We thank the reviewer for the supportive comments.

1. The Abstract is focused on the electrolytes and does not discuss the organic fraction and its contribution. Something should be mentioned about organic bases, such as amines, and organic acids such carboxylics and dicarboxylics.

We revised a sentence in the abstract to explicitly mention organic acid/base partitioning. The role of organic species in driving pH is beginning to be examined, so we highlighted the well-known role of pH on organic acid/base partitioning.

> In the atmosphere, the acidity of condensed phases (aerosol particles, cloud water, and fog droplets) governs the phase partitioning of semi-volatile gases such as HNO_3, NH_3, HCl, and organic acids and bases as well as chemical reaction rates.

2. Same in section 1 around line 22.

A list of specific organic acids/bases were added:

> Semi-volatile species, for which significant fractions typically exist in both the gas and condensed phases, include ammonia (NH_3), nitric acid (HNO_3), hydrochloric acid (HCl), and low molecular weight organic acids (formic, acetic, oxalic, malonic, succinic, glutaric, and maleic acids) and/or bases (e.g. amines).

3. The use of the world "occult" is completely foreign to me. It should at least be defined, but better would be to use a word more familiar.

Occult is now defined (we keep the term for compactness in the figure):

> The acidity of atmospheric deposition for dry, wet, and occult (wind-driven cloud-water) pathways is directly affected by aerosol and cloud pH (Fig. 1).

4. Page 4, line 32. Nicotine (and cocaine for that matter) are organic bases. increasing pH partitions these compounds to the gas phase (so-called free-basing). The gaseous compounds have a much higher deposition efficiency to the respiratory tract than particles increasing the dose.

We clarified the statement to indicate the role of particle acidity was to drive nicotine off surfaces and into the indoor air. We also added a reference to the partitioning mechanism for alkaloids to indicate the behavior may apply to other species as well.

> Aerosol acidity was also recently shown to enhance airborne nicotine levels and resulting thirdhand smoke exposure by promoting volatilization from surfaces (such as clothes) and allowing distribution throughout a building's indoor air (DeCarlo et al., 2018). Similar behavior may be possible for other alkaloids (Pankow, 2001).

5. section 3, page 17, line 26. Change The to This.

Updated

6. Section 5, page 30, line 17: Why do you say that cloud liquid water is not in equilibrium with the gas phase? Well, nothing is completely in equilibrium but the surface area in a cloud is huge so equilibrium is nearly attained.

In a relative sense, most (non-glassy) aerosols are far closer to equilibrium than clouds can ever be. This is because their size, hence equilibration times, is orders of magnitude smaller. For this reason you can ~~always~~ *frequently (word choice revised Feb 2020)* assume thermodynamic equilibrium for submicron, but not supermicron aerosol. Droplets are tens of microns in diameter and reside typically in a moving air parcel (e.g. in a convective cloud) which experiences changes in temperature and local saturation ratio, so the equilibrium assumption is often less satisfied (Seinfeld and Pandis, 1998).

The comment "water is not in equilibrium with the gas phase" refers to the effect of perturbing the RH of the air surrounding the sample. For aerosol, even a 10% change in RH can profoundly impact liquid water, as equilibration with RH is almost instantaneous. Cloud liquid water, on the other hand, is not driven by RH but by the cooling rate that generates them. After sampling, the evaporation biases have a much smaller effect precisely because the liquid volume is so large. We have removed the reference to "water equilibration" to avoid unnecessary confusion.

Sentence to be modified from:

> The same limitations do not exist for fog/cloud water or precipitation, where larger sample volumes can be collected from accessible clouds, the associated water is not in equilibrium with the gas phase (although evaporation artifacts may still cause biases), and solutions are dilute enough to allow for a direct pH measurement. The latter has been done with electrochemical pH probes for decades (Sect. 5.2).

To:

> The sample volumes for fog/cloud water or precipitation are orders of magnitude larger than for aerosols and can be collected from clouds using well established instrumentation. This, together with their dilute concentration allow for a direct pH measurement, which has been done with electrochemical pH probes for decades (Sect. 5.2).

7. The authors many not be aware of the work by Beverly Cohen published in 2000 using a metal plate to assess aerosol acidity.

We were not aware but have located a report and article:

1. Field Evaluation of Nanofilm Detectors for Measuring Acidic Particles in Indoor and Outdoor Air By: Beverly S Cohen, Maire SA Heikkinen, Yair Hazi, Hai Gao, Paul Peters, and Morton Lippmann, https://www.healtheffects.org/system/files/Cohen.pdf
2. Cohen et al., Detecting H+ in ultrafine ambient aerosol using iron nano-film detectors and scanning probe microscopy, https://doi.org/10.1080/104732200301881.

The technique is used to determine the number of acidic vs nonacidic particles. It provides some qualitative information (e.g. H2SO4 and NH4HSO4 are more acidic than (NH4)2SO4). We have not added a reference due to the qualitative nature of the study.

8. Page 33, section 5.1.3, line 31: Comment should be common.

Updated

9. Page 58, lines 22-27: Something should be said here about the role of volatile acids (HCl, HNO3) and bases (NH3, amines). If these exist in the gas phase, they serve to equilibrate acidity across the particle size distribution. If the particles are so acidic that the volatile bases are depleted from the gas phase, I can see how there could be a gradient in acidity with particle size. Likewise for the particles being alkaline and the volatile acids being depleted. As the authors discuss elsewhere, these gases are key to understanding the acidity of particles but unfortunately they are infrequently measured. I encourage a simple discussion of this logic.

We added a new sentence in the paragraph highlighting the role for semivolatile acids and bases:

> Overall, atmospheric particle pH is size dependent and generally higher for coarse mode particles due to variations in inorganic composition with particle size. Differences as large 4 pH units have been reported between fine and coarse particles (Fang et al., 2017; Young et al., 2013). Bulk PM_1 and $PM_{2.5}$ acidity is more similar than fine vs coarse mode acidity (pH_F within 1 – 2 units, e.g., Bougiatioti et al., 2016; Guo et al., 2017b), but submicron (diameter < 1 μm) particles still show higher acidity than bulk $PM_{2.5}$. The reason for this is the strong enrichment of aerosol with NVCs from dust and sea salt at the larger sizes (even in the fine mode) and role of sulfate in new particle formation and surface-area driven condensation at the small sizes (Fig. 2). While semivolatile acids and bases act to homogenize acidity across the size distribution, mass transfer limitations (next section) and the heterogeneity of emission composition lead to variation in pH with size. Significant pH changes can occur in the 1 to 2.5 μm size range (Fang et al., 2017; Ding et al., 2019). The size dependent pH is also seen for sea salt aerosol (Fridlind and Jacobson, 2000) as well as in urban aerosols in China (Ding et al., 2019) where the fine mode is consistently 2-3 pH units lower than the coarse mode. The implications of this acidity gradient are considerable, for metal solubility and their impacts on public health and ecosystem productivity, as well as chemistry and semi-volatile partitioning of pH-sensitive species.

Anonymous Referee #2

Pye et al. provides a detailed review concerning aerosol and cloud acidity. This is a much needed review, as the studies concerning aerosol acidity has increased. I applaud the large author list on this work, as it is very extensive and impressive. The review provides a much needed discussion concerning various aspects of cloud and aerosol pH, including definition, measurements and calculations, observations, and comparisons with models. I foresee this paper becoming an important source, both in the field and for introducing this subject in classes. This paper should be published upon consideration of the following comments:

We thank the reviewer for the supportive comments.

1.) Similar to Reviewer #1, occult is not a term that I am familiar with. If it could be defined, or a synonym could be used, that would be appreciated.

Now defined in response to reviewer #1

2.) I appreciate Table 1, as there are numerous abbreviations throughout the manuscript. However, there appears to be some abbreviations missing, such as NVCs. Please include all abbreviations in the manuscript into Table 1, as it can be hard to find them in this large manuscript.

Appendix A has been expanded to include additional abbreviations. A second appendix (B) was added listing the models, datasets, and other related information. Items in appendix B are often abbreviations (e.g. WRF-Chem), but knowing their definition is not critical to the message of the paper. In some cases (e.g. ISORROPIA, SPECIATE) the name in B is not an abbreviation.

Updated Appendix A and new Appendix B:

Appendix A: Nomenclature

Symbol	Description
a_{H^+}	The activity of hydrogen ions in aqueous solution on a molality basis
$a_{H^+}^{(c)}$	The activity of H^+ ions on a molarity (concentration) basis
$a_{H^+}^{(x)}$	The activity of H^+ ions on a mole fraction basis
α_{HSO4}	Fraction of HSO_4^- dissociated into H^+ and SO_4^{2-}
a_i	The activity of species i (usually molality-based for ions in aqueous solutions)
ACSM	Aerosol chemical speciation monitor
adiGR	Adjusted gas ratio (see Table 2)
ALPHA	Adapted Low-cost Passive High-Absorption
ALWC	Aerosol liquid water content (mass per volume of air)
AMS	Aerosol mass spectrometer
$c^{\ominus}$	The standard state (unit) molarity
c_{H^+}	The molarity or "molar concentration" of hydrogen ions in an aqueous solution (also written using square brackets as $[H^+]$)
CCN	Cloud condensation nuclei
CTM	Chemical transport model
DELTA	Denuder for Long Term Atmospheric sampling
DON	Degree of neutralization (see Table 2)
DSN	Degree of sulfate neutralization (see Table 2)
$f_{H^+}^*$	The (rational) activity coefficient based on the mole fraction concentration scale
$F_{p,i}$	Fraction of species i in the particle vs particle + gas phase
FR	Flex Ratio, identifies the NH_3 emissions level at which the nitrate concentration switches from NH_3-insensitive (or negative sensitivity) to positive NH_3 sensitivity
~~$f_{H^+}^*$~~	~~The (rational) activity coefficient based on the mole fraction concentration scale~~
GR	Gas ratio (see Table 2)
H^+_{air}	Concentration of aerosol H^+ per volume of air (e.g., moles per m^{-3} of air)
$H^+_{air,cb}$	H^+_{air} determined from charge balance (see Table 2)

HO_x	Hydrogen oxides ($OH + HO_2$)
K_a	Acid dissociation constant for $HX \rightleftharpoons H^+ + X^-$
K_b	Acid association constant for $H^+ + X^- \rightleftharpoons HX$ or $H^+ + X \rightleftharpoons XH^+$
K_H	Dimensionless Henry's law constant
K_w	Activity-based equilibrium constant for the dissociation of water into H^+ and OH^- (see Bandura and Lvov (2005) for tabulation of values)
~~LLPS~~	~~Liquid–liquid phase separation~~
KMT	Kinetic mass transfer
LLPS	Liquid–liquid phase separation
$m^{\ominus}$	The standard state (unit) molality
m_{H^+}	Molality of H^+ (mol kg^{-1} solvent)
M_w	Molar mass of water: 0.018015 kg mol^{-1}
n_i	Number (e.g., moles) of species i
NEI	National Emission Inventory (for the United States)
NO_x	Nitrogen oxides ($NO + NO_2$)
NVC	Non-volatile cations
PAHs	polycyclic aromatic hydrocarbons
PFASs	polyfluoroalkyl substances
PFSAs	Perfluoroalkyl sulfonic acids~~perfluroroalkane sulfonic acid~~
PFCAs	Perfluoroalkyl carboxylic acids
pH	Hydrogen ion potential with activity coefficient and concentration expressed on a molality concentration scale (see Table 1)
pH_c	pH on a concentration (molarity) basis
pH_x	pH on a mole fraction basis
pH_T	"Total" pH based on the molality of sulfate and bisulfate ions (see Table 1)
pH_F	"Free ion" approximation of pH obtained when the activity coefficient of H^+ is unity (see Table 1)
$pH_{\pm}$ (H, X)	Approximation of pH using the mean molal ion activity coefficient of an H^+ and anion X pair (see Table 1)
pK_{wi}	$-\log_{10}$ ~~of~~ (K_w K_i)~~(see Bandura and Lvov (2005) for tabulation of values)~~

PM	Particulate matter, synonymous with aerosol
PM_1	Particulate mass with an equivalent diameter below 1 μm
$PM_{2.5}$	Particulate mass with an aerodynamic equivalent diameter below 2.5 μm
PSC	Pitzer-Simonson-Clegg (model)
R	Universal gas constant
r^2	Coefficient of determination
RH	Relative humidity
RRF	Relative response factor, relative change in concentration due to relative change in emission
SO_x	Sulfur oxides (usually $SO_2 + TSO_4$)
T	Temperature
TMI	Transition Metal Ions
TCl	Total chloride (sum of gas-phase hydrochloric acid and aerosol chloride)
TNO_3	Total nitrate (sum of gas-phase nitric acid and particulate nitrate)
TNH_4	Total ammonia (sum of gas-phase ammonia and particulate ammonium)
TSO_4	Total particulate sulfate (sum of sulfate and bisulfate)
VOCs	Volatile organic compounds
WSOC	Water-soluble organic compounds
x_{H^+}	The mole fraction of H^+ in the solution
X_T	Molal sulfate ratio indicating sulfate- rich vs poor domain (Eq. 9)
Z	Charge balance on total gas and particle phases used to estimate initial amount of H^+ (Eq. 19)
ZSR	Zdanovskii-Stokes-Robinson (method for calculation of aerosol water)
γ_{H^+}	The molal activity coefficient of species i
$\gamma_{H^+}^{(c)}$	The molarity-based activity coefficient of H^+
$\gamma_{\pm,HX}$	The mean~~Single~~ ion activity coefficient (for monovalent acid HX)
ρ_0	The density of the reference solvent (water)

Added Feb 2020 to Appendix A:

IN	*Ice nuclei*

Appendix B: Models, data, and related methods discussed in the text

Type	Examples
Activity coefficient models	AIOMFAC, UNIFAC
Gas-particle thermodynamic models	AIOMFAC-GLE, ADDEM, E-AIM, EQSAM, EQUISOLV II, GFEMN, ISORROPIA II, MOSAIC, SCAPE, UHAERO
3-D models	CAM-Chem, CESM, CMAQ, GEOS-Chem, GISS, PM-CAMx, TM4-ECPL, WRF-Chem
Supporting algorithms/chemistry/databases	ASTEM, CAM6, HETV, MAM, MESA, MOZART, MTEM, SPECIATE
Observational data sets (networks, satellites, field campaigns)	ACTRIS, AIRS, AMoN, CalNex, CASTNET, CrIS, CSN, EMEP/EBAS, IASI, IMPROVE, MAN, NAMN, SEARCH, SEAC4RS, SOAS, WINTER

3.) I think a Table that summarizes Section 2.6 would improve the quality of the paper. This will be one of the many reasons people will want to read and cite the paper, concerning a discussion and comparison of the thermodynamic models in order to calculate pH. Including a table that summarizes how each model calculates pH, the pros and cons of each model, any assumptions, and etc., would help the readers remember that discussion better.

We added a table summarizing the four thermodynamic models used most extensively in the paper. One sentence was added to the first paragraph of section 2.6:

> Advantages and disadvantages of four common thermodynamic models are summarized in Table 2.

The following new table was added (*The italicized text was added Feb 2020 after posting the initial response to reviewer 2)*:

Table 2: Common box models used to calculate acidity.

Model	Input	Acidity Output	Advantages	Disadvantages
E-AIM	Gas + particle or equilibrium particle composition (H^+, NH_4^+, Na^+, SO_4^{2-}, HSO_4^-, NO_3^-, Cl^-, Br^-, organic acids, amines) in moles in overall electroneutral conditions (see Eq. 19 for Z); RH, T.	pH at equilibrium	pH via recommended Eq. 1 Considered the most accurate inorganic thermodynamic model Some ionizing organic species (e.g. organic acids, amines) considered	Computationally intensive T and RH restricted for some compositions to preserve accuracy
AIOMFAC-GLE	Gas + particle or equilibrium particle composition (H^+, Li^+, Na^+, K^+, NH_4^+, Mg^{2+}, Ca^{2+}, Cl^-, Br^-, NO_3^-, HSO_4^-, SO_4^{2-}, organic species and/or organic functional groups) in mol m^{-3} air for electroneutral conditions; RH, T	pH at equilibrium	pH via recommended Eq. 1 Accounts for organic--inorganic interactions and liquid-liquid equilibrium in consistent framework Code publicly distributed through repository	Limited support for solid-liquid equilibria of diverse inorganic salts (presently) Optimized for temperatures near 298 K, with limited accuracy for much colder atmospheric temperatures *Organic species do not ionize (Feb 2020 update)*
MOSAIC	Distinct gas and particle composition (H^+, NH_4^+, Na^+, Ca^{2+}, SO_4^{2-}, HSO_4^-, $CH_3SO_3^-$, NO_3^-, Cl^-, and CO_3^{2-}) in mol m^{-3} air; RH, and T. Automatic adjustments applied to non-electroneutral input particle-phase composition.	pH_F by default ($pH_\pm$ with modification) for each particle size bin (or mode) at each time step while dynamically solving gas-particle mass transfer	Provides size-resolved pH_F and $pH_\pm$ to account for compositional heterogeneity across particles of different sizes and origins Does not require equilibrium assumption	Gas-particle and solid-liquid equilibrium constants depend on temperature, but activity coefficients are limited to 298.15 K.
ISORROPIA II	Gas + particle or particle composition (TSO_4, TCl, TNO_3, TNH_4, Na, K, Ca, Mg) in mol m^{-3} or μg m^{-3} air; RH, T. Automatic adjustments applied to non-electroneutral input particle-phase composition.	pH_F by default ($pH_\pm$ with modification) at equilibrium	Computationally efficient Code has widespread public distribution and incorporation in CTMs	Approximations employed (e.g. some activity coefficients treated as 1, minor species do not perturb equilibrium, *higher numerical tolerances (Feb 2020 update)*) Segmented solution approach leads to discontinuous solution surface

4.) Throughout the sections, it is apparent that different people wrote them with different styles coming through in each section. For example, some sections briefly state future research while other sections devote a subsection about future research (and some sections do not have any discussion about questions/future work). Starting with at least Section 3, if not some aspects of Section 2 (i.e., Measuring pH), it would be beneficial for the authors to include a description of what they consider future questions/work to be.

In some cases, concepts span multiple sections. For example, proxies were introduced in section 4, but the box model intercomparison in section 6 had summarizing messages. We have reorganized the paper to improve the flow/connection throughout. The new order will be:

i. Introduction
ii. Definition
iii. Proxies (former 4)
iv. Box model comparison & w/proxies (former 6)
v. Role of processes: Aqueous Chemistry (former 3)
vi. Role of size, composition, mass transfer (former 7)
vii. Observations (former 5)
viii. CTM results
ix. Conclusions

This moves the box model intercomparison (*iv)* immediately after definitions of pH and proxies. The box model intercomparison contains a recap of concepts introduced in the preceding two sections (in Section 4.3: Recommendations on the calculation of pH by approximation and proxy) and thus serves as a synthesis of sections *ii*-*iv*.

New section *v* (old section 3) covers the role of aqueous chemistry. Since the section is already short, summary in nature, and the subject of a companion paper, an additional summary paragraph was not added.

For new Section *vi* (old 7) on size, composition, mass transfer, the last two subsections end with specific conclusions regarding the roles of size, composition, mass transfer, and organics/LLPS. No further conclusions/future directions were added.

Section *vii* (old 5/Observations) is divided into section 7.1 (aerosols) and 7.2 (clouds). Section 7.2 already had a section on the need for future monitoring of cloud pH. Section 7.2.4 was promoted up to 7.3 and expanded to include aerosol pH:

> 7.3 Need for future monitoring of cloud and aerosol pH
>
> Although cloud and fog sampling is generally more challenging than aerosol collection, pH measurement of the collected cloud/fog water is simpler due to its much larger volume and much lower ionic strength. As a result, ~~Over the past several decades,~~ fogs and clouds have been sampled and their pH determined in areas around the globe with more temporal and spatial coverage than for aerosol pH. Depending on inputs of key acids and bases, cloud/fog pH has been observed to range from below 2 to greater than 7~~.~~, slightly higher, but similar to fine aerosol pH that ranges from below 0 to near 7. Programs designed to target reductions in acid rain have had

direct impacts on cloud and fog pH~~.~~, but aerosol pH has been much more constant than cloud pH in the southeastern US and southeastern Canada over time. Analysis of cloud pH observations over the past 25 – 30 years reveals that cloud/fog acidity in many regions has decreased as anthropogenic emissions of the important acid precursors, SO_2 and NO_x, have decreased. A continued rise in cloud/fog pH is likely in many regions with planned, future decreases in NOx and SO_2 emissions and stable or increasing NH_3 emissions. Future changes in emissions could eventually be significant enough to lead to fine aerosol pH changes as well. Increases in cloud pH are expected to enhance the solubility of gas phase organic acids, potentially shortening their atmospheric lifetimes~~.~~ while increases in aerosol pH could lead to more nitrate aerosol formation and allow previously unfavorable kinetic reactions to occur.

As emissions evolve with time, continued characterization of cloud and particle pH is needed to understand how anthropogenic activities affect condensed-phase acidity and downstream endpoints in the earth system. Much remains to be learned about factors controlling cloud/fog pH in the atmosphere and the influence of this acidity on aqueous phase chemistry, including the aqueous phase uptake and oxidation of soluble gases to form secondary inorganic or organic aerosol. More detailed measurements of organic acids and bases, and their influence on cloud pH, will be increasingly important as sulfate and nitrate concentrations decline. Likewise, there is a need for more systematic monitoring of cloud and fog composition in key environments, as opposed to the more ad hoc past sampling approaches driven primarily by the objectives of process-based research. Because fogs and clouds are good integrators of atmospheric acids and bases in both the gas and particle phases, they may offer a convenient and practical basis for ongoing monitoring of atmospheric acidity. Future monitoring strategies should consider long-term monitoring at surface sites as well as periodic measurements of cloud, particle, and gas-phase composition from aircraft in order to enhance our understanding of acidity at higher elevations in the troposphere. Future measurements should also better document heterogeneity of acidity across individual drops within a cloud ~~or~~/ fog or aerosol population, for example ~~looking at~~by determining the size-dependence of ~~drop~~ pH. Aerosol pH estimates will likely continue to be primarily based on thermodynamic models in the near future and thus require simultaneous particle- and gas-phase measurements (specifically of ammonia) to improve the spatial and temporal scales over which fine particle pH is currently characterized.

Section *viii* (CTM predictions) already contains a summary/future directions section.

Multiple minor changes were made throughout the manuscript for the new section order (will be provided in the future tracked changes document).

5.) For Section 3, it would be good to include a couple of items in discussion, including: (a) How many of the reactions have been conducted for dilute, laboratory conditions, therefore, for aerosol, where the ion activity is higher and water is lower, there is large uncertainty in how the reactions may occur. (b) How there is debate occurring the field about various reactions (e.g., production of sulfate in aerosol in China) and the questions/future studies needed to move this questions forward. (c) N2O5 chemistry appears to be missing in your discussion throughout, including in Section 5.

The current paper is already quite long (~140 pages). The topic of kinetic drivers of pH and how pH affects kinetics is a large topic and warrants a separate companion paper. Former section 3 (now 5) was meant to highlight some examples of the kinetics-pH interplay, but not intended to be comprehensive. We will defer the bulk of these reviewer suggestions to the companion paper. However, we added mention of N_2O_5 in the introduction along with two references:

> The concentration of fine particulate matter ($PM_{2.5}$) is directly modulated by pH through its effects on gas–particle partitioning, ~~and~~ pH-dependent condensed-phase reactions~~.~~, and other particle processes influenced by pH. For example, N_2O_5 heterogeneous hydrolysis significantly affects tropospheric chemistry (Dentener and Crutzen, 1993) and depends strongly on particle composition (Chang et al., 2011), including formation of organic coatings due to liquid-liquid phase separation influenced by acidity (see Section 6.3 for a discussion of phase separation in the context of acidity).
>
> Chang, W. L., Bhave, P.V., Brown, S.S., Riemer, N., Stutz, J., and Dabdub, D.: Heterogeneous atmospheric chemistry, ambient measurements, and model calculations of N_2O_5: A review, Aerosol Sci. Technol., 45, 6665-6695, https://doi.org/10.1080/02786826.2010.551672, 2011.
>
> Dentener, F. J., and Crutzen, P. J.: Reaction of N_2O_5 on tropospheric aerosols: Impact on the global distributions of NO_x, O_3, and OH, J. Geophys. Res., 98(D4), 7149– 7163, https://doi.org/10.1029/92JD02979, 1993.

6.) For Section 8, a table that summarizes the CTMs with the thermodynamic models they use and the species they use to calculate pH would help with the discussion.

We added a new table, Table 7, that summarizes the CTM calculations of pH. We included models used in this work only (rather than characterizing all CTMs in literature). A sentence was added to the first paragraph of Section 8:

> Table 7 summarizes the species considered in the calculation of pH for each model displayed in this work.

The following new table was added:

Table 7: Species and methods used to calculate acidity in CTMs. Bulk cloudwater pH is calculated assuming electroneutrality, generally using model-specific algorithms. Dissolved gases in cloudwater are determined using Henry's law coefficients. Configurations are specific to this work.

Model	Aerosol size information	Species/sources considered in aerosol pH calculation	Fine aerosol pH calculation method	Species/sources considered in cloud pH calculation
CMAQ v5.3	Fine aerosol: explicit Aitken and accumulation modes. Coarse mode acidity not explicitly calculated but included in determination of dynamic mass transfer and composition.	TSO_4, TCl, TNO_3, TNH_4, Na, K, Ca, Mg from sea salt, dust, wildland fires, and anthropogenic activities.	ISORROPIA II pH_F for inorganic-only composition of combined fine modes. Condensed water associated with organic species is also predicted (not considered in fine aerosol pH_F in this work).	Aqueous species: H^+, OH^-, HSO_3^-, SO_3^{2-}, HSO_4^-, SO_4^{2-}, HCO_3^-, CO_3^{2-}, HCO_2^-, NH_4^+, NO_3^-, Cl^-, Ca^{2+}, Na^+, K^+, Mg^{2+} Dissolved gases: SO_2, CO_2, NH_3, HCl, HNO_3, HCOOH, H_2SO_4 (as sulfate), N_2O_5 (as $2\times HNO_3$)
GEOS-Chem v12.0.0	Bulk fine aerosol. Coarse mode acidity not explicitly calculated but included in determination of dynamic mass transfer and composition.	TSO_4, HCl, TNO_3, TNH_4, and fine mode Ca, Mg, Na, Cl from anthropogenic, sea salt, and dust sources (dust contributions not considered in default GEOS-Chem predictions but Ca and Mg from dust considered in this work).	ISORROPIA II pH_F.	Aqueous species: SO_4^{2-}, NO_3^-, NH_4^+ Dissolved gases: CO_2, SO_2, NH_3, HNO_3
TM4-ECPL	Fine (externally mixed dust) and coarse (internally mixed dust) aerosol.	SO_4^{2-}, NH_3, NH_4^+, HNO_3 and NO_3^-; sea salt and dust assumed to be externally mixed with fine mode sulfate and not considered in the fine acidity calculation.	ISORROPIA II pH_F for inorganic-only composition of fine and coarse modes (each in equilibrium with gas). Condensed water associated with organic species is also predicted (not considered in fine aerosol pH_F in this work).	Aqueous species: SO_4^{2-}, $CH_3O_3S^-$, NO_3^-, NH_4^+, Na^+, Ca^{2+}, K^+, Cl^- Mg^{2+} Dissolved gases: SO_2, CO_2, HNO_3, NH_3, oxalic acid
WRF-Chem	Four aerosol size bins (0.039–0.156, 0.156–0.625, 0.625–2.5, 2.5–10 µm in diameter) treated dynamically.	sulfate, HNO_3/NO_3^-, NH_3/NH_4^+, $CH_3O_3S^-$, Cl^-, CO_3^{2-}, Na, Ca; HCl not considered with MOZART chemistry (no displacement of Cl^- from sea salt aerosols allowed).	MOSAIC size-resolved pH_F.	Aqueous species: OH^-, HCO_3^-, CO_3^{2-}, CO_3^-, HSO_3^-, SO_3^{2-}, HSO_4^-, SO_4^{2-}, SO_4^-, SO_5^-, HSO_5^-, $HOCH_2SO_3^-$, $^-OCH_2SO_3^-$, NO_2^-, NO_3^-, HO_2^-, O_2^-, $HCOO^-$, Cl^-, Cl_2^-, $ClOH^-$, NH_4^+, Fe^{3+}, Mn^{2+} Dissolved gases: SO_2, CO_2, HNO_3, NH_3, HO_2, HCOOH, H_2O_2
CAM-Chem	Four log-normal modes.	Inorganic aerosol composition considered: SO_4^{2-}, NH_4^+, soil dust, sea salt.	Not considered in this work.	Aqueous species: OH^-, HCO_3^-, NO_3^-, HSO_3^-, SO_3^{2-}, SO_4^{2-}, NH_4^+ Dissolved gases: SO_2, H_2SO_4, HNO_3, CO_2, NH_3

7.) For Section 9, I appreciate that it summarizes the very large review. However, at this point, I really think a description of remaining questions, studies, observations and future outlook is necessary so that we, as a community, know what should be done to move forward.

The synthesized messages in section 9 were developed at a workshop involving the coauthors of this study. Coauthors submitted their thoughts on major messages ahead of discussion then messages were discussed, refined, and agreed upon by the group. As a result, we think the most important major messages (which include both summary information and future directions) have been captured. The individual sections contain additional information. Some future directions (e.g. understanding/improving bisulfate dissociation predictions to improve consistency among box models) were raised and discussed by the group but considered too detailed for the main messages.

We think that section 9 already provides guidance to the community. The following guidance is contained in section 9:

- We recommend researchers use specific nomenclature to document and communicate what metric of acidic they report
- pH is the ideal indicator of acidity and researchers should aim to report that value or an approximation ($pH_{\pm}$ is best approximation)
- The role of kinetic-pH interactions is likely underappreciated and should be further examined to understand where H^+ is chemically generated (this is discussed in the companion paper)
- Experimental determination of aerosol pH is a current knowledge gap
- Heterogeneity of pH across the aerosol/cloud droplet population and within a given particle needs investigation (most methods/models use bulk techniques)
- Ammonia measurements are needed to facilitate determination of aerosol pH
- Ambient characterization of pH is spatially and temporally incomplete (more observations or observationally constrained estimates are needed-Section 7 highlights current areas without measurements and where trends are available).
- pH should be considered in the context of CTM evaluation and endpoints of interest.
- Considerable model diversity in predicted pH exists and Section 8 points to mixing state assumptions and composition as reasons and locations where model diversity is high and could be measured

Other Revisions

1. A few studies reporting observationally-constrained estimates of fine aerosol pH were added to SI Table S6 and fully synchronized with Fig 2b (global distribution histogram) and Fig 14 (map). In cases where only a min and max fine aerosol pH_F value was provided by an observational study (Table S6), a mean value was created by averaging the min and max (revisions in Table S6). When the min/max were averaged, it was noted in the Method column (see tracked changes). Additional cleanup in Table S6 included state abbreviations and minor lat/lon adjustments. We added one sentence regarding new data:

   However, more acidic particles (pH ranging from -0.8 to 3.0) have been observed near the Kilauea volcano in Hawaii (Kroll et al., 2015).

   Data added to SI Table S6:

Location	Altitude (m)	Lati-tude (°N)	Lati-tude (°E)	Time	Aerosol Size	n	Mean (pH)	σ (pH)	Min (pH)	Max (pH)	Method	Reference
Pellston, Michigan, USA		45.56	-84.86	Jul-16	<0.4 µm		1.5				pH paper	Craig et al. 2018
Near Kilauea, Hawaii, USA		19.2026-19.4327	155.4775-155.2739	Jan - Feb 2013	PM1		1.1		-0.8	3.0	E-AIM II with ACSM measured composition	Kroll et al., 2015
Tianjin		39.11	117.16	12-23 August 2015	PM2.5	387	3.4	0.5	2.6	4.6	ISORROPIA (forward, metastable)	Shi et al., 2019
Po Valley Italy	mean of 6 sites	45.4	12.2	winter 2012-2013	PM2.5		3.9	0.3			ISORROPIA (forward, metastable, no NH3)	Masiol et al. 2020
Po Valley Italy	mean of 6 sites	45.4	12.2	summer 2012	PM2.5		2.3	0.3			ISORROPIA (forward, metastable, no NH3)	Masiol et al. 2020

2. The Barbados value in Fig 14 was updated to reflect an average for 0.4 to 1.7 µm size particles rather than only 0.4 to 0.8 µm.
3. A reference (Ding, J., et al, Atmos. Chem. Phys., 2019) was updated with the correct title: 'Aerosol pH and its driving factors in Beijing'.
4. SI references were formatted and cleaned up (including addition of DOIs and a few missing references).
5. We added an acknowledgement to Chris Nolte and Donna Schwede for their helpful comments during EPA internal review.
6. The number of significant digits reported in the main text tables was reduced.
7. References to discussion papers were updated to final versions.
8. Some abbreviations were cleaned up in the text (along with appendix revisions in response to reviewer 2).
9. Minor grammatical edits.
10. Figure 8 (comparison of acidity with proxies using field data) panel order was revised to follow order of discussion in text (minor formatting changes).
11. Strong acidity terminology was clarified. Now, charge/ion balance is used for the quantity in Table 2, Figure 8, and the primary term used in the text for summation over measured anions and cations. The order of some paragraphs was revised in proxy Section 3 as well as some minor wording edits.

12. A sentence in the conclusions, “This is a direct consequence of the liquid water content and other aerosol species being in equilibrium with the ambient relative humidity – while in clouds all the species can vary independently of each other,” was reworded for clarity. Now: “This is a direct consequence of the difference in liquid water content which is higher in clouds than fine aerosols.”
13. Some numbers in the introduction of idealized systems for box model pH calculation in 4.1.1 were not synced with Fig. 3. Section 4.1.1 text updated to match Fig. 3.
14. Multiple observations are available for Tianjin. Figure 5 (diurnal variation) used Shi et al. 2019 not Shi et al. 2017 as was labeled. Caption revised.
15. Figure 5 was updated (formatting and correction to plotting error for Atlanta data).
16. Equation S11 was updated (pH appeared on wrong side) and a typo in Section S1 corrected.
17. Note: For the purposes of tracked changes, section order was updated before changes were recorded to avoid large sections appearing as edits solely due to movement of text.

The Acidity of Atmospheric Particles and Clouds

Havala O. T. Pye[1], Athanasios Nenes[2,3], Becky Alexander[4], Andrew P. Ault[5], Mary C. Barth[6], Simon L. Clegg[7], Jeffrey L. Collett, Jr.[8], Kathleen M. Fahey[1], Christopher J. Hennigan[9], Hartmut Herrmann[10], Maria Kanakidou[11], James T. Kelly[12], I-Ting Ku[8], V. Faye McNeill[13], Nicole Riemer[14], Thomas Schaefer[10], Guoliang Shi[15], Andreas Tilgner[10], John T. Walker[1], Tao Wang[16], Rodney Weber[17], Jia Xing[18], Rahul A. Zaveri[19], Andreas Zuend[20]

[1]Office of Research and Development, U.S. Environmental Protection Agency, Research Triangle Park, NC, 27711, USA
[2]School of Architecture, Civil and Environmental Engineering, Ecole Polytechnique Fédérale de Lausanne, Lausanne, CH-1015, Switzerland
[3]Institute for Chemical Engineering Sciences, Foundation for Research and Technology Hellas, Patras, GR-26504, Greece
[4]Department of Atmospheric Science, University of Washington, Seattle, WA, 98195, USA
[5]Department of Chemistry, University of Michigan, Ann Arbor, MI, 48109-1055, USA
[6]National Center for Atmospheric Research, Boulder, CO, 80307, USA
[7]School of Environmental Sciences, University of East Anglia, Norwich NR4 7TJ, UK
[8]Department of Atmospheric Science, Colorado State University, Fort Collins, CO, 80523, USA
[9]Department of Chemical, Biochemical, and Environmental Engineering, University of Maryland Baltimore County, Baltimore, MD, 21250, USA
[10]Leibniz Institute for Tropospheric Research (TROPOS), Atmospheric Chemistry Department (ACD), Leipzig, 04318, Germany
[11]Department of Chemistry, University of Crete, Voutes, Heraklion Crete, 71003, Greece
[12]Office of Air Quality Planning & Standards, U.S. Environmental Protection Agency, Research Triangle Park, NC, 27711, USA
[13]Department of Chemical Engineering, Columbia University, New York, NY, 10027, USA
[14]Department of Atmospheric Sciences, University of Illinois at Urbana-Champaign, Urbana-Champaign, Illinois, 61801, USA
[15]State Environmental Protection Key Laboratory of Urban Ambient Air Particulate Matter Pollution Prevention and Control, Nankai University, Tianjin, 300071, China
[16]Department of Civil and Environmental Engineering, The Hong Kong Polytechnic University, Hung Hom, Kowloon, Hong Kong, China
[17]School of Earth and Atmospheric Sciences, Georgia Institute of Technology, Atlanta, GA, 30332, USA
[18]School of Environment, Tsinghua University, Beijing, 100084, China
[19]Atmospheric Sciences & Global Change Division, Pacific Northwest National Laboratory, Richland, WA, 99352, USA
[20]Department of Atmospheric and Oceanic Sciences, McGill University, Montreal, Quebec, H3A 0B9, Canada

Correspondence to: Havala O. T. Pye (pye.havala@epa.gov)

Abstract. Acidity, defined as pH, is a central component of aqueous chemistry. In the atmosphere, the acidity of condensed phases (aerosol particles, cloud water, and fog droplets) governs the phase partitioning of semi-volatile gases such as HNO_3, NH_3, ~~and~~ HCl, and organic acids and bases as well as chemical reaction rates. It has implications for the atmospheric lifetime of pollutants, deposition, and human health. Despite its fundamental role in atmospheric processes, only recently has this field seen a growth in the number of studies on particle acidity. Even with this growth, many fine particle pH estimates must be based on thermodynamic model calculations since no operational techniques exist for direct measurements. Current

information indicates acidic fine particles are ubiquitous, but observationally-constrained pH estimates are limited in spatial and temporal coverage. Clouds and fogs are also generally acidic, but to a lesser degree than particles, and have a range of pH that is quite sensitive to anthropogenic emissions of sulfur and nitrogen oxides, as well as ambient ammonia. Historical measurements indicate that cloud and fog droplet pH has changed in recent decades in response to controls on anthropogenic emissions, while the limited trend data for aerosol particles indicates acidity may be relatively constant due to the semi-volatile nature of the key acids and bases and buffering in particles. This paper reviews and synthesizes the current state of knowledge on the acidity of atmospheric condensed phases, specifically particles and cloud droplets. It includes recommendations for estimating acidity and pH, standard nomenclature, a synthesis of current pH estimates based on observations, and new model calculations on the local and global scale.

1 The importance of atmospheric acidity

Human activity and natural processes result in emissions of sulfur, nitrogen, ammonia, dust, and other compounds that affect the composition of the Earth's atmosphere. The acidity of suspended atmospheric media, particles and droplets, influences many processes that involve the atmosphere and all aspects of the Earth system (e.g., watersheds, marine and terrestrial ecosystems) that interface with it, see Fig. 1. Aerosols (also referred to as particulate matter, PM) and cloud droplets throughout the atmosphere exhibit a wide range of acidity, each spanning five orders of magnitude or more in molality units, or five units of pH (Fig. 2). Some anthropogenic emissions (sulfur dioxide, nitrogen oxides, organic acids) increase acidity while others (ammonia, non-volatile cations (NVC), amines) reduce acidity. The orders of magnitude differences in water content between aerosols and clouds leads to distinctly different acidity levels in these media, as well as their response to changes in precursor concentrations. The ability of a chemical species to affect particle or cloud droplet acidity is driven by both its degree of acidity (or basicity), reflected in the~~ir~~ dissociation (or association) constant~~s~~, and by volatility, with less volatile compounds partitioning to a greater degree into liquid aerosols and cloud droplets. Semi-volatile species, for which significant fractions typically exist in both the gas and condensed phases, include ammonia (NH_3), nitric acid (HNO_3), hydrochloric acid (HCl), and low molecular weight organic acids (formic, acetic, oxalic, malonic, succinic, glutaric, and maleic acids) and/or bases (e.g. amines). Sulfuric acid (H_2SO_4), by contrast, has extremely low volatility and can be treated as entirely in the condensed phase for most applications. Metal cations, including those found in dust and sea salt, are also essentially non-volatile. The abundance of these various constituents is a function of emission source and atmospheric processing and ultimately dictates the pH of fine particles (Fig. 1, 2).

Although aerosol and cloud acidity are distinct in many ways, aerosol forms in part from cloud evaporation, and so aerosol composition and acidity may be directly affected by cloud chemistry. Similarly, cloud droplets and ice crystals nucleate on pre-existing particles, and therefore much of the material that modulates cloud acidity originates from the precursor aerosol. In addition, cloud droplets can collide with surfaces resulting in occult deposition (Dollard et al., 1983) or precipitation in the

form of rain. With these connections in mind, both aerosol and cloud acidity are important to human health, ecosystem health and productivity, climate, and environmental management.

The acidity of atmospheric deposition for dry, wet, and occult (wind-driven cloud-water) pathways is directly affected by aerosol and cloud pH (Fig. 1). Thus, programs designed to reduce acid rain (e.g., the Acid Rain Program under Title IV of the 1990 Clean Air Act Amendments in the U.S.), have had implications for particle and cloud droplet acidity. In terrestrial ecosystems, direct effects of acid deposition to foliage include leaching of cations, altered stomatal function and changes in wax structure (Cape, 1993). Acid deposition can exacerbate soil acidification (Binkley and Richter, 1987), resulting in loss of soil base cations, leaching of nitrate and mobilization of aluminium, affecting terrestrial ecosystem health and the quality of water delivered to streams and lakes (Driscoll et al., 2007). Apart from reactive nitrogen, atmospheric deposition is also a significant source of limiting and trace nutrients such as phosphorus, iron, and copper, especially in the remote oceans (Mahowald et al., 2008; Myriokefalitakis et al., 2018). While mineral dust is a major source of these nutrients, combustion sources also emit iron, copper and other trace metals (Reff et al., 2009; Ito et al, 2019). Acid processing of aerosol prior to deposition, may greatly enhance the solubility of all these compounds increasing their bioavailability and ecosystem impacts (Meskhidze et al., 2003; Nenes et al., 2011; Kanakidou et al., 2018). For example, dust aerosols coated by acidic sulfate and nitrate show increased Fe solubility compared to fresh dust particles, particularly in the fine mode, the deposition of which may promote phytoplankton blooms in nutrient-limited regions of the oceans (Meskhidze et al., 2005). The same process occurs for P (e.g., Nenes et al., 2011; Stockdale et al., 2016); however, the extent to which particle pH may similarly increase the solubility and amount of organic forms of nitrogen and phosphorous, a potentially large source to ecosystems (Jickells et al., 2013), is not well known (Kanakidou et al., 2018). Deposition of trace nutrients from acid-promoted dissolution into regions of the ocean where the nutrients are not limiting ~~the~~ to biological productivity may enhance ~~the~~ productivity in ~~other~~ nutrient-limited regions ~~that are nutrient-limited~~ by means of long-range transport by ocean currents. Such a redistribution of nutrients can have important implications for the biogeochemistry of the ocean, the oxygenation state, and the carbon cycle (Ito et al., 2016).

Aerosol acidity is also a governing factor for atmospheric dry deposition of inorganic reactive nitrogen species, which is a key nutrient driving primary productivity in terrestrial and marine ecosystems. The hydrogen ion activity in aqueous aerosols affects the partitioning of total nitrate ($TNO_3 = HNO_3 + NO_3^-$) and total ammonium ($TNH_4 = NH_3 + NH_4^+$) between the gas and aerosol phases. Given the much larger deposition velocity of gases compared to submicron aerosols, pH-mediated partitioning influences the effective deposition velocity and lifetime of TNO_3, TNH_4, and total inorganic N ($TNO_3 + TNH_4$). Acidity therefore also affects the magnitude and spatial patterns of inorganic N deposition to terrestrial and aquatic ecosystems. Lower aerosol pH favors partitioning of TNO_3 toward gaseous HNO_3 rather than aerosol NO_3^- thus shortening its lifetime (Weber et al., 2016). In contrast, TNH_4 ($NH_3 + NH_4^+$) partitions toward gaseous NH_3 at higher pH. Conditions of aerosol pH that promote a short residence time and local dry deposition of TNO_3 may conversely result in longer range transport of TNH_4

and a more spatially extensive pattern of deposition and influence from source regions. The presence of dust and sea salt can influence not only pH but the size distribution (Lee et al., 2008, Lee et al., 2004) and resulting deposition velocity of nitrate aerosol due to higher deposition velocities of coarse compared to fine mode particles (Slinn, 1977). Variations in this scavenging efficiency, dependent upon cloud pH, can also affect atmospheric lifetimes and spatial deposition patterns of TNH_4. HNO_3, due to its strong acidity, is essentially partitioned entirely to cloud droplets for typical cloud pH values (>2). NH_3 also mostly partitions into cloud drops for pH values below 6, but an appreciable fraction can remain in the gas phase for higher pH values. Biases in pH in atmospheric models can therefore influence the amount, speciation, and location of N deposition, with implications for determining ecosystem critical load exceedances for nutrients and acidity (Bobbink et al., 2010).

$PM_{2.5}$ is associated with adverse human health effects, including premature mortality (Di et al., 2017; Lepeule et al., 2012; Pope et al., 2009; EPA, 2009). Aerosol acidity is associated with health effects of air pollution through its influence on atmospheric processes that affect the amount and composition of $PM_{2.5}$ (Fig. 1). The concentration of fine particulate matter ($PM_{2.5}$) is directly modulated by pH through its effects on gas–particle partitioning, ~~and~~ pH-dependent condensed-phase reactions~~.~~, and other particle processes influenced by pH. For example, N_2O_5 heterogeneous hydrolysis significantly affects tropospheric chemistry (Dentener and Crutzen, 1993) and depends strongly on particle composition (Chang et al., 2011), including formation of organic coatings due to liquid-liquid phase separation influenced by acidity (see Section 6.3 for a discussion of phase separation in the context of acidity). The "strong acidity" property of aerosol (Koutrakis et al., 1988) has historically been associated with adverse health effects (Dockery et al., 1993; Dockery et al., 1996; Thurston et al., 1994; Raizenne et al., 1996; Spengler et al., 1996; Gwynn et al., 2000; EPA, 2009). One reason for this could be that aerosol acidity influences solubilization and the concentrations of toxic forms of trace species, such as transition and heavy metals, that have been linked to negative health effects (Kelly and Fussell, 2012; Lippmann, 2014; Rohr and Wyzga, 2012; Chen and Lippmann, 2009, Frampton et al., 1999). Transition metal ions (TMI), such as soluble Cu and Fe from acid dissolution, contribute significantly to the oxidative potential of particles (Fang et al., 2017; Poschl and Shiraiwa, 2015), which has been linked to cardiorespiratory emergency department visits with a stronger association than $PM_{2.5}$ mass (Abrams et al., 2017; Bates et al., 2015). Ye et al. (2018) report a strong association between soluble Fe, which is modulated by particle acidity and aerosol water content, and cardiovascular endpoints. The mechanistic link between acidity, TMI dissolution, and health outcomes recently proposed by Fang et al. (2017) may help explain why sulfate in the ambient atmosphere is associated with adverse health outcomes – in contrast to studies that show little role for sulfate in negative health endpoints (Schlesinger, 2007; Reiss et al., 2007).

Aerosol acidity can affect the gas–particle partitioning of semi-volatile toxic organic pollutants and therefore their environmental fate and pathways for exposure (Vierke et al., 2013). Some per- and polyfluoroalkyl substances (PFASs), including ~~perfluoroalkane~~ perfluoroalkyl sulfonic acids (PFSAs) and perfluoroalkyl carboxylic acids (PFCAs), are strongly acidic and likely to be at least partially dissociated (ionized) under pH conditions typical of most atmospheric aerosols (Ahrens

Formatted: Subscript

Formatted: Subscript

et al., 2012). Once in the particle phase, ~~they~~ pollutants are vulnerable to hydrolysis, which shortens their lifetime in the environment but may lead to the formation of toxic degradation products (Tebes-Stevens et al., 2017). Aerosol acidity was also recently shown to enhance airborne nicotine levels and resulting thirdhand smoke exposure by promoting volatilization from surfaces (such as clothes) and allowing distribution throughout a building's indoor air (DeCarlo et al., 2018). Similar behavior may be possible for other alkaloids (Pankow, 2001). Furthermore, aerosol acidity may also affect particle toxicity on a per mass basis (increase or decrease) by influencing organic aerosol composition (Arashiro et al., 2016; Tuet et al., 2017). Many organic compounds that are toxic (e.g., nitrosamines) can also be formed in the aerosol phase under acidic conditions; at the same time, other potentially toxic compounds (e.g., organonitrates) may hydrolyze under strongly acidic conditions (Rindelaub et al., 2016a). Even for non-toxic organic aerosol facilitated by acidity, the enhanced (or conversely reduced) formation of inert organic mass in the particle promotes the partitioning (or evaporation) of toxic species, such as polycyclic aromatic hydrocabons (PAHs) (Liang et al., 1997), from the gas phase to the particle and thereby alters the location of deposition in the respiratory airways. For a highly soluble organic species, uptake to the aerosol phase can also potentially extend its~~their~~ atmospheric lifetime~~s~~ by ~~protecting the species against~~slowing deposition ~~on~~ to vegetation and ground surfaces.

Since acidity impacts the mass and chemical composition of atmospheric aerosols, which scatter and absorb radiation and serve as cloud condensation nuclei (CCN), acidity can also affect climate. First, particle pH influences, and is related to, the water uptake properties (hygroscopicity) of particles, which in turn can modulate both visibility and the radiative balance throughout the atmosphere (the aerosol direct climate effect). Cloud pH has been linked to the amount and speciation of aerosol upon evaporation, with important radiative effects (Turnock et al., 2019). Changes in acidity can also affect the number of chromophores contained within aerosol (so-called brown carbon) and their efficiency to absorb sunlight in the near-UV range (Hinrichs et al., 2016; Teich et al., 2017; Phillips et al., 2017). Acidity-induced changes in aerosol affect the ability of particles to act as CCN and contribute to the formation of droplets in warm and mixed-phase clouds. For example, insoluble particles, such as dust, facilitate the production of ice crystals in mixed-phase and cold clouds (Seinfeld and Pandis, 2016); acidification of these particles can modify the active sites that ice is formed upon, and thereby affect the distribution of ice and liquid water throughout the atmosphere (Sullivan et al., 2010; Reitz et al., 2011). The distribution of droplets and ice also may in turn regulate the riming efficiency in mixed-phase clouds (Pruppacher and Klett, 2010) and distribution of clouds throughout the atmosphere. Changes in cloud distribution strongly modulate Earth's radiative balance and the hydrological cycle (IPCC, 2007).

Atmospheric acidity also plays an important role in new particle formation, which is thought to contribute up to 50% of the CCN concentrations in the atmosphere, thus acting as a climate regulator (Gordon et al., 2017). Sulfuric acid likely plays a critical role in the formation of stable clusters upon which new particles are formed (Weber et al., 1997; Weber et al., 1998), while bases such as amines and NH_3~~ammonia~~ (Jen et al., 2016) can facilitate stabilization and growth of such clusters. Uptake of organic acids through acid-base chemistry (Zhang et al., 2004; Hodshire et al., 2016) and acid-mediated secondary organic

aerosol formation (e.g., McNeill, 2015) impact the aerosol size distribution with implications for CCN concentrations, cloud droplet formation and climate.

Understanding particle acidity can facilitate improved air quality management strategies and policy planning to mitigate the health and environmental effects of air pollution. Consideration of different policy options and the development of emission reduction strategies often relies on chemical transport model (CTM) simulations of future conditions. Such modeling depends on the capability of CTMs to adequately simulate responses to policy scenarios. The predictive capability of CTMs is closely linked to their ability to track particle acidity through the pathways shown in Fig. 1. Some studies have pursued the development of observation-based indicators for the sensitivity of pollutants to precursor emissions for use in CTM evaluation and air quality management (e.g., Gas Ratio, Sect. 43). However, the use of the sensitivity indicators has been limited because their robustness has not been well established. Recent work (Shah et al., 2018; Vasilakos et al., 2018) has begun to explore the influence of particle acidity on the simulated responsiveness of $PM_{2.5}$ to emissions changes. Vasilakos et al. (2018) demonstrated that reliable predictions of particle pH in CTMs are key to modeling the response of $PM_{2.5}$ components to precursor emission changes. Furthermore, pH biases may propagate to biases in nitrate partitioning, dissolved metal concentrations, inorganic and organic aerosol amount and composition, aerosol size distributions, and ultimately could affect predicted impacts of emissions on ecosystem productivity and public health.

This study reviews the current understanding of aerosol and cloud acidity in the atmosphere. The work is motivated by the central role of aerosol and cloud acidity in numerous complex atmospheric processes of importance to human health and welfare as well as the rapid growth in literature on aerosol acidity in recent years. Despite decades of research on these processes, relatively few observational constraints exist for model evaluation. This review aims to collect values of fine aerosol and cloud pH as well as discuss the approaches used to determine them. We provide an overview of the range of pH acidity scales and methods of approximating pH as well as discuss their challenges and advantages (Sect. 2). In addition, we discuss proxies of pH (Sect. 3), insights from box modeling of particle pH and its approximations and proxies (Sect. 4), the role of chemistry in driving and being modulated by pH (Sect. 35), the role of size and composition (Sect. 6), ~~proxies of pH (Sect. 4),~~ observations of particle (Sect. 57.1) and cloud (Sect. 57.2) pH, ~~insights from box modeling of particle pH and its approximations and proxies (Sect. 6), the role of size and composition (Sect. 7),~~ and regional and global model representations of pH (Sect. 8).

2 The definition of pH and pH scales

Aerosol acidity is generally not directly measured, despite some recent progress (see Sect. 57.1.1-57.1.2). Instead, estimates are obtained from thermodynamic models that involve assumptions, which can vary according to the completeness of the atmospheric dataset being considered. The numerical value of pH also differs according to the concentration scale in use.

Furthermore, pH has a number of different definitions – each devised for a particular application – and can only be measured accurately and with metrological traceability for dilute solutions. These facts are not always well understood. This section summarizes the formal definition of pH and operational definitions and approximations. Thermodynamic models used to calculate fine particle pH are also discussed.

2.1 Definition of acidity in terms of the pH

The degree of acidity or basicity of a solution can be quantified based on the thermodynamic activity (the effective concentration, including non-ideal behavior) of dissolved hydrogen ions (H^+). In ~~its~~ the most common form, this measure of acidity is reported as a dimensionless quantity known as the pH. The International Union of Pure and Applied Chemistry (IUPAC) defines pH as (Buck et al., 2002; IUPAC, 1997):

$$\mathrm{pH} = -\log_{10}(a_{\mathrm{H}^+}) = -\log_{10}\left(\frac{m_{\mathrm{H}^+}}{m^{\ominus}}\,\gamma_{\mathrm{H}^+}\right), \qquad (1)$$

where a_{H^+} denotes the activity of H^+ in aqueous solution on a molality basis, m_{H^+} is the molality of H^+ (mol kg^{-1}, i.e. moles of H^+ ions per kg of solvent, typically pure water), and γ_{H^+} is its molal activity coefficient (see Table 1 for a summary of definitions of pH and Appendix A for notation). The quantity $m^{\ominus} = 1$ mol kg^{-1} is the standard state (unit) molality used to achieve a dimensionless quantity in the logarithm (Covington et al., 1985) (omitted for simplicity in future equations). For solid particles or ice clouds, and potentially for glassy particles, a single pH value is undefined due either to the lack of a liquid aqueous phase or the potential for long intraparticle mixing timescales. In Eq. (1), both a_{H^+} and γ_{H^+} are molality-based with a reference state of infinite dilution in pure water ($\gamma_{\mathrm{H}^+} \longrightarrow 1$ as $m_{\mathrm{H}^+} \longrightarrow 0$). In most calculations involving natural systems the solvent is pure water, and therefore the molality, m_i (mol kg^{-1}), of solute species i is given by $m_i = \frac{n_i}{n_w M_w}$, where n_i is the number of moles of i in the aerosol or cloud water particles, n_w the number of moles of water and M_w the molar mass of water. For some applications involving solutions containing large fractions of organic material that are miscible with water, the definition of the 'solvent' may be altered to include all non-ionic (organic) species. This is largely for practical reasons and because some thermodynamic models of activities in solutions and liquid mixtures (e.g., Yan et al., 1999; Zuend et al., 2008) require it. The activity coefficients used in the calculation of pH must be consistent with both the definition of what constitutes the solvent and also the concentration scale used. Further explanation is given in the Supplementary Information (Sect. S1).

The IUPAC definition of pH (Eq. 1) is regarded as a notional definition, because it involves the activity coefficient of a single ion (Buck et al., 2002; Covington et al., 1985). These are inaccessible experimentally because electrolyte solutions (of any relevant amount of substance) always contain both cations and anions, in proportions yielding an overall electroneutral system. Only mean activity coefficients of neutral cation–anion combinations are measurable quantities, such as $\gamma_{\pm,\mathrm{HCl}} = \left[\gamma_{\mathrm{H}^+}\gamma_{\mathrm{Cl}^-}\right]^{\frac{1}{2}}$ in the case of the 1:1 electrolyte HCl (e.g., Prausnitz et al., 1999; Robinson and Stokes, 2002). Several, but not all, thermodynamic activity coefficient models used in atmospheric science and geochemistry provide a computation of single-ion activity

coefficients within their mathematical framework (see later discussion of aerosol models, Sect. 2.6). However, these single-ion values are purely conventional in that they depend on assumptions inherent in the derivation of the model equations and, unlike mean activity coefficients, are not necessarily comparable between models.

2.2 Alternative pH concentration scales

Older definitions of pH by IUPAC, alongside Eq. (1), define the pH value on a molarity scale (pH_c) (Covington et al., 1985):

$$\mathrm{pH}_c = -\log_{10}\left(a_{\mathrm{H}^+}^{(c)}\right) = -\log_{10}\left(\frac{c_{\mathrm{H}^+}}{c^{\ominus}}\,\gamma_{\mathrm{H}^+}^{(c)}\right). \quad (2)$$

The superscript (c) indicates the molarity basis for the activity ($a_{\mathrm{H}^+}^{(c)}$) and activity coefficient ($\gamma_{\mathrm{H}^+}^{(c)}$), distinct from the molality basis. The reference state is still infinite dilution in pure water ($\gamma_{\mathrm{H}^+}^{(c)} \to 1$ as $c_{\mathrm{H}^+} \to 0$), and the quantity $c^{\ominus} = 1$ mol dm^{-3} is the standard state molarity. The quantity c_{H^+} denotes the molarity or molar concentration of H^+ in an aqueous solution (i.e., mol of H^+ per dm^3 of aqueous solution; IUPAC, 1997). For dilute solutions, c_{H^+} is practically equivalent to the molar amount of ion per dm^3 of pure water. Covington et al. (1985) point out that for most applications involving dilute aqueous solutions, the pH and $\mathrm{pH_c}$ values obtained from molality and molarity scales (for the same mixture) are of negligible numerical difference. The pH difference depends mainly on the density of water, and the difference in molal vs molarity-based pH is approximately 0.001 pH units at 298.15 K, increasing to about 0.02 pH units at 393.15 K (with larger differences expected for concentrated aqueous electrolyte solutions and/or those with mixed solvents).

The mole fraction concentration scale is used by the Extended Aerosol Inorganics Model (*E-AIM*) of Clegg and co-authors (Clegg et al., 2001; Wexler and Clegg, 2002, and references therein). The pH on a mole fraction basis, $\mathrm{pH_x}$, is given by:

$$\mathrm{pH}_x = -\log_{10}\left(a_{\mathrm{H}^+}^{(x)}\right) = -\log_{10}\left(x_{\mathrm{H}^+}\, f_{\mathrm{H}^+}^{*}\right), \quad (3)$$

where x_{H^+} is the mole fraction of H^+ in the solution, $a_{\mathrm{H}^+}^{(x)}$ and $f_{\mathrm{H}^+}^{*}$ are the mole-fraction-based activity and the (rational) activity coefficient, respectively, both defined with respect to an infinite dilution reference state in pure water (superscript $*$ or (x)). The mole fractions of all species i, including water, are calculated as $x_i = n_i/\Sigma_j\, n_j$, where the summation is calculated over all solution species j (ions, uncharged (e.g., organic) solutes, and water).

Conversions among pH values calculated using different concentration scales is necessary to compare model predictions, and to report acidity on a consistent basis. Generally, formulae for the conversion of pH are derived based upon the equivalence of the chemical potentials of solution entities irrespective of concentration scale (see, for example, Robinson and Stokes, 2002). The conversions to pH from the equivalent values on the mole fraction and molarity scales are given below, and the derivations are given in the Supplementary Information (Sect. S1):

$$\mathrm{pH} = \mathrm{pH}_x + \log_{10}\left(M_w \cdot 1\,\frac{\mathrm{mol}}{\mathrm{kg}}\right) \approx \mathrm{pH}_x - 1.74436, \quad (4)$$

$$\mathrm{pH} = \mathrm{pH}_c - \log_{10}\left(\frac{1}{\rho_0} \cdot 10^3 \frac{\mathrm{kg}}{\mathrm{m}^3}\right). \quad (5)$$

where, ρ_0 (kg m^{-3}) is the density of the reference solvent (pure water for the normal case, i.e. when activity coefficients on molality and molarity scale are defined with reference state of infinite dilution in pure water, regardless of a presence of organics in the solution). Because the density ρ_0 depends weakly on temperature, the exact relation between pH and pH_c is non-linear. In the usual case of water as the reference solvent (ρ_0 close to 1000 kg m^{-3}), the logarithmic difference is small (typically < 0.02 pH units), resulting in $\mathrm{pH}_c \approx$ pH (Jia et al., 2018).

2.3 Approximations of pH

Approximate values of pH, based upon the definition of pH (Eq. 1) but making simplifying assumptions, can be obtained in several ways. For example, the activity coefficient γ_{H^+} could be set to unity and pH computed based on only the *free* H^+ molality, symbol $\mathrm{pH_F}$:

$$\mathrm{pH_F} = -\log_{10}(m_{\mathrm{H}^+}) \quad (6)$$

The assumption of $\gamma_{\mathrm{H}^+} = 1$ is appropriate only in highly dilute aqueous solutions, corresponding to ambient relative humidities close to 100%.

Another approach is to use the mean molal ion activity coefficient of an H^+–anion pair in place of γ_{H^+}, i.e. $\gamma_{\mathrm{H}^+} \approx \gamma_{\pm,\mathrm{HX}}$, where X is a monovalent anion such as $\mathrm{HSO_4^-}$, $\mathrm{NO_3^-}$, or $\mathrm{Cl^-}$ (e.g., Wright, 2007). This approximation can be expected to capture the typical increase in γ_{H^+} with increasing H^+ liquid phase concentration (decreasing ambient RH), although only semi-quantitatively. The approximate pH determined in this way is labeled as $\mathrm{pH}_\pm(\mathrm{H,X})$:

$$\mathrm{pH}_\pm(\mathrm{H,X}) = -\log_{10}\left(m_{\mathrm{H}^+}\gamma_{\pm,\mathrm{HX}}\right). \quad (7)$$

The deviation of $\mathrm{pH}_\pm(\mathrm{H,X})$ from pH is related to the ratio of the specified single-ion activity coefficients via $\mathrm{pH}_\pm(\mathrm{H,X}) - \mathrm{pH} = \frac{1}{2}\log_{10}\left(\frac{\gamma_{\mathrm{H}^+}}{\gamma_{\mathrm{X}^-}}\right)$. Consequently, the pH approximation by $\mathrm{pH}_\pm(\mathrm{H,X})$ is very good for $\frac{\gamma_{\mathrm{H}^+}}{\gamma_{\mathrm{X}^-}} \approx 1.0$, which is the case in the highly dilute limit of aqueous electrolyte solutions. Further, it may also hold approximately towards higher electrolyte concentrations if both single-ion activity coefficients tend to deviate from 1.0 to a similar degree (which depends on aerosol composition).

An alternative to $\mathrm{pH_F}$ would be to use the *total* H^+ molality, which can be defined as the sum of dissolved H^+ and $\mathrm{HSO_4^-}$ molalities:

$$\mathrm{pH_T} = -\log_{10}(m_{\mathrm{H}^+} + m_{\mathrm{HSO4^-}}) \quad (8)$$

The use of this definition may be appropriate in contexts where the amount of free H^+ is not of interest and/or the computation of bisulfate dissociation (which will vary with RH, aerosol composition, and temperature) is impractical. The use of $\mathrm{pH_F}$ and

pH_T as alternatives to pH, as well as the assumption that $pH \approx pH_{\pm}(H, X)$, are tested by the intercomparison of thermodynamic model predictions for fine particles in Sect. ~~6~~3.

2.4 Acidity and the pH scale

Expressing the acidity of a solution in terms of pH leads to a scale that has two important characteristics: an increase in acidity is accompanied by a decrease in pH and vice-versa; and it is a logarithmic scale, meaning that a decrease by one pH unit corresponds to a ten-fold increase in H^+ activity. Hence, apparently modest changes in pH represent relatively large changes in acidity.

A pH of 7 represents a neutral aqueous solution with values less than 7 generally considered acidic and values larger than 7 basic in nature. The characterization of pH equal to 7 as neutral is based on the chemical equilibrium between H^+ and OH^- ions arising naturally in aqueous solutions. The auto-dissociation of water ($H_2O \rightleftharpoons OH^-_{(aq)} + H^+_{(aq)}$) is described by the temperature (T)-dependent equilibrium constant on molality basis, $K_w(T)$. The value of pK_w (= $-\log_{10}[K_w]$) is 14.95 at 0°C and 13.99 at 25°C for pressures encountered in the atmospheric (Bandura and Lvov, 2005) resulting in corresponding pH values of about and 7.475and 6.995, respectively, for highly dilute aqueous systems. Both systems are neutral, although the pH values differ.

The pH scale is commonly considered to span values from 0 to 14, but larger and smaller values are also possible as the scale has no specific limits. Current large-scale models (Sect. 8) and observations (Sect. ~~5~~7) indicate that cloud pH has a global mean somewhere between 4 and 6 and ranges from around 2 to above 7 (Fig. 2). The global distribution of fine particle (nominally particles of 2.5 μm in diameter and below, $PM_{2.5}$) pH is bimodal with a population of particles having a mean pH of 1 – 3 and another population, influenced by dust, sea spray, and potentially biomass burning, having an average pH closer to 4 – 5. Fine particle pH can be negative (Sect. ~~5~~7.1), particularly when sulfate is a major component, and is rarely predicted to exceed 7.

2.5 Measuring pH and operational definition of pH

The small sizes and associated liquid volumes of single particles (which are in chemical equilibrium with vapours) prevent the application of standard pH measurement techniques for single aerosol particle and cloud droplet acidity. Instead, samples of larger volumes must be collected (e.g., a population of droplets in the case of cloud water, Sect. ~~5~~7.2) or other methods employed, including measurements of aerosol and gas phase compositions and the application of thermodynamic models (Sect. 2.6) to compute pH values via Eq. (1).

With ~~sufficient~~enough sample volume, particularly in the case of cloud droplets which typically have low ionic strengths, traditional pH measurement techniques can be used. The operational definition of pH is based on the principle of determining

the difference between the pH of a solution of interest and that of a reference (buffer) solution of known pH by measuring the difference in electromotive force, using an electrochemical cell (e.g., a combination electrode coupled to a pH meter). High-precision measurement of absolute pH values of the reference buffer solution used for calibration are made with a so-called primary method using electrochemical cells without transference (Harned cells, see Buck et al. 2002). The uncertainty associated with typical pH measurements, which use glass electrodes, is of the order of 0.014 for ionic strengths < 0.1 mol kg^{-1} and is expected to increase towards higher ionic strength (Buck et al., 2002). Further details on pH measurement methods and their relationship to Eq. (1) are provided in the SI.

The measurement of aerosol pH is problematic because of the difficulty in collecting sufficient sample material without perturbing its acidity and also due to the mismatch between ionic strengths present in atmospheric fine particles (> 1 mol kg^{-1} and sometimes exceeding 100 mol kg^{-1}, Herrmann et al., 2015) and the molal ionic strength for which normal operational techniques are appropriate (no more than about 0.1 mol kg^{-1}). Values of pH based upon primary measurement methods, which are used for instrument calibration, cannot be readily defined at high ionic strength. This is because assumptions regarding the activity coefficient of the Cl^- ion (which is needed to establish the pH value of the buffer) are limited to very dilute solutions. In addition, the calibration of the pH electrodes requires the ionic strengths of the buffer and test solution (e.g. an aerosol sample) to be low and similar in magnitude. A pH electrode, calibrated for dilute conditions, will yield a measured pH that is systematically in error to an unknown degree if placed in a solution of higher ionic strength (e.g., Wiesner et al., 2006). Similar considerations apply to colorimetric methods (see Sect. ~~5~~7.1): the equilibria involving the chemical species that provide the color response depend not solely on a_{H^+}, but on the thermodynamic activities of the sensing species themselves. These will vary with the chemical composition and concentration of the solution. Thus, colorimetric methods also require calibration that is relevant to the solution media they will be used to measure.

2.6 Thermodynamic models for pH calculation

Given the operational difficulties associated with measuring aerosol pH (Sect. 2.5), estimates of the degree of acidity of particles generally depend upon the use of thermodynamic models. In atmospheric science, a number of different thermodynamic models are used to predict equilibrium gas–particle partitioning, liquid-phase activity coefficients, solid–liquid and liquid–liquid equilibria, dynamic mass transfer of semi-volatile species, aerosol liquid water content (ALWC), and pH. Most models can treat both metastable (supersaturated) solutions or stable states (where solids have formed). Here, some of the most widely used models are described, focusing on their general approach, special features, and relevant species in the context of pH calculations. Advantages and disadvantages of four common thermodynamic models are summarized in Table 2.

The thermodynamic modeling approach inherent in some models (e.g., ISORROPIA, MOSAIC, and EQUISOLV II) does not yield single ion activity coefficients that allow for calculation of pH via Eq. 1. For example, ISORROPIA II and MOSAIC

nominally output information for pH_F and studies published prior to this work using those models (see Sect. ~~5~~7.1), were approximating acidity by reporting pH_F. In this work (Sect. ~~6~~4), model source codes were modified to use the mean molal activity coefficients for different cation–anion pairs (e.g., (H^+, HSO_4^-) or (H^+, Cl^-)) in the estimation of pH using $pH_{\pm}(H,X)$. Section ~~6~~.4 and observationally constrained pH estimates focus on equilibrium conditions, although MOSAIC is often used to dynamically calculate the transient H^+ amount.

2.6.1 Extended Aerosol Inorganics Model (E-AIM)

The Extended Aerosol Inorganics Model (E-AIM) is a thermodynamic model to calculate gas/liquid/solid equilibrium in aqueous aerosol systems containing inorganic ions, water, and an arbitrary number of organic compounds with user-defined properties. It uses the Pitzer–Simonson–Clegg (PSC) equations (Pitzer and Simonson, 1986; Clegg et al., 1992; Clegg et al., 1998) for the calculations of solvent and solute activity coefficients (single ion values) on the mole fraction scale. There are four principal models that differ in terms of the species and temperature range considered (Wexler and Clegg, 2002, and references therein; Friese and Ebel, 2010). The models include some or all of the following ions and the solid salts and gases that can be formed from them: H^+, NH_4^+, Na^+, SO_4^{2-}, HSO_4^-, NO_3^-, Cl^-, and Br^-. The possible calculations include the properties of an aqueous solution of defined composition, as well as the equilibrium state of a gas and particle system at defined RH and temperature. In chemical systems containing inorganic ions, the aqueous phase equilibria $H^+ + SO_4^{2-} \rightleftharpoons HSO_4^-$, $NH_4^+ \rightleftharpoons NH_3 + H^+$, and $H_2O \rightleftharpoons H^+ + OH^-$ are solved as well as those between aerosol species NH_3(aq), H^+(aq), NO_3^-(aq), Cl^-(aq) with the gases NH_3, HNO_3, and HCl. Analogous equilibria (i.e., acid dissociation, gas/liquid equilibrium) can also be solved for user-specified mono- and di-carboxylic acids, and mono- and di-amines. The model can be used for both acidic and alkaline aerosols.

The activity coefficients, and contributions to the water activity, of uncharged (or undissociated forms of) organic solutes are calculated using the Universal Quasi-Chemical Functional group Activity Coefficients (UNIFAC) model (Fredenslund et al., 1975). Organic anions are assumed to have the same activity coefficient model interaction parameters as HSO_4^- or SO_4^{2-} (according to their charge), and amine cations are assigned the same parameters as NH_4^+.

The *E-AIM* model is based upon thermodynamic data for pure aqueous solutions and mixtures over a wide range of temperatures. This basis in measurements, and the calculation of ionic activities in terms of interactions between pairs and triplets of solute species, makes *E-AIM* generally the most accurate (inorganic) thermodynamic model used in atmospheric science. Nevertheless, it has some known weaknesses: predictions of rising equilibrium RH with concentration in some aqueous NH_4^-–NO_3^-–SO_4^{2-}–H_2O aerosols at about 250 K and below (Model II); and similar errors in aqueous aerosols at low RH and containing high concentrations of NH_4^+ and Cl^- (Model IV). To address the latter case some restrictions have been placed on the types of calculations that can be carried out (see http://www.aim.env.uea.ac.uk/aim/model4/input4a.html). Most relevant to aerosol pH is the fact that calculated molalities of free H^+, HSO_4^- and SO_4^{2-} in aqueous H_2SO_4 – and therefore in

mixtures containing the three ions – deviate somewhat from measurements of the stoichiometric dissociation constant of HSO_4^- obtained spectroscopically (Knopf et al., 2003; Myhre et al., 2003). Myhre et al. (2003) show that there is good agreement between modeled and measured degrees of dissociation of HSO_4^- (α_{HSO4}) at room temperature up to 30 – 40 wt% acid (equivalent to 75 to 56% equilibrium RH), within the relatively large scatter in the data. At 50 wt% acid, and above, the calculated α_{HSO4} are too low, meaning that the molality of free H^+ is also too low. These differences increase for H_2SO_4 concentrations above 35 wt% (5.5 mol kg^{-1}) and temperatures below about 240 K (Knopf et al., 2003). These errors do not necessarily lead to errors in pH as the stoichiometric activity of H^+ (used in determination of pH, Eq. 1) in aqueous solution is accurately reproduced as indicated by accurate predictions of equilibria with acid gases (HNO_3 and HCl, Fig. 6 to 12 of Carslaw et al., 1995).

2.6.2 AIOMFAC-based equilibrium model

The Aerosol Inorganic–Organic Mixtures Functional groups Activity Coefficient (AIOMFAC) model is a thermodynamic activity coefficient model treating liquid mixtures containing water, inorganic ions, and organic compounds. The model combines a Pitzer-type aqueous ion interaction model with a modified UNIFAC model (Fredenslund et al., 1975; Hansen et al., 1991), which was originally designed for organic mixtures. As in UNIFAC, AIOMFAC applies a group-contribution approach to cover a wide variety of organic compounds by a relatively small set of organic functional groups (~16 main groups). The AIOMFAC expressions, parameterization and validation based on experimental data, as well as known limitations are described in detail elsewhere (Zuend et al., 2011; Zuend et al., 2008).

AIOMFAC presently includes the following inorganic ions: H^+, Li^+, Na^+, K^+, NH_4^+, Mg^{2+}, Ca^{2+}, Cl^-, Br^-, NO_3^-, HSO_4^-, SO_4^{2-}, (I^- forthcoming). Most of these ions can be present simultaneously in an aqueous solution; limitations exist for Li^+ in the presence of bisulfate (HSO_4^-) ions due to a lack of experimental data required for determining associated model parameters. However, using a less-rigorous analogy approach, AIOMFAC can approximate those parameters so that all listed ions can be treated in solution. The bisulfate dissociation equilibrium is solved numerically using the temperature-dependent equilibrium constant parameterization by Knopf et al. (2003). Other inorganic electrolyte species are considered completely dissociated when in liquid solution – with deviations from that assumption accounted for implicitly by activity coefficients. In contrast to the E-AIM model, AIOMFAC does not solve the $H_2O \rightleftharpoons H^+ + OH^-$ dissociation equilibrium (which is acceptable when the pH is at least an order of magnitude lower than the neutral value). The organic functional groups available in calculations for mixed organic–inorganic systems include carboxyl, hydroxyl, ketone, aldehyde, ether, ester, alkenyl, alkyl, hydroperoxide, peroxyacid, peroxide, and aromatic functional groups. However, only a subset of these groups is currently available when HSO_4^-, Mg^{2+} or H^+ are present; see https://aiomfac.lab.mcgill.ca/about.html (Fig. 4 on that website). A few species are available exclusively for a select set of organic or inorganic systems, e.g., an organonitrate group in non-electrolyte systems (Zuend and Seinfeld, 2012) and the methanesulfonate ion in certain organic-free aqueous solutions ($CH_3SO_3^-$ with H^+, Na^+, NH_4^+; Fossum et al., 2018).

An online version of AIOMFAC is available at https://aiomfac.lab.mcgill.ca (and http://www.aiomfac.caltech.edu). Note that the online AIOMFAC model is simply an activity coefficient model, not a complete gas–liquid thermodynamic equilibrium model. A limitation of AIOMFAC is that the composition-dependent degree of dissociation of organic acids (via the carboxyl group) is not accounted for explicitly in the determination of acidity. As such, the pH calculations are only meaningful in the presence of some amount of inorganic H^+. Due to the weak temperature-dependence of activity coefficients, the model is applicable over a temperature range of about 298 ± 30 K, while most of the experimental training data were for temperatures ≥ 293 K. AIOMFAC variants with a more sophisticated temperature dependence have been parameterized for electrolyte-free aqueous organic systems (Ganbavale et al., 2015).

A unique feature of AIOMFAC is its ability to represent non-ideal interactions between organic molecules and inorganic ions in liquid solutions up to high concentrations, a feature that is important for the prediction of liquid–liquid phase separation. Thermodynamic equilibrium models have been developed with AIOMFAC as their core module, including efficient numerical methods for the prediction of liquid–liquid equilibria (Zuend and Seinfeld, 2013) and the equilibrium gas–particle partitioning of water and semi-volatile organic compounds (Zuend and Seinfeld, 2012; Zuend et al., 2010).

Recent work further extends the AIOMFAC-based gas–particle partitioning model by consideration of the gas–liquid equilibria of the following inorganic acids and bases: HNO_3, HCl, HBr, and NH_3, while H_2SO_4 is treated as non-volatile (Ma and Zuend, *in preparation*). This equilibrium model is referred to as AIOMFAC–GLE hereafter. For given input in the form of molar amounts per unit volume of air at given pressure and temperature, the AIOMFAC–GLE model predicts the compositions of co-existing phases (gas phase plus up to two liquid phases) and associated activity coefficients of all species in all (liquid) phases. This enables a straightforward calculation of phase-specific pH values using Eq. (1).

2.6.3 MOSAIC

The Model for Simulating Aerosol Interactions and Chemistry (MOSAIC) is a sectional aerosol model that treats aerosol thermodynamics, size-resolved dynamic gas–particle partitioning, heterogeneous chemistry, and coagulation (Zaveri et al., 2008). It includes all major inorganic salts and electrolytes composed of H^+, NH_4^+, Na^+, Ca^{2+}, SO_4^{2-}, HSO_4^-, $CH_3SO_3^-$, NO_3^-, Cl^-, and CO_3^{2-}. Ions such as K^+ and Mg^{2+} are represented by equivalent amounts of Na^+ while other unspecified inorganic species such as silica, other inert minerals and trace metals found in soil dust aerosols are lumped together as “other inorganic mass” (OIN). MOSAIC also includes carbonaceous species such as black carbon, primary organics, and secondary organics. Although organic–inorganic interactions are not presently treated explicitly in MOSAIC, organics and OIN species can absorb water, which indirectly affects the overall particle pH. The gas-phase species that can partition to the particle phase include H_2SO_4, CH_3SO_3H (methanesulfonic acid), HNO_3, HCl, NH_3, and any number of secondary organics.

At a given time step, the thermodynamics submodule MESA (Multicomponent Equilibrium Solver for Aerosols; Zaveri et al., 2005a) first determines the equilibrium phase state in each size section as a function of particle-phase composition, particle size (accounting for the Kelvin effect), relative humidity and temperature, with aerosol water content calculated using the Zdanovskii–Stokes–Robinson (ZSR) method (Stokes and Robinson, 1966; Zdanovskii, 1948). The dynamic gas–particle partitioning module ASTEM (Adaptive Step Time-split Euler Method) then calculates the driving forces for mass transfer of the gas-phase species over each bin and integrates the associated mass transfer differential equations for all size sections (Zaveri et al., 2008). The mean stoichiometric activity coefficients of electrolytes for the equilibrium phase state and mass transfer driving force calculations are estimated using the Multicomponent Taylor Expansion Method (MTEM; Zaveri et al., 2005b). Briefly, MTEM calculates the mean molal activity coefficient of an electrolyte in a multicomponent solution on the basis of its values in binary solution for all the electrolytes present in the mixture at the solution water activity (a_w), assuming that a_w is equal to the ambient RH. For self-consistency most of the MTEM and ZSR parameters are determined using the comprehensive ~~Pitzer-Simonson-Clegg model (~~PSC~~) (Clegg and Pitzer, 1992; Pitzer and Simonson, 1986; Clegg et al., 1998)~~ model at 298.15 K. The PSC model is the basis of E-AIM.

In partially or fully deliquesced aerosols, the hydrogen ion molality (m_{H^+}) plays a central role in both equilibrium phase state and mass transfer calculations. For computational efficiency, two solution domains are considered on the basis of the so-called molal sulfate ratio, X_T:

$$X_T = \frac{m_{NH_4^+} + m_{Na^+} + 2m_{Ca^{2+}}}{m_{SO_4^{2-}} + m_{HSO_4^-} + m_{CH_3SO_3^-}}. \quad (9)$$

In the sulfate-rich domain (i.e., $X_T < 2$), the partial dissociation of the bisulfate ion ($HSO_4^- \rightleftharpoons H^+ + SO_4^{2-}$) and electroneutrality equations are simultaneously solved to determine m_{H^+}, which is subsequently used to determine the equilibrium gas-phase concentrations of HNO_3, HCl, and NH_3 at the particle surface for computing their driving forces for mass transfer. In the sulfate-poor domain (i.e., $X_T \geq 2$), HSO_4^- is assumed to completely dissociate to SO_4^{2-}, and the use of equilibrium m_{H^+} to calculate the driving forces produces spurious oscillations in the mass transfer of HNO_3, HCl, and NH_3. This problem is solved by introducing the concept of dynamic m_{H^+}, which is determined by simultaneously solving surface equilibrium equations together with the acid-base coupled condensation approximation. At a given time, the dynamic m_{H^+} is thus a function of the gas/liquid equilibrium constants and mass transfer coefficients of HNO_3, HCl, and NH_3 along with their gas- and particle-phase concentrations. When the gases and particles reach a steady state, the dynamic m_{H^+} in each size section is equal to the equilibrium m_{H^+}. See Sect. ~~7~~ 6 for a further discussion of the role of particle size and mass transfer on pH.

2.6.4 ISORROPIA II

ISORROPIA II (Fountoukis and Nenes, 2007; http://isorropia.epfl.ch) is a computationally efficient code that treats the thermodynamics of inorganic K^+–Ca^{2+}–Mg^{2+}–NH_4^+–Na^+–SO_4^{2-}–NO_3^-–Cl^-–H_2O aerosol systems. NH_3, HNO_3, and HCl are considered present in the solution. The current version, version 2.3, of the code is used in this work (see code website for

version history). The discrete adjoint of ISORROPIA, called ANISORROPIA, has also been developed (Capps et al., 2012) using a combination of automatic differentiation of ISORROPIA II and post-convergence treatments (to account for discontinuities in the information flow during solution) to compute the sensitivities of all output parameters of the code to their relevant inputs with analytical precision.

ISORROPIA II can compute the equilibrium composition for two types of inputs: (a) forward, closed-system problems, in which the temperature, relative humidity and total concentrations (gas + aerosol) of aerosol precursors are known, and (b) reverse, open-system problems, in which the temperature, relative humidity, and the concentrations of aerosol NH_4^+, SO_4^{2-}, Na^+, Cl^-, NO_3^-, Ca^{2+}, K^+, and Mg^{2+} are used as input.

To reduce the computational complexity and increase solver speed, ISORROPIA II uses a segmented solution approach, where depending on the relative amounts of each aerosol precursor, major and minor species are defined. The equilibria of the major species together with conservation of mass and electroneutrality provide the equilibrium composition. ISORROPIA II uses mean activity coefficients for the cation–anion pairs in solution. For this, the Kusik and Meissner (1978) model for specific ionic pairs is applied in combination with the Bromley (1973) mixing rule for activity coefficients in the multicomponent mixtures found in the aerosol. ALWC is computed as a function of RH, using the Zdanovskii–Stokes–Robinson relation (Stokes and Robinson, 1966; Zdanovskii, 1948), using a water activity database computed from the E-AIM thermodynamic model, and incorporating the effect of temperature. Although the mean activity coefficients of all major cation–anion pairs are considered, for certain species (e.g., OH^-, and undissociated ammonia, nitric and hydrochloric acid $NH_{3(aq)}$, $HNO_{3(aq)}$, $HCl_{(aq)}$) unity activity coefficients are assumed due to a lack of corresponding data. Also, the first dissociation of sulfuric acid in solution is always assumed to be complete.

2.6.5 EQUISOLV II

EQUISOLV II is a model for calculating gas–aerosol equilibrium in atmospheric systems that contain water vapour, gases including NH_3, HNO_3, and HCl, and soluble inorganic electrolytes distributed across multiple particle size bins (Jacobson, 1999). Equilibrium is solved using a mass flux iteration technique. The model contains the major inorganic ions H^+, NH_4^+, Na^+, K^+, Mg^{2+}, Ca^{2+}, SO_4^{2-}, HSO_4^-, NO_3^-, Cl^-, and CO_3^{2-} (Jacobson et al., 1999) as well as some minor and trace constituents. The thermodynamic treatment is summarized in chapter 17 of Jacobson (2005b).

Mean activity coefficients of the cations and anions in single electrolyte solutions are calculated using polynomials fit to available data and reference values at 25 °C, supplemented by similar fits to values of enthalpies and apparent molar heat capacities of the solutions. Together, using standard relationships, these enable mean activity coefficients to be calculated for different temperatures. Mean ionic activity coefficients in mixtures are estimated using the approach of Bromley (1973), based on values for the constituent pure aqueous solutions at the total ionic strength of the mixture. The equilibrium $HSO_4^- \rightleftharpoons H^+ +$

SO_4^{2-} is calculated explicitly and is based on the same thermodynamic treatment as in E-AIM (Clegg and Brimblecombe, 1995). The approach of Kusik and Meissner (1978) is used to estimate the mean molal activity coefficients $\gamma_{\pm}\,(H^+, HSO_4^-)$ and $\gamma_{\pm}\,(H^+, SO_4^{2-})$ in mixtures in order to obtain the equilibrium concentrations of H^+, HSO_4^-, and SO_4^{2-} (see Sect. 4.2 of (Jacobson et al., 1996). This approach will not yield the same values as the treatment of Clegg and Brimblecombe (1995); see Sect. ~~6~~4.1.

The relationship between the water content of aqueous aerosols containing multiple electrolytes and RH is estimated with the Zdanovskii-Stokes-Robinson relation (Stokes and Robinson, 1966; Zdanovskii, 1948), using polynomials representing single-solute molalities as a function of water activity (equivalent to equilibrium RH), and incorporating the effect of temperature, based upon the same enthalpy and heat capacity data as for the solutions referred to above.

2.6.6 Other thermodynamic models

Many other thermodynamic models have been developed for the prediction of atmospheric aerosol hygroscopicity and related properties, including the Gibbs free energy minimization model GFEMN (Ansari and Pandis, 1999) for inorganic aerosol systems, ADDEM (Topping et al., 2005a,b) which emphasizes consideration of droplet size (Kelvin effect), and UHAERO (Amundson et al., 2007; Amundson et al., 2006) which allows for the computation of complex phase diagrams of both inorganic and organic systems. These models are based on the ~~Pitzer–Simonson–Clegg~~PSC model for activity coefficient and pH calculations, either directly or via polynomial expressions fitted to that model (and are thus related to E-AIM). The models SCAPE and SCAPE 2 (with NVC), for inorganic aerosol thermodynamics (Kim and Seinfeld, 1995; Kim et al., 1993a, b), implement several activity coefficient methods, including Bromley's method (Bromley, 1973), the Kusik and Meissner method (Kusik and Meissner, 1978) and a Pitzer model. The Equilibrium Simplified Aerosol Model (EQSAM) (Metzger et al., 2002; 2006) computes gas/liquid/solid partitioning for aqueous inorganic aerosol systems, including crustal cations and iron (II, III) species. The numerical complexity of thermodynamic equilibrium models has also led to work focused on the design of computational solvers for high efficiency; for example, HETV (Makar et al., 2003) is a vectorized solver for the SO_4–NO_3–NH_4 system based on the ISORROPIA algorithms. All these thermodynamic models provide a theoretical basis and mechanism to link cations and anions in aqueous solution to pH or one of its approximations.

3 Proxies of aerosol pH

pH has been referred to as a master variable as a result of its fundamental role in the condensed phase environment (Strum and Morgan, 1996) including the processes highlighted in the introduction (Sect. 1) and later in Sect. 5~~in the previous section~~. This role suggests that any study interested in understanding processes influenced by particle acidity (e.g., gas–particle partitioning, acid-catalyzed reactions, metal dissolution) should examine pH. Due to the lack of direct measurements of aerosol pH (see

Sect. 2.5, ~~5~~7.1) as well as requirements for data used to calculate pH (Table 2), multiple methods have been employed in the literature as surrogates or proxies for ~~fine~~ particle acidity. In some cases, proxies are used to infer a pH and whether particles are acidic or basic. In other cases, concepts related to pH, such as PM sensitivity to ammonia vs oxidized nitrogen, are interpreted via molar ratios of species, but pH itself is not discussed as a central concept. Since the underlying processes affecting the endpoint of interest (e.g., gas–particle partitioning of semi-volatile species that contribute to PM mass) is often ~~directly~~ dictated by pH, pH is implicitly contained in such analysis. However, since proxies have only an indirect connection to the system's acidity, interpretation of results without information on pH can be challenging, incomplete, and in the worst case, incorrect.

In this section, the most common aerosol pH proxies are defined and historical context for their development and use provided. Proxies are indirectly related to pH and thus differ from the approximations highlighted in Sect. 2.3. Section ~~6~~ 4 expands upon the information presented here and in Section 2 by evaluating the effectiveness of each proxy using box model predictions of ~~pH_f~~ acidity based on ambient data.

3.1 Proxies based on electroneutrality

Two of the most commonly used proxy methods for aerosol pH, the cation/anion equivalent ratio (also called the cation/anion equivalence ratio or molar ratio, Hennigan et al., 2015), and the charge balance (also called the ion balance ~~or~~ and sometimes strong acidity, Table ~~2~~3), are based upon the principle of solution electroneutrality. In both approaches, H^+ is assumed to balance with an excess of anions. In the case of a molar ratio, the amount of H^+ is assumed to scale inversely with the level of the cations relative to anions.

Application of the molar equivalent ratio to infer acidity began with studies comparing measured strong acidity to SO_4^{2-} in aerosol samples (Lee et al., 1993; Lee et al., 1999; Liu et al., 1996), because direct measurements of strong acidity (e.g., via extraction and measurement by pH probe such as EPA Method IO-4.1) have biases associated with sample collection and challenges with data interpretation. The concept of the cation/anion equivalent ratio was first applied to NH_4^+ and SO_4^{2-} measurements to infer the chemical forms (e.g., NH_4HSO_4 vs. $(NH_4)_2SO_4$) of these abundant ions (Junge, 1963; Wall et al., 1988; Moyers et al., 1977; Lewis and Macias, 1980; Macias et al., 1981).

Electroneutrality and the cation/anion equivalent ratio require ~~the incorporation~~consideration of all ionic species present in solution in a given particle. However, practical measurement limitations and assumptions have led to variations of the cation/anion equivalent used throughout the years. One such assumption is that H^+ accounts for the charge deficit between the water-soluble species present in particles that can be readily measured with an ion chromatograph. This typically includes five cation (NH_4^+, Na^+, Ca^{2+}, Mg^{2+}, and K^+) and three anion (Cl^-, NO_3^-, SO_4^{2-}) species (e.g., Quinn et al., 2006; Sun et al., 1998), though it occasionally includes a limited group of organic anions (Kerminen et al., 2001). A similar definition has also been

applied to the non-refractory inorganic species measured with an Aerodyne Aerosol Mass Spectrometer (NH_4^+, NO_3^-, SO_4^{2-}, and partial Cl^-) (Zhang et al., 2005; Quinn et al., 2006). If the aerosol is near neutral (pH ≈ 7) or acidity is dictated by components other than the inorganic ions in the balance (e.g., organic acids) then charge balance will not provide meaningful information (Trebs et al., 2005; Lawrence and Koutrakis, 1996). Further, the carbonate system ($CO_{2(aq)}$–H_2CO_3–HCO_3^-–CO_3^{2-}) must be included in the ion balance when the pH is near neutral, or above (Winkler, 1986).

The molar equivalent ratio is frequently simplified to consider only NH_4^+, NO_3^-, and SO_4^{2-} (Pathak et al., 2009). The justification for this assumption is that these species represent the dominant fraction of inorganic ions, thereby controlling acidity in environments with low levels of crustal species and minor marine influence (Zhang et al., 2005). Non-volatile cations have the potential to drive large-scale patterns in pH_F (see Fig. 2 as well as Sect. 8), thus making proxies without non-volatile cations potentially invalid over large parts of the globe. Several variations of the molar equivalent ratio using these three species have been developed. The degree of sulfate neutralization (DSN), introduced by Pinder et al. (2008a), is defined as:

$$\mathrm{DSN} = ([\mathrm{NH_4^+}] - [\mathrm{NO_3^-}])/[\mathrm{TSO_4}] \quad (10)$$

where each term represents the molar concentration of each species in the particle phase. Measurements of sulfate do not usually distinguish between bisulfate and sulfate (Solomon et al., 2014), so total sulfate, $[\mathrm{TSO_4}]$, is used (where $[\mathrm{TSO_4}] = [\mathrm{HSO_4^-}] + [\mathrm{SO_4^{2-}}]$). The bisulfate anion is often more abundant than the sulfate ion in fine particles; however, TSO_4 is often conceptualized has having an effective charge of negative 2.

Similar to DSN, the degree of neutralization (DON, Adams et al., 1999) has been suggested, defined as:

$$\mathrm{DON} = [\mathrm{NH_4^+}]/(2[\mathrm{TSO_4}] + [\mathrm{NO_3^-}]) \quad (11)$$

Other names have been applied to the DON, including e.g., the neutralization ratio (Lawal et al., 2018). The DON represents the ammonium associated with sulfate + nitrate while DSN represents the ammonium associated only with sulfate. In principle, this suggests that they account for different aspects of particle acidity (Pinder et al., 2008a); however, DSN and DON were highly correlated in California (r^2 = 0.961) and the southeastern U.S. (r^2 = 0.978) (this work, not shown), two locations with very different NO_3^- levels, suggesting that they represent the same physical parameter. The importance of this correlation as an indicator of pH, and its general validity, remains to be studied.

Finally, the simplest form of the cation/anion molar equivalent ratio considers particle acidity based solely on the NH_4^+ / SO_4^{2-} ratio. This simplification further requires that NO_3^- is relatively low (Xue et al., 2011). Acidic conditions are inferred when the measured NH_4^+/ SO_4^{2-} molar ratios is less than two (Turpin et al., 1997), as this is assumed to indicate when mildly acidic ammonium sulfate particles begin containing progressively larger amounts of acidic ammonium bisulfate. Particle acidity and pH are assumed to scale with NH_4^+/ SO_4^{2-}, with decreasing ratios corresponding to decreasing pH (Zhang et al., 2007).

More recently, the total ammonium to sulfate ratio has been proposed as an indicator of pH (Murphy et al., 2017):

$$TNH_4{:}\,TSO_4 = \frac{([NH_3]+[NH_4^+])}{[TSO_4]} \quad (12)$$

Thermodynamic predictions from E-AIM were interpreted using this ratio to show that pH and ammonia volatilization increases as $TNH4{:}\,TSO_4$ varies from below 1 to above 2 (coinciding with formation of sulfate over bisulfate). While the $TNH_4{:}\,TSO_4$ proxy may not give a precise pH estimate, it can provide general information. For example, the ratio of NH_3:SO_2 emissions had been used to predict that aerosol pH may increase in the near future (Murphy et al., 2017) despite relatively constant levels in the recent past (Weber et al., 2016).

In the case of charge balance, the amount of H^+~~,~~ is determined from the total cation/anion deficit; for this reason, it is expressed as hydrogen ion concentration in air, i.e. total molar H^+ amount per unit volume of air containing aerosol particles and/or cloud droplets, H^+_{air} (nmole m^{-3} air or similar). H^+_{air} is related to pH; however, the two are not expected to correlate since the former is an extensive property while the latter is an intensive property of an aerosol distribution. For example, a highly acidic (pH < 1) particle with a low mass may have a lower H^+_{air} than a much larger, moderately acidic (pH > 4) particle. Further, H^+_{air} lacks direct modulation by particulate volume (liquid water, the solvent for H^+) and activity coefficients. ~~For example,~~D ~~d~~iurnal variations in RH have been shown to cause pH_F variations on the order of 1 pH unit in the eastern U.S. (Guo et al., 2015; Battaglia et al., 2017; see Sect. ~~5~~7.1). Like the cation/anion equivalent ratio~~n~~, the charge balance metric also assumes specific forms of dissociation state for multivalent ions (particularly for sulfate) and is strongly influenced by measurement uncertainty for each ionic species, especially when the aerosol is mildly acidic. These are all reasons why Guo et al. (2015) found only a weak correlation between H^+_{air} and pH_F ($r^2 = 0.36$). Measured aerosol composition can also be used to create charge balance estimates of H^+ in air. This method is also referred to as ion balance and sometimes strong acidity in the literature (e.g., Ito et al., 1998). When charge balance is performed on observations, it usually means a summation of all charge equivalent anions and cations in the particle. Excess molar charge equivalents of anions compared to cations are assigned to H^+_{air}:

$$H^+_{air,cb} = 2[TSO_4] + [NO_3^-] + [Cl^-] - ([NH_4^+] + [Na^+] + [K^+] + 2[Ca^{2+}] + 2[Mg^{2+}]). \quad (13)$$

Thermodynamic equilibrium models (Section 2.6) use charge balance (reflecting the requirement for solution electroneutrality) as an equation or constraint together with all other considerations of species equilibria across the phases present, to obtain a unique solution. Some thermodynamic equilibrium models also use the cation/anion equivalent ratio to enhance computational efficiency by identifying major ionic species and compositional domains (e.g., Pilinis and Seinfeld, 1987; Kim et al., 1993b; Nenes et al., 1998). However, thermodynamic models do not use charge balance from input data as a proxy for pH. Thermodynamic models (either manually, or automatically) evaluate inputs, in terms of a charge balance, to ensure that the solution obtained is atmospherically relevant – as e.g., an excess of non-volatile cations may imply a strongly alkaline solution that is not found in the atmosphere. This aspect is discussed in more detail in Sect. 4.

Operationally, H^+_{air} from charge balance is subject to errors associated with measuring aerosol phase composition which are likely to be large and affect interpretation of ambient conditions. These are the same challenges that arise in thermodynamic calculations based on particulate-only inputs where biases or uncertainty in the measured species can propagate to errors in acidity (Hennigan et al., 2015; Song et al., 2018). When H^+_{air} is small in concentration or species contributing to the charge balance are incompletely characterized, the proxy may return a value of zero or negative (indicating a surplus of cations) – neither physically possible - due to limited precision and accuracy in the measurements. Using measured aerosol composition, Murphy et al. (2017) and Hennigan et al. (2015) typically found negative values (indicating no H^+, theoretically impossible) of H^+ from charge balance and an error range large enough to span both positive and negative H^+_{air} estimates at almost all times. State-of-the-art measurements are not sufficiently precise to overcome this limitation (Murphy et al., 2017). The problems associated with this proxy are highlighted in Sect. 4 where charge balance estimates near zero show no correlation with pH.

In the 1980s – 1990s, experimental methods were developed to estimate the apparent net fine particle (<2.5 µm) strong acidity (Koutrakis et al., 1988; Koutrakis et al., 1992; Purdue, 1993). These methods, synthesized in a workshop report (EPA, 1999; Purdue, 1993), resulted in an officially documented method for estimating H^+_{air} from measurements. EPA Method IO-4.1 used filter extracts in combination with measurements from a commercially available pH probe (titration methods are another option) to calculate an estimate of H^+_{air} or H^+ as equivalent mass of sulfuric acid. The method relies on efficient particle collection with minimal filter artifacts and low amounts of nitrate compared to sulfate (EPA, 1999). For example, ammonia could displace H^+ and neutralize acidic particles during collection without an efficient denuder (Koutrakis et al., 1988). Extraction and dilution of ambient samples modifies their chemical environment such that the conditions during measurement are different from those in the ambient atmosphere, potentially affecting gas–particle partitioning of total ammonium and dissociation of weak acids including bisulfate (Purdue, 1993). Variations of this method were developed to limit the extent of dilution by measuring the pH of droplets on the surface of a hydrophobic filter using microelectrodes (Winkler, 1986; Keene et al., 2004). However, the extent of dilution is still enough to shift the sulfate–bisulfate equilibrium outside of conditions present in many atmospheric particles. The use of a strong acidity proxy in many past health studies complicates their interpretation regarding the role of acidity since H^+_{air} is only a proxy for pH.

~~Measured aerosol composition can also be used to create charge balance estimates of H^+ in air. This method is also referred to as ion equivalents and sometimes strong acidity in the literature (e.g., Ito et al., 1998). When charge balance is performed on observations, it usually means a summation of all charge equivalent anions and cations in the particle. Excess molar charge equivalents of anions compared to cations are assigned to H^+_{air}:~~

$$~~H^+_{air,cb} = 2[TSO_4] + [NO_3^-] + [Cl^-] - ([NH_4^+] + [Na^+] + [K^+] + 2[Ca^{2+}] + 2[Mg^{2+}]).~~ \quad (13)$$

~~Thermodynamic equilibrium models use charge balance (reflecting the requirement for solution electroneutrality) as an equation or constraint together with all other considerations of species equilibria across the phases present, to obtain a unique solution. Some thermodynamic equilibrium models also use the cation/anion equivalent ratio to enhance computational efficiency by identifying major ionic species and compositional domains (e.g., Pilinis and Seinfeld, 1987; Kim et al., 1993b; Nenes et al., 1998). However, thermodynamic models do not use charge balance from input data as a proxy for pH. Thermodynamic models (either manually, or automatically) evaluate inputs, in terms of a charge balance, to ensure that the solution obtained is atmospherically relevant – as e.g., an excess surplus of non-volatile cations may imply a strongly alkaline solution that is not found in the atmosphere. This aspect is discussed in more detail in Sect. 6.~~

~~Operationally, H^+_{air} from charge balance is subject to errors associated with measuring aerosol phase composition which are likely to be large and affect interpretation of ambient conditions. These are the same challenges that arise in thermodynamic calculations based on particulate-only inputs where biases or uncertainty in the measured species can propagate to errors in acidity (Hennigan et al., 2015; Song et al., 2018). When H^+_{air} is small in concentration or incomplete consideration of species contributing to the charge balance, charge balance may return a value of zero or negative (indicating a surplus of cations) owing to limited precision and accuracy in the measurements. Using measured aerosol composition, Murphy et al. (2017) and Hennigan et al. (2015) typically found negative values (indicating no H^+, theoretically impossible) of H^+ from charge balance and an error range large enough to span both positive and negative strong acidity estimates at almost all times. State-of-the-art measurements are not sufficiently precise to overcome this limitation (Murphy et al., 2017). The limitations of charge balance are highlighted in Sect. 6 where ion balance estimates near zero show no correlation with pH.~~

Proxies for acidity have been used in a variety of applications. In the past, proxies were specifically applied in the context of acid-catalysed SOA. Evidence for this phenomenon was sought in ambient data based upon landmark studies that demonstrated an important role of acid-catalysed reactions in forming SOA in laboratory systems (Jang et al., 2002; Paulot et al., 2009; Surratt et al., 2010). However, due to a lack of direct particle acidity measurements (see Sect. ~~5~~7.1 for details and discussion), researchers used different acidity proxies to characterize the impacts on SOA formation in the atmosphere. The NH_4^+/SO_4^{2-} molar ratio was used in several studies (Zhang et al., 2007; Peltier et al., 2007; Tanner et al., 2009) to infer that more acidic conditions did not enhance SOA concentrations. Froyd et al. (2010) used airborne measurements of the NH_4^+/SO_4^{2-} ratio to classify acidic and neutral particle regimes, and inferred a causal effect of acidity on isoprene organosulfate formation at low NO_x in the eastern U.S. Strong associations between SOA concentrations or SOA marker compounds and H^+ derived from the charge balance were inferred in multiple locations (Pathak et al., 2011; Feng et al., 2012; Budisulistiorini et al., 2013; Nguyen et al., 2014). Several other studies investigated the relationship between particle acidity and atmospheric SOA using different predicted or derived measures of acidity. H^+_{air} estimates based on operational extraction methods were used extensively in the literature to link SOA formation to acidity (Surratt et al., 2007; Offenberg et al., 2009; Zhang et al., 2012). In Beijing, Guo et al. (2012b) found evidence of acid-catalysed SOA based upon correlations between secondary organic carbon (SOC)

concentrations and H^+ concentrations (nmol m^{-3}) from ISORROPIA, run without gaseous inputs. Li et al. (2013) also observed correlations between SOA markers and acidity in China using pH predictions from E-AIM with aerosol inputs only. No evidence for acid-catalysed SOA formation was found in a separate study in Pittsburgh, PA that analysed correlations between modeled H^+ and measured SOA concentrations (Takahama et al., 2006). Takahama et al. (2006) used gas and particle phase inputs for predictions with the GFEMN model and also observed no correlations between pH_c (with $\gamma_{H^+}^{(c)}$ set to unity) and SOA. The studies employing proxies likely suffered from problems with the proxies, themselves (as discussed above), and confounding factors such as correlations between organic aerosol and sulfate, a major source of acidity, that often occur in regional pollution (Sun et al., 2011; Nguyen et al., 2015). These seemingly contradictory results were resolved once pH_F was used, and the conclusions reached in these prior studies have been revisited based upon detailed understanding of the underlying chemical mechanisms and additional insight suggesting that the aerosol acidity is frequently not a limiting factor in catalysing SOA formation (Surratt et al., 2010; Xu et al., 2015; Weber et al., 2016). Acid-~~catalyzed~~ catalysed isoprene SOA has now been implemented in a wide variety of box model and chemical transport model applications that now rely exclusively on thermodynamic models for acidity estimates (Pye et al., 2013; Marais et al., 2016b; Riedel et al., 2016; Budisulistiorini et al., 2017). So, while proxies can provide some information on the PM system, they should not be over interpreted as a measure of pH.

3.2 Gas Ratio

The Gas Ratio (GR) was defined by Ansari and Pandis (1998) to address the realization that inorganic PM concentrations do not always respond linearly to changes in sulfate concentrations (a common assumption at the time) and sought to develop a parameter that ~~can~~ could be used for policy requiring only measurement network data. The underlying reason for this nonlinear response is that gas–particle partitioning of ammonium and nitrate is sensitive to pH. The Gas Ratio (GR) is defined in molar units as follows:

$$GR = ([TNH_4] - 2[TSO_4])/[TNO_3] \quad (14)$$

and uses total ammonia ($NH_3 + NH_4^+$)~~,~~ and total nitrate ($HNO_3 + NO_3^-$). The numerator of the GR is sometimes referred to as free ammonia, because it is the amount of TNH_3 that would be available to form NH_4NO_3 under the simplistic assumption that appreciable NH_4NO_3 does not form when the molar ratio of TNH_4 to TSO_4 is less than two (i.e., the stoichiometric ratio of $(NH_4)_2SO_4$). The concept of ~~"~~free ammonia~~"~~ is discussed in greater detail below (Sect. ~~6~~4.2.3). The GR has not been used explicitly as a proxy for aerosol pH, but it has been used extensively to define aerosol and composition regimes that relate to acidity.

Ansari and Pandis (1998) characterized inorganic PM response for changes in TNH_4, TNO_3, and TSO_4 as functions of GR, temperature, RH, and system concentrations. Their analysis determined critical values of GR that defined boundaries of the PM response regimes. As West et al. (1999) showed, the GR still requires complementary thermodynamic modeling to robustly explore the PM response for large sulfate reductions. Other applications of the GR include calculation of GR as a function of

altitude (Adams et al., 1999), characterization of the sulfate-nitrate-ammonia-water aerosol system in the context of natural and transboundary pollution over the U.S. (Park et al., 2004), and exploration of the sensitivity of aerosol nitrate to changes in temperature, RH, TNH_4, TNO_3, and sulfate for Pittsburgh (Takahama et al., 2004). In addition, Blanchard and Hidy (2003) considered the GR in a study of the response of nitrate to changes in TNH_4, TNO_3, and sulfate in the southeastern U.S. A relationship was demonstrated between the GR and an excess-NH_3 indicator that resembles free ammonia, but accounts for chloride and non-volatile cations. Pun and Seigneur (2001) used box model simulations to demonstrate that nitrate concentrations in California's San Joaquin Valley ~~(SJV)~~ would be sensitive to HNO_3 levels but not NH_3.

Pinder et al. (2008a) investigated the response of PM to emissions of NOx, SO_2, and NH_3, and demonstrated with AIM thermodynamic modeling that NH_4NO_3 can form at low temperature even when the GR is less than zero, in contrast to previous assumptions. To address this limitation, they developed an adjusted GR (*adjGR*) that modified the calculation of free ammonia:

$$\text{adjGR} = \frac{[\text{TNH}_4]-\text{DSN}\times[\text{TSO}_4]}{[\text{TNO}_3]} = \frac{[\text{TNH}_4]-([\text{NH}_4^+]-[\text{NO}_3^-])}{[\text{TNO}_3]} \quad (15)$$

where DSN is the degree of sulfate neutralization. Using a chemical transport model, Pinder et al. (2008a) demonstrated that the response of nitrate concentrations to changes in SO_2 and NH_3 emissions could be reasonably represented as a function of the adjGR and GR, but the adjGR provided a better fit for cases where DSN differs significantly from a value of two. In a separate study, Pinder et al. (2008b) found a strong relationship between the adjGR and the sensitivity of inorganic PM concentrations to NH_3 levels at sites in the eastern U.S.

Additional metrics similar to GR have been defined. Wang et al. (2011) considered the GR and adjGR in a study of the sensitivity of inorganic aerosols to NH_3 in mainland eastern China. They also defined a new indicator, the Flex Ratio (FR), calculated based on predictions of a statistical response-surface model developed from about 100 CTM simulations probing the sensitivity of PM to NH_3 and NO_x emissions (See Xing et al. (2018) for a precise definition). Nitrate concentrations are more sensitive to NH_3 than NO_x emissions for FR > 1, and nitrate concentrations are more sensitive to NO_x than NH_3 emissions for FR < 1. The FR provides a relatively precise estimate of the transition point between NH_3-rich and NH_3-poor conditions for existing NOx emissions levels. However, use of the FR remains limited due to its dependence on the availability of response-surface model predictions, which are currently limited to regions in Asia (e.g., Xing et al., 2011; Zhao et al., 2015). Wang et al. (2011) reported that the nitrate response regimes indicated by the GR and FR were qualitatively consistent in their study.

~~3.3~~ The studies described above, and other studies (e.g., Campbell et al., 2015; Dennis et al., 2008; Lee et al., 2006; San Martini et al., 2005; Zhang et al., 2009), have used the GR and adjGR to understand the response of the sulfate-nitrate-ammonium-water aerosol system to changes in precursor concentrations and emissions. The GR provides a reasonable indication of the sensitivity of inorganic PM to changes in TNH_4, TNO_3, and sulfate in many cases. However, ~~they~~ the GR and

Formatted: Normal, No bullets or numbering

similar metrics do not consider the role of non-volatile cations and universally applicable ranges of GR for demarcating response zones are difficult to define due to the dependence on other factors (temperature, RH, and system concentrations). The GR has not been used explicitly as a proxy for particle acidity, but the response of nitrate to precursor concentrations can be represented as a function of GR using S-shaped curves (Pinder et al., 2008a) that resemble the sigmoid curves reported for gas–particle partitioning of TNO_3 as a function of pH (Guo et al., 2016). Therefore, some relation is expected between these indicators and particle acidity which is shown in Sect. ~~6~~4.2.3. While the above studies applied different proxies, ~~two~~ recent ~~studies~~work demonstrates the direct role of aerosol pH in modulating the sulfate-nitrate-ammonium-water aerosol system. ~~Nenes et al. (2019) show that pH is a key factor in determining the sensitivity of $PM_{2.5}$ to NH_3 versus HNO_3 levels.~~ Vasilakos et al. (2018) demonstrate that nitrate partitioning in response to changing SO_2 emissions also depends on NVCs, which must be properly accounted for to accurately model pH.

Formatted

~~3.4~~3.3 Semi-volatile species partitioning

Aerosol pH affects the gas–particle partitioning of semi-volatile acidic and basic compounds in the atmosphere, including inorganic (HNO_3, NH_3, HCl) and organic (amines, formic, acetic, and oxalic acid) species. The underlying reason why pH affects partitioning is that the protonated and deprotonated forms of the species vary considerably in their volatility (Keene et al., 1998; Meskhidze et al., 2003; Guo et al., 2017b). Based on this insight, estimates of aerosol pH can be derived from simultaneous measurements of the abundance of a compound in the gas and condensed phases, assuming that the species in question are in thermodynamic equilibrium. For example, HNO_3 partitioning is determined by:

$HNO_3\ (g) \rightleftharpoons HNO_3\ (aq)$ (R1)

$HNO_3\ (aq) \rightleftharpoons H^+\ (aq) + NO_3^-\ (aq)$ (R2)

Reactions R1 and R2 are characterized by the Henry's law constant (K_H) and the acid dissociation constant (K_a), respectively. These equilibrium expressions can be combined (see also the derivations provided in the supporting information of Guo et al., 2017b and Nah et al., 2018) and rearranged to yield:

$$a_{H^+} = \frac{K_H K_a p_{HNO3}}{a_{NO_3^-}} \quad (16)$$

where p_{HNO3} is the partial pressure of nitric acid, $a_{NO_3^-}$ is the nitrate activity in deliquesced aerosols, and a_{H^+} is the H^+ activity in the aqueous aerosols. pH can be expressed as the fraction of total nitrate in the particle ($F_{p,NO3} = [NO_3^-]/[TNO_3]$ by moles), the gas constant (R), temperature, equilibrium constants, and molality-based activity coefficients for species i (γ_i):

$$pH = -\log_{10}\left(\frac{K_H K_a (1-F_{p,NO3}) RT}{\gamma_{NO3} - F_{p,NO3}}\right) \quad (17).$$

An analogous version of Eq. (17) could be applied to any monovalent acid/anion pair (e.g., ~~hydrochloride~~ hydrochloric acid/chloride partitioning). pH based on $F_{p,NH4}$ ($[NH_4^+]/[TNH_4]$ by mole) is slightly different.

$$\mathrm{pH} = -\log_{10}\left(\frac{\gamma_{NH4+}F_{p,NH4}}{K_H K_a (1-F_{p,NH4})RT}\right) \quad (18)$$

where K_a is the acid dissociation constant for NH_4^+:

$$NH_4^+ (aq) \rightleftharpoons H^+ (aq) + NH_3 (aq) \quad (R3)$$

pH from Eq. (17) and (18) becomes uncertain when F_p is in the vicinity of one or zero, especially when considering the effects of observational uncertainty.

Current analytical techniques allow for the direct measurement of nitric acid while the aqueous aerosol nitrate concentration~~,~~ can be derived from the aerosol nitrate mass concentration (μg m^{-3}, directly measured) by using the ALWC (measured or estimated). Conversion from aqueous concentrations to activity requires activity coefficients, which can be computed (e.g., Clegg et al., 1992), obtained from one of the aerosol thermodynamic equilibrium models, or approximated with a relevant ion pair ($pH_\pm$) (Sect. 2). Most studies to date have simplified the above expressions by assuming activity coefficients of unity (molal basis), with aqueous concentrations replacing species activities in Eq. (16) above (Meskhidze et al., 2003; Keene et al., 2004) and the resulting pH (Eq. 17–18) becoming pH_F.

Gas–particle partitioning of TNH_4, total ~~chlorine~~ chloride (TCl = HCl + Cl^-), and TNO_3 are all candidates for estimating pH. The approach was first discussed in relation to the pH of sea salt aerosols in the marine boundary layer (Keene et al., 1998). However, the phase partitioning behaviors of HCl and HNO_3 were inconsistent, as measured HNO_3/NO_3^- implied a pH in the ~1 – 2 range, but HCl/Cl^- levels implied a pH much higher (Keene et al., 1998). These discrepancies were postulated to result from positive biases in the HNO_3 (*g*) measurements, uncertainties in the thermodynamic constants, and kinetic limitations to mass transfer (deviation from equilibrium); however, no mention about the effects of mixing state and ability to predict liquid water content was discussed. The first quantitative estimates of aerosol pH_c (molarity basis, see Eq. 2) via partitioning were done by Keene and Savoie (1998) and used HCl/Cl^- partitioning to characterize sea salt particles mixed with anthropogenic pollution. Meskhidze et al. (2003) used measured HNO_3/NO_3^- partitioning to quantify aerosol pH_F, with specific applications to Fe solubility. Keene et al. (2004) extended the analysis and compared the size-dependent aerosol pH_c predicted by the phase partitioning of NH_3, HCl, and HNO_3 in marine air. They observed general agreement in the pH predictions based on HNO_3 and HCl partitioning, while acidity based on NH_3 partitioning was systematically lower by ~1 – 2 pH units. Keene et al. (2004) assumed $\gamma_{H^+}^{(c)}$ was unity in their calculations and noted this as a likely source of uncertainty. In a study a decade later, Young et al. (2013) compared the aerosol pH_c (by size, with $\gamma_{H^+}^{(c)}$ computed by E-AIM) predicted by NH_3, HNO_3, and HCl phase partitioning at a continental location near Denver, CO. In this study, aerosol pH_c derived from NH_3 and HNO_3 partitioning generally agreed, while pH_c predicted from HCl partitioning was systematically higher by ~1 – 2 pH units than the other methods. The authors attributed these differences to order-of-magnitude uncertainties in the Henry's constant of HCl (Sander, 2015). Similar problems with HCl/Cl^- partitioning were observed in the northeast U.S., potentially due to uncertainties in the thermodynamic properties of HCl or non-volatile cation measurement artifacts (Haskins et al., 2018). Aerosol pH (pH_c and

pH_x both evaluated) derived from NH_3 partitioning agreed well with E-AIM and ISORROPIA predictions under highly polluted conditions in Mexico City (Hennigan et al., 2015). In this study, HNO_3 and HCl data were not available to compare with the NH_3 partitioning calculations, so an evaluation of differences, as was performed by Keene et al. (2004), was not possible.

The partitioning of semi-volatile carboxylic acids should also provide insight into aerosol pH conditions (Keene et al., 2004). Nah et al. (2018) found that oxalic acid partitioning was consistent with its known thermodynamic properties, and thus represented a reasonable proxy for aerosol pH in a study in the southeast USA. However, in the same study, the partitioning of formic and acetic acid implied aerosol pH levels that were ~5 – 6 pH units higher than that predicted by ISORROPIA or other semi-volatile species, including oxalic acid (Nah et al., 2018). The reasons for such dramatic differences are not known, but the formation of organic salts may be one explanation (Paciga et al., 2014; Hakkinen et al., 2014; Tao and Murphy, 2019a).

Efforts to reconcile some of the above differences using model simulations are challenged by large uncertainties in the emissions (Kelly et al., 2016) and secondary formation (Millet et al., 2015) of key species. Although few other comparisons of aerosol pH based upon direct measurements of semi-volatile partitioning have been conducted, semi-volatile species partitioning is used as a key evaluation of thermodynamic model predictions of pH. Guo et al. (2015) compared ISORROPIA predictions of ALWC and NH_3 partitioning with direct measurements in the southeastern U.S. during the Southern Oxidant and Aerosol Study (SOAS). ALWC is required for accurate calculations of a_{H^+} (hence pH) while NH_3 partitioning (for aqueous particles) is dependent upon pH. Guo et al. (2015) observed excellent model–measurement agreement for both ALWC and NH_3 partitioning, suggesting that their pH predictions were similarly accurate. Comparisons of modeled and measured semi-volatile species partitioning are now regularly used to check thermodynamic model predictions of aerosol pH (e.g., Guo et al., 2016; 2017b; 2018b; Murphy et al., 2017; Nah et al., 2018; Song et al., 2018). For example, predictions of HNO_3/NO_3^- partitioning were systematically biased at RH below 40%, suggesting that pH predictions under such RH conditions are likely problematic (Guo et al., 2016).

Practical measurement limitations have precluded more extensive evaluations of direct pH predictions with partitioning predictions of pH. First, the method requires measurable concentrations of a compound in both gas and condensed phases. Conditions in which a species is partitioned almost entirely to one phase preclude the application of this method. For example, Keene et al. (2004) were unable to make quantitative estimates of aerosol pH based upon formic or acetic acid partitioning since the aerosol concentrations were frequently below method detection limits. In certain environments, HNO_3 is partitioned almost entirely in the gas phase, limiting its use for aerosol pH determinations. This limitation also extends to the ability to test and validate the thermodynamic models, whose phase partitioning predictions ~~are seen as~~are a key model check since direct pH measurements are not yet applied to ambient particles (Liu et al., 2017). Second, this approach applies the instantaneous equilibrium assumption, which does not always hold (see Sect. ~~7~~ 6 for a discussion on deviations from

equilibrium). The partitioning method is susceptible to biases associated with sampling semi-volatile components in either the gas or particle phases. Due to their semi-volatile nature, measurements of these compounds can suffer positive (overestimation) or negative (underestimation) artifacts, and the challenges associated with measuring organic (Turpin et al., 2000; Eatough et al., 2003; Lipsky and Robinson, 2006) and inorganic (Ashbaugh and Eldred, 2004; Talbot et al., 1990; Pathak et al., 2004; von Bobrutzki et al., 2010) semi-volatile compounds have been well documented. Despite major advances in analytical capabilities, such challenges persist (Dhawan and Biswas, 2019; Guo et al., 2016; Tao and Murphy, 2019a). Finally, the assumption regarding the phase state of the aqueous aerosol (i.e., whether it is on the efflorescent or the deliquescent branch of the water uptake curve, given hysteresis) has a profound impact on the amount of liquid water present in the aerosol, which in turn affects the ionic strength and ions speciation in solution (hence pH). Although studies have confirmed that the liquid water content can be in agreement with observations (Guo et al., 2015), and in combination with semi-volatile partitioning measurements provide a well-constrained estimate for aerosol pH, the ALWC predictions central to the pH calculations are not routinely evaluated. While organics do not appreciably affect pH in particles consisting of a single aqueous phase (Battaglia et al., 2019), the presence of organic species could result in highly viscous (semi-solid or glassy) particles where the system is not at equilibrium and pH has a heterogeneous distribution throughout the particle. ~~the changes in acidity as particle viscosity increases, shifting the phase towards semi-solid and glassy forms and creating a heterogeneous distribution of H^+ across the particle, are unknown.~~ All these factors eventually limit the precision and range of atmospheric conditions for which pH estimates based on semi-volatile species partitioning can be used. The accuracy of partitioning as well as other proxies ~~an~~ as estimates of pH are further discussed in Sect. ~~6~~4 (specifically Sect. ~~6~~4.2.3 and ~~6~~4.3) based on box model calculations.

4 Box-model guidance for the use of approximations and proxies of acidity for fine particles

This section applies the concepts introduced in previous sections regarding the definition of pH (Sect. 2.1), approximations of pH (Sect. 2.3), and proxies of acidity (Sect. 43). Specifically, E-AIM, AIOMFAC-GLE, MOSAIC, ISORROPIA II, and EQUISOLV II are used to carry out an intercomparison of pH predictions, approximations, and/or proxies using idealized and ambient fine particle compositions. Observations of gas–liquid equilibrium of semi-volatile inorganic compounds were obtained from published studies from North America, Europe, and China representing what can be found in typical regional and global model studies.

4.1 Idealized scenarios

4.1.1 Description of systems

In this section, well-constrained acidity calculations were carried out by the models described in Sect. 2.6. The test cases involve the prediction of gas–liquid equilibrium of water and semi-volatile inorganic compounds as well as pH for a range of equilibrium RH. Three aerosol test systems are compared: (1) an ammonium- and sulfate-rich system, (2) a NaCl-rich, sea-salt-like aerosol system, and (3) a nitrate- and ammonium-rich, but relatively sulfate-poor system. For each system, moderately

acidic and highly acidic conditions were investigated, while covering seven RH levels: 99 %, 90 %, 80 %, 70 %, 60 %, 50 %, and 40 %. All calculations were for a temperature of ~~25 °C~~298 K. Molar input concentrations were chosen to represent realistic atmospheric conditions, for example using gas phase ammonia concentrations of 1.2 – 25 ppb_v typical for suburban to polluted air (Wang et al., 2015) and sulfate amounts resulting in ~ 3 – 8 µg m^{-3} inorganic aerosol mass concentration in the highly acidic cases. The input concentrations and conditions for the systems are summarized in Table ~~4~~3. These input concentrations describe initial (non-equilibrium) total (gas + liquid) molar amounts per unit volume of air – except for water, which is constrained by the given RH. The thermodynamic models equilibrate the different dissolved species and volatile inorganic gases, including solving for the equilibrium ~~dissociation~~ degree of bisulfate dissociation (HSO_4^-) in the liquid aerosol phase, the ammonia–ammonium equilibrium, and the aerosol water content. Mean molal activity coefficients for (H^+, HSO_4^-) or (H^+, Cl^-) cation–anion pairs are used in sulfate-rich and sulfate-poor systems, respectively, to estimate pH using $pH_{\pm}(H,X)$ (Eq. 7). The calculated pH for all systems are summarised in Tables S3 – S5.

System 1: Water + $(NH_4)_2SO_4$ + H_2SO_4 + NH_3

The first test system is an acidic aqueous ammonium + sulfate / bisulfate system. Input concentrations of the electrolytes include $(NH_4)_2SO_4$ (99.9 % by mass or 50 % by mass for moderately and highly acidic cases respectively) and H_2SO_4 with a separate gas phase input of NH_3 (mol m^{-3} air), all of which are then subject to change within a thermodynamic equilibrium calculation. No solid–liquid equilibria were considered. The highest pH values predicted are ~ 4 for the slightly acidic case at 99 % RH, while the lowest pH values of ~ 0.53 ~~to 0.88~~ were predicted for the highly acidic case at 40 % RH.

System 2: Water + Na_2SO_4 + $NaCl$ + H_2SO_4 + HCl

The second system represents an acidified sea-salt-like aerosol solution, in which Mg^{2+} was substituted by charge-equivalent amounts of Na^+. A highly acidic and a moderately acidic variant were created by specifying different amounts of sulfuric acid. The input for this system includes HCl, some of which will exist in the gas phase.

System 3: Water + $(NH_4)_2SO_4$ + H_2SO_4 + NH_3 + HNO_3

The third system represents an acidic, nitrate-rich and comparably sulfate-poor aerosol ($X_T > 2$ in Eq. 9). It involves the gas–liquid equilibration of the inorganic base NH_3 and the acid HNO_3, critical for establishing the equilibrium pH in the system. In the moderately acidic case, the ~~highest~~ pH values at 99 % RH are ~ 2.5 ~~at 99 % RH~~, while the ~~lowest~~ pH values ~~were predicted~~ for the highly acidic case at 40 % RH~~, with the pH ranging between ~ 0.91 and 1.60 depending on the model~~were near 1.5.

4.1.2 Comparison of pH predictions and approximate measures of pH

Results for systems 1, 2, and 3 are shown in Fig. ~~10~~ 3 panels (a), (b), and (c) for moderately acidic and (d), (e), and (f) for highly acidic scenarios. The pH values predicted by those models accounting for the single-ion activity coefficient of H^+ (E-AIM and AIOMFAC-GLE, solid symbols in Fig. ~~10~~3) differ only slightly from each other. For example, the E-AIM and AIOMFAC–GLE calculations for system 1 yield pH differences of 0.03 to 0.2 pH units for RH between 99 % and 80 %, while differences in magnitude of 0.21 to 0.35 pH units result for RH between 70 % and 40 %. Differences are expected to be smaller at high RH, where high water contents result in relatively high dilution and model–model differences in activity coefficients become smaller (see Sect. 2.5 for challenges at high ionic strength). However, this system illustrates that even at 99 % RH the H^+ activity coefficients deviate from a value of one and are as small as 0.4. The pH predictions solely based on free H^+ (pH_F, Eq. 6) frequently deviate from pH by 1 unit for the idealized scenarios considered here (Fig. ~~11~~4). Predictions based on total H^+ (pH_T, Eq. 8) can differ from pH by up to 2 units.

MOSAIC, EQUISOLV II, and ISORROPIA II use mean molal ion activities when computing the dissociation of bisulfate, the gas–liquid equilibrium of ammonia, and other equilibria (single-ion activity coefficients are not computed by these models). Therefore, pH predictions with such models require an approximation, for example the application of the mean molal ion activity approach of Eq. (7) for $pH_{\pm}$. Although not a perfect approximation, $pH_{\pm}$ predictions can be very close to those carried out with the single-ion activity coefficient consideration. For example, for the moderately acidic case in system 1 (Fig. ~~10a~~3a, MOSAIC predictions differ from those by E-AIM by about 0.03 pH units at 99 % RH (0.07 pH units with respect to AIOMFAC–GLE), 0.3 pH units at 80 % RH and 0.46 pH units at 40 % RH (0.75 pH units with respect to AIOMFAC–GLE). For system 1, the MOSAIC- $pH_{\pm}$ value is generally lower than the pH from E-AIM and AIOMFAC–GLE. In the highly acidic system 1 case, the pH difference between MOSAIC and E-AIM is within 0.03 – 0.21 units, except for a 0.33 pH unit difference at 40 % RH. The ISORROPIA II model shows the largest variation in predicted pH over the 99 % to 40 % RH range, especially for the highly acidic case (Fig. ~~10d~~3d). For reasons of enhanced computational efficiency, ISORROPIA II uses look-up tables to determine the water content at a specified RH for a given aerosol system and is run with a higher tolerance level for numerical convergence than, for example, AIOMFAC-GLE. These efficiency adjustments may contribute to a notable difference in predicted water content and resulting $pH_{\pm}$, particularly at 99 % RH, compared to the predictions with more rigorous equilibrium solvers used by the other models.

Generally, the observed differences in pH predicted by the thermodynamic models occur due to a combination of reasons. These include: (1) differing predicted liquid water content at given equilibrium RH (water activity); (2) the predicted degree of bisulfate dissociation, which depends on the aqueous phase composition and the values of the predicted activity coefficients (for H^+, SO_4^{2-}, and HSO_4^-) involved in the equilibrium; (3) the gas–liquid partitioning of NH_3 (or other volatile components for systems 2 & 3), and (4) the use of single-ion vs. mean molal ion activity coefficients in the calculation or approximation of pH. Reasons (1) – (3) affect each other directly, such that any inherent difference among the model equations, for example

the temperature and ionic strength dependence of water and ion activity coefficients, will lead to a different equilibrium solution for the aqueous phase composition and pH. The interplay among composition-dependent activity coefficients and the gas–liquid or ion dissociation equilibria are non-linear and may amplify or dampen effects on predicted pH in a complex manner. Therefore, given the type of test computations with gas–liquid equilibria considered here, differences among models on the order of 0.05 – 0.2 pH units (or even larger at very high ionic strengths resulting at moderate to low RH) are to be expected. Within this range, pinpointing which of the models is closest to the truth is not possible, but in general, pH from models that calculate single-ion activity coefficients (and hence a_{H^+}) using a rigorous numerical approach are to be preferred over those that assume a unity H^+ activity coefficient or those that assume a mean activity coefficient. Figure ~~10~~ 3 indicates that the disagreement between model predictions typically increases with decreasing water activity (RH) for both moderately and highly acidic conditions.

For system 2 (sea-salt like), all models predict the highest acidities (lowest pH) at high RH, with the pH values increasing with decreasing RH for both the slightly and highly acidic calculation variants (Fig. ~~10~~ 3b,e). This is because most of the HCl in the system is present in the gas phase, and this amount remains relatively constant over the whole RH range. Chloride ion activity in the aqueous phase rises as RH decreases and the aqueous solution becomes more concentrated. As a result, H^+ activity decreases with decreasing RH to compensate and so maintain equilibrium with the roughly constant partial pressure of HCl(g). This rise in pH may be unrealistic compared to typical ambient conditions due to the high HCl and absence of ammonia in this test case. The pH predictions by E-AIM model III and AIOMFAC–GLE agree well (absolute differences of 0.01 to 0.06 pH units). The MOSAIC and ISORROPIA II predictions of pH in system 2 were carried out using the ions (H^+, Cl^-) for $pH_\pm$. For the moderately acidic conditions, the MOSAIC and ISORROPIA-derived $pH_\pm$ are in good agreement with E-AIM only at 99 % RH (0.02 units difference), while larger deviations of 0.15 to 0.75 pH units occur for 90 % to 40 % RH. In this moderately acidic case, MOSAIC, ISORROPIA II, and EQUISOLV II tend to systematically overpredict the pH value towards lower RH relative to the other models. In the highly acidic case, the MOSAIC–E-AIM deviation is between 0.07 and 0.43 pH units at RH < 99 %. Such deviations are linked to large variations in the molality-based H^+ activity coefficients ranging from ~ 0.72 at 99 % RH to > 30 at 40 % RH (see AIOMFAC–GLE values in Table S4), which lead to larger errors when mean molal activity coefficients are used to obtain $pH_\pm$. This important influence of the H^+ activity coefficient or its approximation via $\gamma_\pm(H^+, Cl^-)$ is exemplified by comparison of the ISORROPIA II predictions with E-AIM and the other models. The very high activity coefficients of H^+ and Cl^- predicted by E-AIM, which get larger as RH decreases, result in only very low molalities of H^+ left in the aqueous aerosol. ISORROPIA II yields a mean activity coefficient of (H^+, Cl^-) that is very low compared to that of the other models, and varies little with RH, which means that the predicted HCl concentration in the aerosol is substantially higher. This results in the lower, and rather invariant, predicted $pH_\pm$ by ISORROPIA II for RH < 80 %. This example further indicates that assuming activity coefficients of unity in the computation of pH_F based on free H^+ molality (or for pH_T) can lead to errors in this approximation of actual pH values in concentrated solutions (see also Sect. ~~6~~4.2).

The pH predictions by E-AIM model III and AIOMFAC–GLE agree relatively well for system 3, which contains mainly ammonium nitrate (Fig. ~~10~~ 3c,f), especially in the moderately acidic case. There, pH differences are 0.02 units at 99 % RH and about 0.10 – 0.12 units between 90 % and 40 % RH, with AIOMFAC–GLE predicting the slightly lower pH. In the highly acidic case, the differences are similarly low above 70 % RH, while they are ~ 0.18 to 0.25 pH units between 70 % and 40 % RH. The deviations between the E-AIM pH and MOSAIC, ISORROPIA II, or EQUISOLV II $pH_{\pm}$ are clearly larger than those between AIOMFAC–GLE and E-AIM. Even at high RH (> 80 %), the acidity estimates from ISORROPIA II and MOSAIC can differ from each other by almost 1 pH unit (Fig. ~~10f~~3f). Furthermore, the models using mean molal activity coefficients disagree from E-AIM and AIOMFAC-GLE at the highest RH where relatively good agreement is expected due to more dilute conditions. There are several reasons mentioned above that may be responsible for these deviations. The activity coefficient value (reason (4) above) contributes to the difference between MOSAIC/ISORROPIA II/EQUISOLV II and the E-AIM and AIOMFAC–GLE models, because the mean molal ion activity coefficient used as a substitute for γ_{H^+} in first three of these models can either over- or underpredict the single-ion γ_{H^+} depending on the solution composition. The differences in pH predictions by ISORROPIA II compared to those by AIOMFAC-GLE and E-AIM at 99 % and 90 % RH (Fig. ~~10~~ 3f) are mainly because ISORROPIA II yields free H^+ molalities (m_{H^+}) that are similar at the two RH levels, whereas for E-AIM they differ by a factor of four (higher RH, lower molality). This difference seems to be related to variation in the predicted equilibrium gas–aerosol partitioning of total H^+: at 99 % RH the cumulative particle-phase mass concentrations of $H^+ + HSO_4^-$ (~ total particle-phase H^+) per unit volume of air predicted by E-AIM and ISORROPIA II are similar, but at 90 % RH ISORROPIA II predicts a factor of 6 less total H^+ than E-AIM. At similar ~~aerosol liquid water content~~ALWC, this yields a lower m_{H^+} and higher pH than expected at 90 %. Elucidating detailed differences in acidity predictions between the thermodynamic models for nitrate-containing systems like system 3 should be considered in future work.

Figure ~~11~~ 4 compares the different pH estimation options proposed in Sect. 2.3 for use by models that do not predict the single-ion activity coefficient of H^+. All calculations (for the systems shown in Fig. ~~10~~ 3 and discussed above) were carried out using AIOMFAC-GLE for consistency, and E-AIM is expected to yield similar results. The pH approximations based on total or free H^+ molality imply the assumption of an H^+ activity coefficient of unity. The comparison in Fig. 4~~11~~ shows that these two options tend to show larger deviations from the molality-based pH predicted by AIOMFAC–GLE compared to the use of single ion activity coefficients. Both pH_T and pH_F approximate pH within about 0.5 pH units under highly dilute conditions with pH greater than about 3. However, pH_T becomes a poorer approximation of pH when pH values decrease below 3, mainly due to the increasing concentrations of HSO_4^-. In the case of the three systems compared here, pH_F is overall a better estimate for pH than pH_T, such that use of total H^+ is not recommended for atmospheric aerosols. The suitability of pH_F as an approximation may be influenced by the specific system being tested (e.g., RH condition, composition) and needs of the application.

Overall, the AIOMFAC–GLE model results suggest that $pH_{\pm}$ (with (H^+, HSO_4^-) or (H^+, Cl^-) as the ions for the computation of $\gamma_{\pm,HX}^{(m)}$ used in Eq. 7) is better than pH_F or pH_T in approximating pH.. Computation of the mean molal activity coefficient based on (2 H^+, SO_4^{2-}) leads to a better $pH_{\pm}$ approximation only in the moderately acidic case of system 1 (Fig. 4~~11~~a) at RH < 90 %, while it is worse than using (H^+, HSO_4^-) in the highly acidic case of system 1 (open symbols Fig. ~~11a~~4a). Therefore, the use of a 1:1 electrolyte for $pH_{\pm}$ is recommended. This mean molal activity coefficient approach is recommended when ISORROPIA II, EQUISOLV II, or MOSAIC are used as thermodynamic models for the calculation of aerosol properties.

4.2 Ambient scenarios

4.2.1 Description of datasets and calculations

Datasets were selected to cover a broad range of acidity, temperature, RH, and species present that drive aerosol pH (Table 5~~4~~). In addition to the major species NH_4^+/NH_3, SO_4^{2-}, and NO_3^-/HNO_3, the dataset also contained variable concentrations of Cl^-/HCl and the non-volatile species Na^+, Ca^{2+}, K^+ and Mg^{2+} (not shown in the table). A total of more than 7700 data points were available for evaluation from Tianjin, China; the California Nexus (CalNex) campaign; Cabauw, Netherlands; Wintertime Investigation of Transport, Emissions, and Reactivity (WINTER) campaign; and SOAS campaign ~~(Nenes et al., 2019)~~, with ~7200 data points having relative humidities above 35 % and spanning a temperature range from 252 to 305 K (see also Nenes et al., 2019). Given that the MOSAIC box model required – in its current implementation – a manual setup of each input condition, a few data points were selected from the total available in each dataset to compare against the corresponding predictions from the other models. The points were selected to span the range of RH and sulfate amounts encountered in the datasets. Four data points per study location were selected, giving 20 total simulations from MOSAIC to compare against. The MOSAIC inputs are summarized in Supplementary Table S9 with results shown in Fig. S6.

Before thermodynamic calculations are carried out with E-AIM, AIOMFAC-GLE, MOSAIC, and ISORROPIA II, each data point was evaluated to ensure that the resulting thermodynamic solution was atmospherically relevant – i.e., with an alkalinity that does not exceed that of carbonate aerosol (e.g., $CaCO_3$). Specifically, the charge-equivalent amount of cations is not allowed to exceed the abundance of anions which would result in considerable amounts of hydroxyl ion. In the case of E-AIM and AIOMFAC-GLE, the composition data were pre-processed and evaluated before input, while MOSAIC and ISORROPIA II evaluate the data automatically and issue error messages or apply adjustments to the input. The input composition data for each model consists of total amounts of Na^+, K^+, Mg^{2+}, Ca^{2+}, TNH_4, TCl, and TNO_3, in moles per unit volume of air. The prefix T emphasizes the fact that the final three of the amounts are totals of: $NH_4^+{}_{(aq)}$, $NH_{3(aq)}$, and $NH_{3(g)}$; $Cl^-{}_{(aq)}$ and $HCl_{(g)}$; and $NO_3^-{}_{(aq)}$, $HNO_{3(aq)}$, and $HNO_{3(g)}$. The amount of H^+ needed to achieve charge balance is calculated from:

$$Z = [TNH_4] + [Na^+] + [K^+] + 2[Mg^{2+}] + 2[Ca^{2+}] - [TCl] - [TNO_3] - 2[TSO_4], \quad (19)$$

This equation differs from the ~~strong acidity~~ charge balance proxy introduced in Sect. ~~4~~ 3 since it considers the total (gas + particle) amounts of semi-volatile acids and bases rather than exclusively the particle phase as in Eq. (13). If the value of Z is zero, then the system is charge balanced with all TNH_4 present as NH_4^+ (during a model calculation NH_3 can still partition into the gas phase, but this will occur by dissociation of NH_4^+). If the value of Z is greater than zero, there is an excess of cations, and a Z amount of TNH_4 is assumed to exist as NH_3, and the NH_4^+ ion in the system is reduced to [TNH_4 – Z]. If the value of Z is less than zero, there is an excess of anions even when all TNH_4 is present as NH_4^+. In this case, an amount of H^+ equal to –Z is added to the system. For E-AIM and AIOMFAC, the calculation of Z and adjustments specified above yield the starting point for the calculation. The amounts of $NH_4^+{}_{(aq)}$, $NH_{3(aq)}$, $NH_{3(g)}$, $HSO_4^-{}_{(aq)}$, $OH^-{}_{(aq)}$, $HCl_{(g)}$ and $HNO_{3(g)}$ in the system at the specified RH and temperature are determined by solving the relevant equilibrium equations. In MOSAIC, the excess Cl^- and NO_3^- anions are transferred to the gas phase as HCl and HNO_3, in that order, while any excess SO_4^{2-} in the particle phase is balanced by adding H^+ to the system. The adjusted gas- and particle-phase concentrations are then used as the initial conditions for further dynamic gas–particle partitioning. In the case of ISORROPIA II, the aerosol is required to be more acidic than aqueous $CaCO_3$ at given RH, so Z should be less or equal to zero.

The presence of non-volatile cations is handled slightly differently by the models. When calcium is present in ISORROPIA II, the code first forms $CaSO_4$ as a precipitate (Fountoukis and Nenes, 2007). If there is any remaining Ca and its mole-equivalent exceeds those of SO_4^{2-}, NO_3^-, and Cl^- combined, an error message is noted and the code assumes that the excess Ca^{2+} is in the form of $CaCO_3$ and the pH of dissolved $CaCO_3$ is prescribed at the given RH (see Sect. ~~7~~6.1 for a discussion of carbonate chemistry and pH). If all Ca precipitates out as $CaSO_4$, then the ISORROPIA II code examines if the mole-equivalents of Na^+, K^+, and Mg^{2+} exceeds that of the NO_3^-, Cl^-, and remaining SO_4^{2-} combined. If that is the case, an error message is issued, and the excess cations are ignored. Otherwise, the code then uses the inputs of Na^+, free Ca^{2+}, free SO_4^{2-}, etc. to calculate the pH, ALWC, and semi-volatile partitioning of TNH_4, TCl, and TNO_3. A similar approach is taken in MOSAIC, which assumes that the maximum possible amount of $CaSO_4$ precipitates out over the full RH range, and any excess Ca after forming $Ca(NO_3)_2$ and $CaCl_2$ is assumed to be in the form of $CaCO_3$. MOSAIC does not explicitly treat K^+ and Mg^{2+}, which are instead represented by equivalent moles of Na^+. Both E-AIM and AIOMFAC also assume that the maximum possible amount of $CaSO_4$ precipitates out and is not considered in the gas–particle partitioning calculations for RH < 98 %. Furthermore, E-AIM does not consider Ca^{2+}, K^+, and Mg^{2+} in the calculations, but instead uses a charge-equivalent amount of Na^+. For AIOMFAC-GLE model input, the electroneutral set of ions is mapped to a set of representative electrolyte components. To facilitate intercomparison among the models over a wide range in RH, aside from the consideration of the precipitation of solid $CaSO_4$, the models were run using the assumption of the aerosol phase being present as an aqueous electrolyte solution, potentially supersaturated with respect to certain crystalline salts (also referred to as metastable mode in ISORROPIA). Since this assumption becomes invalid at low RH, the statistical evaluation of model–model differences and pH approximations was restricted to the RH range above 35 %, while model calculations were carried out with the supersaturated solution assumption including data points at lower RH.

During the calculation of the equilibrium composition and corresponding aerosol pH by ISORROPIA II here, all non-volatile cations are converted into their mole-equivalent sodium concentrations. Also, data where non-volatile cation concentrations exceed what is required to neutralize the amount of anions (sulfate, nitrate, and chloride) present are not considered. All models were allowed to predict partitioning according to their equations and property databases, therefore differences in pH and activity coefficients are a convolution of all differences in the underlying thermodynamic treatment (equilibrium constants, numerical solver tolerance thresholds, calculated activity coefficients, and aerosol water content). A comprehensive accounting of the effects of these differences will be the focus of future work – and here we present only the differences in pH between models and their different implementations of pH approximations.

4.2.2 pH and its approximations

The pH values predicted by AIOMFAC-GLE (Fig. ~~12a~~5a) and E-AIM (Fig. ~~12b~~5b) for the combined datasets show both the wide range of pH calculated for each of the datasets as well as variability in the results from the two models. E-AIM and AIOMFAC-GLE agree in their trends but differences increase as RH decreases (as the aqueous aerosols become more concentrated). Differences between the models are usually within 0.5 pH units. The most acidic systems are SOAS (Centreville, AL) in the southeastern U.S. (pH range: ~ -2 to 2) and WINTER for measurements aloft in the northeast U.S. (pH range ~ -4 to 2), which in part is related to the very low NH_3 concentrations and lack of non-volatile cations. The extremely high acidity branch of WINTER data is related to measurements carried out aloft, where temperatures as low as 252 K were encountered. The low humidities in that environment decrease aerosol water to very low levels (Guo et al., 2016). The CalNex dataset is characterized by intermediate pH values, ranging between 0 and 2.5, mostly driven by higher NH_3 levels and presence of NVCs. The Tianjin and Cabauw datasets are characterized by the largest concentration of NH_3 and NVCs, and for this reason have the highest pH, reaching a value of 5.

In order to understand the uncertainty introduced by using pH_F or $pH_\pm$ instead of model-predicted pH, model results are examined for each campaign separately. Figure 13 presents the differences between pH predictions and approximations for the Cabauw dataset. Calculations of pH with AIOMFAC-GLE (left column) using the various approximations (pH_F, $pH_\pm$) has notably different structure than that using E-AIM (right column). In both models, the difference between $pH_\pm$ and pH rarely exceed 0.5 pH units, especially for RH above 60 %; pH_F is characterized by larger differences, but still mostly within one pH unit – and reflects the effect of the $\log_{10}(\gamma_{H^+})$ contribution which is largest at the lowest RH. These results are consistent with prior studies that assume that the activity coefficient of H^+ is equal to unity for the purpose of pH estimation (but not for solving the thermodynamic equilibria) (Song at al., 2018).

Results in Fig. ~~13~~ 6 suggest that using a H^+–X^- ion pair and applying an activity coefficient in the calculation of $pH_\pm$ gives less scatter and absolute bias across the dataset than using pH_F within a given model framework (E-AIM or AIOMFAC-GLE). The

ion pair that leads to the best $pH_{\pm}$ estimate varies between AIOMFAC-GLE and E-AIM with H^+–Cl^- and H^+–HSO_4^- showing overall the most promise. The H^+–NO_3^- pair tends to exhibit a large scatter and systematic bias in the case of E-AIM, while it shows the least scatter and bias among all ion pairs in the case of AIOMFAC-GLE. Repeating this exercise for all the other datasets (Supplementary Figures S2 – S5) partly supports these observations – but the pattern and magnitude of the differences (approximate pH minus pH) vary according to the aerosol compositions characteristic of each dataset. For the WINTER data in particular (Fig. S5), biases much larger than 0.5 pH units can be seen at lower humidity (which is especially notable for E-AIM). These deviations can be attributed to the value of the activity coefficient of H^+, which becomes very large for the ultra-high ionic strengths characteristic of the WINTER aerosols at intermediate and low RH. The H^+ activity coefficient, which exceeds 10 and can reach up to 100, tends to decrease the pH between 1 and 2 units beyond what is expected from pH_F (Fig. S5 b). The results from AIOMFAC-GLE and E-AIM in Figure 13 and supplementary Figs. S2 – S5 show that the calculated values of the pH approximations differ between the models in quite complex ways, largely reflecting the different treatments of the activity coefficients. These are reflected both in the value of γ_{H+}, and secondary effects on liquid water uptake, ion dissociation and semi-volatile partitioning.

Both ISORROPIA II and MOSAIC nominally output pH_F (and can be modified to output $pH_{\pm}$); using approximations (pH_F or $pH_{\pm}$) in place of pH introduces uncertainty. ISORROPIA-predicted pH approximations as a function of relative humidity compared to AIOMFAC-GLE (left column) and E-AIM (right column, Fig. ~~1~~47) show that the deviation between pH_F and pH increases as the humidity decreases, with the largest deviations occurring for the extremely acidic aerosol dataset of WINTER. However, for most cases, relative humidities above 60 % are correlated with a deviation from pH that is less than a unit (smaller differences are seen for AIOMFAC-GLE than E-AIM). Comparisons of MOSAIC calculations, against the predictions from ISORROPIA II for the 20 selected cases (Table S9) indicated the two models produce $pH_{\pm}$ (H^+, NO_3^-), $pH_{\pm}$ (H^+, Cl^-), and pH_F metrics that are highly correlated ($r^2 \geq 0.96$) with minimal offset (regression slope within 0.11 pH units of 1:1 line) between the models (Fig. S6). Using the H^+–NO_3^- ion pair to express $pH_{\pm}$ from ISORROPIA provides the closest agreement with pH if AIOMFAC-GLE is used as a reference.

The pH errors between ISORROPIA II and AIOMFAC-GLE/E-AIM for all the datasets combined are summarized in Table ~~6~~5. Using $pH_{\pm}$ (H^+, NO_3^-) as a pH approximation shows the lowest RMSE and mean bias error in the case of AIOMFAC-GLE predictions ~~when considering all field data sets~~, followed by $pH_{\pm}$ (H^+, Cl^-) as the next best approximation. However, when considering E-AIM, the evaluation of all data sets shows that $pH_{\pm}$ (H^+, Cl^-) and $pH_{\pm}$ (H^+, HSO_4^-) are favored over $pH_{\pm}$ (H^+, NO_3^-), as $pH_{\pm}$ (H^+, NO_3^-) shows an RMSE of ~ 1 for the WINTER data, which was characterized by the lowest pH values. The comparison between thermodynamic models for the performance of pH proxies include a convolution of numerous errors in the cases of ISORROPIA II, MOSAIC, and EQUISOLV II; therefore, they cannot be used to determine a priori which choice of anion is best for use in $pH_{\pm}$ (H, X). Some of the $pH_{\pm}$ (H, X) variants also show a larger dependence on RH than others, with the largest deviations from pH typically found towards the problematic region of lower RH (< 50 %); see Fig. ~~1~~36. Based on

the combined evaluations of pH approximations by E-AIM and AIOMFAC-GLE against their own pH predictions (no model–model bias incurred), $pH_{\pm}$ (H^+, Cl^-) has the best agreement for the wide pH range examined, although any of the pH± variants work sufficiently well, especially at RH > 60 %.

4.2.3 Comparison of proxies to aerosol pH

Several studies have compared certain proxies of acidity (Sect. 43, see also Table 23) to thermodynamic model predictions of pH_F (Guo et al., 2015; Guo et al., 2016; Hennigan et al., 2015; Lawal et al., 2018; Murphy et al., 2017; Winkler, 1986). Predictions of pH_F using the semi-volatile partitioning approach (Eq. 18, Figure 8a-c) were evaluated in Mexico City (Hennigan et al., 2015), but more commonly, due to the lack of direct aerosol pH_F measurements for comparison, semi-volatile species partitioning is often used as a critical check of thermodynamic equilibrium model assumptions and predictive skill (Guo et al., 2016; Guo et al., 2017a; Guo et al., 2015; Nah et al., 2018). Connecting the neutrality-based or gas ratio type proxies to a numerical value of pH is less common in literature and the assessment of acidity based on those proxies is usually qualitative (e.g. acidic vs non-acidic categorization or determination of relatively higher/lower acidity). In Fig. 158, comparisons from the literature are extended to include more locations, representing diverse chemical regimes, source influences, and meteorological conditions. Proxies introduced in Sect. 4 3 are compared to ISORROPIA II-predicted values of aerosol pH_F using gas + aerosol inputs for four locations (southeast U.S. in summer, California in summer, northeast U.S. in winter, and Tianjin in China in summer; Table 54).

Figure 15Figure 8d shows that the cation/anion equivalent ratio is fundamentally limited as a proxy for aerosol pH_F. The assumption applied throughout the literature is that a cation deficit (anion equivalents > cation equivalents excluding H^+; ratio < 1; see Sect. 4 3 and Table 32) indicates acidic particles, an anion deficit (ratio > 1) corresponds to alkaline particles. Consequently, a molar equivalent ratio near unity represents near-neutral conditions. Figure 15Figure 8 shows clearly that these interpretations of the molar ratio are not valid. For a given cation/anion equivalent ratio, predicted pH_F values vary by 3 – 4 pH_F units. All of the data with cation/anion equivalent ratios near unity are predicted to be quite acidic, with $pH_F < 3$ (and often < 1). The behavior in Fig. 15 8 is consistent with observations at locations in Canada (Murphy et al., 2017) and more broadly across the U.S. (Lawal et al., 2018). Even the aerosol predicted by the cation/anion equivalent ratio to be alkaline are actually quite acidic, with $pH_F < 3$ for almost all of the data where cation/anion > 1. Even if pH_F underestimates pH by 2 units (the maximum underestimation in Fig. 14 7a,b) particles would still generally be considered acidic. Common simplifying assumptions associated with the molar ratio method that were discussed in Sect. 43.1 (e.g., considering only NH_4^+–NO_3^--SO_4^{2-} or NH_4^+–SO_4^{2-}) were shown by Guo et al. (2018) to be especially problematic in estimating pH_F. Taken together, these results support prior recommendations against use of equivalent ratios as surrogates for particle acidity (Guo et al., 2018b; Hennigan et al., 2015; Lawal et al., 2018; Shi et al., 2017).

Estimates of particle acidity based on an ion charge balance are similarly problematic (~~Fig. 15~~Fig. ~~a~~8c). A charge balance of zero, which corresponds to a cation/anion equivalent ratio of unity, wrongly implies nearly neutral aerosols according to this proxy. Excess cations (negative charge balance, Eq. 13, ~~Fig. 15~~Fig. ~~a~~8c), which corresponds to cation/anion equivalents ratios > 1, wrongly implies alkaline conditions. ~~Figure 15~~Figure 8 agrees with prior recommendations against using the charge balance as a proxy for particle acidity (Guo et al., 2015; Hennigan et al., 2015; Murphy et al., 2017; Winkler, 1986). The equivalent ratio and charge balance methods both suffer from the same deficiencies, which include: sensitivity to limitations in the precision and accuracy of measurements, not accounting for the buffering effects of many species or the modulating effects of aerosol water, and the non-ideal nature of concentrated aqueous particles, which necessitates the computation of species activity coefficients. As noted above, some usages of strong acidity, a once commonly used parameter to access aerosol acidity health impacts is essentially an ion balance and suffers from similar limitations. A further limitation of the charge balance proxy is the use of an extensive quantity (H^+_{air}) to represent an intensive property (pH) of an aerosol distribution, which points to a major design flaw of that approach.

To our knowledge, ~~Fig. 15~~Fig. ~~c~~ 8f represents the first quantitative comparison between GR (the gas ratio proxy, Table ~~3~~2) and predictions of aerosol pH_F. Based on the thermodynamics of gas–particle partitioning, the GR (and adjGR) relationship to pH follows a sigmoidal curve that similarly defines the partitioning of semi-volatile species sensitive to pH (e.g., see Fig. 5 in Pinder et al., 2008a for an illustration of how nitrate PM is a function of GR and adjGR). For the northeast U.S. and California data, the GR follows this sigmoidal behaviour and is strongly correlated with predicted pH_F. Increasing GR corresponds to increasing pH, although the slope and intercept of the two data sets differ substantially since they lie on different areas of the curve. In the southeast U.S., the GR results show much larger absolute values than the other locations, since HNO_3 measurements were unavailable and the aerosol nitrate values were used as input for TNO_3 (Guo et al., 2015). The GR in Tianjin shows no relationship with pH_F (slope = 0.03, ~~r~~R^2 = 0.01), even though the data included complete aerosol and gas phase measurements. Although the GR may be highly correlated with pH_F in some environments, it is not advisable to use the GR as a pH_F proxy given the variability observed in ~~Fig. 15~~Fig. 8. For example, at a given GR, the pH_F range spans ~1 – 4 pH units while the coefficient of determination ranges from 0.01 to 0.75 across the four locations. This suggests that *a posteriori* knowledge of the pH_F–GR relationship is required to use the GR as a proxy for pH. The GR requires aerosol inorganic composition and measurements of both gas-phase NH_3 and HNO_3. Therefore, with such a data set, pH_F (or pH) can be predicted directly with one of the thermodynamic equilibrium models, which is the recommended approach.

A fundamental limiting factor in using the GR as a proxy for pH is its assumptions about free ammonia. The GR method assumes that under ammonia-poor conditions, where TNH_4 is less than $2\times TSO_4$, the aerosol is acidic and TNH_4 will partition predominantly to the aerosol phase (Seinfeld and Pandis, 2016). Similarly, the method assumes that ammonia-rich conditions, which exist when TNH_4 is greater than $2\times TSO_4$, correspond to largely neutralized aerosols and significant gas-phase NH_3 (Seinfeld and Pandis, 2016). While ammonia-rich particles are less acidic in terms of charge balance (Eq. 13) than ammonia

poor particles (all else being equal), a plot of pH vs. GR (Fig. S1) shows that even in ammonia-rich conditions with a high GR, particles do not approach pH near 7. The aerosol is strongly acidic (pH < 1) under ammonia-poor conditions, and a small but significant fraction of TNH_4 can exist in the gas phase even though the pH is low. The fraction of TNH_4 in the gas phase ~~(ε_{NH3})~~ approaches 0.1 while the GR < 0, (corresponding to $TNH_4 < 2 \times TSO_4$). Likewise, the aerosol remains strongly acidic even under ammonia-rich conditions, where TNH_4 exceeds the amount required to neutralize all of the TSO_4 (GR > 0). Even when the amount of TNH_4 greatly exceeds all available TNO_3 and TSO_4, the aerosol remains strongly acidic (approaching a predicted pH of 3.7 as the GR approaches 50 in Fig. S1 example). For such high gas ratios the majority of TNH_4 (~0.95) resides in the gas phase. This phenomenon is somewhat counterintuitive: it seems logical that gas-phase ammonia would react completely with acids as strong as HNO_3 and H_2SO_4 until they were fully neutralized. However, the volatility of NH_3 is an important factor that balances the extent to which it reacts with acidic components in the aerosol phase. This explains the insensitivity of aerosol pH in the southeast U.S., even though sulfate levels are also decreasing while ammonia has remained steady or even increased (Weber et al., 2016).

Aerosol pH calculations based on partitioning of HNO_3 and NH_3 between the gas and aerosol phases show mixed results when compared to predictions by thermodynamic equilibrium models (~~Fig. 15~~Fig. 8~~d-f~~a-c). In the southeast U.S., the ISORROPIA and NH_3 partitioning-derived pH_F values are moderately correlated, with nearly all values within 1 pH_F unit of the 1:1 line (~~Fig. 15~~Fig. ~~f~~8c). In this case, the pH calculated from NH_3 partitioning was systematically lower than the thermodynamic model predictions, a result that was also observed for predictions in Mexico City (Hennigan et al., 2015). In California, the pH_F calculations from NH_3 and HNO_3 partitioning generally did not agree with the thermodynamic model predictions. The model-predicted pH_F was higher (avg. pH_F = 2.67) than the calculation from NH_3 (avg. pH_F = 1.64) and similar to the one based on HNO_3 partitioning (avg. pH_F = 2.45). Although the pH_F calculations from NH_3 and HNO_3 partitioning lie in the same general area of the graph in ~~Fig. 15~~Fig. 8, they were inversely correlated with each other (r = -0.76, not shown), an observation that requires further investigation and likely future studies to reconcile. Keene et al. (2004) also observed disagreement between the pH_F calculations from NH_3 and HNO_3 partitioning. In the northeast U.S., the phase partitioning of HNO_3 gave mixed results, as well. At times, the predicted and calculated pH_F values agreed well, while at other times there were differences of ~2 – 3 pH_F units. The greatest discrepancies were observed at the lowest ~~aerosol liquid water contents~~ALWC (mass fraction basis, ~~Fig. 15~~Fig. ~~e~~8b), a relationship also identified by Guo et al. (2016) and consistent with the idea that activity becomes harder to predict at lower water content (Sect. ~~6~~4.1, Fig. ~~10~~3). Potential problems with pH_F calculated from semi-volatile species partitioning have been discussed (Keene et al., 1998; Keene and Savoie, 1998; Young et al., 2013). The approach requires measurements of at least one semi-volatile gas-phase species and the aerosol inorganic composition, which are input into a thermodynamic model to get the ALWC, a required component to calculate condensed-phase activities in Eq. 16 and needed to use typical Henry's law coefficients in Eq. 17 and 18. Therefore, given the need for all these inputs, thermodynamic models should be used to directly predict pH or one of its approximations.

4.3 Recommendations on the calculation of pH by approximation and proxy

Where single-ion activity predictions are not available, the comparison based on the ambient datasets used here suggests that the best pH approximation is obtained by using Eq. 7 for $pH_{\pm}$. However, identifying a universal H^+–anion pair that best reproduces pH appears to be model-dependent with only $pH_{\pm}$ (H^+, NO_3^-) having the potential to be a worse estimate of pH than pH_F (in the case of E-AIM). Although, on average, all of the approximate measures of pH compare similarly against pH from AIOMFAC-GLE and E-AIM, there is a strong dependence of the bias on RH that is mitigated through the use of $pH_{\pm}$ (as opposed to pH_F), and for this reason it is the recommended approach when ISORROPIA, MOSAIC, EQUISOLV II or similar models are used for calculations of pH in the future. Low RH also coincides with time periods where models (both box and chemical transport models) face challenges in accurately predicting gas–particle partitioning (e.g., Guo et al., 2016; Kelly et al., 2018) thus motivating a need to properly characterize acidity under those conditions.

Based on the analyses and discussion presented in this section and Sect. 43, it is strongly recommended that proxies are avoided in the analysis of particle acidity. Some of the proxies correlate with pH_F, even strongly at times, although this varies greatly with ambient conditions (T, RH), composition, and concentration. This leads to large inconsistencies across locations, and even within a given observational data set. Often, the proxies are not able to qualitatively distinguish acidic from neutral particles or to capture qualitative trends in acidity (e.g., pH increases or decreases with a given indicator). A detailed comparison with thermodynamic equilibrium model predictions constrained with aerosol and gas inputs is required to identify the periods and locations where a proxy may perform adequately; defeating the purpose of using the proxy. With the open access and web-based availability of validated aerosol thermodynamic equilibrium models (Sect. 2.6), scientists are encouraged to use one or more of these tools in future studies of particle acidity.

5 Interactions of aerosol and cloud chemistry with acidity

The previous sections highlighted how cations and anions (along with ambient conditions) drive pH in condensed phases with a focus on equilibrium conditions and models. In addition, kinetic processes such as cation and anion dissolution influence acidity. Furthermore, the acidity of aerosols, clouds, and fogs is tightly coupled with their chemical reactivity. The pH of the atmospheric aqueous phase affects the partitioning of weakly acidic and basic gases to the condensed phase, and the rate of many multiphase chemical reactions. The chemical reactions in the atmospheric aqueous phase, in turn, modulate the pH of the aqueous phase. As a result, the acidity of aerosols, cloud droplets, and fog droplets is not only determined by thermodynamic equilibrium, but also multiphase chemical kinetics. Because of the complex nature of these couplings between acidity and atmospheric aqueous phase chemistry, these issues are presented in more detail in a companion paper currently in preparation (Tilgner et al., 2019 *in prep*). ~~The~~ This section highlights some important systems where acidity interacts with, and is influenced by, condensed-phase chemical reactions.

One important example of a system with chemistry-acidity feedbacks is the multiphase oxidation of sulfur dioxide (SO_2) to form particulate sulfate (S(IV)→S(VI) conversion, also referred to as 'sulfur' oxidation). Sulfate makes up 15% of $PM_{2.5}$ mass globally (Sofiev et al., 2018) and is a major component of $PM_{2.5}$ in areas affected by emissions from combustion of sulfur-containing fossil fuels. Multiphase reactions are the primary driving force for oxidation of SO_2 to sulfate (Calvert et al., 1985). The ionization of SO_2 in the aqueous phase under basic conditions enhances its uptake; the effective Henry's Law constant for SO_2 varies three orders of magnitude (from 17 M atm^{-1} to 1.7×10^4 M atm^{-1}) between pH 3 and pH 6 (Sander, 2015). Therefore, sulfate production, especially under acidic conditions, is largely limited by the amount of SO_2 that can partition to the aqueous phase. Meanwhile, sulfate formation is a major source of acidity in aerosols, fog and cloud droplets (Calvert et al., 1985). In the absence of buffering, S(IV)→ S(VI) oxidation pathways which are more effective at higher pH, such as oxidation of SO_3^{2-} by O_3 (Maahs, 1983; Lagrange et al., 1994) or NO_2 (Lee and Schwartz, 1983; Clifton et al., 1988), will become quenched with increasing sulfate production (~~Fig. 3~~Fig. 9, Supplement Sect. S2). However, buffering may be significant in atmospheric waters; Collett et al. (1999), for example, demonstrated that buffering in a California fog permitted the fog pH to stay 0.3 to 0.7 pH units higher than expected, enhancing the amount of sulfate aerosol present after the fog episode by 50%.

Another important process controlled by the acidity of the aqueous phase is the solubility of transition metal ions such as Fe(III) and Mn(II), which can catalyze S(IV) oxidation. Transition metals are ubiquitous in the atmosphere, having been observed in aerosol samples and cloud/fog/rain water collected around the globe (e.g., Bianco et al., 2017; Hsu et al., 2010). Transition metals (particularly Fe, Cu, and Mn) are active in the aqueous-phase chemistry of clouds, fogs, and deliquesced aerosols, catalyzing reactions and affecting the oxidative capacity of the condensed phase (Deguillaume et al., 2005). Due in part to variation in how transition metal emissions are generated from different source types (e.g., mechanically generated mineral dust vs. condensation/gas-to-particle conversion of gases emitted during combustion), transition metal composition/concentration and source contributions vary across the aerosol size distribution (Deguillaume et al., 2005). This has implications for the chemical environment and acidity that metals from different sources are exposed to, the reactions they participate in, and their potential impacts on human health.

The degree to which transition metals contribute to condensed phase reactions depends on their solubility. TMI solubility typically increases as pH decreases, although the relationship between pH and metal solubility is a complex one (Spokes et al., 1994). Transition metals are often emitted as largely insoluble chemical species, and their solubility increases as the emitted particles 'age' via exposure to acidic gases in the atmosphere. The degree to which pH affects TMI solubility depends on the origin of the particles, degree of particle aging which alters a particle's physicochemical characteristics, and the specific metal (Deguillaume et al., 2005; Deguillaume et al., 2010). Several laboratory studies have attempted to elucidate the pH dependence of transition metal solubilization for different species. Spokes et al. (1994) found that for a Saharan dust sample, the solubilization of Al and Fe, while strongly enhanced at lower pH, was nearly completely reversible with increasing pH. For an

urban aerosol sample, some of the solubilized metals remained in solution with increasing pH, possibly due to complexation of the metal species with organic ligands. Manganese was found in both dust and urban particles to be soluble with decreased pH, with only limited reversibility as the pH was increased.

Acid-catalyzed reactions of hypohalous acids (HOX, where X = Br, Cl or I) in sea salt aerosols influence the oxidative capacity of the troposphere (Saiz-Lopez and von Glasow, 2012; von Glasow and Crutzen, 2014; Simpson et al., 2015). The reactions of HOX with other halogen ions can lead to the release of reactive halogen gases, which are involved in many key tropospheric reaction cycles. Reactions of S(IV) with HOX are another major contributor to sulfate formation in sea salt aerosols (Chen et al., 2016; Vogt et al., 1996; von Glasow et al., 2002). These reactions acidify the aerosol (Chen et al., 2016) but may be considered a sink of reactive halogens, in that they convert HOX to their less-reactive acid form. Reactive halogen gases act directly as important sinks of key oxidants, such as O_3 and HO_2, and therefore indirectly influence other linked systems HO_x (=OH + HO_2) and NO_x (=NO + NO_2) (Oltmans et al., 1989; Schmidt et al., 2016; Sherwen et al., 2016). Moreover, reactive halogen gases, especially the Cl atom, can be powerful oxidants that can rapidly react with important tropospheric organic trace gases, such as non-methane volatile organic compounds (VOCs), and dimethylsulfide (Barnes et al., 2006; Hossaini et al., 2016).

Acidity also impacts the partitioning of weak acids, including organic acids, into aqueous aerosols and cloud/fog droplets by controlling their ionization state in the aqueous phase. The hydration of carbonyl groups in compounds that also contain pH sensitive moieties, such as α-oxocarboxylic acids, is also highly influenced by acidity (Kerber and Fernando, 2010). Increasing acidity leads to a decrease of the effective partitioning towards the particle phase of acids and to an increase in the effective partitioning of bases, and vice versa (see Fig. 410). In the case of ionizable organic species such as organic acids, key aqueous-phase oxidants, such as OH, NO_3 and O_3, can react via different possible reaction pathways and kinetics with the protonated and deprotonated forms (Buxton et al., 1988; Herrmann et al., 2010; Herrmann et al., 2015; Bräuer et al., 2019). Accordingly, the overall reaction rate constant for oxidation of dissociating compounds can be largely pH dependent, especially for reaction with nitrate radicals. For organic acids, the overall rate constant typically increases with increasing pH and more efficient oxidation can be expected under less acidic conditions. For example, the overall second order rate constant for the reaction of nitrate radicals with formic acid (and its ionized, dissociated form) varies from close to 3.8×10^5 $M^{-1}s^{-1}$ at pH = 2.0 to 5.1×10^7 $M^{-1}s^{-1}$ at pH = 5 (Exner et al., 1994). Additionally, the increased partitioning of organic acids under less acidic conditions leads to even higher oxidations rates.

Changes in the pH of a cloud or fog droplet can result from addition of acids or bases to the solution, through partitioning from the gas phase, collision/coalescence of droplets, or aqueous reactions. The magnitude of the pH change can be strongly affected by the presence and ability of weak acids or bases to buffer against that change through proton uptake or release. A buffer is a mixture of a weak acid and its conjugate base (e.g., formic acid and formate) or a mix of a weak base and its conjugate acid

(e.g., ammonia and ammonium). The magnitude of an internal buffering effect is greatest when the solution pH is equal to the pK_a (pK_b) of the weak acid (base) buffer. External buffering can also be important, perhaps best illustrated by the uptake of additional ammonia from the gas phase in response to a decrease in solution pH (Liljestrand, 1985; Jacob et al., 1986a; Jacob et al., 1986b).

The formation of secondary organic aerosol material in atmospheric aerosols via multiphase processes is strongly related to the acidity. Many atmospheric organic accretion reactions, such as aldol condensation (Noziere and Esteve, 2007; Noziere et al., 2010; Sareen et al., 2010; Li et al., 2011), hemiacetal and acetal formation (Jang et al., 2002; Kalberer et al., 2004; Shapiro et al., 2009; Loeffler et al., 2006), and esterification of carboxylic acids (Barsanti and Pankow, 2006) are acid-catalyzed. The acid-catalyzed reactive uptake of epoxide species, especially isoprene epoxydiols (IEPOX) (Paulot et al., 2009; Surratt et al., 2010), to aerosol water has also emerged as a significant source of secondary organic aerosol material (Lin et al., 2012; Marais et al., 2016b, Pye et al., 2013). Because the epoxidic oxygen must be protonated in concert with ring-opening, the reactive uptake of IEPOX to aqueous media is strongly pH-dependent, with the reactive uptake coefficient decreasing rapidly with increasing pH for pH > 1 (Gaston et al., 2014). Therefore, the rate of IEPOX secondary organic aerosol (SOA) formation is slow in cloud water because of the generally higher pH compared to particles (McNeill, 2015), but given the relatively large liquid water content of clouds, which promotes dissolution, IEPOX uptake could be significant in more acidic cloud droplets (pH 3-4) (Tsui et al., 2019).

The trend of decreasing sulfate content in clouds and aerosols across North America and Europe may have implications for partitioning of inorganic (Vasilakos et al., 2018; Shah et al., 2018) and organic gases between the gas and condensed phases, and the dominant mechanisms and rates of multiphase chemical processes in the atmosphere which produce $PM_{2.5}$ mass, under future conditions. Implications of acidity changes for partitioning of semi-volatile compounds and their multiphase chemical processing are outlined in more detail in a companion paper (Tilgner et al., 2019 *in prep*).

6 Role of particle size, composition, and mass transfer kinetics in pH heterogeneity

Traditionally (e.g. Section 4, 7.1), fine particle pH is calculated assuming equilibrium and a uniform distribution of species across all particles ~~(e.g., Sect. 5.1 and 6)~~. Here, the role of differences in particle size, mass transfer, and composition (including presence of organic species) in driving pH in a population of particles is highlighted.

6.1 Role of particle size and composition

The pH of aerosols varies with particle size because of the differences in the chemical composition, hygroscopicity, and gas–particle equilibration time scales between fine and coarse particles. Fine-mode aerosols are produced by new particle formation and growth but are also directly emitted from anthropogenic as well as natural sources (dust and sea salt). At least some of the

chemistry that initiates new particle formation, and thus drives low pH for the smallest sizes, involves sulfuric acid and acid-base reactions (Kulmala et al., 2004). Anthropogenically-derived fine mode aerosols are typically composed of inorganic salts, organic species, and black carbon and are generally acidic. Fine-mode pH is sensitive to the relative amounts of non-volatile cations (if any), sulfate, nitrate, and ammonium present in the particle phase (Fig. 2) and continuously responds to the changing concentrations of their gas-phase counterparts—H_2SO_4(g), HNO_3(g), and NH_3(g) —as well as the ambient RH and temperature.

In contrast, coarse mode aerosols mainly consist of sea-salt and dust particles directly emitted to the atmosphere as a result of wind stress on the surface of the oceans and arid land, respectively. Sea salt and dust contain significant amounts of non-volatile cations such as Na^+, Ca^{2+}, Mg^{2+}, and K^+, whereas, in contrast, the dominant cation in fine mode particles is typically semi-volatile ammonium. Dust, and more generally non-volatile cations, can also originate from mechanical wear or disturbances associated with anthropogenic activity such as road, residential, and commercial construction as well as brake wear and road salt application (Philip et al., 2017; Lough et al., 2005; Kolesar et al., 2018). Both fossil fuel and biomass combustion also emit non-volatile cations in the $PM_{2.5}$ size range (Reff et al., 2009). Whether or not non-volatile cations influence pH depends on their mixing state with deliquesced particles. In other words, particles of the same size but different compositions should be treated as external mixtures when calculating their pH. For example, equilibrium model analysis of bulk ambient aerosol observations by Guo et al. (2016) indicate that the refractory ions were externally mixed from PM_1 because including those ions caused deviation between the predicted and measured nitrate partitioning. A small fraction of non-volatile aerosol components is sometimes present in the fine mode and tends to reduce acidity. For example, K^+ associated with biomass burning has been shown to cause higher pH compared to cases with very low K^+ levels (Bougiatioti et al., 2016).

Sea-salt and dust are naturally basic or alkaline, as they contain carbonates. The pH of ocean water (≈ 8) is relatively uniform and sets the pH_F for unprocessed sea-salt emissions (Keene et al., 1998). The pH of fresh airborne dust is more difficult to assess due to the high degree of heterogeneity in composition and its hygroscopicity; however, it is very likely that ambient dust is not acidic (has pH > 7). Sea salt and dust aerosol can initially maintain high pH (above 5 and close to 7) due to the presence of carbonate (CO_3^{2-}/HCO_3^-). However, the uptake of acid gases such as SO_2(g), HCl(g), HNO_3(g) and H_2SO_4(g) result in a chemical reaction (Usher et al., 2003) such as:

$$CO_3^{2-}(aq) + 2H^+(aq) \dashrightarrow CO_2(g) + H_2O(l) \qquad (R4)$$

Reaction R4 consumes H^+ produced from the uptake of acid gases (e.g., $HNO_3(g) \dashrightarrow H^+(aq) + NO_3^-(aq)$, Reaction R1 and R2 combined), allowing the aerosol to maintain its high pH until the carbonate has been depleted via conversion to CO_2(g). Once the carbonate has been depleted (a process not treated by current equilibrium models, Sect. 2.6), the dust and sea-salt aerosol can become acidified by continued uptake of acid gases. Observations of aged sea salt and dust ~~show~~ indicate an internal mixture with sulfate, nitrate, and chloride due to such reactions (Fairlie et al., 2010; Kirpes et al., 2018; Tobo et al., 2010). Freshly emitted sea-salt aerosol is in the liquid state while Ca-rich dust particles are emitted as solids. Consequently,

acidification of sea salt aerosol is thought to proceed more efficiently due to relatively high mass accommodation coefficients (about 0.1 or higher) for condensing acids on liquid particles compared to solid dust aerosol with much lower uptake coefficients ranging between 10^{-4} and 10^{-3} (Alexander et al., 2005; Fairlie et al., 2010). The increase of aerosol water with increasing RH and the solubilization of gaseous HCl that is present in the marine boundary layer (due to acid displacement reactions) has also been suggested as the reason for increasing acidity of sea-salt aerosols with increasing RH and altitude in the marine environment (von Glasow and Sander, 2001). Further acidification of sea salt aerosols occurs via displacement of Cl^- as HCl(g) due to reactions such as (Mcinnes et al., 1994; Zhao and Gao, 2008):

$$HNO_3(g) + Cl^-(aq) \rightarrow HCl(g) + NO_3^-(aq) \quad (R5)$$

$$H_2SO_4(g) + 2Cl^-(aq) \rightarrow 2HCl(g) + SO_4^{2-}(aq) \quad (R6)$$

Although these reactions do not directly produce additional H^+ ions, the resulting H^+ molal concentration increases due to a decrease in the overall aerosol water content in particles containing $NaNO_3$ and Na_2SO_4, which are less hygroscopic than NaCl.

Overall, atmospheric particle pH is size dependent and generally higher for coarse mode particles due to variations in inorganic composition with particle size. Differences as large 4 pH units have been reported between fine and coarse particles (Fang et al., 2017; Young et al., 2013). Bulk PM_1 and $PM_{2.5}$ acidity is more similar than fine vs coarse mode acidity (pH_F within 1 – 2 units, e.g., Bougiatioti et al., 2016; Guo et al., 2017b), but submicron (diameter < 1 μm) particles still show higher acidity than bulk $PM_{2.5}$. The reason for this is the strong enrichment of aerosol with NVCs from dust and sea salt at the larger sizes (even in the fine mode) and role of sulfate in new particle formation and surface-area driven condensation at the small sizes (Fig. 2). While semivolatile acids and bases act to homogenize acidity across the size distribution, mass transfer limitations (next section) and the heterogeneity of emission composition lead to variation in pH with size. Significant pH changes can occur in the 1 to 2.5 μm size range (Fang et al., 2017; Ding et al., 2019). The size dependent pH is also seen for sea salt aerosol (Fridlind and Jacobson, 2000) as well as in urban aerosols in China (Ding et al., 2019) where the fine mode is consistently 2-3 pH units lower than the coarse mode. The implications of this acidity gradient are considerable, for metal solubility and their impacts on public health and ecosystem productivity, as well as chemistry and semi-volatile partitioning of pH-sensitive species.

6.2 Role of mass transfer

Acidity is dependent on particle composition, and particle composition can be affected by mass transfer rates that vary by particle size. For fine mode particles, the characteristic time for particle growth or shrinkage from one equilibrium state to another after changes in RH is short enough (< 1 s) to justify the assumption of thermodynamic equilibrium with respect to water uptake (Pilinis et al., 1989). In comparison, equilibration of semi-volatile components (HNO_3, HCl, and NH_3) with the fine mode ranges from 20 min or less (Guo et al., 2018b) up to 10 hours (Meng and Seinfeld 1996; Fridlind and Jacobson, 2000). In the case of coarse mode aerosols or large accumulation mode aerosols, mass transfer rates for semi-volatile components can lead to equilibration time scales of several hours. Hanisch and Crowley (2001), for example, found vapors of

HNO_3 reach equilibrium through uptake by sea spray aerosols of 1-3 μm diameter within 3-10 h. In another study of remote marine aerosols, equilibrium in the coarse sea salt mode is reached quickly for NH_3, but HNO_3 and HCl require much longer times, of the order of 10 – 300 hours (Fridlind and Jacobson, 2000). In this case, relatively small amounts of TNH_4 partition to the coarse sea salt particles compared to much larger amounts of HNO_3 needed to displace HCl to reach equilibrium. These time scales are comparable or can even exceed the lifetime of the particles, implying that some particles can be removed by deposition before equilibrium is reached (Fridlind and Jacobson, 2000). In a subsequent theoretical study, Jacobson (2005a) found that under at least some conditions equilibrium can be reached within less than 1 h by large particles (< 6 μm) and within 15 min by particles < 3 μm, while in several other cases coarse particles took longer to reach equilibrium. Thus, aerosols of different sizes within the fine and coarse modes may not always be in mutual equilibrium due to mass transport limitations, and equilibrium alone may not uniquely determine the distribution of condensed semi-volatile gases across the particles of different sizes (Wexler and Seinfeld, 1990, 1992).

Given the above, both mass transport and thermodynamics must be considered to accurately predict the distribution of semi-volatile gases and the associated aerosol pH across the entire aerosol size spectrum. However, simulating mass transfer and thermodynamics for the size- and composition-distributed aerosol is computationally challenging due to numerical stiffness. There are two main sources of numerical stiffness. The first source arises from the large differences in the mass transfer time scales for particles of different sizes. Additional stiffness and non-linearity are introduced by H^+ ions in partially and fully deliquesced aerosols. In such cases, the H^+ ion molal hydrogen ion concentration (m_{H^+}) plays a crucial role in the determination of equilibrium aerosol phase state as well as in the determination of equilibrium gas-phase concentrations of HNO_3, HCl, and NH_3 at the particle surface for computing their driving forces for mass transfer. The characteristic time scale for H^+ ions is quite short relative to other species, especially under "acid-neutral" or "sulfate-poor" conditions, where the pseudosteady-state concentrations of H^+ ions are two or more orders of magnitude smaller than the sum of all other cations (Sun and Wexler, 1998). Since semi-volatile species in different particles of different sizes are coupled via the gas phase, the numerical solver for mass transfer would have to take time steps on the order of the shortest timescale to ensure accuracy for all the species across the entire aerosol size distribution. Such small time-steps are computationally prohibitive for common chemical transport model applications. Several attempts have been made over the past 20 years to reduce the stiffness of the system of nonlinear ordinary differential equations that describe the multicomponent, size-distributed mass transfer problem so that it could be efficiently solved (Capaldo et al., 2000; Hu et al., 2008; Jacobson, 1997; Jacobson, 2002, 2005a; Jacobson et al., 1996; Pilinis et al., 2000; Sun and Wexler, 1998; Zaveri et al., 2008; Zhang and Wexler, 2006).

Here, we illustrate the time-evolution of size-distributed pH using the sectional MOSAIC box model with 60 size bins for a scenario (test case 14 in Zaveri et al., 2008) in which fine mode aerosol composed of $(NH_4)_2SO_4$ and coarse mode aerosol composed of NaCl were exposed to appreciable gas-phase concentrations of H_2SO_4 (1 ppbv), HNO_3 (15 ppbv), HCl (1 ppbv), and NH_3 (10 ppbv) at 85% RH and 298.15 K temperature (~~Fig. 16~~Fig. 11). While the fine mode rapidly absorbs significant

amounts of these gases within the first few minutes of the simulation, it takes nearly 10 h for the aerosol composition, and hence the pH, to become uniform across the bins of different sizes. Furthermore, the displacement of HCl from the coarse mode due to HNO_3 absorption occurs slowly over this time, although significant differences in the pH can be seen across the coarse mode size bins even after 10 h. In conclusion, it is important to treat dynamic mass transfer to accurately simulate size-distributed pH and composition of aerosols. Although challenging, fully dynamic and hybrid (i.e., a combination of equilibrium for fine mode and dynamic for coarse mode) numerical methods have been implemented in 3D chemical transport models (Fast et al., 2006; Jacobson et al., 2007; Zhang et al., 2010).

6.3 Role of organic–inorganic interactions

Aerosol particles are rarely composed of a completely distinct organic-free aqueous inorganic phase and electrolyte-free organic phase – an assumption often made in air quality models for reasons of simplicity. Instead, mixed particles exist consisting of a complex mixture of organic compounds, inorganic ions, and water that may be separated into multiple liquid/solid phases (Bertram et al., 2011; Hallquist et al., 2009; Maria et al., 2004; Murphy et al., 2006; Pöhlker et al., 2012; Song et al., 2012; Zuend et al., 2010). The role of organic–inorganic interactions on the acidity of liquid/amorphous aerosol phases has been addressed in only a few studies and represents an area of research where further efforts are needed. Particle phase acidity could be affected in multiple ways by organic–inorganic interactions: directly by means of non-ideal mixing effects on the activity coefficient of H^+ (and all other species) in a liquid phase of given composition; indirectly via the effect of organics on composition and the equilibrium gas–particle partitioning of water and other semi-volatile components (including NH_3, inorganic and organic acids), as well as the potential for LLPS; and directly by dissociating organic acids that contribute dissolved H^+ or amines that associate with H^+.

A phase-separated particle typically consists of a rather hydrophobic organic-rich phase and an aqueous electrolyte-rich (salt/ion rich) phase (You et al. (2014) and references therein) (~~Fig. 17~~Fig. 12). Note that water and inorganic ions, including H^+, can exist in the organic-rich phase of a liquid–liquid phase separated system (Pye et al., 2018; Zuend and Seinfeld, 2012). Both the detection of LLPS and pH in ambient particles as well as micron-sized droplets in laboratory experiments is a difficult technical challenge (Wei et al., 2018). To our knowledge, no online measurement techniques applicable to field sampling exist for that purpose (see Sect. ~~5~~7.1 for aerosol pH measurement challenges). The current state of knowledge is therefore limited to relatively simple laboratory systems and theoretical considerations. Dallemagne et al. (2016) used a model system in the form of a super-micron-sized ternary aqueous poly(ethylene glycol)-400 (PEG-400) + ammonium sulfate droplet. They studied this system in an RH and temperature-controlled cell with confocal microscopy in the presence of a pH-sensitive fluorescent dye to determine the pH value at different locations in the liquid drop. They report a small, yet distinct change in pH due to the phase transition from a single to two liquid phases for this system when RH decreases: pH = 3.8 ± 0.1 in a single mixed phase at > 90 % RH, while the organic-rich shell phase in a LLPS state exhibited pH = 4.2 ± 0.2 at 80 % RH to pH = 4.1 ± 0.1 at 65 % RH; the pH in the sulfate-rich phase was not determined during LLPS. The pH value of the organic-rich phase was

similar to that of a corresponding salt-free aqueous PEG-400 solution measured using a standard pH probe. Since changes in RH lead to changes in particle water content, here causing the LLPS, the degree to which such changes affected the measured pH in the Dallemagne et al. (2016) study remain unclear.

Losey et al. (2016) controlled the pH in aqueous solution droplets consisting of 3-methylglutaric acid, ammonium sulfate and sodium hydroxide. They found that changes in pH and the degree of methylglutaric acid dissociation (deprotonation), affect the separation RH (SRH), the onset of LLPS during dehumidification. The SRH was ~79 % for pH = 3.65, ~70 % for pH = 5.17, and ~64 % for pH = 6.45. The RH at which the two liquid phases merge into a homogeneous single phase was observed around 80 % RH in this system, approximately independent of pH – indicating that a hysteresis between SRH and merging RH occurs for pH close to neutral, but not at lower pH. While this study did not attempt to measure the pH in distinct liquid phases, it indicates that the established pH, resulting from interactions between inorganic electrolytes and organic acids, affects the LLPS behavior. Losey et al. (2018) further explored similar systems at higher acidity in the presence of sulfuric acid (varying the ammonium-to-sulfate ratio from 2.0 to 1.5 to 1.0). They report that all observed RH levels of phase transitions were affected by the pH established with sulfuric acid. The SRH consistently decreased with increasing amounts of sulfuric acid (toward lower pH); e.g., for 3-methylglutaric acid + ammonium sulfate + sulfuric acid from SRH of ~80 % at pH = 2.68 to SRH of ~30 % at pH = 0.34. Similar lowering of SRH with increasing acidity was also found for a non-acidic organic mixture component (1,2,6-hexanediol). Furthermore, at high acidity (here pH lower than 0.5), several of the studied systems did not show any LLPS down to very low RH. While the quantitative phase transition behaviour depends on the organic component, these experiments by Losey et al. (2018) imply that organic–inorganic interactions can have an impact on mutual solubility and phase transitions, in those cases with increasing mutual solubility towards higher acidity.

While a LLPS will impact the acidity in coexisting liquid phases, the extent to which the pH values will typically differ between the phases – and, related to that, the molar concentrations of hydronium ions and ionic strength – remains an open question. Theoretical considerations aid in constraining the range of expectations in this case. Thermodynamic equilibrium between two liquid phases, each of neutral electric charge, implies that the electrochemical potential of H^+ ions is equivalent in both phases (see Sect. 2). Therefore, the activity-based pH in coexisting phases is expected to be similar, but not necessarily of the exact same value. Computations with the AIOMFAC-based liquid–liquid equilibrium model confirm for case studies that the pH in two liquid phases is of the same order of magnitude, often with a difference of less than 0.2 pH units (Pye et al., 2018). However, H^+ molalities (or concentrations) in the two coexisting phases of atmospheric aerosols are predicted to be very different, often by up to several orders of magnitude; hence, it is important to calculate pH based on H^+ activity, not simply concentration (see also Sect. ~~6~~4.3 recommendations for approximating pH). In Pye et al. (2018), several thermodynamic models were applied to predict the partitioning of ammonia, water, and organic compounds between the gas and particle phases for conditions in the southeastern U.S. during summer 2013. AIOMFAC-based coupled liquid–liquid and gas–particle partitioning computations within that study predicted partial to complete miscibility among organic and inorganic aerosol

components, depending on RH. The AIOMFAC-based model predicted an increase in the concentration of gas-phase ammonia (NH_3) alongside a decrease in acidity when partial miscibility of organics was accounted for. In comparison to calculations with complete phase separation between organic and inorganic ions enforced, the interactions of inorganic ions with organic compounds (in mixed phases) were predicted to promote an enhanced association of H^+ and SO_4^{2-} into HSO_4^-, resulting in a slightly higher pH (0.1 pH units median increase), since the bisulfate ion is predicted to be more miscible with organic compounds than equivalent amounts of H^+ and SO_4^{2-} (Pye et al., 2018). This indicates a pH buffering effect of the degree of bisulfate dissociation; however, additional complexity in understanding the main drivers of such pH changes arises from simultaneous changes in the equilibrium gas–particle partitioning of water, organics, and ammonia.

The impact of amines and organic acids on H^+ is usually neglected in efforts to model pH. Amines may contribute to aerosol alkalinity – especially given their potentially strong proton affinity (Dall'Osto et al., 2019), but they must be in sufficient quantities to compete with NH_3 and other cations. Although not strong sources of protons or cations, these alkaline and acidic organics may still be considered together with other water-soluble organic compounds (WSOCs) in the particulate phase in terms of their ability to influence the aerosol water content. The uptake of water due to organic components is often used to correct the solvent volume and pH_F derived based on the inorganic aerosol composition (e.g., Guo et al., 2015; Bougiatioti et al., 2016). This implies that aerosol pH is reversibly influenced by the amount of water (driven by RH and composition) associated with the aerosol particles, which has been shown to drive some of the diurnal variability of pH (Guo et al., 2015).

For systems where a single mixed aerosol phase is assumed, current work indicates dissociating organic acids do not strongly affect pH and the limited studies to date suggest that inorganic species drive pH (Battaglia et al., 2019; Song et al., 2018; Vasilakos et al., 2018). For the southeastern U.S., pH changes predicted by E-AIM were generally limited to < 0.2 pH units in response to dramatic increases in oxalic acid (Vasilakos et al., 2018). Similarly, E-AIM predicted that increases in oxalic acid concentrations resulted in < 0.1 pH unit changes for polluted Beijing conditions (Song et al., 2018). This is notable since the predicted pH in Beijing (neglecting organics) was consistently above the first acid dissociation constant (pK_{a1}) value for oxalic acid, conditions where pH is predicted to be most sensitive to organic acids (Nah et al., 2018). Nah et al. (2018) showed that for aerosol pH_F varying between 0.9 and 3.8, the inorganic-only predicted pH_F was sufficient to define an effective sigmoid curve for oxalic acid, one of the most abundant of organic acids with a pK_a that is well within this range. Neglecting the effects of oxalate on pH by Nah et al. (2018) did not seem to affect the quality of the partitioning. Battaglia et al., (2019) extended these prior studies to include additional organic acids (oxalic, glutaric, and malonic acids) as well as three non-acid organics (levoglucosan, tetrahydrofuran, and 1-pentanol) mixed with inorganics representative of Beijing winter haze and eastern U.S. summertime compositions. The changes in pH relative to the inorganic-only system were predicted by AIOMFAC to be quite small, generally < 0.2 pH units, when a single aerosol phase was present (Battaglia, Jr., et al., 2019). The response of pH to the same organics at lower RH (< 70%) or under LLPS conditions was not characterized.

While current work suggests organic–inorganic interactions only slightly affect the pH, they can drive both LLPS and other phase transitions. Based on case studies (Pye et al., 2018; Battaglia et al., 2019), the interactions between water and ions are likely the main determinants of the resulting pH value. However, considering the complexity and variability of realistic aerosol compositions, the extent to which organic–inorganic interactions moderate the pH in liquid phases has not yet been studied in depth.

~~7~~

87 Atmospheric observations of acidity

The preceding sections (e.g. Sect. 2.5) have alluded to some of the distinct challenges associated with particle and cloud pH measurements. Measuring the pH of nominally sub-10 µm atmospheric aerosols is not routinely possible, as the methods typically available for bulk condensed phases (e.g., electrochemical pH probes) cannot be applied to the liquid phase of a single particle or a population of particles as a result of the extremely low levels of liquid water. Another issue is the highly concentrated nature of aerosol solutions, whose ionic strengths are often orders of magnitude above the maximum ionic strength currently accepted by the IUPAC definition (0.1 M). As a result, limited direct measurements of aerosol pH exist (Sect. ~~5~~7.1.1 – ~~5~~7.1.2) and observationally-constrained estimates of bulk fine particle acidity are usually created from thermodynamic models (Sect. ~~5~~7.1.3 – ~~5~~7.1.4). The sample volumes for fog/cloud water or precipitation are orders of magnitude larger than for aerosols and can be collected from clouds using well established instrumentation. This, together with their dilute concentration allow for a direct pH measurement, which has been done with electrochemical pH probes for decades (Sect. 7.2).~~The same limitations do not exist for fog/cloud water or precipitation, where larger sample volumes can be collected from accessible clouds, the associated water is not in equilibrium with the gas phase (although evaporation artifacts may still cause biases), and solutions are dilute enough to allow for a direct pH measurement. The latter has been done with electrochemical pH probes for decades (Sect. 5.2).~~

~~8.1~~7.1 Observed aerosol acidity

Challenges associated with measuring semi-volatile species (Sect. 43.3) and maintaining aqueous concentrations found in ambient particles have limited direct measurements of aerosol pH for many years. The abundance of many non-volatile ionic components of the atmospheric aerosol (e.g., sulfate or sodium) can be measured. However, unperturbed equilibrium contact with the gas phase cannot be easily maintained. Determining H^+ activity (or molality in the case of pH_F) requires knowledge of water content, which for non-glassy aerosol is in chemical equilibrium with the gas phase (e.g., Seinfeld and Pandis, 2016). Thus, if the ALWC changes between sampling and analysis, as often occurs in routine monitoring networks, the pH of that particle can shift. A second challenge is that one of the most important cations present in submicron aerosol, NH_4^+, is largely

in equilibrium with gas-phase NH_3, so perturbations during collection and processing may result in large evaporation/condensation biases (e.g., Guo et al., 2018a).

Despite the obstacles related to measuring the pH of aerosols, the importance of aerosol pH has motivated efforts to more directly probe the pH of aerosols. Direct measurements may either provide an ensemble or bulk average pH value (Li and Jang, 2012; Jang et al., 2008; Ganor et al., 1993; Craig et al., 2018), single particle values (Craig et al., 2017; Rindelaub et al., 2016b), or intra-particle pH values (Wei et al., 2018). Considerable effort has also been spent to develop pH estimates using a combination of thermodynamic modeling with measurements of aerosol and gas-phase composition (e.g., Guo et al., 2018a; Guo et al., 2017a; Guo et al., 2015; Bougiatioti et al., 2016; Song et al., 2018; and others).

~~8.1.1~~7.1.1 Bulk pH measurements

For bulk pH values to be reasonable, composition and partitioning of semi-volatiles among the particles in the population should be relatively uniform (see Sect. ~~7~~6 for a discussion on the role of particle mixing state). For a set of submicron particles with homogeneous composition (i.e. an internal mixture, as often found in aged aerosols), this assumption is often satisfied, particularly at higher RH. The simplest bulk method, first utilized in the late 1980s involved adding a known volume of water to a filter and then utilizing a standard electrochemical pH probe to infer so-called strong acidity (Koutrakis et al., 1988). As discussed here and in Sect. 43.1, given the semi-volatile nature of water and non-conservative nature of the H^+ ion (Saxena et al., 1993), this approach has significant shortcomings.

The use of pH sensitive indicators has been one of the most common approaches to avoid sample modification. Although only a handful of studies have used indicators for aerosol studies, multiple approaches have been applied. Jang et al. (2008) used a Teflon filter where the dye metanil yellow was taken up by the filter prior to sampling aerosol. Particle mass was determined gravimetrically, and pH sensitive indicators were analysed with a UV-Visible (UV-Vis) spectrometer. Through a calculation combining mass, absorption features of the protonated (at 545 nm) and deprotonated (at 420 nm) form, and particle volume from a simultaneous aerosol size distribution, the mass of H^+ was determined and then converted to pH. The RH had to be precisely controlled, since any change in water content would limit the reliability of the results. The authors noted the need for an online approach to avoid these complications. This work was expanded in Li and Jang (2012) with the use of an optical flow chamber to help control the RH and improve transfer from the collection point in a Teflon aerosol chamber to the UV-Vis spectrometer for measurement. For a tightly controlled system, the dyed filter approach provided particle pH, but the method has not been reliably applied in the complex ambient atmosphere.

Colorimetric methods have been utilized at different points to determine the pH of aerosols and cloud droplets. Ganor et al. (1993) used pH paper on a four-stage impactor (>10 µm, 3.0-10.0 µm, 0.9-3.0 µm, and < 0.9 µm) to probe larger "haze" particles in Israel under conditions with RH exceeding 80%, cloud droplets, and fog droplets. Two types of pH paper were

used covering two pH ranges, 0.5-5.0 and 5.0-9.0 (indicator not given), with 0.5 pH unit resolution. For these measurements, a size-dependence in acidity was observed, with pH decreasing from 5 to 2 from cloud/fog to large particles using visual identification. Submicron haze aerosol pH was characterized as having an overall pH of 1.5 – 2.5 in Israel (Ganor et al., 1993). Craig et al. (2018) recently quantified the measurement of aerosol pH with a precision of 0.1 pH units using particles impacted on pH paper followed by rapidly taking a cell phone picture later analysed with a simple image processing script in MatLab. For their work, thymol blue (pH = 0 – 2.5) and methyl orange (pH = 2.5 – 4.5) indicator dyes on paper were used for both model aerosol in the laboratory and ambient samples at a forested site in Northern Michigan (pH = 1.5 – 3.5) and in Ann Arbor, Michigan (pH = 3.0 – 3.5). Water and ammonia volatilization due to increased surface area to volume ratios in smaller particles explains the observed increase of particle acidity with decreasing particle size but also the inadequacy of pH paper method to measure the pH of very small particles (Craig et al., 2018). Ganor et al. (1993) and Craig et al. (2018) mentioned that for the colorimetric approach to be effective, the particles must be aqueous with sufficient aerosol water to substantially wet the indicator paper, which was not always the case for ambient sampling. The atmospheric samples in Northern Michigan (Craig et al., 2018) covering three size ranges (2.5-5.0, 0.4-2.5, and < 0.4 μm) and measuring to smaller sizes than in Ganor et al. (1993), showed a distinct decrease in pH toward smaller size. For the smallest stage in Craig et al. (2018), variation in pH was observed across the samples with values ranging from 1.5 – 3.0, possibly due to differences in pH between individual particles in that size range, though further investigation is needed (see Sect. ~~7~~ 6 for a discussion on the relationship between particle size and pH). Craig et al. (2018) made comparisons to the bulk solutions with the thermodynamic model E-AIM, finding good agreement. When applied to the particle data, the thermodynamic model ISORROPIA predict a pH_F lower than measured by roughly a pH unit, while E-AIM was roughly 2 pH units lower. Further testing is needed between thermodynamic models and colorimetric methods to explore differences, particularly since the high ionic strengths in particles that may affect organic dye activity (e.g., via issues raised in Sect. 2.5).

~~8.1.2~~7.1.2 Single particle pH measurements

Several emerging methods have the potential to provide even greater insight into the pH of individual particles but have been focused on model systems. Determining single particle pH is desirable as the variation of pH values for individual particles from the population-level average is not well known. Even a few acidic particles can dominate the average pH value for a population in an environment with fresh emissions (e.g., urban area) where the particles have not reached equilibrium with the gas concentrations surrounding them (Craig and Ault, 2018). This heteorogeneity may be less important in a regional background that has experienced significant atmospheric processing (Guo et al., 2018a). One of the first approaches to single droplet pH measurement was Ganor (1999), which impacted cloud and fog droplets collected on the four stages of a cascade impactor on to a cleaved calcite ($CaCO_3$) crystal. If an acidic droplet containing sulfate was impacted, the microchemical reaction produced gypsum ($CaSO_4 \cdot 2H_2O$) crystals. Fog droplet pH values of 3.0 and 4.0 were observed in Israel for sizes of 1-2 μm and 3-9 μm, respectively. A second single particle method (Dallemagne et al., 2016), used for studying liquid–liquid phase separation (LLPS) in larger particles (10-30 μm) with optical microscopy methods, applied a fluorescent indicator

(Oregon Green 488 carboxylic acid, succinimidyl ester) to probe pH before and after phase separation via fluorescence microscopy (see Sect. ~~7~~6.3 for discussion of organic species and their role in acidity).

A recently developed approach for probing the pH of individual droplets is the acid-conjugate base method (Rindelaub et al., 2016b), which calibrates the peak area for the acid and conjugate base measured with Raman microspectroscopy to molar concentrations, which along with the acid dissociation constant (K_a) and activity coefficient calculations can be used to determine the activity of the H^+ ion. Rindelaub et al. (2016b) originally applied this to monitoring sulfate and bisulfate in proximity to the pK_a of 2. Craig et al. (2017) expanded this method to cover a range of systems (nitric acid–nitrate, bioxalate–oxalate, acetic acid–acetate, and bicarbonate–carbonate, as well as an inorganic–organic mixture). From these systems, a pH of -1 to 10 could be probed, covering the full range of atmospherically- relevant particle pH (Fig. 2). The acid-conjugate base method originally made use of activity coefficients from the extended Debye-Hückel method (Rindelaub et al., 2016b), but has been expanded to other methods in subsequent publications (Craig et al., 2017). In addition to using simplistic model systems, recent work has shown that the protonation state of hydroxyl functional groups (–OH) in organic molecules from SOA formation can be used to estimate pH. Bondy et al. (2018) showed that by modulating pH the protonation state of 2-methylglyceric acid or 2-methylglyceric acid sulfate ester could be used to roughly identify the pH of a system, though further quantification is necessary to assess the accuracy of this approach. This was shown by monitoring the carbonyl (C=O) stretch of the carboxylic acid group on 2-methyl glyceric acid when protonated versus the asymmetric and symmetric vibrations of the carboxylate group (COO^-) when deprotonated. While these vibrations have been successfully measured in ambient aerosols collected during the SOAS summer 2013 campaign, none of the acid-conjugate base methods has been applied on ambient aerosol to evaluate aerosol pH.

Wei et al. (2018) recently probed intraparticle pH variation using Surface-Enhanced Raman Spectroscopy, and showed pH is not always uniform within an individual particle. The researchers took the acid-conjugate base method one step further with nanoprobes by functionalizing a gold nanoparticle dimer with an indicator molecule (4-mercaptobenzoic acid) and monitoring the acid versus conjugate base form of the indicator molecule in 20 μm phosphate buffer solution droplets (pH = 7 – 11). They showed that within a single particle, a gradient of up to 3.6 pH units could be observed between the core (higher pH) and the exterior few microns of the particle (lower pH) due to accumulation of protons at the air/water interface. Such substantial differences in pH within a single particle are unexpected (as they imply a large chemical potential difference of H^+ ions) and further independent measurements are needed to confirm this behavior in atmospheric particles.

~~8.1.3~~7.1.3 Considerations for the development of observationally-derived pH estimates

Only very recently have methods for direct measurement of aerosol pH become available, and they require considerable development before they become routine and generally applied. Until now, most information generated on aerosol acidity relies on measurements of particle composition and gas-phase semi-volatiles, in addition to thermodynamic equilibria or

kinetic modeling (see Sect. 2.6). pH_F (Table 1) is the most ~~comment~~ common approximation of pH reported in literature. The accuracy of these estimates depends on and is evaluated by the agreement between observed and modeled gas–particle partitioning of pH-sensitive species – typically TNH_4, TNO_3, and TCl, as well as accuracy of predicted aerosol liquid water (Guo et al., 2015; Guo et al., 2017b; Guo et al., 2018b; Meskhidze et al., 2003; Song et al., 2018). NH_3 is an ideal species to measure since gas–particle partitioning of TNH_4 is sensitive to most ambient pH levels and NH_4^+~~ammonium~~ is often the dominant particle cation. However, NH_3~~ammonia~~ measurements are challenging and often not co-located with aerosol composition measurements. Bougiatioti et al. (2016) estimated that neglecting gas-phase NH_3 levels of about 0.1 to 0.7 μg m^{-3} in the thermodynamic equilibrium calculation of fine aerosol pH could lead to an underestimation in the pH_F of around 0.5 units, while Guo et al. (2015) found neglecting gas-phase NH_3 leads to an underestimation of pH_F by one unit. Although this magnitude of underestimation is not universally applicable when NH_3 is missing from the thermodynamic calculations, it may be a reasonable bound for most of the atmosphere. Weber et al. (2016) and Guo et al. (2017a) estimated that on average, a 5-fold to 10-fold increase in the NH_3 levels leads a one unit change in pH. For cases were more than 90% of TNH_4 ~~total ammonium~~ is in the aerosol, neglecting gas-phase NH_3 should give similar (1 unit) underestimations in pH. Accurately bounding the error requires aerosol pH calculations to be evaluated against observations in both the aerosol and gas phases.

Routine air quality monitoring networks provide limited opportunity for pH estimation. European networks (European Monitoring and Evaluation Programme (EMEP)/EBAS, http://ebas.nilu.no/, and Research Infrastructure for the observation of Aerosol, Clouds and Trace Gases (ACTRIS), http://actris.nilu.no/Data/Policy/) provide mainly bulk PM_{10} aerosol chemical composition data which prohibits equilibrium assumptions due to the contributions from coarse mode mass. Most routine networks in the U.S. measure $PM_{2.5}$, but the Interagency Monitoring of Protected Visual Environments (IMPROVE, http://vista.cira.colostate.edu/Improve/) network lacks measurements of NH_4^+~~ammonium~~ and the Chemical Speciation Network (CSN, https://www.epa.gov/amtic/chemical-speciation-network-csn) NH_4^+~~ammonium~~ is biased low compared to other networks and measurements (Pye et al., 2018; Silvern et al., 2017). The Clean Air Status and Trends Network (CASTNET, https://www.epa.gov/castnet) provides measurements of NH_4^+, NO_3^-, and SO_4^{2-}, along with HNO_3, SO_2, and base cations, at approximately 92 sites across the U.S.. However, CASTNET does not size select particles. For IMPROVE and CSN, concurrent relevant gas-phase measurements are generally not available. Up until 2015, the Southeastern Aerosol Research and Characterization Study (SEARCH) in the ~~United States~~U.S. provided complete hourly particle and gas-phase semi-volatile measurements with high accuracy and precision (Edgerton et al., 2006; Hansen et al., 2003). Recent instrumental developments (MARGA, Liu et al., 2014) enable concurrent measurements of inorganic substances that influence aerosol pH and are present in the gas phase (namely HCl, HNO_3, HNO_2, SO_2, NH_3) or in the aerosol phase (Cl^-, NO_3^-, SO_4^{2-}, NH_4^+, K^+, Ca^{2+}, Mg^{2+}). Online NH_3 instruments are becoming more available and with sensitivity down to very low concentrations (von Bobrutzki et al., 2010). In combination with aerosol data, gas-phase measurements generate datasets that can constrain aerosol pH.

For submicron aerosol (PM_1), the development and operation of aerosol mass spectrometers (AMS, Zhang et al. 2007; Jimenez et al.; 2009) and aerosol chemical speciation monitors (ACSM, Ng et al. 2011) during the last decade provides a powerful tool to build a database of nonrefractory submicron aerosol composition. This database could constrain aerosol pH when complemented by gas-phase measurements, mainly of NH_3, as well as measurements of the non-volatile, refractory aerosol components. Such studies, usually performed on a campaign basis, have enabled the estimation of aerosol pH at various locations around the globe, including the southeastern US, Greece, and mainland China (Table S6), and ACSM measurements could be more routinely available in the future (e.g., ACTRIS, Schmale et al., 2017). However, the contribution of organosulfates and organonitrates to AMS measured total sulfate and nitrate (Farmer et al., 2010; Dovrou et al., 2019) must be considered to provide robust inorganic aerosol composition for acidity predictions. In locations such as the eastern U.S. in summer where organosulfates already account for 15% of total sulfate (Riva et al., 2019), AMS measured total sulfate, when used in a thermodynamic model as inorganic sulfate, can lead to erroneous predictions of particle composition and thus pH (Pye et al., 2018).

The largest challenge using network or campaign data to estimate pH is that simultaneous information on NH_3 and NH_4^+ is often not available. The National Atmospheric Deposition Program/Ammonia Monitoring Network (AMoN) measures NH_3 on a biweekly schedule at 104 active sites in the U.S. (as of July 29, 2019) (http://nadp.isws.illinois.edu/AMoN). Colocation with CASTNET NH_4^+ measurements provides NH_3 + NH_4^+ at approximately 70 sites (Puchalski et al., 2019). The U.K. National Ammonium Monitoring Network (NAMN) has been established to measure the spatial distribution and long-term trends in atmospheric gaseous NH_3 and aerosol NH_4^+ (Sutton, 2001; Sutton et al., 1998). In 2016, the network measured gaseous NH_3 on a monthly basis by DEnuder for Long Term Atmospheric (DELTA) sampling at 56 sites and by Adapted Low-cost Passive High-Absorption (ALPHA) samplers at a further 38 sites, 9 of these sites used for calibration, in order to quantify the spatiotemporal varibility of NH_3 and NH_4^+ concentrations and deposition across the UK, http://www.pollutantdeposition.ceh.ac.uk/content/ammonia-network). Observations show spatially variable changes in NH_3 with both reductions, mainly to the north, and increases, to the south between 1997 and 2007. In nature reserve areas in the Netherlands, atmospheric NH_3~~ammonia~~ concentrations have been monitored by the Measuring Ammonia in Nature (MAN) network (http://man.rivm.nl) since 2005 (Lolkema et al., 2015). In 2015 that network contained 60 natural areas with a total of 236 sampling points were NH_3 was monitored using passive samplers. While no significant trend has been found on average, at 6 stations a significant increasing trend was recorded.

The amount of knowledge on the atmospheric distribution of NH_3 has increased rapidly in the satellite era since the NH_3 tropospheric column observations from space by the Atmospheric Infrared Sounder (AIRS) sensor on-board the Aqua satellite (Warner et al., 2016), the Infrared Atmospheric Sounding Interferometer (IASI) (Clarisse et al., 2009), and the Cross-track Infrared Sounder (CrIS) (Shephard and Cady-Pereira, 2015) became available. These satellite observations have shown ~~the~~ high NH_3 levels associated with animal feeding operations and fertilizer applications as well as biomass burning (especially

wild fires). These data provided a global view of NH_3 column distribution, construction of which was inhibited by the spatial and temporal variability of NH_3 concentrations reflecting its spatially varying sources and its short tropospheric lifetime of up to a couple of hours (Dentener and Crutzen, 1994). While there is not yet established methodology to derive aerosol pH from space observations, the improvement of near surface information on atmospheric composition in combination with ground-level observation network data (perhaps even augmented by model fields of such data) will likely advance our understanding. Considerably more challenging, however, is constraining the vertical distributions of aerosol pH – especially since the lower temperatures and less abundant water progressively challenge the assumption of thermodynamic equilibrium and may require the treatment of particle history and hysteresis (e.g., Wang et al., 2008).

~~8.1.4~~7.1.4 Spatial and temporal variability of aerosol pH

Current observationally-constrained estimates of indicate fine mode aerosol is ubiquitously acidic. During winter with low temperature and high relative humidity, aerosol pH_F is higher than during summer following the liquid water availability and temperature (~~Fig. 5~~Fig. 13a). This seasonal trend has been widely observed in the eastern U.S. (Guo et al., 2016; Guo et al., 2015), Beijing (Tan et al., 2018), Inner Mongolia (Wang et al., 2019a), Hong Kong (Xue et al., 2011), Po Valley, Italy (Squizzato et al., 2013), Cabauw, Netherlands (Guo et al., 2018b), and eastern Canada (Tao and Murphy, 2019b) with pH_F differences between seasons spanning from 0.6 to 2.3 pH_F units. Wang et al. (2019b) reported the lowest mean aerosol pH_F in summer and attributed it to the higher contribution of secondary sulfate than in the other seasons and the highest mean aerosol pH_F in spring likely associated with the influence of dust. The most complete dataset containing seasonality comes from Canada, where observationally-derived monthly mean pH values for $PM_{2.5}$ were constructed for 6 sites over 10 years (Tao and Murphy, 2019b). The Canadian dataset shows summertime minimum pH and wintertime maximum with 1 pH unit of difference (~2 versus ~3, respectively). Aerosol acidity increases with increasing temperature (0.1 unit increase in pH per 2 K decrease in temperature) and decreasing relative humidity. Summer pH is largely dictated by temperature while both meteorological factors and aerosol composition affect winter pH. Beijing shows a similar pH_F trend with winter having higher pH_F than summer (pH_F of 4.1 vs 1.8) (Tan et al., 2018). However, Beijing data also shows summer 2016–2017 pH_F (Ding et al., 2019) being almost 2 units higher than that in summer 2014 (Tan et al., 2018), potentially indicating effective air pollution mitigation strategies. The summer minimum in fine aerosol pH is a common feature of all available pH datasets and is associated with the effects of high ambient temperatures and low aerosol water content. Temperature has also been shown to strongly affect the partitioning of total ammonium through its effects on solubility and dissociation (Hennigan et al., 2015). Composition can also play a role in seasonality as shown in data for Inner Mongolia (Wang et al., 2019a) and at Po Valley (Squizzato et al., 2013) where maximum fine aerosol pH_F was found in spring likely due to the influence of desert dust aerosol from Gobi and from Sahara deserts respectively during those time periods. The absolute values in Mongolia show partial neutralization of the aerosol with pH_F between 5 and 6.1, while those for Po Valley are more acidic, being 1.3 pH_F units higher in spring (pH_F = 3.6) than in the summer (pH_F = 2.3).

Similarly, resulting from diurnal changes in temperature and relative humidity, higher pH_F is observed during the night compared to that during the day (~~Fig. 5~~Fig. 13b). For example, acidity shows diurnal variation in China of almost 2 pH_F units (Cheng et al., 2015), in southern Canada of 0.5 – 5 pH units (Murphy et al., 2017), in the U.S. of 0.65 – 1.5 pH_F units (Battaglia et al., 2017; Guo et al., 2015; Nah et al., 2018), and about 1 pH_F unit in southern California (Guo et al., 2017b). Finokalia experiences ~1 pH_F unit lower pH_F during the day than night because of low aerosol water content and high temperatures (Bougiatioti et al., 2016). This pattern is amplified by the urban Heat Island Effect through its impact on temperature (Battaglia et al., 2017).

~~Figure 6~~Figure 14 summarizes the current estimates of ambient fine aerosol pH based on literature data summarized in Table S6. Studies that used only aerosol composition for calculating pH ("reverse mode" aerosol calculations, which are uncertain, e.g., see Hennigan et al., 2015) or ion-balance based approaches are excluded from the figure. Mean fine aerosol pH_F ranges from around 1 to 6 although specific locations and episodes may experience higher or lower acidity. Highly acidic fine aerosols are found in South East Asia, the eastern U.S., and other locations. Mainland China, Europe, Canada, Mexico, and the western U.S. have on average similar levels of aerosol acidity (2.5 to 3). This spatial variability in pH reflects variability in the chemical composition of fine aerosols that result from the combined effect of changes in sources and meteorology.

Overall, the eastern U.S. aerosol is predicted to be one of the most acidic locations, with average pH_F near a value of 1 (Battaglia et al., 2017; Craig et al., 2018; Fang et al., 2017; Weber et al., 206; Pye et al. 2018; Xu et al., 2015; Guo et al., 2016; Guo et al., 2015), and higher pH_F, by about 1 unit, observed in locations of intensive agriculture with high NH_3 concentrations (Nah et al., 2018) and those influenced by larger particles (Fang et al., 2017; Craig et al., 2018). Higher aerosol pH (2 – 3 in pH_F) was estimated for Los Angeles in summer (Guo et al., 2017b), similar to observationally derived values for the Eastern Mediterranean (0.5 – 2.8 pH_F, Bougiatioti et al., 2016). The pH_F of PM_1 and $PM_{2.5}$ in Pasadena during the CalNex-2010 campaign were slightly different with the larger $PM_{2.5}$ particles having pH_F 0.8 units higher than PM_1 (Guo et al., 2017b) due to the larger water content and more abundant NVC at larger sizes. Greater acidity in submicron (PM_1) versus larger ($PM_{2.5}$) fine-mode particles is a robust feature in multiple data sets (e.g., Bougiatioti et al., 2016; Fang et al., 2017; Fridlind and Jacobson, 2000; Ding et al., 2019; see Sect. ~~7~~6.1 for a discussion of pH as a function of particle size). Guo et al. (2016) estimated the mean pH_F at 0.77 ± 0.96 for PM_1 aerosol aloft based on aerosol chemical composition measurements during the Wintertime Investigation of Transport, Emissions, and Reactivity (WINTER) campaign in the northeastern U.S. and thermodynamic modeling.

For mainland China, fine aerosol pH_F estimates vary, but tend to be mildly acidic (average pH_F approximately 4) and span from negative values (in Chengdu) to as high as 6.1 for $PM_{2.5}$ aerosol (Liu et al., 2017; Jia et al., 2018; Song et al. 2018; Tian et al., 2018; Cheng et al., 2015; He et al., 2018; Tan et al., 2018; Shi et al., 2017; Guo et al., 2017a; Ding et al., 2019; Jia et al.,

2018b; Wang et al., 2019), while in Southeast Asia (Singapore and Hong Kong) fine aerosol is highly acidic (average pH_F approximately 1) (Behera et al., 2013; Yao et al., 2007). Ding et al. (2019) estimated coarse particles were generally neutral or alkaline, based on observations in Beijing and modeling with ISORROPIA II. The strong acidity in Southeast Asia is consistent with reported high solubility of particulate iron sampled in the South China sea (Li et al., 2017). Altogether, these data suggest that there is a large spatial gradient of pH across China and Southeast Asia, reflecting the highly variable sources of acidity and alkalinity within each region (Shi et al., 2019).

Higher aerosol pH_F of 4.60 and 4.75 has been inferred from observations for Hawaii (Pszenny et al., 2004) and for Sao Paulo (Vieira-Filho et al., 2016). In the case of Hawaii, the higher pH_F is due to the neutralizing effect of non-volatile cations from sea salt. However, more acidic particles (pH ranging from -0.8 to 3.0) have been observed near the Kilauea volcano in Hawaii (Kroll et al., 2015). Sao Paulo is affected by combustion sources and thus emissions of nitrate and NVC that increase the aerosol pH_F. Bougiatioti et al. (2016) reported that under the influence of biomass burning, aerosol pH_F increases to values around 3, indicative of the impact of non-volatile cations, particularly potassium, as well as ammonia and nitrate emitted from wood burning. In general, aerosol pH_F increases when gas-phase NH_3 increases and can further be elevated by co-condensation of nitrate and water and the presence of non-volatile ions (Guo et al., 2018a; Shi et al., 2019).

Information on pH trends over time is limited, due to the scarcity of relevant data. pH data for mainland China published prior to 2010 (Tables S6, S7) showed highly acidic aerosol with pH_F of -0.16 ± 0.75 in contrast to more recent estimates (mean pH_F of 3.42 ± 1.75 for 2011 – 2016). Pre-2010 estimates are subject to large uncertainty resulting from their calculation method of relying only on aerosol composition information as input. Thermodynamic analysis of data, when carried out in a way that minimizes pH biases (mostly focused on using total gas and particle composition inputs and higher RH conditions) suggests acidity trends that may, at first glance, seem counterintuitive. One of the few such examples published that provides important insights can be found for the eastern U.S. during summer. Emissions controls over the last 20 years lead to significant reduction in sulfate aerosol, and ammonia levels remained constant or even slightly increased. Despite these important changes, summertime aerosol acidity remained the same (Weber et al., 2016). The insensitivity of aerosol pH to changes in emissions controls in this region is largely driven by the semi-volatility of ammonium, which requires a fraction of it to remain in the gas phase as dictated by thermodynamic equilibrium. Similar behaviour was found by Tao and Murphy (2019b) in Canada, where summertime aerosol pH did not increase over 10 years despite substantial decreases of sulfate and constant levels of ammonia. In the same study, the seasonality and interannual variability of pH_F was found to be strongly driven by the temperature changes and the resulting shift in thermodynamic partitioning and water uptake. The modeling study of Lawal et al. (2018) also showed little response of aerosol pH_F throughout the Continental U.S. to emission reductions despite the considerable improvements in air quality over the period 2001-2011. For this, they used a thermodynamic (ISORROPIA II) and the chemical transport (CMAQ) model together with the aerosol pH relevant observations from three monitoring networks (AMoN, SEARCH, and CASTNET). However, if sulfate aerosol continues to decrease, aerosol pH may eventually begin increasing (as proposed by

Tao and Murphy, 2019b). In the southeastern US, when sulfate approaches the 0.2 – 0.3 μg m^{-3}, level, small amounts of NVCs start affecting pH causing it to increase (Weber et al., 2016). Weber et al. (2016) also calculated that only large increases in NH_3 together with sulfate reductions can lead to an increase in pH. Thus, for sulfate between 0.1 and 10 μg m^{-3}, pH approaches 2.5 when NH_3 is over 10 μg m^{-3} and ammonium nitrate is formed. In any location, unusually high levels of NH_3 (an order of magnitude above the background or higher) associated with localized emissions, (e.g., confined animal feeding operations) can also increase pH (Nah et al., 2018). For locations characterized by high levels of ammonia, strong emissions of nitrate, and/or high levels of NVCs, pH may be driven by the water uptake and the mild acidity associated with ammonium nitrate aerosol. Furthermore, meteorology (RH, T) is an important driver of pH and meteorological trends influenced by climate change or interannual variability, can dominate over any composition changes (Tao and Murphy, 2019b). The eventual response of aerosol pH to changing emissions and meteorology can be determined with models – but careful evaluation of them with in-situ data is critical to ensure that they are in the correct acidity regime (e.g., Vasilakos et al., 2018; Shah et al., 2018).

8.27.2 Observed cloud and fog acidity

Sample collection is usually the largest challenge associated with measuring cloud droplet pH. Once obtained, the pH of collected cloud and fog water is typically measured using an electronic pH meter and a combination glass electrode. The approach to pH measurement in cloud and fog water has been similar over the past several decades. Semi-micro or micro-electrodes are available to analyze small volumes of available fog/cloud water, with some pH microelectrodes capable of measuring as little as 10 μL of sample. The electrodes are typically calibrated using pH 4 (phthalate-based) and 7 (phosphate-based) buffer solutions, although higher and lower pH calibration buffers are also available (see also supplementary information Sect. S1). Buck et al. (2002) provide an overview of key buffer requirements (stability, ionic strength, certification, low pH change with temperature) and a list of primary buffer standard compositions.

8.2.17.2.1 What determines the pH in a cloud/fog droplet?

The pH of a fog or cloud drop is determined by the balance between acids and bases in solution. The initial composition of a droplet is determined by the dissolution of soluble material contained within an aerosol particle that serves as the CCN. Further changes to composition come from subsequent scavenging of other, non-activated, interstitial particles and from uptake of water-soluble gases and aqueous-phase reactions (Sect. ~~3~~5). While early measurements of cloud and fog composition focused on inorganic species, it has become increasingly clear that organic matter also contributes significantly to droplet composition (Herckes et al., 2013) and, potentially, to droplet pH.

Uptake of gaseous carbon dioxide is an important factor governing cloud pH, especially in remote environments. Equilibration of a pure water drop with current levels of atmospheric CO_2 at 298 K results in a droplet pH of approximately 5.6, a value often referred to as the pH of natural rain or cloud water. Cloud pH values above or below this value are often referred to as alkaline or acidic, respectively.

Sulfuric and nitric acids frequently make significant contributions to cloud/fog drop pH while ammonia is typically the most abundant base. Sulfuric acid is taken up through particle scavenging, including scavenging of ammoniated sulfate particles, and is also formed *in situ* through aqueous phase oxidation of sulfur dioxide. Nitric acid is a highly soluble gas, in part because of its strong acidity which leads to nearly complete deprotonation in a cloud drop to form nitrate. Addition of nitrate to cloud water also comes from scavenging of particles containing solids or dissolved nitrate salts. These include ammonium nitrate, but also calcium or sodium nitrate, which are frequently formed by reaction of nitric acid or its precursors with sea salt or soil dust particles (e.g., ten Brink, 1998; Lee et al., 2008). Cloud water ammonium is derived by uptake of gaseous ammonia, as well as from particles containing salts of ammonium with nitrate, sulfate, and organic acids. As a result of these various scavenging and oxidation pathways, it is common for cloud/fog composition to be dominated by concentrations of sulfate, nitrate, and ammonium (e.g., Weathers et al., 1988; Collett et al., 2002).

A variety of weak organic acids and bases, including carboxylic/dicarboxylic acids and amines, can also influence the pH of fog or cloud drops. Carboxylic and dicarboxylic acids are frequently reported (e.g., Kawamura and Kaplan, 1984; Weathers et al., 1988; Munger et al., 1989; Facchini et al., 1992; Collett et al., 1999; van Pinxteren et al., 2005; Boris et al., 2016) as contributors to cloud or fog acidity, even in remote environments, due to the abundance of these compounds, including formic acid, acetic acid, pyruvic acid, succinic acid, and oxalic acid, in the atmosphere. For these weak acids and bases, the extent of partitioning from the gas phase is a sensitive function of droplet pH. Partitioning of weak carboxylic acids, such as formic and acetic acids, into the aqueous phase is strongly favored at pH values above the acid's pKa value, due to the deprotonation of the acid in such high-pH solutions.

~~8.2.2~~7.2.2 Recent observations of cloud/fog pH and long-term trends

Clouds and fogs have been observed to exhibit a wide range of pH values (Table S8). Typical values fall between pH 3 and 6. The most acidic observation reported was in an evaporating fog in Corona Del Mar in coastal Southern California, with a pH of 1.69 (Hileman, 1983). Other highly acidic pH values include 1.95 for a fog at Mt. Oyama in Japan (Mori et al., 1997), 1.94 for a fog in Duebendorf, Switzerland (Sigg et al., 1987), and 1.7 for a fog in Kahler Asten, Germany (Kroll and Winkler, 1988). Such acidic values are typically associated with large inputs of sulfuric and nitric acids, although hydrochloric acid has also been an important source of acidity in some urban areas (e.g., the Duebendorf fog). High pH fogs or clouds have also been reported in situations with large inputs of ammonia or alkaline soil dust. For example, Collett et al. (1999) reported pH values up to 7.43 for radiation fogs in California's Central Valley, a region with high ammonia concentrations stemming from major

agricultural activities. Wang et al. (2011) collected cloud water at Mt. Tai, China and observed cloud pH values during periods of strong soil dust influence in the range of 6.5 – 6.7. Changing regional transport patterns and resulting variations in inputs of acids and bases to Mt. Tai clouds, however, resulted in a wide range of values between 2.56 and 7.64 overall at this site. pH as high as 7.76, in Ca^{2+} rich advection fogs, has been observed at a roadside location near Sao Paulo, Brazil (Vasconcellos et al., 2018). Fog pH values above 7 have also been reported in polluted fogs in Kanpur, India (Kaul et al.,2011; maximum pH 8.07), in Ca^{2+}-rich fogs in Xishuangbanna, China (Zhu et al., 2000; maximum pH 9.15), in marine-influenced clouds at Puy de Dome, France (Deguillaume et a., 2013; maximum pH 7.6), and in other locations (see Table S8).

~~Figure 7~~Figure 15 (and Table S8) depicts pH observations from locations around the globe including observations at continental and marine locations for fogs and clouds collected by airborne and ground-based sampling platforms. Panels represent different time periods, from pre-1985 to post 2005, to highlight how strong regional changes in anthropogenic emissions, especially sulfur and nitrogen oxides, are incorporated in clouds thus affecting pH. Measurements pre-1985 are mostly associated with studies in the United States, Europe, Japan, and Australia. More global interest and coverage was seen in the later 1980s and 90s, with several measurement sites active in east Asia, Africa, and South America. Since 2005, there has been continued interest in cloud and fog observations in some regions, including in China and India, two countries facing increasingly severe air quality challenges. Globally, observed pH values range from highly acidic to more alkaline. While measurement locations are not constant over time, there appears to be a decrease in incidence of more acid clouds and fogs in North America and Europe since the 1980s and early 1990s, while trends in the incidence of acid fogs and clouds in East Asia are less clear.

While the global scientific community lacks long-term monitoring programs for cloud/fog composition, there are a few locations around the world where such measurements have been made routinely, or at least periodically, over periods of a decade or more. ~~Figure 8~~Figure 16 shows temporal trends in cloud/fog pH from a number of sites in the United States and Japan. Fog pH values from radiation fogs in California's Central Valley show a significant increase from the 1980s to the current decade. Herckes et al. (2015) attributed the rapid pH rise in the early part of the record, particularly at sites in the southern part of the valley, to decreases in SO_2 emissions. A steady climb is also apparent in cloud pH values measured at Whiteface Mountain, located in upstate New York in the northeastern U.S., consistent with reductions in regional NO_x and SO_2 emissions. Schwab et al. (2016) previously reported decreases in cloud water SO_4^{2-}, NO_3^-, NH_4^+, and H^+ concentrations at Whiteface Mountain of 3.8%, 3.7%, 2.8%, and 4.3% per year, respectively, over the period 1994-2013. Over this twenty-year period the cloud pH increased approximately 0.4 pH units per decade. Cloud pH values have been measured at remote locations in the Luquillo Mountains on the Caribbean island of Puerto Rico since 1967. Mean values reported in several studies up through 2012 (Lazrus et al., 1970; Weathers et al., 1988; Asbury et al., 1994; Gioda et al., 2009; Gioda et al., 2011; Gioda et al., 2013; Reyes-Rodríguez et al., 2009; Valle-Díaz et al., 2016) fall between 4.6 and 5.8, with no apparent trend. The pH values observed and the lack of a clear trend here are consistent with the fairly clean conditions in the region. Long-term

records of cloud or fog composition are even rarer in Asia. Between the 1960s and 1990s in central Japan (~~Fig. 8~~Fig. 16), conditions are fairly acidic, with mean pH values mostly between 3 and 4. Measurements after 2000 suggest a possible increase in cloud pH in the region. Long-term (unpublished) cloud pH measurements exist for a few locations in Japan and Taiwan; future anticipated publication may shed more light on acidity trends in the region.

~~Figure 9~~Figure 17 examines changes in cloud and fog pH measured from 1980 to present in Europe. By combining data from multiple locations, a more complete assessment of pH trends on the continent is possible. While there is considerable variability within individual record years and between years, the data overall suggest a trend toward increased pH, with values at the present time typically about one pH unit higher than in 1980. This increase, also seen in the U.S., is consistent with decreasing European emissions of key acid precursors: SO_2 and NO_x.

~~Given the obvious connections between clouds and precipitation, similarities~~ Similarities in the temporal trends of cloud pH with pH trends reported in precipitation are ~~worth noting~~likely given the obvious connections between clouds and precipitation. Vet et al. (2014) analyze a large set of precipitation measurements from around the world, considering precipitation composition and its temporal changes by region, with the analyses focused especially on the period 2000 – 2007. They report that changes in SO_2 and NO_x emissions in many regions of the globe result in measurable changes in sulfate and nitrate wet deposition that in turn produce changes in pH and H^+ wet deposition. Vet et al. (2014) note that 75% of European sites and 85% of North American sites saw increases in precipitation pH over this time period. A more spatially heterogeneous pattern of changing precipitation pH is reported for Asia. Looking at a longer time period, Duan et al. (2016) report a decreasing average precipitation pH in China from 1999 – 2006 with pH increasing after 2006, a pattern that is the inverse of temporal trends in China's SO_2 emissions.

~~8.2.3~~7.2.3 pH variation across drops within a cloud/fog

Up to this point, a single pH value for a cloud or fog has been discussed. In reality, each droplet within a fog or cloud is likely to have a unique composition. Within a cloud, droplets have a range of sizes as they grow, following initial cloud drop activation on CCN, by condensation (water vapor depositing on cloud drops) and coalescence (droplets typically of different sizes impacting and forming a single, larger drop). Cloud drops form when a critical supersaturation, associated with the critical (dry) diameter of the particle, is met following Köhler theory. Köhler theory indicates that larger CCNs activate at lower supersaturations and are therefore the first CCNs to be dissolved in droplets. A simple model representing the initial stages of condensational growth (Twohy et al., 1989) found that larger cloud drops activate on larger CCNs. Larger particles are typically mechanically generated and oftentimes are comprised of more alkaline components, including soil dust and sea salt. Smaller particles, typically made up of sulfate, nitrate, ammonium, and organic species, tend to be more acidic (Hoag et al., 1999). Given that the composition of the CCNs varies with size, then the fog/cloud solute composition will vary with drop size as

observed in a variety of clouds and fogs (Noone et al., 1988; Ogren et al., 1989; Munger, 1989; Bator and Collett, 1997; Laj et al., 1998; van Pinxteren et al., 2016; Moore et al., 2004; Guo et al., 2012a; Herckes et al., 2013).

Other cloud physical processes also affect the solute composition as a function of cloud drop size. Because of the larger surface area to volume ratio in smaller drops compared to larger cloud drops, water vapor condensation will favor more rapid growth (per unit volume) of small drops, quickly diluting their solute concentrations. Furthermore, droplets formed from smaller hygroscopic particles are much more diluted at the point of cloud droplet formation (CCN activation), compared to coarse mode particles (e.g., Nenes and Seinfeld, 2003). Coalescence tends to occur among larger and intermediate cloud drops of sufficiently different sizes because of their different fall speeds. Thus, coalescence tends to mix the composition of the larger drops leaving the composition of very small drops less affected by this process. The same is true for mixed phase, ice-water, clouds, where falling ice crystals capture large cloud drops most effectively. Once drops or ice crystals are large enough to fall out of the cloud (i.e. precipitation as rain or snow), removal from the atmosphere (by wet deposition) of larger drops and their dissolved solutes and trace gases will occur.

The rate of mass transfer of other trace components between the gas and aqueous (cloud/fog droplet) phases also depends upon the size of the droplet. The kinetic mass transfer coefficient often used to describe the mass transfer between the gas and aqueous phases in cloud chemistry models incorporates a representation of gas phase diffusion and interfacial mass transfer limitations and illustrates the dependence of mass transfer on droplet size, with the overall transfer rate related to the inverse of the droplet radius (or inverse of the square of the radius) (Schwartz, 1986). This size dependence of the mass transfer coefficient can contribute to mass transfer occurring to and from droplets at variable rates across the droplet size spectrum, sometimes leading to slower aqueous concentration increases in large droplets from the uptake of soluble gas phase species compared to smaller droplets (Ervens et al., 2003).

Measurements of pH in cloud water samples collected by size fractionating cloud water collectors (Collett et al., 1994) revealed that pH was lower in small drops compared to large drops for clouds and fogs sampled at various locations in the United States. The variation of pH across the droplet size spectrum has important implications for aqueous-phase chemistry, especially for S(IV) oxidation to form sulfate (Seidl, 1989; Hegg and Larson, 1990; Pandis et al., 1990; Lin and Chameides, 1991; Roelofs, 1993; Fahey et al., 2005; Gurciullo and Pandis, 1997; Reilly et al., 2001; Tilgner et al., 2013; Hu et al., 2019; Rao and Collett, 1998), which increases the acidity of the drops. Bulk cloud pH_F calculations (i.e. average characteristics, a common treatment in chemical transport models, Sect. 8.2) tend to underestimate the fraction of dissolved S(IV) in the form of SO_3^{2-} (where S(IV) = $SO_2{\cdot}H_2O + HSO_3^- + SO_3^{2-}$), which causes the underestimation of sulfate production rates (Fahey and Pandis, 2003; Hegg et al., 1992; Hoag et al., 1999; Moore et al., 2004; Roelofs, 1993). This is particularly true for S(IV) oxidation by ozone (O_3), since the rate constant for $SO_3^{2-} + O_3$ is several orders of magnitude larger than for $HSO_3^- + O_3$. Barth (2006) found that pH variation across cloud drop sizes is also important for aqueous-phase formaldehyde oxidation forming formic acid, which, as

a weak acid, can reduce the pH of the drops. Furthermore, Tilgner et al. (2013) demonstrate that a size-resolved multiphase chemistry treatment results in higher acidity production in smaller droplets leading to more acidic, smaller CCN particles after cloud processing while larger particles tend to be less acidic.

Both the composition and pH variation across the droplet population lead to differences in reactivity for different size droplets. Not only does the composition of droplets vary across the size spectrum in terms of reactants/oxidants, but many reactions and effective Henry's Law coefficients are pH dependent (Sect. ~~3~~5). Additionally, droplets of different size settle and deposit at different rates. In fogs, where the net effect of processing can be a cleansing of the atmosphere, larger droplets deposit faster than smaller ones, so those species enriched in larger droplets will be removed from the atmosphere faster than those species enriched in smaller droplets (Collett et al., 2001; Collett et al., 2008; Fahey et al., 2005). Nevertheless, most chemistry transport models still use a bulk water composition (i.e. average characteristics) to compute aqueous phase chemistry. Parameterizations informed by how bulk and size-resolved pH differ can be employed to better represent aqueous-phase oxidation within clouds (see Sect. 8.2).

~~8.2.4~~7.3 Need for future monitoring of cloud and aerosol pH

Formatted: Heading 2

Although cloud and fog sampling is generally more challenging than aerosol collection, pH measurement of the collected cloud/fog water is simpler due to its much larger volume and much lower ionic strength. As a result, ~~Over the past several decades,~~ fogs and clouds have been sampled and their pH determined in areas around the globe with more temporal and spatial coverage than for aerosol pH. Depending on inputs of key acids and bases, cloud/fog pH has been observed to range from below 2 to greater than 7~~.~~, slightly higher, but similar to fine aerosol pH that ranges from below 0 to near 7. Programs designed to target reductions in acid rain have had direct impacts on cloud and fog pH~~.~~, but aerosol pH has been much more constant than cloud pH in the southeastern US and southeastern Canada over time. Analysis of cloud pH observations over the past 25 – 30 years reveals that cloud/fog acidity in many regions has decreased as anthropogenic emissions of the important acid precursors, SO_2 and NO_x, have decreased. A continued rise in cloud/fog pH is likely in many regions with planned, future decreases in NO_x and SO_2 emissions and stable or increasing NH_3 emissions. Future changes in emissions could eventually be significant enough to lead to fine aerosol pH changes as well. Increases in cloud pH are expected to enhance the solubility of gas phase organic acids, potentially shortening their atmospheric lifetimes~~.~~ while increases in aerosol pH could lead to more nitrate aerosol formation and allow previously unfavorable kinetic reactions to occur.

As emissions evolve with time, continued characterization of cloud and particle pH is needed to understand how anthropogenic activities affect condensed-phase acidity and downstream endpoints in the earth system. Much remains to be learned about factors controlling cloud/fog pH in the atmosphere and the influence of this acidity on aqueous phase chemistry, including the aqueous phase uptake and oxidation of soluble gases to form secondary inorganic or organic aerosol. More detailed

measurements of organic acids and bases, and their influence on cloud pH, will be increasingly important as sulfate and nitrate concentrations decline. Likewise, there is a need for more systematic monitoring of cloud and fog composition in key environments, as opposed to the more *ad hoc* past sampling approaches driven primarily by the objectives of process-based research. Because fogs and clouds are good integrators of atmospheric acids and bases in both the gas and particle phases, they may offer a convenient and practical basis for ongoing monitoring of atmospheric acidity. Future monitoring strategies should consider long-term monitoring at surface sites as well as periodic measurements of cloud, particle, and gas-phase composition from aircraft in order to enhance our understanding of acidity at higher ~~elevations~~ altitudes in the troposphere. Future measurements should also better document heterogeneity of acidity across individual drops within a cloud ~~or~~/ fog or aerosol population, for example ~~looking at~~by determining the size-dependence of ~~drop~~ pH. Aerosol pH estimates will likely continue to be primarily based on thermodynamic models in the near future and thus require simultaneous particle- and gas-phase measurements (specifically of ammonia) to improve the spatial and temporal scales over which fine particle pH is currently characterized.

~~9 Role of particle size, composition, and mass transfer kinetics in pH heterogeneity~~

~~Traditionally, fine particle pH is calculated assuming equilibrium and a uniform distribution of species across all particles (e.g., Sect. 5.1 and 6). Here, the role of differences in particle size, mass transfer, and composition (including presence of organic species) in driving pH in a population of particles is highlighted.~~

~~9.1 Role of particle size and composition~~

~~The pH of aerosols varies with particle size because of the differences in the chemical composition, hygroscopicity, and gas-particle equilibration time scales between fine and coarse particles. Fine-mode aerosols are produced by new particle formation and growth but are also directly emitted from anthropogenic as well as natural sources (dust and sea salt). At least some of the chemistry that initiates new particle formation, and thus drives low pH for the smallest sizes, involves sulfuric acid and acid-base reactions (Kulmala et al., 2004). Anthropogenically derived fine mode aerosols are typically composed of inorganic salts, organic species, and black carbon and are generally acidic. Fine-mode pH is sensitive to the relative amounts of non-volatile cations (if any), sulfate, nitrate, and ammonium present in the particle phase (Fig. 2) and continuously responds to the changing concentrations of their gas-phase counterparts $H_2SO_4(g)$, $HNO_3(g)$, and $NH_3(g)$ as well as the ambient RH and temperature.~~

~~In contrast, coarse mode aerosols mainly consist of sea-salt and dust particles directly emitted to the atmosphere as a result of wind stress on the surface of the oceans and arid land, respectively. Sea salt and dust contain significant amounts of non-volatile cations such as Na^+, Ca^{2+}, Mg^{2+}, and K^+, whereas the dominant cation in fine mode particles is typically semi-volatile~~

ammonium. Dust, and more generally non-volatile cations, can also originate from mechanical wear or disturbances associated with anthropogenic activity such as road, residential, and commercial construction as well as brake wear and road salt application (Philip et al., 2017; Lough et al., 2005; Kolesar et al., 2018). Both fossil fuel and biomass combustion also emit non-volatile cations in the $PM_{2.5}$ size range (Reff et al., 2009). Whether or not non-volatile cations influence pH depends on their mixing state with deliquesced particles. In other words, particles of the same size but different compositions should be treated as external mixtures when calculating their pH. For example, equilibrium model analysis of bulk ambient aerosol observations by Guo et al. (2016) indicate that the refractory ions were externally mixed from PM_1 because including those ions caused deviation between the predicted and measured nitrate partitioning. A small fraction of non-volatile aerosol components is sometimes present in the fine mode and tends to reduce acidity. For example, K^+ associated with biomass burning has been shown to cause higher pH compared to cases with very low K^+ levels (Bougiatioti et al., 2016).

Sea-salt and dust are naturally basic or alkaline, as they contain carbonates. The pH of ocean water (~ 8) is relatively uniform and sets the pH_i for unprocessed sea-salt emissions (Keene et al., 1998). The pH of fresh airborne dust is more difficult to assess due to the high degree of heterogeneity in composition and its hygroscopicity; however, it is very likely that ambient dust is not acidic (has pH > 7). Sea-salt and dust aerosol can initially maintain high pH (above 5 and close to 7) due to the presence of carbonate (CO_3^{2-}/HCO_3^-). However, the uptake of acid gases such as $SO_2(g)$, $HCl(g)$, $HNO_3(g)$ and $H_2SO_4(g)$ result in a chemical reaction (Usher et al., 2003) such as:

$$CO_3^{2-}(aq) + 2H^+(aq) \rightarrow CO_2(g) + H_2O(l) \quad \text{(R4)}$$

Reaction R4 consumes H^+ produced from the uptake of acid gases (e.g., $HNO_3(g) \rightarrow H^+(aq) + NO_3^-(aq)$, Reaction R1 and R2 combined), allowing the aerosol to maintain its high pH until the carbonate has been depleted via conversion to $CO_2(g)$. Once the carbonate has been depleted (a process not treated by current equilibrium models, Sect. 2.6), the dust and sea-salt aerosol can become acidified by continued uptake of acid gases. Observations of aged sea salt and dust show an internal mixture with sulfate, nitrate, and chloride due to such reactions.(Fairlie et al., 2010; Kirpes et al., 2018; Tobo et al., 2010). Freshly emitted sea-salt aerosol is in the liquid state while Ca-rich dust particles are emitted as solids. Consequently, acidification of sea salt aerosol is thought to proceed more efficiently due to relatively high mass accommodation coefficients (about 0.1 or higher) for condensing acids on liquid particles compared to solid dust aerosol with much lower uptake coefficients ranging between 10^{-4} and 10^{-2} (Alexander et al., 2005; Fairlie et al., 2010). The increase of aerosol water with increasing RH and the solubilization of gaseous HCl that is present in the marine boundary layer (due to acid displacement reactions) has also been suggested as the reason for increasing acidity of sea-salt aerosols with increasing RH and altitude in the marine environment (von Glasow and Sander, 2001). Further acidification of sea salt aerosols occurs via displacement of Cl^- as $HCl(g)$ due to reactions such as (Mcinnes et al., 1994; Zhao and Gao, 2008):

$$HNO_3(g) + Cl^-(aq) \rightarrow HCl(g) + NO_3^-(aq) \quad \text{(R5)}$$

$$H_2SO_4(g) + 2Cl^-(aq) \rightarrow 2HCl(g) + SO_4^{2-}(aq) \quad \text{(R6)}$$

Although these reactions do not directly produce additional H^+ ions, the resulting H^+ molal concentration increases due to a decrease in the overall aerosol water content in particles containing $NaNO_3$ and Na_2SO_4, which are less hygroscopic than NaCl.

Overall, atmospheric particle pH is size dependent and generally higher for coarse mode particles due to variations in inorganic composition with particle size. Differences as large 4 pH units have been reported between fine and coarse particles (Fang et al., 2017; Young et al., 2013). Bulk PM_1 and $PM_{2.5}$ acidity is more similar than fine vs coarse mode acidity (pH_f within 1 – 2 units, e.g., Bougiatioti et al., 2016; Guo et al., 2017b), but submicron (diameter < 1 μm) particles still show higher acidity than bulk $PM_{2.5}$. The reason for this is the strong enrichment of aerosol with NVCs from dust and sea salt at the larger sizes (even in the fine mode) and role of sulfate in new particle formation and surface-area driven condensation at the small sizes (Fig. 2). Significant pH changes can occur in the 1 to 2.5 μm size range (Fang et al., 2017; Ding et al., 2019). The size dependent pH is also seen for sea salt aerosol (Fridlind and Jacobson, 2000) as well as in urban aerosols in China (Ding et al., 2019) where the fine mode is consistently 2-3 pH units lower than the coarse mode. The implications of this acidity gradient are considerable, for metal solubility and their impacts on public health and ecosystem productivity, as well as chemistry and semi-volatile partitioning of pH-sensitive species.

9.2 Role of mass transfer

Acidity is dependent on particle composition, and particle composition can be affected by mass transfer rates that vary by particle size. For fine mode particles, the characteristic time for particle growth or shrinkage from one equilibrium state to another after changes in RH is short enough (< 1 s) to justify the assumption of thermodynamic equilibrium with respect to water uptake (Pilinis et al., 1989). In comparison, equilibration of semi-volatile components (HNO_3, HCl, and NH_3) with the fine mode ranges from 20 min or less (Guo et al., 2018b) up to 10 hours (Meng and Seinfeld 1996; Fridlind and Jacobson, 2000). In the case of coarse mode aerosols or large accumulation mode aerosols, mass transfer rates for semi-volatile components can lead to equilibration time scales of several hours. Hanisch and Crowley (2001), for example, found vapors of HNO_3 reach equilibrium through uptake by sea spray aerosols of 1-3 μm diameter within 3-10 h. In another study of remote marine aerosols, equilibrium in the coarse sea salt mode is reached quickly for NH_3, but HNO_3 and HCl require much longer times, of the order of 10 – 300 hours (Fridlind and Jacobson, 2000). In this case, relatively small amounts of TNH_4 partition to the coarse sea salt particles compared to much larger amounts of HNO_3 needed to displace HCl to reach equilibrium. These time scales are comparable or can even exceed the lifetime of the particles, implying that some particles can be removed by deposition before equilibrium is reached (Fridlind and Jacobson, 2000). In a subsequent theoretical study, Jacobson (2005a) found that under at least some conditions equilibrium can be reached within less than 1 h by large particles (< 6 μm) and within 15 min by particles < 3 μm, while in several other cases coarse particles took longer to reach equilibrium. Thus, aerosols of different sizes within the fine and coarse modes may not always be in mutual equilibrium due to mass transport limitations,

and equilibrium alone may not uniquely determine the distribution of condensed semi-volatile gases across the particles of different sizes (Wexler and Seinfeld, 1990, 1992).

Given the above, both mass transport and thermodynamics must be considered to accurately predict the distribution of semi-volatile gases and the associated aerosol pH across the entire aerosol size spectrum. However, simulating mass transfer and thermodynamics for the size- and composition-distributed aerosol is computationally challenging due to numerical stiffness. There are two main sources of numerical stiffness. The first source arises from the large differences in the mass transfer time scales for particles of different sizes. Additional stiffness and non-linearity are introduced by H^+ ions in partially and fully deliquesced aerosols. In such cases, the H^+ ion molal hydrogen ion concentration (m_{H^+}) plays a crucial role in the determination of equilibrium aerosol phase state as well as in the determination of equilibrium gas-phase concentrations of HNO_3, HCl, and NH_3 at the particle surface for computing their driving forces for mass transfer. The characteristic time scale for H^+ ions is quite short relative to other species, especially under "acid-neutral" or "sulfate-poor" conditions, where the pseudosteady-state concentrations of H^+ ions are two or more orders of magnitude smaller than the sum of all other cations (Sun and Wexler, 1998). Since semi-volatile species in different particles of different sizes are coupled via the gas phase, the numerical solver for mass transfer would have to take time steps on the order of the shortest timescale to ensure accuracy for all the species across the entire aerosol size distribution. Such small time steps are computationally prohibitive for common chemical transport model applications. Several attempts have been made over the past 20 years to reduce the stiffness of the system of nonlinear ordinary differential equations that describe the multicomponent, size-distributed mass transfer problem so that it could be efficiently solved (Capaldo et al., 2000; Hu et al., 2008; Jacobson, 1997; Jacobson, 2002, 2005a; Jacobson et al., 1996; Pilinis et al., 2000; Sun and Wexler, 1998; Zaveri et al., 2008; Zhang and Wexler, 2006).

Here, we illustrate the time-evolution of size-distributed pH using the sectional MOSAIC box model with 60 size bins for a scenario (test case 14 in Zaveri et al., 2008) in which fine mode aerosol composed of $(NH_4)_2SO_4$ and coarse mode aerosol composed of NaCl were exposed to appreciable gas-phase concentrations of H_2SO_4 (1 ppbv), HNO_3 (15 ppbv), HCl (1 ppbv), and NH_3 (10 ppbv) at 85% RH and 298.15 K temperature (Fig. 16). While the fine mode rapidly absorbs significant amounts of these gases within the first few minutes of the simulation, it takes nearly 10 h for the aerosol composition, and hence the pH, to become uniform across the bins of different sizes. Furthermore, the displacement of HCl from the coarse mode due to HNO_3 absorption occurs slowly over this time, although significant differences in the pH can be seen across the coarse mode size bins even after 10 h. In conclusion, it is important to treat dynamic mass transfer to accurately simulate size-distributed pH and composition of aerosols. Although challenging, fully dynamic and hybrid (i.e., a combination of equilibrium for fine mode and dynamic for coarse mode) numerical methods have been implemented in 3D chemical transport models (Fast et al., 2006; Jacobson et al., 2007; Zhang et al., 2010).

9.3 Role of organic–inorganic interactions

Aerosol particles are rarely composed of a completely distinct organic-free aqueous inorganic phase and electrolyte-free organic phase – an assumption often made in air quality models for reasons of simplicity. Instead, mixed particles exist consisting of a complex mixture of organic compounds, inorganic ions, and water that may be separated into multiple liquid/solid phases (Bertram et al., 2011; Hallquist et al., 2009; Maria et al., 2004; Murphy et al., 2006; Pöhlker et al., 2012; Song et al., 2012; Zuend et al., 2010). The role of organic–inorganic interactions on the acidity of liquid/amorphous aerosol phases has been addressed in only a few studies and represents an area of research where further efforts are needed. Particle phase acidity could be affected in multiple ways by organic–inorganic interactions: directly by means of non-ideal mixing effects on the activity coefficient of H^+ (and all other species) in a liquid phase of given composition; indirectly via the effect of organics on composition and the equilibrium gas–particle partitioning of water and other semi-volatile components (including NH_3, inorganic and organic acids), as well as the potential for LLPS; and directly by dissociating organic acids that contribute dissolved H^+ or amines that associate with H^+.

A phase-separated particle typically consists of a rather hydrophobic organic-rich phase and an aqueous electrolyte-rich (salt/ion rich) phase (You et al. (2014) and references therein) (Fig. 17). Note that water and inorganic ions, including H^+, can exist in the organic-rich phase of a liquid–liquid phase separated system (Pye et al., 2018; Zuend and Seinfeld, 2012). Both the detection of LLPS and pH in ambient particles as well as micron-sized droplets in laboratory experiments is a difficult technical challenge (Wei et al., 2018). To our knowledge, no online measurement techniques applicable to field sampling exist for that purpose (see Sect. 5.1 for aerosol pH measurement challenges). The current state of knowledge is therefore limited to relatively simple laboratory systems and theoretical considerations. Dallemagne et al. (2016) used a model system in the form of a super-micron-sized ternary aqueous poly(ethylene glycol)-400 (PEG-400) + ammonium sulfate droplet. They studied this system in an RH and temperature-controlled cell with confocal microscopy in the presence of a pH-sensitive fluorescent dye to determine the pH value at different locations in the liquid drop. They report a small, yet distinct change in pH due to the phase transition from a single to two liquid phases for this system when RH decreases: pH = 3.8 ± 0.1 in a single mixed phase at > 90 % RH, while the organic-rich shell phase in a LLPS state exhibited pH = 4.2 ± 0.2 at 80 % RH to pH = 4.1 ± 0.1 at 65 % RH; the pH in the sulfate-rich phase was not determined during LLPS. The pH value of the organic-rich phase was similar to that of a corresponding salt-free aqueous PEG-400 solution measured using a standard pH probe. Since changes in RH lead to changes in particle water content, here causing the LLPS, the degree to which such changes affected the measured pH in the Dallemagne et al. (2016) study remain unclear.

Losey et al. (2016) controlled the pH in aqueous solution droplets consisting of 3-methylglutaric acid, ammonium sulfate and sodium hydroxide. They found that changes in pH and the degree of methylglutaric acid dissociation (deprotonation), affect the separation RH (SRH), the onset of LLPS during dehumidification. The SRH was ~ 79 % for pH = 3.65, ~ 70 % for pH = 5.17, and ~ 64 % for pH = 6.45. The RH at which the two liquid phases merge into a homogeneous single phase was observed

around 80 % RH in this system, approximately independent of pH – indicating that a hysteresis between SRH and merging RH occurs for pH close to neutral, but not at lower pH. While this study did not attempt to measure the pH in distinct liquid phases, it indicates that the established pH, resulting from interactions between inorganic electrolytes and organic acids, affects the LLPS behavior. Losey et al. (2018) further explored similar systems at higher acidity in the presence of sulfuric acid (varying the ammonium-to-sulfate ratio from 2.0 to 1.5 to 1.0). They report that all observed RH levels of phase transitions were affected by the pH established with sulfuric acid. The SRH consistently decreased with increasing amounts of sulfuric acid (toward lower pH); e.g., for 3-methylglutaric acid + ammonium sulfate + sulfuric acid from SRH of ~ 80 % at pH = 2.68 to SRH of ~ 30 % at pH = 0.34. Similar lowering of SRH with increasing acidity was also found for a non-acidic organic mixture component (1,2,6-hexanediol). Furthermore, at high acidity (here pH lower than 0.5), several of the studied systems did not show any LLPS down to very low RH. While the quantitative phase transition behaviour depends on the organic component, these experiments by Losey et al. (2018) imply that organic–inorganic interactions can have an impact on mutual solubility and phase transitions, in those cases with increasing mutual solubility towards higher acidity.

While a LLPS will impact the acidity in coexisting liquid phases, the extent to which the pH values will typically differ between the phases – and, related to that, the molar concentrations of hydronium ions and ionic strength – remains an open question. Theoretical considerations aid in constraining the range of expectations in this case. Thermodynamic equilibrium between two liquid phases, each of neutral electric charge, implies that the electrochemical potential of H^+ ions is equivalent in both phases (see Sect. 2). Therefore, the activity-based pH in coexisting phases is expected to be similar, but not necessarily of the exact same value. Computations with the AIOMFAC-based liquid–liquid equilibrium model confirm for case studies that the pH in two liquid phases is of the same order of magnitude, often with a difference of less than 0.2 pH units (Pye et al., 2018). However, H^+ molalities (or concentrations) in the two coexisting phases of atmospheric aerosols are predicted to be very different, often by up to several orders of magnitude; hence, it is important to calculate pH based on H^+ activity, not simply concentration (see also Sect. 6.3 recommendations for approximating pH). In Pye et al. (2018), several thermodynamic models were applied to predict the partitioning of ammonia, water, and organic compounds between the gas and particle phases for conditions in the southeastern U.S. during summer 2013. AIOMFAC-based coupled liquid–liquid and gas–particle partitioning computations within that study predicted partial to complete miscibility among organic and inorganic aerosol components, depending on RH. The AIOMFAC-based model predicted an increase in the concentration of gas-phase ammonia (NH_3) alongside a decrease in acidity when partial miscibility of organics was accounted for. In comparison to calculations with complete phase separation between organic and inorganic ions enforced, the interactions of inorganic ions with organic compounds (in mixed phases) were predicted to promote an enhanced association of H^+ and SO_4^{2-} into HSO_4^-, resulting in a slightly higher pH (0.1 pH units median increase), since the bisulfate ion is predicted to be more miscible with organic compounds than equivalent amounts of H^+ and SO_4^{2-} (Pye et al., 2018). This indicates a pH buffering effect of the degree of bisulfate dissociation; however, additional complexity in understanding the main drivers of such pH changes arises from simultaneous changes in the equilibrium gas–particle partitioning of water, organics, and ammonia.

The impact of amines and organic acids on H^+ is usually neglected in efforts to model pH. Amines may contribute to aerosol alkalinity – especially given their potentially strong proton affinity (Dall'Osto et al., 2019), but they must be in sufficient quantities to compete with NH_3 and other cations. Although not strong sources of protons or cations, these alkaline and acidic organics may still be considered together with other water-soluble organic compounds (WSOCs) in the particulate phase in terms of their ability to influence the aerosol water content. The uptake of water due to organic components is often used to correct the solvent volume and pH_E derived based on the inorganic aerosol composition (e.g., Guo et al., 2015; Bougiatioti et al., 2016). This implies that aerosol pH is reversibly influenced by the amount of water (driven by RH and composition) associated with the aerosol particles, which has been shown to drive some of the diurnal variability of pH (Guo et al., 2015).

For systems where a single mixed aerosol phase is assumed, current work indicates dissociating organic acids do not strongly affect pH and the limited studies to date suggest that inorganic species drive pH (Battaglia et al., 2019; Song et al., 2018; Vasilakos et al., 2018). For the southeastern U.S., pH changes predicted by E-AIM were generally limited to < 0.2 pH units in response to dramatic increases in oxalic acid (Vasilakos et al., 2018). Similarly, E-AIM predicted that increases in oxalic acid concentrations resulted in < 0.1 pH unit changes for polluted Beijing conditions (Song et al., 2018). This is notable since the predicted pH in Beijing (neglecting organics) was consistently above the first acid dissociation constant (pK_{a1}) value for oxalic acid, conditions where pH is predicted to be most sensitive to organic acids (Nah et al., 2018). Nah et al. (2018) showed that for aerosol pH_E varying between 0.9 and 3.8, the inorganic-only predicted pH_E was sufficient to define an effective sigmoid curve for oxalic acid, one of the most abundant of organic acids with a pK_a that is well within this range. Neglecting the effects of oxalate on pH by Nah et al. (2018) did not seem to affect the quality of the partitioning. Battaglia et al., (2019) extended these prior studies to include additional organic acids (oxalic, glutaric, and malonic acids) as well as three non-acid organics (levoglucosan, tetrahydrofuran, and 1-pentanol) mixed with inorganics representative of Beijing winter haze and eastern U.S. summertime compositions. The changes in pH relative to the inorganic-only system were predicted by AIOMFAC to be quite small, generally < 0.2 pH units, when a single aerosol phase was present (Battaglia, Jr., et al., 2019). The response of pH to the same organics at lower RH (< 70%) or under LLPS conditions was not characterized.

While current work suggests organic–inorganic interactions only slightly affect the pH, they can drive both LLPS and other phase transitions. Based on case studies (Pye et al., 2018; Battaglia et al., 2019), the interactions between water and ions are likely the main determinants of the resulting pH value. However, considering the complexity and variability of realistic aerosol compositions, the extent to which organic–inorganic interactions moderate the pH in liquid phases has not yet been studied in depth.

~~10~~8 Regional and global model representations and usage of pH_F

Chemical transport models and climate models are the ultimate integrators of knowledge that link emissions to the endpoints of public health, climate, and deposition. Aerosol acidity, however, is almost never considered or reported in these large frameworks (although there are exceptions, e.g., TM4-ECPL reported model-predicted pH_F for clouds and particles; Fig. S2 of Myriokefalitakis et al., 2015), so potentially large differences in acidity may be a driver of bias that has been unidentified to date. In the following section, major features of a set of models (Community Multiscale Air Quality modeling system, CMAQ; Goddard Earth Observing System with Chemistry model, GEOS-Chem; TM4-ECPL; and Weather Research and Forecasting coupled with chemistry WRF-Chem) are summarized in terms of fine aerosol pH_F predictions (Sect. 8.1). The cloud pH_F from a subset of the CTMs listed above and the Community Atmosphere Model with Chemistry (CAM-Chem; Lamarque et al., 2012; Tilmes et al., 2015), a component of the NCAR Community Earth System Model (CESM), are also included (Sect. 8.2). Table 7 summarizes the species considered in the calculation of pH for each model displayed in this work.

~~10.1~~8.1 Aerosol pH_F

All three-dimensional CTMs presented here use thermodynamic models to predict aerosol composition and thus $PM_{2.5}$ predictions are sensitive to pH_F. Thermodynamic models for the inorganic system were initially implemented to predict the gas–particle partitioning of semi-volatiles including nitric acid and ammonia due to their importance in forming fine particulate matter, but later studies have leveraged the predicted acidity for acid-mediated reactions. In TM4-ECPL, the pH of clouds and aerosol water affects the equilibria and thus chemistry of organic acids as well as the partitioning of reactive nitrogen and the solubilization of the trace elements iron and phosphorus. TM4-ECPL explicitly accounts for interconversion of Fe (II) and Fe (III) and formation of oxalate (the partitioning of which is also pH-sensitive, e.g., Nah et al., 2018) that acts as a ligand and contributes to secondary organic aerosol. This chemistry has been used to understand changes in oceanic deposition of Fe and P from preindustrial, present-day, and future atmospheres (Myriokefalitakis et al., 2015; Myriokefalitkis et al., 2016) as well as with regional focus on the Mediterranean region (Kanakidou et al., 2019). The CMAQ v5.1+ (Pye et al., 2013) and GEOS-Chem v11-02+ (Marais et al., 2016a) models use particle acidity, although in slightly different forms, to mediate the uptake of isoprene epoxydiols and resulting production of secondary organic aerosol in $PM_{2.5}$. For purposes of acid-catalyzed particle-phase reactions, GEOS-Chem uses ISORROPIA II-predicted pH_F (Marais et al., 2016a) while CMAQ v5.1 and later consider the entire internally mixed fine-mode particle phase abundance in calculating the concentration of H^+ (Pye et al., 2013). In CMAQ, organic constituents act to dilute H^+ (increase pH_F when the solvent includes organics) relative to an externally-mixed or phase-separated assumption (Schmedding et al., 2019). This leads to a moderate correlation between acidity (expressed as 10^{-pHF}) and isoprene-derived organic aerosol constituents (r^2=0.3-0.5) (Budisulistiorini et al., 2017) for the SE US, in contrast to acidity pH_F estimates under an externally-mixed or inorganic-only solvent assumption that show no significant correlation with isoprene SOA (Budisulistiorini et al., 2015). The WRF-Chem model, configured with MOZART chemistry and MOSAIC aerosols with the MESA thermodynamic model, uses particle acidity to calculate SOA production from glyoxal (Knote et al.,

2014). Even though aqueous production of sulfate in clouds is mediated by cloud pH, heterogeneous sulfate production on aqueous aerosol (via pathways in ~~Fig. 3~~Fig. 9) is generally not considered in models, but future efforts may include these pathways due to model underestimates of sulfate in regions like Beijing, China (e.g., Shao et al., 2019; Cheng et al., 2016) and Fairbanks, Alaska (Molders and Leelasakultum, 2012).

Chemical transport models use a variety of thermodynamic box models depending on their needs for accuracy and efficiency or treatment of specific systems and processes. The MESA thermodynamic model is used in CTMs configured with the MOSAIC aerosol model (e.g. WRF-Chem; Fast et al., 2006). ISORROPIA II is employed in several CTMs including GEOS-Chem (v8-03-01 and later), the CMAQ (v5.0 and later) modeling system, NASA GISS, WRF Polyphemus 1.6, the Tracer Model (TM) v4,5-ECPL family of models (Appel et al., 2013; Metzger et al., 2018; Myriokefalitakis et al., 2011; Pye et al., 2009), PM-CAMx (both regular and UF versions), and some versions of WRF-Chem (e.g., Zhang et al., 2013). GEOS-Chem, CMAQ, and TM4-ECPL assume the fine particles are in metastable equilibrium with the gas phase and employ the forward (i.e., gas and aerosol precursors as input) calculation mode of ISORROPIA II to partition semi-volatiles, calculate liquid water content, and pH_F. While stable vs metastable assumptions strongly affect the amount of liquid water content and may influence the resulting composition of the aqueous phase, Song et al. (2018) found that calculations assuming stable and metastable state yield similar results in terms of pH_F when the aerosol is deliquesced for conditions in China. The generality of this finding, especially when the complex phase diagram associated with eutectics of multiple salts is fully considered, remains to be determined.

The pH of the coarse mode is treated to varying degrees in models. TM4-ECPL (Myriokefalitakis et al., 2015) applies the equilibrium assumption to internally mixed sulfate, nitrate, ammonium, sea-salt and dust aerosols in the coarse mode after equilibrating the fine mode aerosol. CMAQ, starting with v4.7, uses a hybrid approach to mass transfer (Kelly et al., 2010) where the internally mixed Aitken and accumulation modes are in equilibrium with the gas phase, and mass transfer with the coarse mode is treated dynamically using the difference between the ambient and equilibrium vapor pressure of semi-volatiles (computed with ISORROPIA II in reverse mode in CMAQ v5.0 and later) as a driving force for condensation/evaporation (Capaldo et al., 2000). This driving force, however, is not allowed to exceed the gas-to-particle diffusional limit prescribed in CMAQ which would result in numerical instability when the aerosol pH is mildly acidic to alkaline (see Sect. ~~7~~6.2 for additional discussion) (Pilinis et al., 2000). While ISORROPIA is not recommended for estimating pH_F in field or laboratory applications when only particle composition is available (reverse mode, open system, see discussion in Hennigan et al., 2015 and Song et al., 2018), the reverse mode can be used for a driving force in a chemical transport model since CTMs represent a closed system, species concentrations are not subject to measurement error, and the driving force can be capped at the diffusion limitation. For coarse particles in CMAQ, H^+ determined via charge balance (assuming all particulate sulfur is in the form of sulfate, Eq. 13) is output for diagnostic purposes but is not used within the model. GEOS-Chem does not perform thermodynamic calculations for coarse particles. However, it does keep track of coarse-mode sea-salt and dust alkalinity, which

is relevant for calculating heterogeneous reactions on coarse particles. For example, heterogeneous S(IV)+O_3 only happens in the model when the sea-salt and dust aerosol is still alkaline (Alexander et al., 2005). Heterogeneous reactions between hypohalous acids and halide ions (e.g., HOBr+Br-) on sea salt aerosol are acid catalyzed, so these reactions are only allowed to occur in the model after the sea-salt alkalinity has been titrated (titrated coarse-mode pH is assumed to be equal to 5) (Sherwen et al., 2016). The Weather Research and Forecasting model (Powers et al., 2017; Skamarock et al., 2008) coupled with chemistry (WRF-Chem version 3.9.1; Fast et al., 2006; Grell et al., 2005) has four aerosol configurations, including a bulk aerosol scheme, two modal aerosol schemes, and a sectional aerosol scheme (8 or 4 bin). Figures 19 and 21 use the 4-bin sectional aerosol scheme (bins 0.039–0.156, 0.156–0.625, 0.625–2.5, 2.5–10 μm in diameter) with MOSAIC coupled to MOZART (Model for Ozone and Related Chemical Tracers, version 4) gas-phase chemistry and cloud water chemistry (Knote et al., 2015; Zaveri et al., 2008). Within MOSAIC, the multi-component equilibrium solver for aerosols (MESA, Zaveri et al., 2005a) solves inorganic aerosol thermodynamics for each aerosol size bin (see also Sect. 2.6.3 for a description of MOSAIC).

Even models using the same thermodynamic algorithms can produce different pH_F estimates since CTMs differ in their assumptions regarding equilibrium, mixing state, emission speciation, composition distribution across size, and chemical constituents important for driving pH (see Table 7). Especially notable are differences that occur with respect to the presence, abundance, and mixing state of non-volatile cations, the presence of which tends to increase pH_F – and may further elevate pH_F by co-condensation of nitrate and its associated water uptake (e.g., Guo et al., 2018a). In TM4-ECPL, SO_4^{2-}, NH_3, NH_4^+, HNO_3 and NO_3^- are explicitly treated. Additional cations in TM4-ECPL (for fine-submicron- and coarse modes) are specified based on the composition of mineral dust and sea salt. However, TM4-ECPL does not include Ca and Mg from dust in the fine mode calculations, as also proposed by Ito and Feng (2010), since TM4-ECPL considers all submicron dust and sulfate aerosol to be externally mixed in the atmosphere. The opposite assumption is made for coarse particles in TM4-ECPL since sulfate and nitrate are produced by heterogeneous processes on coarse particles (leading to an internal mixture) and coarse particle lifetime is short (decreasing the likelihood of distinct source plumes interacting). GEOS-Chem, employing a bulk scheme for fine aerosol, considers SO_4^{2-}, NH_3(g), NH_4^+, HNO_3(g), NO_3^-, Na^+, Ca^{2+}, Mg^{2+}, and Cl^- from fine-mode sea-salt aerosol. Cations from dust are not included in GEOS-Chem fine aerosol pH_F calculations by default (version 12.0.0), but Ca^{2+} and Mg^{2+} from fine-mode dust aerosol (assuming 3% and 0.6% by mass dissolution, respectively; Fairlie et al., 2010) were added to simulations in this work (see Fig. S7). CMAQ v5.0 and later, with Aitken and accumulation modes for fine aerosol, considers non-volatile cations from sea-salt, wildfires, wind-blown dust, and anthropogenic sources such as fugitive road dust, agricultural soils, and coal combustion as described by the EPA National Emission Inventory (NEI) and SPECIATE database (Reff et al., 2009). WRF-Chem configured as MOZART-MOSAIC represents the major aerosol species including sulfate, MSA^-, NO_3^-, Cl^-, CO_3^{2-}, NH_4^+, Na^+, Ca^{2+} in the charge balance for H^+ (other inorganic species, primarily dust particles, are considered inert, Sect. 2.6.3). Since HCl is not present in MOZART gas-phase chemistry, displacement of Cl^- from sea salt aerosols cannot be represented.

Chemical transport model predictions of particle acidity in the literature as well as in this paper (Fig. 18-19) are expressed as pH_F and assume molarity- and molality-based concentrations lead to equivalent pH_F with water as the solvent (Sect. 2.2 and Jia et al., 2018). CTMs, particularly those that use ISORROPIA or assume externally mixed inorganic and organic particles, assume the solvent for H^+ is water associated with inorganic electrolytes. In WRF-Chem with MOSAIC, species that do not contribute directly to the ion balance (e.g., organics and inert mass) can absorb water, and thereby indirectly influence the pH_F via solvent abundance. TM4-ECPL and CMAQ v5.3 can calculate pH_F including solvent water associated with both inorganic and organic constituents, but in this paper, only water associated with electrolytes is considered in pH_F.

The limited literature to date evaluating CTM-predicted pH_F indicates agreement between models and observationally-constrained estimates within 1 pH_F unit or better (summarized in Table S10). Observationally-constrained pH_F from the eastern U.S. in summer at the surface (0.9 ± 0.6, Guo et al., 2015), summer aloft (1.1 ± 0.4, Xu et al., 2016) and winter aloft (0.8 ± 1.0, Guo et al., 2016) all indicate strongly acidic particles and are in good agreement with GEOS-Chem aloft predicted pH_F of 1.3 during the SEAC4RS 2013 (Marais et al., 2016a) and WINTER 2015 (Shah et al., 2018) campaigns. CMAQ agreement with observations in the eastern U.S. are sensitive to assumptions regarding non-volatile cations with surface-level predictions of pH_F showing good agreement with observations in the work of Vasilakos et al. (2018) (pH_F = 0.82) and when non-volatile cations were excluded in the work of Pye et al. (2018) (pH_F = 0.9 ± 0.9). For Centreville, Alabama in the work by Vasilakos et al. (2018), CMAQ predicted excessively acidic aerosol during the day and similar to or higher than observationally-constrained pH_F estimates by 1 unit at night. Reductions in non-volatile cations, which may be overpredicted due to errors in nocturnal mixing (Appel et al., 2013), reduced the nocturnal pH_F in CMAQ making it more consistent with observations (Vasilakos et al., 2018). pH_F evaluation in other locations is more limited. Guo et al. (2017b) indicate a pH_F for wintertime Beijing of 4.2, consistent with GEOS-Chem simulations of Beijing for Autumn/winter (pH_F=4.3, range: 3.6 to 5.0; Shao et al., 2019) and CMAQ (pH_F of 4.5 ± 0.8 for Beijing February 2016, this work). Shao et al. (2019) found that including Ca^{2+}, K^+, and Mg^{2+} from dust in the aerosol pH_F calculations had a small effect on predicted aerosol pH_F (increase of 0.1) in Beijing in autumn and winter, consistent with Guo et al. (2017b).

An evaluation of CTM-predicted pH_F can be leveraged to understand the responsiveness of a model to changes in atmospheric composition. For example, Vasilakos et al. (2018) show that modeling pH_F correctly in CMAQ is critical to accurately partition nitrate between the gas and aerosol-phase and thus capture trends in $PM_{2.5}$ nitrate as sulfate is reduced in the United States. Shah et al. (2018) provide insight into the effectiveness of past and future emission reductions by tracking pH_F predicted by GEOS-Chem. Shah et al. (2018) predict that pH_F for winter in the eastern U.S. increases from 0.39 to 1.7 between 2007 and 2023 using GEOS-Chem. As a result, nitrate aerosol concentrations are predicted to decrease less than the reductions of NO_x emissions and total nitrate would imply. Since regulatory guidance for model application encourages the use of relative response factors (RRFs) by $PM_{2.5}$ component (EPA, 2018), a pH_F evaluation can be particularly useful since a bias in pH_F can result in a bias in gas–particle partitioning sensitivity. However, absolute abundances are also important in model applications,

and thus a pH_F evaluation complements evaluation against speciated $PM_{2.5}$ measurements from networks and intensive campaigns.

Figures 18 and 19 show results from four CTMs to give a sense of whether common spatial features exist among models predicting fine particle pH_F. Differences in fine particle pH_F between models are likely caused by differences in model resolution as well as emission and meteorology scenarios as the ISORROPIA II and MESA/MOSAIC thermodynamic models produce similar values (Sect. ~~6~~4). pH_F is strongly influenced by non-volatile cations in broad regions affected by dust and sea spray. Some of the least acidic fine aerosols ($4 < pH_F < 7$) are predicted in sea spray rich regions and where strong westerlies occur over the southern oceans just north of Antarctica. These pH_F values are consistent with those of fresh sea spray shortly (minutes) after emission (pH ~5, Keene et al., 1998). Other areas over the ocean, for example, the northern Pacific south of Alaska, show more acidic aerosol, likely influenced by sulfur from shipping in combination with lower concentrations of sea-spray cations due to colder water temperatures and relatively low wind speed. For all models that include high latitudes in the domain, extremely acidic particles are predicted in the Arctic and over Greenland ($pH_F < 1$). No estimates of Arctic aerosol pH_F are available in the literature, but several studies have inferred low amounts of ammonium and high acidity from proxies (Fisher et al., 2011; Croft et al., 2016), yet sources of NH_3 from seabirds may neutralize particle acidity in the Arctic (Wentworth et al., 2016). Other work has noted that sulfur dioxide is able to escape scavenging more effectively during lifting than ammonia or ammonium sulfate (Park et al., 2004) thus providing for long-range transport of acidity over alkalinity. The decrease in pH_F (increase in acidity) due to scavenging also appears in the westerly outflow from China (Fig. 18), consistent with the higher fraction of soluble iron found in particles collected in the region (Li et al., 2017). A similar pattern is also found in the easterly outflow region from central America (Fig. 18), although observational confirmation is still needed.

Fine mode pH_F downwind of deserts varies by model but is between 4 and 6 for dust-dominant conditions in CMAQ and GEOS-Chem. TM4-ECPL does not include~~s~~ Ca and Mg from dust in the fine mode (external mixture) while it considers those NVCs in the coarse mode calculations of aerosol pH. This assumption leads to an aerosol pH_F in TM4 over the Sahara of ~2-3 for the fine mode and ~6-7 for the coarse mode (Fig. 18c,d) further implying that dust cations, if present and internally mixed in the fine mode, can affect aerosol by ~4 pH_F units (see also Fig. S7 for GEOS-Chem fine aerosol pH predictions with and without dust NVC). pH_F ~6-7 fine aerosols are predicted in GEOS-Chem over the Sahara and Atlantic outflow of dust, most notably in the winter and spring and to a lesser degree in the summer and fall. SO_2 emissions are non-zero in Saudi Arabia (Krotkov et al., 2016) leading to lower pH_F for the middle East compared to other desert regions such as the Sahara.

Anthropogenically-dominated locations, such as Europe, Asia, and the United States show different aerosol pH_F values but are universally predicted to be acidic. All the models in Fig. 18 show a gradient in pH_F over Europe with locations in the northern part of western Europe (near Germany) showing higher predicted fine aerosol pH (pH_F ~2-3) compared to the Mediterranean Sea where pH_F values can be less than 1 and approach 0. This gradient is consistent with enhanced ammonia in northern Europe

(Clarisse et al., 2009) and the limited European pH data, which includes observationally-constrained estimates for Cabauw in the Netherlands (pH_F ~3.6; Guo et al., 2018b), for aerosol extracts from Germany (pH ~1-2; Scheinhardt et al., 2013), and for Finokalia, Crete ($pH_F = 1.25 \pm 1.14$ excluding water associated with organics; Bougiatioti et al., 2016). Predicted aerosol pH_F indicates moderate acidity (pH_F ~3-4) for locations such as Beijing, China and northern India. The eastern U.S. is one of the more acidic anthropogenically dominated locations with $0 < pH_F < 4$ (Fig. 19), consistent with or slightly higher than observationally constrained estimates (Sect. ~~5~~7.1.4). The fine horizontal resolution in WRF-Chem and CMAQ continental U.S. simulations captures localized increases in pH_F due to ammonia from agricultural activity in eastern North Carolina, the Great Plains, Idaho's Snake River Valley, and California's San Joaquin Valley (Fig. 19a,d).

The MOSAIC aerosol model in WRF-Chem provides information on how predicted aerosol pH_F varies among different-size aerosols with different composition (Fig. S8). The $PM_{2.5}$ aerosol pH_F (aerosol water weighted average for bins 0.039–0.156, 0.156–0.625, and 0.625–2.5 μm in diameter, Fig. 19d) shows higher values in regions where NaCl aerosol dominates (off coast of California, over the Great Salt Lake), moderate pH_F values over the Great Plains and off the East Coast, low pH_F in the Ohio River Valley (due to large SO_x emissions and sulfate formation), and the lowest pH_F in the Southwest U.S. (where aerosol water is low). CMAQ (Fig. 19a) predicts similar spatial trends over the U.S. for the fine aerosol pH_F (Aitken + accumulation modes), but generally predicts less spatial heterogeneity with more acidic particles (by ~1-2 pH_F units) over the midwest, and slightly less acidic particles (by ~1 pH_F) in the southwest. GEOS-Chem and WRF-Chem exhibit differences over Nevada of 5 pH_F units during summer. WRF-Chem indicates more acidic particles in the submicron range compared to $PM_{2.5}$. The most notable differences between $PM_{2.5}$ (liquid water weighted sum over bins 1-3) and submicron pH_F (liquid water weighted sum over bins 1-2) in WRF-Chem occur over the oceans, Gulf of Mexico, and Gulf of California where predicted $pH_F > 5.6$ for the larger fine (0.6 to 2.5 μm) bin. Similar values are not seen in the smaller aerosol bins except for one plume of $pH_F > 5.6$ (in bin 2, 0.156–0.625 μm). The two smallest aerosol size bins have very similar pH values over the continent, while the largest fine bin (bin 3) has similar pH values over the continent well inland from the coast and higher pH values near the coasts over land. Similarly TM4-ECPL shows differences of about 4 pH_F units between fine (submicron) and coarse mode particles from Arizona and Montana (Fig. 18c,d). Since different sources contribute differently across the size range, heterogeneity in size resolved pH_F predictions also implies mixing state assumptions in bulk schemes affect pH_F estimates and a single pH_F value across a broad size range does not capture the range of states present in the atmosphere (see also Sect. ~~7~~6 for a discussion on mixing state).

Coarse mode aerosol pH_F in the WRF-Chem MOSAIC (aerosol size bin 4, 2.5–10 μm size range, Fig. 19e) is generally higher than $PM_{2.5}$ values (Fig. 19d), especially over the oceans where NaCl dominates (note that WRF-Chem v4.1 and earlier does not include HCl thereby producing higher aerosol pH_F over oceans than expected). In the more arid regions of the southwest U.S. and northern Mexico, coarse mode aerosol pH_F is quite acidic, while elsewhere over the conterminous U.S. coarse mode aerosol pH_F ranges from 1 to 6, with low values over the Ohio River Valley. Coarse mode aerosol pH_F in TM4-ECPL (Fig.

18d) shows values near 4-6 over the central-western U.S. and Canada and $pH_F < 2$ in the eastern U.S. Coarse mode aerosol pH_F has similarly low values in other anthropogenic regions (part of Europe, India, and East Asia) as well as southern Africa, Indonesia, and most of South America. Over the oceans and remote regions, coarse mode aerosol pH_F predicted by TM4-ECPL has a value of 6 or greater.

~~10.~~2~~8~~.2 Cloud pH

Compared to aerosol pH, cloud pH calculations have a longer history in CTMs and climate models, given that sulfate is the dominant secondary pollutant in fine particulate matter that is produced primarily in cloud droplets. Recent work has shown that when cloud pH increases from a combination of SO_x emission controls and increasing NH_3 from intensified agriculture, the efficiency at which SO_2 converts to sulfate via in-cloud O_3 oxidation can increase thus reducing the effectiveness of SO_x controls close to emission regions (Paulot et al., 2017).

Compared to CTMs, climate models are more limited in their treatment of semi-volatile inorganic species (e.g., particulate nitrate may not be considered as in CAM5; Liu et al., 2012), but generally include sea salt and dust (even if assumed inert) as well as sulfate. Modeling studies of acid rain with regional models (Carmichael and Peters, 1986; Chang et al., 1987; Venkatram et al., 1988) and sulfate production in climate models (Barth et al., 2000; Feichter et al., 1996; Koch et al., 1999) include pH since pH dictates the rate of aqueous reactions that convert SO_2 to sulfate (Sect. ~~3~~5). Early global model studies (Barth et al., 2000; Feichter et al., 1996; Park et al., 2004) either prescribed cloud pH, or diagnosed pH from the concentration of cloud-water S(IV) / S(VI) and assumed ammonium-to-sulfate ratio. Even recent studies (e.g., Turnock et al., 2019) may prescribe cloud pH to simulate sulfate production. In most CTMs, the calculation of cloud pH_F is more comprehensive. Five such models are described here and pH_F estimates are presented in Fig. 20-21. Chemical composition tracked for cloud chemistry can be the same as or different from that used in aerosol chemistry (Table 7).

CESM2.0, including CAM6-chem (released in 2018, Fig. 20a, 21a), includes an updated tropospheric chemistry mechanism (MOZART-T1) and represents aerosols using a Modal Aerosol Model (MAM; Liu et al., 2012; Liu et al., 2016) with 4 lognormal modes and including the species sulfate, ammonium, primary and secondary organic matter, black carbon, soil dust, and sea salt. MAM considers the thermodynamic partitioning of H_2SO_4 (gas) and NH_3. The MAM scheme does include cloud chemistry that represents S(IV) oxidation by ozone and hydrogen peroxide to form sulfate and non-reactive uptake of HNO_3 and NH_3. The pH is estimated using an iterative method to solve the electroneutrality equation using OH^-, HCO_3^-, NO_3^-, HSO_3^-, SO_3^{2-}, SO_4^{2-}, and NH_4^+. The pH_F is determined at each chemistry time step and grid point where liquid cloud water exists.

In CMAQ, there are two varieties of the cloud chemistry module: the default cloud chemistry routine that assumes instantaneous equilibrium to describe the distribution of species between gas/aqueous/ionic forms and the routines that include

kinetic mass transfer (KMT) considerations. CMAQ's default cloud chemistry module is based on the work of Walcek and Taylor (1986). pH_F (Fig. 20b, 21b) is estimated throughout the course of the chemistry calculations by solving the system of nonlinear algebraic equations resulting from electroneutrality and ionic/Henry's Law equilibrium assumptions. Activity coefficients, estimated with the Davies equation, are applied to ionic species in solution. For the standard chemical mechanism (i.e., five S(IV) oxidation reactions and two SOA reactions), the following species are considered in the ion balance and ionic strength calculations: H^+, OH^-, HSO_3^-, SO_3^{2-}, HSO_4^-, SO_4^{2-}, HCO_3^-, CO_3^{2-}, HCO_2^-, NH_4^+, NO_3^-, Cl^-, Ca^{2+}, Na^+, K^+, Mg^{2+}. Fe^{3+} and Mn^{2+}, potentially important players in catalyzing aqueous S oxidation, are included in the ionic strength calculation but do not impact droplet pH_F as they are assumed to be associated with generic anions, A^- and B^-. pH_F evolves as S(IV) is oxidized to S(VI) and additional species are scavenged from interstitial aerosol, allowing species to redistribute between phases and different (non)ionic forms for the duration of cloud processing. In CMAQ's KMT family of cloud chemistry modules, individual species/ions are tracked, including $[H^+]$, and evolve dynamically, using forward and reverse reactions to represent ionic equilibria (Fahey et al., 2017). Initial pH_F is estimated from known concentrations of activated aerosol species (i.e., all accumulation and coarse mode species), and electroneutrality.

Bulk cloud pH_F calculations were first implemented into GEOS-Chem as described in Alexander et al. (2012). Prior to this, cloud pH was assumed to equal 4.5 in GEOS-Chem. In GEOS-Chem (version 12.0.0 with MERRA-2 reanalysis) (Fig. 20c, 21c), bulk cloud pH_F is calculated using local concentrations of SO_4^{2-}, $SO_2(g)$, $NH_3(g)$, NH_4^+, $HNO_3(g)$, NO_3^-, and $CO_2(g)$. The cloud water pH_F calculation utilizes the electroneutrality equation and the following forms of dissolved species (in moles L^{-1}): SO_4^{2-}, OH^-, HCO_3^-, CO_3^{2-}, HSO_3^-, SO_3^{2-}, NO_3^-, NH_4^+. The concentration of HSO_4^- is assumed negligible, which is valid given that most pH_F values > 3 where the second dissociation of sulfuric acid is virtually complete. The model assumes a cloud mass scavenging efficiency of 0.7 for SO_4^{2-}, NO_3^-, and NH_4^+ aerosol based on observations (Hegg and Hobbs, 1986; Hegg et al., 1984; Schumann, 1991; Sellegri et al., 2003). The concentrations of all species but SO_4^{2-} in the electroneutrality equation are calculated based on cloud liquid water content, temperature, each species' effective Henry's law constants. For example, NO_3^- is calculated as follows:

$$[\mathrm{NO_3^-}] = \left(\frac{K_H K_a}{[\mathrm{H^+}]}\right) p_{\mathrm{HNO_3}} \quad (20)$$

where activities are approximated as aqueous concentrations, K_H is the Henry's law constant (Reaction R1) for HNO_3, K_a is the dissociation constant (Reaction R2) for HNO_3, and p_{HNO_3} is the partial pressure of $HNO_3(g)$. The resulting cubic equation is solved numerically. GEOS-Chem does not account for the effect of organic acids or cations originating from sea salt or dust (e.g., Na^+, Ca^{2+}) on cloud water pH_F. HCl is also not part of the cloud pH_F calculation because HCl is not yet a transported species in the standard version of the model (version 12.0.0). This can easily be implemented into the cloud pH_F calculation when the chlorine chemistry in GEOS-Chem is updated (Wang et al., 2019b).

Cloud pH_F in GEOS-Chem (Fig. 20c, 21c), as well as other models, is utilized for the calculation of sulfate production rates from in-cloud oxidation of SO_2(g). Bulk schemes, such as those described above, tend to underestimate sulfate production compared to calculations accounting for heterogeneity in pH with drop size (see Sect. ~~5~~7.2.3 for a discussion of drivers of heterogeneity). To account for this bias, GEOS-Chem utilizes parameterizations developed by Fahey and Pandis (2001) and Yuen et al. (1996). The Fahey and Pandis (2001) parameterization is a decision algorithm that determines whether or not cloud droplet heterogeneity will impact sulfate production rates. The impact of cloud droplet heterogeneity on sulfate production rates tends to be most prevalent in the presence of alkaline aerosols such as sea salt (Alexander et al., 2012; Fahey and Pandis, 2001). If cloud water is acidic enough, heterogeneity will not matter. The Fahey and Pandis (2001) algorithm considered this effect and identifies a condition where bulk cloud pH_F will underestimate sulfate production rates. GEOS-Chem corrects for this low bias in the sulfate production rate utilizing the Yuen et al. (1996) parameterization, which was developed by comparing calculated sulfate production rates from a bulk cloud model with a cloud resolving model that accounts for cloud droplet size heterogeneity. Since the Yuen et al. (1996) parameterization was developed for warm clouds, its use is restricted to temperatures above 268 K in GEOS-Chem. Additionally, the Yuen et al. (1996) parametrization is only used in GEOS-Chem over the oceans, because the parameterization considers alkalinity typical of sea salt aerosols. The impact of cloud droplet heterogeneity on sulfate production rates was implemented into GEOS-Chem by Alexander et al. (2012).

In TM4-ECPL (Fig. 20d, 21d), in-cloud pH_F is controlled by strong acids (SO_4^{2-}, methanesulfonate, HNO_3, NO_3^-), bases (ammonium ion, NH_4^+), as well as by the dissociations of hydrated CO_2, SO_2, NH_3 and of oxalic acid (Myriokefalitakis et al., 2011). Cloud droplet heterogeneity and dust and sea salt aerosol components are not considered for cloud pH_F calculations.

The cloud chemistry configured with the WRF-Chem v3.9.1 with MOZART gas chemistry and 4-bin MOSAIC aerosol scheme is a bulk cloud water approach that is subsequently partitioned into the 4 cloud water bins (which connect to the 4 aerosol size bins). The Fahey and Pandis (2001) aqueous chemistry scheme is implemented and calculates sulfate formation as well as formaldehyde oxidation and non-reactive uptake of nitric acid, hydrochloric acid, ammonia, and other trace gases. The pH_F is found using a bisection method to solve the electroneutrality equation, which includes the following species: OH^-, HCO_3^-, CO_3^{2-}, CO_3^-, HSO_3^-, SO_3^{2-}, HSO_4^-, SO_4^{2-}, SO_4^-, SO_5^-, HSO_5^-, $HOCH_2SO_3^-$, $^-OCH_2SO_3^-$, NO_2^-, NO_3^-, HO_2^-, O_2^-, $HCOO^-$, Cl^-, Cl_2^-, $ClOH^-$, and NH_4^+. While trace metal ion chemistry is included in the aqueous-phase formation of sulfate, these metals are not part of the pH_F calculation. The pH_F is determined at each chemistry time step and grid point where liquid cloud water exists (Fig. 21e).

Model predicted cloud-droplet pH_F (Fig. 20-21) reflects atmospheric sources of inorganic species, similar to fine mode aerosol pH_F, but is further modulated by the presence of clouds and abundance of condensed water. Since cloud droplets are more dilute than particles, pH_F is generally higher than for fine aerosol. The southern ocean clouds have pH_F 4.5-6 with TM4-ECPL showing more acidic cloud droplets ($pH_F = 4.5$) in the southern oceans compared to GEOS-Chem and CAM-Chem (pH_F ~5-

6) due to lack of sea spray and dust aerosol components in TM4-ECPL cloud pH_F calculations. Cloud droplet pH_F is often greater over oceans than continents at the same latitude. GEOS-Chem and CAM-Chem show slightly different north-south trends in cloud pH over the Southern Ocean with GEOS-Chem indicating clouds decrease in acidity from Antarctica to the equator and CAM-Chem indicating increasing acidity. One cloudwater pH measurement gives a value about 5 for off coast of Chile/Peru (~~Fig. 7~~Fig. 15), but more measurements are needed, particularly in the southern hemisphere. Note that CAM-Chem, GEOS-Chem, TM4-ECPL, and WRF-Chem do not include dust cations in the cloud pH calculations (CMAQ does include fine and coarse dust) and deserts and their downwind areas such as the Sahara and western U.S. (e.g., Hand et al., 2017) show diversity on the order of 3-4 pH_F units among the models. Measured cloud pH over northern Africa is 6-7 (~~Fig. 7~~Fig. 15), consistent with CMAQ. TM4-ECPL, which does not consider dust cations in cloud pH calculations, predicts $pH_F < 4$ cloud droplets in arid regions such as over the Sahara, southwest U.S., and inland Asia where liquid cloud water may be very low. Dust regions also coincide with limited cloud coverage so aqueous chemistry is less important. Several models (CMAQ, CAM-Chem, GEOS-Chem, WRF-Chem, TM4-ECPL) correctly capture locally enhanced acidity for the cloud droplets in the vicinity of the Ohio River Valley in the eastern United States as well as in upstate New York at Whiteface Mountain where pH is 4.5-5.0 since 2010 (Table S11). The pH_F gradient from northern to southern Europe is reversed for cloud water compared to aerosols with Germany and Poland showing more acidic cloud droplets than over Italy and Spain (GEOS-Chem, CMAQ, TM4-ECPL). For both clouds and particles, aerosol pH_F is higher in northern China (e.g., Beijing) compared to southern China (e.g., the Pearl River Delta) except in TM4-ECPL. CAM-Chem, CMAQ, GEOS-Chem, and WRF-Chem do not predict present-day average cloud droplet pH_F below 3 (which is not strictly the lower limit in observed cloud pH, ~~Fig. 7~~Fig. 15). For select locations and models (Table S11), predicted cloud pH was generally within 2 pH units of observations and often showed better agreement.

~~10.~~3~~8~~.3 Recommendations for improving models

Evaluation of CTM predictions of fine aerosol pH_F in literature (Table S10) suggest reasonable agreement between models and observations (pH_F within 1 unit for fine aerosols). However, observed estimates of pH_F (Sect. ~~5~~7.1) are extremely limited in location and do not fully cover the diversity of environments and values covered by CTM predictions. Furthermore, the models that have been most evaluated (e.g., CMAQ, GEOS-Chem) tend to use a relatively complete set of inorganic species and advanced thermodynamic routines such as ISORROPIA II but this may not reflect the entire CTM or climate model community (e.g., CAM-Chem). CTM predictions here indicate that assumptions regarding non-volatile cations, from both dust and sea salt, play a large role in CTM predictions of pH_F. Prior to the inclusion of Ca, K, and Mg ions from dust in GEOS-Chem aerosol pH_F calculations (this work, Fig. S7), CMAQ and GEOS-Chem showed large pH_F differences (multiple pH_F units) in dust outflow regions. Similarly, cloud droplet pH_F predictions varied by up to 3-4 pH_F units between models in non-volatile cation-rich environments. Despite cloud droplets generally occupying a smaller range in pH_F than particles (Fig. 2), models examined here provide no indication that cloud droplet pH_F is predicted more consistently across models than aerosol

pH_F. Spatial and temporal variability in clouds, which are challenging to predict and represented differently across models, could contribute to some of this model variability. (Note that for 10 of the 11 cases where select models were compared to observations, models tended to systematically underestimate ~~of~~ or overestimate rather than bracket the observed cloud pH_F value, Table S11). Model-to-model differences in many locations amount to multiple pH_F units and observational constraints would be needed to evaluate models. In addition to measuring inorganic aerosol constituents and gas-phase semi-volatiles to perform thermodynamic calculations, particle mixing state, and cloud properties may also need to be characterized with measurements. Remote locations (including over oceans, most of the southern hemisphere, and likely aloft) are locations with diverse CTM predictions of cloud and particle pH_F and are particularly lacking observational constraints of pH_F.

~~11~~9 Conclusions

Aerosol and cloud acidity are key drivers of atmospheric chemistry and processes that link emissions to impacts on air quality, human health, ecosystems, and climate. Despite their importance, limited information exists on the spatiotemporal distribution of atmospheric acidity, its drivers, and its influences. For aerosol acidity, only recently have data become available that can be used for model evaluation and improvement. This review aims to provide a comprehensive overview of the state of knowledge of atmospheric acidity, considering particulate matter as well as clouds and fogs. Apart from a review of the published literature, the study also includes a rigorous set of definitions for acidity, the methods used to measure and infer the in-situ levels of acidity in each condensed-phase type, and a synthesis and critical evaluation of current estimates. Across the review, the following major messages emerge (see the sections listed for more discussion):

- The various pH definitions in use for characterizing aerosol and cloud-water acidity differ in important ways from each other and from the definition of pH by IUPAC, which is based on the negative base-10 logarithm of the molal activity of H^+. A nomenclature is provided for the community to document how different studies calculate and express aerosol acidity. The use of the definition of pH by IUPAC (Eq. 1), involving the activity coefficient of H^+, is recommended to best and consistently quantify the pH. (Sect. 2.)

- ~~While thermodynamic partitioning and ionic equilibria are the dominant factors that drive aerosol pH levels, models are frequently lacking H^+ that is kinetically generated as a result of transient gas- and liquid-phase chemical reactions. The representation of kinetic processes is necessary to determine sulfate levels important for driving pH. The consequences of varying acidity for organic particle and cloud chemistry have only started to be investigated. (Sect. 3 and companion paper *in prep*.)~~

- Methods for measuring cloud-water pH are relatively established, but methods for measuring aerosol pH remain challenging. Measuring aerosol pH is difficult due to the extremely high ionic strengths that are typically found in aqueous aerosol, the low amounts of mass, and the extreme sensitivity to environmental perturbations, as well as the

chemical heterogeneity found in particles across size, location, and time. Methods for determining the pH of bulk aerosol samples and individual particles continue to be developed and will address an important measurement gap that still exists for determining the acidity of aerosol. Particularly important is the application of such methods to understand the pH environment from particle to particle and within particles, especially under conditions where the aerosol is not at equilibrium or not internally mixed. (Sect. 2, 6, 7~~5, 7~~.)

- None of the observationally-based aerosol acidity proxies in use today are suitable as a universal indicator of pH. Under certain conditions (strongly acidic conditions), certain proxies may be of limited use and when combined with gas-phase measurements exhibit some correlation with pH. However, the uncertainty of these proxies remains very large, and even the best ones require verification with models. The best estimates of particle pH are obtained from thermodynamic model calculations when gas–particle partitioning observations are available for evaluation as well as for constraining the calculations. These estimates generally require a thermodynamic equilibrium assumption, which is reasonable for submicron aerosol. Direct measurement of NH_3 is extremely important, since combined with aerosol data, it provides a constraint on model-derived acidity estimates and a metric for evaluation. Other semi-volatile inorganic acidic gases (like HNO_3 and HCl) also provide constraints on acidity but are subject to higher uncertainty due to interaction with the coarse mode. (Sect. ~~4~~ 3 and elsewhere.)

- Different box model-based estimates of pH using the same inputs differ on average by 0.3 pH units (but can vary up to one pH unit, increasing with decreasing RH) depending on the model framework used and the approach for estimating the H^+ activity coefficient. When single-ion activity coefficients are unavailable, an approximation based on the mean molal activity coefficient of a relevant ion pair (e.g., $\gamma_{\pm}(H^+, Cl^-)$ yielding a $pH_{\pm}$) can reduce the bias in acidity by up to 0.43 pH units for atmospherically relevant conditions. The ion pair that leads to the best single-ion activity coefficient for H^+ may be model dependent; for example, $\gamma_{\pm}(H^+, NO_3^-)$ yields the best $pH_{\pm}$ from ISORROPIA II. (Sect. ~~6~~4.)

- While thermodynamic partitioning and ionic equilibria are the dominant factors that drive aerosol pH levels, models are frequently lacking H^+ that is kinetically generated as a result of transient gas- and liquid-phase chemical reactions. The representation of kinetic processes is necessary to determine sulfate levels important for driving pH. The consequences of varying acidity for organic particle and cloud chemistry have only started to be investigated. (Sect. 5 and companion paper *in prep*.)

- The limited observationally-constrained pH estimates to date establish that acidic aerosol is ubiquitous and can be extremely acidic (pH as low as -1 averaged over long timescales and episodically even lower). Aerosol pH depends on the size, composition, and mixing state of particles. Fine mode aerosols are often dominated by ammonium, sulfate, nitrate, and organics and are systematically more acidic (up to 5 pH units) than coarse mode aerosols, which are rich

in non-volatile cations originating from sea salt and dust. Most observationally-constrained estimates of particle acidity to date are the approximation, pH_F. Since the accuracy of pH_F as a measure of pH depends on RH and composition (Sect. 6), characterization of ambient pH is incomplete. (Sect. ~~5~~7.1.)

- Although aerosols and clouds both tend to be acidic, the response of acidity to changes in precursor emissions is distinctly different in the two media. Published studies suggest that reductions in sulfur dioxide and nitrogen oxide emissions across the U.S. and Canada have had little impact on aerosol pH, and pH is relatively insensitive to ~~ammonia~~ changes in NH_3. Conversely, clouds and fogs exhibit a broad pH range that is quite sensitive to the relative abundance of H_2SO_4, HNO_3, and NH_3 ~~sulfuric and nitric acids and ammonia~~ with multiple locations showing increases in cloud pH as anthropogenic emissions are controlled. This is a direct consequence of the difference in liquid water content which is higher in clouds than fine aerosols~~and other aerosol species being in equilibrium with the ambient relative humidity – while in clouds all the species can vary independently of each other~~. (Sect. ~~5~~7.)

- Large-scale model variation in predicted pH_F, up to 5 pH units in specific locations, is likely not driven by the thermodynamic representations in models, but by the composition that feeds the thermodynamic calculations (especially the emission and microphysical interactions of non-volatile cations with other aerosol components). For locations with observationally-constrained pH estimates, agreement between models and observations can be within one pH unit. In addition, the global acidity distribution in models and observations can be surprisingly similar (Figure 2). Cloud pH does not seem ~~to be~~ better constrained than aerosol pH, suggesting that there is considerable work to be done refining simulations to reach agreement with observational values and trends. Spatial gradients in CTM pH predictions (that do not coincide with availability of measurements) suggest regions where future measurements should be made. The level of agreement required between models and observations depends on the target of a specific assessment (e.g., PM sensitivity to emissions, deposition of nutrients and acidity~~nutrient deposition~~, metals solubility). Therefore, model frameworks should evaluate their endpoint of interest (e.g., ~~nutrient~~ deposition, $PM_{2.5}$ concentration) and consider how an error in predicted pH could lead to a bias. The error in pH may be important for some applications, but not others. (Sect. 8.)

Perhaps one of the more important outcomes of this review is the recognition that cloud and aerosol pH emerge as an important property for influencing a wide range of CTM predictions, and therefore improvements to how aerosol and cloud pH are represented in CTMs could potentially enhance policy and programs informed by these models. pH determines the innate response of a model to emission changes, can provide insights that established approaches (evaluation of gas/aerosol composition) are not able to provide, and determines the chemical regime for PM formation, ~~nutrient~~ deposition, and soluble metals. Including and reporting pH (or an approximation thereof) in future studies will increase the understanding of the effects of emissions, human activity, and climate change on society and the Earth System as a whole.

Appendix A: Nomenclature

Symbol	Description
a_{H^+}	The activity of hydrogen ions in aqueous solution on a molality basis
$a_{H^+}^{(c)}$	The activity of H^+ ions on a molarity (concentration) basis
$a_{H^+}^{(x)}$	The activity of H^+ ions on a mole fraction basis
α_{HSO4}	Fraction of HSO_4^- dissociated into H^+ and SO_4^{2-}
a_i	The activity of species *i* (usually molality-based for ions in aqueous solutions)
ACSM	Aerosol chemical speciation monitor
adjGR	Adjusted gas ratio (see Table 3)
ALPHA	Adapted Low-cost Passive High-Absorption
ALWC	Aerosol liquid water content (mass per volume of air)
AMS	Aerosol mass spectrometer
$c^{\ominus}$	The standard state (unit) molarity
c_{H^+}	The molarity or "molar concentration" of hydrogen ions in an aqueous solution (also written using square brackets as $[H^+]$)
CCN	Cloud condensation nuclei
CTM	Chemical transport model
DELTA	Denuder for Long Term Atmospheric sampling
DON	Degree of neutralization (see Table 3)
DSN	Degree of sulfate neutralization (see Table 3)
$f_{H^+}^*$	The (rational) activity coefficient based on the mole fraction concentration scale
$F_{p,i}$	Fraction of species *i* in the particle vs particle + gas phase
FR	Flex Ratio, identifies the NH_3 emissions level at which the nitrate concentration switches from NH_3-insensitive (or negative sensitivity) to positive NH_3 sensitivity
~~$f_{H^+}^*$~~	~~The (rational) activity coefficient based on the mole fraction concentration scale~~
GR	Gas ratio (see Table 3)
H^+_{air}	Concentration of aerosol H^+ per volume of air (e.g., moles per m^{-3} of air)
$H^+_{air,cb}$	H^+_{air} determined from charge balance (see Table 3)

Formatted: Normal
Formatted: Left
Formatted Table
Formatted: Font: Times New Roman
Formatted: Subscript
Formatted: Font: Italic

HO_x	Hydrogen oxides ($OH + HO_2$)
IN	Ice nuclei
K_a	Acid dissociation constant for $HX \rightleftharpoons H^+ + X^-$
K_b	Acid association constant for $H^+ + X^- \rightleftharpoons HX$ or $H^+ + X \rightleftharpoons XH^+$
K_H	Dimensionless Henry's law constant
K_w	Activity-based equilibrium constant for the dissociation of water into H^+ and OH^- (see Bandura and Lvov (2005) for tabulation of values)
~~LLPS~~	~~Liquid–liquid phase separation~~
KMT	Kinetic mass transfer
LLPS	Liquid–liquid phase separation
$m^{\ominus}$	The standard state (unit) molality
m_{H^+}	Molality of H^+ (mol kg^{-1} solvent)
M_w	Molar mass of water: 0.018015 kg mol^{-1}
n_i	Number (e.g., moles) of species i
NEI	National Emission Inventory (for the United States)
NO_x	Nitrogen oxides ($NO + NO_2$)
NVC	Non-volatile cations
PAHs	polycyclic aromatic hydrocarbons
PFASs	polyfluoroalkyl substances
PFSAs	Perfluoroalkyl sulfonic acids~~perfluroroalkane sulfonic acid~~
PFCAs	Perfluoroalkyl carboxylic acids
pH	Hydrogen ion potential with activity coefficient and concentration expressed on a molality concentration scale (see Table 1)
pH_c	pH on a concentration (molarity) basis
pH_x	pH on a mole fraction basis
pH_T	"Total" pH based on the molality of sulfate and bisulfate ions (see Table 1)
pH_F	"Free ion" approximation of pH obtained when the activity coefficient of H^+ is unity (see Table 1)
$pH_{\pm}(H, X)$	Approximation of pH using the mean molal ion activity coefficient of an H^+ and anion X pair (see Table 1)

Formatted: Subscript
Formatted: Subscript
Formatted: Font: Italic
Formatted Table
Formatted: Font: Italic, Subscript
Formatted: Superscript
Formatted: Superscript
Formatted: Subscript
Formatted: Superscript
Formatted: Font: Italic
Formatted: Font: Italic, Subscript

pK_{wi}	-$\log_{10}$ of (K_w K_i) (see Bandura and Lvov (2005) for tabulation of values)
PM	Particulate matter, synonymous with aerosol
PM_1	Particulate mass with an equivalent diameter below 1 μm
$PM_{2.5}$	Particulate mass with an aerodynamic equivalent diameter below 2.5 μm
PSC	Pitzer-Simonson-Clegg (model)
R	Universal gas constant
r^2	Coefficient of determination
RH	Relative humidity
RRF	Relative response factor, relative change in concentration due to relative change in emission
SO_x	Sulfur oxides (usually SO_2 + TSO_4)
T	Temperature
TMI	Transition Metal Ions
TCl	Total chloride (sum of gas-phase hydrochloric acid and aerosol chloride)
TNO_3	Total nitrate (sum of gas-phase nitric acid and particulate nitrate)
TNH_4	Total ammonia (sum of gas-phase ammonia and particulate ammonium)
TSO_4	Total particulate sulfate (sum of sulfate and bisulfate)
VOCs	Volatile organic compounds
WSOC	Water-soluble organic compounds
x_{H^+}	The mole fraction of H^+ in the solution
X_T	Molal sulfate ratio indicating sulfate- rich vs poor domain (Eq. 9)
Z	Charge balance on total gas and particle phases used to estimate initial amount of H^+ (Eq. 19)
ZSR	Zdanovskii-Stokes-Robinson (method for calculation of aerosol water)
γ_{H^+}	The molal activity coefficient of species i
$\gamma_{H^+}^{(c)}$	The molarity-based activity coefficient of H^+
$\gamma_{\pm,HX}$	The mean Single ion activity coefficient (for monovalent acid HX)
ρ_0	The density of the reference solvent (water)

Formatted: Font: Italic
Formatted: Superscript
Formatted: Subscript
Formatted: Subscript
Formatted: Subscript
Formatted: Font: Italic
Formatted: Font: Italic
Formatted: Font: Italic

Appendix B: Models, data, and related methods discussed in the text

Type	Examples
Activity coefficient models	AIOMFAC, UNIFAC
Gas-particle thermodynamic models	AIOMFAC-GLE, ADDEM, E-AIM, EQSAM, EQUISOLV II, GFEMN, ISORROPIA II, MOSAIC, SCAPE, UHAERO
3-D models	CAM-Chem, CESM, CMAQ, GEOS-Chem, GISS, PM-CAMx, TM4-ECPL, ~~WRF-Chem~~
Supporting algorithms/chemistry/databases	ASTEM, CAM6, HETV, MAM, MESA, MOZART, MTEM, SPECIATE
Observational data sets (networks, satellites, field campaigns)	ACTRIS, AIRS, AMoN, CalNex, CASTNET, CrIS, CSN, EMEP/EBAS, IASI, IMPROVE, MAN, NAMN, SEARCH, SEAC4RS, SOAS, WINTER

Formatted: No underline
Formatted: No underline
Formatted: Font: Bold, No underline
Formatted Table
Formatted: Font: Bold, No underline
Formatted: Right: 0.05"
Formatted: No underline
Formatted: Right: 0.05"
Formatted: No underline
Formatted: Font: Not Bold
Formatted: No underline
Formatted: No underline
Formatted: Right: 0.05"
Formatted: Font: Not Bold
Formatted: No underline
Formatted: No underline
Formatted: Right: 0.05"
Formatted: No underline
Formatted: Font: Not Bold
Formatted: No underline
Formatted: Right: 0.05"
Formatted: No underline
Formatted: No underline
Formatted: Font: Not Italic

Code and data availability.
E-AIM can be run at http://www.aim.env.uea.ac.uk/aim/.

AIOMFAC can be run at https://aiomfac.lab.mcgill.ca for single liquid phases; code is available at https://github.com/andizuend/AIOMFAC.

MOSAIC is available upon request from its author (Rahul Zaveri).

ISORROPIAII is available at http://isorropia.epfl.ch (access to source code requires login provided by AN upon request).

EQUISOLV II output was obtained from its creator, Mark Jacobson (jacobson@stanford.edu).

CAM6-Chem code is available as part of CESM available at http://github.com/ESCOMP/cesm.

CMAQ v5.2 and v5.3 code is available at https://github.com/USEPA/CMAQ and at doi:10.5281/zenodo.107987.

GEOS-Chem code is available at https://github.com/geoschem.

TM4-ECPL code is available from its authors (Stelios Myriokefalitakis and Maria Kanakidou) upon request

Instructions for obtaining WRF-Chem are available at http://www2.mmm.ucar.edu/wrf/users/download/get_source.html.

Box model inputs used in Sect. ~~6~~ 4 and observed cloud and fine aerosol pH estimates from literature (Section 7) will be deposited in electronic tabular format in the Environmental Protection Agency Science Hub repository upon final publication (https://catalog.data.gov/harvest/about/epasciencehub, doi:10.23719/1504059).

Supplement. The supplement related to this article is available online and includes additional documentation for definitions of pH, methods used to estimate sulfur production as a function of pH (~~Fig. 3~~Fig. 9), and details regarding the proxy evaluation (~~Fig. 15~~Fig. 8). In addition, figures further exploring the gas ratio, suitability of pH approximations, an ISORROPIA–MOSIAC intercomparison, and additional CTM predictions are shown. Data used as box model input (idealized scenarios), to create spatial maps of particle and cloud pH, and for CTM-observation comparisons of pH are available in the supplement.

Author contributions. HOTP provided overall project coordination including preparation and finalization of synthesized drafts. HOTP and AN designed the overall scope of this study. AN coordinated the supplement. JW and JK led Sect. 1 on the importance of acidity with contributions from AN. AZ led Sect. 2 on definitions of pH. ~~VFM led Sect. 3 on the role of kinetics and mechanisms of pH.~~ CH led Sect. ~~4~~ 3 on proxies of pH. AN led Sect. 4 on the box model intercomparison. Section 4 contains significant portions of text originally created by the Sect. 2 (idealized scenario calculations) and Sect. 3 (proxy calculations) teams. VFM led Sect. 5 on the role of kinetics and mechanisms of pH. RAZ led Sect. 6 on the role of particle size and mixing state. MK and AN led Sect. ~~5~~7.1 on observations of atmospheric particle pH. JC led Sect. ~~5~~7.2 on observations of cloud water pH. ~~AN led Sect. 6 on the box model intercomparison. Section 6 contains significant portions of text originally created by the Sect. 2 (idealized scenario calculations) and Sect. 4 (proxy calculations) teams. RAZ led Sect. 7 on the role of particle size and mixing state.~~ HOTP led Sect. 8 on large-scale model predictions of pH. Major messages (Sect. 9) written by

AN, were created at a workshop organized by HOTP and hosted at EPA in Research Triangle Park. Authors prepared text, figures, and tables in collaboration.

Competing interests. The authors declare that they have no conflict of interest.

Disclaimer. The U.S. Environmental Protection Agency through its Office of Research and Development collaborated in the research described here. The research has been subjected to Agency administrative review and approved for publication but may not necessarily reflect official Agency policy. The views expressed in this article are those of the authors and do not necessarily represent the views or policies of the U.S. Environmental Protection Agency.

Acknowledgements. We thank the EPA for funding and hosting the workshop *The State of Acidity in the Atmosphere: Particles and Clouds* and Ken Elstein, Brooke Hemming, and Randa Boykin for their assistance during the workshop. We thank Chris Nolte and Donna Schwede for helpful comments on the manuscript during EPA internal review. We are grateful to Mark Z. Jacobson for participating in the model intercomparison (section ~~6~~4) and for providing the results of EQUISOLV II calculations. We thank Barron Henderson for assistance with CMAQ plots, Homaira Sharif for assistance with reference formatting in the main text, and Bo Xu for help assembling the appendix. We thank Barron Henderson and Sharon Phillips for their technical leadership on EPA contracts resulting in CMAQv5.2 output for hemispheric and continental US simulations, respectively. AN was supported by the project PyroTRACH (ERC-2016-COG) funded by H2020-EU.1.1. – Excellent Science – European Research Council (ERC), project ID 726165. The work by JC and ITK was supported by grant number NSF-AGS-1650786. CJH acknowledges support from the National Science Foundation through project CHE-1454763. NR acknowledges support from NSF AGS-1254428. AZ acknowledges support by the Natural Sciences and Engineering Research Council of Canada (NSERC, RGPIN/04315-2014). TW acknowledges support by the Hong Kong Research Grants Council (T24-504/17-N). RAZ acknowledges support from the Office of Science of the U.S. Department of Energy as part of the Atmospheric System Research program (DE-AC05-76RL01830).

Figures

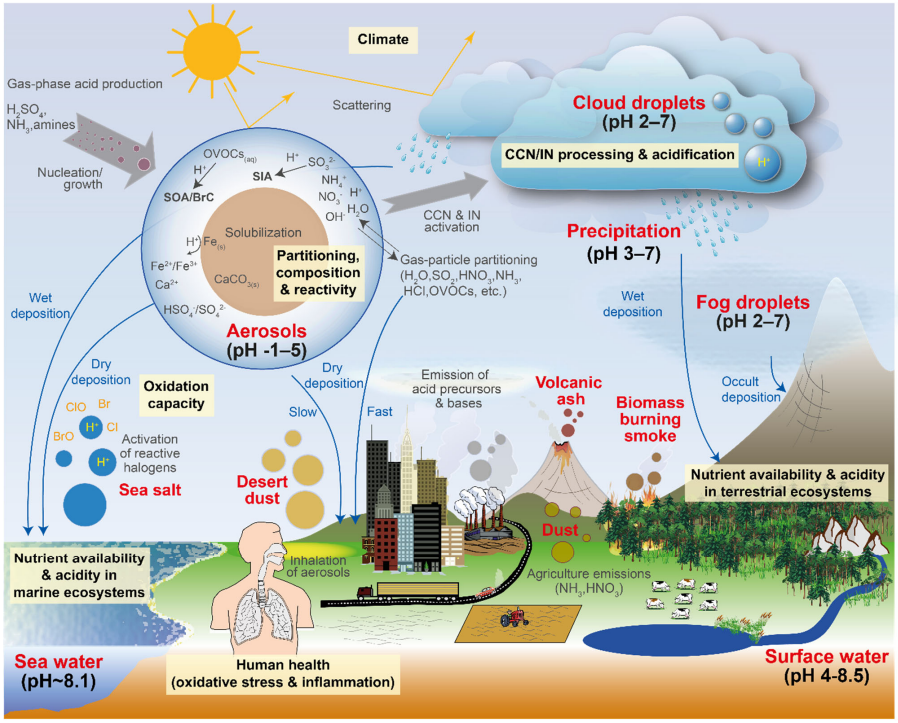

Figure 1. Sources and receptors of aerosol and cloud droplet acidity. Major primary sources and occurrence in the atmosphere are identified in bold red text: sea salt, dust, biomass burning (sources); and aerosols, fog droplets, cloud droplets, precipitation (occurrence). Key aerosol processes are indicated by arrows and grey text: nucleation/growth, light scattering, CCN and ice nuclei (IN) activation, and gas–particle partitioning. ~~The aerosol~~S ~~s~~inks (wet, dry and occult deposition) are indicated by blue lines and text. The effects that aerosols have in the atmosphere, and on terrestrial and marine ecosystems and human health, are highlighted in yellow. Approximate pH ranges of aqueous aerosols and droplets, seawater, and terrestrial surface waters are also given.

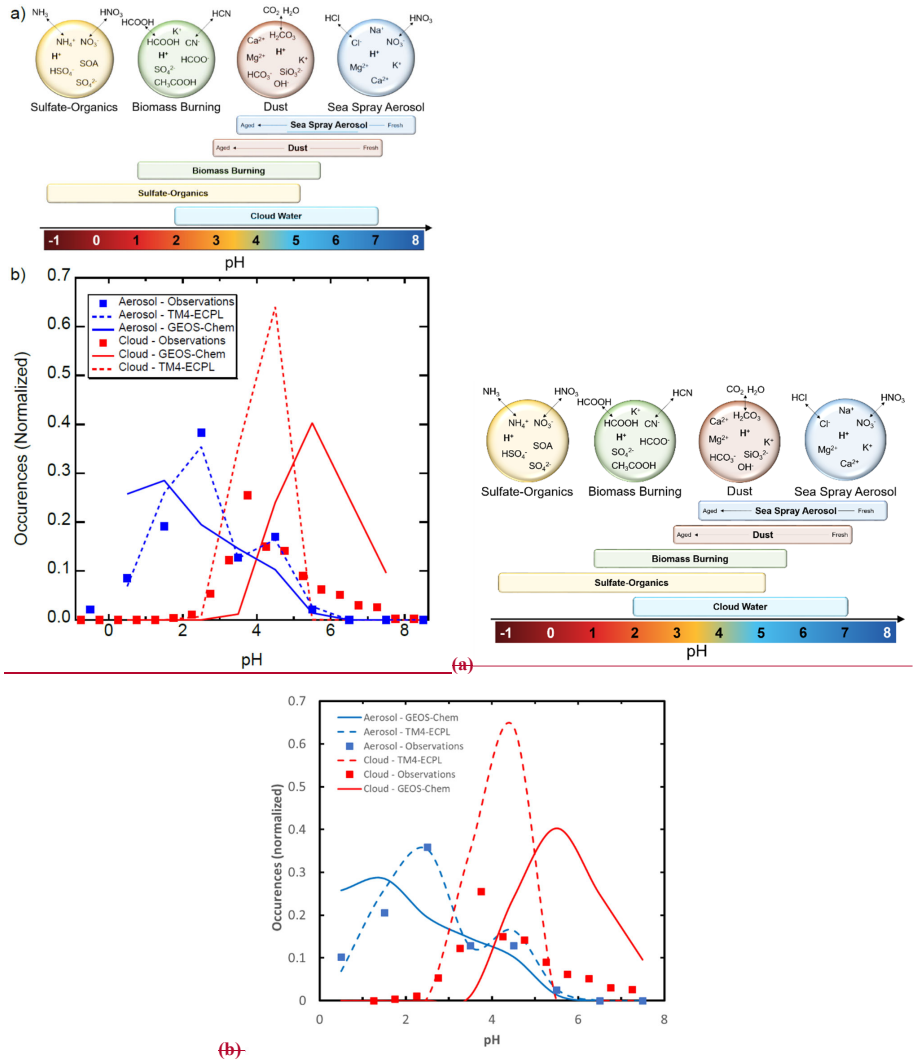
a)
Sulfate-Organics
Biomass Burning
Dust
Sea Spray Aerosol
Aged
Sea Spray Aerosol
Fresh
Aged
Dust
Fresh
Biomass Burning
Sulfate-Organics
Cloud Water
-1 0 1 2 3 4 5 6 7 8
pH
b)
Occurences (Normalized)
Aerosol - Observations
Aerosol - TM4-ECPL
Aerosol - GEOS-Chem
Cloud - Observations
Cloud - GEOS-Chem
Cloud - TM4-ECPL
pH
Sulfate-Organics
Biomass Burning
Dust
Sea Spray Aerosol
Sea Spray Aerosol
Dust
Biomass Burning
Sulfate-Organics
Cloud Water
pH

~~(a)~~

Occurences (normalized)
Aerosol - GEOS-Chem
Aerosol - TM4-ECPL
Aerosol - Observations
Cloud - TM4-ECPL
Cloud - Observations
Cloud - GEOS-Chem
pH

~~(b)~~

Figure 2. Characteristics of (a) aerosol and cloud pH drivers and (b) global distribution of fine-mode aerosol (ground level) and cloudwater pH (column average weighted by liquid water content) from observations (Sect. 57) and global simulations (Sect. 8).

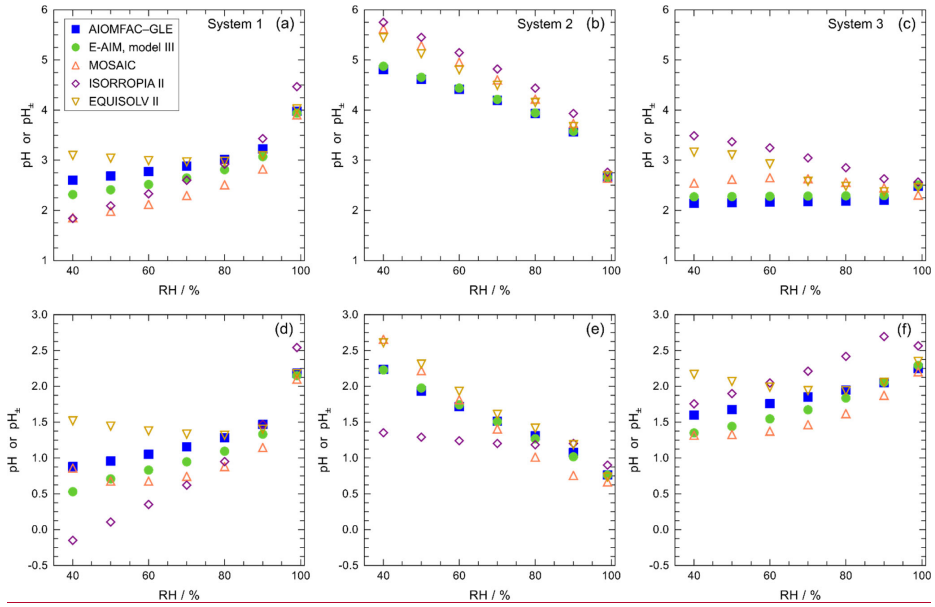

Figure 3. Comparison of pH predictions by six aerosol thermodynamics models for seven RH levels, including gas–liquid partitioning of volatile components (see details in Table 4). Upper panels show moderately acidic cases, lower panels highly acidic cases (with different *y*-axis scaling). Systems are described in Sect. 4.1: (a, d) system 1 is sulfate-rich aqueous $(NH_4)_2SO_4 + H_2SO_4 + NH_3$; (b, e) system 2 is acidified sea-salt-like aqueous aerosol $(Na_2SO_4 + NaCl + H_2SO_4 + HCl)$; (c, f) system 3 is nitrate-rich aqueous $(NH_4)_2SO_4 + H_2SO_4 + NH_3 + HNO_3$. Models E-AIM and AIOMFAC-GLE (solid symbols, green and blue respectively) predict pH based on the single-ion activity coefficient of H^+, the other models (open symbols, MOSAIC in upward orange triangle, ISORROPIA II in purple diamond, EQUISOLV II in downward yellow triangle) approximate pH by a version of pH_S; the specific mean ion activity coefficients used for pH_S by those models are listed in supplemental Tables S3 – S5 for each system.

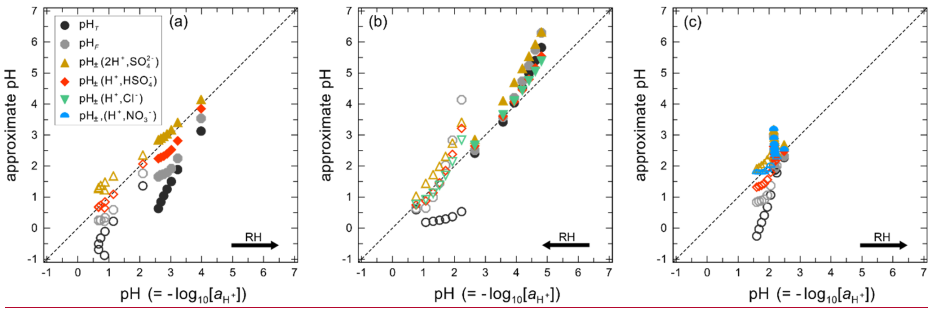

Figure 4. Comparison of different approximate pH values *vs*. the molal pH by system (panels a, b, c for system 1, 2 ,3) introduced in Sect. 4.1 and also shown in Fig. 3, all calculated by AIOMFAC–GLE. Solid symbols show the moderately acidic cases and open symbols the highly acidic cases. pH approximations are based on total H^+ (pH_T), free H^+ (pH_F), and pH_S (defined in Table 1). For the pH_S variants, the H^+ activity coefficient was approximated by the mean molal activity coefficient of H^+ combined with either SO_4^{2-}, HSO_4^-, Cl^- or NO_3^- (Cl^- only for system 2; NO_3^- only for system 3). Arrows on the lower right indicate the relationship between increasing RH and pH for each system; the highest RH shown is 99 % in all cases. Colors indicate different pH approximations (pH_T vs pH_F vs pH_S) including activity coefficient approximations based on different ion pairs (for pH_S).

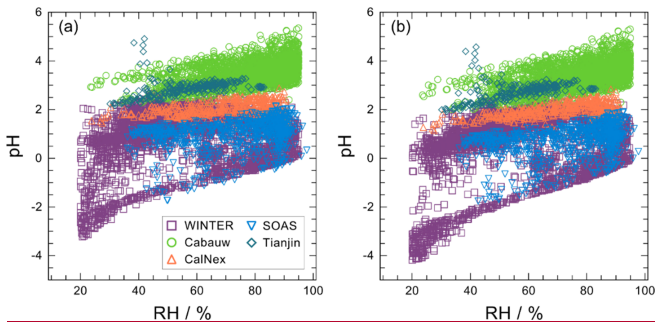

Figure 5. A comparison of calculated pH using (a) AIOMFAC-GLE, and (b) E-AIM as a function of RH for all field campaign datasets examined (SOAS Centreville, Cabauw, CalNex, Tianjin and WINTER, see Sect. 4.2 and Table 5 for a description of the data sets).

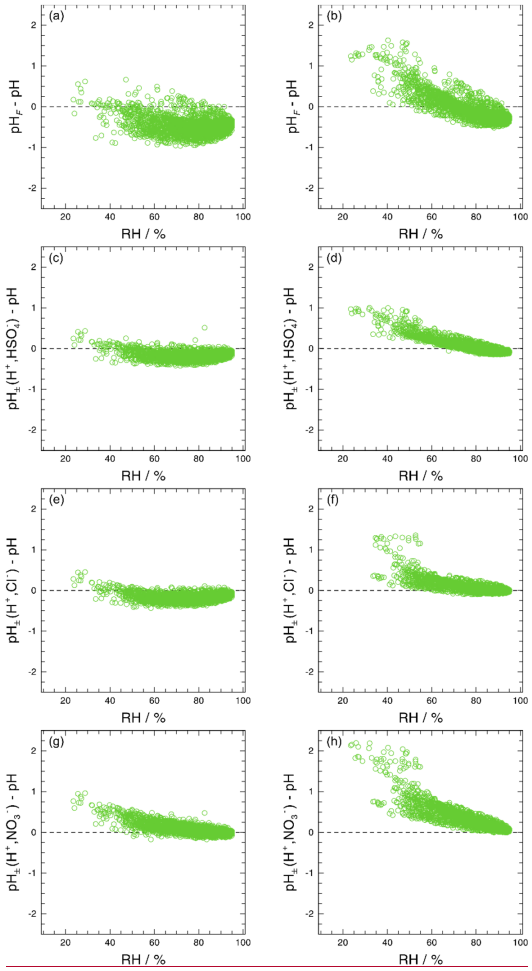

Figure 6. Comparison of different approximate metrics of pH, using the Cabauw data and calculated by AIOMFAC-GLE (left column), and E-AIM (right column). The results are shown as differences from pH as follows: (a, b) pH_F - pH; (c, d) $pH_{\pm}(H^+,HSO_4^-)$ - pH; (e, f) $pH_{\pm}(H^+,Cl^-)$ - pH; (g, h) $pH_{\pm}(H^+,NO_3^-)$ - pH.

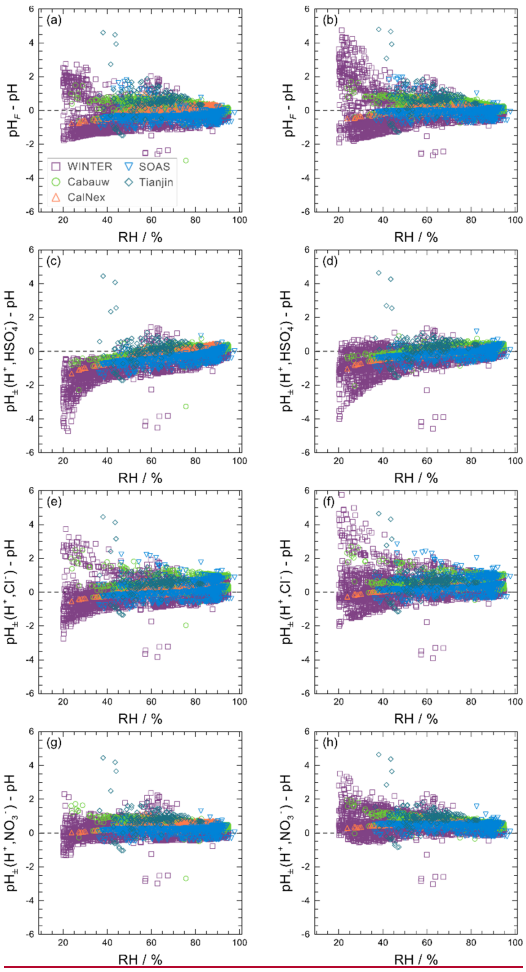

Figure 7. ISORROPIA-calculated pH using the different metrics, and its difference against pH values calculated with AIOMFAC-GLE (left column) and, E-AIM (right column). Data shown for all the field campaign observations considered in this study (Table 5).

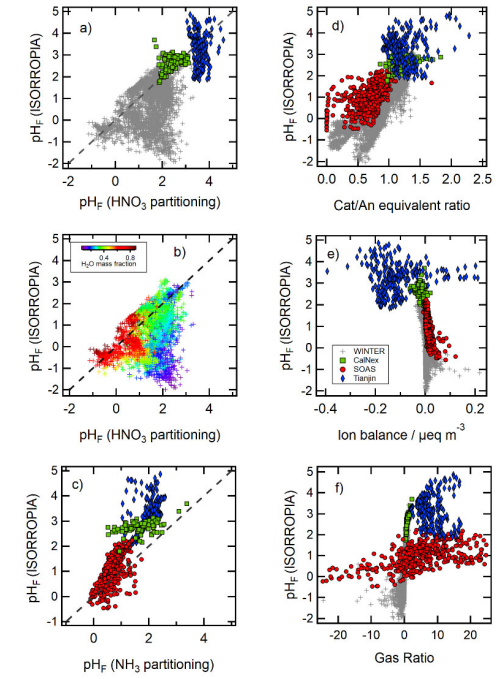

Figure 8. Comparison of pH_F calculated by ISORROPIA with proxies: (a-b) pH_F calculated using HNO_3 partitioning (Eq. 16), (c) pH_F calculated using NH_3 partitioning (Eq. 18), (d) cation/anion equivalent ratio, (e) ion balance (charge balance), and (f) gas ratio (GR). The ambient data sets are described in detail in Table 5. The proxy methods were calculated as in Table 3, unless otherwise stated. Note the convention for the ion balance calculation in (e) results in a positive value when there is a cation deficit. The dotted lines in a-c represent the 1:1 line, shown for visual effect. The legend in panel (e) applies to all panels except (b), which only shows data for the WINTER data set, colored according to the aerosol water mass fraction (relative to the total predicted aerosol mass). In panel (f), 8 (out of 3626 total) points for the WINTER data set and 98 (out of 587 total) points for the SOAS data set are off scale, for clarity.

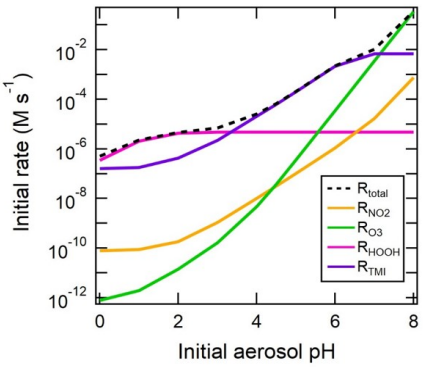

Figure ~~39~~. The rates of four in-particle sulfate production pathways (oxidation by O_3, NO_3, and HOOH and catalyzed by transition metal ions (TMI) Fe(III) and Mn(II)) as a function of initial aerosol pH, for Beijing winter haze conditions. See Supporting Information Sect. S2 for more details.

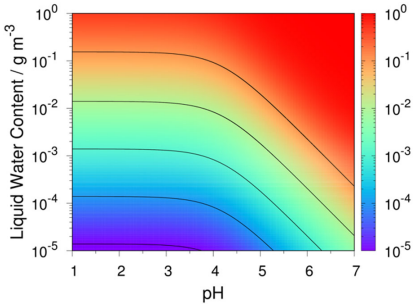

Figure 410. Calculated dissolved aqueous-phase fraction of benzoic acid as a function of liquid water content and aqueous phase acidity. The black lines are the isolines of the aqueous fractions of 10^{-i} (i = 1,...,6).

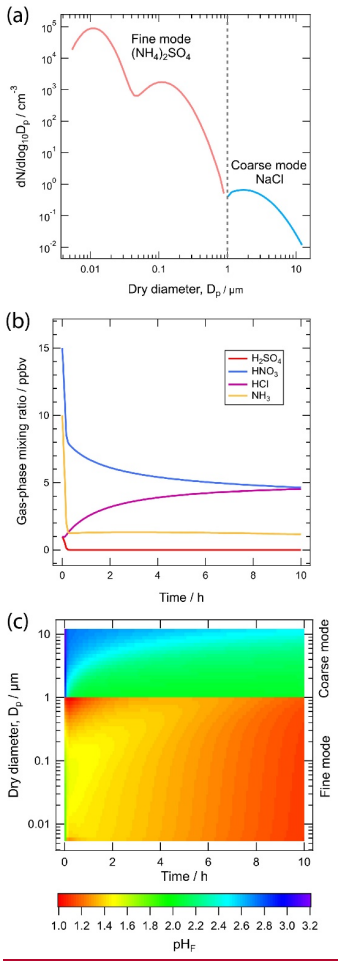

Figure 11. Simulated evolution of size-distributed aerosol pH using the sectional MOSAIC aerosol box model: (a) Initial aerosol number size distributions for the fine and coarse modes, (b) Time evolution of gas-phase species, and (c) Time evolution of aerosol pH as a function of size (bins labeled based on what was initially in the fine and coarse modes).

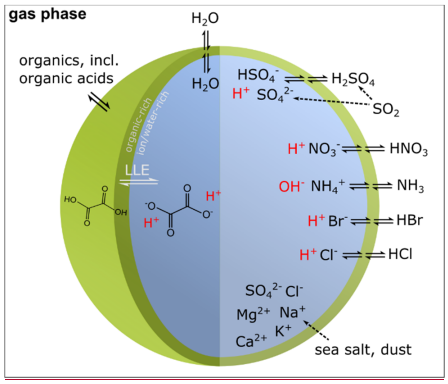

Figure 12. Sketch of a multicomponent aerosol particle consisting of an organic-rich and an aqueous inorganic-ion rich phase in LLPS; here adopting a core–shell morphology. Shown are equilibria of water, organic compounds, as well as inorganic acids and bases contributing to the overall particulate matter mass, ionic strength and the pH. The dynamically established pH exerts control on the gas–particle partitioning of semi-volatile acids and bases, such as HNO_3, HCl and NH_3. All species may partition into all phases; however, inorganic ions tend to favour the aqueous phase, while organic compounds of moderate to low polarity will predominantly partition to an organic-rich phase.

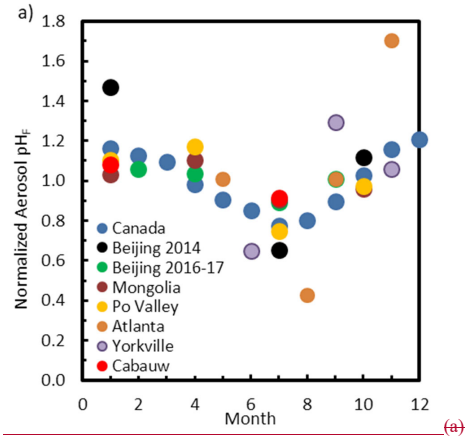
a)
Normalized Aerosol pH$_F$
Month
Canada
Beijing 2014
Beijing 2016-17
Mongolia
Po Valley
Atlanta
Yorkville
Cabauw

(a)

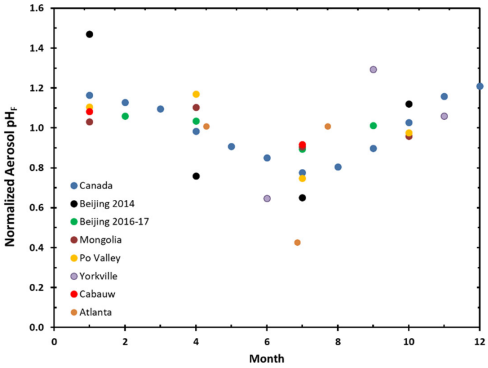
Normalized Aerosol pH$_F$
Month
Canada
Beijing 2014
Beijing 2016-17
Mongolia
Po Valley
Yorkville
Cabauw
Atlanta

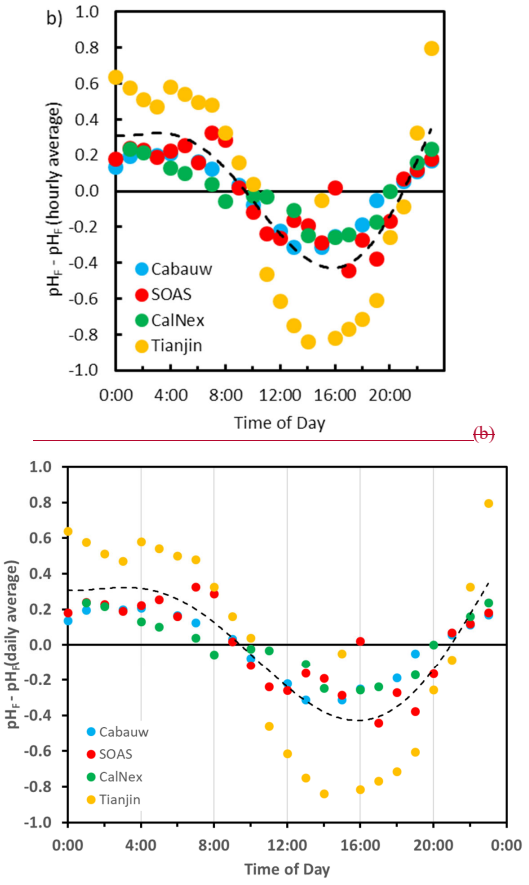

Figure ~~5~~13. (a) Seasonality of fine aerosol acidity (pH_F ~~normalized to the~~divided by the annual average) from the literature. Annual average pH for Canada (Tao and Murphy, 2019b), Beijing 2014 (Tan et al., 2018), Beijing 2016-2017 (Ding et al., 2019), Inner Mongolia (Wang et al., 2019a), Po Valley (Squizzato et al., 2013), Cabauw (Guo et al., 2018b), Atlanta (Guo et al., 2015), and Yorkville (Guo et al., 2015; Nah et al., 2018) is 2.5, 2.8, 4.3, 5.5, 3.1, 3.6, 1.3, 1.7, respectively. (b) Diurnal cycle of aerosol pH_F at four select sites (see Sect. ~~5~~ 7 and Table S6 for a description of data), expressed as the departure from its daily ~~mean~~ average diurnal value (3.7, 0.6, 2.1, 3.2, for Cabauw (Guo et al., 2018b), SOAS-Centreville (Guo et al., 2015), CalNex-Pasadena (Guo et al., 2017b), and Tianjin

(Shi et al., ~~2017~~2019), respectively). In deriving the diurnal profiles, each dataset is grouped in hourly bins, from which average hourly values are calculated. Estimates are pH_F except for Tao and Murphy (2019b) who estimate pH.

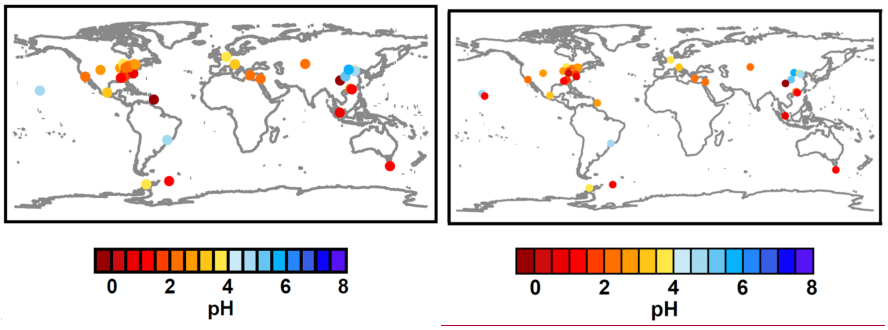

~~Figure 6~~Figure 14. Observationally estimated ground-level fine aerosol pH. Estimates are primarily based on observationally-constrained thermodynamic equilibrium model predictions reported as pH_F. Values correspond to present-day conditions. Measurement locations, measurement time periods, reported pH values, and citations are listed in Table S6. Values shown in the Figure will be available in tabular format via data.gov (see data availability statement).

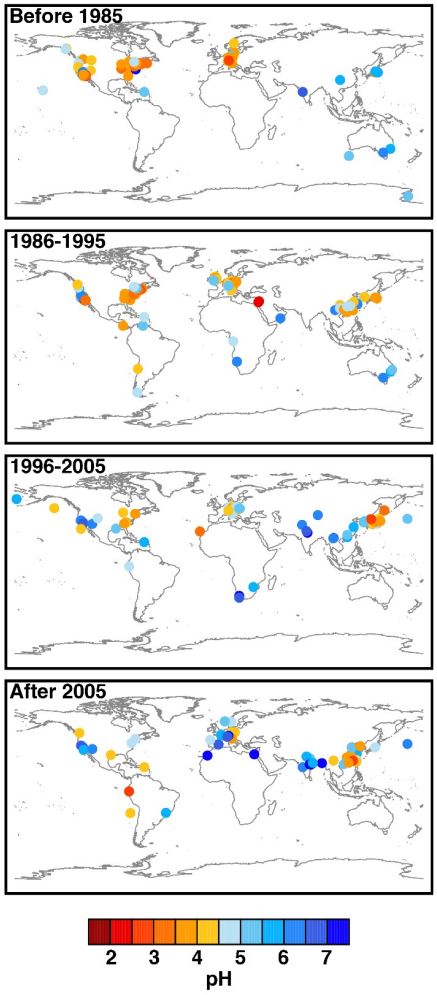

~~Figure 7~~Figure 15. Values of pH in fog and cloud water samples collected around the globe. The measurements are divided into 4 time periods to provide better comparison across an era of changing anthropogenic emissions. Plotted points represent

reported mean pH values. In cases where mean pH was not reported or calculable from reported data, either the reported median pH or the average of reported minimum and maximum H^+ concentrations converted to pH are plotted. Measurement locations, measurement time periods, reported pH values, and citations are listed in Table S8. Values shown will be available in tabular format via data.gov (see data availability statement).

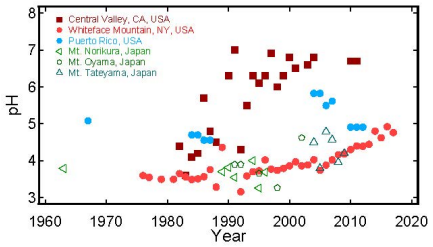

~~Figure 8~~Figure 16**.** Mean cloud/fog pH values reported for individual measurement locations and years, from the 1960s to present. Sites are included from the western and northeastern United States, from the Caribbean island of Puerto Rico, and from locations in central Japan. See text and Table S8 for references.

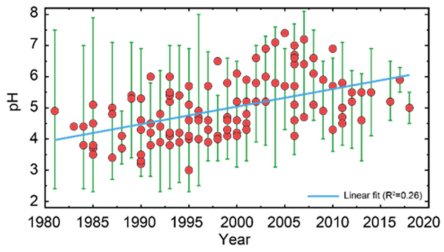

~~Figure 9~~Figure 17. Trend in measured pH values of fogs and clouds sampled in Europe from the 1980s to present. See Table S8 for a list of sites and references. The dots represent the average or median values measured at the site and the green interval bars the range (minimum, maximum) in the reported data distributions. The trend line indicates an increase of approximately 0.56 pH units per decade.

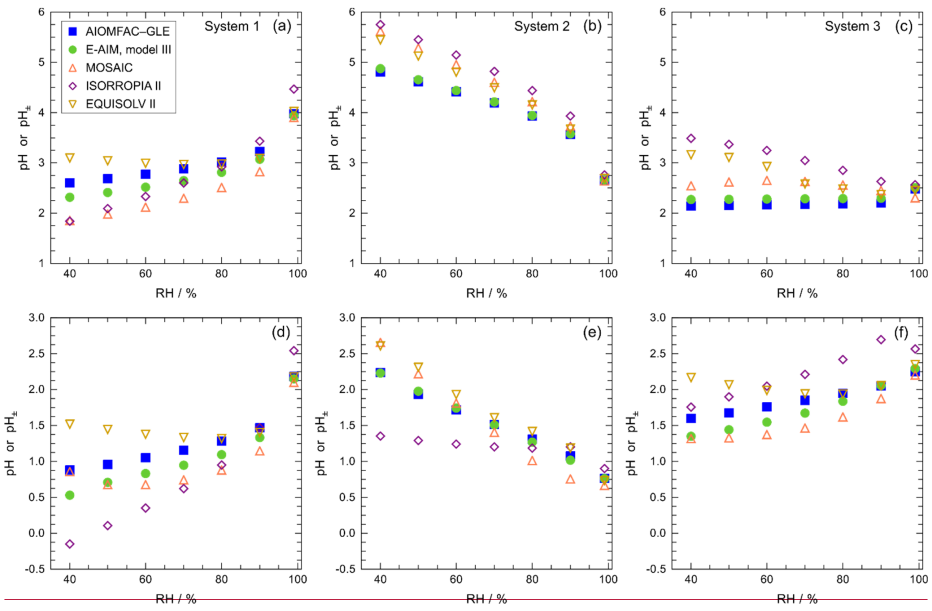

Figure 10. Comparison of pH predictions by six aerosol thermodynamics models for seven RH levels, including gas–liquid partitioning of volatile components (see details in Table 3). Upper panels show moderately acidic cases, lower panels highly acidic cases (with different *y*-axis scaling). Systems are described in Sect. 6.1: (a, d) System 1: sulfate-rich aqueous $(NH_4)_2SO_4 + H_2SO_4 + NH_3$; (b, e) system 2: acidified sea-salt-like aqueous aerosol $(Na_2SO_4 + NaCl + H_2SO_4 + HCl)$; (c, f) system 3: nitrate-rich aqueous $(NH_4)_2SO_4 + H_2SO_4 + NH_3 + HNO_3$. Models E-AIM and AIOMFAC (solid symbols, green and blue respectively) predict pH based on the single-ion activity coefficient of H^+, the other models (open symbols, MOSAIC in upward orange triangle, ISORROPIA II in purple diamond, EQUISOLV II in downward yellow triangle) approximate pH by a version of pH_x; the specific mean ion activity coefficients used for pH_x by those models are listed in supplemental Tables S3 – S5 for each system.

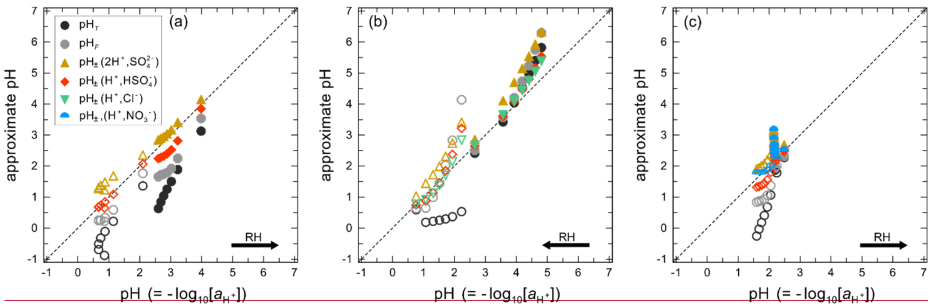

Figure 11. Comparison of different approximate pH values *vs.* the molal pH by system (panels a, b, c for system 1, 2 ,3) introduced in Sect. 6.1 and also shown in Fig. 10, all calculated by AIOMFAC-GLE. Solid symbols show the moderately acidic cases and open symbols the highly acidic cases. pH approximations are based on total H^+ (pH_T), free H^+ (pH_F), and pH_∞ (defined in Table 1). For the pH_∞ variants, the H^+ activity coefficient was approximated by the mean molal activity coefficient of H^+ combined with either SO_4^{2-}, HSO_4^-, Cl^- or NO_3^- (Cl^- only for system 2; NO_3^- only for system 3). Arrows on the lower right indicate the relationship between increasing RH and pH for each system; the highest RH shown is 99 % in all cases. Colors indicate different pH approximations (pH_T vs pH_F vs pH_∞) including activity coefficient approximations based on different ion pairs (for pH_∞).

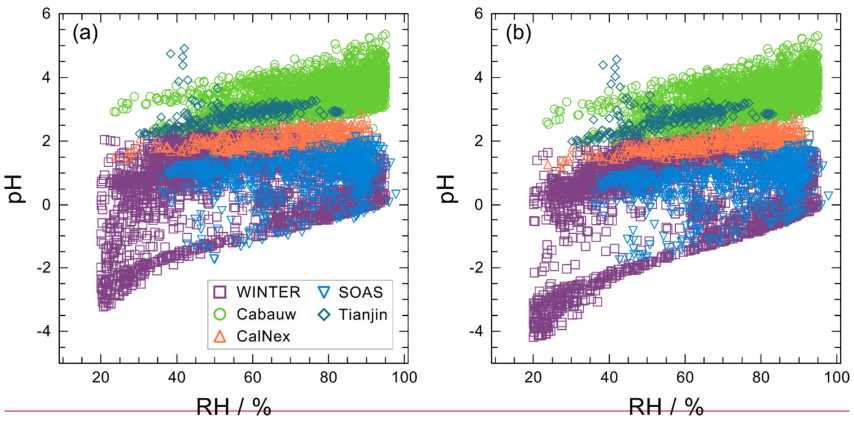

Figure 12. A comparison of calculated pH using (a) AIOMFAC-GLE, and (b) E-AIM as a function of RH for all field campaign datasets examined (SOAS Centreville, Cabauw, CalNex, Tianjin and WINTER, see Sect. 6.2 and Table 4 for a description of the data sets).

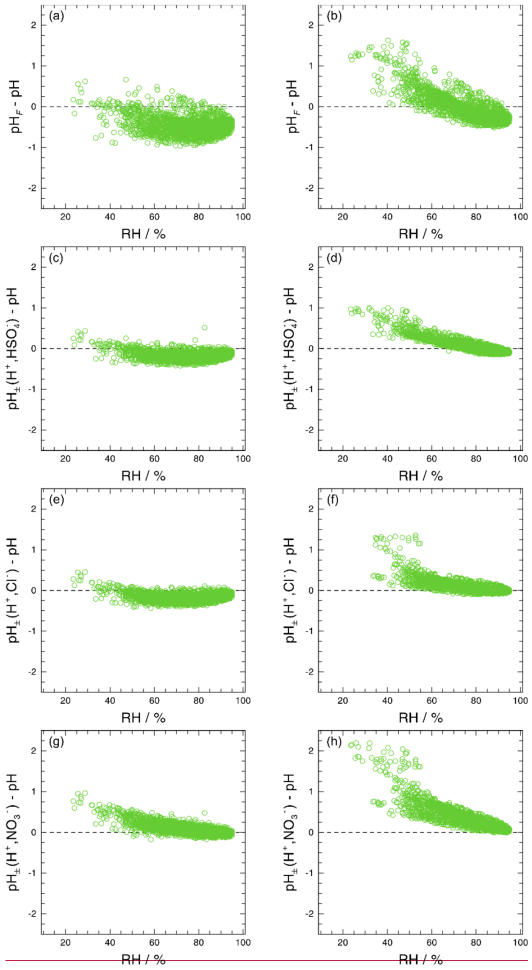

Figure 13. Comparison of different approximate metries of pH, using the Cabauw data and calculated by AIOMFAC-GLE (left column), and E-AIM (right column). The results are shown as differences from pH as follows: (a, b) pH_F – pH; (c, d) $pH_{\pm}(H^+,HSO_4^-)$ – pH; (e, f) $pH_{\pm}(H^+,Cl^-)$ – pH; (g, h) $pH_{\pm}(H^+,NO_3^-)$ – pH.

Formatted: Left

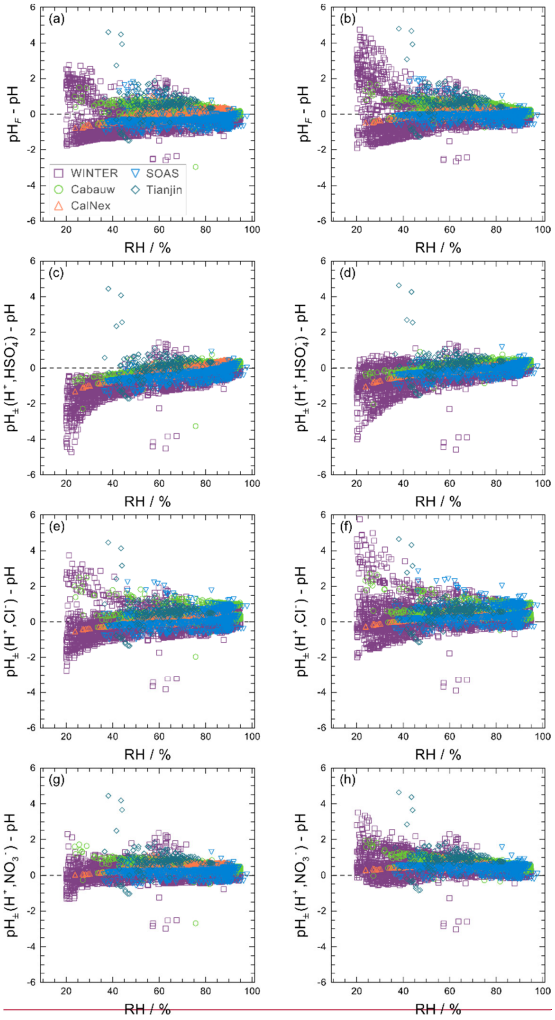

~~**Figure 14.** ISORROPIA-calculated pH using the different metrics, and its difference against pH values calculated with AIOMFAC-GLE (left column) and, E-AIM (right column). Data shown for all the field campaign observations considered in this study (Table 4).~~

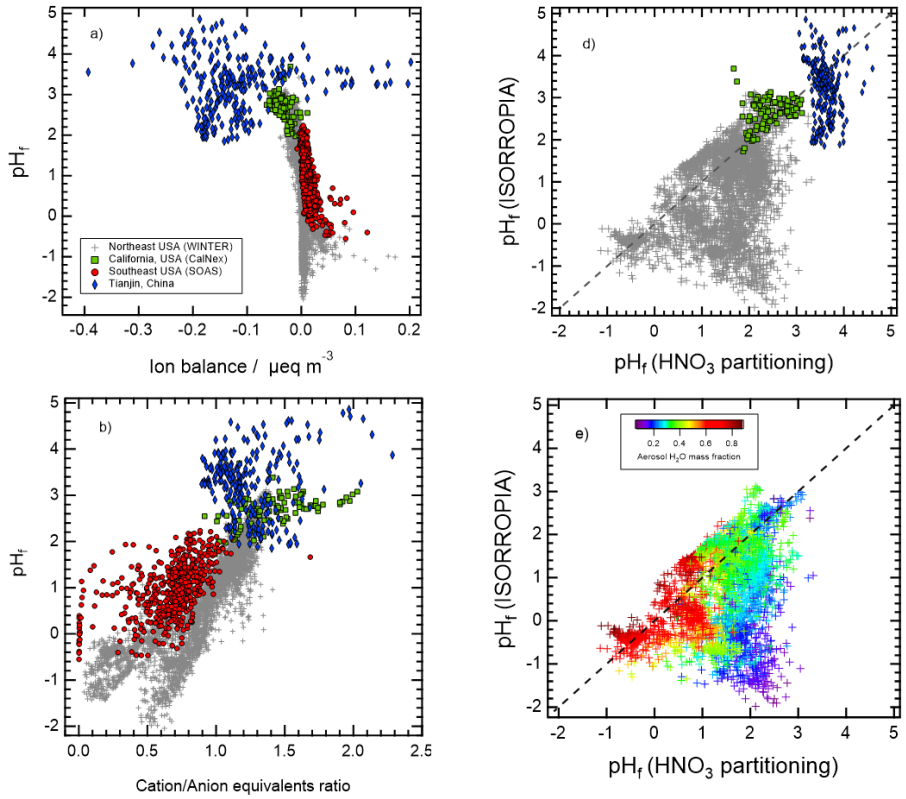
a)
Northeast USA (WINTER)
California, USA (CalNex)
Southeast USA (SOAS)
Tianjin, China
pH$_f$
Ion balance / μeq m^{-3}
b)
pH$_f$
Cation/Anion equivalents ratio
d)
pH$_f$ (ISORROPIA)
pH$_f$ (HNO$_3$ partitioning)
e)
Aerosol H$_2$O mass fraction
pH$_f$ (ISORROPIA)
pH$_f$ (HNO$_3$ partitioning)

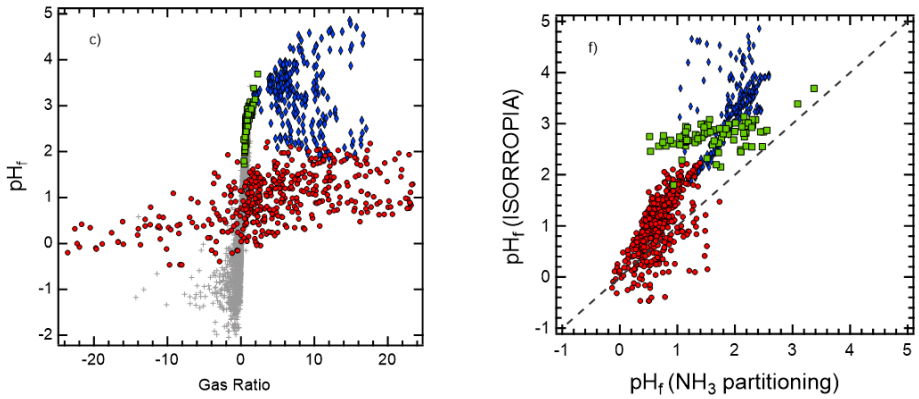

Figure 15. Comparison of pH_f calculated by ISORROPIA with proxies: (a) the charge balance, (b) cation/anion molar equivalent ratio, (c) gas ratio (GR), (d, e) HNO_3 gas–particle partitioning (Eq. 17), and (f) NH_3 gas–particle partitioning (Eq. 18). The ambient data sets are described in detail in Table 4. The proxy methods were calculated as in Table 2, unless otherwise noted. Note the convention for the charge balance calculation in (a) results in a positive value when there is a cation deficit. The dashed lines in d–f represent the 1:1 line, shown for visual effect. The legend in panel (a) applies to all panels except (c), which only shows data for the WINTER data set, colored according to the aerosol water mass fraction (relative to the total predicted aerosol mass).

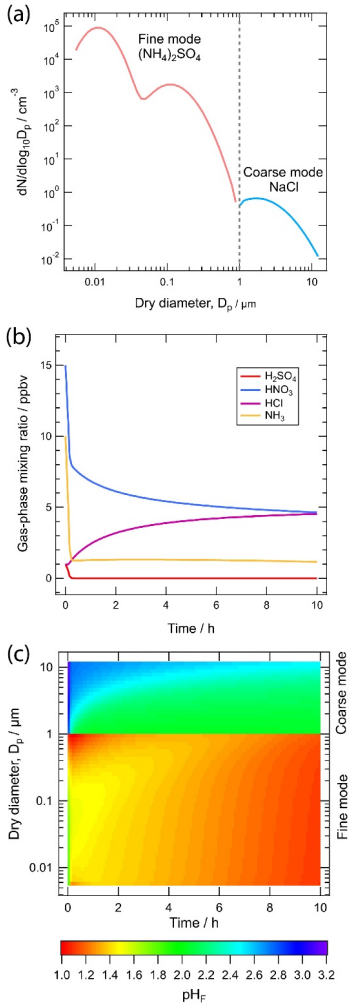

~~**Figure 16.** Simulated evolution of size-distributed aerosol pH using the sectional MOSAIC aerosol box model: (a) Initial aerosol number size distributions for the fine and coarse modes, (b) Time evolution of gas-phase species, and (c) Time evolution of aerosol pH as a function of size (bins labeled based on what was initially in the fine and coarse modes).~~

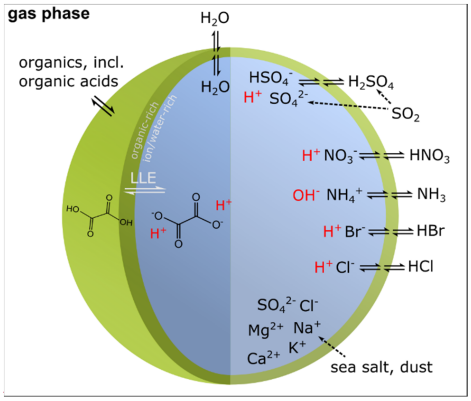

Figure 17. Sketch of a multicomponent aerosol particle consisting of an organic-rich and an aqueous inorganic-ion rich phase in LLPS; here adopting a core–shell morphology. Shown are equilibria of water, organic compounds, as well as inorganic acids and bases contributing to the overall particulate matter mass, ionic strength and the pH. The dynamically established pH exerts control on the gas–particle partitioning of semi-volatile acids and bases, such as HNO_3, HCl and NH_3. All species may partition into all phases; however, inorganic ions tend to favour the aqueous phase, while organic compounds of moderate to low polarity will predominantly partition to an organic-rich phase.

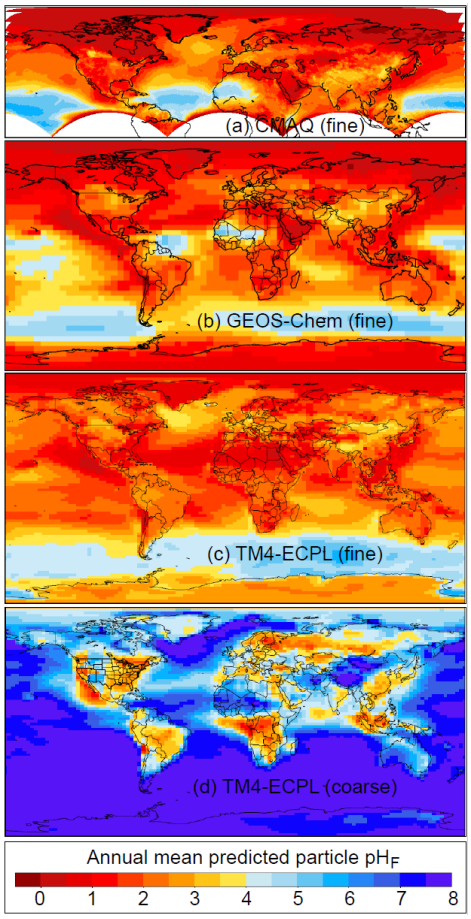

Figure 18. Particle pH_F at the surface predicted by (a) CMAQv5.2 for Aitken + accumulation modes (2016 northern hemisphere annual average), (b) GEOS-Chem for bulk fine aerosol (2015 annual average, version 12.0.0 with additional dust cations), (c) TM4-ECPL for PM_1 (2009 annual average), and (d) TM4-ECPL for coarse aerosol (2009 annual average). Values averaged over ~~aerosol liquid water~~ALWC content greater than 0.01 μg m^{-3}. The solvent for H^+ is water associated with inorganic electrolytes.

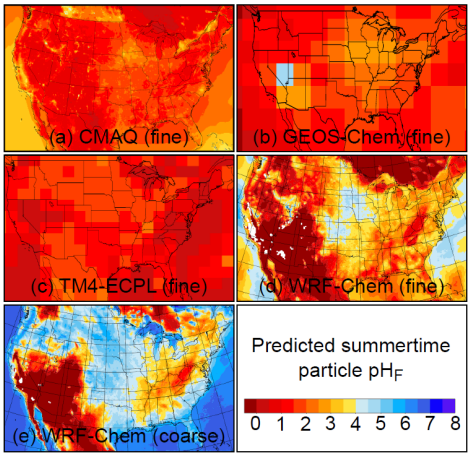

Figure 19. Particle pH_F predicted at the surface for June over the contiguous United States by (a) CMAQv5.2 for Aitken + accumulation modes (2016), (b) GEOS-Chem for bulk fine aerosol (2015), (c) TM4-ECPL for PM_1 (2009), (d) WRF-Chem v3.9.1 with MOSAIC for $PM_{2.5}$ aerosols (June 1-14, 2013, liquid water weighted average), and (3) WRF-Chem for coarse aerosol (2.5 to 10 µm). Values averaged over ~~aerosol liquid water content~~ALWC greater than 0.01 µg m^{-3}. The solvent for H^+ is water associated with inorganic electrolytes in a-c and total aerosol water (including water associated with organics and OIN) in d-e.

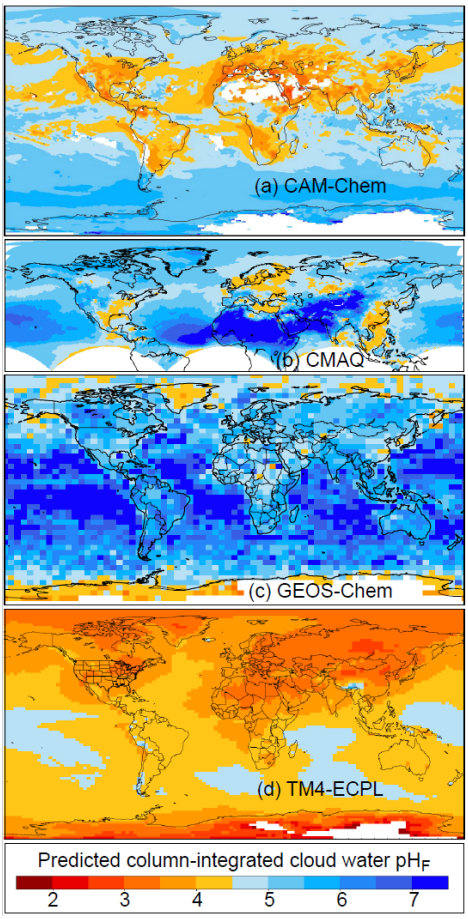

Figure 20. Liquid-water-weighted vertical column integrated cloud water pH_F predicted by: (a) CAM6-Chem (convective clouds excluded, June 2015), (b) CMAQv5.3 (resolved clouds only, 2016 annual average), (c) GEOS-Chem (2015 annual average), and (d) TM4-ECPL (2009 annual average). Note different color scale compared to particle predictions. White indicates no cloud water.

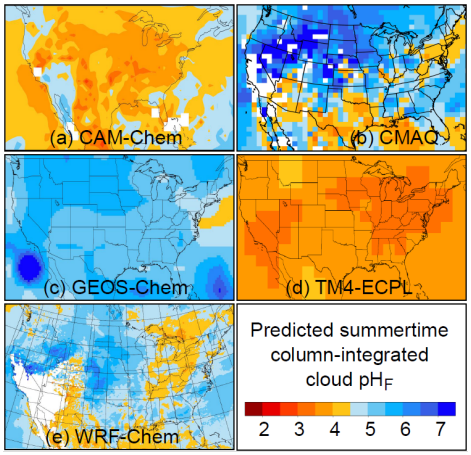

Figure 21. Liquid-water-weighted vertical column June average cloud water pH_F over the contiguous United States predicted by: (a) CAM6-Chem (convective clouds excluded, 2015), (b) CMAQv5.3 (resolved clouds only, 2016), (c) GEOS-Chem (2015), (d) TM4-ECPL (2009), and (e) WRF-Chem (2013). White indicates no cloud water.

Tables

Table 1. Definitions and notation for pH and various molality-based pH approximations. All activity coefficients are on a molality basis, relative to a reference state of infinite dilution in pure water. Note, for mathematical rigor (omitted above for simplicity), all expressions in the $\log_{10}$ need to be normalized by unit molality $m^{\ominus}$.[b]

Symbol and defining expression	Remarks
$\mathrm{pH} = -\log_{10}(a_{\mathrm{H}^+}) = -\log_{10}\left(m_{\mathrm{H}^+}\gamma_{\mathrm{H}^+}\right)$	recommended IUPAC definition of pH
$\mathrm{pH_F} = -\log_{10}(m_{\mathrm{H}^+})$	*free* H^+ approximation of pH
$\mathrm{pH}_{\pm}(\mathrm{H,X}) = -\log_{10}\left(m_{\mathrm{H}^+}\gamma_{\pm,\mathrm{HX}}\right)$	approximation of pH based on mean molal ion activity coefficient [a] of H^+ and anion X, with X = Cl^-, NO_3^- or HSO_4^- (choice to be specified in parenthesis or as subscript)
$\mathrm{pH_T} = -\log_{10}(m_{\mathrm{H}^+} + m_{\mathrm{HSO4^-}})$	*total* H^+ approximation of pH

[a] For 1:1 electrolytes, $\gamma_{\pm,\mathrm{HX}} = \sqrt[2]{\gamma_{\mathrm{H}^+}\cdot\gamma_{\mathrm{X}}}$. The difference between $\mathrm{pH}_{\pm}(\mathrm{H,X})$ and pH is related to the activity coefficient ratio, $\mathrm{pH}_{\pm}(\mathrm{H,X}) - \mathrm{pH} = \frac{1}{2}\log_{10}\left(\frac{\gamma_{\mathrm{H}^+}}{\gamma_{\mathrm{X}^-}}\right)$.

[b] With explicit normalization, $\mathrm{pH_F} = -\log_{10}\left(\frac{m_{\mathrm{H}^+}}{m^{\ominus}}\right)$.

Formatted: Right: 0.33"

Table 2: Common box models used to calculate acidity.

Model	Input	Acidity Output	Advantages	Disadvantages
E-AIM	Gas + particle or equilibrium particle composition (H^+, NH_4^+, Na^+, SO_4^{2-}, HSO_4^-, NO_3^-, Cl^-, Br^-, organic acids, amines) in moles in overall electroneutral conditions (see Eq. 19 for Z); RH, T.	pH at equilibrium	pH via recommended Eq. 1 Considered the most accurate inorganic thermodynamic model Some ionizing organic species (e.g. organic acids, amines) considered	Computationally intensive T and RH restricted for some compositions to preserve accuracy
AIOMFAC-GLE	Gas + particle or equilibrium particle composition (H^+, Li^+, Na^+, K^+, NH_4^+, Mg^{2+}, Ca^{2+}, Cl^-, Br^-, NO_3^-, HSO_3^-, SO_3^{2-}, organic species and/or organic functional groups) in mol m^{-3} air for electroneutral conditions; RH, T	pH at equilibrium	pH via recommended Eq. 1 Accounts for organic--inorganic interactions and liquid-liquid equilibrium in consistent framework Code publicly distributed through repository	Limited support for solid-liquid equilibria of diver inorganic salts (presently) Optimized for temperatures near 298 K, with limited accuracy for much colder atmospheric temperatures Organic species do not ionize
MOSAIC	Distinct gas and particle composition (H^+, NH_4^+, Na^+, Ca^{2+}, SO_4^{2-}, HSO_4^-, $CH_3SO_3^-$, NO_3^-, Cl^-, and CO_3^{2-}) in mol m^{-3} air; RH, and T. Automatic adjustments applied to non-electroneutral input particle-phase composition.	pH_F by default ($pH_\pm$ with modification) for each particle size bin (or mode) at each time step while dynamically solving gas-particle mass transfer	Provides size-resolved pH_F and $pH_\pm$ to account for compositional heterogeneity across particles of different sizes and origins Does not require equilibrium assumption	Gas-particle and solid-liquid equilibrium constants depend on temperature, but activity coefficients are limited to 298.15 K.
ISORROPIA II	Gas + particle or particle composition (TSO_4, TCl, TNO_3, TNH_4, Na, K, Ca, Mg) in mol m^{-3} or µg m^{-3} air; RH, T. Automatic adjustments applied to non-electroneutral input particle-phase	pH_F by default ($pH_\pm$ with modification) at equilibrium	Computationally efficient Code has widespread public distribution and incorporation in CTMs	Approximations employed (e.g. some activi coefficients treated as 1, minor species do not pertu equilibrium, higher numerical tolerances) Segmented solution approach leads to discontinuo solution surface

composition.

Table ~~2~~3. Definitions of proxy methods. For all quantities the units are moles of chemical species per unit volume of air (e.g., mol m-3). The quantity $[\mathbf{TSO_4}]$ is total particulate sulfate, or **the sum of** $[\mathbf{HSO_4^-}] + [\mathbf{SO_4^{2-}}]$.

Proxy	Definition
Cation/anion equivalent ratio	$\text{Cation}/\text{Anion} = \frac{[NH_4^+] + [Na^+] + [K^+] + 2[Ca^{2+}] + 2[Mg^{2+}]}{2[TSO_4] + [NO_3^-] + [Cl^-]}$
Degree of sulfate neutralization	$DSN = ([NH_4^+] - [NO_3^-])/[TSO_4]$
Degree of neutralization	$DON = [NH_4^+]/(2[TSO_4] + [NO_3^-])$
TNH_4: TSO_4	$TNH_4\text{: } TSO_4 = \frac{([NH_3] + [NH_4^+])}{[TSO_4]}$
Ion balance (H^+ from charge balance)~~Strong acidity (charge balance)~~	$H^+_{air,cb} = 2[TSO_4] + [NO_3^-] + [Cl^-] - ([NH_4^+] + [Na^+] + [K^+] + 2[Ca^{2+}] + 2[Mg^{2+}])$
Gas ratio (GR)	$GR = ([NH_3] + [NH_4^+] - 2[TSO_4])/([HNO_3] + [NO_3^-])$
Adjusted gas ratio (adjGR)	$adjGR = ([NH_3] + [NO_3^-])/([HNO_3] + [NO_3^-])$

Table 34. Input concentrations (total gas+aerosol) for each of the highly and moderately acidic cases of inorganic systems 1 – 3. Compositions are specified in terms of moles of electrolyte and gas-phase species per m^3 of air and rounded to 3 significant figures. Model calculations were carried out for seven equilibrium RH from 99% to 40%, at 298.15 K and 101.325 kPa pressure.

System no., case	$n_{(NH4)2SO4}$ (mol m^{-3})	n_{H2SO4} (mol m^{-3})	n_{NH3} (mol m^{-3})	n_{HNO3} (mol m^{-3})	n_{Na2SO4} (mol m^{-3})	n_{NaCl} (mol m^{-3})	n_{HCl} (mol m^{-3})
1, moderately acidic	2.500000×10^-08	3.37×10^11	1.00×10^-06	0	0	0	0
1, highly acidic	1.50×10^-08	2.02×10^08	5.00×10^-08	0	0	0	0
2, moderately acidic	0	1.00×10^10	0	0	5.61×10^09	1.04×10^07	1.00×10^-08
2, highly acidic	0	5.00×10^08	0	0	5.61×10^09	1.04×10^07	1.00×10^-06
3, moderately acidic	2.50×10^-08	3.37×10^11	1.00×10^-06	1.00×10^-06	0	0	0
3, highly acidic	2.50×10^-08	3.37×10^11	1.00×10^-07	1.00×10^-07	0	0	0

Formatted ... [1]
Formatted ... [2]
Formatted ... [3]
Formatted ... [4]
Formatted ... [5]
Formatted ... [6]
Formatted: Font: 10 pt
Formatted ... [7]
Formatted ... [8]
Formatted ... [9]
Formatted ... [10]
Formatted: Font: 10 pt
Formatted ... [11]
Formatted ... [12]
Formatted ... [13]
Formatted ... [14]
Formatted ... [15]
Formatted ... [16]
Formatted ... [17]
Formatted ... [18]
Formatted ... [19]
Formatted ... [20]
Formatted ... [21]
Formatted ... [22]

Table 45. Characteristics of the datasets used for the box model intercomparison. Values are reported as mean followed be standard deviation in parenthesis. n is the number of data points. ~~(RH, T, and concentration are the same as those in Nenes et al., 2019).~~

Dataset ID (reference)	Location (Period)	RH (%)	T (K)	Sulfate (μg m^{-3})	Total Ammonium (μg m^{-3})	Total Nitrate (μg m^{-3})	n
Tianjin (Shi et al., 2019)	Tianjin, China (9/Aug/2015-22/Aug/2015)	576.6 (12.4)	3021.8 (2.793)	21.46 (10.9911)	37.7438 (7.688)	18.12 (121.50)	227
~~CALNEX~~CalNex (Guo et al., 2017b)	Pasadena, CA, USA (17/May/2010-15/Jun/2010)	71.3 (1516.5)	291.1 (4.264)	2.86 9 (1.70)	3.44 (1.81)	10.23. (9.74)	482
Cabauw (Guo et al., 2018b)	Cabauw, Netherlands (2/May/2012-04/Jun/2013)	78.2 (154.8)	282.2 (7.37)	1.92 (1.657)	9.3 (6.8)	4.1 (3.9)	2612
WINTER (Guo et al., 2016)	Eastern USA aloft (03/Feb/2015)	56.1 (198.9)	2710.8 (76.52)	1.02 (0.108)	0.53 (0.44)	2.12 (2.108)	3121
SOAS (Guo et. al, 2015)	Centreville, USA (06/Jun/2013-14/Jul/2013)	72.7 3 (17.4)	2987.9 (3.453)	1.81 (1.218)	0.78 (0.50)	0.12 (0.15)	780

Table 5~~6~~. (a) Comparison of ISORROPIA II-derived pH approximations against pH. (b, c) Comparison of pH approximations against pH when computed by the same model in (b) AIOMFAC-GLE and in (c) E-AIM.

	RMSE compared to AIOMFAC-GLE pH	MB compared to AIOMFAC-GLE pH	RMSE compared to E-AIM pH	MB compared to E-AIM pH
(a) pH approximation by ISORROPIA II[(1)]				
pH_F	0.46~~57~~	-0.06~~65~~	0.45~~2~~	0.10~~097~~
$pH_\pm$ (H^+, HSO_4^-)	0.51~~05~~	-0.23~~0~~	0.39~~3~~	-0.07~~68~~
$pH_\pm$ (H^+, Cl^-)	0.45~~49~~	0.17~~0~~	0.53~~27~~	0.33~~1~~
$pH_\pm$ (H^+, NO_3^-)	0.51~~3~~	0.37~~2~~	0.63~~4~~	0.53~~4~~
(b) pH approximation by AIOMFAC-GLE[(2)]				
pH_F	0.61~~1~~	-0.54~~4~~	-	-
$pH_\pm$ (H^+, HSO_4^-)	0.27~~2~~	-0.24~~35~~	-	-
$pH_\pm$ (H^+, Cl^-)	0.23~~0~~	-0.20~~0~~	-	-
$pH_\pm$ (H^+, NO_3^-)	0.18~~1~~	0.07~~3~~	-	-
(c) pH approximation by E-AIM[(2)]				
pH_F	-	-	0.55~~46~~	0.12~~3~~
$pH_\pm$ (H^+, HSO_4^-)	-	-	0.35~~4~~	0.18~~2~~
$pH_\pm$ (H^+, Cl^-)	-	-	0.50~~497~~	0.23~~3~~
$pH_\pm$ (H^+, NO_3^-)	-	-	0.73~~28~~	0.49~~3~~

[(1)] The pH, as defined by Eq. (1), was calculated using both AIOMFAC-GLE and E-AIM. The comparisons are presented in terms of the root mean square error (RMSE) and mean bias (MB) as pH(approx.) - pH, all in pH units. Results were calculated using all of the SOAS, Cabauw, CalNex, WINTER, and Tianjin datasets (combined) described in Table ~~4~~ 5 (n = 7222 points), with RMSE and MB calculations limited to data points with RH > 35 %.

[(2)] Calculations by (b) AIOMFAC-GLE and (c) E-AIM covering the same combined data sets as in (a).

Table 7: Species and methods used to calculate acidity in CTMs. Bulk cloud water pH is calculated assuming electroneutrality, generally using model-specific algorithms. Dissolved gases in cloud water are determined using Henry's law coefficients. Configurations are specific to this work.

Model	Aerosol size information	Species/sources considered in aerosol pH calculation	Fine aerosol pH calculation method	Species/sources considered in cloud pH calculation
CMAQ v5.3	Fine aerosol: explicit Aitken and accumulation modes. Coarse mode acidity not explicitly calculated but included in determination of dynamic mass transfer and composition.	TSO_4, TCl, TNO_3, TNH_4, Na, K, Ca, Mg from sea salt, dust, wildland fires, and anthropogenic activities.	ISORROPIA II pH_F for inorganic-only composition of combined fine modes. Condensed water associated with organic species is also predicted (not considered in fine aerosol pH_F in this work).	Aqueous species: H^+, OH^-, HSO_3^-, SO_3^{2-}, HSO_4^-, SO_4^{2-}, HCO_3^-, CO_3^{2-}, HCO_2^-, NH_4^+, NO_3^-, Cl^-, Ca^{2+}, Na^+, K^+, Mg^{2+} Dissolved gases: SO_2, CO_2, NH_3, HCl, HNO_3, HCOOH, H_2SO_4 (as sulfate), N_2O_5 (as $2\times HNO_3$)
GEOS-Chem v12.0.0	Bulk fine aerosol. Coarse mode acidity not explicitly calculated but included in determination of dynamic mass transfer and composition.	TSO_4, HCl, TNO_3, TNH_4, and fine mode Ca, Mg, Na, Cl from anthropogenic, sea salt, and dust sources (dust contributions not considered in default GEOS-Chem predictions but Ca and Mg from dust considered in this work).	ISORROPIA II pH_F.	Aqueous species: SO_4^{2-}, NO_3^-, NH_4^+ Dissolved gases: CO_2, SO_2, NH_3, HNO_3
TM4-ECPL	Fine (externally mixed dust) and coarse (internally mixed dust) aerosol.	SO_4^{2-}, NH_3, NH_4^+, HNO_3 and NO_3^-; sea salt and dust assumed to be externally mixed with fine mode sulfate and not considered in the fine acidity calculation.	ISORROPIA II pH_F for inorganic-only composition of fine and coarse modes (each in equilibrium with gas). Condensed water associated with organic species is also predicted (not considered in fine aerosol pH_F in this work).	Aqueous species: SO_4^{2-}, $CH_3O_3S^-$, NO_3^-, NH_4^+, Na^+, Ca^{2+}, K^+, Cl^- Mg^{2+} Dissolved gases: SO_2, CO_2, HNO_3, NH_3, oxalic acid
WRF-Chem	Four aerosol size bins (0.039–0.156, 0.156–0.625, 0.625–2.5, 2.5–10 µm in diameter) treated dynamically.	sulfate, HNO_3/NO_3^-, NH_3/NH_4^+, $CH_3O_3S^-$, Cl^-, CO_3^{2-}, Na, Ca; HCl not considered with MOZART chemistry (no displacement of Cl^- from sea salt aerosols allowed).	MOSAIC size-resolved pH_F.	Aqueous species: OH^-, HCO_3^-, CO_3^{2-}, CO_3^-, HSO_3^-, SO_3^{2-}, HSO_4^-, SO_4^{2-}, SO_4^-, SO_5^-, HSO_5^-, $HOCH_2SO_3^-$, $OCH_2SO_3^-$, NO_2^-, NO_3^-, HO_2^-, O_2^-, $HCOO^-$, Cl^-, Cl_2^-, $ClOH^-$, NH_4^+, Fe^{3+}, Mn^{2+} Dissolved gases: SO_2, CO_2, HNO_3, NH_3, HO_2, HCOOH, H_2O_2
CAM-Chem	Four log-normal modes.	Inorganic aerosol composition considered: SO_4^{2-}, NH_4^+, soil dust, sea salt.	Not considered in this work.	Aqueous species: OH^-, HCO_3^-, NO_3^-, HSO_3^-, SO_3^{2-}, SO_4^{2-}, NH_4^+ Dissolved gases: H_2SO_4, HNO_3, NH_3

Formatted: Caption, Space Before: 0 pt, After: 0 pt
Formatted: Font: 9.5 pt, Font color: Auto
Formatted: Centered
Formatted Table
Formatted: Left
Formatted: Left, Line spacing: single
Formatted: Left, Line spacing: single
Formatted: Left, Line spacing: single
Formatted: Font: 9.5 pt, Font color: Text 1
Formatted: Centered
Formatted: Left
Formatted: Left
Formatted: Left
Formatted: Left, Line spacing: single
Formatted: Left, Line spacing: single
Formatted: Font: 9.5 pt, Font color: Text 1
Formatted: Centered
Formatted: Left
Formatted: Left
Formatted: Left, Line spacing: single
Formatted: Left, Line spacing: single
Formatted: Left
Formatted: Font: 9.5 pt, Font color: Text 1
Formatted: Centered
Formatted: Left
Formatted: Left
Formatted: Left, Line spacing: single
Formatted: Left
Formatted: Left, Line spacing: single
Formatted: Font: 9.5 pt, Font color: Text 1
Formatted: Centered
Formatted: Left, Line spacing: single
Formatted: Left
Formatted: Left
Formatted: Left, Line spacing: single
Formatted: Font: 9.5 pt, Font color: Auto
Formatted: Centered
Formatted: Left
Formatted: Left

References

Abrams, J. Y., Weber, R. J., Klein, M., Sarnat, S. E., Chang, H. H., Strickland, M. J., Verma, V., Fang, T., Bates, J. T., Mulholland, J. A., Russell, A. G., and Tolbert, P. E.: Associations between Ambient Fine Particulate Oxidative Potential and Cardiorespiratory Emergency Department Visits, Environ. Health Persp., 125, 107008-107008, https://doi.org/10.1289/EHP1545, 2017.

Adams, P. J., Seinfeld, J. H., and Koch, D. M.: Global concentrations of tropospheric sulfate, nitrate, and ammonium aerosol simulated in a general circulation model, J. Geophys. Res-Atmos., 104, 13791-13823, https://doi.org/10.1029/1999jd900083, 1999.

Ahrens, L., Harner, T., Shoeib, M., Lane, D., and Murphy, J.: Improved Characterization of Gas–Particle Partitioning for Per- and Polyfluoroalkyl Substances in the Atmosphere Using Annular Diffusion Denuder Samplers, Environ. Sci. Technol., 46, 7199-7206, https://doi.org/10.1021/es300898s, 2012.

Aleksic, N., Roy, K., Sistla, G., Dukett, J., Houck, N., and Casson, P.: Analysis of cloud and precipitation chemistry at Whiteface Mountain, NY, Atmos. Environ., 43, 2709-2716, , https://doi.org/10.1016/j.atmosenv.2009.02.053, 2009.

Alexander, B., Park, R., Jacob, D., Li, Q., Yantosca, R., Savarino, J., Lee, C., and Thiemens, M.: Sulfate formation in sea-salt aerosols: Constraints from oxygen isotopes, J. Geophys. Res.-Atmos., 110, https://doi.org/10.1029/2004JD005659, 2005.

Alexander, B., Allman, D., Amos, H., Fairlie, T., Dachs, J., Hegg, D., and Sletten, R.: Isotopic constraints on the formation pathways of sulfate aerosol in the marine boundary layer of the subtropical northeast Atlantic Ocean, J. Geophys. Res-Atmos., 117, https://doi.org/10.1029/2011JD016773, 2012.

Amundson, N. R., Caboussat, A., He, J. W., Martynenko, A. V., Savarin, V. B., Seinfeld, J. H., and Yoo, K. Y.: A new inorganic atmospheric aerosol phase equilibrium model (UHAERO), Atmos. Chem. Phys., 6, 975-992, https://doi.org/10.5194/acp-6-975-2006, 2006.

Amundson, N. R., Caboussat, A., He, J. W., Martynenko, A. V., Landry, C., Tong, C., and Seinfeld, J. H.: A new atmospheric aerosol phase equilibrium model (UHAERO): organic systems, Atmos. Chem. Phys., 7, 4675-4698, https://doi.org/10.5194/acp-7-4675-2007, 2007.Ansari, A. S. and Pandis, S. N.: Response of inorganic PM to precursor concentrations, Environ. Sci. Technol., 32, 2706-2714, https://doi.org/10.1021/es971130j, 1998.

Ansari, A. S. and Pandis, S. N.: Prediction of multicomponent inorganic atmospheric aerosol behavior, Atmospheric Environment, 33, 745-757, https://doi.org/10.1016/S1352-2310(98)00221-0, 1999.

Appel, K. W., Pouliot, G. A., Simon, H., Sarwar, G., Pye, H. O. T., Napelenok, S. L., Akhtar, F., and Roselle, S. J.: Evaluation of dust and trace metal estimates from the Community Multiscale Air Quality (CMAQ) model version 5.0, Geosci. Model Dev., 6, 883-899, https://doi.org/10.5194/gmd-6-883-2013, 2013.

Arashiro, M., Lin, Y. H., Sexton, K. G., Zhang, Z., Jaspers, I., Fry, R. C., Vizuete, W. G., Gold, A., and Surratt, J. D.: In vitro exposure to isoprene-derived secondary organic aerosol by direct deposition and its effects on COX-2 and IL-8 gene expression, Atmos. Chem. Phys., 16, 14079-14090, https://doi.org/10.5194/acp-16-14079-2016, 2016.

Asbury, C. E., McDowell, W. H., Trinidad-Pizarro, R., and Berrios, S.: Solute deposition from cloud water to the canopy of a puerto rican montane forest, Atmos. Environ., 28, 1773-1780, https://doi.org/10.1016/1352-2310(94)90139-2, 1994.

Ashbaugh, L. L. and Eldred, R. A.: Loss of particle nitrate from Teflon sampling filters: Effects on measured gravimetric mass in California and in the IMPROVE network, J. Air Waste Manage. Assoc., 54, 93-104, https://doi.org/10.1080/10473289.2004.10470878, 2004.

Bandura, A. V. and Lvov, S. N.: The Ionization Constant of Water over Wide Ranges of Temperature and Density, J. Phys. Chem. Ref. Data, 35, 15-30, https://doi.org/10.1063/1.1928231, 2005.

Barnes, I., Hjorth, J., and Mihalopoulos, N.: Dimethyl sulfide and dimethyl sulfoxide and their oxidation in the atmosphere, Chem. Rev., 106, 940-975, https://doi.org/10.1021/Cr020529+, 2006.

Barsanti, K. C. and Pankow, J. F.: Thermodynamics of the formation of atmospheric organic particulate matter by accretion reactions - Part 3: Carboxylic and dicarboxylic acids, Atmos. Environ., 40, 6676-6686, https://doi.org/10.1016/j.atmosenv.2006.03.013, 2006.

Barth, M. C.: The importance of cloud drop representation on cloud photochemistry, Atmos. Res., 82, 294-309, https://doi.org/10.1016/j.atmosres.2005.10.008, 2006.

Barth, M. C., P. J. Rasch, J. T. Kiehl, C. M. Benkovitz, Schwartz, S. E.: Sulfur chemistry in the National Center for Atmospheric Research Community Climate Model: Description, evaluation, features and sensitivity to aqueous chemistry, J. Geophys. Res., 105, 1387-1415, , https://doi.org/10.1029/1999JD900773, 2000.

Bates, J. T., Weber, R. J., Abrams, J., Verma, V., Fang, T., Klein, M., Strickland, M. J., Sarnat, S. E., Chang, H. H., Mulholland, J. A., Tolbert, P. E., and Russell, A. G.: Reactive Oxygen Species Generation Linked to Sources of Atmospheric Particulate Matter and Cardiorespiratory Effects, Environ. Sci. Technol., 49, 13605-13612, https://doi.org/10.1021/acs.est.5b02967, 2015.

Bator, A. and Collett Jr, J. L.: Cloud chemistry varies with drop size, J. Geophys. Res.-Atmos., 102, 28071-28078, https://doi.org/10.1029/97JD02306, 1997.

Battaglia, M. A., Douglas, S., and Hennigan, C. J.: Effect of the Urban Heat Island on Aerosol pH, Environ. Sci. Technol., 51, 13095-13103, https://doi.org/10.1021/acs.est.7b02786, 2017.

~~Battaglia, M. A., Weber, R. J., Nenes, A., and Hennigan, C. J.: Effects of Water-soluble Organic Carbon on Aerosol pH, Atmos. Chem. Phys. Discuss., 2019, 1-36, https://doi.org/10.5194/acp-2019-344, 2019.~~Battaglia Jr., M. A., Weber, R. J., Nenes, A., and Hennigan, C. J.: Effects of water-soluble organic carbon on aerosol pH, Atmos. Chem. Phys., 19, 14607–14620, https://doi.org/10.5194/acp-19-14607-2019, 2019.

Behera, S. N., Betha, R., Liu, P., and Balasubramanian, R.: A study of diurnal variations of PM2.5 acidity and related chemical species using a new thermodynamic equilibrium model, Sci. Total Environ., 452-453, 286-295, https://doi.org/10.1016/j.scitotenv.2013.02.062, 2013.

Bertram, A. K., Martin, S. T., Hanna, S. J., Smith, M. L., Bodsworth, A., Chen, Q., Kuwata, M., Liu, A., You, Y., and Zorn, S. R.: Predicting the relative humidities of liquid-liquid phase separation, efflorescence, and deliquescence of mixed particles of ammonium sulfate, organic material, and water using the organic-to-sulfate mass ratio of the particle and the oxygen-to-carbon elemental ratio of the organic component, Atmos. Chem. Phys., 11, 10995-11006, https://doi.org/10.5194/acp-11-10995-2011, 2011.

Bianco, A., Vaitilingom, M., Bridoux, M., Chaumerliac, N., Pichon, J., Piro, J., and Deguillaume, L.: Trace Metals in Cloud Water Sampled at the Puy De Dome Station, Atmosphere, 8, https://doi.org/10.3390/atmos8110225, 2017.

Binkley, D. and Richter, D.: Nutrient Cycles and H+ Budgets of Forest Ecosystems, in: Advances in Ecological Research, edited by: Macfadyen, A. and Ford, E. D., Academic Press, London, 1-51, https://doi.org/10.1016/S0065-2504(08)60086-0, 1987.

Blanchard, C. L. and Hidy, G. M.: Effects of changes in sulfate, ammonia, and nitric acid on particulate nitrate concentrations in the southeastern United States, J. Air Waste Manage. Assoc., 53, 283-290, https://doi.org/10.1080/10473289.2003.10466152, 2003.

Bobbink, R., Hicks, K., Galloway, J., Spranger, T., Alkemade, R., Ashmore, M., Bustamante, M., Cinderby, S., Davidson, E., Dentener, F., Emmett, B., Erisman, J. W., Fenn, M., Gilliam, F., Nordin, A., Pardo, L., and De Vries, W.: Global assessment of nitrogen deposition effects on terrestrial plant diversity: a synthesis, Ecol. Appl., 20, 30-59, https://doi.org/10.1890/08-1140.1, 2010.

Bondy, A. L., Craig, R. L., Zhang, Z., Gold, A., Surratt, J. D., and Ault, A. P.: Isoprene-Derived Organosulfates: Vibrational Mode Analysis by Raman Spectroscopy, Acidity-Dependent Spectral Modes, and Observation in Individual Atmospheric Particles, J. Phys. Chem. A, 122, 303-315, https://doi.org/10.1021/acs.jpca.7b10587, 2018.

Boris, A. J., Lee, T., Park, T., Choi, J., Seo, S. J., and Collett, J. L.: Fog composition at Baengnyeong Island in the eastern Yellow Sea: detecting markers of aqueous atmospheric oxidations, Atmos. Chem. Phys., 16, 437-453, https://doi.org/10.5194/acp-16-437-2016, 2016.

Bougiatioti, A., Nikolaou, P., Stavroulas, I., Kouvarakis, G., Weber, R., Nenes, A., Kanakidou, M., and Mihalopoulos, N.: Particle water and pH in the eastern Mediterranean: source variability and implications for nutrient availability, Atmos. Chem. Phys., 16, 4579-4591, https://doi.org/10.5194/acp-16-4579-2016, 2016.

Bräuer, P., Mouchel-Vallon, C., Tilgner, A., Mutzel, A., Böge, O., Rodigast, M., Poulain, L., van Pinxteren, D., Wolke, R., Aumont, B., and Herrmann, H.: Development of a protocol for the auto-generation of explicit aqueous-phase oxidation schemes of organic compounds, Atmos. Chem. Phys., 19, 9209–9239, https://doi.org/10.5194/acp-19-9209-2019, 2019.~~Bräuer, P., Mouchel-Vallon, C., Tilgner, A., Mutzel, A., Böge, O., Rodigast, M., Poulain, L., van Pinxteren, D., Wolke, R., Aumont, B., and Herrmann, H.: Development of a protocol for the auto-generation of explicit aqueous-phase oxidation schemes of organic compounds, Atmos. Chem. and Phys. Discuss., https://doi.org/10.5194/acp-2018-1318, 2019.~~

Bromley, L. A.: Thermodynamic properties of strong electrolytes in aqueous solutions, AIChE J., 19, 313-320, https://doi.org/10.1002/aic.690190216, 1973.

Buck, R. P., Rondinini, S., Covington, A. K., Baucke, F. G. K., Brett Christopher, M. A., Camoes, M. F., Milton, M. J. T., Mussini, T., Naumann, R., Pratt, K. W., Spitzer, P., and Wilson, G. S.: Measurement of pH. Definition, standards, and procedures (IUPAC Recommendations 2002). In: Pure and Applied Chemistry, 11, https:// doi.org/10.1351/pac200274112169, 2002.

Budisulistiorini, S. H., Canagaratna, M. R., Croteau, P. L., Marth, W. J., Baumann, K., Edgerton, E. S., Shaw, S. L., Knipping, E. M.,Worsnop, D. R., and Jayne, J. T.: Real-time continuous characterization of secondary organic aerosol derived from isoprene epoxydiols in downtown Atlanta, Georgia, using the Aerodyne Aerosol Chemical Speciation Monitor, Environ. Sci. Technol., 47, 5686-5694, https://doi.org/10.1021/es400023n, 2013.

Budisulistiorini, S. H., Li, X., Bairai, S. T., Renfro, J., Liu, Y., Liu, Y. J., McKinney, K. A., Martin, S. T., McNeill, V. F., Pye, H. O. T., Nenes, A., Neff, M. E., Stone, E. A., Mueller, S., Knote, C., Shaw, S. L., Zhang, Z., Gold, A., and Surratt, J. D.: Examining the effects of anthropogenic emissions on isoprene-derived secondary organic aerosol formation during the 2013 Southern Oxidant and Aerosol Study (SOAS) at the Look Rock, Tennessee ground site, Atmos. Chem. Phys., 15, 8871-8888, https://doi.org/10.5194/acp-15-8871-2015, 2015.

Budisulistiorini, S. H., Nenes, A., Carlton, A. G., Surratt, J. D., McNeill, V. F., and Pye, H. O. T.: Simulating Aqueous-Phase Isoprene-Epoxydiol (IEPOX) Secondary Organic Aerosol Production During the 2013 Southern Oxidant and Aerosol Study (SOAS), Environ. Sci. Technol., 51, 5026-5034, https://doi.org/10.1021/acs.est.6b05750, 2017.

Buxton, G. V., Greenstock, C. L., Helman, W. P., and Ross, A. B.: Critical-review of rate constants for reactions of hydrated electrons, hydrogen-atoms and hydroxyl radicals (OH/O-) in aqueous-solution, J. Phys. Chem. Ref. Data, 17, 513-886, https://doi.org/10.1063/1.555805, 1988.

Calvert, J. G., Lazrus, A., Kok, G. L., Heikes, B. G., Walega, J. G., Lind, J., and Cantrell, C. A.: Chemical mechanisms of acid generation in the troposphere, Nature, 317, 27-35, https://doi.org/10.1038/317027a0, 1985.

Campbell, P., Zhang, Y., Yahya, K., Wang, K., Hogrefe, C., Pouliot, G., Knote, C., Hodzic, A., San Jose, R., Perez, J. L., Guerrero, P. J., Baro, R., and Makar, P.: A multi-model assessment for the 2006 and 2010 simulations under the Air Quality Model Evaluation International Initiative (AQMEII) phase 2 over North America: Part I. Indicators of the sensitivity of O-3 and PM2.5 formation regimes, Atmos. Environ., 115, 569-586, https://doi.org/10.1016/j.atmosenv.2014.12.026, 2015.

Capaldo, K. P., Pilinis, C., and Pandis, S. N.: A computationally efficient hybrid approach for dynamic gas/aerosol transfer in air quality models, Atmos. Environ., 34, 3617-3627, https://doi.org/10.1016/S1352-2310(00)00092-3, 2000.

Cape, J. N.: Direct damage to vegetation caused by acid rain and polluted cloud: definition of critical levels for forest trees, Environ. Pollut., 82, 167-180, https://doi.org/10.1016/0269-7491(93)90114-4, 1993.

Capps, S. L., Henze, D. K., Hakami, A., Russell, A. G., and Nenes, A.: ANISORROPIA: the adjoint of the aerosol thermodynamic model ISORROPIA, Atmos. Chem. Phys., 12, 527-543, https://doi.org/10.5194/acp-12-527-2012, 2012.

Carmichael, G. R. and Peters, L. K.: A second generation model for regional-scale transport/chemistry/deposition, Atmos. Environ., 20, 173-188, https://doi.org/10.1016/0004-6981(86)90218-0, 1986.

Carslaw, K. S., Clegg, S. L., and Brimblecombe, P.: A Thermodynamic Model of the System HCl-HNO3-H2SO4-H2O, Including Solubilities of HBr, from <200 to 328 K, J. Phys. Chem., 99, 11557-11574, https://doi.org/10.1021/j100029a039, 1995.

Chang, J. S., Brost, R. A., Isaksen, I. S. A., Madronich, S., Middleton, P., Stockwell, W. R., and Walcek, C. J.: A three-dimensional Eulerian acid deposition model: Physical concepts and formulation, J. Geophys. Res.-Atmos., 92, 14681-14700, https://doi.org/10.1029/JD092iD12p14681, 1987.

Chang, W. L., Bhave, P.V., Brown, S.S., Riemer, N., Stutz, J., and Dabdub, D.: Heterogeneous atmospheric chemistry, ambient measurements, and model calculations of N_2O_5: A review, Aerosol Sci. Technol., 45, 6665-6695, https://doi.org/10.1080/02786826.2010.551672, 2011.

Chen, L. C. and M. Lippmann, M: Effects of metals within ambient air particulate matter (PM) on human health, Inhal. Toxicol., 21, 1-31, https://doi.org/10.1080/08958370802105405, 2009.

Chen, Q., Geng, L., Schmidt, J., Xie, Z., Kang, H., Dachs, J., Cole-Dai, J., Schauer, A., Camp, M., and Alexander, B.: Isotopic constraints on the role of hypohalous acids in sulfate aerosol formation in the remote marine boundary layer, Atmos. Chem. and Phys., 16, 11433-11450, 10.5194/acp-16-11433-2016, 2016.

Cheng, C., Wang, G., Meng, J., Wang, Q., Cao, J., Li, J., and Wang, J.: Size-resolved airborne particulate oxalic and related secondary organic aerosol species in the urban atmosphere of Chengdu, China, Atmos. Res., 161-162, 134-142, https://doi.org/10.1016/j.atmosres.2015.04.010, 2015.

Formatted: Subscript

Formatted: Subscript

Cheng, Y., Zheng, G., Wei, C., Mu, Q., Zheng, B., Wang, Z., Gao, M., Zhang, Q., He, K., Carmichael, G., Poschl, U., and Su, H.: Reactive nitrogen chemistry in aerosol water as a source of sulfate during haze events in China, Science Advances, 2, https://doi.org/10.1126/sciadv.1601530, 2016.

Clarisse, L., Clerbaux, C., Dentener, F., Hurtmans, D., and Coheur, P.-F.: Global ammonia distribution derived from infrared satellite observations, Nat. Geosci., 2, 479, https://doi.org/10.1038/ngeo551, 2009.

Clegg, S. L. and Brimblecombe, P.: Application of a Multicomponent Thermodynamic Model to Activities and Thermal Properties of 0-40 mol kg-1 Aqueous Sulfuric Acid from <200 to 328 K, J. Chem. Eng. Data, 40, 43-64, https://doi.org/10.1021/je00017a012, 1995.

Clegg, S., and Pitzer, K.: Thermodynamics of multicomponent, miscible, ionic solutions: generalized equations for symmetrical electrolytes, J. Phys. Chem., 96, 3513-3520, https://doi.org/10.1021/j100187a061, 1992.

Clegg, S. L., Pitzer, K. S., and Brimblecombe, P.: Thermodynamics of Multicomponent, Miscible, Ionic-Solutions .2. Mixtures Including Unsymmetrical Electrolytes, J. Phys. Chem., 96, 9470-9479, https://doi.org/10.1021/J100202a074, 1992.

Clegg, S. L., Brimblecombe, P., and Wexler, A. S.: Thermodynamic Model of the System H+−NH4+−Na+−SO42-−NO3-−Cl-−H2O at 298.15 K, J. Phys. Chem. A, 102, 2155-2171, https://doi.org/10.1021/jp973043j, 1998.

Clifton, C. L., Altstein, N., and Huie, R. E.: Rate-constant for the reaction of NO2 with sulfur (IV) of the pH range 5.3-13, Environ. Sci. Technol., 22, 586-589, https://doi.org/10.1021/es00170a018, 1988.

Collett, J., Hoag, K., and Rao, X.: Internal acid buffering in San Joaquin Valley fog drops and its influence on aerosol processing, Atmos. Environ., 33, 4833-4847, https://doi.org/10.1016/S1352-2310(99)00221-6, 1999.

Collett, J. L., Bator, A., Rao, X., and Demoz, B. B.: Acidity variations across the cloud drop size spectrum and their influence on rates of atmospheric sulfate production, Geophys. Res. Lett., 21, 2393-2396, https://doi.org/10.1029/94GL02480, 1994.

Collett, J. L., Sherman, D. E., Moore, K. F., Hannigan, M. P., and Lee, T.: Aerosol particle processing and removal by fogs: observations in chemically heterogeneous central California radiation fogs, Water, Air and Soil Pollution: Focus, 1, 303-312, http://dx.doi.org/10.1023/A:1013175709931, 2001.

Collett, J. L., Bator, A., Sherman, D. E., Moore, K. F., Hoag, K. J., Demoz, B. B., Rao, X., and Reilly, J. E.: The chemical composition of fogs and intercepted clouds in the United States, Atmos. Res., 64, 29-40, https://doi.org/10.1016/S0169-8095(02)00077-7, 2002.

Collett, J. L., Herckes, P., Youngster, S., and Lee, T.: Processing of atmospheric organic matter by California radiation fogs, Atmos. Res., 87, 232-241, https://doi.org/10.1016/j.atmosres.2007.11.005, 2008.

Covington, A. K., Bates, R. G., and Durst, R. A.: (1985). Definitions of pH scales, standard reference values, measurement of pH, and related terminology, Pure Appl. Chem. 57 (3): 531–542, https://doi.org/10.1351/pac198557030531, 1985.

Craig, R. L., and Ault, A. P.: Aerosol Acidity: Direct Measurement from a Spectroscopic Method, in: Multiphase Environmental Chemistry in the Atmosphere, ACS Symposium Series, 1299, American Chemical Society, 171-191, https://doi.org/10.1021/bk-2018-1299.ch009, 2018.

Craig, R. L., Nandy, L., Axson, J. L., Dutcher, C. S., and Ault, A. P.: Spectroscopic Determination of Aerosol pH from Acid–Base Equilibria in Inorganic, Organic, and Mixed Systems, J. Phys. Chem. A, 121, 5690-5699, https://doi.org/10.1021/acs.jpca.7b05261, 2017.

Craig, R. L., Peterson, P. K., Nandy, L., Lei, Z., Hossain, M. A., Camarena, S., Dodson, R. A., Cook, R. D., Dutcher, C. S., and Ault, A. P.: Direct Determination of Aerosol pH: Size-Resolved Measurements of Submicrometer and Supermicrometer Aqueous Particles, Anal. Chem., https://doi.org/10.1021/acs.analchem.8b00586, 2018.

Croft, B., Wentworth, G. R., Martin, R. V., Leaitch, W. R., Murphy, J. G., Murphy, B. N., Kodros, J. K., Abbatt, J. P. D., and Pierce, J. R.: Contribution of Arctic seabird-colony ammonia to atmospheric particles and cloud-albedo radiative effect, Nature Commun., 7, 13444, https://doi.org/10.1038/ncomms13444, 2016.

Dallemagne, M. A., Huang, X. Y., and Eddingsaas, N. C.: Variation in pH of Model Secondary Organic Aerosol during Liquid-Liquid Phase Separation, J. Phys. Chem. A, 120, 2868-2876, https://doi.org/10.1021/acs.jpca.6b00275, 2016.

Dall'Osto, M., Airs, R. L., Beale, R., Cree, C., Fitzsimons, M. F., Beddows, D., Harrison, R. M., Ceburnis, D., O'Dowd, C., Rinaldi, M., Paglione, M., Nenes, A., Decesari, S., and Simó, R.: Simultaneous Detection of Alkylamines in the Surface Ocean and Atmosphere of the Antarctic Sympagic Environment, ACS Earth and Space Chemistry, 3, 854-862, https://doi.org/10.1021/acsearthspacechem.9b00028, 2019.

DeCarlo, P. F., Avery, A. M., and Waring, M. S.: Thirdhand smoke uptake to aerosol particles in the indoor environment, Science Advances, 4, https://doi.org/10.1126/sciadv.aap8368, 2018.

Deguillaume, L., Leriche, M., Desboeufs, K., Mailhot, G., George, C., and Chaumerliac, N.: Transition metals in atmospheric liquid phases: Sources, reactivity, and sensitive parameters, Chem. Rev., 105, 3388-3431, https://doi.org/10.1021/cr040649c, 2005.

Deguillaume, L., Desboeufs, K., Leriche, M., Long, Y., and Chaumerliac, N.: Effect of iron dissolution on cloud chemistry: from laboratory measurements to model results, Atmospheric Pollution Research, 1, 220-228, https://doi.org/10.5094/APR.2010.029, 2010.

Dennis, R. L., Bhave, P. V., and Pinder, R. W.: Observable indicators of the sensitivity of PM2.5 nitrate to emission reductions - Part II: Sensitivity to errors in total ammonia and total nitrate of the CMAQ-predicted non-linear effect of SO2 emission reductions, Atmos. Environ., 42, 1287-1300, https://doi.org/10.1016/j.atmosenv.2007.10.036, 2008.

Dentener, F. J., and Crutzen, P. J.: A three-dimensional model of the global ammonia cycle, J. Atmos. Chem., 19, 331-369, https://doi.org/10.1007/BF00694492, 1994.

Dentener, F. J., and Crutzen, P. J.: Reaction of N_2O_5 on tropospheric aerosols: Impact on the global distributions of NO_x, O_3, and OH, J. Geophys. Res., 98(D4), 7149– 7163, https://doi.org/10.1029/92JD02979, 1993.

Dhawan, S. and Biswas, P.: Sampling artifacts in denuders during phase partitioning measurements of semi-volatile organic compounds, Aerosol Sci. Tech., 53, 73-85, https://doi.org/10.1080/02786826.2018.1546373, 2019.

Di, Q., Wang, Y., Zanobetti, A., Wang, Y., Koutrakis, P., Choirat, C., Dominici, F., and Schwartz, J. D.: Air Pollution and Mortality in the Medicare Population, New Engl. J. Med., 376, 2513-2522, https://doi.org/10.1056/NEJMoa1702747, 2017.

Dickson, A. G.: pH buffers for sea water media based on the total hydrogen ion concentration scale, Deep Sea Research Part I: Oceanographic Research Papers, 40, 107-118, https://doi.org/10.1016/0967-0637(93)90055-8, 1993.

Ding, J., Zhao, P., Su, J., Dong, Q., and Du, X.: Aerosol pH and its ~~influencing~~ driving factors in Beijing, Atmos. Chem. Phys., 19, 7939-7954, https://doi.org/10.5194/acp-19-7939-2019, 2019.

Formatted: Subscript

Formatted: Subscript

Formatted: Subscript

Formatted: Subscript

Dockery, D. W., Pope, C. A., Xu, X., Spengler, J. D., Ware, J. H., Fay, M. E., Ferris, B. G., and Speizer, F. E.: An Association between Air Pollution and Mortality in Six U.S. Cities, New Engl. J. Med., 329, 1753-1759, 1993.

Dockery, D. W., Cunningham, J., Damokosh, A. I., Neas, L. M., Spengler, J. D., Koutrakis, P., Ware, J. H., Raizenne, M., and Speizer, F. E.: Health effects of acid aerosols on North American children: respiratory symptoms, Environ. Health Persp., 104, 500-505, https://doi.org/10.1289/ehp.96104500, 1996.

Dollard, G. J., Unsworth, M. H., and Harve, M. J.: Pollutant transfer in upland regions by occult precipitation, Nature, 302, 241-243, https://doi.org/10.1038/302241a0, 1983.

Dovrou, E., Lim, C. Y., Canagaratna, M. R., Kroll, J. H., Worsnop, D. R., and Keutsch, F. N.: Measurement techniques for identifying and quantifying hydroxymethanesulfonate (HMS) in an aqueous matrix and particulate matter using aerosol mass spectrometry and ion chromatography, Atmos. Meas. Tech., 12, 5303–5315, https://doi.org/10.5194/amt-12-5303-2019, 2019.~~Dovrou, E., Lim, C. Y., Canagaratna, M. R., Kroll, J. H., Worsnop, D. R., and Keutsch, F. N.: Measurement techniques of identifying and quantifying sulfur compounds in fog and cloud water, Atmos. Meas. Tech. Discuss., https://doi.org/10.5194/amt-2019-127, in review, 2019.~~

Driscoll, C. T., Lambert, K. F., and Chen, L.: Acidic deposition: Sources and ecological effects Acid in the Environment: Lessons Learned and Future Prospects, edited by: Visgilio, G. R. and Whitelaw, D. M., https://doi.org/10.1007/978-0-387-37562-5, 2007.

Duan, L., Yu, Q., Zhang, Q., Wang, Z., Pan, Y., Larssen, T., Tang, J., and Mulder, J.: Acid deposition in Asia: Emissions, deposition, and ecosystem effects, Atmos. Environ., 146, 55-69, https://doi.org/10.1016/j.atmosenv.2016.07.018, 2016.

Eatough, D. J., Long, R. W., Modey, W. K., and Eatough, N. L.: Semi-volatile secondary organic aerosol in urban atmospheres: meeting a measurement challenge, Atmos. Environ., 37, 1277-1292, https://doi.org/10.1016/S1352-2310(02)01020-8, 2003.

Edgerton, E. S., Hartsell, B. E., Saylor, R. D., Jansen, J. J., Hansen, D. A., and Hidy, G. M.: The Southeastern Aerosol Research and Characterization Study, Part 3: Continuous Measurements of Fine Particulate Matter Mass and Composition, J. Air Waste Manage. Assoc., 56, 1325-1341, https://doi.org/10.1080/10473289.2006.10464585, 2006.

EPA: Compendium of Methods for the Determination of Inorganic Compoundsin Ambient Air: Compendium Method IO-4.1, Determination of the strong acidity of atmospheric particles fine-particles (<2.5 um), Cincinnati, OH, EPA/625/R-96/010a, 1999.

EPA: Integrated Science Assessment (ISA) for particulate matter (Final Report, Dec 2009), U.S. Environmental Protection Agency, Washington, DC, EPA/600/R-08/139F, 2009, 2009.

EPA,: Modeling Guidance for Demonstrating Attainment of Air Quality Goals for Ozone, PM2.5, and Regional Haze., U.S. Environmental Protection Agency, Office of Air Quality Planning and Standards, Research Triangle Park, NC. EPA 454/R-18-009, available at: https://www3.epa.gov/ttn/scram/guidance/guide/O3-PM-RH-Modeling_Guidance-2018.pdf, 2018.

Ervens, B., Herckes, P., Feingold, G., Lee, T., Collett, J. L., and Kreidenweis, S. M.: On the Drop-Size Dependence of Organic Acid and Formaldehyde Concentrations in Fog, J. Atmos. Chem., 46, 239-269, https://doi.org/10.1023/A:1026393805907, 2003.

Exner, M., Herrmann, H., and Zellner, R.: Rate constants for the reactions of the NO3 radical with HCOOH/HCOO- and CH3COOH/CH3COO- in aqueous-solution between 278 K and 328 K, J. Atmos. Chem., 18, 359-378, https://doi.org/10.1007/BF00712451, 1994.

Facchini, M. C., Fuzzi, S., Lind, J. A., Fierlinger-Oberlinninger, H., Kalina, M., Puxbaum, H., Winiwarter, W., Arends, B. G., Wobrock, W., Jaeschke, W., Berner, A., and Kruisz, C.: Phase-partitioning and chemical reactions of low molecular weight organic compounds in fog, Tellus B, 44, 533-544, https://doi.org/10.3402/tellusb.v44i5.15566, 1992.

Fahey, K. M. and Pandis, S. N.: Optimizing model performance: variable size resolution in cloud chemistry modeling, Atmos. Environ., 35, 4471-4478, https://doi.org/10.1016/S1352-2310(01)00224-2, 2001.

Fahey, K. M. and Pandis, S.N.: Size-resolved aqueous-phase atmospheric chemistry in a three-dimensional chemical transport model. J. Geophys. Res., 108, 4690-4701, https://doi.org/10.1029/2003JD003564, 2003.

Fahey, K. M., Carlton, A. G., Pye, H. O. T., Baeka, J., Hutzell, W. T., Stanier, C. O., Baker, K. R., Appel, K. W., Jaoui, M., and Offenberg, J. H.: A framework for expanding aqueous chemistry in the Community Multiscale Air Quality (CMAQ) model version 5.1, Geosci. Model Dev., 10, 1587-1605, https://doi.org/10.5194/gmd-10-1587-2017, 2017.

Fahey, K. M., Pandis, S., Collett Jr, J., and Herckes, P.: The influence of size-dependent droplet composition on pollutant processing by fogs, Atmos. Environ., 39, 4561-4574, https://doi.org/10.1016/j.atmosenv.2005.04.006, 2005.

Fairlie, T., Jacob, D., Dibb, J., Alexander, B., Avery, M., van Donkelaar, A., and Zhang, L.: Impact of mineral dust on nitrate, sulfate, and ozone in transpacific Asian pollution plumes, Atmos. Chem. Phys., 10, 3999-4012, https://doi.org/10.5194/acp-10-3999-2010, 2010.

Fang, T., Guo, H., Zeng, L., Verma, V., Nenes, A., and Weber, R.: Highly Acidic Ambient Particles, Soluble Metals, and Oxidative Potential: A Link between Sulfate and Aerosol Toxicity, Environ. Sci. Technol., 51, 2611-2620, https://doi.org/10.1021/acs.est.6b06151, 2017.

Farmer, D. K., Matsunaga, A., Docherty, K. S., Surratt, J. D., Seinfeld, J. H., Ziemann, P. J., and Jimenez, J. L.: Response of an aerosol mass spectrometer to organonitrates and organosulfates and implications for atmospheric chemistry, P. Natl. Acad. Sci. U. S. A., 107, 6670, https://doi.org/10.1073/pnas.0912340107, 2010.

Fast, J. D., Gustafson, W. I., Easter, R. C., Zaveri, R. A., Barnard, J. C., Chapman, E. G., Grell, G. A., and Peckham, S. E.: Evolution of ozone, particulates, and aerosol direct radiative forcing in the vicinity of Houston using a fully coupled meteorology-chemistry-aerosol model, J. Geophys. Res-Atmos., 111, D21305, https://doi.org/10.1029/2005jd006721, 2006.

Feichter, J., Kjellström, E., Rodhe, H., Dentener, F., Lelieveldi, J., and Roelofs, G.-J.: Simulation of the tropospheric sulfur cycle in a global climate model, Atmos. Environ., 30, 1693-1707, https://doi.org/10.1016/1352-2310(95)00394-0, 1996.

Feng, J.L., Guo, Z.G., Zhang, T.R., Yao, X.H., Chan, C.K., and Fang, M.: Source and formation of secondary particulate matter in $PM_{2.5}$ in Asian continental outflow. J. of Geophys. Res.-Atmos., 117, https://doi.org/10.1029/2011JD016400, 2012.

Fisher, J. A., Jacob, D. J., Wang, Q., Bahreini, R., Carouge, C. C., Cubison, M. J., Dibb, J. E., Diehl, T., Jimenez, J. L., Leibensperger, E. M., Lu, Z., Meinders, M. B. J., Pye, H. O. T., Quinn, P. K., Sharma, S., Streets, D. G., van Donkelaar, A., and Yantosca, R. M.: Sources, distribution, and acidity of sulfate–ammonium aerosol in the Arctic in winter–spring, Atmos. Environ., 45, 7301-7318, https://doi.org/10.1016/j.atmosenv.2011.08.030, 2011.

Fossum, K. N., Ovadnevaite, J., Ceburnis, D., Dall'Osto, M., Marullo, S., Bellacicco, M., Simó, R., Liu, D., Flynn, M., Zuend, A., and O'Dowd, C.: Summertime Primary and Secondary Contributions to Southern Ocean Cloud Condensation Nuclei, Sci. Rep., 8, 13844, https://doi.org/10.1038/s41598-018-32047-4, 2018.

Fountoukis, C. and Nenes, A.: ISORROPIA II: a computationally efficient thermodynamic equilibrium model for K^+-Ca^{2+}-Mg^{2+}-NH_4^+-Na^+-SO_4^{2-}-NO_3^--Cl^--H_2O aerosols, Atmos. Chem. Phys., 7, 4639-4659, https://doi.org/10.5194/acp-7-4639-2007, 2007.

Frampton, M. W., Ghio, A. J., Samet, J. M., Carson, J. L., Carter, J. D., and Devlin, R. B.: Effects of aqueous extracts of PM10 filters from the Utah Valley on human airway epithelial cells, Am. J. Physiol., 277, L960-L967, https://doi.org/10.1152/ajplung.1999.277.5.L960, 1999.

Fredenslund, A., Jones, R. L., and Prausnitz, J. M.: Group-Contribution Estimation of Activity Coefficients in Nonideal Liquid Mixtures, AIChE J., 21, 1086-1099, https://doi.org/10.1002/aic.690210607, 1975.

Fridlind, A. M. and Jacobson, M. Z.: A study of gas-aerosol equilibrium and aerosol pH in the remote marine boundary layer during the First Aerosol Characterization Experiment (ACE 1), J. Geophys. Res. Atmos., 105, 17325-17340, https://doi.org/10.1029/2000jd900209, 2000.

Friese, E. and Ebel, A.: Temperature Dependent Thermodynamic Model of the System H+−NH4+−Na+−SO42−−NO3−−Cl−−H2O, J. Phys. Chem. A, 114, 11595-11631, https://doi.org/10.1021/jp101041j, 2010.

Froyd, K. D., Murphy, S. M., Murphy, D. M., de Gouw, J. A., Eddingsaas, N. C., and Wennberg, P. O.: Contribution of isoprene-derived organosulfates to free tropospheric aerosol mass, P. Natl. Acad. Sci. U. S. A., 107, 21360-21365, https://doi.org/10.1073/pnas.1012561107, 2010.

Ganbavale, G., Zuend, A., Marcolli, C., and Peter, T.: Improved AIOMFAC model parameterisation of the temperature dependence of activity coefficients for aqueous organic mixtures, Atmos. Chem. Phys., 15, 447-493, https://doi.org/10.5194/acp-15-447-2015, 2015.

Ganor, E.: A method for identifying sulfuric acid in single cloud and fog droplets, Atmos. Environ., 33, 4235-4242, https://doi.org/10.1016/S1352-2310(99)00170-3, 1999.

Ganor, E., Levin, Z., and Pardess, D.: Determining the acidity and chemical composition of fog, haze and cloud droplets in Israel, Atmos. Environ. A, 27, 1821-1832, https://doi.org/10.1016/0960-1686(93)90287-9, 1993.

Gaston, C., Riedel, T., Zhang, Z., Gold, A., Surratt, J., and Thornton, J.: Reactive Uptake of an Isoprene-Derived Epoxydiol to Submicron Aerosol Particles, Environ. Sci. Technol., 48, 11178-11186, https://doi.org/10.1021/es5034266, 2014.

Gioda, A., Mayol-Bracero, O. L., Morales-García, F., Collett, J., Decesari, S., Emblico, L., Facchini, M. C., Morales-De Jesús, R. J., Mertes, S., Borrmann, S., Walter, S., and Schneider, J.: Chemical Composition of Cloud Water in the Puerto Rican Tropical Trade Wind Cumuli, Water, Air, Soil Poll., 200, 3-14, https://doi.org/10.1007/s11270-008-9888-4, 2009.

Gioda, A., Reyes-Rodríguez, G. J., Santos-Figueroa, G., Collett, J. L., Decesari, S., Ramos, M. d. C. K. V., Bezerra Netto, H. J. C., de Aquino Neto, F. R., and Mayol-Bracero, O. L.: Speciation of water-soluble inorganic, organic, and total nitrogen in a background marine environment: Cloud water, rainwater, and aerosol particles, J. Geophys. Res-Atmos., 116, https://doi.org/10.1029/2010JD015010, 2011.

Gioda, A., Mayol-Bracero, O. L., Scatena, F. N., Weathers, K. C., Mateus, V. L., and McDowell, W. H.: Chemical constituents in clouds and rainwater in the Puerto Rican rainforest: Potential sources and seasonal drivers, Atmos. Environ., 68, 208-220, https://doi.org/10.1016/j.atmosenv.2012.11.017, 2013.

Gordon, H., Kirkby, J., Baltensperger, U., Bianchi, F., Breitenlechner, M., Curtius, J., Dias, A., Dommen, J., Donahue, N. M., Dunne, E. M., Duplissy, J., Ehrhart, S., Flagan, R. C., Frege, C., Fuchs, C., Hansel, A., Hoyle, C. R., Kulmala, M., Kürten, A., Lehtipalo, K., Makhmutov, V., Molteni, U., Rissanen, M. P., Stozkhov, Y., Tröstl, J., Tsagkogeorgas, G., Wagner, R., Williamson, C., Wimmer, D., Winkler, P. M., Yan, C., and Carslaw, K. S.: Causes and importance of new particle formation in the present-day and preindustrial atmospheres, J. Geophys. Res-Atmos., 122, 8739-8760, https://doi.org/10.1002/2017JD026844, 2017.

Grell, G. A., Peckham, S. E., Schmitz, R., McKeen, S. A., Frost, G., Skamarock, W. C., and Eder, B.: Fully coupled "online" chemistry within the WRF model, Atmos. Environ., 39, 6957-6975, https://doi.org/10.1016/j.atmosenv.2005.04.027, 2005.

Guo, H., Xu, L., Bougiatioti, A., Cerully, K. M., Capps, S. L., Hite, J. R., Carlton, A. G., Lee, S. H., Bergin, M. H., Ng, N. L., Nenes, A., and Weber, R. J.: Fine-particle water and pH in the southeastern United States, Atmos. Chem. Phys., 15, 5211-5228, https://doi.org/10.5194/acp-15-5211-2015, 2015.

Guo, H., Sullivan, A. P., Campuzano-Jost, P., Schroder, J. C., Lopez-Hilfiker, F. D., Dibb, J. E., Jimenez, J. L., Thornton, J. A., Brown, S. S., Nenes, A., and Weber, R. J.: Fine particle pH and the partitioning of nitric acid during winter in the northeastern United States, J. Geophys. Res-Atmos., 121, 10,355-310,376, https://doi.org/10.1002/2016JD025311, 2016.

Guo, H., Weber, R., and Nenes, A.: High levels of ammonia do not raise fine particle pH sufficiently to yield nitrogen oxide-dominated sulfate production, Sci. Rep., 7, https://doi.org/10.1038/s41598-017-11704-0, 2017a.

Guo, H. Y., Liu, J. M., Froyd, K. D., Roberts, J. M., Veres, P. R., Hayes, P. L., Jimenez, J. L., Nenes, A., and Weber, R. J.: Fine particle pH and gas–particle phase partitioning of inorganic species in Pasadena, California, during the 2010 CalNex campaign, Atmos. Chem. Phys., 17, 5703-5719, https://doi.org/10.5194/acp-17-5703-2017, 2017b.

Guo, H., Nenes, A., and Weber, R. J.: The underappreciated role of non-volatile cations in aerosol ammonium-sulfate molar ratios, Atmos. Chem. Phys., 18, 17307-17323, https://doi.org/10.5194/acp-18-17307-2018, 2018a.

Guo, H., Otjes, R., Schlag, P., Kiendler-Scharr, A., Nenes, A., and Weber, R. J.: Effectiveness of ammonia reduction on control of fine particle nitrate, Atmos. Chem. Phys., 18, 12241-12256, https://doi.org/10.5194/acp-18-12241-2018, 2018b.

Guo, J., Wang, Y., Shen, X., Wang, Z., Lee, T., Wang, X., Li, P., Sun, M., Jeffrey, L. C. J., Jr., Wang, W., and Wang, T.: Characterization of cloud water chemistry at Mount Tai, China: Seasonal variation, anthropogenic impact, and cloud processing, Atmos. Environ., 60, 467-476, https://doi.org/10.1016/j.atmosenv.2012.07.016, 2012a.

Guo, S., Hu, M, Guo, Q. F., Zhang, X., Zheng, M., Zheng, J., Chang, C. C., Schauer, J. J., and Zhang, R. Y.: Primary sources and secondary formation of organic aerosols in Beijing, China, Environ. Sci. Technol., 46, 9846-9853, https://doi.org/10.1021/es2042564, 2012b.

Gurciullo, C. S., and Pandis, S. N.: Effect of composition variations in cloud droplet populations on aqueous-phase chemistry, J. Geophys. Res -Atmos., 102, 9375-9385, https://doi.org/10.1029/96JD03651, 1997.

Gwynn, R. C., Burnett, R. T., and Thurston, G. D.: A time-series analysis of acidic particulate matter and daily mortality and morbidity in the Buffalo, New York, region, Environ. Health Persp., 108, 125-133, https://doi.org/10.1289/ehp.00108125, 2000.

Hakkinen, S. A. K., McNeill, V. F., and Riipinen, I.: Effect of Inorganic Salts on the Volatility of Organic Acids, Environ. Sci. Technol., 48, 13718-13726, https://doi.org/10.1021/es5033103, 2014.

Hallquist, M., Wenger, J. C., Baltensperger, U., Rudich, Y., Simpson, D., Claeys, M., Dommen, J., Donahue, N. M., George, C., Goldstein, A. H., Hamilton, J. F., Herrmann, H., Hoffmann, T., Iinuma, Y., Jang, M., Jenkin, M. E., Jimenez, J. L., Kiendler-Scharr, A., Maenhaut, W., McFiggans, G., Mentel, T. F., Monod, A., Prevot, A. S. H., Seinfeld, J. H., Surratt, J. D., Szmigielski, R., and Wildt, J.: The formation, properties and impact of secondary organic aerosol: current and emerging issues, Atmos. Chem. Phys., 9, 5155-5236, https://doi.org/10.5194/acp-9-5155-2009, 2009.

Hand, J. L., Gill, T. E., and Schichtel, B. A.: Spatial and seasonal variability in fine mineral dust and coarse aerosol mass at remote sites across the United States, J. Geophys. Res.-Atmos., 122, 3080-3097, https://doi.org/10.1002/2016jd026290, 2017.

Hanisch, F. and Crowley, J. N.: Heterogeneous reactivity of gaseous nitric acid on Al2O3, CaCO3, and atmospheric dust samples: A Knudsen cell study, J. Phys. Chem. A, 105, 3096-3106, https://doi.org/10.1021/jp001254+, 2001.

Hansen, D. A., Edgerton, E. S., Hartsell, B. E., Jansen, J. J., Kandasamy, N., Hidy, G. M., and Blanchard, C. L.: The Southeastern Aerosol Research and Characterization Study: Part 1—Overview, J. Air Waste Manage. Assoc., 53, 1460-1471, https://doi.org/10.1080/10473289.2003.10466318, 2003.

Hansen, H. K., Rasmussen, P., Fredenslund, A., Schiller, M., and Gmehling, J.: Vapor-liquid-equilibria by UNIFAC group contribution. 5. Revision and extension, Ind. Eng. Chem. Res., 30, 2352-2355, https://doi.org/10.1021/ie00058a017, 1991.

Haskins, J. D., Jaegle, L., Shah, V., Lee, B. H., Lopez-Hilfiker, F. D., Campuzano-Jost, P., Schroder, J. C., Day, D. A., Guo, H. Y., Sullivan, A. P., Weber, R., Dibb, J., Campos, T., Jimenez, J. L., Brown, S. S., and Thornton, J. A.: Wintertime Gas–Particle Partitioning and Speciation of Inorganic Chlorine in the Lower Troposphere Over the Northeast United States and Coastal Ocean, J. Geophys. Res.-Atmos., 123, 12897-12916, https://doi.org/10.1029/2018JD028786, 2018.

Hegg, D. A. and Hobbs, P. V.: Sulfate and nitrate chemistry in cumuliform clouds, Atmos. Environ., 20(5), 901–909, https://doi.org/10.1016/0004-6981(86)90274-X, 1986.

Hegg, D. A., and Larson, T. V.: The effects of microphysical parameterization on model predictions of sulfate production in clouds, Tellus B, 42, 272-284, https://doi.org/10.1034/j.1600-0889.1990.t01-2-00006.x, 1990.

Hegg, D. A., Hobbs, P. V., and Radke, L. F.: Measurements of the scavenging of sulfate and nitrate in clouds, Atmos. Environ., 18, 1939-1946, https://doi.org/10.1016/0004-6981(84)90371-8, 1984.

Hegg, D. A., Yuen, P.-F., and Larson, T. V.: Modeling the effects of heterogeneous cloud chemistry on the marine particle size dis tribution. J. Geophys. Res., 97, 12 927-12 933, https://doi.org/10.1029/92JD01184,1992

Hennigan, C. J., Izumi, J., Sullivan, A. P., Weber, R. J., and Nenes, A.: A critical evaluation of proxy methods used to estimate the acidity of atmospheric particles, Atmos. Chem. Phys., 15, 2775-2790, https://doi.org/10.5194/acp-15-2775-2015, 2015.

Herckes, P., Valsaraj, K. T., and Collett, J. L., Jr.: A review of observations of organic matter in fogs and clouds: Origin, processing and fate, Atmos. Res., 132, 434-449, https://doi.org/10.1016/j.atmosres.2013.06.005, 2013.

Herckes, P., Marcotte, A. R., Wang, Y., and Collett, J. L.: Fog composition in the Central Valley of California over three decades, Atmos. Res., 151, 20-30, https://doi.org/10.1016/j.atmosres.2014.01.025, 2015.

Herrmann, H., Hoffmann, D., Schaefer, T., Brauer, P., and Tilgner, A.: Tropospheric Aqueous-Phase Free-Radical Chemistry: Radical Sources, Spectra, Reaction Kinetics and Prediction Tools, ChemPhysChem, 11, 3796-3822, https://doi.org/10.1002/cphc.201000533, 2010.

Herrmann, H., Schaefer, T., Tilgner, A., Styler, S., Weller, C., Teich, M., and Otto, T.: Tropospheric Aqueous-Phase Chemistry: Kinetics, Mechanisms, and Its Coupling to a Changing Gas Phase, Chem. Rev., 115, 4259-4334, https://doi.org/10.1021/cr500447k, 2015.

Hileman, B.: Acid fog, Environ. Sci. Technol., 17, 117A-120A, https://doi.org/10.1021/es00109a714, 1983.

Hinrichs, R. Z., Buczek, P., and Trivedi, J. J.: Solar Absorption by Aerosol-Bound Nitrophenols Compared to Aqueous and Gaseous Nitrophenols, Environ. Sci. Technol., 50, 5661-5667, https://doi.org/10.1021/acs.est.6b00302, 2016.

Hoag, K. J., Collett Jr, J. L., and Pandis, S. N.: The influence of drop size-dependent fog chemistry on aerosol processing by San Joaquin Valley fogs, Atmos. Environ., 33, 4817-4832, https://doi.org/10.1016/S1352-2310(99)00268-X, 1999.

Hodshire, A. L., Lawler, M. J., Zhao, J., Ortega, J., Jen, C., Yli-Juuti, T., Brewer, J. F., Kodros, J. K., Barsanti, K. C., Hanson, D. R., McMurry, P. H., Smith, J. N., and Pierce, J. R.: Multiple new-particle growth pathways observed at the US DOE Southern Great Plains field site, Atmos. Chem. Phys., 16, 9321-9348, https://doi.org/10.5194/acp-16-9321-2016, 2016.

Hossaini, R., Chipperfield, M. P., Saiz-Lopez, A., Fernandez, R., Monks, S., Feng, W. H., Brauer, P., and von Glasow, R.: A global model of tropospheric chlorine chemistry: Organic versus inorganic sources and impact on methane oxidation, J. Geophys. Res.-Atmos., 121, 14271-14297, https://doi.org/10.1002/2016jd025756, 2016.

Hsu, S., Wong, G., Gong, G., Shiah, F., Huang, Y., Kao, S., Tsai, F., Lung, S., Lin, F., Lin, I., Hung, C., and Tseng, C.: Sources, solubility, and dry deposition of aerosol trace elements over the East China Sea, Mar. Chem., 120, 116-127, https://doi.org/10.1016/j.marchem.2008.10.003, 2010.

Hu, X.-M., Zhang, Y., Jacobson, M. Z., and Chan, C. K.: Coupling and evaluating gas/particle mass transfer treatments for aerosol simulation and forecast, J. Geophys. Res.-Atmos.,113, D11208, https://doi.org/10.1029/2007JD009588, 2008

Hu, J., Yin, Y., and Chen, Q.: The Acidity Distribution of Drops in a Deep Convective Cloud, J. Geophys. Res.-Atmos., 124, 424-440, 2019.

IPCC: Climate Change 2007: Synthesis Report. Contribution of Working Groups I, II and III to the Fourth Assessment Report of the Intergovernmental Panel on Climate Change [Core Writing Team, edited by Pachauri, R.K. and Reisinger, A.], IPCC, Geneva, Switzerland, 104 pp, https://www.ipcc.ch/report/ar4/syr/, 2007.

Ito, A. and Feng, Y.: Role of dust alkalinity in acid mobilization of iron, Atmos. Chem. Phys., 10, 9237-9250, https://doi.org/10.5194/acp-10-9237-2010, 2010.

Ito, K., Chasteen, C. C., Chung, H. K., Poruthoor, S. K., Zhang, G. F., and Dasgupta, P. K.: A continuous monitoring system for strong acidity in aerosols, Anal. Chem., 70, 2839-2847, https://doi.org/10.1021/Ac980135b, 1998.

Ito A., Myriokefalitakis S., Kanakidou M., Mahowald NM., Scanza R A., Hamilton D. S., Baker A. R., Jickells T., Sarin M, Bikkina S., Gao Y., Shelley R.U., Buck C.S., Landing W.M., Bowie A.R., Perron M.M.G., Guieu C., Meskhidze, N., Johnson, M.S., Feng, Y., Kok, J.F., Nenes, A., and Duce, R.A.:, Johnson MS., Feng Y, Kok JF., Nenes A, Duce RA., Pyrogenic iron: The missing link to high iron solubility in aerosols, Science Advances, 5(5), https://doi.org/10.1126/sciadv.aau7671N, 2019.

Ito, T., Nenes, A., Johnson, M. S., Meskhidze, N., and Deutsch, C.: Acceleration of oxygen decline in the tropical Pacific over the past decades by aerosol pollutants, Nat. Geosci., 9, 443, https://doi.org/10.1038/ngeo2717, 2016.

IUPAC: Compendium of Chemical Terminology, 2nd edition (the “Gold Book”), Blackwell Scientific Publications, Oxford (1997). Online version: (2019), available at: http://publications.iupac.org/books/author/mcnaught.html, 1997.

Jacob, D. J., Munger, J. W., Waldman, J. M., and Hoffmann, M. R.: The H2SO4-HNO3-NH3 system at high humidities and in fogs: 1. Spatial and temporal patterns in the San Joaquin Valley of California, J. Geophys. Res.-Atmos., 91, 1073-1088, https://doi.org/10.1029/JD091iD01p01073, 1986a.

Jacob, D. J., Waldman, J. M., Munger, J. W., and Hoffmann, M. R.: The H2SO4-HNO3-NH3 system at high humidities and in fogs: 2. Comparison of field data with thermodynamic calculations, J. Geophys. Res.-Atmos., 91, 1089-1096, https://doi.org/10.1029/JD091iD01p01089, 1986b.

Jacobson, M. Z.: Development and application of a new air pollution modeling system—II. Aerosol module structure and design, Atmos. Environ., 31, 131-144, https://doi.org/10.1016/1352-2310(96)00202-6, 1997.

Jacobson, M. Z.: Studying the effects of calcium and magnesium on size-distributed nitrate and ammonium with EQUISOLV II. Atmos. Environ. 33, 3635-3649, https://doi.org/10.1016/S1352-2310(99)00105-3, 1999.

Jacobson, M. Z.: Analysis of aerosol interactions with numerical techniques for solving coagulation, condensation, dissolution, and reversible chemistry among multiple size distributions, J. Geophys. Res., 107, 4366, https://doi.org/10.1029/2001JD002044, 2002.

Jacobson, M. Z.: A solution to the problem of nonequilibrium acid/base gas–particle transfer at long time step, Aerosol Sci. Tech., 39, 92-103, https://doi.org/10.1080/027868290904546, 2005a.

Jacobson, M. Z.: Fundamentals of Atmospheric Modeling, 2nd Edition, Cambridge University Press, New York, 828pp, 2005b.

Jacobson, M. Z., Kaufman, Y. J., and Rudich Y.: Examining feedbacks of aerosols to urban climate with a model that treats 3-D clouds with aerosol inclusions, J. Geophys. Res.-Atmos.,112, D24205, https://doi.org/10.1029/2007JD008922, 2007.

Jacobson, M. Z., Tabazadeh, A., and Turco, R. P.: Simulating equilibrium within aerosols and nonequilibrium between gases and aerosols, J. Geophys. Res.-Atmos., 101, 9079-9091, https://doi.org/10.1029/96jd00348, 1996.

Jang, M., Czoschke, N. M., Lee, S., and Kamens, R. M.: Heterogeneous atmospheric aerosol production by acid-catalyzed particle-phase reactions, Science, 298, 814-817, https://doi.org/10.1126/science.1075798, 2002.

Jang, M., Cao, G., and Paul, J.: Colorimetric particle acidity analysis of secondary organic aerosol coating on submicron acidic aerosols, Aerosol Sci. Tech., 42, 409-420, https://doi.org/10.1080/02786820802154861, 2008.

Jen, C. N., Bachman, R., Zhao, J., McMurry, P. H., and Hanson, D. R.: Diamine-sulfuric acid reactions are a potent source of new particle formation, Geophys. Res. Lett., 43, 867-873, https://doi.org/10.1002/2015GL066958, 2016.

Jia, S., Wang, X., Zhang, Q., Sarkar, S., Wu, L., Huang, M., Zhang, J., and Yang, L.: Technical note: Comparison and interconversion of pH based on different standard states for aerosol acidity characterization, Atmos. Chem. Phys., 18, 11125-11133, https://doi.org/10.5194/acp-18-11125-2018, 2018.

Jickells, T., Baker, A. R., Cape, J. N., Cornell, S. E., and Nemitz, E.: The cycling of organic nitrogen through the atmosphere, Philosophical Transactions of the Royal Society B: Biological Sciences, 368, 20130115, https://doi.org/10.1098/rstb.2013.0115, 2013.

Jimenez, J. L., Canagaratna, M. R., Donahue, N. M., Prevot, A. S. H., Zhang, Q., Kroll, J. H., DeCarlo, P. F., Allan, J. D., Coe, H., Ng, N. L., Aiken, A. C., Docherty, K. S., Ulbrich, I. M., Grieshop, A. P., Robinson, A. L., Duplissy, J., Smith, J. D., Wilson, K. R., Lanz, V. A., Hueglin, C., Sun, Y. L., Tian, J., Laaksonen, A., Raatikainen, T., Rautiainen, J., Vaattovaara, P., Ehn, M., Kulmala, M., Tomlinson, J. M., Collins, D. R., Cubison, M. J., Dunlea, E. J., Huffman, J. A., Onasch, T. B., Alfarra, M. R., Williams, P. I., Bower, K., Kondo, Y., Schneider, J., Drewnick, F., Borrmann, S., Weimer, S., Demerjian, K., Salcedo, D., Cottrell, L., Griffin, R., Takami, A., Miyoshi, T., Hatakeyama, S., Shimono, A., Sun, J. Y., Zhang, Y. M., Dzepina, K., Kimmel, J. R., Sueper, D., Jayne, J. T., Herndon, S. C., Trimborn, A. M., Williams, L. R., Wood, E. C., Middlebrook, A. M., Kolb, C. E., Baltensperger, U., and Worsnop, D. R.: Evolution of Organic Aerosols in the Atmosphere, Science, 326, 1525-1529, https://doi.org/10.1126/science.1180353, 2009.

Junge, C. E.: Air chemistry and radioactivity, International geophysics series, 4, Academic Press, New York,, 382 p. pp., 1963.

Kalberer, M., Paulsen, D., Sax, M., Steinbacher, M., Dommen, J., Prevot, A., Fisseha, R., Weingartner, E., Frankevich, V., Zenobi, R., and Baltensperger, U.: Identification of polymers as major components of atmospheric organic aerosols, Science, 303, 1659-1662, https://doi.org/10.1126/science.1092185, 2004.

Kanakidou, M., Myriokefalitakis, S., and Tsigaridis, K.: Aerosols in atmospheric chemistry and biogeochemical cycles of nutrients, Environ. Res. Lett., 13, 063004, https://doi.org/10.1088/1748-9326/aabcdb, 2018.

Kanakidou M., Myriokefalitakis, S., Tsagkaraki, M., Atmospheric inputs of nutrients to the Mediterranean Sea, Deep Sea Research II, https://doi.org/10.1016/j.dsr2.2019.06.014, 2019

Karydis, V. A., Tsimpidi, A. P., Pozzer, A., Astitha, M., and Lelieveld, J.: Effects of mineral dust on global atmospheric nitrate concentrations, Atmos. Chem. Phys., 16, 1491-1509, https://doi.org/10.5194/acp-16-1491-2016, 2016.

Kawamura, K. and Kaplan, I. R.: Capillary gas chromatography determination of volatile organic acids in rain and fog samples, Anal. Chem., 56, 1616-1620, https://doi.org/10.1021/ac00273a018, 1984.

Keene, W. C. and Savoie, D. L.: The pH of deliquesced sea-salt aerosol in polluted marine air, Geophys. Res. Lett., 25, 2181-2184, https://doi.org/10.1029/98gl01591, 1998.

Keene, W. C., Sander, R., Pszenny, A. A. P., Vogt, R., Crutzen, P. J., and Galloway, J. N.: Aerosol pH in the marine boundary layer: A review and model evaluation, J. Aerosol Sci., 29, 339-356, https://doi.org/10.1016/S0021-8502(97)10011-8, 1998.

Keene, W. C., Pszenny, A. A. P., Maben, J. R., Stevenson, E., and Wall, A.: Closure evaluation of size-resolved aerosol pH in the New England coastal atmosphere during summer, J. Geophys. Res.-Atmos., 109, D23307, https://doi.org/10.1029/2004jd004801, 2004.

Kelly, F. J. and Fussell, J. C.: Size, source and chemical composition as determinants of toxicity attributable to ambient particulate matter, Atmos. Environ., 60, 504– 526, https://doi.org/10.1016/j.atmosenv.2012.06.039, 2012.

Kelly, J. T., Bhave, P. V., Nolte, C. G., Shankar, U., and Foley, K. M.: Simulating emission and chemical evolution of coarse sea-salt particles in the Community Multiscale Air Quality (CMAQ) model, Geosci. Model Dev., 3, 257-273, https://doi.org/10.5194/gmd-3-257-2010, 2010.

Kelly, J. T., Baker, K. R., Nolte, C. G., Napelenok, S. L., Keene, W. C., and Pszenny, A. A. P.: Simulating the phase partitioning of NH3, HNO3, and HCl with size-resolved particles over northern Colorado in winter, Atmos. Environ., 131, 67-77, https://doi.org/10.1016/j.atmosenv.2016.01.049, 2016.

Kelly, J. T., Parworth, C. L., Zhang, Q., Miller, D. J., Sun, K., Zondlo, M. A., et al.: Modeling NH_4NO_3 over the San Joaquin Valley during the 2013 DISCOVER-AQ campaign. J. Geophys. Res.-Atmos., 123, 4727– 4745, https://doi.org/10.1029/2018JD028290, 2018.

Kerber, R.C. and Fernando, M. S.: α-Oxocarboxylic Acids, J. Chem. Educ. 87, 10, 1079-1084, https://doi.org/10.1021/ed1003096, 2010.

Kerminen, V. M., Hillamo, R., Teinila, K., Pakkanen, T., Allegrini, I., and Sparapani, R.: Ion balances of size-resolved tropospheric aerosol samples: implications for the acidity and atmospheric processing of aerosols, Atmos. Environ., 35, 5255-5265, https://doi.org/10.1016/S1352-2310(01)00345-4, 2001.

Kim, Y. P. and Seinfeld, J. H.: Atmospheric Gas–Aerosol Equilibrium: III. Thermodynamics of Crustal Elements Ca2+, K+, and Mg2+, Aerosol Sci. Tech., 22, 93-110, https://doi.org/10.1080/02786829408959730, 1995.

Kim, Y. P., Seinfeld, J. H., and Saxena, P.: Atmospheric Gas-Aerosol Equilibrium I. Thermodynamic Model, Aerosol Sci. Tech., 19, 157-181, https://doi.org/10.1080/02786829308959628, 1993a.

Kim, Y. P., Seinfeld, J. H., and Saxena, P.: Atmospheric Gas-Aerosol Equilibrium II. Analysis of Common Approximations and Activity Coefficient Calculation Methods, Aerosol Sci. Tech., 19, 182-198, https://doi.org/10.1080/02786829308959629, 1993b.

Kirpes, R., Bondy, A., Bonanno, D., Moffet, R., Wang, B., Laskin, A., Ault, A., and Pratt, K.: Secondary sulfate is internally mixed with sea spray aerosol and organic aerosol in the winter Arctic, Atmos. Chem. Phys., 18, 3937-3949, https://doi.org/10.5194/acp-18-3937-2018, 2018.

Knopf, D. A., Luo, B. P., Krieger, U. K., and Koop, T.: Thermodynamic dissociation constant of the bisulfate ion from Raman and ion interaction modeling studies of aqueous sulfuric acid at low temperatures, J. Phys. Chem. A, 107, 4322-4332, https://doi.org/10.1021/jp027775+, 2003.

Knote, C., Hodzic, A., Jimenez, J. L., Volkamer, R., Orlando, J. J., Baidar, S., Brioude, J., Fast, J., Gentner, D. R., Goldstein, A. H., Hayes, P. L., Knighton, W. B., Oetjen, H., Setyan, A., Stark, H., Thalman, R., Tyndall, G., Washenfelder, R., Waxman, E., and Zhang, Q.: Simulation of semi-explicit mechanisms of SOA formation from glyoxal in aerosol in a 3-D model, Atmos. Chem. Phys., 14, 6213-6239, https://doi.org/10.5194/acp-14-6213-2014, 2014.

Knote, C., Hodzic, A., and Jimenez, J. L.: The effect of dry and wet deposition of condensable vapors on secondary organic aerosols concentrations over the continental US, Atmos. Chem. Phys., 15, 1-18, https://doi.org/10.5194/acp-15-1-2015, 2015.

Koch, D., Jacob, D., Tegen, I., Rind, D., and Chin, M.: Tropospheric sulfur simulation and sulfate direct radiative forcing in the Goddard Institute for Space Studies general circulation model, J. Geophys. Res.-Atmos., 104, 23799-23822, https://doi.org/10.1029/1999JD900248, 1999.

Kolb, D.: The pH concept, J. Chem. Educ., 56, 49, https://doi.org/10.1021/ed056p49, 1979.

Kolesar, K. R., Mattson, C. N., Peterson, P. K., May, N. W., Prendergast, R. K., Prattab, K. A.: Increases in wintertime PM2.5 sodium and chloride linked to snowfall and road salt application, Atmos. Environ., 177, 195-202, https://doi.org/10.1016/j.atmosenv.2018.01.008, 2018.

Koutrakis, P., Wolfson, J. M., and Spengler, J. D.: An Improved Method for Measuring Aerosol Strong Acidity: Results from a Nine-month Study in St. Louis, Missouri and Kingston, Tennessee, Atmos. Environ., 22, 6, https://doi.org/10.1016/0004-6981(88)90308-3, 1988.

Koutrakis, P., Thompson, K. M., Wolfson, J. M., Spengler, J. D., Keeler, G. J., and Slater, J. L.: Determination of Aerosol Strong Acidity Losses Due to Interactions of Collected Particles - Results from Laboratory and Field Studies, Atmos. Environ. A, 26, 987-995, https://doi.org/10.1016/0960-1686(92)90030-O, 1992.

Kroll, G., and Winkler, P.: Estimation of wet deposition via fog, in: Environmental Meteorology, edited by: Grefen, K. and Löbel, J., Springer, 227-236, 1988.

Kroll, J. H., Cross, E. S., Hunter, J. F., Sidhant, P., TREX XII, TREX XI, Wallace, L. M. M., Croteau, P. L., Jayne, J. T., Worsnop, D. R., Heald, C. L., Murphy, J. G., and Frankel, S. L.: Atmospheric evolution of sulfur emissions from Kilauea: Real-time measurements of oxidation, dilution, and neutralization within a volcanic plume, Environ. Sci. Technolo., 49, 4129-4137, https://doi.org/10.1021/es506119x, 2015.

Krotkov, N. A., McLinden, C. A., Li, C., Lamsal, L. N., Celarier, E. A., Marchenko, S. V., Swartz, W. H., Bucsela, E. J., Joiner, J., Duncan, B. N., Boersma, K. F., Veefkind, J. P., Levelt, P. F., Fioletov, V. E., Dickerson, R. R., He, H., Lu, Z. F., and Streets, D.

G.: Aura OMI observations of regional SO2 and NO2 pollution changes from 2005 to 2015, Atmos. Chem. Phys., 16, 4605-4629, https://doi.org/10.5194/acp-16-4605-2016, 2016.

Kulmala, M., Vehkamaki, H., Petaja, T., Dal Maso, M., Lauri, A., Kerminene, V.-M., Birmili, W., McMurry, P. H.: Formation and growth rates of ultrafine atmospheric particles: a review of observations, J. Aerosol Sci., 35, 143-176, https://doi.org/10.1016/j.jaerosci.2003.10.003, 2004.

Kusik, C. and Meissner, H.: Electrolyte activity coefficients in inorganic processing, AICHE Sym. S., 74, 14-20, 1978.

Lagrange, J., Pallares, C., and Lagrange, P.: Electrolyte effects on aqueous atmospheric oxidation of sulfur dioxide by ozone, J. Geophys. Res.-Atmos., 99, 14595-14600, https://doi.org/10.1029/94JD00573, 1994.

Laj, P., Fuzzi, S., Lazzari, A., Ricci, L., Orsi, G., Berner, A., Dusek, U., Schell, D., Günther, A., and Wendisch, M.: The Size Dependent Composition of Fog Droplets, Beitrage zur Physik der Atmosphare-Contributions to Atmospheric Physics, 71, 115-130, 1998.

Lamarque, J. F., Emmons, L. K., Hess, P. G., Kinnison, D. E., Tilmes, S., Vitt, F., Heald, C. L., Holland, E. A., Lauritzen, P. H., Neu, J., Orlando, J. J., Rasch, P. J., and Tyndall, G. K.: CAM-chem: description and evaluation of interactive atmospheric chemistry in the Community Earth System Model, Geosci. Model Dev., 5, 369-411, https://doi.org/10.5194/gmd-5-369-2012, 2012.

Lawal, A. S., Guan, X. B., Liu, C., Henneman, L. R. F., Vasilakos, P., Bhogineni, V., Weber, R. J., Nenes, A., and Russell, A. G.: Linked Response of Aerosol Acidity and Ammonia to SO2 and NOx Emissions Reductions in the United States, Environ. Sci. Technol., 52, 9861-9873, https://doi.org/10.1021/acs.est.8b00711, 2018.

Lawrence, J., and Koutrakis, P.: Measurement and speciation of gas and particulate phase organic acidity in an urban environment, 2. Speciation, J. Geophys. Res.-Atmos., 101, 9171-9184, https://doi.org/10.1029/95jd03357, 1996.

Lazrus, A. L., Baynton, H. W., and Lodge Jr, J. P.: Trace constituents in oceanic cloud water and their origin, Tellus, 22, 106-114, https://doi.org/10.1111/j.2153-3490.1970.tb01941.x, 1970.

Lee, Y.-N. and Schwartz, S. E.: Kinetics of Oxidation of Aqueous Sulfur(IV) by Nitrogen Dioxide, in: Precipitation Scavenging, Dry Deposition, and Resuspension. Volume 1: Precipitation Scavenging, edited by: Pruppacher, H. R., Semonin, R. G., and Slinn, W. G., Elsevier, New York, Amsterdam, Oxford, 453-470, 1983.

Lee, H. S., Wadden, R. A., and Scheff, P. A.: Measurement and Evaluation of Acid Air-Pollutants in Chicago Using an Annular Denuder System, Atmos. Environ. A, 27, 543-553, https://doi.org/10.1016/0960-1686(93)90211-G, 1993.

Lee, H. S., Kang, C. M., Kang, B. W., and Kim, H. K.: Seasonal variations of acidic air pollutants in Seoul, South Korea, Atmos. Environ., 33, 3143-3152, https://doi.org/10.1016/S1352-2310(98)00382-3, 1999.

Lee, S., Ghim, Y. S., Kim, Y. P., and Kim, J. Y.: Estimation of the seasonal variation of particulate nitrate and sensitivity to the emission changes in the greater Seoul area, Atmos. Environ., 40, 3724-3736, https://doi.org/10.1016/j.atmosenv.2006.03.029, 2006.

Lee, T., Yu, X.-Y., Ayre, B., Kreidenweis, S. M., Malm, W. C., Collete, J. L.: Observations of fine and coarse particle nitrate at several rural locations in the United States. Atmos. Environ., 42, 2720-2732, https://doi.org/10.1016/j.atmosenv.2007.05.016, 2008.

Lee, T., Kreidenweis, S. M., and Collett, J. L.: Aerosol ion characteristics during the big bend regional aerosol and Visibility observational study. J Air Waste Manag Assoc., 54, 585-592, https://doi.org/10.1080/10473289.2004.10470927, 2004

Lepeule, J., Laden, F., Dockery, D., and Schwartz, J.: Chronic Exposure to Fine Particles and Mortality: An Extended Follow-up of the Harvard Six Cities Study from 1974 to 2009, Environ. Health Perspect., 120, 965-970, https://doi.org/10.1289/ehp.1104660, 2012.

Lewis, C. W. and Macias, E. S.: Composition of Size-Fractionated Aerosol in Charleston, West-Virginia, Atmos. Environ., 14, 185-194, https://doi.org/10.1016/0004-6981(80)90277-2, 1980.

Li, J. Y. and Jang, M.: Aerosol Acidity Measurement Using Colorimetry Coupled With a Reflectance UV-Visible Spectrometer, Aerosol Sci. Tech., 46, 833-842, https://doi.org/10.1080/02786826.2012.669873, 2012.

Li, J. J., Wang, G. H., Cao, J. J., Wang, X. M., and Zhang, R. J.: Observation of biogenic secondary organic aerosols in the atmosphere of a mountain site in central China: temperature and relative humidity effects, Atmos. Chem. Phys., 13, 11535-11549, https://doi.org/10.5194/acp-13-11535-2013, 2013.

Li, W., Xu, L., Liu, X., Zhang, J., Lin, Y., Yao, X., Gao, H., Zhang, D., Chen, J., Wang, W., Harrison, R. M., Zhang, X., Shao, L., Fu, P., Nenes, A., and Shi, Z.: Air pollution–aerosol interactions produce more bioavailable iron for ocean ecosystems, Science Advances, 3, e1601749, https://doi.org/10.1126/sciadv.1601749, 2017.

Li, Z., Schwier, A., Sareen, N., and McNeill, V.: Reactive processing of formaldehyde and acetaldehyde in aqueous aerosol mimics: surface tension depression and secondary organic products, Atmos. Chem. Phys., 11, 11617-11629, https://doi.org/10.5194/acp-11-11617-2011, 2011.

Liang, C., Pankow, J. F., Odum, J. R., and Seinfeld, J. H.: Gas/Particle Partitioning of Semivolatile Organic Compounds To Model Inorganic, Organic, and Ambient Smog Aerosols, Environ. Sci. Technol., 31, 3086-3092, https://doi.org/10.1021/es9702529, 1997.

Liljestrand, H. M.: Average rainwater pH, concepts of atmospheric acidity, and buffering in open systems, Atmos. Environ., 19, 487-499, https://doi.org/10.1016/0004-6981(85)90169-6, 1985.

Lin, G., Penner, J., Sillman, S., Taraborrelli, D., and Lelieveld, J.: Global modeling of SOA formation from dicarbonyls, epoxides, organic nitrates and peroxides, Atmos. Chem. Phys., 12, 4743-4774, https://doi.org/10.5194/acp-12-4743-2012, 2012.

Lin, X. and Chameides, W. L.: Model studies of the impact of chemical inhomogeneity on SO 2 oxidation in warm stratiform clouds, J. Atmos. Chem., 13, 109-129, https://doi.org/10.1007/BF00115969, 1991.

Lippmann, M.: Toxicological and epidemiological studies of cardiovascular effects of ambient air fine particulate matter (PM2.5) and its chemical components: coherence and public health implications, Crit. Rev. Toxicol., 44, 299– 347, https://doi.org/10.3109/10408444.2013.861796, 2014.

Lipsky, E. M., and Robinson, A. L.: Effects of dilution on fine particle mass and partitioning of semivolatile organics in diesel exhaust and wood smoke, Environ. Sci. Technol., 40, 155-162, https://doi.org/10.1021/es050319p, 2006.

Liu, J. M., Scheuer, E., Dibb, J., Ziemba, L. D., Thornhill, K. L., Anderson, B. E., Wisthaler, A., Mikoviny, T., Devi, J. J., Bergin, M., and Weber, R. J.: Brown carbon in the continental troposphere, Geophys. Res. Lett., 41, 2191-2195, https://doi.org/10.1002/2013GL058976, 2014.

Liu, L. J. S., Burton, R., Wilson, W. E., and Koutrakis, P.: Comparison of aerosol acidity in urban and semirural environments, Atmos. Environ., 30, 1237-1245, https://doi.org/10.1016/1352-2310(95)00438-6, 1996.

Liu, M. X., Song, Y., Zhou, T., Xu, Z. Y., Yan, C. Q., Zheng, M., Wu, Z. J., Hu, M., Wu, Y. S., and Zhu, T.: Fine particle pH during severe haze episodes in northern China, Geophys. Res. Lett., 44, 5213-5221, https://doi.org/10.1002/2017gl073210, 2017.

Liu, X., Easter, R. C., Ghan, S. J., Zaveri, R., Rasch, P., Shi, X., Lamarque, J. F., Gettelman, A., Morrison, H., Vitt, F., Conley, A., Park, S., Neale, R., Hannay, C., Ekman, A. M. L., Hess, P., Mahowald, N., Collins, W., Iacono, M. J., Bretherton, C. S., Flanner, M. G., and Mitchell, D.: Toward a minimal representation of aerosols in climate models: description and evaluation in the Community Atmosphere Model CAM5, Geosci. Model. Dev., 5, 709-739, https://doi.org/doi: 10.5194/gmd-5-709-2012, 2012.

Liu, X., Ma, P. L., Wang, H., Tilmes, S., Singh, B., Easter, R. C., Ghan, S. J., and Rasch, P. J.: Description and evaluation of a new four-mode version of the Modal Aerosol Module (MAM4) within version 5.3 of the Community Atmosphere Model, Geosci. Model. Dev., 9, 505-522, https://doi.org/doi: 10.5194/gmd-9-505-2016, 2016.

Loeffler, K., Koehler, C., Paul, N., and De Haan, D.: Oligomer formation in evaporating aqueous glyoxal and methyl glyoxal solutions, Environ. Sci. Technol., 40, 6318-6323, https://doi.org/10.1021/es060810w, 2006.

Lolkema, D. E., Noordijk, H., Stolk, A. P., Hoogerbrugge, R., van Zanten, M. C., and van Pul, W. A. J.: The Measuring Ammonia in Nature (MAN) network in the Netherlands, Biogeosciences, 12, 5133-5142, https://doi.org/10.5194/bg-12-5133-2015, 2015.

Losey, D. J., Parker, R. G., and Freedman, M. A.: pH Dependence of liquid–liquid phase separation in organic aerosol, J. Phys. Chem.Lett., 7, 3861-3865, https://doi.org/10.1021/acs.jpclett.6b01621, 2016.

Losey, D. J., Ott, E.-J. E., and Freedman, M. A.: Effects of high acidity on phase transitions of an organic aerosol, J. Phys. Chem. A, 122, 3819-3828, https://doi.org/10.1021/acs.jpca.8b00399, 2018.

Lough, G. C., Schauer, J. J., Park, J.-S., Shafer, M. M., DeMinter, J. T., and Weinstein, J. P.: Emissions of Metals Associated with Motor Vehicle Roadways, Environ. Sci. Technol., 39 (3) 826-836 https://pubs.acs.org/doi/10.1021/es048715f, 2005.

Maahs, H. G.: Measurements of the oxidation rate of sulfur (IV) by ozone in aqueous solution and their relevance to SO2 conversion in non-urban tropospheric clouds, Atmos. Environ., 17, 341-345, https://doi.org/10.1016/0004-6981(83)90050-1, 1983.

Macias, E. S., Zwicker, J. O., Ouimette, J. R., Hering, S. V., Friedlander, S. K., Cahill, T. A., Kuhlmey, G. A., and Richards, L. W.: Regional Haze Case Studies in the Southwestern United-States, 1. Aerosol Chemical-Composition, Atmos. Environ., 15, 1971-1986, https://doi.org/10.1016/0004-6981(81)90231-6, 1981.

Mahowald, N., Jickells, T. D., Baker, A. R., Artaxo, P., Benitez-Nelson, C. R., Bergametti, G., Bond, T. C., Chen, Y., Cohen, D. D., Herut, B., Kubilay, N., Losno, R., Luo, C., Maenhaut, W., McGee, K. A., Okin, G. S., Siefert, R. L., and Tsukuda, S.: Global distribution of atmospheric phosphorus sources, concentrations and deposition rates, and anthropogenic impacts, Global Biogeochem. Cycles, 22, https://doi.org/10.1029/2008GB003240, 2008.

Makar, P. A., Bouchet, V. S., and Nenes, A.: Inorganic chemistry calculations using HETV—a vectorized solver for the SO42−–NO3−–NH4+ system based on the ISORROPIA algorithms, Atmos. Environ., 37, 2279-2294, https://doi.org/10.1016/S1352-2310(03)00074-8, 2003.

Marais, E., Jacob, D., Jimenez, J., Campuzano-Jost, P., Day, D., Hu, W., Krechmer, J., Zhu, L., Kim, P., Miller, C., Fisher, J., Travis, K., Yu, K., Hanisco, T., Wolfe, G., Arkinson, H., Pye, H., Froyd, K., Liao, J., and McNeill, V.: Aqueous-phase mechanism for secondary organic aerosol formation from isoprene: application to the southeast United States and co-benefit of SO2 emission controls, Atmos. Chem. Phys., 16, 1603-1618, https://doi.org/10.5194/acp-16-1603-2016, 2016a.

Marais, E. A., Jacob, D. J., Jimenez, J. L., Campuzano-Jost, P., Day, D. A., Hu, W., Krechmer, J., Zhu, L., Kim, P. S., Miller, C. C., Fisher, J. A., Travis, K., Yu, K., Hanisco, T. F., Wolfe, G. M., Arkinson, H. L., Pye, H. O. T., Froyd, K. D., Liao, J., and McNeill, V. F.: Aqueous-phase mechanism for secondary organic aerosol formation from isoprene: application to the southeast United States and co-benefit of SO2 emission controls, Atmos. Chem. Phys., 16, 1603-1618, https://doi.org/10.5194/acp-16-1603-2016, 2016b.

Maria, S. F., Russell, L. M., Gilles, M. K., and Myneni, S. C. B.: Organic aerosol growth mechanisms and their climate-forcing implications, Science, 306, https://doi.org/10.1126/science.1103491, 2004.

Mcinnes, L., Covert, D., Quinn, P., and Germani, M.: Measurements of chloride depletion and sulfur enrichment in individual sea-salt particles collected from the remote marine boundary-layer, J. Geophys. Res.-Atmos., 99, 8257-8268, https://doi.org/10.1029/93JD03453, 1994.

McNeill, V.: Aqueous Organic Chemistry in the Atmosphere: Sources and Chemical Processing of Organic Aerosols, Environ. Sci. Technol., 49, 1237-1244, https://doi.org/10.1021/es5043707, 2015.

Meng, Z. and Seinfeld, J. H.: Time scales to achieve atmospheric gas-aerosol equilibrium for volatile species, Atmos. Environ., 30, 2889-2900, https://doi.org/10.1016/1352-2310(95)00493-9, 1996.

Meskhidze, N., Chameides, W. L., Nenes, A., and Chen, G.: Iron mobilization in mineral dust: Can anthropogenic SO_2 emissions affect ocean productivity?, Geophys. Res. Lett., 30, 2085, https://doi.org/10.1029/2003gl018035, 2003.

Meskhidze, N., Chameides, W. L., and Nenes, A.: Dust and pollution: A recipe for enhanced ocean fertilization?, J. Geophys. Res.-Atmos., 110, D03301, https://doi.org/10.1029/2004jd005082, 2005.

Metzger, S. M., Dentener, F. J., Lelieveld, J., and Pandis, S. N.: Gas/aerosol partitioning I: A computationally efficient model, J. Geophys. Res., 107(D16), doi:10.1029/2001JD001102, 2002.

Metzger, S., Mihalopoulos, N., and Lelieveld, J.: Importance of mineral cations and organics in gas-aerosol partitioning of reactive nitrogen compounds: case study based on MINOS results, Atmos. Chem. Phys., 6, 2549–2567, https://doi.org/10.5194/acp-6-2549-2006, 2006.

Metzger, S., Abdelkader, M., Steil, B., and Klingmuller, K.: Aerosol water parameterization: long-term evaluation and importance for climate studies, Atmos. Chem. Phys., 18, 16747-16774, https://doi.org/10.5194/acp-18-16747-2018, 2018.

Millet, D. B., Baasandorj, M., Farmer, D. K., Thornton, J. A., Baumann, K., Brophy, P., Chaliyakunnel, S., de Gouw, J. A., Graus, M., Hu, L., Koss, A., Lee, B. H., Lopez-Hilfiker, F. D., Neuman, J. A., Paulot, F., Peischl, J., Pollack, I. B., Ryerson, T. B., Warneke, C., Williams, B. J., and Xu, J.: A large and ubiquitous source of atmospheric formic acid, Atmos. Chem. Phys., 15, 6283-6304, https://doi.org/10.5194/acp-15-6283-2015, 2015.

Molders, N. and Leelasakultum, K.: Fairbanks North Star Borough PM2.5 Non-Attainment Area CMAQ Modeling, University of Alaska Fairbanks, Geophysical Institute, College of Natural Science and Mathematics, Department of Atmospheric Sciences 398831 CMAQ-DEC 2012 2012.

Moore, K. F., Sherman, D. E., Reilly, J. E., and Collett, J. L.: Drop size-dependent chemical composition in clouds and fogs. Part I. Observations, Atmos. Environ., 38, 1389-1402, https://doi.org/10.1016/j.atmosenv.2003.12.013, 2004.

Mori, T., Okochi, H., and Igawa, M.: An Episode of pH 1.95 Acid Fog Containing High Concentration of HCl in Mt. Oyama, Tanzawa Mountains, Journal of Japan Society for Atmospheric Environment/Taiki Kankyo Gakkaishi, 32, 157-161, https://doi.org/10.11298/taiki1995.32.157, 1997.

Moyers, J. L., Ranweiler, L. E., Hopf, S. B., and Korte, N. E.: Evaluation of Particulate Trace Species in Southwest Desert Atmosphere, Environ. Sci. Technol., 11, 789-795, https://doi.org/10.1021/Es60131a002, 1977.

Munger, J. W.: The Chemical Composition of Fogs and Clouds in Southern California, Dissertation (Ph.D.), California Institute of Technology, 1989.

Munger, J. W., Collett, Jr., J., Daube, Jr., B. C., and Hoffmann, M. R.: Carboxylic acids and carbonyl compounds in southern California clouds and fogs, Tellus B, 41B, 230-242, https://doi.org/10.1111/j.1600-0889.1989.tb00303.x, 1989.

Murphy, D. M., Cziczo, D. J., Froyd, K. D., Hudson, P. K., Matthew, B. M., Middlebrook, A. M., Peltier, R. E., Sullivan, A., Thomson, D. S., and Weber, R. J.: Single-particle mass spectrometry of tropospheric aerosol particles, J. Geophys. Res.-Atmos., 111, D23s32, https://doi.org/10.1029/2006jd007340, 2006.

Murphy, J. G., Gregoire, P. K., Tevlin, A. G., Wentworth, G. R., Ellis, R. A., Markovic, M. Z., and VandenBoer, T. C.: Observational constraints on particle acidity using measurements and modelling of particles and gases, Faraday Discuss., 200, 379-395, https://doi.org/10.1039/c7fd00086c, 2017.

Myhre, C. E. L., Christensen, D. H., Nicolaisen, F. M., and Nielsen, C. J.: Spectroscopic study of aqueous H2SO4 at different temperatures and compositions: Variations in dissociation and optical properties, J. Phys. Chem. A, 107, 1979-1991, https://doi.org/10.1021/jp026576n, 2003.

Myriokefalitakis, S., Tsigaridis, K., Mihalopoulos, N., Sciare, J., Nenes, A., Kawamura, K., Segers, A., and Kanakidou, M.: In-cloud oxalate formation in the global troposphere: a 3-D modeling study, Atmos. Chem. Phys., 11, 5761, https://doi.org/10.5194/acp-11-5761-2011, 2011.

Myriokefalitakis, S., Daskalakis, N., Mihalopoulos, N., Baker, A. R., Nenes, A., and Kanakidou, M.: Changes in dissolved iron deposition to the oceans driven by human activity: a 3-D global modelling study, Biogeosciences, 12, 3973-3992, https://doi.org/10.5194/bg-12-3973-2015, 2015.

Myriokefalitakis S., Nenes A., Baker A.R., Mihalopoulos N., and Kanakidou M.: Bioavailable atmospheric phosphorous supply to the global ocean: a 3-D global modelling study, Biogeosciences, 13, 6519–6543, https://doi.org/10.5194/bg-13-6519-2016, 2016.

Myriokefalitakis, S., Ito, A., Kanakidou, M., Nenes, A., Krol, M. C., Mahowald, N. M., Scanza, R. A., Hamilton, D. S., Johnson, M. S., Meskhidze, N., Kok, J. F., Guieu, C., Baker, A. R., Jickells, T. D., Sarin, M. M., Bikkina, S., Shelley, R., Bowie, A., Perron, M. M. G., and Duce, R. A.: Reviews and syntheses: the GESAMP atmospheric iron deposition model intercomparison study, Biogeosciences, 15, 6659-6684, https://doi.org/10.5194/bg-15-6659-2018, 2018.

Nah, T., Guo, H., Sullivan, A., Chen, Y., Tanner, D., Nenes, A., Russell, A., Ng, N., Huey, L., and Weber, R.: Characterization of aerosol composition, aerosol acidity, and organic acid partitioning at an agriculturally intensive rural southeastern US site, Atmos. Chem. Phys., 18, 11471-11491, https://doi.org/10.5194/acp-18-11471-2018, 2018.

Nenes, A. and Seinfeld, J. H.: Parameterization of cloud droplet formation in global climate models, J. Geophys. Res.-Atmos., 108, https://doi.org/10.1029/2002JD002911, 2003.

Nenes, A., Pandis, S. N., and Pilinis, C.: ISORROPIA: A new thermodynamic equilibrium model for multiphase multicomponent inorganic aerosols, Aquat. Geochem., 4, 123-152, https://doi.org/10.1023/a:1009604003981, 1998.

Nenes, A., Krom, M. D., Mihalopoulos, N., Van Cappellen, P., Shi, Z., Bougiatioti, A., Zarmpas, P., and Herut, B.: Atmospheric acidification of mineral aerosols: a source of bioavailable phosphorus for the oceans, Atmos. Chem. Phys., 11, 6265-6272, https://doi.org/10.5194/acp-11-6265-2011, 2011.

Nenes, A., Pandis, S. N., Weber, R. J., and Russell, A.: Aerosol pH and liquid water content determine when particulate matter is sensitive to ammonia and nitrate availability, Atmos. Chem. Phys. Discuss., https://doi.org/10.5194/acp-2019-840, in review, 2019.

Ng, N. L., Herndon, S. C., Trimborn, A., Canagaratna, M. R., Croteau, P. L., Onasch, T. B., Sueper, D., Worsnop, D. R., Zhang, Q., Sun, Y. L., and Jayne, J. T.: An Aerosol Chemical Speciation Monitor (ACSM) for Routine Monitoring of the Composition and Mass Concentrations of Ambient Aerosol, Aerosol Sci. Tech., 45, 780-794, https://doi.org/10.1080/02786826.2011.560211, 2011.

Nguyen, Q. T., Christensen, M. K., Cozzi, F., Zare, A., Hansen, A. M. K., Kristensen, K., Tulinius, T. E., Madsen, H. H., Christensen, J. H., Brandt, J., Massling, A., Nøjgaard, J. K., and Glasius, M.: Understanding the anthropogenic influence on formation of biogenic secondary organic aerosols in Denmark via analysis of organosulfates and related oxidation products, Atmos. Chem. Phys., 14, 8961-8981, https://doi.org/10.5194/acp-14-8961-2014, 2014.

Nguyen, T. K. V., Capps, S. L., and Carlton, A. G.: Decreasing Aerosol Water Is Consistent with OC Trends in the Southeast U.S., Environ. Sci. Technol., 49, 7843–7850, https://doi.org/10.1021/acs.est.5b00828, 2015.

Noone, K. J., Charlson, R. J., Covert, D. S., Ogren, J. A., and Heintzenberg, J.: Cloud droplets: Solute concentration is size dependent, J. Geophys. Res.-Atmos., 93, 9477-9482, https://doi.org/10.1029/JD093iD08p09477, 1988.

Noziere, B. and Esteve, W.: Light-absorbing aldol condensation products in acidic aerosols: Spectra, kinetics, and contribution to the absorption index, Atmos. Environ., 41, 1150-1163, https://doi.org/10.1016/j.atmosenv.2006.10.001, 2007.

Noziere, B., Dziedzic, P., and Cordova, A.: Inorganic ammonium salts and carbonate salts are efficient catalysts for aldol condensation in atmospheric aerosols, Phys. Chem. Chem. Phys., 12, 3864-3872, https://doi.org/10.1039/b924443c, 2010.

Offenberg, J. H., Lewandowski, M., Edney, E. O., Kleindienst, T. E., and Jaoui, M.: Influence of Aerosol Acidity on the Formation of Secondary Organic Aerosol from Biogenic Precursor Hydrocarbons, Environ. Sci. Technol., 43, 7742-7747, https://doi.org/10.1021/Es901538e, 2009.

Ogren, J. A., Heintzenberg, J., Zuber, A., Noone, K. J., and Charlson, R. J.: Measurements of the size-dependence of solute concentrations in cloud droplets, Tellus B, 41, 24-31, https://doi.org/10.3402/tellusb.v41i1.15044, 1989.

Oltmans, S. J., Schnell, R. C., Sheridan, P. J., Peterson, R. E., Li, S. M., Winchester, J. W., Tans, P. P., Sturges, W. T., Kahl, J. D., and Barrie, L. A.: Seasonal surface ozone and filterable bromine relationship in the high arctic, Atmos. Environ., 23, 2431-2441, https://doi.org/10.1016/0004-6981(89)90254-0, 1989.

Paciga, A. L., Riipinen, I., and Pandis, S. N.: Effect of Ammonia on the Volatility of Organic Diacids, Environ. Sci. Technol., 48, 13769-13775, https://doi.org/10.1021/es5037805, 2014.

Pandis, S. N., Seinfeld, J. H., and Pilinis, C.: Chemical composition differences in fog and cloud droplets of different sizes, Atmos. Environ. A., 24, 1957-1969, https://doi.org/10.1016/0960-1686(90)90529-V, 1990.

Pankow, J. F.: A consideration of the role of gas/particle partitioning in the deposition of nictoine and other tobacco smoke compounds in the respiratory tract, Chem. Res. Toxicol., 14, 1465-1481, https://doi.org/10.1021/tx0100901, 2001.

Park, R. J., Jacob, D. J., Field, B. D., Yantosca, R. M., and Chin, M.: Natural and transboundary pollution influences on sulfate-nitrate-ammonium aerosols in the United States: Implications for policy, J. Geophys. Res.-Atmos., 109, D15204, https://doi.org/10.1029/2003jd004473, 2004.

Pathak, R. K., Yao, X. H., and Chan, C. K.: Sampling artifacts of acidity and ionic species in PM2.5, Environ. Sci. Technol., 38, 254-259, https://doi.org/10.1021/es0342244, 2004.

Pathak, R. K., Wu, W. S., and Wang, T.: Summertime PM2.5 ionic species in four major cities of China: nitrate formation in an ammonia-deficient atmosphere, Atmos. Chem. Phys., 9, 1711-1722, https://doi.org/10.5194/acp-9-1711-2009, 2009.

Pathak, R.K., Wang, T., Ho, K.F., and Lee, S.C.: Characteristics of summertime $PM_{2.5}$ organic and elemental carbon in four major Chinese cities: Implications of high acidity for water-soluble organic carbon (WSOC). Atmos. Environ., 45(2), 318-325, https://doi.org/10.1016/j.atmosenv.2010.10.021, 2011.

Paulot, F., Crounse, J., Kjaergaard, H., Kurten, A., St. Clair, J., Seinfeld, J., and Wennberg, P.: Unexpected Epoxide Formation in the Gas-Phase Photooxidation of Isoprene, Science, 325, 730-733, https://doi.org/10.1126/science.1172910, 2009.

Paulot, F., Fan, S., and Horowitz, L. W.: Contrasting seasonal responses of sulfate aerosols to declining SO2 emissions in the Eastern U.S.: Implications for the efficacy of SO2 emission controls, Geophys. Res. Lett., 44, 455-464, https://doi.org/10.1002/2016GL070695, 2017.

Peltier, R. E., Sullivan, A. P., Weber, R. J., Wollny, A. G., Holloway, J. S., Brock, C. A., de Gouw, J. A., and Atlas, E. L.: No evidence for acid-catalyzed secondary organic aerosol formation in power plant plumes over metropolitan Atlanta, Georgia, Geophys. Res. Lett., 34, L06801, https://doi.org/10.1029/2006gl028780, 2007.

Philip, S., Martin, R., Snider, G., Weagle, C., van Donkelaar, A., Brauer, M., Henze, D., Klimont, Z., Venkataraman, C., Guttikunda, S., and Zhang, Q.: Anthropogenic fugitive, combustion and industrial dust is a significant, underrepresented fine particulate matter source in global atmospheric models, Environ. Res. Lett., 12, https://doi.org/10.1088/1748-9326/aa65a4, 2017.

Phillips, S. M., Bellcross, A. D., and Smith, G. D.: Light absorption by brown carbon in the southeastern United States is pH-dependent, Environ. Sci. Technol., 51, 6782-6790, https://doi.org/10.1021/acs.est.7b01116, 2017.

Pilinis, C. and Seinfeld, J. H.: Continued development of a general equilibrium model for inorganic multicomponent atmospheric aerosols, Atmos. Environ., 21, 2453-2466, https://doi.org/10.1016/0004-6981(87)90380-5, 1987.

Pilinis, C., Seinfeld, J. H., and Grosjean, D.: Water content of atmospheric aerosols, Atmos. Environ., 23, 1601-1606, https://doi.org/10.1016/0004-6981(89)90419-8, 1989.

Pilinis, C., Capaldo, K. P., Nenes, A., and Pandis, S. N.: MADM - A new multicomponent aerosol dynamics model, Aerosol Sci. Tech., 32, 482-502, https://doi.org/10.1080/027868200303597, 2000.

Pinder, R. W., Dennis, R. L., and Bhave, P. V.: Observable indicators of the sensitivity of PM2.5 nitrate to emission reductions - Part I: Derivation of the adjusted gas ratio and applicability at regulatory-relevant time scales, Atmos. Environ., 42, 1275-1286, https://doi.org/10.1016/j.atmosenv.2007.10.039, 2008a.

Pinder, R. W., Gilliland, A. B., and Dennis, R. L.: Environmental impact of atmospheric NH3 emissions under present and future conditions in the eastern United States, Geophys. Res. Lett., 35, L12808, https://doi.org/10.1029/2008gl033732, 2008b.

Pitzer, K. S. and Simonson, J. M.: Thermodynamics of multicomponent, miscible, ionic systems: theory and equations, J. Phys. Chem., 90, 3005-3009, https://doi.org/10.1021/j100404a042, 1986.

Pöhlker, C., Wiedemann, K. T., Sinha, B., Shiraiwa, M., Gunthe, S. S., Smith, M., Su, H., Artaxo, P., Chen, Q., Cheng, Y., Elbert, W., Gilles, M. K., Kilcoyne, A. L. D., Moffet, R. C., Weigand, M., Martin, S. T., Pöschl, U., and Andreae, M. O.: Biogenic

potassium salt particles as seeds for secondary organic aerosol in the amazon, Science, 337, 1075-1078, https://doi.org/10.1126/science.1223264, 2012.

Pope, C. A., Ezzati, M., and Dockery, D. W.: Fine-Particulate Air Pollution and Life Expectancy in the United States, New Engl. J. Med., 360, 376-386, https://doi.org/10.1056/NEJMsa0805646, 2009.

Poschl, U. and Shiraiwa, M.: Multiphase chemistry at the atmosphere-biosphere interface influencing climate and public health in the anthropocene, Chem. Rev., 115, 4440-4475, https://doi.org/10.1021/cr500487s, 2015.

Powers, J. G., Klemp, J. B., Skamarock, W. C., Davis, C. A., Dudhia, J., Gill, D. O., Coen, J. L., Gochis, D. J., Ahmadov, R., Peckham, S. E., Grell, G. A., Michalakes, J., Trahan, S., Benjamin, S. G., Alexander, C. R., Dimego, G. J., Wang, W., Schwartz, C. S., Romine, G. S., Liu, Z. Q., Snyder, C., Chen, F., Barlage, M. J., Yu, W., and Duda, M. G.: The Weather Research and Forecasting Model: Overview, System Efforts, and Future Directions, B. Am. Meteorol. Soc., 98, 1717-1737, https://doi.org/10.1175/Bams-D-15-00308.1, 2017.

Prausnitz, J. M., Lichtenthaler, R. N., and Azevedo, E. G. d.: Molecular thermodynamics of fluid-phase equilibria, 3rd edition, Prentice-Hall international series in the physical and chemical engineering sciences, Prentice Hall PTR, Upper Saddle River, N.J., 1999.

Pruppacher, H. R. and J. D. Klett, Microphysics of Clouds and Precipitation, Atmos. Oceanogr. Sci. Libr., vol. 18, 2nd edition, 954 pp., Springer Netherlands, https://doi.org/10.1007/978-0-306-48100-0, 2010.

Pszenny, A., Moldanová, J., Keene, W., Sander, R., Maben, J., Martinez, M., Crutzen, P., Perner, D., and Prinn, R.: Halogen cycling and aerosol pH in the Hawaiian marine boundary layer, Atmos. Chem. Phys, 4, 147-168, https://doi.org/10.5194/acp-4-147-2004, 2004.

Puchalski, M.A., Walker, J.T., Beachley, G.M., Zondlo, M.A., and Benedict, K.B.:. Need for improved monitoring of spatial and temporal trends of reduced nitrogen. EM, July 2019.

Pun, B. K. and Seigneur, C.: Sensitivity of particulate matter nitrate formation to precursor emissions in the California San Joaquin Valley, Environ. Sci. Technol., 35, 2979-2987, https://doi.org/10.1021/es0018973, 2001.

Purdue, L. J.: Determination of the strong acidity of atmospheric fine-particles (<2.5 μm) using annular denuder technology, U.S. Environmental Protection Agency, Washington, D.C., EPA/600/R-93/037 (NTIS PB93178234), 1993.

Pye, H. O. T., Liao, H., Wu, S., Mickley, L. J., Jacob, D. J., Henze, D. K., and Seinfeld, J. H.: Effect of changes in climate and emissions on future sulfate-nitrate-ammonium aerosol levels in the United States, J. Geophys. Res.-Atmos., 114, https://doi.org/10.1029/2008jd010701, 2009.

Pye, H. O. T., Pinder, R. W., Piletic, I. R., Xie, Y., Capps, S. L., Lin, Y. H., Surratt, J. D., Zhang, Z. F., Gold, A., Luecken, D. J., Hutzell, W. T., Jaoui, M., Offenberg, J. H., Kleindienst, T. E., Lewandowski, M., and Edney, E. O.: Epoxide Pathways Improve Model Predictions of Isoprene Markers and Reveal Key Role of Acidity in Aerosol Formation, Environ. Sci. Technol., 47, 11056-11064, https://doi.org/10.1021/es402106h, 2013.

Pye, H. O. T., Zuend, A., Fry, J. L., Isaacman-VanWertz, G., Capps, S. L., Appel, K. W., Foroutan, H., Xu, L., Ng, N. L., and Goldstein, A. H.: Coupling of organic and inorganic aerosol systems and the effect on gas–particle partitioning in the southeastern US, Atmos. Chem. Phys., 18, 357-370, https://doi.org/10.5194/acp-18-357-2018, 2018.

Quinn, P. K., Bates, T. S., Coffman, D., Onasch, T. B., Worsnop, D., Baynard, T., de Gouw, J. A., Goldan, P. D., Kuster, W. C., Williams, E., Roberts, J. M., Lerner, B., Stohl, A., Pettersson, A., and Lovejoy, E. R.: Impacts of sources and aging on

submicrometer aerosol properties in the marine boundary layer across the Gulf of Maine, J. Geophys. Res.-Atmos., 111, D23s36, https://doi.org/10.1029/2006jd007582, 2006.

Raizenne, M., Neas, L. M., Damokosh, A. I., Dockery, D. W., Spengler, J. D., Koutrakis, P., Ware, J. H., and Speizer, F. E.: Health effects of acid aerosols on North American children: pulmonary function, Environ. Health Persp., 104, 506-514, https://doi.org/10.1289/ehp.96104506, 1996.

Rao, X. and Collett, J. L.: The Drop Size-Dependence of Iron and Manganese Concentrations in Clouds and Fogs: Implications for Sulfate Production, J. Atmos. Chem., 30, 273-289, https://doi.org/10.1023/A:1006044614291, 1998.

Reff, A., Bhave, P. V., Simon, H., Pace, T. G., Pouliot, G. A., Mobley, J. D., and Houyoux, M.: Emissions Inventory of PM2.5 Trace Elements across the United States, Environ. Sci. Technol., 43, 5790-5796, https://doi.org/10.1021/es802930x, 2009.

Reilly, J. E., Rattigan, O. V., Moore, K. F., Judd, C., Sherman, D. E., Dutkiewicz, V. A., Kreidenweis, S. M., Husain, L., and Collett Jr, J. L.: Drop size-dependent S (IV) oxidation in chemically heterogeneous radiation fogs, Atmos. Environ., 35, 5717-5728, https://doi.org/10.1016/S1352-2310(01)00373-9, 2001.

Reiss, R., Anderson, E. L., Cross, C. E., Hidy, G., Hoel, D., McClellan, R. and Moolgavkar, S.: Evidence of Health Impacts of Sulfate- and Nitrate-Containing Particles in Ambient Air, Inhal. Toxicol., 19, 419-449, https://doi.org/10.1080/08958370601174941, 2007.

Reitz, P., Spindler, C., Mentel, T. F., Poulain, L., Wex, H., Mildenberger, K., Niedermeier, D., Hartmann, S., Clauss, T., Stratmann, F., Sullivan, R. C., DeMott, P. J., Petters, M. D., Sierau, B., and Schneider, J.: Surface modification of mineral dust particles by sulphuric acid processing: implications for ice nucleation abilities, Atmos. Chem. Phys., 11, 7839-7858, https://doi.org/10.5194/acp-11-7839-2011, 2011.

Reyes-Rodríguez, G. J., Gioda, A., Mayol-Bracero, O. L., and Collett, J.: Organic carbon, total nitrogen, and water-soluble ions in clouds from a tropical montane cloud forest in Puerto Rico, Atmos. Environ., 43, 4171-4177, https://doi.org/10.1016/j.atmosenv.2009.05.049, 2009.

Riedel, T. P., Lin, Y. H., Zhang, Z., Chu, K., Thornton, J. A., Vizuete, W., Gold, A., and Surratt, J. D.: Constraining condensed-phase formation kinetics of secondary organic aerosol components from isoprene epoxydiols, Atmos. Chem. Phys., 16, 1245-1254, https://doi.org/10.5194/acp-16-1245-2016, 2016.

Rindelaub, J. D., Borca, C. H., Hostetler, M. A., Slade, J. H., Lipton, M. A., Slipchenko, L. V., and Shepson, P. B.: The acid-catalyzed hydrolysis of an α-pinene-derived organic nitrate: kinetics, products, reaction mechanisms, and atmospheric impact, Atmos. Chem. Phys., 16, 15425-15432, https://doi.org/10.5194/acp-16-15425-2016, 2016a.

Rindelaub, J. D., Craig, R. L., Nandy, L., Bondy, A. L., Dutcher, C. S., Shepson, P. B., and Ault, A. P.: Direct Measurement of pH in Individual Particles via Raman Microspectroscopy and Variation in Acidity with Relative Humidity, J. Phys. Chem. A, 120, 911-917, https://doi.org/10.1021/acs.jpca.5b12699, 2016b.

Riva, M., Chen, Y., Zhang, Y., Lei, Z., Olson, N., Boyer, H. C., Narayan, S., Yee, L. D., Green, H., Cui, T., Zhang, Z., Baumann, K. D., Fort, M., Edgerton, E. S., Budisulistiorini, S., Rose, C. A., Ribeiro, I., e Oliveira, R. L., Santos, E., Szopa, S., Machado, C., Zhao, Y., Alves, E., de Sa, S., Hu, W., Knipping, E., Shaw, S., Duvoisin Junior, S., Souza, R. A. F. d., Palm, B. B., Jimenez, J. L., Glasius, M., Goldstein, A. H., Pye, H. O. T., Gold, A., Turpin, B. J., Vizuete, W., Martin, S. T., Thornton, J., Dutcher, C. S., Ault, A. P., and Surratt, J. D.: Increasing Isoprene Epoxydiol-to-Inorganic Sulfate Aerosol (IEPOX:Sulfinorg) Ratio Results in Extensive Conversion of Inorganic Sulfate to Organosulfur Forms: Implications for Aerosol Physicochemical Properties, Environ. Sci. Technol., https://doi.org/10.1021/acs.est.9b01019, 2019.

Robinson, R. A., and Stokes, R. H.: Electrolyte solutions, 2nd, revised edition, Dover Publications, Mineola, NY, 2002.

Roelofs, G. J. H.: A Cloud Chemistry Sensitivity Study and Comparison of Explicit and Bulk Cloud Model Performance, Atmos. Environ. A, 27, 2255-2264, https://doi.org/10.1016/0960-1686(93)90396-G, 1993.

Rohr, A.C. and Wyzga R. E.: Attributing health effects to individual particulate matter constituents, Atmos. Environ., 62, 130–152, https://doi.org/10.1016/j.atmosenv.2012. 07.036, 2012.

Saiz-Lopez, A. and von Glasow, R.: Reactive halogen chemistry in the troposphere, Chem. Soc. Rev., 41, 6448-6472, https://doi.org/10.1039/c2cs35208g, 2012.

San Martini, F. M., West, J. J., de Foy, B., Molina, L. T., Molina, M. J., Sosa, G., and McRae, G. J.: Modeling inorganic aerosols and their response to changes in precursor concentration in Mexico City, J. Air Waste Manage. Assoc., 55, 803-815, https://doi.org/10.1080/10473289.2005.10464674, 2005.

Sander, R.: Compilation of Henry's law constants (version 4.0) for water as solvent, Atmos. Chem. Phys., 15, 4399-4981, https://doi.org/10.5194/acp-15-4399-2015, 2015.

Sareen, N., Schwier, A., Shapiro, E., Mitroo, D., and McNeill, V.: Secondary organic material formed by methylglyoxal in aqueous aerosol mimics, Atmos. Chem. Phys., 10, 997-1016, https://doi.org/10.5194/acp-10-997-2010, 2010.

Saxena, P., Mueller, P. K., Kim, Y. P., Seinfeld, J. H., and Koutrakis, P.: Coupling thermodynamic theory with measurements to characterize acidity of atmospheric particles, Aerosol Sci. Tech., 19, 279-293, https://doi.org/10.1080/02786829308959636, 1993.

Scheinhardt, S., Müller, K., Spindler, G., and Herrmann, H.: Complexation of trace metals in size-segregated aerosol particles at nine sites in Germany, Atmos. Environ., 74, 102-109, https://doi.org/10.1016/j.atmosenv.2013.03.023, 2013.

Schlesinger, R. B.: The Health Impact of Common Inorganic Components of Fine Particulate Matter (PM2.5) in Ambient Air: A Critical Review, Inhal. Toxicol., 19, 811-832, https://doi.org/10.1080/08958370701402382, 2007.

Schmale, J., Henning, S., Henzing, B., Keskinen, H., Sellegri, K., Ovadnevaite, J., Bougiatioti, A., Kalivitis, N., Stavroulas, I., Jefferson, A., Park, M., Schlag, P., Kristensson, A., Iwamoto, Y., Pringle, K., Reddington, C., Aalto, P., Äijälä, M., Baltensperger, U., Bialek, J., Birmili, W., Bukowiecki, N., Ehn, M., Fjæraa, A. M., Fiebig, M., Frank, G., Fröhlich, R., Frumau, A., Furuya, M., Hammer, E., Heikkinen, L., Herrmann, E., Holzinger, R., Hyono, H., Kanakidou, M., Kiendler-Scharr, A., Kinouchi, K., Kos, G., Kulmala, M., Mihalopoulos, N., Motos, G., Nenes, A., O'Dowd, C., Paramonov, M., Petäjä, T., Picard, D., Poulain, L., Prévôt, A. S. H., Slowik, J., Sonntag, A., Swietlicki, E., Svenningsson, B., Tsurumaru, H., Wiedensohler, A., Wittbom, C., Ogren, J. A., Matsuki, A., Yum, S. S., Myhre, C. L., Carslaw, K., Stratmann, F., and Gysel, M.: Collocated observations of cloud condensation nuclei, particle size distributions, and chemical composition, Scientific Data, 4, 170003, https://doi.org/10.1038/sdata.2017.3, 2017.

Schmedding, R., Ma, M., Zhang, Y., Farrell, S., Pye, H. O. T., Chen, Y., Wang, C.-T., Rasool, Q. Z., Budisulistiorini, S. H., Ault, A. P., Surratt, J. D., and Vizuete, W.: α-Pinene-Derived organic coatings on acidic sulfate aerosol impacts secondary organic aerosol formation from isoprene in a box model, Atmos. Environ., 213, 456-462, https://doi.org/10.1016/j.atmosenv.2019.06.005, 2019.

Schmidt, J., Jacob, D., Horowitz, H., Hu, L., Sherwen, T., Evans, M., Liang, Q., Suleiman, R., Oram, D., Le Breton, M., Percival, C., Wang, S., Dix, B., and Volkamer, R.: Modeling the observed tropospheric BrO background: Importance of multiphase chemistry and implications for ozone, OH, and mercury, J. Geophys. Res.-Atmos., 121, 11819-11835, https://doi.org/10.1002/2015JD024229, 2016.

Schumann, T.: Aerosol and Hydrometeor Concentrations and Their Chemical-Composition during Winter Precipitation Along a Mountain Slope, 3. Size-Differentiated in-Cloud Scavenging Efficiencies, Atmos. Environ. A, 25, 809-824, https://doi.org/10.1016/0960-1686(91)90079-M, 1991.

Schwab, J. J., Casson, P., Brandt, R., Husain, L., Dutkewicz, V., Wolfe, D., Demerjian, K. L., Civerolo, K. L., Rattigan, O. V., and Felton, H. D.: Atmospheric chemistry measurements at Whiteface Mountain, NY: cloud water chemistry, precipitation chemistry, and particulate matter, Aerosol Air Qual. Res, 16, 841-854, https://doi.org/ 10.4209/aaqr.2015.05.0344, 2016.

Schwartz, S.: Mass-transport considerations pertinent to aqueous phase reactions of gases in liquid-water clouds, in: NATO ASI Series, Vol. G6, 425-471, 1986.

Seidl, W.: Ionic concentrations and initial S (IV)-oxidation rates in droplets during the condensational stage of cloud, Tellus B, 41, 32-50, 1989.

Seinfeld, J. H. and Pandis, S. N.: Atmospheric chemistry and physics: from air pollution to climate change, John Wiley & Sons, 2016.

Sellegri, K., Laj, P., Dupuy, R., Legrand, M., Preunkert, S., and Putaud, J. P.: Size-dependent scavenging efficiencies of multicomponent atmospheric aerosols in clouds, J. Geophys. Res.-Atmos., 108, 4334, https://doi.org/10.1029/2002jd002749, 2003.

Shah, V., Jaeglé, L., Thornton, J. A., Lopez-Hilfiker, F. D., Lee, B. H., Schroder, J. C., Campuzano-Jost, P., Jimenez, J. L., Guo, H., Sullivan, A. P., Weber, R. J., Green, J. R., Fiddler, M. N., Bililign, S., Campos, T. L., Stell, M., Weinheimer, A. J., Montzka, D. D., and Brown, S. S.: Chemical feedbacks weaken the wintertime response of particulate sulfate and nitrate to emissions reductions over the eastern United States, P. Natl. Acad. Sci. U. S. A., 115, 8110, https://doi.org/10.1073/pnas.1803295115, 2018.

Shao, J., Chen, Q., Wang, Y., Lu, X., He, P., Sun, Y., Shah, V., Martin, R. V., Philip, S., Song, S., Zhao, Y., Xie, Z., Zhang, L., and Alexander, B.: Heterogeneous sulfate aerosol formation mechanisms during wintertime Chinese haze events: air quality model assessment using observations of sulfate oxygen isotopes in Beijing, Atmos. Chem. Phys., 19, 6107-6123, https://doi.org/10.5194/acp-19-6107-2019, 2019.

Shapiro, E., Szprengiel, J., Sareen, N., Jen, C., Giordano, M., and McNeill, V.: Light-absorbing secondary organic material formed by glyoxal in aqueous aerosol mimics, Atmos. Chem. Phys., 9, 2289-2300, https://doi.org/10.5194/acp-9-2289-2009, 2009.

Shephard, M. W. and Cady-Pereira, K. E.: Cross-track Infrared Sounder (CrIS) satellite observations of tropospheric ammonia, Atmos. Meas. Tech., 8, 1323–1336, https://doi.org/10.5194/amt-8-1323-2015, 2015.

Sherwen, T., Schmidt, J., Evans, M., Carpenter, L., Grossmann, K., Eastham, S., Jacob, D., Dix, B., Koenig, T., Sinreich, R., Ortega, I., Volkamer, R., Saiz-Lopez, A., Prados-Roman, C., Mahajan, A., and Ordonez, C.: Global impacts of tropospheric halogens (Cl, Br, I) on oxidants and composition in GEOS-Chem, Atmos. Chem. Phys., 16, 12239-12271, https://doi.org/10.5194/acp-16-12239-2016, 2016.

Shi, G. L., Xu, J., Peng, X., Xiao, Z. M., Chen, K., Tian, Y. Z., Guan, X. B., Feng, Y. C., Yu, H. F., Nenes, A., and Russell, A. G.: pH of Aerosols in a Polluted Atmosphere: Source Contributions to Highly Acidic Aerosol, Environ. Sci. Technol., 51, 4289-4296, https://doi.org/10.1021/acs.est.6b05736, 2017.

Shi, X., Nenes, A., Xiao, Z., Song, S., Yu, H., Shi, G., Zhao, Q., Chen, K., Feng, Y., and Russell, A. G.: High-Resolution Data Sets Unravel the Effects of Sources and Meteorological Conditions on Nitrate and Its Gas–Particle Partitioning, Environ. Sci. Technol., 53, 3048-3057, https://doi.org/10.1021/acs.est.8b06524, 2019.

Sigg, L., Stumm, W., Zobrist, J., and Zurcher, F.: The chemistry of fog - factors regulating its composition, Chimia, 41, 159-165, https://doi.org/10.1002/chin.198747400,1987.

Silvern, R. F., Jacob, D. J., Kim, P. S., Marais, E. A., Turner, J. R., Campuzano-Jost, P., and Jimenez, J. L.: Inconsistency of ammonium–sulfate aerosol ratios with thermodynamic models in the eastern US: a possible role of organic aerosol, Atmos. Chem. Phys., 17, 5107-5118, https://doi.org/10.5194/acp-17-5107-2017, 2017.

Simpson, W. R., Brown, S. S., Saiz-Lopez, A., Thornton, J. A., and von Glasow, R.: Tropospheric Halogen Chemistry: Sources, Cycling, and Impacts, Chem. Rev., 115, 4035-4062, https://doi.org/10.1021/cr5006638, 2015.

Skamarock, W. C., Klemp, J. B., Dudhia, J., Gill, D. O., Barker, D. M., Duda, M., Huang, X. Y., Wang, W., and Powers, J. G.: A Description of the Advanced Research WRF Version 3, National Center for Atmospheric Research NCAR/TN–475+STR, 2008.

Slinn, W. G. N.: Some approximations for the wet and dry removal of particles and gases from the atmosphere, Water Air Soil Poll., 5, 513, https://doi.org/10.1007/BF00285550, 1977.

Sofiev, M., Winebrake, J., Johansson, L., Carr, E., Prank, M., Soares, J., Vira, J., Kouznetsov, R., Jalkanen, J., and Corbett, J.: Cleaner fuels for ships provide public health benefits with climate tradeoffs, Nature Commun., 9, https://doi.org/10.1038/s41467-017-02774-9, 2018.

Solomon, P. A., Crumpler, D., Flanagan, J. B., Jayanty, R. K. M., Rickman, E. E., and McDade, C. E.: US National PM2.5 Chemical Speciation Monitoring Networks-CSN and IMPROVE: Description of networks, J. Air Waste Manage. Assoc., 64, 1410-1438, https://doi.org/10.1080/10962247.2014.956904, 2014.

Song, M., Marcolli, C., Krieger, U. K., Zuend, A., and Peter, T.: Liquid-liquid phase separation in aerosol particles: Dependence on O:C, organic functionalities, and compositional complexity, Geophys. Res. Lett, 39 (13), https://doi.org/10.1029/2012GL052807, 2012.

Song, S. J., Gao, M., Xu, W. Q., Shao, J. Y., Shi, G. L., Wang, S. X., Wang, Y. X., Sun, Y. L., and McElroy, M. B.: Fine-particle pH for Beijing winter haze as inferred from different thermodynamic equilibrium models, Atmos. Chem. Phys., 18, 7423-7438, https://doi.org/10.5194/acp-18-7423-2018, 2018.

Spengler, J. D., Koutrakis, P., Dockery, D. W., Raizenne, M., and Speizer, F. E.: Health effects of acid aerosols on North American children: air pollution exposures, Environ. Health Persp., 104, 492-499, https://doi.org/10.1289/ehp.96104492, 1996.

Spokes, L., Jickells, T., and Lim, B.: Solubilization of aerosol trace-metals by cloud processing - a laboratory study, Geochim. Cosmochim. Acta, 58, 3281-3287, https://doi.org/10.1016/0016-7037(94)90056-6, 1994.

Squizzato, S., Masiol, M., Brunelli, A., Pistollato, S., Tarabotti, E., Rampazzo, G., and Pavoni, B.: Factors determining the formation of secondary inorganic aerosol: a case study in the Po Valley (Italy), Atmos. Chem. Phys., 13, 1927-1939, https://doi.org/10.5194/acp-13-1927-2013, 2013.

Stockdale, A., Krom, M. D., Mortimer, R. J. G., Benning, L. G., Carslaw, K. S., Herbert, R. J., Shi, Z., Myriokefalitakis, S., Kanakidou, M., and Nenes, A.: Understanding the nature of atmospheric acid processing of mineral dusts in supplying bioavailable phosphorus to the oceans, P. Natl. Acad. Sci. U. S. A., 113, 14639, https://doi.org/10.1073/pnas.1608136113, 2016.

Stokes, R. H. and Robinson, R. A.: Interactions in aqueous nonelectrolyte solutions, I. Solute-solvent equilibria, J. Phys. Chem., 70, 2126-2130, https://doi.org/10.1021/j100879a010, 1966.

Strumm, W. and Morgan, J. J.: Aquatic Chemistry: Chemical Equilibria and Rates in Natural Waters 3rd Edition, Wiley-Interscience, 1040 p, 1995.

Sullivan, R. C., Petters, M. D., DeMott, P. J., Kreidenweis, S. M., Wex, H., Niedermeier, D., Hartmann, S., Clauss, T., Stratmann, F., Reitz, P., Schneider, J., and Sierau, B.: Irreversible loss of ice nucleation active sites in mineral dust particles caused by sulphuric acid condensation, Atmos. Chem. Phys., 10, 11471-11487, https://doi.org/10.5194/acp-10-11471-2010, 2010.

Sun, Q. and Wexler, A. S.: Modeling urban and regional aerosols -- condensation and evaporation near acid neutrality, Atmos. Environ., 32, 3257-3531, https://doi.org/10.1016/S1352-2310(98)00059-4, 1998.

Sun, J. Y., Qin, D. H., Mayewski, P. A., Dibb, J. E., Whitlow, S., Li, Z. Q., and Yang, Q. Z.: Soluble species in aerosol and snow and their relationship at Glacier 1, Tien Shan, China, J. Geophys. Res.-Atmos., 103, 28021-28028, https://doi.org/10.1029/98jd01802, 1998.

Sun, Y. L., Zhang, Q., Schwab, J. J., Chen, W. N., Bae, M. S., Lin, Y. C., Hung, H. M., and Demerjian, K. L.: A case study of aerosol processing and evolution in summer in New York City, Atmos. Chem. Phys., 11, 12737-12750, https://doi.org/10.5194/acp-11-12737-2011, 2011.

Surratt, J. D., Lewandowski, M., Offenberg, J. H., Jaoui, M., Kleindienst, T. E., Edney, E. O., and Seinfeld, J. H.: Effect of acidity on secondary organic aerosol formation from isoprene, Environ. Sci. Technol., 41, 5363-5369, https://doi.org/10.1021/Es0704176, 2007.

Surratt, J. D., Chan, A. W. H., Eddingsaas, N. C., Chan, M. N., Loza, C. L., Kwan, A. J., Hersey, S. P., Flagan, R. C., Wennberg, P. O., and Seinfeld, J. H.: Reactive intermediates revealed in secondary organic aerosol formation from isoprene, P. Natl. Acad. Sci. U. S. A., 107, 6640-6645, https://doi.org/10.1073/pnas.0911114107, 2010.

Sutton, E. A.: A spatial analysis of atmospheric ammonia and ammonium in the U.K., The Scientific World, 1, 275–286, https://doi.org/10.1100/tsw.2001.313, 2001.

Sutton, M. A., Tang, Y. S., Miners, B. P., Coyle, M., Smith, R. J., and Fowler, D.: Spatial and temporal patterns of ammonia concentration in the UK Results of the National Ammonia Monitoring Network, Final Report to the DETR Insitute of Terrestrial Ecologym Edinburg, 79, 1998.

Takahama, S., Wittig, A. E., Vayenas, D. V., Davidson, C. I., and Pandis, S. N.: Modeling the diurnal variation of nitrate during the Pittsburgh Air Quality Study, J. Geophys. Res.-Atmos., 109, D16s06, https://doi.org/10.1029/2003jd004149, 2004.

Takahama, S., Davidson, C.I., and Pandis, S.N.: Semicontinuous measurements of organic carbon and acidity during the Pittsburgh air quality study: Implications for acid-catalyzed organic aerosol formation. Environ. Sci. Technol., 40 (7), 2191-2199, https://doi.org/10.1021/es050856+, 2006.

Talbot, R. W., Vijgen, A. S., and Harriss, R. C.: Measuring tropospheric nitric acid: Problems and prospects for nylon filter and mist chamber techniques, J. Geophys. Res.-Atmos., 95, 7553-7561, https://doi.org/10.1029/JD095iD06p07553, 1990.

Tan, T., Hu, M., Li, M., Guo, Q., Wu, Y., Fang, X., Gu, F., Wang, Y., and Wu, Z.: New insight into PM2.5 pollution patterns in Beijing based on one-year measurement of chemical compositions, Sci. Total Environ., 621, 734-743, https://doi.org/10.1016/j.scitotenv.2017.11.208, 2018.

Tanner, R. L., Olszyna, K. J., Edgerton, E. S., Knipping, E., and Shaw, S. L.: Searching for evidence of acid-catalyzed enhancement of secondary organic aerosol formation using ambient aerosol data, Atmos. Environ., 43, 3440-3444, https://doi.org/10.1016/j.atmosenv.2009.03.045, 2009.

Tao, Y. and Murphy, J. G.: Evidence for the Importance of Semivolatile Organic Ammonium Salts in Ambient Particulate Matter, Environ. Sci. Technol., 53, 108-116, https://doi.org/10.1021/acs.est.8b03800, 2019a.

Tao, Y. and Murphy, J. G.: The sensitivity of PM2.5 acidity to meteorological parameters and chemical composition changes: 10-year records from six Canadian monitoring sites, Atmos. Chem. Phys., 19, 9309–9320, https://doi.org/10.5194/acp-19-9309-2019,~~Tao, Y. and Murphy, J. G.: The sensitivity of PM2.5 acidity to meteorological parameters and chemical composition changes: 10-year records from six Canadian monitoring sites, Atmos. Chem. Phys. Discuss., 2019, 1-21, https://doi.org/10.5194/acp-2019-238,~~ 2019b.

Tebes-Stevens, C., Patel, J., Jones, W., and Weber, E.: Prediction of Hydrolysis Products of Organic Chemicals under Environmental pH Conditions, Environ. Sci. Technol., 51, 5008-5016, https://doi.org/10.1021/acs.est.6b05412, 2017.

Teich, M., van Pinxteren, D., Wang, M., Kecorius, S., Wang, Z., Müller, T., Močnik, G., and Herrmann, H.: Contributions of nitrated aromatic compounds to the light absorption of water-soluble and particulate brown carbon in different atmospheric environments in Germany and China, Atmos. Chem. Phys., 17, 1653-1672, https://doi.org/10.5194/acp-17-1653-2017, 2017.

ten Brink, H. M.: Reactive uptake of HNO3 and H2SO4 in sea-salt (NaCl) particles, J. Aerosol Sci., 29, 57-64, https://doi.org/10.1016/S0021-8502(97)00460-6, 1998.

Thurston, G. D., Ito, K., Hayes, C. G., Bates, D. V., and Lippmann, M.: Respiratory hospital admissions and summertime haze air pollution in Toronto, Ontario: consideration of the role of acid aerosols, Environ. Res., 65, 271-290, https://doi.org/10.1006/enrs.1994.1037, 1994.

Tilgner, A., Bräuer, P., Wolke, R., and Herrmann, H.: Modelling multiphase chemistry in deliquescent aerosols and clouds using CAPRAM3. 0i, J. Atmos. Chem., 70, 221-256, https://doi.org/10.1007/s10874-013-9267-4, 2013.

Tilmes, S., Lamarque, J. F., Emmons, L. K., Kinnison, D. E., Ma, P. L., Liu, X., Ghan, S., Bardeen, C., Arnold, S., Deeter, M., Vitt, F., Ryerson, T., Elkins, J. W., Moore, F., Spackman, J. R., and Martin, M. V.: Description and evaluation of tropospheric chemistry and aerosols in the Community Earth System Model (CESM1.2), Geosci. Model Dev., 8, 1395-1426, https://doi.org/10.5194/gmd-8-1395-2015, 2015.

Tobo, Y., Zhang, D., Matsuki, A. and Iwasaka, Y.: Asian dust particles converted into aqueous droplets under remote marine atmospheric conditions, Proc. Natl. Acad. Sci. USA, 107: 17905–17910. https://doi.org/10.1073/pnas.1008235107, 2010.

Topping, D. O., McFiggans, G. B., and Coe, H.: A curved multi-component aerosol hygroscopicity model framework: Part 2 – Including organic compounds, Atmos. Chem. Phys., 5, 1223-1242, https://doi.org/10.5194/acp-5-1223-2005, 2005a.

Topping, D. O., McFiggans, G. B., and Coe, H.: A curved multi-component aerosol hygroscopicity model framework: Part 1 – Inorganic compounds, Atmos. Chem. Phys., 5, 1205-1222, https://doi.org/10.5194/acp-5-1205-2005, 2005b.

Trebs, I., Metzger, S., Meixner, F. X., Helas, G. N., Hoffer, A., Rudich, Y., Falkovich, A. H., Moura, M. A. L., da Silva, R. S., Artaxo, P., Slanina, J., and Andreae, M. O.: The NH_4^+-NO_3^--Cl^--SO_4^{2-}-H_2O aerosol system and its gas phase precursors at a pasture site in the Amazon Basin: How relevant are mineral cations and soluble organic acids?, J. Geophys. Res.-Atmos., 110, D07303, https://doi.org/10.1029/2004jd005478, 2005.

Tsui, W. G., Woo, J. L., and McNeill, V. F.: Impact of Aerosol-Cloud Cycling on Aqueous Secondary Organic Aerosol Formation, Preprints, https://doi.org/10.20944/preprints201909.0319.v1, 2019.

Tuet, W. Y., Chen, Y., Xu, L., Fok, S., Gao, D., Weber, R. J., and Ng, N. L.: Chemical oxidative potential of secondary organic aerosol (SOA) generated from the photooxidation of biogenic and anthropogenic volatile organic compounds, Atmos. Chem. Phys., 17, 839-853, https://doi.org/10.5194/acp-17-839-2017, 2017.

Turnock, S. T., Mann, G. W., Woodhouse, M. T., Dalvi, M., O'Connor, F. M., Carslaw, K. S., and Spracklen, D. V.: The Impact of Changes in Cloud-Water pH on Aerosol Radiative Forcing, Geophys. Res. Lett., in press, https://doi.org/10.1029/2019GL082067, 2019.

Turpin, B. J., Saxena, P., Allen, G., Koutrakis, P., McMurry, P., and Hildemann, L.: Characterization of the Southwestern Desert Aerosol, Meadview, AZ, J. Air Waste Manage. Assoc., 47, 344-356, https://doi.org/10.1080/10473289.1997.10464451, 1997.

Turpin, B. J., Saxena, P., and Andrews, E.: Measuring and simulating particulate organics in the atmosphere: problems and prospects, Atmos. Environ., 34, 2983-3013, https://doi.org/10.1016/S1352-2310(99)00501-4, 2000.

Twohy, C., Austin, P., and Charlson, R.: Chemical consequences of the initial diffusional growth of cloud droplets: a clean marine case, Tellus B, 41, 51-60, https://doi.org/10.1111/j.1600-0889.1989.tb00124.x, 1989.

Usher, C. R., Michel, A. E., and Grassian, V. H.: Reactions on mineral dust, Chem. Rev., 103, 4883-4940, https://doi.org/10.1021/cr020657y, https://doi.org/10.1021/cr020657y, 2003.

Valle-Díaz, C. J., Torres-Delgado, E., Colón-Santos, S. M., Lee, T., Collett Jr, J. L., McDowell, W. H., and Mayol-Bracero, O. L.: Impact of long-range transported African dust on cloud water chemistry at a tropical montane cloud forest in northeastern Puerto Rico, Aerosol Air Qual. Res., 16, 653-664, https://doi.org/10.4209/aaqr.2015.05.0320, 2016.

van Pinxteren, D., Plewka, A., Hofmann, D., Müller, K., Kramberger, H., Svrcina, B., Bächmann, K., Jaeschke, W., Mertes, S., Collett, J. L., and Herrmann, H.: Schmücke hill cap cloud and valley stations aerosol characterisation during FEBUKO (II): Organic compounds, Atmos. Environ., 39, 4305-4320, https://doi.org/10.1016/j.atmosenv.2005.02.014, 2005.

van Pinxteren, D., Fomba, K. W., Mertes, S., Müller, K., Spindler, G., Schneider, J., Lee, T., Collett, J. L., and Herrmann, H.: Cloud water composition during HCCT-2010: Scavenging efficiencies, solute concentrations, and droplet size dependence of inorganic ions and dissolved organic carbon, Atmos. Chem. Phys., 16, 3185-3205, https://doi.org/10.5194/acp-16-3185-2016, 2016.

Vasconcellos, P. C., Goncalves, F. L. T., Avila, S. G., Censon, V. K., and Bauer, H.: The chemical composition of winter fogs at Sao Paulo highway sites, J. Braz. Chem. Soc. 29, 1951-1958, http://dx.doi.org/10.21577/0103-5053.20180072, 2018.

Vasilakos, P., Russell, A., Weber, R., and Nenes, A.: Understanding nitrate formation in a world with less sulfate, Atmos. Chem. Phys., 18, 12765-12775, https://doi.org/10.5194/acp-18-12765-2018, 2018.

Venkatram, A., Karamchandani, P. K., and Misra, P. K.: Testing a comprehensive acid deposition model, Atmos. Environ., 22, 737-747, https://doi.org/10.1016/0004-6981(88)90011-X, 1988.

Vet, R., Artz, R. S., Carou, S., Shaw, M., Ro, C.-U., Aas, W., Baker, A., Bowersox, V. C., Dentener, F., Galy-Lacaux, C., Hou, A., Pienaar, J. J., Gillett, R., Forti, M. C., Gromov, S., Hara, H., Khodzher, T., Mahowald, N. M., Nickovic, S., Rao, P. S. P., and Reid, N. W.: A global assessment of precipitation chemistry and deposition of sulfur, nitrogen, sea salt, base cations, organic acids, acidity and pH, and phosphorus, Atmos. Environ., 93, 3-100, https://doi.org/10.1016/j.atmosenv.2013.10.060, 2014.

Vieira-Filho, M., Pedrotti, J. J., and Fornaro, A.: Water-soluble ions species of size-resolved aerosols: Implications for the atmospheric acidity in São Paulo megacity, Brazil, Atmos. Res., 181, 281-287, https://doi.org/10.1016/j.atmosres.2016.07.006, 2016.

Vierke, L., Ahrens, L., Shoeib, M., Palm, W.-U., Webster, E. M., Ellis, D. A., Ebinghaus, R., and Harner, T.: In situ air–water and particle–water partitioning of perfluorocarboxylic acids, perfluorosulfonic acids and perfluorooctyl sulfonamide at a wastewater treatment plant, Chemosphere, 92, 941-948, https://doi.org/10.1016/j.chemosphere.2013.02.067, 2013.

Vogt, R., Crutzen, P., and Sander, R.: A mechanism for halogen release from sea-salt aerosol in the remote marine boundary layer, Nature, 383, 327-330, 10.1038/383327a0, 1996.

von Bobrutzki, K., Braban, C. F., Famulari, D., Jones, S. K., Blackall, T., Smith, T. E. L., Blom, M., Coe, H., Gallagher, M., Ghalaieny, M., McGillen, M. R., Percival, C. J., Whitehead, J. D., Ellis, R., Murphy, J., Mohacsi, A., Pogany, A., Junninen, H., Rantanen, S., Sutton, M. A., and Nemitz, E.: Field inter-comparison of eleven atmospheric ammonia measurement techniques, Atmos. Meas. Tech., 3, 91-112, https://doi.org/10.5194/amt-3-91-2010, 2010.

von Glasow, R. and Crutzen, P. J.: 5.2 - Tropospheric Halogen Chemistry, in: Treatise on Geochemistry (Second Edition), edited by: Holland, H. D., and Turekian, K. K., Elsevier, Oxford, 19-69, 2014.

von Glasow, R. and Sander, R.: Variation of sea salt aerosol pH with relative humidity, Geophys. Res. Lett., 28, 247-250, https://doi.org/10.1029/2000gl012387, 2001.

von Glasow, R., Sander, R., Bott, A., and Crutzen, P.: Modeling halogen chemistry in the marine boundary layer - 2. Interactions with sulfur and the cloud-covered MBL, J. Geophys. Res.-Atmos., 107, https:/doi.org/10.1029/2001JD000943, 2002.

Walcek, C. J. and Taylor, G. R.: A Theoretical Method for Computing Vertical Distributions of Acidity and Sulfate Production within Cumulus Clouds, J. Atmos. Sci., 43, 339-355, https://doi.org/10.1175/1520-0469(1986)043<0339:Atmfcv>2.0.Co;2, 1986.

Wall, S. M., John, W., and Ondo, J. L.: Measurement of Aerosol Size Distributions for Nitrate and Major Ionic Species, Atmos. Environ., 22, 1649-1656, https://doi.org/10.1016/0004-6981(88)90392-7, 1988.

Wang, H., Ding, J., Xu, J., Wen, J., Han, J., Wang, K., Shi, G., Feng, Y., Ivey, C. E., Wang, Y., Nenes, A., Zhao, Q., and Russell, A. G.: Aerosols in an arid environment: The role of aerosol water content, particulate acidity, precursors, and relative humidity on secondary inorganic aerosols, Sci. Total Environ., 646, 564-572, https://doi.org/10.1016/j.scitotenv.2018.07.321, 2019a.

Wang, J., Hoffmann, A. A., Park, R. J., Jacob, D. J., and Martin, S. T.: Global distribution of solid and aqueous sulfate aerosols: Effect of the hysteresis of particle phase transitions, J. Geophys. Res.-Atmos., 113, https://doi.org/10.1029/2007JD009367, 2008.

Wang, S., Nan, J., Shi, C., Fu, Q., Gao, S., Wang, D., Cui, H., Saiz-Lopez, A., and Zhou, B.: Atmospheric ammonia and its impacts on regional air quality over the megacity of Shanghai, China, Sci. Rep., 5, 15842, https://doi.org/10.1038/srep15842, 2015.

Wang, S. X., Xing, J., Jang, C. R., Zhu, Y., Fu, J. S., and Hao, J. M.: Impact Assessment of Ammonia Emissions on Inorganic Aerosols in East China Using Response Surface Modeling Technique, Environ. Sci. Technol., 45, 9293-9300, https://doi.org/10.1021/es2022347, 2011.

Wang, X., Jacob, D. J., Eastham, S. D., Sulprizio, M. P., Zhu, L., Chen, Q. J., Alexander, B., Sherwen, T., Evans, M. J., Lee, B. H., Haskins, J. D., Lopez-Hilfiker, F. D., Thornton, J. A., Huey, G. L., and Liao, H.: The role of chlorine in global tropospheric chemistry, Atmos. Chem. Phys., 19, 3981-4003, https://doi.org/10.5194/acp-19-3981-2019, 2019b.

Warner, J. X., Wei, Z., Strow, L. L., Dickerson, R. R., and Nowak, J. B.: The global tropospheric ammonia distribution as seen in the 13-year AIRS measurement record, Atmos. Chem. Phys., 16, 5467-5479, https://doi.org/10.5194/acp-16-5467-2016, 2016.

Weathers, K. C., Likens, G. E., Bormann, F. H., Bicknell, S. H., Bormann, B. T., Daube, B. C., Eaton, J. S., Galloway, J. N., Keene, W. C., Kimball, K. D., McDowell, W., Siccama, T. G., Smiley, D., and Tarrant, R. A..: Cloudwater chemistry from ten sites in North America, Environ. Sci. Technol., 22, 1018-1026, https://doi.org/10.1021/es00174a004, 1988.

Weber, R. J., Marti, J. J., McMurry, P. H., Eisele, F. L., Tanner, D. J., and Jefferson, A.: Measurements of new particle formation and ultrafine particle growth rates at a clean continental site, J. Geophys. Res.-Atmos., 102, 4375-4385, https://doi.org/10.1029/96JD03656, 1997.

Weber, R. J., McMurry, P. H., Mauldin, L., Tanner, D. J., Eisele, F. L., Brechtel, F. J., Kreidenweis, S. M., Kok, G. L., Schillawski, R. D., and Baumgardner, D.: A study of new particle formation and growth involving biogenic and trace gas species measured during ACE 1, J. Geophys. Res.-Atmos., 103, 16385-16396, https://doi.org/10.1029/97JD02465, 1998.

Weber, R. J., Guo, H., Russell, A. G., and Nenes, A.: High aerosol acidity despite declining atmospheric sulfate concentrations over the past 15 years, Nat. Geosci., 9, 282, https://doi.org/10.1038/ngeo2665, 2016.

Wei, H., Vejerano, E. P., Leng, W., Huang, Q., Willner, M. R., Marr, L. C., and Vikesland, P. J.: Aerosol microdroplets exhibit a stable pH gradient, P. Natl. Acad. Sci. U. S. A., https://doi.org/10.1073/pnas.1720488115, 2018.

Wentworth, G. R., Murphy, J. G., Croft, B., Martin, R. V., Pierce, J. R., Côté, J.-S., Courchesne, I., Tremblay, J.-É., Gagnon, J., Thomas, J. L., Sharma, S., Toom-Sauntry, D., Chivulescu, A., Levasseur, M., and Abbatt, J. P. D.: Ammonia in the summertime Arctic marine boundary layer: sources, sinks, and implications, Atmos. Chem. Phys., 16, 1937–1953, https://doi.org/10.5194/acp-16-1937-2016, 2016.

West, J. J., Ansari, A. S., and Pandis, S. N.: Marginal PM2.5: Nonlinear aerosol mass response to sulfate reductions in the Eastern United States, J. Air Waste Manage. Assoc., 49, 1415-1424, https://doi.org/10.1080/10473289.1999.10463973, 1999.

Wexler, A. S. and Clegg, S. L.: Atmospheric aerosol models for systems including the ions H+, NH4+, Na+, SO42−, NO3−, Cl−, Br−, and H2O, J. Geophys. Res.-Atmos., 107, ACH 14-11-ACH 14-14, https://doi.org/10.1029/2001jd000451, 2002.

Wexler, A. S. and Seinfeld, J. H.: The distribution of ammonium salts among a size and composition dispersed aerosol, Atmos. Environ., 24, 1231-1246, https://doi.org/10.1016/0960-1686(90)90088-5, 1990.

Wexler, A. S. and Seinfeld, J. H.: Analysis of aerosol ammonium nitrate: Departures from equilibrium during SCAQS, Atmos. Environ., 26, 579-591, https://doi.org/10.1016/0960-1686(92)90171-G, 1992.

Wiesner, A. D., Katz, L. E., and Chen, C.-C.: The impact of ionic strength and background electrolyte on pH measurements in metal ion adsorption experiments, Journal of Colloid and Interface Science, 301, 329-332, https://doi.org/10.1016/j.jcis.2006.05.011, 2006.

Winkler, P.: Relations Between Aerosol Acidity and Ion Balance, in: Chemistry of Multiphase Atmospheric Systems, edited by: Jaeschke, W., 6, Springer-Verlag, New York, 269-298, 1986.

Wright, M. R.: An Introduction to Aqueous Electrolyte Solutions, John Wiley & Sons, Chichester, UK, 2007.

Xing, J., Wang, S. X., Jang, C., Zhu, Y., and Hao, J. M.: Nonlinear response of ozone to precursor emission changes in China: a modeling study using response surface methodology, Atmos. Chem. Phys., 11, 5027-5044, https://doi.org/10.5194/acp-11-5027-2011, 2011.

Xing, J., Ding, D., Wang, S., Zhao, B., Jang, C., Wu, W., Zhang, F., Zhu, Y., and Hao, J.: Quantification of the enhanced effectiveness of NOx control from simultaneous reductions of VOC and NH3 for reducing air pollution in the Beijing–Tianjin–Hebei region, China, Atmos. Chem. Phys., 18, 7799-7814, https://doi.org/10.5194/acp-18-7799-2018, 2018.

Xu, L., Guo, H., Boyd, C. M., Klein, M., Bougiatioti, A., Cerully, K. M., Hite, J. R., Isaacman-VanWertz, G., Kreisberg, N. M., Knote, C., Olson, K., Koss, A., Goldstein, A. H., Hering, S. V., de Gouw, J., Baumann, K., Lee, S.-H., Nenes, A., Weber, R. J., and Ng, N. L.: Effects of anthropogenic emissions on aerosol formation from isoprene and monoterpenes in the southeastern United States, P. Natl. Acad. Sci. U. S. A., 112, 37-42, https://doi.org/10.1073/pnas.1417609112, 2015.

Xu, L., Middlebrook, A. M., Liao, J., de Gouw, J. A., Guo, H. Y., Weber, R. J., Nenes, A., Lopez-Hilfiker, F. D., Lee, B. H., Thornton, J. A., Brock, C. A., Neuman, J. A., Nowak, J. B., Pollack, I. B., Welti, A., Graus, M., Warneke, C., and Ng, N. L.: Enhanced formation of isoprene-derived organic aerosol in sulfur-rich power plant plumes during Southeast Nexus, J. Geophys. Res.-Atmos., 121, 11137-11153, https://doi.org/10.1002/2016jd025156, 2016.

Xue, J., Lau, A. K. H., and Yu, J. Z.: A study of acidity on PM2.5 in Hong Kong using online ionic chemical composition measurements, Atmos. Environ., 45, 7081-7088, https://doi.org/10.1016/j.atmosenv.2011.09.040, 2011.

Yan, W., Topphoff, M., Rose, C., and Gmehling, J.: Prediction of vapor–liquid equilibria in mixed-solvent electrolyte systems using the group contribution concept, Fluid Phase Equilib., 162, 97-113, 10.1016/S0378-3812(99)00201-0, 1999.Yao, X., Ling, T. Y., Fang, M., and Chan, C. K.: Size dependence of in situ pH in submicron atmospheric particles in Hong Kong, Atmos. Environ., 41, 382-393, https://doi.org/10.1016/j.atmosenv.2006.07.037, 2007.

Ye, D., Klein, M., Mulholland, J., A., Russell, A., G., Weber, R., Edgerton, E., S., Chang, H., H., Sarnat, J., A., Tolbert, P., E., and Ebelt Sarnat, S.: Estimating Acute Cardiovascular Effects of Ambient PM2.5 Metals, Environ. Health Persp., 126, 027007, https://doi.org/10.1289/EHP2182, 2018.

You, Y., Smith, M. L., Song, M., Martin, S. T., and Bertram, A. K.: Liquid–liquid phase separation in atmospherically relevant particles consisting of organic species and inorganic salts, Int. Rev. Phys. Chem., 33, 43-77, https://doi.org/10.1080/0144235X.2014.890786, 2014.

Young, A. H., Keene, W. C., Pszenny, A. A. P., Sander, R., Thornton, J. A., Riedel, T. P., and Maben, J. R.: Phase partitioning of soluble trace gases with size-resolved aerosols in near-surface continental air over northern Colorado, USA, during winter, J. Geophys. Res.-Atmos., 118, 9414-9427, https://doi.org/10.1002/Jgrd.50655, 2013.

Yuen, P. F., Hegg, D. A., Larson, T. V., and Barth, M. C.: Parameterization of heterogeneous droplet chemistry for use in bulk cloud models, J. Appl. Meteorol., 35, 679-689, https://doi.org/10.1175/1520-0450(1996)035<0679:Pohdcf>2.0.Co;2, 1996.

Zaveri, R., Easter, R., and Peters, L.: A computationally efficient Multicomponent Equilibrium Solver for Aerosols (MESA), J. Geophys. Res., 110, D24203, https://doi.org/10.1029/2004JD005618, 2005a.

Zaveri, R. A., Easter, R. C., and Wexler, A. S.: A new method for multicomponent activity coefficients of electrolytes in aqueous atmospheric aerosols, J. Geophys. Res.-Atmos., 110, https://doi.org/10.1029/2004jd004681, 2005b.

Zaveri, R. A., Easter, R. C., Fast, J. D., and Peters, L. K.: Model for Simulating Aerosol Interactions and Chemistry (MOSAIC), J. Geophys. Res.-Atmos., 113, https://doi.org/10.1029/2007jd008782, 2008.

Zdanovskii, A. B.: New methods of calculating solubilities of electrolytes in multicomponent systems, Zh. Fiz. Khim., 22, 1478-1485, 1948.

Zhang, K. M. and Wexler, A. S.: An asynchronous time-stepping (ATS) integrator for atmospheric applications: Aerosol dynamics, Atmos. Environ., 40, 4574-4588, https://doi.org/10.1016/j.atmosenv.2006.03.048, 2006.

Zhang, H. F., Worton, D. R., Lewandowski, M., Ortega, J., Rubitschun, C. L., Park, J. H., Kristensen, K., Campuzano-Jost, P., Day, D. A., Jimenez, J. L., Jaoui, M., Offenberg, J. H., Kleindienst, T. E., Gilman, J., Kuster, W. C., de Gouw, J., Park, C., Schade, G. W., Frossard, A. A., Russell, L., Kaser, L., Jud, W., Hansel, A., Cappellin, L., Karl, T., Glasius, M., Guenther, A., Goldstein, A. H., Seinfeld, J. H., Gold, A., Kamens, R. M., and Surratt, J. D.: Organosulfates as Tracers for Secondary Organic Aerosol (SOA) Formation from 2-Methyl-3-Buten-2-ol (MBO) in the Atmosphere, Environ. Sci. Technol., 46, 9437-9446, https://doi.org/10.1021/Es301648z, 2012.

Zhang, Q., Canagaratna, M. R., Jayne, J. T., Worsnop, D. R., and Jimenez, J. L.: Time- and size-resolved chemical composition of submicron particles in Pittsburgh: Implications for aerosol sources and processes, J. Geophys. Res.-Atmos., 110, D07s09, https://doi.org/10.1029/2004jd004649, 2005.

Zhang, Q., Jimenez, J. L., Worsnop, D. R., and Canagaratna, M.: A case study of urban particle acidity and its influence on secondary organic aerosol, Environ. Sci. Technol., 41, 3213-3219, https://doi.org/10.1021/es061812j, 2007.

Zhang, R., Suh, I., Zhao, J., Zhang, D., Fortner, E. C., Tie, X., Molina, L. T., Molina, M. J.: Atmospheric New Particle Formation Enhanced by Organic Acids, Science, 304, 1486-1490, https://doi.org/10.1126/science.1095139, 2004.

Zhang, Y., Wen, X. Y., Wang, K., Vijayaraghavan, K., and Jacobson, M. Z.: Probing into regional O-3 and particulate matter pollution in the United States: 2. An examination of formation mechanisms through a process analysis technique and sensitivity study, J. Geophys. Res.-Atmos., 114, D22305, https://doi.org/10.1029/2009jd011900, 2009.

Zhang, Y., Pan, Y., Wang, K., Fast, J. D., and Grell, G. A.: WRF/Chem-MADRID: Incorporation of an aerosol module into WRF/Chem and its initial application to the TexAQS2000 episode, J. Geophys. Res.-Atmos.,115, D18202, https://doi.org/10.1029/2009JD013443, 2010.

Zhang, Y., Sartelet, K., Wu, S.-Y., and Seigneur, C.: Application of WRF/Chem-MADRID and WRF/Polyphemus in Europe – Part 1: Model description, evaluation of meteorological predictions, and aerosol–meteorology interactions, Atmos. Chem. Phys., 13, 6807-6843, https://doi.org/10.5194/acp-13-6807-2013, 2013.

Zhao, Y. and Gao, Y.: Acidic species and chloride depletion in coarse aerosol particles in the US east coast, Sci. Total Environ., 407, 541-547, https://doi.org/10.1016/j.scitotenv.2008.09.002, 2008.

Zhao, B., Wang, S. X., Xing, J., Fu, K., Fu, J. S., Jang, C., Zhu, Y., Dong, X. Y., Gao, Y., Wu, W. J., Wang, J. D., and Hao, J. M.: Assessing the nonlinear response of fine particles to precursor emissions: development and application of an extended response surface modeling technique v1.0, Geosci. Model Dev., 8, 115-128, https://doi.org/10.5194/gmd-8-115-2015, 2015.

Zuend, A. and Seinfeld, J.: Modeling the gas–particle partitioning of secondary organic aerosol: the importance of liquid-liquid phase separation, Atmos. Chem. Phys., 12, 3857-3882, https://doi.org/10.5194/acp-12-3857-2012, 2012.

Zuend, A. and Seinfeld, J. H.: A practical method for the calculation of liquid–liquid equilibria in multicomponent organic–water–electrolyte systems using physicochemical constraints, Fluid Phase Equilibr., 337, 201-213, https://doi.org/10.1016/j.fluid.2012.09.034, 2013.

Zuend, A., Marcolli, C., Luo, B., and Peter, T.: A thermodynamic model of mixed organic-inorganic aerosols to predict activity coefficients, Atmos. Chem. Phys., 8, 4559-4593, https://doi.org/10.5194/acp-8-4559-2008, 2008.

Zuend, A., Marcolli, C., Peter, T., and Seinfeld, J. H.: Computation of liquid-liquid equilibria and phase stabilities: implications for RH-dependent gas/particle partitioning of organic-inorganic aerosols, Atmos. Chem. Phys., 10, 7795-7820, https://doi.org/10.5194/acp-10-7795-2010, 2010.

Zuend, A., Marcolli, C., Booth, A., Lienhard, D., Soonsin, V., Krieger, U., Topping, D., McFiggans, G., Peter, T., and Seinfeld, J.: New and extended parameterization of the thermodynamic model AIOMFAC: calculation of activity coefficients for organic-inorganic mixtures containing carboxyl, hydroxyl, carbonyl, ether, ester, alkenyl, alkyl, and aromatic functional groups, Atmos. Chem. Phys., 11, 9155-9206, https://doi.org/10.5194/acp-11-9155-2011, 2011.

Page 132: [1] Formatted **Pye, Havala** **12/16/2019 4:24:00 PM**

Font: 10 pt

Page 132: [1] Formatted **Pye, Havala** **12/16/2019 4:24:00 PM**

Font: 10 pt

Page 132: [1] Formatted **Pye, Havala** **12/16/2019 4:24:00 PM**

Font: 10 pt

Page 132: [2] Formatted **Pye, Havala** **12/16/2019 4:30:00 PM**

Font: 10 pt, Superscript

Page 132: [2] Formatted **Pye, Havala** **12/16/2019 4:30:00 PM**

Font: 10 pt, Superscript

Page 132: [3] Formatted **Pye, Havala** **12/16/2019 4:31:00 PM**

Font: 10 pt, Superscript

Page 132: [3] Formatted **Pye, Havala** **12/16/2019 4:31:00 PM**

Font: 10 pt, Superscript

Page 132: [4] Formatted **Pye, Havala** **12/16/2019 4:24:00 PM**

Font: 10 pt

Page 132: [4] Formatted **Pye, Havala** **12/16/2019 4:24:00 PM**

Font: 10 pt

Page 132: [4] Formatted **Pye, Havala** **12/16/2019 4:24:00 PM**

Font: 10 pt

Page 132: [5] Formatted **Pye, Havala** **12/16/2019 4:30:00 PM**

Font: 10 pt, Superscript

Page 132: [5] Formatted **Pye, Havala** **12/16/2019 4:30:00 PM**

Font: 10 pt, Superscript

Page 132: [6] Formatted **Pye, Havala** **12/16/2019 4:31:00 PM**

Font: 10 pt, Superscript

Page 132: [6] Formatted **Pye, Havala** **12/16/2019 4:31:00 PM**

Font: 10 pt, Superscript

Page 132: [7] Formatted **Pye, Havala** **12/16/2019 4:30:00 PM**

Font: 10 pt, Superscript

Page 132: [7] Formatted **Pye, Havala** **12/16/2019 4:30:00 PM**

Font: 10 pt, Superscript

Page 132: [8] Formatted **Pye, Havala** **12/16/2019 4:31:00 PM**

Font: 10 pt, Superscript

Page 132: [8] Formatted **Pye, Havala** **12/16/2019 4:31:00 PM**

Font: 10 pt, Superscript

Page 132: [9] Formatted **Pye, Havala** **12/16/2019 4:31:00 PM**

Font: 10 pt, Superscript

Page 132: [9] Formatted **Pye, Havala** **12/16/2019 4:31:00 PM**

Font: 10 pt, Superscript

Page 132: [10] Formatted **Pye, Havala** **12/16/2019 4:31:00 PM**

Font: 10 pt, Superscript

Page 132: [10] Formatted **Pye, Havala** **12/16/2019 4:31:00 PM**

Font: 10 pt, Superscript

Page 132: [11] Formatted **Pye, Havala** **12/16/2019 4:30:00 PM**

Font: 10 pt, Superscript

Page 132: [11] Formatted **Pye, Havala** **12/16/2019 4:30:00 PM**

Font: 10 pt, Superscript

Page 132: [12] Formatted **Pye, Havala** **12/16/2019 4:31:00 PM**

Font: 10 pt, Superscript

Page 132: [12] Formatted **Pye, Havala** **12/16/2019 4:31:00 PM**

Font: 10 pt, Superscript

Page 132: [13] Formatted **Pye, Havala** **12/16/2019 4:31:00 PM**

Font: 10 pt, Superscript

Page 132: [13] Formatted **Pye, Havala** **12/16/2019 4:31:00 PM**

Font: 10 pt, Superscript

Page 132: [14] Formatted **Pye, Havala** **12/16/2019 4:31:00 PM**

Font: 10 pt, Superscript

Page 132: [14] Formatted **Pye, Havala** **12/16/2019 4:31:00 PM**

Font: 10 pt, Superscript

Page 132: [15] Formatted **Pye, Havala** **12/16/2019 4:24:00 PM**

Font: 10 pt

Page 132: [15] Formatted **Pye, Havala** **12/16/2019 4:24:00 PM**

Font: 10 pt

Page 132: [15] Formatted **Pye, Havala** **12/16/2019 4:24:00 PM**

Font: 10 pt

Page 132: [16] Formatted **Pye, Havala** **12/16/2019 4:30:00 PM**

Font: 10 pt, Superscript

Page 132: [16] Formatted **Pye, Havala** **12/16/2019 4:30:00 PM**

Font: 10 pt, Superscript

Page 132: [17] Formatted **Pye, Havala** **12/16/2019 4:31:00 PM**

Font: 10 pt, Superscript

Page 132: [17] Formatted **Pye, Havala** **12/16/2019 4:31:00 PM**

Font: 10 pt, Superscript

Page 132: [18] Formatted **Pye, Havala** **12/16/2019 4:31:00 PM**

Font: 10 pt, Superscript

Page 132: [18] Formatted **Pye, Havala** **12/16/2019 4:31:00 PM**

Font: 10 pt, Superscript

Page 132: [19] Formatted **Pye, Havala** **12/16/2019 4:24:00 PM**

Font: 10 pt

Page 132: [19] Formatted **Pye, Havala** **12/16/2019 4:24:00 PM**

Font: 10 pt

Page 132: [19] Formatted **Pye, Havala** **12/16/2019 4:24:00 PM**

Font: 10 pt

Page 132: [20] Formatted **Pye, Havala** **12/16/2019 4:31:00 PM**

Font: 10 pt, Superscript

Page 132: [20] Formatted **Pye, Havala** **12/16/2019 4:31:00 PM**

Font: 10 pt, Superscript

Page 132: [21] Formatted **Pye, Havala** **12/16/2019 4:31:00 PM**

Font: 10 pt, Superscript

Page 132: [21] Formatted **Pye, Havala** **12/16/2019 4:31:00 PM**

Font: 10 pt, Superscript

Page 132: [22] Formatted **Pye, Havala** **12/16/2019 4:31:00 PM**

Font: 10 pt, Superscript

Page 132: [22] Formatted **Pye, Havala** **12/16/2019 4:31:00 PM**

Font: 10 pt, Superscript

Supporting information for:
The Acidity of Atmospheric Particles and Clouds

Havala O. T. Pye[1], Athanasios Nenes[2,3], Becky Alexander[4], Andrew P. Ault[5], Mary C. Barth[6], Simon L. Clegg[7], Jeffrey L. Collett, Jr.[8], Kathleen M. Fahey[1], Christopher J. Hennigan[9], Hartmut Herrmann[10], Maria Kanakidou[11], James T. Kelly[12], I-Ting Ku[8], V. Faye McNeill[13], Nicole Riemer[14], Thomas Schaefer[10], Guoliang Shi[15], Andreas Tilgner[10], John T. Walker[1], Tao Wang[16], Rodney Weber[17], Jia Xing[18], Rahul A. Zaveri[19], Andreas Zuend[20]

[1]Office of Research and Development, U.S. Environmental Protection Agency, Research Triangle Park, NC, 27711, USA
[2]School of Architecture, Civil and Environmental Engineering, Ecole Polytechnique Fédérale de Lausanne, Lausanne, CH-1015, Switzerland
[3]Institute for Chemical Engineering Sciences, Foundation for Research and Technology Hellas, Patras, GR-26504, Greece
[4]Department of Atmospheric Science, University of Washington, Seattle, WA, 98195, USA
[5]Department of Chemistry, University of Michigan, Ann Arbor, MI, 48109-1055, USA
[6]National Center for Atmospheric Research, Boulder, CO, 80307, USA
[7]School of Environmental Sciences, University of East Anglia, Norwich NR4 7TJ, UK
[8]Department of Atmospheric Science, Colorado State University, Fort Collins, CO, 80523, USA
[9]Department of Chemical, Biochemical, and Environmental Engineering, University of Maryland Baltimore County, Baltimore, MD, 21250, USA
[10]Leibniz Institute for Tropospheric Research (TROPOS), Atmospheric Chemistry Department (ACD), Leipzig, 04318, Germany
[11]Department of Chemistry, University of Crete, Voutes, Heraklion Crete, 71003, Greece
[12]Office of Air Quality Planning & Standards, U.S. Environmental Protection Agency, Research Triangle Park, NC, 27711, USA
[13]Department of Chemical Engineering, Columbia University, New York, NY, 10027, USA
[14]Department of Atmospheric Sciences, University of Illinois at Urbana-Champaign, Urbana-Champaign, Illinois, 61801, USA
[15]State Environmental Protection Key Laboratory of Urban Ambient Air Particulate Matter Pollution Prevention and Control, Nankai University, Tianjin, 300071, China
[16]Department of Civil and Environmental Engineering, The Hong Kong Polytechnic University, Hung Hom, Kowloon, Hong Kong, China
[17]School of Earth and Atmospheric Sciences, Georgia Institute of Technology, Atlanta, GA, 30332, USA
[18]School of Environment, Tsinghua University, Beijing, 100084, China
[19]Atmospheric Sciences & Global Change Division, Pacific Northwest National Laboratory, Richland, WA, 99352, USA
[20]Department of Atmospheric and Oceanic Sciences, McGill University, Montreal, Quebec, H3A 0B9, Canada

Correspondence to: Havala O. T. Pye (pye.havala@epa.gov)

Number of pages: ~~64~~67
Figures: 8
Tables: 11

S1 Supplementary information for the definition of pH

S1.1 Operational definition and pH measurements

Operational definition of pH

The notional character of the pH definition was recognized decades ago and has led to operational definitions of pH in terms of primary standard methods for pH measurements. These standard methods have been agreed upon by expert consensus, such as during the IUPAC-sponsored conference on "Harmonization of pH Scale Recommendations" in the year 1980 and refinements since then (Covington et al. 1985; Buck et al., 2002). The operational definition of pH is based on the principle of determining the difference between the pH of a solution of interest and that of a reference (buffer) solution of known pH by means of measuring the difference in electromotive force, i.e. an electric potential difference, using two electrochemical cells. High-precision measurement of absolute pH values are made with a so-called primary method using electrochemical cells without transference as described in great detail by Buck et al. (2002) and briefly introduced in this section.

The main purpose of the rather laborious absolute pH measurements is to establish the pH values and associated uncertainties of well-defined, stable standard buffer solutions (so-called primary standard buffers) at certain concentrations and over a meaningful temperature range, e.g. the primary standard of 0.05 mol kg^{-1} potassium hydrogen phthalate (in water) has a determined pH value of 4.005 at 25 °C, 3.997 at 10 °C and 4.000 at 0 °C. Tabulated values of primary standard buffer solutions, covering acidic to alkaline pH ranges, serve as calibration standards for a wider range of so-called secondary standard buffer solutions, covering the pH scale from 1.7 to 13.4 (see tables 1 & 2 in Buck et al., 2002). Primary or secondary standard solutions of known pH are then used in instrument calibration and the quantification of the pH of a sample solution of interest. As stated by Buck et al., (2002), the declaration of a pH measurement by a "primary method" requires assuring full traceability of the results of all measurements and consideration of their uncertainties as well as of limitations in the theory employed in the determination of experimental variables.

Absolute pH measurement with a Harned cell

IUPAC recommends the Harned cell, a cell without liquid junction, as a primary method of pH measurement. Using the conventional notation from electrochemistry, the Harned cell is defined by:

$$\mathrm{Pt} \mid \mathrm{H_2(g)}\ (p = 101.325\ \mathrm{kPa}) \mid \text{buffer S}, \mathrm{Cl^-(aq)} \mid \mathrm{AgCl(s)} \mid \mathrm{Ag}. \qquad \text{(C1)}$$

Here, cell (C1) contains an aqueous standard buffer solution S of known composition as well as chloride ions (typically in form of an aqueous solution of KCl or NaCl). The cell includes a silver–silver-chloride electrode and a hydrogen–platinum electrode (platinum as catalyst), allowing for concentration-dependent measurements of the electrical potential. The potential difference E_1 of the cell is found by using the cell reaction $\mathrm{AgCl(s)} + \frac{1}{2}\mathrm{H_2(g)} \rightleftharpoons \mathrm{Ag(s)} + \mathrm{H^+(aq)} + \mathrm{Cl^-(aq)}$ and application of Nernst's equation to yield (Buck et al., 2002),

$$E_1 = E^{\ominus} - \frac{RT}{F} \ln\left[a_{\mathrm{H^+}} \frac{m_{\mathrm{Cl^-}}}{m^{\ominus}} \gamma_{\mathrm{Cl^-}}\right], \qquad \text{(S1)}$$

where $E^{\ominus}$ is the standard potential difference of the cell at absolute temperature T when the hydrogen gas pressure is corrected to 101.325 kPa. R is the ideal gas constant (8.3144598 J K^{-1} mol^{-1}) and F the Faraday constant (9.6485332×10^4 C mol^{-1}). Equation (S1) can be rearranged to express the molality-based acidity function $\mathrm{p}(a_{\mathrm{H}}\gamma_{\mathrm{Cl}})$, which is a linear function of the measured potential difference $(E_1 - E^{\ominus})$ and the logarithm of the chloride ion molality,

$$\mathrm{p}(a_{\mathrm{H}}\gamma_{\mathrm{Cl}}) = -\log_{10}\left(a_{\mathrm{H}^+}\gamma_{\mathrm{Cl}^-}\right) = \frac{E_1 - E^{\ominus}}{(RT/F)\ln(10)} + \log_{10}\left(\frac{m_{\mathrm{Cl}^-}}{m^{\ominus}}\right). \quad \text{(S2)}$$

Calculation of the (molal) pH value of solution S from Eq. (S2) seems straightforward, $\mathrm{pH(S)} = \mathrm{p}(a_{\mathrm{H}}\gamma_{\mathrm{Cl}}) + \log_{10}\left(\gamma_{\mathrm{Cl}^-}\right)$. However, it requires an independent assumption about the value of the single-ion activity coefficient of the chloride ion (immeasurable). The Bates–Guggenheim convention established a means for a standardized way of determining γ_{Cl^-} under specified conditions (outlined below). The standard potential difference $E^{\ominus}$ is also determined using the Harned cell, with only aqueous HCl present at a specified molality; $m_{\mathrm{HCl}} = 0.01$ mol kg^{-1} is recommended. This buffer-free Harned cell configuration is

$$\mathrm{Pt} \mid \mathrm{H_2} \mid \mathrm{HCl(aq)}, (m_{\mathrm{HCl}} = 0.01 \text{ mol kg}^{-1}) \mid \mathrm{AgCl} \mid \mathrm{Ag}. \quad \text{(C1a)}$$

The Nernst equation for cell C1a involves the molality of HCl and the mean molal activity coefficient $\gamma_{\pm,\mathrm{HCl}}$, which is known for various temperatures from experimental data, e.g. $\gamma_{\pm,\mathrm{HCl}} = 0.9042$ for $m_{\mathrm{HCl}} = 0.01$ mol kg^{-1} (in pure water) at 298.15 K (Bates and Robinson, 1980). Hence, a precise measurement of the electrical cell potential $E_{1\mathrm{a}}$ allows for an unambiguous calculation of $E^{\ominus}$ via

$$E^{\ominus} = E_{1\mathrm{a}} + \frac{2\,RT}{F}\ln\left[\,0.01\,\gamma_{\pm,\mathrm{HCl}}\right]. \quad \text{(S3)}$$

As mentioned above, to arrive at a pH value by means of the acidity function (Eq. S2), $\log_{10}\left(\gamma_{\mathrm{Cl}^-}\right)$ needs to be quantified independently. In brief, the IUPAC (Buck et al., 2002) recommends the following two-step procedure: (i) the value of the acidity function at zero chloride molality $\mathrm{p}(a_{\mathrm{H}}\gamma_{\mathrm{Cl}})^0$ is determined as the intercept of Eq. (S2) by means of a linear extrapolation using several measurements with cell C1 at different molalities of NaCl or KCl (small additions of chloride while maintaining a total molal ionic strength $I < 0.1$ mol kg^{-1}); (ii) the chloride ion activity coefficient, $\gamma^0_{\mathrm{Cl}^-}$, at zero chloride molality (the trace activity coefficient) is determined using Debye–Hückel theory. In aqueous solutions of low ionic strength ($I < 0.1$ mol kg^{-1}), the Debye–Hückel equation for single-ion activity coefficients is applicable (but imperfect). The Bates–Guggenheim convention adopts the expression

$$\log_{10}(\gamma^0_{\mathrm{Cl}^-}) = -A\frac{\sqrt{I}}{1 + b\sqrt{I/m^{\ominus}}}, \quad \text{(S4)}$$

with parameter A as the temperature-dependent Debye–Hückel constant; parameter b set to 1.5, assumed constant for temperatures in the range from 5 – 50 °C; and $I = \frac{1}{2}\sum_i m_i z_i^2$, the ionic strength of the (standard) solution with z_i the normalized integer charge of ion i. Values of A are tabulated in the appendix of Buck et al. (2002), e.g. $A = 0.5100$

$\mathrm{mol}^{-1/2}\,\mathrm{kg}^{-1/2}$ at 298.15 K. Employing this convention and parameters, the primary method allows determining the pH of different standard solutions S based on Eqs. (S2 – S4) as follows:

$$\mathrm{pH(S)} = \lim_{m_{\mathrm{Cl}^-}\to 0}\left[\frac{E_1 - E^{\ominus}}{(RT/F)\ln(10)} + \log_{10}\left(\frac{m_{\mathrm{Cl}^-}}{m^{\ominus}}\right) - A\frac{\sqrt{I}}{1+1.5\sqrt{I/m^{\ominus}}}\right]. \qquad \text{(S5)}$$

The experimental uncertainty for a typical primary pH measurement is of the order 0.004 pH units. However, the uncertainty associated with the assumptions made by the Bates–Guggenheim convention add an estimated 0.01 pH units of uncertainty (95 % confidence interval) for $I < 0.1$ mol kg^{-1}, while increasing uncertainty is expected towards higher ionic strength (Buck et al., 2002). Most of the latter uncertainty arises from assumptions about the true dissociation of ions in buffer solutions (affecting the value of I) and the effective distance of closest approach of ions (factored into $b = 1.5$). We refer to the IUPAC recommendations detailed in Buck et al. (2002) and the pH uncertainty evaluation by Meinrath and Spitzer (2000) for recommended measurement protocols, calibration and considerations of uncertainties as well as various technical details of the procedures introduced.

Practical pH measurements with glass electrodes

In practice, secondary methods are frequently used, among them cells with a glass electrode instead of a H_2|Pt electrode. These secondary methods use cells with transference, which contain liquid junctions (e.g. a salt bridge), leading to irreversible migration of ions and associated non-negligible liquid junction potentials contributing to the measured potential difference of interest. The modern pH meters used widely in laboratories and industry are based on H^+-ion-responsive glass electrodes. This choice of electrode is for reasons of convenience and reliability. The key part of the electrode is a glass membrane (a thin piece of H^+-sensitive glass), often shaped in the form of a bulb, attached to a stem of glass of high electric resistivity containing an internal reference electrode and filling solution of fixed chloride concentration. pH meters come in many shapes and sizes, including flat models, capillary probes and devices with ion-selective electrodes specific for other ions, e.g. nitrate, chloride, sodium and ammonium (Kolb, 1979; Buck et al., 2002). The glass-electrode electrochemical cell is defined by

$$\text{ref. electrode} \,\big|\, \mathrm{KCl(aq)}, \left(m_{\mathrm{KCl}} \geq 3.5\ \mathrm{mol\ kg^{-1}}\right) \vdots\vdots \text{solution (S or X)} \,\big|\, \text{glass electrode.} \qquad \text{(C2)}$$

The reference electrode is usually of the silver–silver chloride type, with a salt bridge, e.g. a porous plug junction in contact with the solution to be tested. The working principle of a glass electrode is based on the development of an electrical potential at H^+-sensitive glass–liquid interfaces. The potential at the outside glass surface depends on the pH of the sample solution measured, while the potential at the inside surface is established by the constant pH of the filling solution (e.g. concentrated $KCl_{(aq)}$). Sometimes the glass and reference electrodes are combined into a single-probe *combination electrode*.

The pH of sample solution X is determined via the measured potential difference $E_2(\mathrm{X}) - E_2(\mathrm{S})$ using an adequate standard buffer solution of known $\mathrm{pH(S)}$,

$$\mathrm{pH(X)} = \mathrm{pH(S)} - \frac{E_2(\mathrm{X}) - E_2(\mathrm{S})}{(RT/F)\ln(10)}. \qquad \text{(S6)}$$

The direct application of Eq. (S6) is an example of a simple one-point calibration. Higher precision measurements are carried out by using a two-point or multi-point calibration procedure, in which at least two standard buffers are used that bracket the (unknown) pH(X). Ideally, the standard buffers chosen are close (above and below) in pH to pH(X), leading to reduced uncertainties. Two-point or multipoint calibrations are needed to achieve a target pH uncertainty of about 0.02 – 0.03 near 25 °C. Details about such methods, proper instrument calibration procedures and associated uncertainties are outlined in Buck et al. (2002) as well as the manuals and guidelines of commercial pH-meter manufacturers. Moreover, these references point out that special considerations are necessary for pH measurements in non-aqueous solutions or solutions containing substantial amounts of organic components, which may affect the behavior of the electrodes and junctions.

S1.2 Derivation of pH scale conversions

Conversions among pH values calculated using different concentration scales (molarity, molality, mole fraction, etc.) are possible and necessary for an adequate comparison of model predictions. It is recommended to convert all pH values to the molality scale. For clarity, the molality-scale pH is denoted by symbol "pH" while the pH on other scales is indicated by a subscript (e.g. pH_x for the mole-fraction-based pH). Generally, formulas for the conversion of pH scales are derived using the equivalence of the (electro-)chemical potential of single ions expressed in any concentration scale. For example, in the case of an electroneutral liquid phase (i.e. cancellation of the local electrostatic potential within the phase), the chemical potential of H^+, $\mu^l_{H^+}$, is given by

$$\mu^l_{H^+} = \mu^{\ominus,(m)}_{H^+} + RT \ln\left(\frac{m_{H^+}}{m^\ominus}\,\gamma_{H^+}\right) = \mu^{\ominus,(x)}_{H^+} + RT \ln\left(x_{H^+} f^*_{H^+}\right). \quad \text{(S7)}$$

Here, the chemical potential is expressed either using the molality scale (first equality on right hand side) or the mole fraction scale (second equality). In a general case, neither of the two standard state chemical potentials ($\mu^{\ominus,(m)}_{H^+}, \mu^{\ominus,(x)}_{H^+}$) nor the two activity coefficients are of equivalent values, yet the correct combinations according to Eq. (S7) yield an equivalent $\mu^l_{H^+}$. By using this fact combined with the detailed definitions of the different activity coefficient scales and reference states, a correct mapping between scales is possible, which then allows also for a conversion between pH values defined on corresponding scales. Note, when solvents other than water are involved one needs to correctly account for the definitions of the activity coefficients in terms of their reference states (e.g. infinite dilution in pure water or in a specific water–organic mixed solvent), then follow the derivation steps analogous to those outlined below. In the case described here, the reference states of γ_{H^+} and $f^*_{H^+}$ are both that of infinite dilution of H^+ in pure water, where $\gamma_{H^+} \to 1$ and $f^*_{H^+} \to 1$ (regardless of whether other solvent compounds are present or not), such that both activity coefficients are equivalent at that reference point. This is consistent with models that only treat organic-free aqueous electrolyte systems as well as with models treating organic–inorganic electrolyte solutions, such as AIOMFAC. Using these definitions leads to (e.g. Zuend, 2007, pp. 45 – 47)

$$\ln(\gamma_{H^+}) = \ln\left(f^*_{H^+}\right) + \ln\left(\frac{x_{H^+}}{M_w\, m_{H^+}}\right), \quad \text{(S8)}$$

where M_w denotes the molar mass of water. Using the definition of molality, $m_{H^+} = \frac{n_{H^+}}{\sum_s n_s M_s}$, (compatible with the AIOMFAC model) Eq. (S8) can be expressed as

$$\ln(\gamma_{H^+}) = \ln\left(f^*_{H^+}\right) + \ln\left(\frac{1}{M_w} \sum_s x_s M_s\right). \quad \text{(S9)}$$

Here, the summation over index s covers non-electrolyte species only, i.e. water and organic mixture components, while $x_s = \frac{n_s}{\sum_s n_s + \sum_i n_i}$ is the mole fraction of 'solvent' s computed by accounting for all solution species, including molar amounts of H^+ and other ions ($\sum_i n_i$). For the case of an aqueous electrolyte solution absent any organic components or when water is defined as the only solvent (e.g. in the E-AIM model), molality is defined by $m_{H^+} = \frac{n_{H^+}}{n_w M_w}$ and $x_w = \frac{n_w}{n_w + \sum_i n_i}$. In this case, Eq. (S9) simplifies to

$$\ln(\gamma_{H^+}) = \ln\left(f^*_{H^+}\right) + \ln(x_w). \quad \text{(S10)}$$

Using Eq. (S9) with the definitions of pH on molality and mole fraction scales (Eqs. 1 and 2 from main text) results in

$$\mathrm{pH}_x - \mathrm{pH} = \log_{10}\left(\frac{m_{H^+}}{m^\ominus} \frac{\sum_s n_s M_s}{M_w\, n_{H^+}}\right) ~~\text{pH}~~, \quad \text{(S11)}$$

with $m_{H^+} = \frac{n_{H^+}}{\sum_s n_s M_s}$ this simplifies to

$$\mathrm{pH} = \mathrm{pH}_x + \log_{10}\left(m^\ominus M_w\right) \approx \mathrm{pH}_x - 1.74436. \quad \text{(S12)}$$

The exact same conversion formula (Eq. S12) results for solutions for which the molality is defined via $m_{H^+} = \frac{n_{H^+}}{n_w M_w}$ which led to Eq. S10. This is the case because the reference state in both cases is that of infinite dilution of ion "*i*" in pure water. As a reminder, $m^\ominus$ stands for unit molality (1 mol kg^{-1}). Therefore, pH values defined on molality and mole fraction scales are offset by a constant value of about -1.74436.

The analogous conversion between molarity and molality-based pH is given by (Jia et al., 2018)

$$\mathrm{pH}_c = \mathrm{pH} - \log_{10}\left(\frac{c^\ominus}{m^\ominus \rho_0} \cdot 10^3 \frac{\mathrm{dm}^3}{\mathrm{m}^3}\right). \quad \text{(S13)}$$

Here, ρ_0 is the density of the reference solvent, water, in units of kg m^{-3}, while $10^3 \frac{\mathrm{dm}^3}{\mathrm{m}^3}$ is a conversion factor necessary when concentrations are expressed in non-SI units of mol dm^{-3} (or moles per liter). Because liquid-state density of the reference solvent depends weakly on temperature, the exact relation between pH and pH_c is non-linear. However, in the case of water near room temperature (ρ_0 close to 1000 kg m^{-3}), the logarithm in Eq. (S13) yields a small number, resulting in $\mathrm{pH}_c \approx$ ~~pH_m~~~~pH_m~~pH (Jia et al., 2018).

S2. Supplementary information for sulfate production in Figure 3

The reaction rates for the S(IV) – S(VI) conversion processes listed in Table S1 were calculated using the conditions for Beijing Winter Haze published in Cheng et al. (2016): 271 K, 40 ppb SO_2, 66 ppb NO_2, 3 ppb O_3, 0.01 ppb HOOH, 3.16×10^{-3} M [Mn^{+2}], and

$$[Fe^{+3}] = \begin{cases} 10^{-3}\ M \text{ for } pH < 3 \\ 10^{3}[H^{+}]^{3}\ M \text{ for } pH \geq 3 \end{cases}. \quad \text{(S14)}$$

Henry's Law constants are available in Table S2.

S3. Supplementary information for proxy estimates in Figure 15

(a) Inorganic ion balance: There are 5 points for the Tianjin data set off scale. The lines represent the linear fits to each data set based on a least squares regression analysis. The fit parameters are as follows: northeast USA (slope = -45.63, intercept = 0.71, R^2 = 0.32, n = 3623), southeast USA (slope = -27.11, intercept = 1.31, R^2= 0.36, n = 555), California (slope = -12.27, intercept = 2.25, R^2= 0.34, n = 102), Tianjin (slope = -1.346, intercept = 3.16, R^2= 0.02, n = 241). Note that a positive value for the ion balance represents conditions with Σ(anion equivalents) > Σ(cation equivalents).

(b) Cation/anion molar equivalents ratio: There are 7 points for the Tianjin data set off scale. The lines represent the linear fits to each data set based on a least squares regression analysis. The fit parameters are as follows: northeast USA (slope = 2.88, intercept = -1.88, R^2= 0.72, n = 3623), southeast USA (slope = 1.34, intercept = 0.07, R^2= 0.27, n = 524), California (slope = 0.69, intercept = 1.70, R^2= 0.27, n = 102), Tianjin (slope = 0.65, intercept = 2.45, R^2= 0.28, n = 241).

(c) Gas ratio: The lines represent the linear fits to each data set based on a least squares regression analysis. The fit parameters are as follows: northeast USA (slope = 1.73, intercept = 0.44, R^2= 0.75, n = 3534), southeast USA (slope = 0.012, intercept = 0.89, R^2= 0.21, n = 525), California (slope = 0.76, intercept = 1.93, R^2= 0.72, n = 102, GR values below -2 excluded from the fit), Tianjin (slope = 0.03, intercept = 3.10, R^2= 0.01, n = 241).

(d) pH from HNO_3 partitioning: The lines represent the linear fits to each data set based on a least squares regression analysis. The fit parameters are as follows: northeast USA (slope = 0.54, intercept = -0.06, R^2= 0.16, n = 3268), California (slope = 0.27, intercept = 2.01, R^2= 0.09, n = 102), Tianjin (slope = -0.27, intercept = 4.20, R^2= 0.00, n = 234, five points with pH_F > 7 were excluded from the fit).

(f) pH from NH_3 partitioning: The lines represent the linear fits to each data set based on a least squares regression analysis. The fit parameters are as follows: southeast USA (slope = 1.15, intercept = 0.25, R^2= 0.41, n = 486), California (slope = 0.22, intercept = 2.41, R^2= 0.22, n = 102), Tianjin (slope = 1.18, intercept = 0.95, R^2= 0.41, n = 234, five points with pH_F > 7 were excluded from the fit).

Supplementary Figures

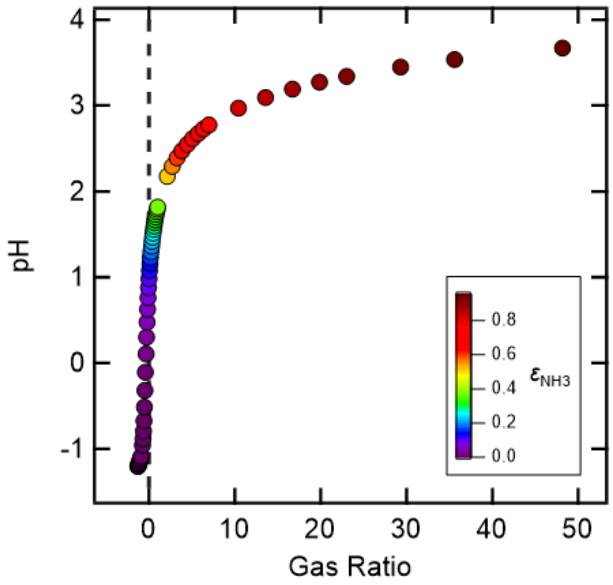

Figure S1. Aerosol pH modeled in E-AIM (model II) versus the Gas Ratio (GR = ([TNH_4] – 2[TSO_4])/[TNO_3]). Conditions for the simulations were: Temperature = 298 K, RH = 0.7, [TSO4] = 10 µg m^{-3}, [TNO_3] = 10 µg m^{-3}, [TNH4] varied from 0 – 130 µg m^{-3}. Color of the symbols corresponds to the fraction of TNH_4 in the gas phase (ε_{NH3} = [NH_3]/([NH_3] + [NH_4^+])). The dotted line at GR = 0 indicates the transition from "ammonia-poor" ([TNH_4] < 2[TSO_4]) to "ammonia-rich" ([TNH_4] > 2[TSO_4]) conditions.

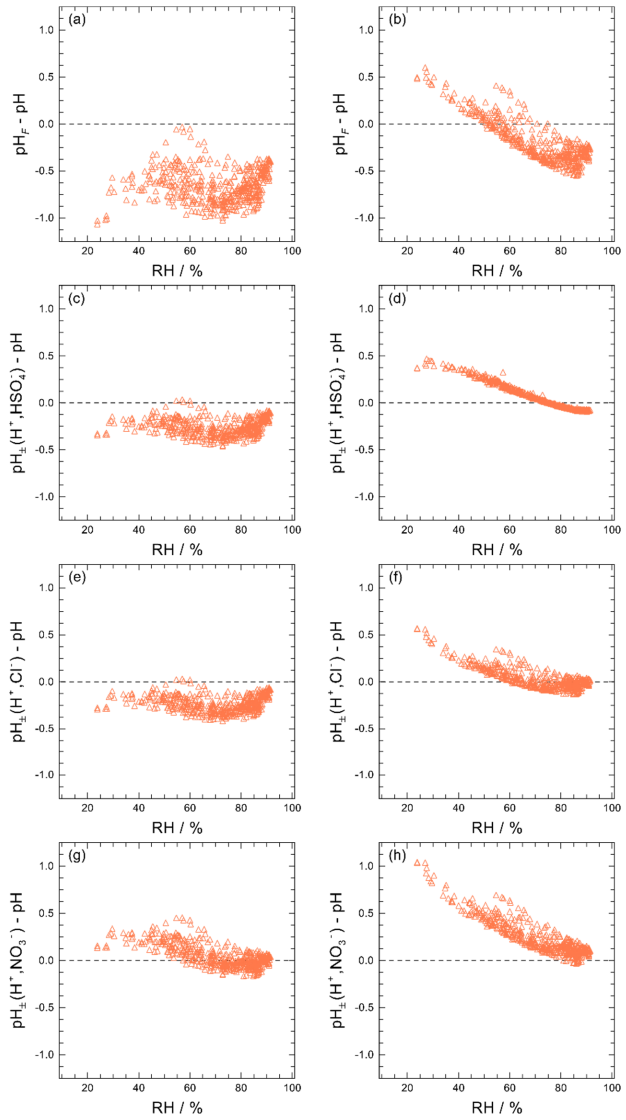

Figure S2. Comparison of different metrics of calculating pH using the CalNex data for AIOMFAC-GLE (left column) and E-AIM (right column).

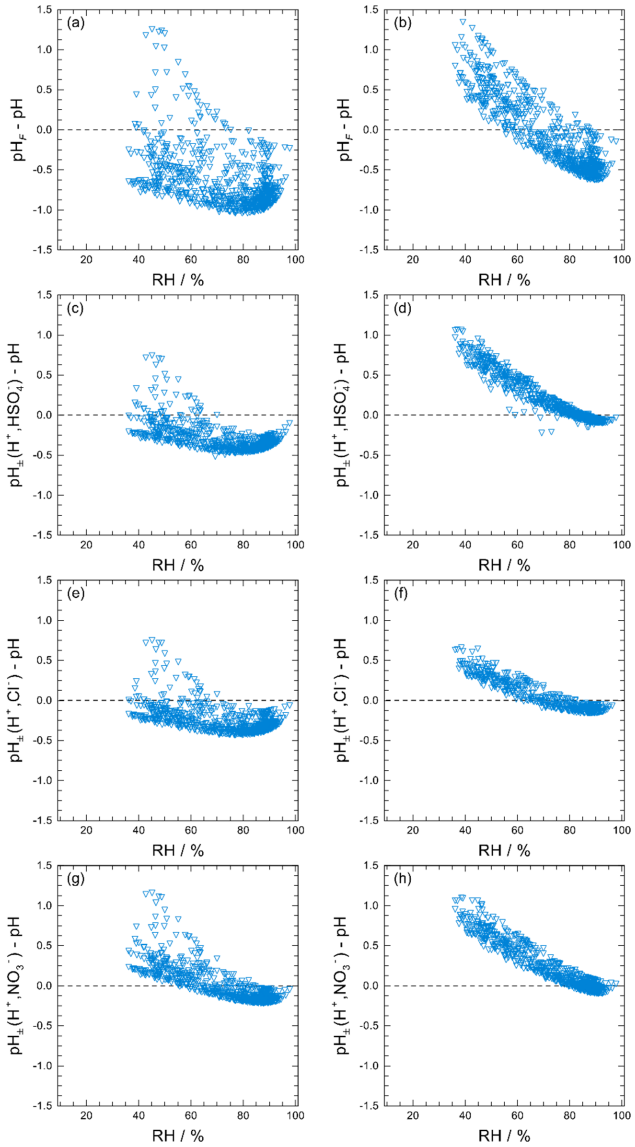

Figure S3. Comparison of different metrics of calculating pH using the SOAS data for AIOMFAC-GLE (left column) and E-AIM (right column).

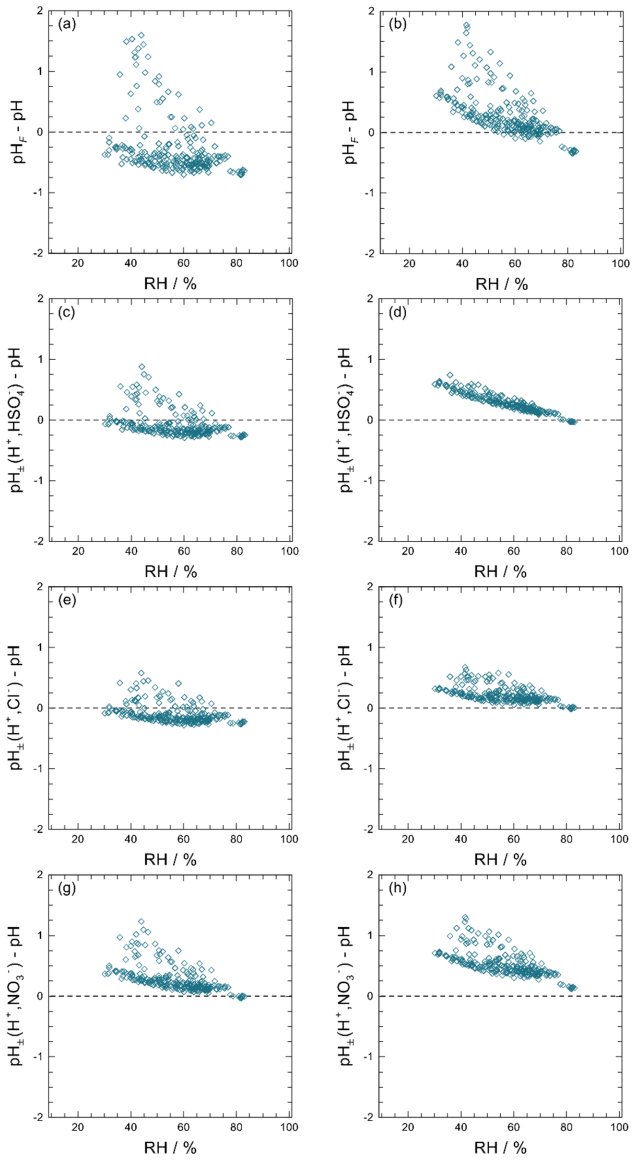

Figure S4. Comparison of different metrics of calculating pH using the Tianjin data for AIOMFAC-GLE (left column) and E-AIM (right column).

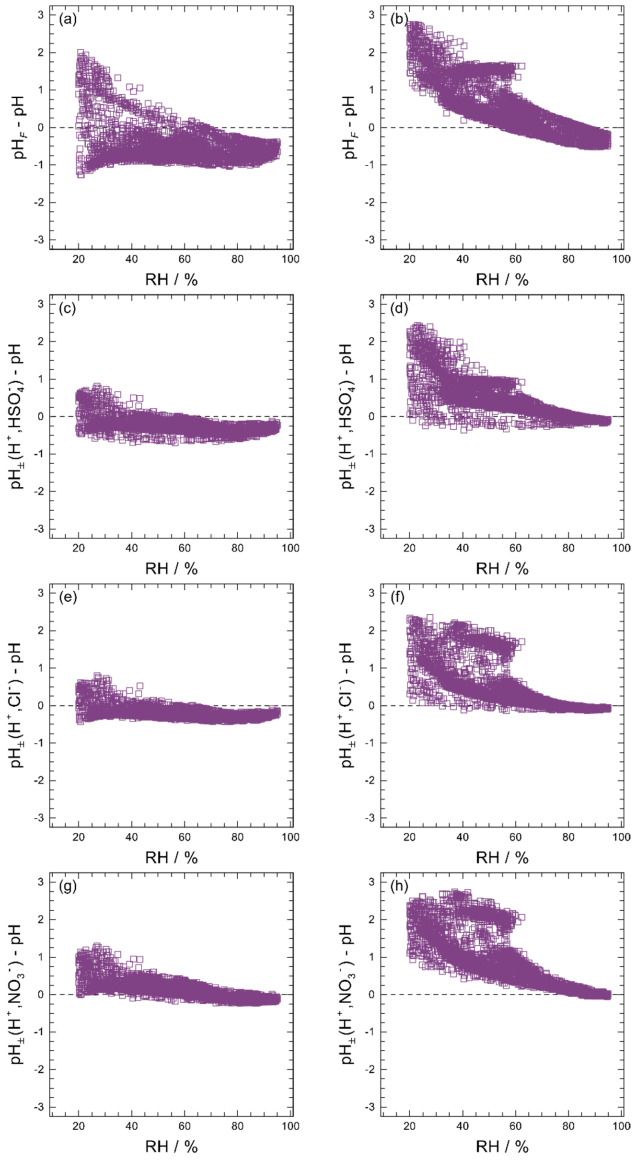

Figure S5. Comparison of different metrics of calculating pH using the WINTER data for AIOMFAC-GLE (left column) and E-AIM (right column).

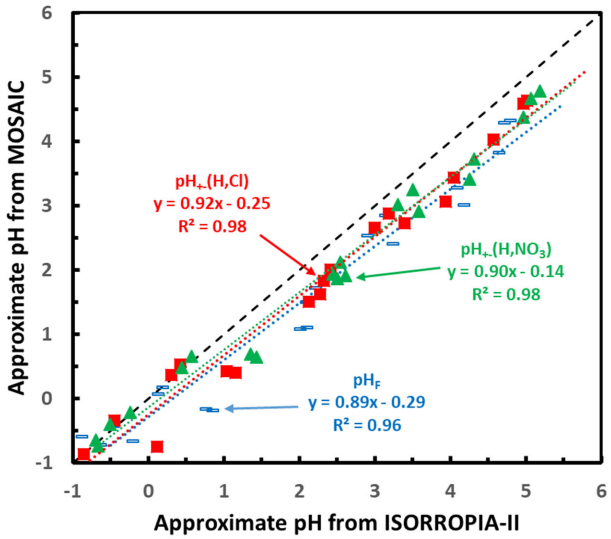

Figure S6. MOSAIC-calculated pH using the different metrics plotted against the corresponding pH values calculated using ISORROPIA II for the data presented in Table S7. Each pH metric is presented with a distinct symbol, and the corresponding linear fit to the data is shown in the corresponding symbol colour.

(a) Fine aerosol pH_F without NVC from dust

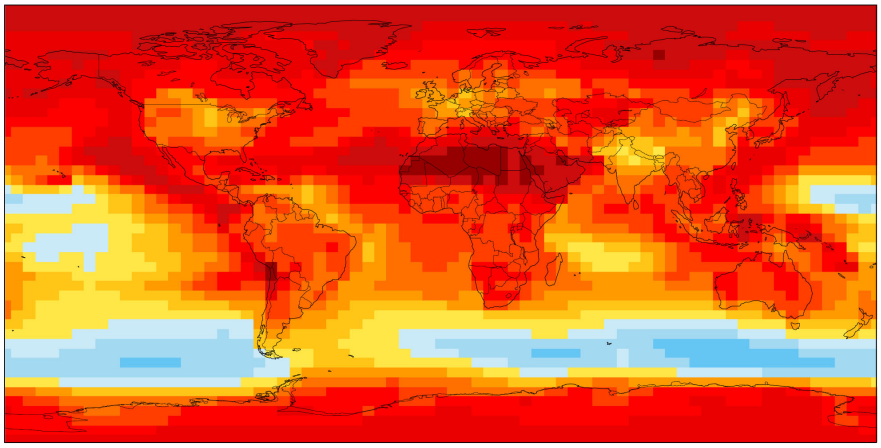

−0.5 0.7 1.9 3.1 4.4 5.6 6.8 8.0

(b) Change in fine aerosol pH_F due to NVC from dust

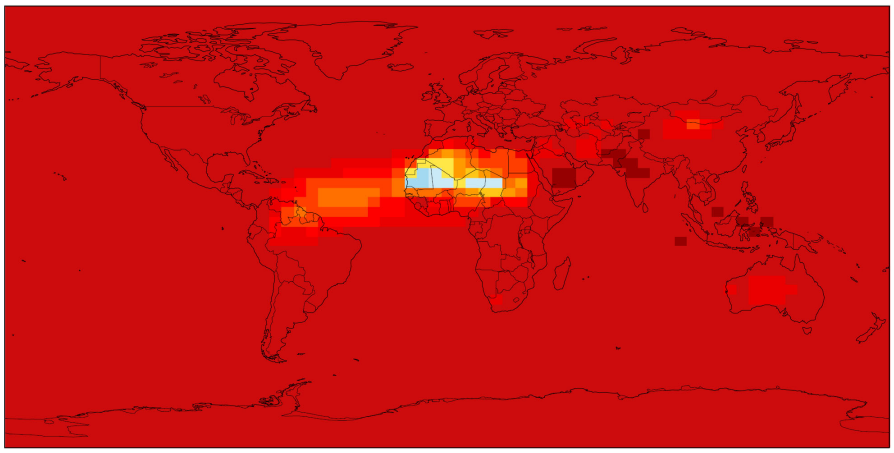

−0.5 0.7 1.9 3.1 4.4 5.6 6.8 8.0

Figure S7. (a) GEOS-Chem annual-mean predicted fine aerosol pH_F excluding non-volatile cations (NVCs) from dust (default GEOS-Chem approach). (b) Increase in pH_F from the inclusion of NVCs from dust. Main text GEOS-Chem figures include NVC from dust in calculations of fine aerosol pH_F.

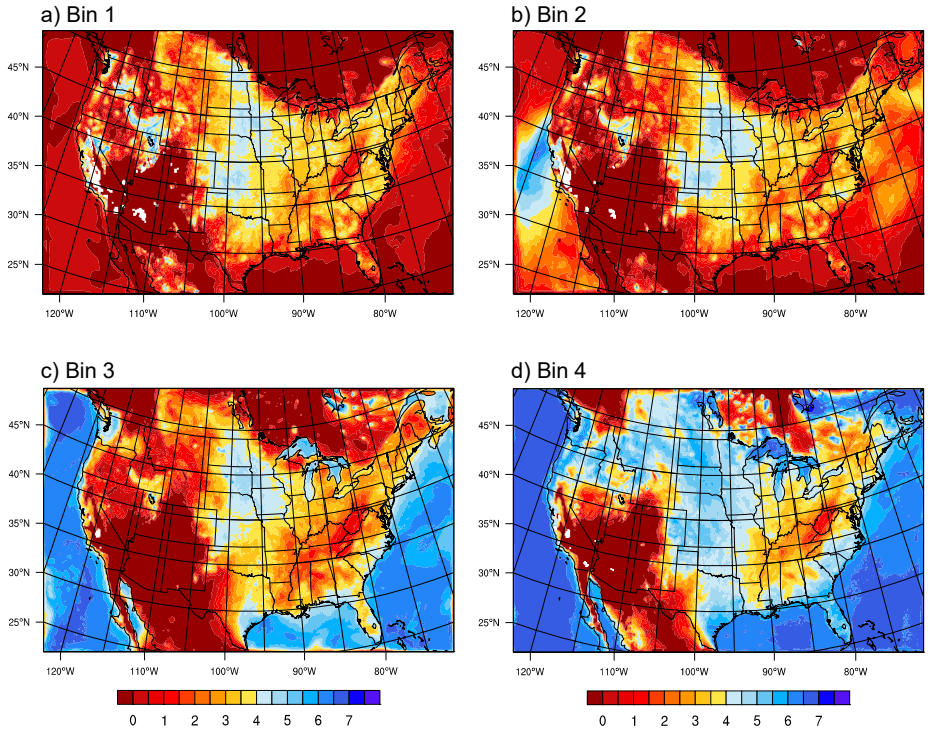
a) Bin 1
b) Bin 2
c) Bin 3
d) Bin 4
45°N
40°N
35°N
30°N
25°N
120°W
110°W
100°W
90°W
80°W
0 1 2 3 4 5 6 7

278 **Supplementary Tables**

279

280 **Table S1.** Reaction rates for the S(IV) –S(VI) conversion processes in Figure 3.

281

Rate	Parameters	Reference
$R_{HOOH} = k_1 K_1 \frac{[\mathrm{H^+}][\mathrm{HSO_3^-}]}{1 + K_1[\mathrm{H^+}]}[\mathrm{HOOH}]$	$k_1 = 7.2 \times 10^7 \exp(-4000\left(\frac{1}{T} - \frac{1}{298}\right))$ $\mathrm{M^{-1}s^{-1}}$ $K_1 = 16\ \mathrm{M^{-1}}$	McArdle and Hoffmann (1983); Zellner (~~19941~~1996)
$R_{TMI} = R_{Fe} + R_{Mn}$ R_{Fe} $= \begin{cases} \frac{k_2[Fe^{+3}][S(IV)]}{[H^+](1 + K_2[S(IV)]^{2/3})} & M \text{ for } pH < 3 \\ k_3[Fe^{+3}]^2[S(IV)] \text{ for } 3 \le pH < 5 \\ k_4[S(IV)] \text{for } pH \ge 5 \end{cases}$ $R_{Mn} = \begin{cases} k_5[\mathrm{Mn^{+2}}][S(IV)] \text{ for } pH < 6 \\ 680[H^+]^2 \text{ for } pH \ge 6 \end{cases}$	$k_2 = 6\ \mathrm{s^{-1}}$ $K_2 = 150\ \mathrm{M^{-2/3}}$ $k_3 = 10^9 \mathrm{M^{-2}\ s^{-1}}$ $k_4 = 10^{-3}\ \mathrm{s^{-1}}$ $k_5 = 10^3\ \mathrm{M^{-1}s^{-1}}$ $k_6 = 680\ \mathrm{M^{-1}s^{-1}}$	Martin and Hill (1987); Martin et al. (1991)
$R_{O3} = \left(k_7[\mathrm{SO_2 \cdot H_2O}] + k_8[\mathrm{HSO_3^-}] + k_9[\mathrm{SO_3^{-2}}]\right)[\mathrm{O_3}]$	$k_7 = 2.4 \times 10^4\ \mathrm{M^{-1}s^{-1}}$ $k_8 = 3.7 \times 10^5 \exp(-5530\left(\frac{1}{T} - \frac{1}{298}\right))\ \mathrm{M^{-1}s^{-1}}$ $k_9 = 1.5 \times 10^9 \exp(-5280\left(\frac{1}{T} - \frac{1}{298}\right))\ \mathrm{M^{-1}s^{-1}}$	Hoffmann (1986)
$R_{NO2} = k_{10}[\mathrm{NO_2}][S(IV)]$	k_{10} $= \begin{cases} 1.4 \times 10^5\ \mathrm{M^{-1}s^{-1}} \text{ for } pH < 5.3 \\ 1.24 \times 10^7\ \mathrm{M^{-1}s^{-1}} \text{ for } pH = 5.3 \\ 1.6 \times 10^7\ \mathrm{M^{-1}s^{-1}} \text{ for } pH = 8.7 \\ linear\ interpolation\ for\ 5.3 < pH < 8.7 \end{cases}$	Lee and Schwartz (1983); Clifton (1988); Cheng et al. (2016)

282

283

Table S2. Henry's Law constants (Sander 2015) used for the S(IV) –S(VI) conversion processes in Figure 3.

Henry's Law Constant	Value
H_{SO2}	$1.317225 \exp\left(2900\left(\frac{1}{T}-\frac{1}{298}\right)\right)$ M atm^{-1}
H_{NO2}	$1.22\times10^{-2} \exp\left(2400\left(\frac{1}{T}-\frac{1}{298}\right)\right)$ M atm^{-1}
H_{O3}	$1.01\times10^{-2} \exp\left(2800\left(\frac{1}{T}-\frac{1}{298}\right)\right)$ M atm^{-1}
H_{HOOH}	$8.41\times10^{4} \exp\left(7600\left(\frac{1}{T}-\frac{1}{298}\right)\right)$ M atm^{-1}

Table S3. Predictions of molality-based pH and related H^+ properties for system 1, water + $(NH_4)_2SO_4$ + H_2SO_4 + NH_3 at 298.15 K. Model calculations include the partial dissociation of HSO_4^- and the gas–liquid equilibria of NH_3 and water.

	E-AIM, model III			AIOMFAC–GLE			MOSAIC			ISORROPIA II			EQUISOLV II		
RH	m_{H^+} (mol kg^{-1})	γ_{H^+}	pH	m_{H^+} (mol kg^{-1})	γ_{H^+}	pH	m_{H^+} (mol kg^{-1})	$\gamma_\pm(H^+, HSO_4^-)$	pH±	m_{H^+} (mol kg^{-1})	$\gamma_\pm(H^+, HSO_4^-)$	pH±	m_{H^+} (mol kg^{-1})	$\gamma_\pm(H^+, Cl^-)$	pH±
	moderately acidic; water-free input composition: 99.9% ammonium sulfate by mass; higher NH_3*(g)*														
99%	2.466×10^{-4}	4.681×10^{-1}	**3.94**	2.900×10^{-4}	3.634×10^{-1}	**3.98**	2.873×10^{-4}	4.331×10^{-1}	**3.91**	5.740×10^{-5}	5.852×10^{-1}	**4.47**	1.556×10^{-4}	6.061×10^{-1}	**4.03**
90%	6.359×10^{-3}	1.336×10^{-1}	**3.07**	5.639×10^{-3}	1.054×10^{-1}	**3.23**	6.504×10^{-3}	2.284×10^{-1}	**2.83**	6.221×10^{-4}	6.015×10^{-1}	**3.43**	1.675×10^{-3}	4.808×10^{-1}	**3.09**
80%	1.636×10^{-2}	9.445×10^{-2}	**2.81**	1.208×10^{-2}	7.936×10^{-2}	**3.02**	1.591×10^{-2}	1.941×10^{-1}	**2.51**	1.562×10^{-3}	7.658×10^{-1}	**2.92**	1.799×10^{-3}	5.879×10^{-1}	**2.98**
70%	2.738×10^{-2}	8.258×10^{-2}	**2.65**	1.624×10^{-2}	8.042×10^{-2}	**2.88**	2.538×10^{-2}	2.003×10^{-1}	**2.29**	2.732×10^{-3}	9.249×10^{-1}	**2.60**	1.424×10^{-3}	7.607×10^{-1}	**2.97**
60%	3.928×10^{-2}	7.733×10^{-2}	**2.52**	1.814×10^{-2}	9.192×10^{-2}	**2.78**	3.577×10^{-2}	2.110×10^{-1}	**2.12**	4.223×10^{-3}	1.100	**2.33**	9.985×10^{-4}	1.020	**2.99**
50%	5.261×10^{-2}	7.408×10^{-2}	**2.41**	1.918×10^{-2}	1.074×10^{-1}	**2.69**	4.719×10^{-2}	2.205×10^{-1}	**1.98**	6.210×10^{-3}	1.313	**2.09**	6.429×10^{-4}	1.418	**3.04**
40%	6.883×10^{-2}	7.053×10^{-2}	**2.31**	2.195×10^{-2}	1.136×10^{-1}	**2.60**	5.861×10^{-2}	2.369×10^{-1}	**1.86**	9.091×10^{-3}	1.607	**1.84**	4.017×10^{-4}	1.989	**3.10**
	highly acidic; water-free input composition: 50% ammonium sulfate by mass; moderate NH_3*(g)*														
99%	1.447×10^{-2}	4.910×10^{-1}	**2.15**	1.717×10^{-2}	3.825×10^{-1}	**2.18**	1.760×10^{-2}	4.529×10^{-1}	**2.10**	4.890×10^{-3}	5.864×10^{-1}	**2.54**	1.084×10^{-2}	6.136×10^{-1}	**2.18**
90%	2.47×10^{-1}	1.89×10^{-1}	**1.33**	2.582×10^{-1}	1.312×10^{-1}	**1.47**	2.504×10^{-1}	2.847×10^{-1}	**1.15**	5.504×10^{-2}	6.161×10^{-1}	**1.47**	7.329×10^{-2}	5.404×10^{-1}	**1.40**
80%	4.69×10^{-1}	1.72×10^{-1}	**1.09**	4.629×10^{-1}	1.123×10^{-1}	**1.28**	5.018×10^{-1}	2.629×10^{-1}	**0.88**	1.400×10^{-1}	7.976×10^{-1}	**0.95**	7.065×10^{-2}	6.798×10^{-1}	**1.32**
70%	5.85×10^{-1}	1.93×10^{-1}	**0.95**	5.527×10^{-1}	1.260×10^{-1}	**1.16**	6.425×10^{-1}	2.815×10^{-1}	**0.74**	2.455×10^{-1}	9.738×10^{-1}	**0.62**	5.225×10^{-2}	8.939×10^{-1}	**1.33**
60%	5.92×10^{-1}	2.49×10^{-1}	**0.83**	5.664×10^{-1}	1.568×10^{-1}	**1.05**	7.228×10^{-1}	2.916×10^{-1}	**0.68**	3.793×10^{-1}	1.169	**0.35**	3.445×10^{-2}	1.217	**1.38**
50%	4.89×10^{-1}	4.00×10^{-1}	**0.71**	5.578×10^{-1}	1.971×10^{-1}	**0.96**	7.654×10^{-1}	2.750×10^{-1}	**0.68**	5.565×10^{-1}	1.408	**0.11**	2.104×10^{-2}	1.710	**1.44**
40%	3.57×10^{-1}	8.26×10^{-1}	**0.53**	5.997×10^{-1}	2.204×10^{-1}	**0.88**	6.284×10^{-1}	2.207×10^{-1}	**0.86**	8.116×10^{-1}	1.735	**-0.15**	1.247×10^{-2}	2.431	**1.52**

[a] E-AIM was run using model III and the comprehensive calculation mode including NH_3 equilibration; no solids considered. It predicts mole-fraction-based activity coefficients of H^+; pH_x was converted to pH using Eq. (4).

[b] The AIOMFAC–GLE model was used, including gas–liquid partitioning of NH_3; no solids.

[c] MOSAIC calculations were run with dynamic gas–particle of NH_3 considered; no solids. pH ≈ $pH_\pm$ predicted by use of the listed mean molal ion activity coefficients (Eq. 7).

[d] Models ISORROPIA II and EQUISOLV II approximate pH ≈ $pH_\pm$(H,X) by use of the listed mean molal ion activity coefficients (Eq. 7), with X = Cl^-, HSO_4^- or NO_3^-, as indicated by the $\gamma_\pm(H^+,X)$ used.

Table S4. Predictions of molality-based pH and related H^+ properties for system 2, water + Na_2SO_4 + NaCl + H_2SO_4 + HCl at 298.15 K. Model calculations include the partial dissociation of HSO_4^- and the gas–liquid equilibria of HCl and water.

	E-AIM, model III			**AIOMFAC–GLE**			**MOSAIC**			**ISORROPIA II**			**EQUISOLV II**		
RH	m_{H^+} (mol kg^{-1})	γ_{H^+}	**pH**	m_{H^+} (mol kg^{-1})	γ_{H^+}	**pH**	m_{H^+} (mol kg^{-1})	$\gamma_\pm(H^+,Cl^-)$	**pH±**	m_{H^+} (mol kg^{-1})	$\gamma_\pm(H^+,Cl^-)$	**pH±**	m_{H^+} (mol kg^{-1})	$\gamma_\pm(H^+,Cl^-)$	**pH±**
	moderately acidic; water-free input composition: 99.9% sea salt mimic by mass														
99%	2.902×10^{-3}	7.464×10^{-1}	**2.66**	3.068×10^{-3}	7.157×10^{-1}	**2.66**	3.375×10^{-3}	6.732×10^{-1}	**2.64**	2.441×10^{-3}	7.065×10^{-1}	**2.76**	2.730×10^{-3}	7.464×10^{-1}	**2.69**
90%	2.063×10^{-4}	1.280	**3.58**	2.661×10^{-4}	1.019	**3.57**	1.848×10^{-4}	1.002	**3.73**	1.325×10^{-4}	8.819×10^{-1}	**3.93**	2.358×10^{-4}	8.977×10^{-1}	**3.67**
80%	4.119×10^{-5}	2.753	**3.95**	6.242×10^{-5}	1.870	**3.93**	3.554×10^{-5}	1.699	**4.22**	2.748×10^{-5}	1.320	**4.43**	4.726×10^{-5}	1.486	**4.15**
70%	1.072×10^{-5}	5.739	**4.21**	1.844×10^{-5}	3.482	**4.19**	8.380×10^{-6}	2.955	**4.61**	7.70610^{-6}	1.970	**4.82**	1.393×10^{-5}	2.307	**4.49**
60%	3.066×10^{-6}	1.184×10^{1}	**4.44**	5.810×10^{-6}	6.676	**4.41**	2.171×10^{-6}	5.120	**4.95**	2.509×10^{-6}	2.863	**5.14**	4.435×10^{-6}	3.551	**4.80**
50%	8.852×10^{-7}	2.495×10^{1}	**4.66**	1.800×10^{-6}	1.357×10^{1}	**4.61**	5.856×10^{-7}	8.873	**5.28**	8.659×10^{-7}	4.125	**5.45**	1.319×10^{-6}	5.677	**5.13**
40%	2.410×10^{-7}	5.570×10^{1}	**4.87**	5.098×10^{-7}	3.054×10^{1}	**4.81**	1.507×10^{-7}	1.589×10^{1}	**5.62**	2.957×10^{-7}	6.011	**5.75**	3.941×10^{-7}	9.127	**5.44**
	highly acidic; water-free input composition: 50% sea salt mimic by mass														
99%	2.308×10^{-1}	7.516×10^{-1}	**0.76**	2.346×10^{-1}	7.371×10^{-1}	**0.76**	4.678×10^{-1}	4.626×10^{-1}	**0.66**	1.958×10^{-1}	6.392×10^{-1}	**0.90**	2.444×10^{-1}	7.542×10^{-1}	**0.73**
90%	1.553×10^{-1}	6.213×10^{-1}	**1.02**	2.226×10^{-1}	3.782×10^{-1}	**1.07**	2.861×10^{-1}	6.114×10^{-1}	**0.76**	9.878×10^{-2}	6.366×10^{-1}	**1.20**	7.194×10^{-2}	9.059×10^{-1}	**1.19**
80%	4.226×10^{-2}	1.274	**1.27**	1.019×10^{-1}	4.768×10^{-1}	**1.31**	7.857×10^{-2}	1.238	**1.01**	9.186×10^{-2}	7.088×10^{-1}	**1.19**	3.079×10^{-2}	1.247	**1.42**
70%	1.020×10^{-2}	3.031	**1.51**	3.565×10^{-2}	8.540×10^{-1}	**1.52**	1.445×10^{-2}	2.714	**1.41**	8.089×10^{-2}	7.734×10^{-1}	**1.20**	1.485×10^{-2}	1.654	**1.61**
60%	2.404×10^{-3}	7.525	**1.74**	9.379×10^{-3}	2.052	**1.72**	2.685×10^{-3}	5.715	**1.81**	6.869×10^{-2}	8.383×10^{-1}	**1.24**	4.959×10^{-3}	2.367	**1.93**
50%	5.259×10^{-4}	1.999×10^{1}	**1.98**	1.471×10^{-3}	7.878	**1.94**	5.072×10^{-4}	1.197×10^{1}	**2.22**	5.659×10^{-2}	9.076×10^{-1}	**1.29**	1.344×10^{-3}	3.630	**2.31**
40%	9.912×10^{-5}	5.966×10^{1}	**2.23**	7.366×10^{-5}	7.891×10^{1}	**2.24**	7.971×10^{-5}	2.758×10^{1}	**2.66**	4.495×10^{-2}	9.872×10^{-1}	**1.35**	5.058×10^{-4}	4.885	**2.61**

See also footnotes to Table S~~3~~1.

Table S5. Predictions of molality-based pH and related H^+ properties for system 3, water + $(NH_4)_2SO_4$ + H_2SO_4 + NH_3 + HNO_3 at 298.15 K. Model calculations include the partial dissociation of HSO_4^- and the gas–liquid equilibria of NH_3, HNO_3, and water.

	E-AIM, model III			**AIOMFAC–GLE**			**MOSAIC**			**ISORROPIA II**			**EQUISOLV II**		
RH	m_{H^+} (mol kg^{-1})	γ_{H^+}	**pH**	m_{H^+} (mol kg^{-1})	γ_{H^+}	**pH**	m_{H^+} (mol kg^{-1})	$\gamma_\pm(H^+,NO_3^-)$	**pH±**	m_{H^+} (mol kg^{-1})	$\gamma_\pm(H^+,NO_3^-)$	**pH±**	m_{H^+} (mol kg^{-1})	$\gamma_\pm(H^+,HSO_4^-)$	**pH±**
	moderately acidic; water-free input composition: 99.9% ammonium sulfate by mass; high NH_3*(g) and* HNO_3*(g)*														
99%	4.426×10^{-3}	7.059×10^{-1}	**2.51**	4.803×10^{-3}	6.836×10^{-1}	**2.48**	8.020×10^{-3}	6.157×10^{-1}	**2.31**	4.128×10^{-3}	6.580×10^{-1}	**2.57**	5.987×10^{-3}	5.940×10^{-1}	**2.45**
90%	6.697×10^{-3}	7.539×10^{-1}	**2.30**	1.166×10^{-2}	5.400×10^{-1}	**2.20**	7.217×10^{-3}	4.905×10^{-1}	**2.45**	4.477×10^{-3}	5.188×10^{-1}	**2.63**	5.348×10^{-3}	7.976×10^{-1}	**2.37**
80%	4.574×10^{-3}	1.120	**2.29**	1.047×10^{-2}	6.241×10^{-1}	**2.18**	6.436×10^{-3}	4.255×10^{-1}	**2.56**	2.450×10^{-3}	5.759×10^{-1}	**2.85**	3.331×10^{-3}	9.921×10^{-1}	**2.48**
70%	3.131×10^{-3}	1.651	**2.29**	8.065×10^{-3}	8.301×10^{-1}	**2.17**	6.194×10^{-3}	3.787×10^{-1}	**2.63**	1.291×10^{-3}	6.910×10^{-1}	**3.05**	2.328×10^{-3}	1.123	**2.58**
60%	2.321×10^{-3}	2.249	**2.28**	5.484×10^{-3}	1.247	**2.16**	7.266×10^{-3}	3.077×10^{-1}	**2.65**	6.602×10^{-4}	8.602×10^{-1}	**3.25**	1.009×10^{-3}	1.169	**2.93**
50%	1.908×10^{-3}	2.768	**2.28**	3.003×10^{-3}	2.326	**2.16**	1.157×10^{-2}	2.063×10^{-1}	**2.62**	3.727×10^{-4}	1.152	**3.37**	6.708×10^{-4}	1.162	**3.11**
40%	1.874×10^{-3}	2.862	**2.27**	1.076×10^{-3}	6.628	**2.15**	2.611×10^{-2}	1.083×10^{-1}	**2.55**	1.842×10^{-4}	1.776	**3.49**	5.270×10^{-4}	1.310	**3.16**
	highly acidic; water-free input composition: 99.9% ammonium sulfate mass; moderate NH_3*(g) and* HNO_3*(g)*														
99%	7.955×10^{-3}	6.386×10^{-1}	**2.29**	9.703×10^{-3}	5.797×10^{-1}	**2.25**	1.074×10^{-2}	5.88×10^{-1}	**2.20**	4.357×10^{-3}	6.247×10^{-1}	**2.57**	7.270×10^{-3}	6.152×10^{-1}	**2.35**
90%	3.28×10^{-2}	2.69×10^{-1}	**2.06**	4.292×10^{-2}	2.053×10^{-1}	**2.05**	5.929×10^{-2}	2.251×10^{-1}	**1.87**	5.112×10^{-3}	3.936×10^{-1}	**2.70**	1.413×10^{-2}	6.271×10^{-1}	**2.05**
80%	9.54×10^{-2}	1.53×10^{-1}	**1.84**	8.792×10^{-2}	1.281×10^{-1}	**1.95**	1.383×10^{-1}	1.736×10^{-1}	**1.62**	1.211×10^{-2}	3.139×10^{-1}	**2.42**	1.629×10^{-2}	7.085×10^{-1}	**1.94**
70%	1.68×10^{-1}	1.27×10^{-1}	**1.67**	1.183×10^{-1}	1.194×10^{-1}	**1.85**	2.103×10^{-1}	1.629×10^{-1}	**1.47**	2.236×10^{-2}	2.746×10^{-1}	**2.21**	1.313×10^{-2}	8.727×10^{-1}	**1.94**
60%	2.36×10^{-1}	1.21×10^{-1}	**1.55**	1.304×10^{-1}	1.332×10^{-1}	**1.76**	2.856×10^{-1}	1.482×10^{-1}	**1.37**	3.619×10^{-2}	2.485×10^{-1}	**2.05**	9.261×10^{-3}	1.109	**1.99**
50%	2.97×10^{-1}	1.22×10^{-1}	**1.44**	1.339×10^{-1}	1.573×10^{-1}	**1.68**	3.722×10^{-1}	1.259×10^{-1}	**1.33**	5.526×10^{-2}	2.282×10^{-1}	**1.90**	5.967×10^{-3}	1.436	**2.07**
40%	3.49×10^{-1}	1.28×10^{-1}	**1.35**	1.449×10^{-1}	1.738×10^{-1}	**1.60**	4.690×10^{-1}	1.021×10^{-1}	**1.32**	8.352×10^{-2}	2.105×10^{-1}	**1.75**	3.722×10^{-3}	1.840	**2.16**

See also footnotes to Table S~~3~~1.

Table S6. Observationally-constrained estimates of aerosol acidity. In most cases pH_F is reported although there are some exceptions (e.g. E-AIM predictions are usually pH). This data is available in excel format at doi:10.23719/1504059.

Location	Altitude (m)	Latitude (°N)	Latitude (°E)	Time	Aerosol Size	n	Mean (pH)	σ (pH)	Min (pH)	Max (pH)	Method	Reference
Eastern United States and vicinity												
Chicago, IL, USA urban		41.93	-87.72	Jan & Jul 2011-2015	PM2.5	46	2.5		1.4	3.65	ISORROPIA (forward, aerosol and NH_3, no HNO_3 input, no organics, internally mixed aerosol), average of min/max	Battaglia et al., 2017
Chicago, IL, USA rural		41.93	-87.72	Jul 2011-2015	PM2.5		2.1		1.6	2.6	ISORROPIA (forward, aerosol and NH_3, no HNO_3 input, no organics, internally mixed aerosol), average of min/max	Battaglia et al., 2017
Chicago, IL, USA rural		41.93	-87.72	Jan 2011-2015	PM2.5		3.5		3.4	3.65	ISORROPIA (forward, aerosol and NH_3, no HNO_3 input, no organics, internally mixed aerosol), average of min/max	Battaglia et al., 2017
Pellston, MI, USA		45.55	-84.78	Jul-16	<0.4 µm		1.5				pH paper	Craig et al., 2018
Pellston, MI, USA		45.556	-84.7886	Jul 2016	0.4-2.5 µm		3.5				pH indicator paper/ colorimetric image	Craig et al., 2018
Ann Arbor, MI, USA		42.28	-83.743	Aug 2016	0.4-2.5 µm		3.5				pH indicator paper/ colorimetric image	Craig et al., 2018
Pittsburgh, PA, USA		40.44	-79.98	7-22 Sep 2002	PM1	3599	2.5		-0.5	5.5	Aerosol Inorganics Model (AIM II), average of min/max	Zhang et al., 200
North East US (Ohio River Valley and the Adirondack region)	aircraft and ground	40	-83	1979-1980			0.1	0.6				Ferek et al.,198
Baltimore, MD, USA rural		39.06	-76.88	Jan 2011-2015Jan & Jul 2011-2015	PM2.5	8639	2.5		0.72.3	2.7	ISORROPIA (forward, aerosol and NH_3, no HNO_3 input, no organics, internally mixed aerosol), average of min/max	Battaglia et al., 2017
Baltimore, MD, USA rural		39.06	-76.88	Jan 2011-2015	PM2.5	4786	1.6		2.31.1	2.71	ISORROPIA (forward, aerosol and NH_3, no HNO_3 input, no organics, internally mixed aerosol), average of min/max	Battaglia et al., 2017
Baltimore, MD, USA urban		39.06	-76.88	Jan-Jul 2011-2015	PM2.5	86	1.8		0.71	2.12.55	ISORROPIA (forward, aerosol and NH_3, no HNO_3 input, no organics, internally mixed aerosol), average of min/max	Battaglia et al., 2017

Formatted: Font: (Default) Times New Roman, 8 pt
Formatted: Font: (Default) Times New Roman, 8 pt
Formatted Table
Formatted: Font: (Default) Times New Roman, 8 pt
Formatted: Font: (Default) Times New Roman, 8 pt
Formatted: Font: (Default) Times New Roman, 8 pt
Formatted: Font: (Default) Times New Roman, 8 pt
Formatted: Font: (Default) Times New Roman, 8 pt
Formatted: Font: (Default) Times New Roman, 8 pt
Formatted: Font: (Default) Times New Roman, 8 pt

Location	Altitude (m)	Latitude (°N)	Latitude (°E)	Time	Aerosol Size	n	Mean (pH)	σ (pH)	Min (pH)	Max (pH)	Method	Reference
Hampton, VA, C130 flights	up to 5000m	37.03	-76.35	Feb 2015 - Mar 2015	PM1		0.8	1	-0.5	1.9	ISORROPIA metastable, with HNO_3, no observed NH_3 used, iterated to reach convergence in NH_3	Guo et al., 2016
Yorkville, ~~Georgia~~GA, USA		33.93	-85.05	Jun 2012	PM1		1.1	0.6			ISORROPIA (forward, no NH_3, pH bias correction)	Guo et al., 2015
Yorkville, ~~Georgia~~GA, USA		33.93	-85.05	Dec 2012	PM1		1.8	1			ISORROPIA (forward, no NH_3, pH bias correction)	Guo et al., 2015
Yorkville, GA, USA		33.93	-85.05	Sep 2016 - Oct 2016	PM1		2.2	0.6	0.9	3.8	ISORROPIA (forward, metastable, NH_3, HNO_3 input, internally mixed)	Nah et al., 2018
Atlanta, GA, USA		33.80	-84.40	Mar- Apr 2015	PM1		1.5		1	2	ISORROPIA (forward, iterative, no NH_3, HNO_3, HCl data, fine PM internally mixed), average of min/max	Fang et al., 2017
Atlanta, GA, USA		33.80	-84.40	Mar - Apr 2015	coarse		3.5				ISORROPIA (forward external mixed)	Fang et al., 2017
Atlanta, ~~Georgia~~GA, USA (GIT)	30-40 m	33.78	-84.40	Jul 2012	PM1		1.1	0.4			ISORROPIA (forward, no NH_3, pH bias correction)	Guo et al., 2015
JST, Atlanta, ~~Georgia~~GA, USA		33.78	-84.42	Aug 2011	PM1		0.55				ISORROPIA (forward, no NH_3, pH bias correction)	Guo et al., 2015 (from Vasilakos et al., 2018)
JST, Atlanta, GA, USA~~Georgia~~		33.78	-84.42	May 2012	PM1		1.3	0.7			ISORROPIA (forward, no NH_3, pH bias correction)	Guo et al., 2015
JST, Atlanta, ~~Georgia~~GA, USA		33.78	-84.42	Nov 2012	PM1		2.2	0.9			ISORROPIA (forward, no NH_3, pH bias correction)	Guo et al., 2015
Atlanta, ~~Georgia~~GA, USA (RS)		33.78	-84.39	Sep 2012	PM1		1.3	0.7			ISORROPIA (forward, no NH_3, pH bias correction)	Guo et al., 2015
Centreville, AL, USA	126 m	32.90	-87.25	Jun 1998-Aug 2013	PM2.5		1.19		0	2	ISORROPIA (forward, no NH_3, 1 unit lower in the original study due to lack of NH_3 measurements)	Weber et al., 2016 corrected by 1 unit due to NH_3
Centreville, AL, USA	126 m	32.90	-87.25	1 Jun - 15 Jul 2013	PM1		0.94	0.59	-0.9	2.2	ISORROPIA (forward no NH_3, no correction)	Guo et al., 2015
Centreville, AL, USA		32.90	-87.25	Jun-Jul 2013	PM2.5		1.3	2.1			AIOMFAC (inorganic only, aerosol-only inputs, including activity coefficient)	Pye et al., 2018
Centreville, AL, USA		32.90	-87.25	Jun -Jul 2013	PM2.5		1.5	1.1			AIOMFAC (equilibrium organic-inorganic, aerosol-only inputs, including	Pye et al., 2018

Location	Altitude (m)	Latitude (°N)	Latitude (°E)	Time	Aerosol Size	n	Mean (pH)	σ (pH)	Min (pH)	Max (pH)	Method	Reference
											activity coefficient)	
Centreville, AL, USA		32.90	-87.25	Jun- Jul 2013	PM2.5		1.1	0.7			ISORROPIA (aerosol+gas inputs)	Pye et al., 2018
Barbados, West Indies~~, USA~~		13.10	-58.38	Jul - Aug 1989	0.4-0.8 µm		-0.2		-0.7	0.4	aerosol solution pH calculated from aerosol composition, neutralization by NH_3 and $CaCO_3$, average of min/max	Zhu et al., 1992
Barbados, West Indies~~, USA~~		13.10	-58.38	Jul - Aug 1989	0.8-1.7 µm		5.7		-0.2	11.6	aerosol solution pH calculated from aerosol composition, neutralization by NH_3 and $CaCO_3$, average of min/max	Zhu et al., 1992
Southeast US (SENEX) aircraft				summer 2013	PM1		1.4	0.4			ISORROPIA	Xu et al., 2015
Southeast US (SOAS & SCAPE)				1 Jun - 15 Jul 2013 & May 2012- Feb 2013	PM1		1		0	2	ISORROPIA, average of min/max	Xu et al., 2015
North America excluding Eastern US												
Egbert, ON, Canada		44.23	-79.78	20 Jul - 30 Sep 2012	PM2.5		2.1	approx ± 1	2.5	5	E-AIM Model II (sulfate-nitrate-ammonium; AIM-IC measurements; pH=mole fraction activity coeff*mole fraction H*55.508)	Murphy et al., 2017
Harrow, ON, Canada		42.03	-82.89	15 Jun- 15 Jul 2007	PM2.5		1.6	approx ± 1		>2	E-AIM Model II (sulfate-nitrate-ammonium; AIM-IC measurements; pH=mole fraction activity coeff*mole fraction H*55.508)	Murphy et al., 2017
Colorado, BAO-NOAA, USA	1584m	40.05	-105.01	18 Feb - 12 Mar 2011	various sizes < 1 µm		~~about~~ 2.5	about 1.5	about 1	about 4	E-AIM(Inferred From Measured Phase Partitioning based on HCl, NH_3 and HNO_3, for various sizes	Young et al., 2013
Pasadena, Los Angeles, CA CALNEX, SW USA		34.14	-118.12	15 May - 15 Jun 2010	PM 1		1.9	0.5	1.4	2.5	ISORROPIA forward, with NH_3 and HNO_3	Guo et al., 2017a
Pasadena, Los Angeles, CA CALNEX, SW USA		34.14	-118.12	1-15 Jun 2010	PM 2.5		2.7	0.3	2.2	3	ISORROPIA forward, internally mixed with seasalt	Guo et al., 2017a
Mexico City, Mexico, T1 site		19.71	-98.98	Mar-Apr 2006	PM 1		3.31	1	1.9	7	ISORROPIA forward NH_3 >0, HNO_3 >0	Hennigan et al., 2015
Mexico City, Mexico, T1 site		19.71	-98.98	Mar-Apr 2006	PM 1		3.24	1	2	5	E-AIM forward NH_3 >0, HNO_3 >0	Hennigan et al., 2015

Location	Altitude (m)	Latitude (°N)	Latitude (°E)	Time	Aerosol Size	n	Mean (pH)	σ (pH)	Min (pH)	Max (pH)	Method	Reference
Toronto, Canada		43.658	-79.397	2007-2013	PM 2.5	766	2.6		1.48	4.39	E-AIM I (gas + particles NH_3, HNO_3)	Tao et al.and Murphy, 2019
Toronto Canada		43.659	-79.395	2014-2016	PM 2.5	301	2.65		1.35	4.02	E-AIM I (gas + particles NH_3, HNO_3)	Tao et al.and Murphy, 2019
Ottawa Canada		45.434	-75.676	2007-2016	PM 2.5	851	2.54		1.18	4.67	E-AIM I (gas + particles NH_3, HNO_3)	Tao et alandMurphy., 2019
Simcoe Canada		42.857	-80.27	2007-2016	PM 2.5	713	2.41		0.84	4.38	E-AIM I (gas + particles NH_3, HNO_3)	Tao et al.and Murphy, 2019
Montreal Canada		45.652	73.574	2007-2016	PM 2.5	840	2.35		0.51	4.72	E-AIM I (gas + particles NH_3, HNO_3)	Tao et al.and Murphy, 2019
Windsor Canada		42.293	-83.073	2007-2010	PM 2.5	256	2.12		0.94	3.2	E-AIM I (gas + particles NH_3, HNO_3)	Tao et al.and Murphy, 2019
Windsor Canada		42.293	-83.073	2012-2016	PM 2.5	456	2.35		0.4	3.98	E-AIM I (gas + particles NH_3, HNO_3)	Tao et al.,and Murphy, 2019
St Anicet Canada		45.121	-74.288	2007-2016	PM 2.5	742	2.51		0.9	4.65	E-AIM II (gas + particles NH_3, HNO_3)	Tao et al.,and Murphy, 2019
North Pacific												
Oahu, Hawaii, USA		21.366 67367	- 157.716 7717	4-29 Sep 2000			4.6		2.6	5.3	MOCCA model & measurements	Pszenny et al., 2004
Near Kilauea, Hawaii, USA		19.318	-155.376	Jan - Feb 2013	PM1		1.1		-0.8	3.0	E-AIM II with ACSM measured composition, average of min/max	Kroll et al., 2015
Mainland China												
Beijing, China (PKU)		39.99	116.30	Nov 2015 - Dec 2016	PM2.5		4.2		3	4.9	ISORROPIA forward with NH_3, HNO_3, HCl tested with AIM, good agreement with a difference of 0.3 units	Liu et al., 2017
Guangzhou, China	15 m	23.13	113.26	1 Jul - 31 Jul 2013	PM2.5		2.5	0.3	1.4	3.1	E-AIM IV forward with NH_3, HNO_3, HCl	Jia et al., 2018
Guangzhou, China	15 m	23.13	113.26	1 Jul- 31 Jul 2013	PM2.5		2.8	0.4	1.55	3.5	ISORROPIA forward mode, no NVC, with NH_3, HNO_3, HCl	Jia et al., 2018
Guangzhou, China	15 m	23.13	113.26	1 Jul- 31 Jul 2013	PM2.5		2.6	0.3	1.5	3.1	AIOMFAC	Jia et al., 2018
Beijing	49 m	39.97	116.37	17 Nov- 12 Dec 2014	PM2.5		4.6	0.5	4	5.1	ISORROPIA forward, Ca^{2+} and Mg^{2+} were not measured, pH values would be increased by 0.1 unit	Song et al., 2018
Beijing	49 m	39.97	116.37	17 Nov- 12 Dec 2014	PM2.5		4	0.4	3.6	4.4	E-AIM forward, Ca^{2+} and Mg^{2+} were not measured, pH values would	Song et al., 2018

Location	Altitude (m)	Lati-tude (°N)	Lati-tude (°E)	Time	Aerosol Size	n	Mean (pH)	σ (pH)	Min (pH)	Max (pH)	Method	Reference
											be increased by 0.1 unit	
Beijing	8m	39.97	116.37	24 Jan - 1 Feb 2013	PM2.1		1.1	0.05	1.1	1.2	AIM-IV, no gases	Tian et al., 2018
Chengdu	20 m	30.66	104.02	5 Jan - 24 Jan 2011 **night**	PM2.1		-1.2	1.1	-2.3	0.3	E-AIM Model II, no gases	Cheng et al., 2015
Chengdu	20 m	30.66	104.02	5 Jan - 24 Jan 2011 **day**	PM2.1		0.7	1	-0.2	2.1	E-AIM Model II, no gases	Cheng et al., 2015
Beijing	20 m	40.41	116.68	Oct 2014- Jan 2015	PM2.5		4.70	1.1	3.4	7.6	ISORROPIA (metastable)	He et al., 2018
Beijing	20 m	39.99	116.31	1 Jan- 31 Dec 2014	PM2.5		3.02	1.62	3	4.9	ISORROPIA (forward mode, metastable)	Tan et al., 2018
Beijing	20 m	39.99	116.31	winter 2014	PM2.5		4.11	1.37			ISORROPIA (forward mode, metastable)	Tan et al., 2018
Beijing	20 m	39.99	116.31	fall 2014	PM2.5		3.13	1.2			ISORROPIA (forward mode, metastable)	Tan et al., 2018
Beijing	20 m	39.99	116.31	spring 2014	PM2.5		2.12	0.72			ISORROPIA (forward mode, metastable)	Tan et al., 2018
Beijing	20 m	39.99	116.31	summer 2014	PM2.5		1.82	0.53			ISORROPIA (forward mode, metastable)	Tan et al., 2018
Tianjin	22 m	39.11	117.16	25 Dec 2014- 2 Jun 2015	PM2.5		4.9	1.4	0.33	13.6	ISORROPIA (forward, metastable)	Shi et al., 2017
Tianjin		39.11	117.16	12-23 August 2015	PM2.5	387	3.4	0.5	2.6	4.6	ISORROPIA (forward, metastable)	Shi et al., 2019
Beijing~~, China~~		39.99	116.30		PM 1		4.5				ISORROPIA forward, metastable with NH_3 & HNO_3	Guo et al., 2017b
X'ian~~, China~~		34.23	108.89		PM2.5		5		4.6	5.4	ISORROPIA forward, metastable with NH_3 & HNO_3	Guo et al., 2017b
Beijing		39.983 33	116.28	winter (Feb 2017)	PM2.5		4.5	0.7			ISORROPIA forward	Ding et al., 2019
Beijing		39.983 33	116.28	spring (Apr - May 2016)	PM2.5		4.4	1.2			ISORROPIA forward	Ding et al., 2019
Beijing		39.983 33	116.28	summer (Jul - Aug 2017)	PM2.5		3.8	1.2			ISORROPIA forward	Ding e tal., 2019
Beijing		39.983 33	116.28	fall (Sep - Oct2017).	PM2.5		4.3	0.8			ISORROPIA forward	Ding et al., 2019
Guangzhou~~, China~~		23.13	113.26	Jul -Sep 2013	PM2.5		2.4	0.3	1.5	3.4	E-AIM-III, open system, with NH_3, HNO_3, HCl	Jia et al., 2018
Hohhot, Inner Mongolia~~, China~~		40.48	111.41	summer 2014	PM2.5		5				ISORROPIA (forward metastable, no NH_3)	Wang et al., 2019
Hohhot, Inner Mongolia~~, China~~		40.48	111.41	autumn 2014	PM2.5		5.3				ISORROPIA (forward metastable, no NH3)	Wang et al., 2019

Formatted: Font: 8 pt

Location	Altitude (m)	Latitude (°N)	Latitude (°E)	Time	Aerosol Size	n	Mean (pH)	σ (pH)	Min (pH)	Max (pH)	Method	Reference
Hohhot, Inner Mongolia, China		40.48	111.41	winter 2015	PM2.5		5.7				ISORROPIA (forward metastable, no NH_3)	Wang et al., 2019
Hohhot, Inner Mongolia, China		40.48	111.41	spring 2015	PM2.5		6.1				ISORROPIA (forward metastable, no NH_3)	Wang et al., 2019
Hohhot, Inner Mongolia, China		40.48	111.41	annual 2014-2015	PM2.5		5.6		1.1	8.4	ISORROPIA (forward metastable, no NH_3)	Wang et al., 2019
ASIA (excluding mainland China)												
Singapore	20 m	1.30	103.78	Sep - Nov 2011	PM2.5		0.6	0.4	-0.2	1.5	AIM-IV	Behera et al., 2013
Hong Kong (HKUST)		22.34	114.26	24 Jul 1997 - 29 May 1998	PM2.5		0.3	1.3	about -0.9	1.5	AIM-II (for RH >=70% range only)	Yao et al., 2007
Hong Kong (HKUST)		22.34	114.26	18 Nov 1996 - 5 Nov 1997	PM2.5		-1	1	-2.5	about 0.4	AIM-II (for RH<70% range only)	Yao et al., 2007
Hong Kong (three sites)		22.34	114.26		PM2.5	25	-0.4	1.5	-2.2	1.1	AIM-II (range only)	Yao et al., 2006 (data from Pathak et al., 2004)
Hong Kong (three sites)		22.34	114.26		PM2.5	25	3.9		-1.2	7.5	ISORROPIA (gases + aerosols)	Yao et al., 2006
Hong Kong (three sites)		22.34	114.26		PM2.5	25	2.3		-1.3	7.3	SCAPE2	Yao et al., 2006
Middle East												
Israel (Tel Aviv)		32.11	34.86	summer 1988-1989			2	2	1.5	2.5	Haze	Ganor et al., 1993
Europe												
Po Valley Italy		45.40	12.20	Mar 2009 - Jan 2010	PM2.5	267	3.1	0.6			E-AIM thermodynamic model 4 (average for three sites, four seasons)	Squizzato et al., 2013
Po Valley Italy		45.40	12.20	spring 2009	PM2.5	73	3.6	0.7			E-AIM thermodynamic model 4 (average for three sites)	Squizzato et al., 2013
Po Valley Italy		45.40	12.20	summer 2009	PM2.5	69	2.3	0.7			E-AIM thermodynamic model 4 (average for three sites)	Squizzato et al., 2013
Po Valley Italy		45.40	12.20	fall 2009	PM2.5	62	3	0.9			E-AIM thermodynamic model 4 (average for three sites)	Squizzato et al., 2013
Po Valley Italy		45.40	12.20	winter 2009-2010	PM2.5	63	3.4	0.5			E-AIM thermodynamic model 4 (average for three sites)	Squizzato et al., 2013
Po Valley Italy	mean of 6 sites	45.4	12.2	winter 2012-2013	PM2.5		3.9	0.3			ISORROPIA (forward, metastable, no NH3)	Masiol et al., 2020
Po Valley Italy	mean of 6 sites	45.4	12.2	summer 2012	PM2.5		2.3	0.3			ISORROPIA (forward, metastable, no NH3)	Masiol et al., 2020

Formatted Table
Formatted: Font: (Default) Times New Roman
Formatted: Font: (Default) Times New Roman
Formatted: Font: (Default) Times New Roman
Formatted: Font: (Default) Times New Roman
Formatted: Font: (Default) Times New Roman
Formatted: Font: (Default) Times New Roman, Font color: Auto
Formatted: Font: (Default) Times New Roman, Font color: Auto
Formatted: Font: (Default) Times New Roman
Formatted: Font: (Default) Times New Roman, Font color: Auto
Formatted: Font: (Default) Times New Roman
Formatted: Font: (Default) Times New Roman, Font color: Auto
Formatted: Font: (Default) Times New Roman, Font color: Auto
Formatted: Font: (Default) Times New Roman, Font color: Auto
Formatted: Font: (Default) Times New Roman
Formatted: Font: (Default) Times New Roman
Formatted: Font: (Default) Times New Roman
Formatted: Font: (Default) Times New Roman, Font color: Auto
Formatted: Font: (Default) Times New Roman, Font color: Auto
Formatted: Font: (Default) Times New Roman, Font color: Auto
Formatted: Font: (Default) Times New Roman, Font color: Auto
Formatted: Font: (Default) Times New Roman
Formatted: Font: (Default) Times New Roman, Font color: Auto
Formatted: Font: (Default) Times New Roman, Font color: Auto
Formatted: Font: (Default) Times New Roman
Formatted: Font: (Default) Times New Roman
Formatted: Font: (Default) Times New Roman

Location	Altitude (m)	Latitude (°N)	Latitude (°E)	Time	Aerosol Size	n	Mean (pH)	σ (pH)	Min (pH)	Max (pH)	Method	Reference
Finokalia, Crete	250 m asl	35.33	25.67	Jun - Nov 2012	PM1	37	1.3	1.1	-0.97	3.75	ISORROPIA (forward, no NH_3)	Bougiatioti et al., 2016
Finokalia, Crete-Biomass burning influenced	250 m asl	35.33	25.67	Jun - Nov 2012	PM1	7	2.77	0.88			ISORROPIA (biomass burning influenced air, no NH_3)	Bougiatioti et al., 2016
Cabauw, Netherlands		51.97	4.93	Jul 2012 - Jun 2013	PM 2.5		3.7	0.6			ISORROPIA (Forward mode, gas+aerosol)	Guo et al., 2018
Cabauw, Netherlands		51.97	4.93	Jun - Aug 2013	PM 2.5		3.3	0.5			ISORROPIA (Forward mode, gas+aerosol)	Guo et al., 2018
Cabauw, Netherlands		51.97	4.93	Dec - Feb 2012	PM 2.5		3.9	0.4			ISORROPIA (Forward mode, gas+aerosol)	Guo et al., 2018
South Hemisphere												
Sao Paulo, Brazil		-23.55	-46.63	8 Aug - 5 Sep 2012	size resolved PM		4.8		4.1	5.4	E-AIM, average of min/max	Vieira-Filho et al., 2016
Pacific Ocean/South of Australia-ACE1		-47.5	147.5	18 Nov- 11 Dec 1995	fine	19	1		0	2	EQUISOLV	Fridlind and Jacobson, 2000
South Ocean Weddel, PEGASO, sea-ice influence zone		-61	-45	9 Jan-24 Jan 2015	PM2.5	3	1.36667	0.75056	0.5	1.8	ISORROPIA (forward mode, no NH_3)	Dall'Osto et al., 2019
South Ocean, Weddel, PEGASO		-64	-65	24 Jan-9 Feb 2015	PM2.5	3	3.76667	0.41633	3.3	4.1	ISORROPIA (forward mode, no NH_3)	Dall'Osto et al., 2019

Table S7. Published aerosol acidity values not used in this study.

Location	Altitude (m)	Latitude (°N)	Latitude (°E)	Time	Aerosol Size	n	Mean (pH)	σ (pH)	Min (pH)	Max (pH)	Method	Reference
Beijing		40.41	116.68	Oct 2014- Jan 2015	PM2.5		7.6	0.1			ISORROPIA (stable state)	He et al., 2018
Xi'an		34.23	108.89	17 Nov - 12 Dec 2012	PM2.5		6.7	1.3	4.14	11	ISORROPIA (forward, gas aerosols)	Wang et al., 2016
Beijing		39.99	116.30	21 Jan - 4 Feb 2015	PM2.5		7.63	0.03	7.6	7.7	ISORROPIA (forward, gas aerosols)	Wang et al., 2016
Hong Kong (TST site)		22.26	114.07	5 Dec - 16 Dec 2000	PM2.5	10					AIM2 (only free H+ is available)	Pathak et al., 2004
Hong Kong (HKUST site)		22.33	114.26	12 Mar - 17 Mar 2002	PM2.5	6					AIM2 (only free H+ is available)	Pathak et al., 2004
Jinan	20 m	36.65	117.01	Apr, Aug, Oct, Dec 2006 & Jan 2007	PM1.8		-1.2		-3	1.5	AIM-II, no gases, no organic acids	Cheng et al., 2011
Jinan	20 m	36.65	117.01	Apr, Aug, Oct, Dec 2006 & Jan 2007	PM1.8		-1.1		-2.5	1	AIM-II, no gases, with organic acids	Cheng et al., 2011
Beijing	285 m asl	40.35	116.30	29 Jun- 2 Aug 2005	PM2.5	25	-0.52	0.62			E-AIM Model II only aerosol input	Pathak et al., 2009

Shanghai	15 m	31.45	121.10	5 May - 15 Jun 2005	PM2.5	40	-0.77	0.67			E-AIM Model II only aerosol input	Pathak et al., 2009
Lanzhou		36.13	103.68	18 Jun - 17 Jul 2006	PM2.5	25	-0.38	0.64			E-AIM Model II only aerosol input	Pathak et al., 2009
Guangzhou	17 m	22.69	113.56	15 May - 27 May 2004	PM2.5	13	0.61	0.71			E-AIM Model II only aerosol input	Pathak et al., 2009
Beijing		40.32	116.32	28 Jan 2005-28 Apr 2006	PM2.5		0.65	1.08	about -0.6	about 3	E-AIM Model II (two sites averaged), only aerosol input	He et al., 2012
Chongqing		29.57	106.53	28 Jan 2005-28 Apr 2006	PM2.5		1.45	0.77	about 0.5	about 4	E-AIM Model II (three sites averaged), only aerosol input	He et al., 2012
Beijing	10 m	40.00	116.33	1 Jan - 31 Jan 2013	PM2.5		5.8	0.4	5.4	6.2	ISORROPIA mean of forward and reverse, NH_3 estimated from NO_x	Cheng et al., 2016 in Song et al., 2018
Hong Kong	20 m	22.34	114.26	21 Oct - 25 Oct 2008	PM2.5	127	0.59	0.43	-0.8	2.4	AIM-III (aerosol only input)	Xue et al., 2011
Hong Kong	20 m	22.34	114.26	6 Nov - 13 Nov 2008	PM2.5	180	-0.45	0.59	-2	0.4	AIM-III (aerosol only input)	Xue et al., 2011
Hong Kong	20 m	22.34	114.26	29 Jun - 3 Jul 2009	PM2.5	213	-0.08	0.81	-1.6	3.2	AIM-III (aerosol only input)	Xue et al., 2011

323
324

Table S8. Observed cloud acidity (pH) – sorted by region. This data is available in excel format at doi:10.23719/1504059.

(a) Africa

Location	Altitude (m)	Latitude (°N)	Longitude (°E)	Period (mo/yr)	N	Mean (pH)	Median (pH)	Min (pH)	Max (pH)	Reference
Congo										
Mayombé Massif, Dimonika	290	-4	12.5	Nov-Sept 1986-1987	14	4.9				Lacaux et al., 1992
Egypt										
Delta Barrage, Egypt	18	30.2	31.12	2015-2016		7.6				Salem et al., 2017
Namibia										
Namib Desert, Namibia	420	-22.74	15.89	Apr-Oct 1994-1995	7	6.2	6.4	5.6	6.6	Eckardt and Schemenauer, 1998
South Africa										
Cape Columbine, South Africa		-32.83	17.85	Aug 1997	1	6.5				Olivier, 2002
Cape Columbine, South Africa		-32.83	17.85	May 1998	1	7.3				Olivier, 2002
Lepelfontein, South Africa	200	-31.05	17.85	Sept 2000	1	7.2				Olivier and De Rautenbach, 2002
Soutpansberg, South Africa	1004	-22.93	30.36	Aug 2001	1	5.9				Olivier and De Rautenbach, 2002
Morocco										
Boutmezguida, Anti-Atlas Mts., Morocco	1225	29.2	-10.02	Nov-June 2013-2015		7.3		7	8.5	Dodson and Bargach, 2015; Schunk et al., 2018

(b) Antarctica

Location	Altitude (m)	Latitude (°N)	Longitude (°E)	Period (mo/yr)	N	Mean (pH)	Median (pH)	Min (pH)	Max (pH)	Reference
Antarctic	600-1490	-77.82	166.69	Dec 1982	7	5.3		4.9	6.2	Saxena et al., 1985

(c) Asia

Location	Altitude (m)	Latitude (°N)	Longitude (°E)	Period (mo/yr)	N	Mean (pH)	Median (pH)	Min (pH)	Max (pH)	Reference
Bangladesh										
Bangladesh, coastal Bhola		22.17	90.75	2015-2016	15	7.1		6.9	7.3	Ahmed et al., 2018
Mainland China and Hong Kong										
Anning Industrial Zone, China		24.92	102.46	Dec 1988	19	6.12		5.4	7.5	Huang et al., 1992
Beijing, China		39.93	166.28	1998-1999	3	5.3				Jiang et al., 2010
Beijing, China		39.93	166.28	2005-2006	2	6.2				Jiang et al., 2010
Changsha, China		28.22	112.96	1993	13	4.9		3.4	5.6	Shen et al., 1996
Chengdu, China				Sept 1989	48	3.8	4.1	2.9	6.8	Lei et al., 1997
Chengdu, China		32.2	118.71	1989	58	4.6		3.2	6.8	Shen et al., 1996
Chongqing, China		29.43	106.89	Sept-Oct 1985	18	5.85				Lei et al., 1997
Chongqing, China		29.43	106.89	1985	16	6.2		4.9	7.8	Shen et al., 1996
Chongqing, China		29.43	106.89	Oct 1989	39	3.9	4.6	3	6	Lei et al., 1997
Chongqing, China		29.43	106.89	1989	46	4.6		3.2	6.0	Shen et al., 1996

Location	Altitude (m)	Latitude (°N)	Longitude (°E)	Period (mo/yr)	N	Mean (pH)	Median (pH)	Min (pH)	Max (pH)	Reference
Chongqing, China		29.43	106.89	1984-1990	182	4.4		3.0	8	Li et al., 1996; Li and Peng, 1994
Guangzhou, China		23.15	113.29	Mar 1988	29	3.8	3.9	3.4	4.2	Lei et al., 1997
Guangzhou, China		23.15	113.29	1988	47	3.9		3.4	6.3	Shen et al., 1996
Guangzhou, China		23.15	113.29	Oct 1989	41	4.1	4.6	3.4	6	Lei et al., 1997
Guangzhou, China	82	23.13	113.30	Feb-Mar 2005	3	5.7				Wu et al., 2009
Guilin, China		25.24	110.18	Mar-Apr 1988	13	4.1	4.2	3.6	5.7	Lei et al., 1997
Guilin, China		25.24	110.18	1988	20	3.9		3.3	5.3	Shen et al., 1996
Guiyang, China		26.65	106.63	1989	48	4.6		3.4	6.0	Shen et al., 1996
Jinan, China		36.67	117.05	Jan 2013		2.9		2.62	4.2	Wang et al., 2014
Jingdong County, China	2476	24.54	101.03	2015-2016	117		4.1	3.5	6.9	Nieberding et al., 2018
Jinghong, China	582	22.01	100.80	Dec 1997	3	6.3		5.8	6.8	Zhu et al., 2000
Lushan, China	~1250	29.58	116.02	May 1987	60	5.1		4.9	5.4	Ding et al., 1991
Mengyangzhen, China	771	22.09	100.90	Dec 1997	8	8.3		7.9	9.2	Zhu et al., 2000
Mount Heng, Hunan, China	1269	27.3	112.70	Mar-May 2009	194	3.8		2.9	6.9	Sun et al., 2010
Mt. Lu, Jiujiang city, China	1165	29.58	116.00	Aug-Sept 2011	11	3.5		3.2	3.9	Li et al., 2013
Mt. Tai, China	1534	36.3	117.22	Mar-Apr 2007		4.6	3.7	2.6	7.6	Wang et al., 2011
Mt. Tai, China	1545	36.3	117.22	2007-2008	482	4.6	4.3	2.6	7.6	Guo et al., 2012; Liu et al., 2012; Shen et al., 2012
Mt. Tai, China	1545	36.3	117.22	July-Oct 2014	39	5.9		3.8	6.9	Li et al., 2017
Mt. Tai, China	1534	36.3	117.22	June-Aug 2015	17	4.9		3.8	6.3	Zhu et al., 2018
Mt. Tai Mao Shan, China	957	22.4	114.27	Oct-Nov 2016		3.6		3.0	5.9	Li et al. 2019
Nangchang, China		28.68	115.84	1993	51	4.7		3.4	6.5	Shen et al., 1996
Nanjing, China		32.20	118.73	Dec 2001	13	5.6		4.3	7.3	Li et al., 2008
Nanjing, China	22	32.2	118.71	Dec 2006	11	5.7		4.1	7.6	Tang et al., 2008
Nanjing, China	22	32.2	118.71	2006-2007	37	5.9		4.1	7.3	Yang et al., 2012
Nanling Dayaoshan Mountain, China	815	25.083	113.1	Jan 1999	21	6.1				Wu et al., 2004
Nanling Dayaoshan Mountain, China	815	25.083	113.1	Feb-Mar 2001	36	5.2				Wu et al., 2004
Shanghai, China		31.26	121.45	June-Jul 1986	22	5.5	6.2	4.5	7.4	Lei et al., 1997
Shanghai, China		31.26	121.50	1992-1993	80	6.0		4.5	7.8	Minghua and Demin, 1999
Shanghai, China		31.20	121.50	1989-1991	28	5.2		4.3	6.5	Bao et al., 1995
Shanghai, China		31.3	121.48	2009-2010	26	6.0		4.7	6.6	Li et al., 2011
Urumqi, China		43.41	87.27	Mar-May 2003	19	6.35				Xu et al., 2011
Xiamen, China		24.49	118.10	Mar-Apr 1993	5	3.6		2.9	4.5	Liu et al., 1996
Zhanjiang, Donghai Island, China		21.28	110.2	Mar-Apr 2010	19	5.2		4.8	6.1	Xu et al., 2011
Zhoushan, China		30.00	122.21	May 1987	31	6.0		3.8	7.3	Mo et al., 1989

Location	Altitude (m)	Latitude (°N)	Longitude (°E)	Period (mo/yr)	N	Mean (pH)	Median (pH)	Min (pH)	Max (pH)	Reference
India										
Agra, India	169	27.17	78.08	1998-2000	37	7.2		7	7.6	Lakhani et al., 2007
Akaltara, India	283	22.02	82.43	Feb 2011	1	7.5				Ambade, 2014
Bilaspur, India	346	22.09	82.15	Feb 2011	1	7.2				Ambade, 2014
Delhi, India	217	28.62	77.2	Winter 2001-2003	43	6.7		6.6	6.7	Ali et al., 2004
Dongargarh, India	335	21.02	80.08	Feb 2011	1	7.5				Ambade, 2014
Kanpur, India	142	26.5	80.3	Jan-Feb 2010		7.2		6.0	8.1	Kaul et al., 2011
Kanpur, India		26.46	80.33	2012-2014	66	5.4		5.1	7.3	Chakraborty et al., 2016
Korba, India	252	22.35	82.68	Jan-Feb 2011	4	5.6		5	6.4	Ambade, 2014
New Delhi, India	218	28.35	77.12	Winter 2014-2015	24	5.5		5.1	7.0	Nath and Yadav, 2018
Pune region, India	559	18.52	73.86	1983-1985	47	6.6		6.3	7.6	Khemani et al., 1987
Raipur, India	298	21.23	81.63	2010-2011	14	6.8		6.3	7.4	Ambade, 2014
Rajnandgaon, India	307	21.1	81.03	Feb 2011	1	7.3				Ambade, 2014
Sinhagad, India	1450	18.35	73.75	2007-2010	123	6		4.7	7.4	Budhavant et al., 2014
Japan										
Bijodaira, Mt Tateyama, Japan	977	36.58	137.46	Sept-Oct 2009		4.4		3.9	6	Watanabe et al., 2011
Lake Mashu, Japan	542	43.55	144.5	2006-2012	258	4.6				Yamaguchi et al., 2015
Lake Mashu, Japan	542	43.55	144.5	Jul-Oct 2006		4.5				Yamaguchi et al., 2015
Lake Mashu, Japan	542	43.55	144.5	Jul-Oct 2007		4.6				Yamaguchi et al., 2015
Lake Mashu, Japan	542	43.55	144.5	Jul-Oct 2008		4.3				Yamaguchi et al., 2015
Lake Mashu, Japan	542	43.55	144.5	Jul-Oct 2009		4.5				Yamaguchi et al., 2015
Lake Mashu, Japan	542	43.55	144.5	Jul-Oct 2010		5.1				Yamaguchi et al., 2015
Lake Mashu, Japan	542	43.55	144.5	Jul-Oct 2011		4.8				Yamaguchi et al., 2015
Lake Mashu, Japan	542	43.55	144.5	Jul-Oct 2012		4.6				Yamaguchi et al., 2015
Midagahara, Mt Tateyama, Japan	1930	36.57	137.56	Sept-Oct 2009		4.7		3.8	6.2	Watanabe et al., 2011
Mt. Awaga, Aogakicho, Japan	962	35.33	135.03	May-Nov 1999	14	4.1		4	4.5	Aikawa et al., 2006
Mt. Fuji, Japan	3776	35.4	138.7	Sept 2002	34	4.6		4	6.8	Watanabe et al., 2006
Mt. Mokko, Iwate, Japan	1465	39.93	140.85	Aug-Sept 1997	16	4.1		3.6		Ogawa et al., 1999
Mt. Mokko, Iwate, Japan	1465	39.93	140.83	Sept 1998	62	4.4				Adzuhata et al., 2001b
Mt. Mokko, Iwate, Japan	1465	39.93	140.83	June-Sept 1999	20	4.6				Adzuhata et al., 2001a
Mt. Norikura, Japan	3026	36.34	137.52	July 1963	10	3.8		3.4	4.3	Okita, 1968
Mt. Norikura, Japan	3026	36.34	137.52	Aug 1989	2	3.7		3.6	3.8	Qian et al., 1992
Mt. Norikura, Japan	3026	36.34	137.52	July 1990	12	3.8		3.6	4.2	Qian et al., 1992
Mt. Norikura, Japan	2770	36.34	137.52	Aug 1991	55	3.6		3.3	4.3	Minami and Ishizaka, 1996

Location	Altitude (m)	Latitude (°N)	Longitude (°E)	Period (mo/yr)	N	Mean (pH)	Median (pH)	Min (pH)	Max (pH)	Reference
Mt. Norikura, Japan	2770	36.34	137.52	July & Sept 1994	68	4		3.7	6.7	Watanabe et al., 1999
Mt. Norikura, Japan	2770	36.34	137.52	Aug 1995	7	3.3		3.1	3.5	Watanabe et al., 1999
Mt. Norikura, Japan	2770	36.34	137.52	Oct 1996	32	3.7		3.4	5.1	Watanabe et al., 1999
Mt. Oyama, Japan	700	35.56	139.21	1991-1992	1169	4.0	4.3	2.6	6.8	Hosono et al., 1994
Mt. Oyama, Japan	680	35.56	139.21	1995	175	3.7		2.6	6.1	Igawa et al., 1998
Mt. Oyama, Japan	680	35.56	139.21	Aug-Sept 1998		3.3		3.1	5.6	Watanabe et al., 2001a
Mt. Rokko, Kobe City, Japan	931	34.79	135.26	1997-1998	55	3.8		2	5.8	Aikawa et al., 2001
Mt. Rokko, Kobe City, Japan	931	34.79	135.26	June-Nov 1999	14	3.7		3.3	3.9	Aikawa et al., 2006
Mt. Rokko, Kobe City, Japan	931	34.79	135.26	1997-2001	403	3.8	3.8	3.2	4.9	Aikawa et al., 2005
Mt. Tsukuba, Japan	876	36.39	140.12	Nov 1963	5	5.9		5.6	6.5	Okita, 1968
Murododaria, Mt Tateyama, Japan	2450	36.61	137.63	July-Aug 2004	11	4.5		4	5.4	Watanabe et al., 2010; Watanabe et al., 2011
Murododaria, Mt Tateyama, Japan	2450	36.61	137.63	Autumn 2005	14	3.8		3.5	5.5	Watanabe et al., 2010; Watanabe et al., 2011
Murododaria, Mt Tateyama, Japan	2450	36.61	137.63	Sept-Oct 2006	7	4.8		4.5	6.3	Watanabe et al., 2010; Watanabe et al., 2011
Murododaria, Mt Tateyama, Japan	2450	36.61	137.63	Sept-Oct 2007		4.6		4.3	5.5	Watanabe et al., 2011
Murododaria, Mt Tateyama, Japan	2450	36.61	137.63	Sept-Oct 2008		4.0		3.7	4.7	Watanabe et al., 2011
Murododaria, Mt Tateyama, Japan	2450	36.61	137.63	Sept-Oct 2009		4.2		3.8	5.7	Watanabe et al., 2011
Shiobara, Japan		36.97	139.82	July 1963	2	5.9		5.9	5.9	Okita, 1968
Pakistan										
Kala Bagh, Nathiagali, Pakistan		34.3	73.2	July 1996	18	6.3		5.3	6.8	Ghauri et al., 2001
South Korea										
Chongwon, South Korea	39	36.63	127.49	Sept 1994	32	4.6		4.2	6.4	Chung et al., 1999
Chongwon, South Korea	39	36.63	127.49	Apr-Nov 1995	36	5.3		4.9	5.8	Chung et al., 1999
Chongwon, South Korea	39	36.63	127.49	Jan-Oct 1996	45	5.5		4.4	5.8	Chung et al., 1999
Daekwanreung, South Korea	840	37.68	128.45	2002-2003	203	5.2		3.6	6.8	Kim et al., 2006
Mt. Sobaek, South Korea	1340	36.93	128.43	Aug 1995	27	4.4				Nam et al., 2001
Taiwan										
Chilan Mountain, Taiwan	1650	24.59	121.5	Apr-May 2011	36		4.5	3.7	5.2	Simon et al., 2016
Kinmen Weather Station, Taiwan	48	24.41	118.29	Mar-Apr 2014	15		3.0	2.3	3.4	Simon et al., 2016
Lulin Atmospheric Background Station, Taiwan	2826	23.47	120.87	Apr-May 2011	14		3.9	3.4	4.5	Simon et al., 2016
Mt. Bamboo, Taiwan	1050	25.19	121.54	Jan 2011	291		4.2	3.2	6.4	Klemm et al., 2015
Xitou Flux Tower, Taiwan	1150	23.66	120.8	Sept-Nov 2013	69		4.1	3.2	6.0	Simon et al., 2016

333
334 (d) Australia

Location	Altitude (m)	Latitude (°N)	Longitude (°E)	Period (mo/yr)	N	Mean (pH)	Median (pH)	Min (pH)	Max (pH)	Reference
Barrington Tops	400	-31.92	151.58	Jan-Apr 1989		5.6				Post et al., 1991
Craigieburn	1600	-37.56	144.93	1985-1986	3	6.4				Verhoeven et al., 1987
Dorrigo	900	-30.33	152.67	Jan-Apr 1989		5.4				Post et al., 1991
Sydney	1500-1800	-34.11	151.28	July-Aug 1976	28	5.9		4.6	6.6	Scott, 1978
Tasmania		-40.68	114.68	1981 & 1983	55	5.4		4.1	7.0	Gillett and Ayers, 1989

335
336 (e) Central and South America

Location	Altitude (m)	Latitude (°N)	Longitude (°E)	Period (mo/yr)	N	Mean (pH)	Median (pH)	Min (pH)	Max (pH)	Reference
Brazil										
São Paulo City, Brazil		-23.56	-46.66	2009	8	5.9		5.0	7.7	Vasconcellos et al., 2018
Chile										
El Tofo, Chile	780	-29.43	-71.25	1987	2	5.2		5.0	5.8	Schemenauer and Cereceda, 1992b
El Tofo, Chile	780	-29.43	-71.25	1987	5	3.6		3.5	5.6	Schemenauer and Cereceda, 1992b
El Tofo, Chile	780	-29.43	-71.25	1987	8	4.5		4.0	6.7	Schemenauer and Cereceda, 1992b
Torres del Paine (+Punta Arenas)	50-400	-51.17	-71.97	1987-1994	22	4.8	5.2	4.2	6.3	Weathers and Likens, 1996
Venezuela										
Altos de Pipe, Miranda State	1747	10.33	-66.92	June-Aug 1989	6	4.9				Gordon et al., 1994
Altos de Pipe, Miranda State	1747	10.33	-66.92	Jun, Oct-Dec 1989	13	5.4		4.8		Sanhueza et al., 1992
Altos de Pipe, Miranda State	1747	10.33	-66.92	Mar-May 1990	10	5.0				Gordon et al., 1994
Pico del Avila, Distrito Federal	2150	10.54	-66.88	June-Aug 1989	19	5.0				Gordon et al., 1994
Pico del Avila, Distrito Federal	2150	10.54	-66.88	Mar-May 1990	51	4.6				Gordon et al., 1994
Costa Rica										
Monteverde, Costa Rica	1470	10.3	-84.4	1988-1992	34	3.9		3.3	5.6	Clark et al., 1998
Ecuador										
El Tiro, Ecuador	2825	-4.00	-79.16	2003-2004	59		4.6	3.9	5.6	Beiderwieden et al., 2005
El Tiro, Ecuador*	2870	-4.00	-79.16	2005-2009		4.7				Giannoni et al., 2013
Cerro del Consuelo, Ecuador*	3180	-4.00	-79.16	2004-2009		5.4				Giannoni et al., 2016
ECSF, Ecuador*	1960	-4.00	-79.16	2005-2009		4.9				Giannoni et al., 2013
TS1, Ecuador*	2660	-4.00	-79.16	2005-2009		5.3				Giannoni et al., 2013
Antenas*	3180	-4.00	-79.16	2005-2009		5.5				Giannoni et al., 2013

337 *These sampling locations are close to each other, thus the average pH value was calculated and shown in Figure
338 5.2.
339
340 (f) Europe

Location	Altitude (m)	Latitude (°N)	Longitude (°E)	Period (mo/yr)	N	Mean (pH)	Median (pH)	Min (pH)	Max (pH)	Reference
Austria										
Mt. Sonnblick, Austria	3106	47.05	12.96	May & Nov 1991	15	4.5	4.5	3.8	5.2	Brantner et al., 1994
Mt. Sonnblick, Austria	3106	47.05	12.96	Sept 1996		4.7				Hitzenberger et al., 2000
Mt. Sonnblick, Austria	3106	47.05	12.96	Apr-May1997		5.7				Hitzenberger et al., 2000

Location	Altitude (m)	Latitude (°N)	Longitude (°E)	Period (mo/yr)	N	Mean (pH)	Median (pH)	Min (pH)	Max (pH)	Reference
Rax, Austria	1644	47.7	15.75	Ap1999 & Mar 2000	12	4.1	3.9	3.36	5.26	Löflund et al., 2002
Czech Rep.										
Beskydy Mts., Czech Rep.	1324	49.53	18.43	May- Apr 2003-2004	48	5.2		3.8	6.7	Skybova, 2006
Cervenohorske sedlo, Czech Rep.	1013	50.12	17.16	1999	12	4.7	4.4	3.9	5.9	Zapletal et al., 2007
Cervenohorske sedlo, Czech Rep.	1013	50.12	17.16	2000	12	5.2	5.8	3.1	6.5	Zapletal et al., 2007
Cervenohorske sedlo, Czech Rep.	1013	50.12	17.16	2001	12	4.8	4.5	3.9	6.0	Zapletal et al., 2007
Cervenohorske sedlo, Czech Rep.	1013	50.12	17.16	2002	12	5.2	4.9	3.9	7.0	Zapletal et al., 2007
Flaje, Krusné Hory Mts., Czech Rep.	740	50.68	13.6	Mar-Mar1995-1996	27	3.0		2.3	4.1	Bridges et al., 2002
Mt. Churanov, Czech Rep.,	1122	49.06	13.61	Mar-Nov 1999-2000	23	4.6	4.4	3.4	6.6	Fisak et al., 2002
Mt. Milesovka, Czech Rep.,	837	50.56	13.9	Sept-Nov1999-2000	141	4.6	4.5	3.4	6.1	Fisak et al., 2002
Mt. Milesovka, Czech Rep.,	837	50.56	13.9	May-June 2006	5	4.1	4.2	3.8	4.7	Fisak et al., 2009a; Fisak et al., 2009b
Sumava Mts., Czech Rep.	1123	49.06	13.61	Oct-Oct 1989-1992	40	4.2		2.9	7.0	Elias and Tesar, 1994
Sumava Mts., Czech Rep.	1123	49.06	13.61	Feb-Oct 1988-1991	30	3.2	3.67	2.9	6.4	Elias et al., 1995
France										
Mt. Le Donon, Vosges, France	750	48.5	7.2	Mar 1990	4	3.3		2.8	4.7	Lammel and Metzig, 1991
Near Paris, France	68	48.7	2.2	2012-2013	9	5.2		3.7	6.2	Degefie et al., 2015
Puy de Dôme, France	1465	48	2	2001-2011	143	5.5	5.6	3.1	7.6	Deguillaume et al., 2013
Puy de Dôme, France	1465	48	2	2010-2013	23	5.6	5.5	3.9	7.1	Wirgot et al., 2017
Strasbourg, France	145	48.58	7.77	Feb-Nov 1991	31	3.8	3.7	2.8	5.8	Millet et al., 1997
Strasbourg, France	145	48.58	7.77	Jan-Dec 1992	21	3.9	3.8	2.3	6.2	Millet et al., 1996; Millet et al., 1997
Strasbourg, France	145	48.58	7.77	Oct-Jan 1993-1994	7	5.2	5.5	2.4	6.3	Millet et al., 1997
Strasbourg, France	145	48.58	7.77	1991-1999	54	4.6	4.7	2.3	6.6	Herckes et al., 2002
Germany										
Bavarian Alps, Germany	1780	47.52	11.15	Mar-May 1985-1986	104	4.5	4.9	3.9*	6.0#	Munzert, 1988
Bayreuth, Germany	≈350	≈49.95	≈11.58	Sept-Oct 1987	2	5.0		4.7	5.2	Trautner et al., 1989
Collmberg, Germany	316	51.3	13.01	~1960	9	4.2				Mrose, 1966
Kap Arkona, Germany	46	54.67	13.44	~1960	42	3.8				Mrose, 1966
Lugstein, Ore Mt., Germany	880	50.7	13.75	Dec-May 1997-1998	27	4		3.3	5.4	Lange et al., 2003
Mt. Brocken, Germany	1142	51.79	10.67	~1960	19	5.1				Mrose, 1966
Mt. Brocken, Germany	1142	51.79	10.67	1992	35	4.4				Acker et al., 1998a
Mt. Brocken, Germany	1142	51.79	10.67	1993		4.2				Acker et al., 1998a
Mt. Brocken, Germany	1142	51.79	10.67	1994		3.9				Acker et al., 1998a
Mt. Brocken, Germany	1142	51.79	10.67	1995		4.0				Acker et al., 1998a
Mt. Brocken, Germany	1142	51.79	10.67	1996		4.0		2.5	>8	Acker et al., 1998a; Acker et al., 1998b

Location	Altitude (m)	Latitude (°N)	Longitude (°E)	Period (mo/yr)	N	Mean (pH)	Median (pH)	Min (pH)	Max (pH)	Reference
Mt. Brocken, Germany	1142	51.79	10.67	1997		4.3	4.3	3.4	6.8	Möller, 2007; Plessow et al., 2001
Mt. Brocken, Germany	1142	51.79	10.67	1998		4.1				Möller, 2007
Mt. Brocken, Germany	1142	51.79	10.67	1999		4.3				Möller, 2007
Mt. Brocken, Germany	1142	51.79	10.67	2000		4.2				Möller, 2007
Mt. Kleiner Feldberg, Germany	825	50.22	8.44	-		2.8				Schrimpff, 1983
Mt. Kleiner Feldberg, Germany	825	50.22	8.44	1983-1986	250	3.8		2.4	7	~~Günther~~ Schmitt, 1986
Mt. Kleiner Feldberg, Germany	825	50.22	8.44	Oct-Nov 1990		4.3		3.5	5.9	Wobrock et al., 1994
Mt. Kleiner Feldberg, Germany	825	50.22	8.44	Oct-Nov 1995	114	4.1	4.1	2.7	5	Deutsch et al., 2001
Mt. Kleiner Feldberg, Germany	825	50.22	8.44	Apr-May 1997	25	4.6	4.6	4.1	4.9	Deutsch et al., 2001
Mt. Ochsenkopf, Germany	1024	50.03	11.81	May-June 1985	14	3.7				Verhoeven et al., 1987
Mt. Ochsenkopf, Germany	1024	50.03	11.81	Nov 1987	1	3.4				Trautner et al., 1989
Mt. Schmücke, Germany	937	50.65	10.77	Oct & Nov 2001/2002	22	4.5		4	5.1	Brüggemann et al., 2005
Mt. Schmücke, Germany	937	50.65	10.77	2010	60	4.3	4.6	3.6	5.3	van Pinxteren et al., 2016
Mt. Schöllkopf, Black Forest, Germany	540	48.43	8.39	Dec 1988	5	4.1	4.1	4	4.9	Lammel and Metzig, 1991
Mt. Waldstein, Germany	776	50.14	11.87	Summer 1997	56	4.3	4.3	3.3	5.7	Wrzesinsky and Klemm, 2000
Mt. Waldstein, Germany	776	50.14	11.87	June-Dec 2000	56	4.1				Thalmann et al., 2002
Mt. Waldstein, Germany	776	50.14	11.87	Apr-Mar 2001-2002	247		4.3	3.3	5.4	Klemm and Wrzesinsky, 2007
Ochsenkopf, Germany	1024	50.0314	11.81	May-June, 1985		3.7				Verhoeven et al., 1987
Taunus Mts, Germany	800	50.22	8.41	Autumn, 1983-1986		3.8		2.3	7.9	Schmitt, 1989
Zinnwald, Germany	877	50.73	13.76	Dec-May 1997-1998	51	4		3.3	4.5	Zimmermann and Zimmermann, 2002
Italy										
Po-Valley, S. Pietro Capofiume, Italy	10	44.65	11.62	Winter 1980-1982	36	4.9	5	2.4	7.5	Fuzzi et al., 1983
Po-Valley, S. Pietro Capofiume, Italy	10	44.65	11.62	Feb &Nov 1984	5	3.8	3.6	3.5	4.3	Fuzzi et al., 1985
Po-Valley, S. Pietro Capofiume, Italy	10	44.65	11.62	Nov 1985	63	3.5		2.5	6.7	Fuzzi, 1988
Po-Valley, S. Pietro Capofiume, Italy	10	44.65	11.62	Nov 1985/1986	10	5.1	5.1	4	6.3	Winiwarter et al., 1988
Po-Valley, S. Pietro Capofiume, Italy	10	44.65	11.62	Feb-Mar 1989	62	5.4	5.2	3.4	7.1	Facchini et al., 1990
Po-Valley, S. Pietro Capofiume, Italy	10	44.65	11.62	Nov-Apr 1989-1990	182	3.5	5.4	3.2	6.9	Fuzzi et al., 1992a; Fuzzi et al., 1992b
Po-Valley, S. Pietro Capofiume, Italy	10	44.65	11.62	Nov-Mar 1992-1993			5.4	3.1	7.0	Fuzzi et al., 1996
Po-Valley, S. Pietro Capofiume, Italy	10	44.65	11.62	Feb-Mar 1994	7	5.4	5.5	2.6	7.0	Fuzzi et al., 1997
Po-Valley, S. Pietro Capofiume, Italy	10	44.65	11.62	1996-1997	17	4.6	4.6	3.1	6.4	Facchini et al., 1999
Po-Valley, S. Pietro Capofiume, Italy	10	44.65	11.62	1990-2000		5.5				Giulianelli et al., 2014
Po-Valley, S. Pietro Capofiume, Italy	10	44.65	11.62	2000-2010		6.5				Giulianelli et al., 2014

Location	Altitude (m)	Latitude (°N)	Longitude (°E)	Period (mo/yr)	N	Mean (pH)	Median (pH)	Min (pH)	Max (pH)	Reference
Po-Valley, S. Pietro Capofiume, Italy	10	44.65	11.62	Nov2013	2		4.6	3.3	5.8	Brege et al., 2018
Vallombrosa, Italy	950	43	11	Nov-May 1992-1995	20	4.2	3.8	3.2	6.2	Cini et al., 2002
Norway										
Bakka, Norway	27	60.77	5	Fall 2011		5.0				Wang et al., 2015
Hakadal, Norway	170	60.12	10.83	Fall 2011		4.7		4.4	5.5	Wang et al., 2015
Sundsbø, Norway	28	60.77	5.2	Fall 2011		5.0				Wang et al., 2015
Poland										
Mt. Szrenica, Poland	1332	50.79	15.51	Winter 1993		3.8				Błaś et al., 2008
Mt. Szrenica, Poland	1332	50.79	15.51	Summer 1995		4.1	4.4	3.1	6.7	Błaś et al., 2008; Kmiec et al., 1997
Mt. Szrenica, Poland	1332	50.79	15.51	Dec-Dec 2005-2006	55	4.6		3.5	7.4	Błaś et al., 2010
Zakopane, Poland	911	49.28	17.97	Dec-Dec 2005-2006	4	5.1		4.6	5.8	Błaś et al., 2010
Spain										
Valencia region, Spain	≈842	≈39.3	≈-0.38	Apr-Dec 2008	71	6.6		5.3	7.5	Corell, 2010
Xistral Mts., Spain	700	43.54	-7.5	Sept-Apr 2011-2012	14	4.5		3.8	5.2	Fernández-González et al., 2014
Sweden										
Areskutan, Sweden	1250	63.43	13.09	Summer 1983-1984	125	4.4				Ogren and Rodhe, 1986
Switzerland										
Bern-Belpmoos, Switzerland	515	46.9	7.51	Oct-Mar 1983-1985	40	4.4	5.6	3.1	6.7	Fuhrer, 1986
Dübendorf, Switzerland		47.40	8.61	Dec 1985	21	2.7	4.2	1.9	6.0	Johnson et al., 1987
Eawag, Dübendorf, Switzerland	440	47.40	8.61	Nov-Dec 1986 & Dec 1987	20	3.3		2.1	6	Capel et al., 1990
Eawag, Dübendorf, Switzerland	440	47.40	8.61	Oct 1989 – Jan 1990	24	3.5		2.5	6.3	Xue et al., 1991; Zuo, 1994
Eawag, Dübendorf, Switzerland	440	47.40	8.61	1991-1992		4.1		3.28	6.17	Kotronarou ~~et al.~~ and Sigg, 1993
Jungfraujoch, Switzerland	3450	46.55	7.98	Oct-Nov 1993	72	4.9				Baltensperger et al., 1998
Mt. Lägeren, Switzerland	682	47.48	8.36	Sept-Dec 1986-1987	97	4.8	4.6	2.7	7.1	Joos and Baltensperger, 1991
Mt. Lägeren, Switzerland	682	47.48	8.36	Summer 2006-2007		7	7.3	5.6	7.5	Michna et al., 2015
Mt. Lägeren, Switzerland	682	47.48	8.36	2007		7.2	7.3	7	8.1	Michna et al., 2015
Mt. Lägeren, Switzerland	682	47.48	8.36	May-Apr 2001-2002		4.3	3.9	3.7	5.8	Burkard et al., 2003
Mt. Rigi, Switzerland	1620	47.06	8.49	May-Dec 1990 & Apr 1991	38	4.6		3.0	6.9	Collett Jr. et al., 1993
Niesen Kulm, Switzerland	2330	46.65	7.01	2006-2007		6.4	6.8	6	7.7	Michna et al., 2015
Niesen Schwandegg, Switzerland	1650	46.64	7.67	2006-2007		6.6	6.8	5.8	7.6	Michna et al., 2015
Seeboden, Switzerland	1030	47.07	8.47	1990-1991		5.3		3.8	6.9	Collett Jr et al., 1993
UK										
Dunslair Heights, UK	602	55.68	-3.13	1993-1994		4.1				Fowler et al., 1995
Great Dun Fell, UK	850	54.69	-2.45	1988		3.7	3.7	3.2	4.2	Radojevic et al., 1990
Great Dun Fell, UK	847	54.69	-2.45	Apr-May 1993		4.1	4.2	3.1	5.8	Laj et al., 1997; Sedlak et al., 1997
Holmes Moss, UK	550	53.53	-1.86	1993-1994		4.2				Fowler et al., 1995

Location	Altitude (m)	Latitude (°N)	Longitude (°E)	Period (mo/yr)	N	Mean (pH)	Median (pH)	Min (pH)	Max (pH)	Reference
Plynlimon, UK	390	52	-4.6	1995		5.1		2.9	6.9	Wilkinson et al., 1997

Remarks: *10% percentile, #90% percentile, ~estimated latitude/longitude/height a.m.s.l.

(g) Island/Marine

Location	Altitude (m)	Latitude (°N)	Longitude (°E)	Period (mo/yr)	N	Mean (pH)	Median (pH)	Min (pH)	Max (pH)	Reference
Baengnyeong Island, Yellow Sea	100	37.97	124.62	June-July 2014	11	3.9		3.5	5	Boris et al., 2016
Bering Sea		58.22	-178.29	1998	1	5.5				Sasakawa and Uematsu, 2005
East Peak, Luquillo, Puerto Rico	1051	18.27	-65.75	2004-2005	8	5.8		4.8	6.4	Gioda et al., 2009
East Peak, Luquillo, Puerto Rico	1051	18.27	-65.75	2004-2007	45	5.5		3.5	6.3	Gioda et al., 2013; Gioda et al., 2011
East Peak, Luquillo, Puerto Rico	1051	18.27	-65.75	June-Aug 2007	9	5.6		5.0	7.4	Reyes-Rodríguez et al., 2009
East Peak, Luquillo, Puerto Rico	1051	18.27	-65.75	2010-2012	94	4.9		4.0	7.3	Valle-Díaz et al., 2016
Eastern Pacific Ocean		30.5	-121.5	July 2001	50		4.0	3.3	4.8	Straub et al., 2007
Hilo City, Hawaii		19.74	-155.04	June 1980	6	4.5		4.2	4.7	Parungo et al., 1982
Luquillo Mountains, Puerto Rico	1020	18.32	-65.75	Nov-Dec 1967	7	5.1		4.9	5.4	Lazrus et al., 1970
Luquillo Mountains, Puerto Rico	1050	18.3	-65.78	1986-1987	12	4.6				Asbury et al., 1994
Northeastern North Pacific		49.58	-145	1999	1	4.1				Sasakawa and Uematsu, 2005
Northwestern North Pacific		37.85	142.40	Dec 1996	4	4.1		3.8	5.2	Watanabe et al., 2001b
Northwestern North Pacific		37.85	142.40	July 1998	13	4.2				Sasakawa and Uematsu, 2002
Northwestern North Pacific		44	155	1999	1	3.9				Sasakawa and Uematsu, 2005
Northwestern North Pacific		44	155	2000	21	4.2				Sasakawa and Uematsu, 2005
Northwestern North Pacific		44	155	2001	30	3.7				Sasakawa and Uematsu, 2005
Pico del Ingles, Tenerife, Canary Islands	992	28.5	-16.3	1995 & 1996		3.3		3	4.4	Borys et al., 1998
Puerto Rico	1020	18.32	-65.75	May-Nov 1984-1985		4.7	5.0	4.1	6.9	Weathers et al., 1988
Sea of Japan		39.54	134.28	Feb 1997	1	3.8				Watanabe et al., 2001b
Sea of Japan		39.54	134.28	July 1998	2	2.8				Sasakawa and Uematsu, 2002
Sea of Okhotsk		47.68	145.93	July 1998	5	3				Sasakawa and Uematsu, 2002
Sea of Okhotsk		47.68	145.93	2000	4	4				Sasakawa and Uematsu, 2005
Southeast Pacific		-24	-78	Oct-Nov 2008	72	4.3		2.9	7.2	Benedict et al., 2012
Tenerife, Canary Islands		28.34	-16.64	July 1997	2	3.6		3.7	3.4	Zhang and Anastasio, 2001
Tenerife, Canary Islands		28.34	-16.64	July 1997	1	3.4				Anastasio and McGregor, 2001

(h) Middle East

Location	Altitude (m)	Latitude (°N)	Longitude (°E)	Period (mo/yr)	N	Mean (pH)	Median (pH)	Min (pH)	Max (pH)	Reference
Dhofar, Oman	900	17.26	54.28	July 1990	7	6.4		7.0	7.9	Schemenauer and Cereceda, 1992a
Mt. Carmel, Israel	1120	32.74	35.05	1988	1	2				Ganor et al., 1993
Mt. Meron, Israel	341	33.00	35.41	1992	1	2				Ganor et al., 1993
Tel Aviv University		32.11	34.80	1987 & 1989	3	2.1				Ganor et al., 1993

(i) North America

Location	Altitude (m)	Latitude (°N)	Longitude (°E)	Period (mo/yr)	N	Mean (pH)	Median (pH)	Min (pH)	Max (pH)	Reference
USA										
Albany, NY		42.66	-73.77	Oct 1982	24	5.6		4.3	6.4	Fuzzi et al., 1984
Angiola, CA	60	35.58	-119.53	2000-2001	36		6.7	5.9	8.0	Herckes et al., 2007
Angora Peak, OR	820	45.79	-123.92	July 1993	6	4.6		4.2	5.0	Rao and Collett, 1995
Appledore Island		42.99	-70.61	1987	4	3.5		3.1	6.5	Jagels et al., 1989
Bakersfield FACT, CA		35.35	-119.09	Jan 1994	2	6.4		6.0	6.6	Collett Jr et al., 1999
Bakersfield, CA		35.37	-119	1982-1983	108	2.9		2.6	7	Jacob et al., 1984
Bakersfield, CA	76	35.37	-119	1983-1984	16	5.7		5.1	6.9	Jacob et al., 1986a
Bakersfield, CA	76	35.37	-119	1984-1985	35	4.0		2.9	7.6	Jacob et al., 1986b
Bakersfield, CA		35.37	-119	Jan 1993	5	6.7		6.4	7.1	Erel et al., 1993
Bakersfield, CA	130	35.37	-119.03	Jan 1994	4	6.7		6.5	6.9	Rao and Collett, 1995
Bakersfield, CA	130	35.37	-119.03	Feb 1995	5	5.5		4.9	6.9	Siefert et al., 1998
Bakersfield, CA	130	35.37	-119.03	Dec 1995	4	6.7		6.3	7.0	Collett Jr et al., 1999
Bar Harbor, ME	10	44.38	-68.23	Aug 1984	3	3.0		2.9	3	Weathers et al., 1986
Bar Harbor, ME	5	44.4	-68.23	1984-1985	15	3.2	3.6	2.4	5.4	Weathers et al., 1988
Bar Harbor, ME	< 10	44.4	-68.23	1984-1985	16	3.2	3.7	2.4	5.4	Kimball et al., 1988
Baton Rouge, LA		30.82	-90.79	2002-2004	15	6.1		4.7	6.7	Raja et al., 2005
Baton Rouge, LA		30.82	-90.79	2004-2005	21	5		2.7	6.4	Raja et al., 2008
Brooklyn, NY		40.68	-73.94	1954	11	4.7		3.5	6.3	Houghton, 1955
Buttonwillow, CA	24	35.40	-119.47	1983-1984	7	5.3		5.0	6.8	Jacob et al., 1986a
Buttonwillow, CA	24	35.40	-119.47	Jan 1985	11	5.9		5.3	5.9	Jacob et al., 1986b
Camels Hump mountain, Vermont		44.86	-72.59	Mar-Sept 1991	47	3.2		2.9	4.5	Hemmerlein and Perkins, 1993
Cape Elizabeth		43.56	-70.20	1987	3	2.8		2.5	3.6	Jagels et al., 1989
Casitas Pass, CA		34.39	-119.42	June 1985	42	4.0		3.3	4.9	Munger, 1989
Casitas Pass, CA	290	34.39	-119.42	June 2015	20	5.9		5.3	6.7	Boris et al., 2018
Catoctin Mountain, MD	860	40.22	-77.42	Jan-May 1987	9	5.3				Anderson and Landsberg, 1979
Charleston, SC	~520	32.78	-79.94	Feb 1982	27	3.6				Daum et al., 1984
Cheeka Peak Observatory, WA	460	48.35	-124.67	May 1993	102	4.2				Vong et al., 1997
Clingman's Dome, TN	2014	35.56	-83.50	June-Oct 1994	9	4.4		3.8	6.1	Anderson et al., 1999; Baumgardner Jr et al., 2003
Clingman's Dome, TN	2014	35.56	-83.50	June-Oct 1995	136	3.9		2.7	6.3	Anderson et al., 1999; Baumgardner Jr et al., 2003
Clingman's Dome, TN	2014	35.56	-83.50	June-Oct 1996	103	3.7		3.1	4.9	Anderson et al., 1999; Baumgardner Jr et al., 2003
Clingman's Dome, TN	2014	35.56	-83.50	June-Oct 1997	318	3.8		2.8	5.9	Anderson et al., 1999; Baumgardner Jr et al., 2003
Clingman's Dome, TN	2014	35.56	-83.50	June-Oct 1998	268	3.6		2.8	5.8	Anderson et al., 1999; Baumgardner Jr et al., 2003
Clingman's Dome, TN	2014	35.56	-83.50	June-Sept 1999	173	3.7		2.7	5.5	Anderson et al., 1999; Baumgardner Jr et al., 2003
Clingman's Peak, NC	1987	35.61	-83.50	1986	48	3.7				Dasch, 1988

Location	Altitude (m)	Latitude (°N)	Longitude (°E)	Period (mo/yr)	N	Mean (pH)	Median (pH)	Min (pH)	Max (pH)	Reference
Columbus, OH		39.96	-82.99	May 1990	17	3.8		3.5	4.1	Burkhard et al., 1994
Corona del Mar, CA		33.60	-117.87	Dec 1982	1	2.2				Jacob et al., 1985
Corvallis, OR		44.5661	-123.26	1988-1989	20	5.6	5.7	4.5	6.8	Muir, 1991
Damariscove Island, ME	<10	43.77	-69.62	July-Oct 1985	4	3.4	4.1	2.9	4.2	Kimball et al., 1988
Damariscove Island		43.7579	-69.62	1987	5	2.7		2.4	3.7	Jagels et al., 1989
Davis, CA		38.32	-121.47	Jan-Feb 1991	6	6.3		5.8	7.3	Sagebiel and Seiber, 1993
Davis, CA		38.32	-121.47	Dec 1998	9	6.1		5.5	6.5	Reilly et al., 2001
Davis, CA		38.32	-121.47	Jan 1999	43	6.3		5.3	6.8	Reilly et al., 2001
Davis, CA	50	38.5	-121.75	1998-1999	51	6.3		5.7	6.9	Moore et al., 2004
Davis, CA		38.54	-121.76	1997-2001	16	6.5	6.7	5.6	7.5	Zhang and Anastasio, 2001
Davis, CA		38.54	-121.63	Jan 2011	11		6.8	6.4	7.2	Ehrenhauser et al., 2012
Del Mar, CA		32.96	-117.27	Jan 1983	5	2.9				Jacob et al., 1985
Delaware Bay		39.31	-75.23	Mar 1992	2	3.1		2.9	3.8	Erel et al., 1993
Douglas Island	800	58.27	-134.5	1984-1985	20	4.5	4.8			Bormann et al., 1989
East coast		34.04	-77.89	Jan-Mar 1986	11	3.9				Barth et al., 1989
Eastern+Western Washington		48.41	-119.68	1982-1983	31	3.9		3.3	5.2	Hegg et al., 1984a; Hegg et al., 1984b
Etiwanda		34.13	-117.52	May 1982	1	2.4				Richards et al., 1983
Fontana		34.10	-117.44	May 1982	3	2.8		2.7	3.4	Richards et al., 1983
Fresh Water Bay, AK (Douglas Island, AK)	25	57.88	-135.17	1984-1985	18	4.6	4.4	3.8	5.3	Weathers et al., 1988
Fresno, CA		36.74	-119.78	Dec 1995	2	6.1		5.9	6.4	Collett Jr et al., 1999
Fresno, CA		36.74	-119.78	Jan 1996	1	6		6		Collett Jr et al., 1999
Fresno, CA		36.83	-119.75	Jan 2010	11		6.7	6.4	7.3	Ehrenhauser et al., 2012
Henninger Flats, CA	780	34.18	-118.1	June 1982	42		2.9	5.4	5.7	Waldman et al., 1985
Henninger Flats, CA	780	34.18	-118.1	May-June 1982	86		3.0	5.4	5.7	Waldman et al., 1985
Henninger Flats, CA	780	34.18	-118.1	May-June 1991	21	2.8		2.5	3.9	Erel et al., 1993
Henninger Flats, CA	780	34.18	-118.1	June-July 1987	76	3.3		2.6	4.8	~~William~~ Munger et al., 1990
Houston, TX		29.78	-95.12	Feb 2006	11	4.3		3.2	7.2	~~Suresh~~ Raja et al., 2008
Hubbard Brook, NH	765	43.93	-71.75	Aug 1984	1	3.0				Weathers et al., 1986
Hubbard Brook, NH	765	43.93	-71.75	1984-1985	10	3.9		3.2	4.6	Weathers et al., 1988
Huntington Beach		33.66	-117.99	May 1982	4	3.3		3.1	3.6	Richards et al., 1983
Indianapolis, IN		39.84	-86.17	1985-1986	10	3.4		2.9	4.1	Muir et al., 1986
Isle au Haut, ME	<10	44.03	-68.38	Sept 1985	2	3.6	3.6	3.4	3.8	Kimball et al., 1988
Isle au Haut, ME	<10	44.03	-68.38	1987	11	3.2		2.7	4.0	Jagels et al., 1989
Kearney Agricultural Center, CA		36.60	-119.51	Jan 1991	4	7.0		6.5	7.8	Sagebiel and Seiber, 1993
Kent Island		39.22	-73.34	1954	19	7.2		7	7.4	Houghton, 1955
Kent Island		39.22	-73.34	1987	15	3.5		3.0	5.8	Jagels et al., 1989
Kern Wildlife Refuge, CA		35.76	-119.58	Dec 1995	2	7.0		6.8	7.4	Collett Jr et al., 1999
Kern Wildlife Refuge, CA		35.76	-119.58	Jan 1996	5	7.0		6.9	7.1	Rao and Collett, 1998
La Jolla Peak, CA	475	34.12	-119.05	July 1993	10	3.4		3.1	3.9	Rao and Collett, 1995
La Jolla Peak, CA	475	34.12	-119.05	June 1994	13	3.2		2.8	3.7	Rao and Collett, 1998
Lakes-of-the-clouds, NH	1534	44.27	-71.32	1984-1985	35	3.7	4.0	2.9	4.8	Weathers et al., 1988
Lakes-of-the-clouds, NH	1534	44.27	-71.32	1984-1985	32	3.7	4.0	2.9	4.7	Kimball et al., 1988
Lakes-of-the-clouds, NH	1534	44.27	-71.32	1984-2010	1216		4.1			Murray et al., 2013

Location	Altitude (m)	Latitude (°N)	Longitude (°E)	Period (mo/yr)	N	Mean (pH)	Median (pH)	Min (pH)	Max (pH)	Reference
Lawrence Berkeley Laboratory	246	37.90	-122.2	July-Sept 1986	13	4		3.4	6.2	Gundel et al., 1994
Lennox, CA		33.94	-118.36	Dec 1981	11	2.8		2.7	3.0	~~William~~ Munger et al., 1983
Lennox, CA		33.94	-118.36	Jan 1983	5	3.6				~~William~~ Munger et al., 1983
Lennox, CA		33.94	-118.36	Jan 1981	16	3.0		2.7	3.6	Jacob et al., 1985
Loft Mountain, VA	990	38.25	-78.67	Aug 1984	1	3.1				Weathers et al., 1986
Loft Mountain, VA	500	38.25	-78.67	1984-1985	20	3.6	3.8	3.0	5.5	Weathers et al., 1988
Long Beach, CA		33.77	-118.2	Jan 1983	2	4.9				Jacob et al., 1985
Long Beach, CA		33.77	-118.2	May 1992	1	3.0				Richards et al., 1983
Los Angeles		34.06	-118.25	Jan 1980	10	5.3		4.6	4.8	Hegg and Hobbs, 1981
Los Angeles Basin	600-700	33.8	-118	May 1982		3		2.3	3.6	Richards, 1995
Los Angeles Basin	600-700	33.8	-118	June 1984		3		2.8	3.6	Richards, 1995
Los Angeles Basin	600-700	33.8	-118	May-June 1985		3.4		2.9	3.8	Richards, 1995
Los Angeles, 16 sites		34.06	-118.25	Winter 1980-1982	10		3.3	2.7	7.1	Brewer et al., 1983
Lower Kaweah, CA (SNP)[1]	1856	36.57	-118.77	1985-1986	12	5.0		4.4	5.7	Collett Jr et al., 1989
Lower Kaweah, CA (SNP)[1]	1856	36.57	-118.77	1987-1988	70	4.8		3.9	6.5	Collett Jr et al., 1990b
Lower Kaweah, CA (SNP)[1]	1856	36.57	-118.77	Apr 1988	5	4.5		4.4	4.6	Collett Jr et al., 1990a
Marys Peak, OR	1245	44.5	-123.57	June-Nov 1985	14	4.7	5.2			Bormann et al., 1989
Marys Peak, OR	1249	44.43	-123.63	1984-1985	12	4.6	4.7	4.1	5.5	Weathers et al., 1988
McKittrick, CA	262	35.31	-119.62	1983-1984	58	4.0		2.7	5.2	Jacob et al., 1986a
McKittrick, CA	262	35.31	-119.62	Jan 1984	24	4.2		3.7	5.0	Jacob et al., 1986b
Mohonk Mountain, NY	467	41.78	-74.4	Aug 1984	1	2.8				Weathers et al., 1986
Mohonk Mountain, NY	467	41.78	-74.4	1984-1985	23	3.5	3.6	2.8	4.4	Weathers et al., 1988
Monterey, CA		36.6	-121.89	Sept 1987	5	5.6		5.1	6.8	Schomburg et al., 1991
Moosilauke, NH	962	44.02	-71.83	1986-1988	200	3.7				Li and Aneja, 1992; Mohnen and Vong, 1993; Vong and Guttorp, 1991
Moro Rock, CA (SNP)[1]	1965	36.55	-118.77	Apr 1988	9	4.5		4.3	4.8	Collett Jr et al., 1990a
Morro Bay, CA		35.37	-120.85	July 1982	2	6.2				Jacob et al., 1985
Mount Gibbes, (Mt. Mitchell, NC)	2006	35.76	-82.29	Summer 1986	132	3.8		2.7	5.4	Aneja et al., 1992
Mount Gibbes, (Mt. Mitchell, NC)	2006	35.76	-82.29	Autumn 1986	15	3.9		3.3	4.2	Aneja et al., 1992
Mount Gibbes, (Mt. Mitchell, NC)	2006	35.76	-82.29	Summer 1987	39	4.0		3.5	4.9	Aneja et al., 1992
Mount Gibbes, (Mt. Mitchell, NC)	2006	35.76	-82.29	Autumn 1987	13	4.5		4.0	6.7	Aneja et al., 1992
Mount Gibbes, (Mt. Mitchell, NC)	2006	35.76	-82.29	Summer 1988	53	3.4		2.8	4.5	Aneja et al., 1992
Mount Gibbes, (Mt. Mitchell, NC)	2006	35.76	-82.29	Autumn 1988	46	3.9		3.1	5.3	Aneja et al., 1992
Mount Gibbes, (Mt. Mitchell, NC)	2006	35.76	-82.29	June 1993	15	3.1		2.5	3.8	DeFelice, 1997
Mount Gibbes, (Mt. Mitchell, NC)	2006	35.76	-82.29	June-Aug 1996	5	4.0		3.8	4.2	Menon et al., 2000
Mount Lafayette, NH	1220	44.16	-71.64	Aug 1984	1	3.0				Weathers et al., 1986
Mount Washington, NH		44.41	-71.31	1954	35	4.5		3	5.9	Houghton, 1955
Mount Washington, NH	1524	44.41	-71.31	Aug 1984	1	3.0				Weathers et al., 1986
Mt. Desert Rock, ME	<10	43.97	-68.13	July-Sept 1985	5	3.6	3.6	3.3	5.0	Kimball et al., 1988

Location	Altitude (m)	Latitude (°N)	Longitude (°E)	Period (mo/yr)	N	Mean (pH)	Median (pH)	Min (pH)	Max (pH)	Reference
Mt. Elden, AZ	2834	35.24	-111.6	2005-2007	8		6.3	5.1	6.6	Hutchings et al., 2009
Mt. Mitchell, NC	1950	35.74	-82.29	1986-1988	477	3.6				Mohnen and Vong, 1993; Vong and Guttorp, 1991
Mt. Mitchell, NC	2038	35.74	-82.29	May-Sept 1986	149	3.5		2.7	4.8	Lin and Saxena, 1991; Saxena and Lin, 1990
Mt. Mitchell, NC	2038	35.74	-82.29	May-Sept 1987	86	3.5		2.8	5.9	Lin and Saxena, 1991; Saxena and Lin, 1990
Mt. Mitchell, NC	2038	35.73	-82.27	July-Oct 1987	495	3.3		2.9	4.8	Kim and Aneja, 1992
Mt. Mitchell, NC	2038	35.73	-82.27	June-Sept 1988	978	3.4		2.4	5.6	Kim and Aneja, 1992
Mt. Mitchell, NC	2038	35.73	-82.27	May-Aug 1989	413	3.6		2.8	4.9	Kim and Aneja, 1992
Mt. Mitchell, NC	1980	35.77	-82.27	Aug 1993	16	2.9		2.7	3.3	Rao and Collett, 1995
Mt. Mitchell, NC (Polluted)	2038	35.74	-82.29	1993-1994	14	3.2		3.1	3.3	Deininger and Saxena, 1997
Mt. Mitchell, NC (Black Mountain)	2006	35.73	-82.27	Summer 1987	139	3.3		2.9	4.5	Aneja et al., 1990
Mt. Mitchell, NC (Black Mountain)	2006	35.73	-82.27	Fall 1987	47	4.1		3.6	4.5	Aneja et al., 1990
Mt. Mitchell, NC (Continental)	2038	35.74	-82.29	1993-1994	8	3.5		3.1	4.2	Deininger and Saxena, 1997
Mt. Mitchell, NC (Marine)	2038	35.74	-82.29	1993-1994	11	3.3		3.0	3.8	Deininger and Saxena, 1997
Muskegon, MI	670, 1525	43.84	-86.18	Mar 1977	2	3.8				Scott and Laulainen, 1979
Olidale, CA		35.42	-119.02	Jan 1982	3	3.2		2.1	3.1	Munger et al., 1983
Parlier, CA		36.61	-119.53	Jan 1986	5	5.7		5.4	7	Glotfelty et al., 1990
Pasadena, CA		34.14	-118.13	Dec 1981	8	3.2		2.9	5.3	Munger et al., 1983
Pasadena, CA		34.14	-118.13	Jan 1982	1	2.3				Munger et al., 1983
Pomona-Corona, CA		33.88	-117.57	May 1992	2	2.6				Richards et al., 1983
Pt. Reyes, CA		38.05	-113	Aug 1982	17	4.1				Jacob et al., 1985
Puget Sound Basin, WA		47.75	-112.48	Jan-May 1984	17	4.1		3.7	5.3	Hegg and Hobbs, 1986
Redwood National Park, CA	287	41.25	-124.03	1984-1985	13	4.3	4.4	3.7	5.2	Weathers et al., 1988
Riverside, CA	350	33.97	-117.32	Jan-Mar 1986	16	3.3		2.3	5.7	Munger et al., 1990
Roque Island, ME	<10	44.58	-67.53	July-Sept 1985	3	3.8	3.7	3.6	4.9	Kimball et al., 1988
Roque Island, ME		44.58	-67.53	1987	5	3.5		3.3	3.7	Jagels et al., 1989
Rye Harbor, NH		43	-70.75	Mar-Sept 1990	56	3.4		2.6	4.8	Klemm et al., 1994; Klemm et al., 1992
San Joaquin Valley, CA		36.74	-119.79	1983-1984	13	6.1		5.2	6.8	Miller et al., 1987
San Joaquin Valley, CA (BF, KWR, Fresno)		36.74	-119.79	1995-1996	59		6.5	5.0	7.4	Collett Jr et al., 1998
San Marcos Pass, CA		34.51	-199.82	Aug 1983	14	4.5				Jacob et al., 1985
San Nicholas Island, CA		33.25	-119.5	Aug 1982	7	3.9				Jacob et al., 1985
San Pedro Hill, CA	450	33.74	-118.41	June-July 1987	242	3.3		2.4	5.0	Munger et al., 1990
San Pedro Hill, CA	450	33.74	-118.41	June-July 1991	21	2.8		2.2	4.2	Erel et al., 1993
San Pedro Hill, CA	450	33.74	-118.41	June 1992	3	4.3		4.2	4.4	Erel et al., 1993
San Pedro Hill, CA	450	33.74	-118.41	1994	6	3.8		3.2	4.1	Siefert et al., 1998
Seal Beach, CA		33.74	-118.1	Nov 1981	2	3		3.0	3.0	Richards et al., 1983
Shenandoah National Park, VA	1037	38.62	-78.35	Sept 1990	2	3.6		3.3	4.8	Keene et al., 1995

Location	Altitude (m)	Latitude (°N)	Longitude (°E)	Period (mo/yr)	N	Mean (pH)	Median (pH)	Min (pH)	Max (pH)	Reference
Shenandoah, VA	1040	38.2	-78.33	1986-1988	55	3.7				Li and Aneja, 1992; Mohnen and Vong, 1993; Vong and Guttorp, 1991
Mt. Sutro, CA		37.78	-122.41	Aug 1982	1	4.0				Jacob et al., 1985
Steamboat Springs, CO	3220	40.46	-106.74	Jan 1997	27	4.3		3.9	5.1	Collett Jr et al., 2002
Steamboat Springs, CO	3220	40.46	-106.74	Jan 1997	40	5.1		3.9	6.5	Xu et al., 1999
Sugarloaf Mountain, ME	1280	45.03	-70.32	Aug-Oct 1985	14	3.4	3.9	2.9	4.9	Kimball et al., 1988
Susquehanna University, PA	-	40.79	76.88	2007-2015	146	4.7	6.5	3.1	7.4	Straub, 2017; Straub et al., 2012
Tennessee Vally, Whitetop Mountain, VA	1682	36.52	-82.08	Apr-Oct 1986	14	3.6		2.9	4.6	Joslin et al., 1988
Turtleback Dome, CA (YNP)[2]	1590	37.72	-119.71	Apr-Nov 1988	43	4.5		3.8	5.2	Collett Jr et al., 1990b
University of California at Davis		38.54	-121.76	Jan-Feb 1997	2	6.8				Anastasio and McGregor, 2001
University of California at Davis		38.54	-121.76	Jan-Feb 1998	5	6.5				Anastasio and McGregor, 2001
University of California at Davis		38.54	-121.76	Jan 1999	1	6				Anastasio and McGregor, 2001
University of Michigan, Biological Station, MI	2452	45.67	-84.47	Aug 2005	19	4.4		2.2	5.2	Hill et al., 2007
Upland, CA		34.10	-117.65	Jan 1982	3	2.4		2.9	2.2	~~William~~ Munger et al., 1983
Visalia, CA	43	36.33	-119.29	1983-1984	13	7		5.5	7.2	Jacob et al., 1986a
Western Washington		47.61	-122.33	Apr-May 1979	23	4.3		3.7	6.5	Hegg and Hobbs, 1981
Western Washington		47.61	-122.33	1979-1981	16	4.7		4.3	7	Hegg and Hobbs, 1982
Whiteface Mountain, NY	1500	44.48	-73.9	July-Aug 1976	50	3.6		3.4	4.2	Castillo et al., 1983
Whiteface Mountain, NY	1500	44.48	-73.9	Aug-Sept 1977		3.6		2.7	4.7	Falconer and Falconer, 1980
Whiteface Mountain, NY	1500	44.48	-73.9	Aug-Sept 1979		3.5		2.7	4.7	Falconer and Falconer, 1980
Whiteface Mountain, NY	1500	44.48	-73.9	Summer 1981	114	3.5				Castillo et al., 1985
Whiteface Mountain, NY	1500	44.48	-73.9	Summer 1982	167	3.7				Mohnen and Kadlecek, 1989
Whiteface Mountain, NY	1500	44.48	-73.9	Summer 1982	68	3.9				Castillo et al., 1985
Whiteface Mountain, NY	1500	44.48	-73.9	1983	400	3.6				Mohnen and Kadlecek, 1989
Whiteface Mountain, NY	1500	44.48	-73.9	June-Aug 1983	72	3.7		3.1	4.7	Van Valin et al., 1987
Whiteface Mountain, NY	1500	44.48	-73.9	1984	249	3.5				Mohnen and Kadlecek, 1989
Whiteface Mountain, NY	1500	44.48	-73.9	Winter 1985	38	3.5				Mohnen and Kadlecek, 1989
Whiteface Mountain, NY	1500	44.48	-73.9	1984-1985	10	3.9		3.2	4.6	Weathers et al., 1988
Whiteface Mountain, NY	1483	44.38	-73.08	1986-1988	634	4.1				Li and Aneja, 1992; Mohnen and Vong, 1993; Vong and Guttorp, 1991
Whiteface Mountain, NY	1438	44.38	-73.08	1986-1988	66	3.9				Li and Aneja, 1992; Mohnen and Vong, 1993; Vong and Guttorp, 1991
Whiteface Mountain, NY	1500	44.48	-73.9	1986	375	3.6				Mohnen and Kadlecek, 1989

Location	Altitude (m)	Latitude (°N)	Longitude (°E)	Period (mo/yr)	N	Mean (pH)	Median (pH)	Min (pH)	Max (pH)	Reference
Whiteface Mountain, NY	1500	44.48	-73.9	Summer 1987	91	3.8				Mohnen and Kadlecek, 1989
Whiteface Mountain, NY	1512	44.39	-73.09	July 1987	16	3.5		3.1	4.4	Khwaja et al., 1995
Whiteface Mountain, NY	1512	44.39	-73.09	Aug 1987	6	3.4		3.6	4	Khwaja et al., 1995
Whiteface Mountain, NY	1512	44.39	-73.09	July-Aug 1988	10	3.3		3.1	3.7	Husain, 1989
Whiteface Mountain, NY	1512	44.39	-73.09	Aug 1989	2	4.4				Husain et al., 1991; Miller et al., 1993
Whiteface Mountain, NY		44.39	-73.09	July-Aug 1992	73	3.2		2.9	4.5	Dutkiewicz et al., 1996
Whiteface Mountain, NY	1512	44.39	-73.09	Jun e 1993	23	3.6		3.0	4.7	Siefert et al., 1998
Whiteface Mountain, NY		44.39	-73.09	Sept-Oct 1993	73	3.6		3.3	4	Dutkiewicz et al., 1996
Whiteface Mountain, NY	1620	44.39	-73.09	Sept 1993	4	4.6		4.4	4.7	Rao and Collett, 1995
Whiteface Mountain, NY	1512	44.39	-73.09	June-July 1994	26	3.9		3.2	5.4	Siefert et al., 1998
Whiteface Mountain, NY	1483	44.37	-73.90	June-Oct 1994	223	3.6		2.5	5.8	Anderson et al., 1999; Baumgardner Jr et al., 2003
Whiteface Mountain, NY	1483	44.37	-73.90	June-Oct 1995	523	3.7		2.6	6.5	Anderson et al., 1999; Baumgardner Jr et al., 2003
Whiteface Mountain, NY	1483	44.37	-73.90	June 1995	367	3.4		2.9	4.2	Husain et al., 2000
Whiteface Mountain, NY	1483	44.37	-73.90	June-Oct 1996	569	3.8		2.8	5.9	Anderson et al., 1999; Baumgardner Jr et al., 2003
Whiteface Mountain, NY	1483	44.37	-73.90	June-Oct 1997	393	3.7		2.9	6.1	Anderson et al., 1999; Baumgardner Jr et al., 2003
Whiteface Mountain, NY	1483	44.37	-73.90	June-Oct 1998	387	3.8		2.8	5.9	Anderson et al., 1999; Baumgardner Jr et al., 2003
Whiteface Mountain, NY	1483	44.37	-73.90	June-Sept 1999	473	3.7		2.9	6.1	Anderson et al., 1999; Baumgardner Jr et al., 2003
Whiteface Mountain, NY	1484	44.4	-73.85	July 1998	49	3.1		2.9	3.8	Moore et al., 2004
Whiteface Mountain, NY	1484	44.4	-73.85	July-Oct 1994		3.7				Aleksic et al., 2009
Whiteface Mountain, NY	1484	44.4	-73.85	May-Oct 1995		3.7				Aleksic et al., 2009
Whiteface Mountain, NY	1484	44.4	-73.85	June-Oct 1996		4.0				Aleksic et al., 2009
Whiteface Mountain, NY	1484	44.4	-73.85	June-Oct 1997		3.8				Aleksic et al., 2009
Whiteface Mountain, NY	1484	44.4	-73.85	June-Oct 1998		3.7		2.8	4.7	Aleksic et al., 2009; Rattigan et al., 2001
Whiteface Mountain, NY	1484	44.4	-73.85	June-Oct 1999		3.8				Aleksic et al., 2009
Whiteface Mountain, NY	1484	44.4	-73.85	June-Sept 2000		3.9				Aleksic et al., 2009
Whiteface Mountain, NY	1484	44.4	-73.85	June-Oct 2001		4.0				Aleksic et al., 2009
Whiteface Mountain, NY	1484	44.4	-73.85	June-Sept 2002		3.9				Aleksic et al., 2009
Whiteface Mountain, NY	1484	44.4	-73.85	July-Sept 2003		3.9				Aleksic et al., 2009
Whiteface Mountain, NY	1484	44.4	-73.85	July-Aug 2004		4.0				Aleksic et al., 2009

Location	Altitude (m)	Latitude (°N)	Longitude (°E)	Period (mo/yr)	N	Mean (pH)	Median (pH)	Min (pH)	Max (pH)	Reference
Whiteface Mountain, NY	1484	44.4	-73.85	June-Sept 2005		3.7				Aleksic et al., 2009
Whiteface Mountain, NY	1484	44.4	-73.85	May-Sept 2006		3.9				Aleksic et al., 2009
Whiteface Mountain, NY	1484	44.4	-73.85	Aug-Sept 2014	8	4.8		4.1	5.3	Cook et al., 2017
Whitetop Mountain, VA	1689	36.64	-81.61	Summer 1986	32	3.5		2.8	4.3	Reisinger and Imhoff, 1989
Whitetop Mountain, VA	1689	36.64	-81.61	Summer 1987	18	3.2		2.9	3.7	Reisinger and Imhoff, 1989
Whitetop Mountain, VA	1689	36.64	-81.61	1986-1988	601	3.8				Li and Aneja, 1992; Mohnen and Vong, 1993
Whitetop Mountain, VA	1686	36.64	-81.61	June-Oct 1994	141	3.8		2.8	5.4	Anderson et al., 1999; Baumgardner Jr et al., 2003
Whitetop Mountain, VA	1686	36.64	-81.61	June-Oct 1995	550	3.8		2.6	5.2	Anderson et al., 1999; Baumgardner Jr et al., 2003
Whitetop Mountain, VA	1686	36.64	-81.61	June-Oct 1996	181	3.8		2.8	5.5	Anderson et al., 1999; Baumgardner Jr et al., 2003
Whitetop Mountain, VA	1686	36.64	-81.61	June-Oct 1997	501	3.9		2.8	6.1	Anderson et al., 1999; Baumgardner Jr et al., 2003
Whitetop Mountain, VA	1686	36.64	-81.61	June-Oct 1998	271	3.7		2.7	5.3	Anderson et al., 1999; Baumgardner Jr et al., 2003
Whitetop Mountain, VA	1686	36.64	-81.61	June-Sept 1999	143	4.2		2.7	5.4	Anderson et al., 1999; Baumgardner Jr et al., 2003
Canada										
Mt. Tremblant	860	46.21	-74.56	1985	11	4.7				Schemenauer et al., 1995
Mt. Tremblant	860	46.21	-74.56	1986	31	5.0				Schemenauer et al., 1995
Mt. Tremblant	860	46.21	-74.56	1987	79	5.0				Schemenauer et al., 1995
Mt. Tremblant	860	46.21	-74.56	1988	52	4.8				Schemenauer et al., 1995
Mt. Tremblant	860	46.21	-74.56	1989	48	4.7				Schemenauer et al., 1995
Mt. Tremblant	860	46.21	-74.56	1990	75	4.9				Schemenauer et al., 1995
Mt. Tremblant	860	46.21	-74.56	1991	66	5.0				Schemenauer et al., 1995
North Bay		46.33	-79.43	Jan-Feb 1984	148		3.6	2.3	5.5	Isaac and Daum, 1987
Nova Scotia	8	44.68	-63.42	Aug 1975	15	3.4		3	6.2	Bressan and Larson, 1979
Ontario		34.05	-117.6	1988	117	3.4				Liu et al., 1993
Roundtop Ridge	850	45.09	-72.56	July-Dec 1985	2	4.0				Schemenauer, 1986
Roundtop Ridge	845	45.09	-72.56	1986	22	4.6				Schemenauer et al., 1995
Roundtop Ridge	845	45.09	-72.56	1987	52	5.1				Schemenauer et al., 1995
Roundtop Ridge	845	45.09	-72.56	1988	63	5.2				Schemenauer et al., 1995
Roundtop Ridge	845	45.09	-72.56	1989	53	5				Schemenauer et al., 1995
Roundtop Ridge	845	45.09	-72.56	1990	54	5.1				Schemenauer et al., 1995
Roundtop Ridge	845	45.09	-72.56	1991	35	4.9				Schemenauer et al., 1995
Whistler Mountain		50.06	-122.96	2010		4.4				Ervens et al., 2013

[1] SNP: Sequoia National Park [2] YNP: Yosemite National Park

Table S9. Select data from the complete datasets used for comparing MOSAIC against ISORROPIA-II. Concentrations are expressed in μg m^{-3}, temperature in K and relative humidity as percent (%). Related information is available in excel format at doi:10.23719/1504059.

ID	Na μg m^{-3}	SO_4 μg m^{-3}	TNH_4 μg m^{-3}	TNO3 μg m^{-3}	Cl μg m^{-3}	Ca μg m^{-3}	K μg m^{-3}	Mg μg m^{-3}	RH %	T K	Campaign, Characteristics
1	0.000	1.490	12.851	4.729	0.071	0.000	0.000	0.039	61.5	271.093	Cabauw, High pH, High NO_3, Low SO_4, Low RH
2	0.000	8.479	19.306	15.144	0.278	0.000	0.037	0.022	92.9	271.079	Cabauw, High pH, High NO_3, High SO_4, High RH
3	0.000	7.964	32.317	16.207	0.074	0.000	0.000	0.000	86.6	271.936	Cabauw, High pH, High NO_3, High SO_4, High RH
4	0.000	1.088	49.943	3.851	0.381	0.058	0.000	0.045	71.4	296.264	Cabauw, High pH, High NO_3, Low SO_4, Sulfate poor, Intermediate RH
5	0.000	2.037	0.589	0.043	0.010	0.000	0.000	0.0000	88.5	297.3	SOAS, Low pH, High SO4, Low NO_3, High RH
6	0.000	0.847	0.517	0.013	0.020	0.000	0.000	0.000	65.3	293.9	SOAS, Low pH, High SO4, Low NO_3, Low RH
7	0.000	2.150	1.136	0.060	0.010	0.000	0.000	0.000	69.0	300.5	SOAS, Low pH, High SO4, Low NO_3, Low RH
8	0.000	1.040	0.253	0.013	0.007	0.000	0.000	0.000	90.2	294	SOAS, Low pH, High SO4, Low NO_3, High RH
9	0.000	0.776	1.965	1.095	0.603	0.000	0.000	0.000	60.8	288.15	CalNex, Intermediate pH, Comparable SO_4, NO_3, Low RH, Low PM
10	0.000	6.430	6.178	33.384	4.355	0.000	0.000	0.000	54.0	298.45	CalNex, Intermediate pH, Comparable SO_4, NO_3, Low RH, High PM
11	0.000	3.130	3.672	11.086	0.369	0.000	0.000	0.0000	90.2	286.883	CalNex, Intermediate pH, Comparable SO_4, NO_3, High RH, High PM
12	0.000	0.878	0.847	3.751	0.502	0.000	0.000	0.000	90.8	286.85	CalNex, Intermediate pH, Comparable SO_4, NO_3, High RH, Low PM
13	0.000	0.059	0.058	0.057	0.000	0.000	0.000	0.000	0.603	277.42	WINTER, Low RH, High SO_4, low pH
14	0.000	0.001	0.001	0.002	0.000	0.000	0.000	0.000	0.646	264.91	WINTER, Low RH, Low SO_4, low pH
15	0.000	0.000	0.000	0.001	0.000	0.000	0.000	0.000	0.868	256.02	WINTER, High RH, High SO_4, low pH
16	0.000	0.041	0.005	0.096	0.000	0.000	0.000	0.000	0.801	275.51	WINTER, High RH, Low SO_4, low pH
17	0.041	0.106	2.223	0.202	0.227	0.030	0.030	0.001	0.612	298.25	Tianjin, Low RH, High SO_4
18	0.032	0.447	2.376	0.539	0.063	0.042	0.020	0.001	0.625	303.15	Tianjin, Low RH, Low SO_4
19	0.031	0.209	2.035	0.182	0.140	0.034	0.017	0.001	0.595	302.05	Tianjin, High RH, High SO_4
20	0.026	0.394	2.411	0.809	0.089	0.024	0.013	0.001	0.819	300.25	Tianjin, High RH, Low SO_4

Table S10. Locations used in the box model intercomparison and literature evaluating fine aerosol pH in CTMs.

Region/ Season	Specific Location(s)	Time	Observationally-constrained aerosol pH_F	CMAQ fine aerosol pH_F	GEOS-Chem fine aerosol pH_F	WRF-Chem pH_F
Southeast US Summer	Centreville, AL, USA; various	Summer 2013	0.9 ± 0.6 (a), 1.1 ± 0.4 (b)	1.6 ± 0.5 (i), 0.82 (j), 1.8 ± 1.0 (k), 0.9 ± 0.9 (l)	1.3 (o)	1.5 (r)
Eastern US Winter	Aircraft mission WINTER	February 2015	0.8 ± 1.0 (c)		1.3 (p)	
Los Angeles Basin Summer	Pasadena, CA, USA	May-June 2010	2.7 ± 0.3 (d)	3.0 ± 1.7 (i)		3.4 (r) 3.5 (s)
China Winter	Beijing, China	Winter	4.2 (e)	4.5 ± 0.8 (m)	4.3 ± 0.7 (q)	
China Summer	Tianjin, China	August 2015	3.4 ± 0.5 (f)	3.1 ± 1.5 (n)		
Netherlands	Cabauw	June, July, December 2012-2013	3.7 (g)	3.2 ± 0.7 (n)		
Mediterranean Summer/Fall	Finokalia, Crete	Aug- Nov 2012	1.25 ± 1.14 (h)	0.4 ± 1 (n)		

Data sources:
[a]Guo et al. (2015) SOAS Centreville, AL ground site ISORROPIA estimates
[b]Xu et al. (2016) SENEX aircraft summer 2013 ISORROPIA estimates
[c]Guo et al. (2016) WINTER 2015 aircraft campaign ISORROPIA estimates
[d]Guo et al. (2017a) PM2.5 for the last week of CalNex
[e]Guo et al. (2017b) Beijing PM1 ISORROPIA estimates
[f]Shi et al. (2019) ISORROPIA estimates
[g]Guo et al. (2018)
[h]Bougiatioti et al. (2016) excluding water associated with organics. pH=1.38 ± 1.1 including organic water.
[i]This work, CMAQv5.2 June 2016 predicted mean and standard deviation of hourly predictions (108×108km horizontal resolution)
[j]Vasilakos et al. (2018) CMAQ prediction for summer 2011 Centreville, AL
[k]Calculated from CMAQ simulations of Pye et al. (2018) for CTR June 2013 including nonvolatile cations
[l]Calculated from CMAQ simulations of Pye et al. (2018) for CTR June 2013 excluding nonvolatile cations
[m]This work, CMAQv5.2 February 2016 predicted mean and standard deviation
[n]This work, CMAQv5.2 annual average 2016
[o]Marais et al. (2016) SEAC4RS aircraft campaign predicted by GEOS-Chem
[p]Shah et al., (2018) WINTER 2015 aircraft campaign predicted by GEOS-Chem
[q]Shao et al. (~~2018~~2019) Beijing Autumn/Winter, mean and range, predicted by GEOS-Chem
[r]This work, WRF-Chem with MOSAIC LWC-weighted $PM_{2.5}$
[s]Knote et al. (2014) CALNex, CARES WRF-Chem simulation

Table S11. Select cloud pH measurements (See Table S8) and spatially-corresponding (vertically averaged) cloud pH from CTMs

Location	Latitude (°)	Longitude (°)	Altitude (km)	Time Period (observed)	Cloud/fog pH_F obs (mean)	Model[1]	Vertical average pH
Delta Barrage, Egypt	30.2	31.12		2015-2016	7.6	CAM-chem CMAQ	5.6 5.3
Mt. Boutmezguida, Morocco	29.2	-10.02	1.23	Nov 2013-Jun 2015	7.3	CAM-chem CMAQ	3.6 6.6
Mt. Tai, China	36.3	117.22	1.55	Jun-Aug 2015	4.9	CAM-chem CMAQ	4.4 4.6
Shanghai, China	31.3	121.48		2009-2010	6.0	CAM-chem CMAQ	4.2 4.3
Fresno, CA	36.83	-119.75		Jan 2010	6.7 (median)	CAM-chem CMAQ WRF-Chem	n/a 6.4 n/a
Whiteface Mtn, NY	44.4	-73.85	1.48	Aug-Sep 2014	4.8	CAM-chem CMAQ WRF-Chem	4.2 4.6 4.6
Po Valley, Italy	44.65	11.62		Nov 2013	4.6 (median)	CAM-chem CMAQ	n/a 5.3
Puy de Dome, France	48	2	1.46	2010-2013	5.6	CAM-chem CMAQ	4.1 5.2
Near Paris, France	48.7	2.2		2012-2013	5.2	CAM-chem CMAQ	4.1 4.6
Sundsbø, Norway	60.77	5.2		Fall 2011	5.0	CAM-chem CMAQ	4.8 4.6
California Marine Stratocumulus	36.98	-123.1	0.08 - 1.0	Summer aircraft flights between 2005 and 2018	4.4	CAM-chem CMAQ WRF-Chem	3.8 5.3 5.5

Notes:

[1]CAM-chem simulation time period is June 2015; CMAQ simulation time period is Jan-Dec 2016; WRF-Chem simulation time period is June 1-15, 2013;

References

Acker, K., D. Möller, D., W. Marquardt, W., E. Brüggemann, E., W. Wieprecht, W., R. Auel, R., and D. Kalaß, D: Atmospheric research program for studying changing emission patterns after German unification, Atmos. Environ., 32(20), 3435-3443, https://doi.org/10.1016/S1352-2310(98)00041-7, 1998a.

Acker, K., D. Möller, D., W. Wieprecht, W., D. Kalaß, D., and R. Auel, R.: Investigations of ground-based clouds at the Mt. Brocken, Fresenius', J. Anal. Chem., 361(1), 59-64, https://doi.org/10.1007/s002160050834, 1998b.

Adzuhata, T., J. Inotsume, J., T. Okamura, T., R. Kikuchi, R., T. Ozeki, T., M. Kajikawa, M., and N. Ogawa, N.: Evaluation of ionic pollutants of acid fog and rain using a factor analysis and back trajectories, Anal .Sci., 17(1), 71-76, https://doi.org/10.2116/analsci.17.71, 2001a.

Adzuhata, T., T. Okamura, T., J. Inotsume, J., R. Kikuchi, R., T. Ozeki, T., M. Kajikawa, M., and N. Ogawa, N.: Chemical characterization of acid fog and rain in northern Japan using back trajectory and oblique rotational factor analysis, Wat. Air Soil Pol., 130(1-4), 337-342, https://doi.org/10.1023/A:1013812613373, 2001b.

Ahmed, M., A. Hossain, A., T. Akther, T., M. Shohel, M., and A. Salam: Chemical Composition and Source Identification of Fog Water at an Indo-Gangetic Plain (IGP) Outflow Location (Coastal Bhola Island), Bangladesh, Journal of Environmental Pollution and ManagementJ. Env. Poll. Manag., 1, 104, **[Did not find DOI]**, 2018.

Aikawa, M., T. Hiraki, T., M. Shoga, M., and M. Tamaki, M.: Fog and precipitation chemistry at Mt. Rokko in Kobe, April 1997-March 1998, in: Acid rain Rain 2000, edited, pp. 1517-1522, Springer, https://doi.org/10.1023/A:1013945905410, 2001.

Aikawa, M., T. Hiraki, T., M. Shoga, M., and M. Tamaki, M.: Chemistry of fog water collected in the Mt. Rokko area (Kobe City, Japan) between April 1997 and March 2001, Wat. Air Soil Pol., 160(1-4), 373-393, https://doi.org/10.1007/s11270-005-3117-1, 2005.

Aikawa, M., T. Hiraki, T., and M. Tamaki, M.: Comparative field study on precipitation, throughfall, stemflow, fog water, and atmospheric aerosol and gases at urban and rural sites in Japan, Sci. Total. Environ.STOTEN, 366(1), 275-285, https://doi.org/10.1016/j.scitotenv.2005.06.027, 2006.

Aleksic, N., K. Roy, K., G. Sistla, G., J. Dukett, J., N. Houck, N., and P. Casson, P.: Analysis of cloud and precipitation chemistry at Whiteface Mountain, NY, Atmos. Environ., 43(17), 2709-2716, https://doi.org/10.1016/j.atmosenv.2009.02.053, 2009.

Ali, K., G. Momin, G., S. Tiwari, S., P. Safai, P., D. Chate, D., and P. Rao, P.: Fog and precipitation chemistry at Delhi, North India, Atmos. Environ., 38(25), 4215-4222, https://doi.org/10.1016/j.atmosenv.2004.02.055, 2004.

Ambade, B.: Characterization and source of fog water contaminants in central India, Nat. Hazards, 70(2), 1535-1552, https://doi.org/10.1007/s11069-013-0892-7, 2014.

Anastasio, C., and K. G.McGregor, K. G.: Chemistry of fog waters in California's Central Valley: 1. In situ photoformation of hydroxyl radical and singlet molecular oxygen, Atmos. Environ., 35(6), 1079-1089, https://doi.org/10.1016/S1352-2310(00)00281-8, 2001.

Anderson, D. E., and H. E. Landsberg, H. E.: Detailed structure of pH in hydrometeors, Environ. Sci. Technol., Env. Sci. Techn., 13(8), 992-994, https://doi.org/10.1021/es60156a010, 1979.

Anderson, J. B., R. E. Baumgardner, R. E., V. A. Mohnen, V. A., and J. J. Bowser, J. J.: Cloud chemistry in the eastern United States, as sampled from three high-elevation sites along the Appalachian Mountains, Atmos. Environ., 33(30), 5105-5114, https://doi.org/10.1016/S1352-2310(99)00193-4, 999.

Formatted: Font: Bold, Font color: Dark Red

Aneja, V. P., ~~C. S.~~ Claiborn, C. S., ~~R. L.~~ Bradow, R. L., ~~R. J.~~ Paur, R. J., and ~~R. E.~~ Baumgardner, R. E.: ~~-~~ Dynamic chemical characterization of montane clouds, Atmos. Environ., 24(3), 563-572, https://doi.org/10.1016/0960-1686(90)90011-B, 1990.

Aneja, V. P., ~~W. P.~~ Robarge, W. P., ~~C. S.~~ Claiborn, C. S., ~~A.~~ Murthy, A., ~~D.~~ Soo-Kim, D., ~~Z.~~ Li, Z., and ~~E. B.~~ Cowling, E. B.: ~~-~~ Chemical climatology of high elevation spruce-fir forests in the southern Appalachian Mountains, Environ. Pollut., ~~Env. Pol.,~~ 75(1), 89-96, https://doi.org/10.1016/0269-7491(92)90061-e, 1992.

Asbury, C. E., ~~W. H.~~ McDowell, W. H., ~~R.~~ Trinidad-Pizarro, R., and ~~S.~~ Berrios, S.: ~~-~~ Solute deposition from cloud water to the canopy of a Puerto Rican montane forest, Atmos. Environ., 28(10), 1773-1780, https://doi.org/10.1016/1352-2310(94)90139-2, 1994.

Baltensperger, U., Schwikowski, M., Jost, D., Nyeki, S., Gäggeler, H., and O. Poulida: Scavenging of atmospheric constituents in mixed phase clouds at the high-alpine site Jungfraujoch part I: Basic concept and aerosol scavenging by clouds, Atmos. Environ., 32(23), 3975-3983, https://doi.org/10.1016/S1352-2310(98)00051-X, 1998.

Bao, B.-T., J.-X. Shu, and B.-Q. Zhu: ~~-~~ Study on physicochemical properties of urban fog in Shanghai, Journal of Nanjing Institute of Meteorology, ~~J. Nanjing Inst. Met.,~~ 18(1), 114-118, **[Did not find DOI]**, 1995.

Barth, M., ~~D.~~ Hegg, D., ~~P.~~ Hobbs, P., ~~J.~~ Walega, J., ~~G.~~ Kok, G., ~~B.~~ Heikes, B., and ~~A.~~ Lazrus, A.: ~~-~~ Measurements of atmospheric gas-phase and aqueous-phase hydrogen peroxide concentrations in winter on the east coast of the United States, Tellus B, 41(1), 61-69, https://doi.org/10.3402/tellusb.v41i1.15049, 1989.

Bates, R. G., and Robinson, R. A.: Standardization of silver-silver chloride electrodes from 0 to 60°C, Journal of Solution Chemistry, 9, 455–456, 10.1007/BF00647735, 1980.~~Bates and Robinson, 1980 - Add~~

Battaglia, M. A., Douglas, S., and ~~-~~Hennigan, C. J.: Effect of the Urban Heat Island on Aerosol pH, Environ. Sci. Technol., ~~Env. Sci. Techn.,~~ 31, ~~-~~ https://doi.org/10.1021/acs.est.7b0278, https://doi.org/10.1021/acs.est.7b02786, 2017.

Baumgardner Jr., R. E., ~~S. S.~~ Isil, S. S., ~~T. F.~~ Lavery, T. F., ~~C. M.~~ Rogers, C. M., and ~~V. A.~~ Mohnen, V. A.: Estimates of cloud water deposition at mountain acid deposition program sites in the Appalachian Mountains, J. Air Waste Manage.~~JAWMA,~~ 53(3), 291-308, https://doi.org/10.1080/10473289.2003.10466153, 2003.

Behera, S. N., Betha, R., Liu, P., and Balasubramanian, R.: A study of diurnal variations of PM 2.5 acidity and related chemical species using a new thermodynamic equilibrium model, Sci. Total. Environ.,~~STOTEN,~~ 452–453, 286–295, ~~-~~ https://doi.org/10.1016/j.scitotenv.2013.02.062, ~~-~~, 2013.

Beiderwieden, E., ~~T.~~ Wrzesinsky, T., and ~~O.~~ Klemm, O.: ~~-~~ Chemical characterization of fog and rain water collected at the eastern Andes cordillera, Hydrol. Earth Syst. Sc.~~Hydr. and Earth Syst. Sci.~~ Disc., 2(3), 863-885, https://doi.org/10.5194/hess-9-185-2005, 2005.

Benedict, K. B., ~~T.~~ Lee, T., and ~~J. L.~~ Collett, J. L.: ~~-~~ Cloud water composition over the southeastern Pacific Ocean during the VOCALS regional experiment, Atmos. Environ., 46, 104-114, https://doi.org/10.1016/j.atmosenv.2011.10.029, 2012.

Błaś, M., ~~M.~~ Sobik, M., and ~~R.~~ Twarowski, R.: Changes of cloud water chemical composition in the Western Sudety Mountains, Poland, Atmos. Res., 87(3-4), 224-231, https://doi.org/10.1016/j.atmosres.2007.11.004, 2008.

Błaś, M., Polkowska, Ż., Sobik, M., Klimaszewska, K., Nowiński, K., and Namieśnik, J.: Fog water chemical composition in different geographic regions of Poland, Atmos. Res., 95(4), 455-469, https://doi.org/10.1016/j.atmosres.2009.11.008, 2010.

Formatted: Font: Not Bold, Font color: Auto

Boris, A., T. Lee, T., T. Park, T., J. Choi, J., S. Seo, S., and J. Collett Jr., J.: Fog composition at Baengnyeong Island in the eastern Yellow Sea: detecting markers of aqueous atmospheric oxidations, Atmos. Chem. Phys., 16(2), 437-453, https://doi.org/10.5194/acp-16-437-2016, 2016.

Boris, A. J., D. C., Napolitano, D. C., P. Herckes, P., A. L. Clements, A. L., and J. L. Collett Jr. J. L.: Fogs and Air Quality on the Southern California Coast, Aerosol Air Qual. Res., Aeros. Air Qual. Res., 18(1), 224-239, https://doi.org/10.4209/aaqr.2016.11.0522, 2018.

Bormann, B., R. Tarrant, R., M. McClellan, M., and T. Savage, T.: Chemistry of rainwater and cloud water at remote sites in Alaska and Oregon, J. Env. Qual., 18(2), 149-152, https://doi.org/10.2134/jeq1989.00472425001800020003x, 1989.

Borys, R., D. Lowenthal, D., M. Wetzel, M., F. Herrera, F., A. Gonzalez, A., and J. Harris, J.: Chemical and microphysical properties of marine stratiform cloud in the North Atlantic, J. Geophs. Res., 103(D17), 22073-22085, https://doi.org/10.1029/98JD02087, 1998.

Bougiatioti, A., Nikolaou, P., Stavroulas, I., Kouvarakis, G., Weber, R., Nenes, A., Kanakidou, M., and Mihalopoulos, N.: Particle water and pH in the eastern Mediterranean: Source variability and implications for nutrient availability, Atmos. Chem. Phys., 16, 4579–4591, https://doi.org/10.5194/acp-16-4579-201, 2016.

Brantner, B., H. Fierlinger, H., H. Puxbaum, H., and A. Berner, A.: Cloudwater chemistry in the subcooled droplet regime at Mount Sonnblick (3106 m asl, Salzburg, Austria), Water Air Soil PollWater, Air, and Soil Pol., 74(3-4), 363-384, https://doi.org/10.1007/BF00479800, 1994.

Brege, M., M. Paglione, M., S. Gilardoni, S., S. Decesari, S., M. C. Facchini, M. C., and L. R. Mazzoleni, L. R.: Molecular insights on aging and aqueous-phase processing from ambient biomass burning emissions-influenced Po Valley fog and aerosol, Atmos. Chem. Phys., 18(17), 13197-13214, https://doi.org/10.5194/acp-18-13197-2018, 2018.

Bressan, D. J., and R. E. Larson, R. E.: The history of air forming various marine fogs off Nova Scotia in August 1975, J. Geophs. Res., 84(C4), 1746-1754, https://doi.org/10.1029/JC084iC04p01746, 1979.

Brewer, R. L., R. J. Gordon, R. J., L. S. Shepard, L. S., and E. C. Ellis, E. C.: Chemistry of mist and fog from the Los Angeles urban area, Atmos. Environ. (1967), 17(11), 2267-2270, https://doi.org/10.1016/0004-6981(83)90224-X, 1983.

Bridges, K., T. Jickells, T., T. Davies, T., Z. Zeman, Z., and I. Hunova, I.: Aerosol, precipitation and cloud water chemistry observations on the Czech Krusne Hory plateau adjacent to a heavily industrialised valley, Atmos. Environ., 36(2), 353-360, https://doi.org/10.1016/S1352-2310(01)00388-0, 2002.

Brüggemann, E., T. Gnauk, T., S. Mertes, S., K. Acker, K., R. Auel, R., W. Wieprecht, W., D. Möller, D., J. Collett Jr., J., H. Chang, H., and D. Galgon, D.: Schmücke hill cap cloud and valley stations aerosol characterisation during FEBUKO (I): Particle size distribution, mass, and main components, Atmos. Environ., 39(23-24), 4291-4303, https://doi.org/10.1016/j.atmosenv.2005.02.013, 2005.

Buck, R. P., Rodini, S., Covington, A. K., et al.:Baucke, F. G. K., Brett, C. M., Camoes, M. F., Milton, M. J. T., Mussini, T., Naumann, R., Pratt, K. W., Spitzer, P., and Wilson, G. S.: Measurement of pH. Definition, Standards, and Procedures, Pure and Applied Chemistry, 74(11), 2169–2200, https://doi.org/10.1351/pac200274112169 ,2002.

Budhavant, K., P. Rao, P., P. Safai, P., L. Granat, L., and H. Rodhe, H.: Chemical composition of the inorganic fraction of cloud-water at a high altitude station in West India, Atmos. Environ., 88, 59-65, https://doi.org/10.1016/j.atmosenv.2014.01.039, 2014.

Formatted: Font: (Default) Times New Roman, 10 pt, Not Bold

Burkard, R., P. Bützberger, P., and W. Eugster, W.: Vertical fogwater flux measurements above an elevated forest canopy at the Lägeren research site, Switzerland, Atmos. Environ., 37(21), 2979-2990, https://doi.org/10.1016/S1352-2310(03)00254-1, 2003.

Burkhard, E., V. A. Dutkiewicz, V. A., and L. Husain, L.: A study of SO2, SO42− and trace elements in clear air and clouds above the midwestern United States, Atmos. Environ., 28(8), 1521-1533, https://doi.org/10.1016/1352-2310(94)90211-9, 1994.

Błaś, M., Ż. Polkowska, M. Sobik, K. Klimaszewska, K. Nowiński, and J. Namieśnik: Fog water chemical composition in different geographic regions of Poland, Atmos. Res., 95(4), 455-469, 2010.

Capel, P. D., R. Gunde, R., F. Zuercher, F., and W. Giger, W.: Carbon speciation and surface tension of fog, Environ. Sci. Technol., Env. Sci. Techn., 24(5), 722-727, https://doi.org/10.1021/es00075a017, 1990.

Castillo, R., J. Kadlecek, and S. McLaren: Selected Whiteface Mountain cloud water concentrations summers 1981 and 1982, Wat. Air Soil Pol., 24(3), 323-328, 1985.

Castillo, R. A., J. E. Jiusto, J. E., and E. Mclaren, E.: The pH and ionic composition of stratiform cloud water, Atmos. Environ. (1967), 17(8), 1497-1505, https://doi.org/10.1016/0004-6981(83)90303-7, 1983.

Castillo, R., J. Kadlecek, J., and S. McLaren, S.: Selected Whiteface Mountain cloud water concentrations summers 1981 and 1982, Wat. Air Soil Pol., 24(3), 323-328, https://doi.org/10.1007/BF00161791, 1985.

Chakraborty, A., B. Ervens, B., T. Gupta, T., and S. N. Tripathi, S. N.: Characterization of organic residues of size-resolved fog droplets and their atmospheric implications, J. Geophs. Res., 121(8), 4317-4332, https://doi.org/10.1002/2015JD024508, 2016.

Chung, Y., H. Kim, and M. Yoon: Observations of visibility and chemical compositions related to fog, mist and haze in south Korea, Wat. Air Soil Pol., 111(1-4), 139-157, 1999.

Cheng, C., Wang, G., Meng, J., Wang, Q., Cao, J., Li, J., and Wang, J: Size-resolved airborne particulate oxalic and related secondary organic aerosol species in the urban atmosphere of Chengdu, China, Atmos. Res., 161–162, 134–142., https://doi.org/10.1016/j.atmosres.2015.04.010, 2015.

Cheng, S., Yang, L., Zhou, X., Xue, L., and Gao, X: Size-fractionated water-soluble ions, situ pH and water content in aerosol on hazy days and the in fl uences on visibility impairment in Jinan, China, Atmos. Environ., 45, 4631–4640., https://doi.org/10.1016/j.atmosenv.2011.05.057, 2011.

Cheng, Y., Zheng, G., Wei, C., Mu, Q., Zheng, B., Wang, Z., Gao, M., Zhang, Q., He, K., Carmichael, G., Pöschl, U., Su, H., and Asia, E: Reactive nitrogen chemistry in aerosol water as a source of sulfate during haze events in China., Science. Advances., 2, e1601530, 1–11, https://doi.org/10.1002/2015JD024508 2016.

Chung, Y., H. Kim, H., and M. Yoon, M.: Observations of visibility and chemical compositions related to fog, mist and haze in south Korea, Wat. Air Soil Pol., 111(1-4), 139-157, https://doi.org/10.1023/A:1005077415764, 1999.

Cini, R., F. Prodi, F., G. Santachiara, G., F. Porcu, F., S. Bellandi, S., A. Stortini, A., C. Oppo, C., R. Udisti, R., and F. Pantani, F.: Chemical characterization of cloud episodes at a ridge site in Tuscan Appennines, Italy, Atmos. Res., 61(4), 311-334, https://doi.org/10.1016/S0169-8095(01)00139-9, 2002.

Clark, K. L., N. M. Nadkarni, N. M., D. Schaefer, D., and H. L. Gholz, H. L.: Cloud water and precipitation chemistry in a tropical montane forest, Monteverde, Costa Rica, Atmos. Environ., 32(9), 1595-1603, https://doi.org/10.1016/S1352-2310(97)00384-1, 1998.

Clifton, C. L., Alstein, N., and Huie, R. E.: Rate constant for the reaction of nitrogen dioxide with sulfur (IV) over the pH range 5.3-13, Environ. Sci. Technol., 22(5), 586-589, https://doi.org/10.1021/es00170a018, 1988.

~~Clifton (1988) Add~~

Collett Jr., J., ~~B.~~ Daube Jr., B. ~~J. W.~~ Munger, J. W., and ~~M. R.~~ Hoffmann, M. R.: Cloud water chemistry in Sequoia National Park, Atmos. Environ., 23(5), 999-1007, https://doi.org/10.1016/0004-6981(89)90303-X, 1989.

Collett Jr., J. L., ~~B. C.~~ Daube Jr., B. C., ~~D.~~ Gunz, D., and ~~M. R.~~ Hoffmann, M. R.: Intensive studies of Sierra Nevada cloudwater chemistry and its relationship to precursor aerosol and gas concentrations, Atmos. Environ., 24(7), 1741-1757, https://doi.org/10.1016/0960-1686(90)90507-J, 1990a.

Collett Jr., J. L., ~~B. C.~~ Daube Jr., B. C., and ~~M. R.~~ Hoffmann, M. R.: The chemical composition of intercepted cloudwater in the Sierra Nevada, Atmos. Environ., 24(4), 959-972, https://doi.org/10.1016/0960-1686(90)90298-2, 1990b.

Collett Jr., J., ~~B.~~ Oberholzer, B., and ~~J.~~ Staehelin, J.: Cloud chemistry at Mt Rigi, Switzerland: dependence on drop size and relationship to precipitation chemistry, Atmos. Environ., 27(1), 33-42, https://doi.org/10.1016/0960-1686(93)90068-A, 1993.

Collett Jr., J. L., ~~K. J.~~ Hoag, K. J., ~~D. E.~~ Sherman, D. E., ~~A.~~ Bator, A., and ~~L. W.~~ Richards, L. W.: Spatial and temporal variations in San Joaquin Valley fog chemistry, Atmos. Environ., 33(1), 129-140, https://doi.org/10.1016/S1352-2310(98)00136-8, 1998.

Collett Jr., J. L., ~~K. J.~~ Hoag, K. J., ~~X.~~ Rao, X., and ~~S. N.~~ Pandis, S. N.: Internal acid buffering in San Joaquin Valley fog drops and its influence on aerosol processing, Atmos. Environ., 33(29), 4833-4847, https://doi.org/10.1016/S1352-2310(99)00221-6, 1999.

Collett Jr, J. L., ~~A.~~ Bator, A., ~~D. E.~~ Sherman, D. E., ~~K. F.~~ Moore, K. F., ~~K. J.~~ Hoag, K. J., ~~B. B.~~ Demoz, B. B., ~~X.~~ Rao, X., and ~~J. E.~~ Reilly, J. E.: The chemical composition of fogs and intercepted clouds in the United States, Atmos. Res., 64(1-4), 29-40, https://doi.org/10.1016/S0169-8095(02)00077-7, 2002.

~~Collett Jr, J. L., B. C. Daube Jr, D. Gunz, and M. R. Hoffmann: Intensive studies of Sierra Nevada cloudwater chemistry and its relationship to precursor aerosol and gas concentrations, Atmos. Environ., 24(7), 1741-1757, 1990a.~~

~~Collett Jr, J. L., B. C. Daube Jr, and M. R. Hoffmann: The chemical composition of intercepted cloudwater in the Sierra Nevada, Atmos. Environ., 24(4), 959-972, 1990b.~~

~~Collett Jr, J. L., K. J. Hoag, X. Rao, and S. N. Pandis: Internal acid buffering in San Joaquin Valley fog drops and its influence on aerosol processing, Atmos. Environ., 33(29), 4833-4847, 1999.~~

~~Collett Jr, J. L., K. J. Hoag, D. E. Sherman, A. Bator, and L. W. Richards: Spatial and temporal variations in San Joaquin Valley fog chemistry, Atmos. Environ., 33(1), 129-140, 1998.~~

Cook, R. D., ~~Y.-H.~~ Lin, Y.-H., ~~Z.~~ Peng, Z., ~~E.~~ Boone, E., ~~R. K.~~ Chu, R. K., ~~J. E.~~ Dukett, J. E., ~~M. J.~~ Gunsch, M. J., ~~W.~~ Zhang, W., ~~N.~~ Tolic, N., and ~~A.~~ Laskin, A.: Biogenic, urban, and wildfire influences on the molecular composition of dissolved organic compounds in cloud water, Atmos. Chem. Phys., 17(24), 15167-15180, https://doi.org/10.5194/acp-17-15167-2017, 2017.

Formatted: Font: 10 pt, Bold, Font color: Dark Red

Formatted: Font: 10 pt, Bold, Font color: Dark Red

Formatted: Space After: 10 pt

Formatted: Font: Bold, Font color: Dark Red

Formatted: Font: Bold, Font color: Dark Red

Corell, D.: Fog and rain water chemistry in the western Mediterranean basin (Valencia region, Spain), 5th International Conference on Fog, Fog Collection and Dew, Münster, Germany, 25–30 July, [Did not find DOI], 2010.

Covington, A. K., Bates, R. G., and Durst, R. A.: Definition of pH scales, standard reference values, measurement of pH and related terminology, Pure and Applied Chemistry, Pure Appl. Chem. 57(3):531-542, https://doi.org/10.1351/pac198355091467, 1985.

Craig, R. L., Peterson, P. K., Nandy, L., Lei, Z., Hossain, M. A., Camarena, S., Dodson, R. A., Cook, R. D., Dutcher, C. S., and Ault, A. P.: Direct Determination of Aerosol pH: Size-Resolved Measurements of Submicrometer and Supermicrometer Aqueous Particles, Anal. Chem., https://doi.org/10.1021/acs.analchem.8b00586, 2018.

Dall'Osto, M., Airs, R. L., Beale, R., Cree, C., Fitzsimons, M. F., Beddows, D., Harrison, R. M., Ceburnis, D., Dowd, C. O., Rinaldi, M., Paglione, M., Nenes, A., Decesari, S., and Simo, R.: Simultaneous Detection of Alkylamines in the Surface Ocean and Atmosphere of the Antarctic Sympagic Environment., ACS Earth andSpace Chemistry, 3, 854-862, https://doi.org/10.1021/acsearthspacechem.9b00028, 2019.

Dasch, J. M.: Hydrological and chemical inputs to fir trees from rain and clouds during a 1-month study at Clingmans Peak, NC, Atmos. Environ., 22(10), 2255-2262, https://doi.org/10.1016/0004-6981(89)90194-7, 1988.

Daum, P., S. Schwartz, S., and L. Newman, L.: Acidic and related constituents in liquid water stratiform clouds, J. Geophs. Res., 89(D1), 1447-1458, https://doi.org/10.1029/JD089iD01p01447, 1984.

DeFelice, T.: Investigation of wet acidic deposition episodes capable of damaging red spruce in the Mt. Mitchell State Park, Atmos. Res., 43(4), 325-344, https://doi.org/10.1016/S0169-8095(96)00042-7, 1997.

Degefie, D., T. S. El-Madany, T.-S., M. Held, M., J. Hejkal, J., E. Hammer, E., J. C. Dupont, J.-C., M. Haeffelin, M., E. Fleischer, E., and O. Klemm, O.: Fog chemical composition and its feedback to fog water fluxes, water vapor fluxes, and microphysical evolution of two events near Paris, Atmos. Res., 164, 328-338, https://doi.org/10.1016/j.atmosres.2015.05.002, 2015.

Deguillaume, L., T. Charbouillot, T., M. Joly, M., M. Vaïtilingom, M., M. Parazols, M., A. Marinoni, A., P. Amato, P., A. M. Delort, A.-M., V. Vinatier, V., and A. Flossmann, A.: Classification of clouds sampled at the puy de Dôme (France) from 10 yr monitoring: mean features of their physico-chemical properties, Atmos. Chem. Phys. Disc., 13(8), https://doi.org/10.5194/acp-14-1485-2014, 2013.

Deininger, C., and V. Saxena, V.: A validation of back trajectories of air masses by principal component analysis of ion concentrations in cloud water, Atmos. Environ., 31(2), 295-300, https://doi.org/10.1016/1352-2310(96)00152-5, 1997.

Deutsch, F., P. Hoffmann, P., and H. Ortner, H.: Field experimental investigations on the Fe (II)-and Fe (III)-content in cloudwater samples, J. Atmos. Chem., 40(1), 87-105, https://doi.org/10.1023/A:1010684628804, 2001.

Ding, G.-A., X. M. Ji, X.-M., X. M. Fang, X.-M., J. M. Fu, J.-M., F. Wu, F., W. H. Su, W.-H., W. Z. Song, W.-Z., W. Li, W., X. R. Yu, X.-R., and Z. F. Jiang, Z.-F.: Characters of cloud-fog in Lu Shan mountain, Acta Meteorol. Sin.ACTA Met. Sinica, 49(2), 190-197, https://doi.org/10.11676/qxxb1991.027, 1991.

Ding, J., Zhao, P., Su, J., Dong, Q., Du, X., and Zhang, Y: Aerosol pH and its driving factors in Beijing, Atmos. Chem. Phys., 19, 7939–7954, https://doi.org/10.5194/acp-19-7939-2019, 2019.

Dodson, L. L., and J. Bargach, J.: Harvesting Fresh Water from Fog in Rural Morocco: Research and Impact Dar Si Hmad's Fogwater Project in Aït Baamrane, Procedia EngineeringProcedia Eng., 107, 186-193, https://doi.org/10.1016/j.proeng.2015.06.073, 2015.

Dutkiewicz, V. A., E. Burkhard, E. M. Hussain, M., and L. Husain, L.: Scavenging and solubility of trace element bearing aerosols in frontal clouds at Whiteface Mountain, NY, Atmos. Res., 41(3-4), 337-348, https://doi.org/10.1016/0169-8095(96)00018-X, 1996.

Eckardt, F. D., and R. S. Schemenauer, R. S.: Fog water chemistry in the Namib Desert, Namibia, Atmos. Environ., 32(14-15), 2595-2599, https://doi.org/10.1016/S1352-2310(97)00498-6, 1998.

Ehrenhauser, F. S., K. Khadapkar, K., Y. Wang, Y., J. W. Hutchings, J. W., O. Delhomme, O., R. R. Kommalapati, R. R., P. Herckes, P., M. J. Wornat, M. J., and K. T. Valsaraj, K. T.: Processing of atmospheric polycyclic aromatic hydrocarbons by fog in an urban environment, J. Environ. Monitor., 14(10), 2566-2579, https://doi.org/10.1039/C2EM30336A, 2012.

Elias, V., and M. Tesar, M.: Cloud-water chemistry and estimated rates of occult deposition in a forested area of the Sumava Mts (south Bohemia, Czech Republic), Ser. Proc. Rep. - Int. Assoc. Hyd. Sci., 221, 417-424, **[Did not find DOI]**, 1994.

Elias, V., M. Tesar, M. and J. Buchtele, J.: Occult precipitation: sampling, chemical analysis and process modelling in the Sumava Mts., (Czech Republic) and in the Taunus Mts. (Germany), J. Hydrol., 166(3-4), 409-420, https://doi.org/10.1016/0022-1694(94)05096-G, 1995.

Erel, Y., S. O. Pehkonen, S. O., and M. R. Hoffmann, M. R.: Redox chemistry of iron in fog and stratus clouds, J. Geophs. Res., 98(D10), 18423-18434, http://doi.org/10.1029/93JD01575, 1993.

Ervens, B., Y. Wang, Y., J. Eagar, J., W. R. Leaitch, W. R., A. M. Macdonald, A. M., K. T. Valsaraj, K. T., and P. Herckes, P.: Dissolved organic carbon (DOC) and select aldehydes in cloud and fog water: the role of the aqueous phase in impacting trace gas budgets, Atmosp. Chem. Phys., 13(10), 5117-5135, https://doi.org/10.5194/acp-13-5117-2013, 2013.

Facchini, M. C., J. Lind, J., G. Orsi, G., and S. Fuzzi, S.: Chemistry of carbonyl compounds in Po Valley fog water, Sci. Total. Environ., STOTEN, 91, 79-86, https://doi.org/10.1016/0048-9697(90)90289-7, 1990.

Facchini, M. C., S. Fuzzi, S., S. Zappoli, S., A. Andracchio, A., A. Gelencsér, A., G. Kiss, G., Z. Krivácsy, Z., E. Mészáros, E., H. C. Hansson, H. C., and T. Alsberg, T.: Partitioning of the organic aerosol component between fog droplets and interstitial air, J. Geophs. Res., 104(D21), 26821-26832, https://doi.org/10.1029/1999JD900349, 1999.

~~Facchini, M. C., J. Lind, G. Orsi, and S. Fuzzi: Chemistry of carbonyl compounds in Po Valley fog water, STOTEN, 91, 79-86, 1990.~~

Falconer, R., and P. Falconer, P.: Determination of cloud water acidity at a mountain observatory in the Adirondack Mountains of New York State, J. Geophs. Res., 85(C12), 7465-7470, https://doi.org/10.1029/JC085iC12p07465, 1980.

Fang, T., Guo, H., Zeng, L., Verma, V., Nenes, A., and Weber, R. J.: Highly acidic ambient particles, soluble metals and oxidative potential: A link between sulfate and aerosol toxicity, Environ. Sci. Technol., 1–27, https://doi.org/10.1021/acs.est.6b06151, 2017.

Ferek, R. J., Lasrus, A. L., Haagenson, P. L., and Winchester, J. W.: Strong and Weak Acidity of Aerosols Collected over the Northeastern United States, Environ. Sci. Technol., Env. Sci. Tech., 17, 315–324, https://doi.org/10.1021/es00112a003, 1983.

Fernández-González, R., I. Yebra-Pimentel, I., E. Martínez-Carballo, E., J. Simal-Gándara, J., and X. Pontevedra-Pombal, X.: Atmospheric pollutants in fog and rain events at the northwestern mountains of the Iberian Peninsula, Sci. Total. Environ., STOTEN, 497, 188-199, https://doi.org/10.1016/j.scitotenv.2014.07.093, 2014.

Fisak, J., Tesar, M., Rezacova, D., Elias, V., Weignerova, V., and Fottova, D.: Pollutant concentrations in fog and low cloud water at selected sites of the Czech Republic, Atmos. Res., 64(1-4), 75-87, https://doi.org/10.1016/S0169-8095(02)00081-9, 2002.

Fisak, J., Stoyanova, V., Chaloupecký, P., Řezáčová, D., Tsacheva, T., Kupenova, T., and Marinov, M.: Soluble and insoluble pollutants in fog and rime water samples, Soil Water Res., 4, S123-S130, https://doi.org/10.17221/473-SWR, 2009a.

Fisak, J., V. Stoyanova, V., M. Tesar, M., P. Petrova, P., N. Daskalova, N., T. Tsacheva, T., and M. Marinov, M.: The pollutants in rime and fog water and in air at Milesovka Observatory (Czech Republic), Biologia, 64(3), 492-495, https://doi.org/10.2478/s11756-009-0080-0, 2009b.

Fisak, J., M. Tesar, D. Rezacova, V. Elias, V. Weignerova, and D. Fottova: Pollutant concentrations in fog and low cloud water at selected sites of the Czech Republic, Atmos. Res., 64(1-4), 75-87, 2002.

Fišák, J., V. Stoyanova, P. Chaloupecký, D. Řezáčová, T. Tsacheva, T. Kupenova, and M. Marinov: Soluble and insoluble pollutants in fog and rime water samples, Soil Water Res, 4, S123-S130, 2009.

Fowler, D., I. Leith, I., J. Binnie, J., A. Crossley, A., D. Inglis, D., T. Choularton, T., M. Gay, M., J. Longhurst, J., and D. Conland, D.: Orographic enhancement of wet deposition in the United Kingdom: continuous monitoring, Wat. Air Soil Pol., 85(4), 2107-2112, https://doi.org/10.1007/BF01186145, 1995.

Fridlind, A. M., and Jacobson, M. Z.: A study of gas-aerosol equilibrium and aerosol pH in the remote marine boundary layer during the First Aerosol Characterization Experiment (ACE 1), J. Geophs. Res., 105, 17325–17340, https://doi.org/10.1029/2000JD900209, 2000.

Fuhrer, J.: Chemistry of fogwater and estimated rates of occult deposition in an agricultural area of Central Switzerland, Agr. Ecosyst. Environ.Agr. Eco. Env., 17(3-4), 153-164, https://doi.org/10.1016/0167-8809(86)90038-1, 1986.

Fuzzi, S., G. Orsi, G., and M. Mariotti, M.: Radiation fog liquid water acidity at a field station in the Po Valley, J. Aerosol. Sci., 14(2), 135-138, https://doi.org/10.1016/0021-8502(83)90037-X, 1983.

Fuzzi, S., R. A. Castillo, R. A., J. E. Jiusto, J. E., and G. G. Lala, G. G.: Chemical composition of radiation fog water at Albany, New York, and its relationship to fog microphysics, J. Geophs. Res., 89(D5), 7159-7164, https://doi.org/10.1029/JD089iD05p07159, 1984.

Fuzzi, S., Orsi, G., and Mariotti, M.: Wet deposition due to fog in the Po Valley, Italy, J. Atmos. Chem., 3(2), 289-296, https://doi.org/10.1007/BF00210501, 1985.

Fuzzi, S.: Fog chemistry and deposition in the Po Valley, Italy, in: Acid deposition at high elevation sites, edited, pp. 443-452, Springer, https://doi.org/10.1007/978-94-009-3079-7_25, 1988.

Fuzzi, S., R. A. Castillo, J. E. Jiusto, and G. G. Lala: Chemical composition of radiation fog water at Albany, New York, and its relationship to fog microphysics, J. Geoph. Res., 89(D5), 7159-7164, 1984.

Fuzzi, S., M. Facchini, M., G. Orsi, G., J. Lind, J., W. Wobrock, W., M. Kessel, M., R. Maser, R., W. Jaeschke, W., K. Enderle, K., and B. Arends, B.: The Po valley fog experiment 1989, Tellus B, 44(5), 448-468, https://doi.org/10.1034/j.1600-0889.1992.t01-4-00002.x, 1992a.

Fuzzi, S., M. C. Facchini, M. C., G. Orsi, G., and D. Ferri, D.: Seasonal trend of fog water chemical composition in the Po Valley, Environ, Pollut., 75(1), 75-80, https://doi.org/10.1016/0269-7491(92)90059-j, 1992b.

Fuzzi, S., M. C. Facchini, M. C., G. Orsi, G., G. Bonforte, G., W. Martinotti, W., G. Ziliani, G., P. Mazzalit, P., P. Rossi, P., P. Natale, P., and M. M. Grosa, M. M.: The NEVALPA project: a regional network for fog chemical climatology over the Po valley basin, Atmos. Environ., 30(2), 201-213, https://doi.org/10.1016/1352-2310(95)00298-D, 1996.

Fuzzi, S., M. C. Facchini, G. Orsi, and D. Ferri: Seasonal trend of fog water chemical composition in the Po Valley, Env. Poll., 75(1), 75-80, 1992b.

Fuzzi, S., P. Mandrioli, P., and A. Perfetto, A.: Fog droplets—an atmospheric source of secondary biological aerosol particles, Atmos. Environ., 31(2), 287-290, https://doi.org/10.1016/1352-2310(96)00160-4, 1997.

Fuzzi, S., G. Orsi, and M. Mariotti: Radiation fog liquid water acidity at a field station in the Po Valley, J. Aer. Sci., 14(2), 135-138, 1983.

Fuzzi, S., G. Orsi, and M. Mariotti: Wet deposition due to fog in the Po Valley, Italy, J. Atmos. Chem., 3(2), 289-296, 1985.

Ganor, E., Z. Levin, Z., and D. Pardess, D.: Determining the acidity and chemical composition of fog, haze and cloud droplets in Israel, Atmos. Environ., 27(12), 1821-1832, https://doi.org/10.1016/0960-1686(93)90287-9, 1993.

Ghauri, B. M., M. I. Mirza, M. I., R. Richter, R., V. A. Dutkiewicz, V. A., A. Rusheed, A., A. R. Khan, A. R., and L. Husain, L.: Composition of aerosols and cloud water at a remote mountain site (2.8 kms) in Pakistan, Chemosphere, 3(1), 51-63, https://doi.org/10.1016/S1465-9972(00)00038-6, 2001.

Gillett, R., and G. Ayers, G.: Maritime cloudwater acidity near Tasmania, Clean Air, 23(3), 106-109, **[Did not find DOI]**, 1989.

Giannoni, S. M., R. Rollenbeck, R., P. Fabian, P., and J. Bendix, J.: Complex topography influences atmospheric nitrate deposition in a neotropical mountain rainforest, Atmos. Environ., 79, 385-394, https://doi.org/10.1016/j.atmosenv.2013.06.023, 2013.

Giannoni, S. M., K. Trachte, K., R. Rollenbeck, R., L. Lehnert, L., J. Fuchs, J., and J. Bendix, J.: Atmospheric salt deposition in a tropical mountain rainforest at the eastern Andean slopes of south Ecuador–Pacific or Atlantic origin?, Atmos. Chem. Phys., 16(15), 10241-10261, https://doi.org/10.5194/acp-16-10241-2016, 2016.

Gioda, A., O. L. Mayol-Bracero, O. L., F. Morales-García, F., J. Collett, J., S. Decesari, S., L. Emblico, L., M. C. Facchini, M. C., R. J. Morales-De Jesús, R. J., S. Mertes, S., and S. Borrmann, S.: Chemical composition of cloud water in the Puerto Rican tropical trade wind cumuli, Wat. Air Soil Pol., 200(1-4), 3-14, https://doi.org/10.1007/s11270-008-9888-4, 2009.

Gioda, A., G. J. Reyes-Rodríguez, G. J., G. Santos-Figueroa, G., J. L. Collett, J. L., S. Decesari, S., M. d. C. K. Ramos, M. d. C. K., H. J. Bezerra Netto, H. J., F. R. de Aquino Neto, F. R., and O. L. Mayol-Bracero, O. L.: Speciation of water-soluble inorganic, organic, and total nitrogen in a background marine environment: Cloud water, rainwater, and aerosol particles, J. Geophs. Res., 116(D5), https://doi.org/10.1029/2010JD015010, 2011.

Gioda, A., O. L. Mayol-Bracero, O. L., F. N. Scatena, F. N., K. C. Weathers, K. C., V. L. Mateus, V. L., and W. H. McDowell, W. H.: Chemical constituents in clouds and rainwater in the Puerto Rican rainforest: potential sources and seasonal drivers, Atmos. Environ., 68, 208-220, https://doi.org/10.1016/j.atmosenv.2012.11.017, 2013.

~~Gioda, A., G. J. Reyes-Rodríguez, G. Santos-Figueroa, J. L. Collett, S. Decesari, M. d. C. K. Ramos, H. J. Bezerra Netto, F. R. de Aquino Neto, and O. L. Mayol-Bracero: Speciation of water-soluble inorganic, organic, and total nitrogen in a background marine environment: Cloud water, rainwater, and aerosol particles, J. Geoph. Res., 116(D5), 2011.~~

Giulianelli, L., ~~S.~~ Gilardoni, S., ~~L.~~ Tarozzi, L., ~~M.~~ Rinaldi, M., ~~S.~~ Decesari, S., ~~C.~~ Carbone, C., ~~M.~~ Facchini, M., and ~~S.~~ Fuzzi, S.: Fog occurrence and chemical composition in the Po valley over the last twenty years, Atmos. Environ., 98, 394-401, https://doi.org/10.1016/j.atmosenv.2014.08.080, 2014.

Glotfelty, D. E., ~~M. S.~~ Majewski, M. S., and ~~J. N.~~ Seiber, J. N.: ~~.~~ Distribution of several organophosphorus insecticides and their oxygen analogs in a foggy atmosphere, Environ. Sci. Technol., ~~Env. Sci. Techn.,~~ 24(3), 353-357, https://doi.org/10.1021/es00073a010, 1990.

Gordon, C. A., ~~R.~~ Herrera, R., and ~~T. C.~~ Hutchinson, T. C.: ~~.~~ Studies of fog events at two cloud forests near Caracas, Venezuela—II. Chemistry of fog, Atmos. Environ., 28(2), 323-337, https://doi.org/10.1016/1352-2310(94)90108-2, 1994.

Gundel, L., ~~W.~~ Benner, W., and ~~A.~~ Hansen, A.: Chemical composition of fog water and interstitial aerosol in Berkeley, California, Atmos. Environ., 28(16), 2715-2725, https://doi.org/10.1016/1352-2310(94)90443-X, 1994.

Guo, H., Xu, L., Bougiatioti, A., Cerully, K. M., Capps, S. L., Hite, J. R., Carlton, A. G., Lee, S. H., Bergin, M. H., Ng, N. L., Nenes, A., and Weber, R. J.: Fine-particle water and pH in the southeastern United States, Atmos. Chem. Phys., 15, 5211–5228, https://doi.org/10.5194/acp-15-5211-2015, 2015.

Guo, H., Liu, J., Froyd, K. D., Roberts, J. M., Veres, P. R., Hayes, P. L., Jimenez, J. L., Nenes, A., and Weber, R. J.: Fine particle pH and gas – particle phase partitioning of inorganic species in Pasadena, California, during the 2010 CalNex campaign, Atmos. Chem. Phys., 17, 5703–5719, https://doi.org/10.5194/acp-17-5703-2017, 2017a.

Guo, H., Weber, R. J., and Nenes, A.: High levels of ammonia do not raise fine particle pH sufficiently to yield nitrogen oxide-dominated sulfate production, Sci. Rep., 1–7, https://doi.org/10.1038/s41598-017-11704-0, 2017b.

Guo, H., Otjes, R., Schlag, P., Kiendler-~~scharr~~Scharr, A., Nenes, A., and Weber, R. J.: ~~.~~ Effectiveness of ammonia reduction on control of fine particle nitrate, ~~.~~ Atmos. Chem. Phys., 18, 12241–1225, https://doi.org/10.5194/acp-18-12241-2018, 2018.

~~Guo, H., Sullivan, A.P., Campuzano-jost, P., Schroder, J.C., Nenes, A., Weber, R.J.: Fine particle pH and the partitioning of nitric acid during winter in the northeastern United States, J. Geophys. Res., 121, 1–22. https://doi.org/10.1002/2016JD025311, 2016.~~

~~Guo, H., Weber, R.J., Nenes, A.: High levels of ammonia do not raise fine particle pH sufficiently to yield nitrogen oxide-dominated sulfate production, Sci. Rep., 1–7. https://doi.org/10.1038/s41598-017-11704-0, 2017b.~~

~~Guo, H., Xu, L., Bougiatioti, A., Cerully, K.M., Capps, S.L., Hite, J.R., Carlton, A.G., Lee, S.H., Bergin, M.H., Ng, N.L., Nenes, A., Weber, R.J.: Fine-particle water and pH in the southeastern United States, Atmos. Chem. Phys., 15, 5211–5228. https://doi.org/10.5194/acp-15-5211-2015, 2015.~~

Guo, J., ~~Y.~~ Wang, Y., ~~X.~~ Shen, X., ~~Z.~~ Wang, Z., ~~T.~~ Lee, T., ~~X.~~ Wang, X., ~~P.~~ Li, P., ~~M.~~ Sun, M. ~~J. L.~~ Collett Jr., J. L., and ~~W.~~ Wang, W.: ~~.~~ Characterization of cloud water chemistry at Mount Tai, China: Seasonal variation, anthropogenic impact, and cloud processing, Atmos. Environ., 60, 467-476, https://doi.org/10.1016/j.atmosenv.2012.07.016, 2012.

He, K., Zhao, Q., Ma, Y., Duan, F., Yang, F., Shi, Z., and Chen, G.: Spatial and seasonal variability of PM 2.5 acidity at two Chinese megacities: insights into the formation of secondary inorganic aerosols, Atmos. Chem. Phys., 12, 1377–1395, https://doi.org/10.5194/acp-12-1377-2012, 2012.

He, P., Alexander, B., Geng, L., Chi, X., Fan, S., Zhan, H., Kang, H., Zheng, G., Cheng, Y., Su, H., Liu, C., and Xie, Z.: Isotopic constraints on heterogeneous sulfate production in Beijing haze, Atmos. Chem. Phys., 18, 5515–5528, https://doi.org/10.5194/acp-18-5515-201, 2018.

Hegg, D. A., and ~~P. V.~~ Hobbs, P. V.: Cloud water chemistry and the production of sulfates in clouds, Atmos. Environ. (1967), 15(9), 1597-1604, https://doi.org/10.1016/0004-6981(81)90144-X, 1981.

Hegg, D. A., and ~~P. V.~~ Hobbs, P. V.: Measurements of sulfate production in natural clouds, Atmos. Environ., 16(11), 2663-2668, https://doi.org/10.1016/0004-6981(82)90348-1, 1982.

Hegg, D. e. A., and ~~P. V.~~ Hobbs, P. V.: Sulfate and nitrate chemistry in cumuliform clouds, Atmos. Environ., 20(5), 901-909, https://doi.org/10.1016/0004-6981(86)90274-X, 1986.

Hegg, D. A., ~~P. V.~~ Hobbs, P. V., and ~~L. F.~~ Radke, L. F.: Measurements of the scavenging of sulfate and nitrate in clouds, Atmos. Environ., 18(9), 1939-1946, https://doi.org/10.1016/0004-6981(84)90371-8, 1984a.

Hegg, D. A., ~~L. F.~~ Radke, L. F., and ~~P. V.~~ Hobbs, P. V.: Measurements of transformations in the physical and chemical properties of clouds associated with onshore flow in Washington State, J. Clim. Appl. Met., 23(6), 979-984, https://doi.org/10.1175/1520-0450(1984)023<0979:MOTITP>2.0.CO;2, 1984b.

~~Hegg, D. e. A., and P. V. Hobbs: Sulfate and nitrate chemistry in cumuliform clouds, Atmos. Environ., 20(5), 901-909, 1986.~~

Hemmerlein, M. T., and ~~T. D.~~ Perkins, T. D.: Techniques for pollution monitoring in remote sites: III. Near real-time monitoring of cloud water conductivity and pH, Wat. Air Soil Pol., 71(1-2), 43-50, https://doi.org/10.1007/BF00475511, 1993.

Hennigan, C. J., Izumi, J., Sullivan, A. P., Weber, and R. J., Nenes, A.: A critical evaluation of proxy methods used to estimate the acidity of atmospheric particles, Atmos. Chem. Phys., 15, 2775–2790, https://doi.org/10.5194/acp-15-2775-2015, https://doi.org/10.5194/acp-15-2775-2015, 2015.

Herckes, P., ~~H.~~ Wortham, H., ~~P.~~ Mirabel, P., and ~~M.~~ Millet, M.: Evolution of the fogwater composition in Strasbourg (France) from 1990 to 1999, Atmos. Res., 64(1-4), 53-62, https://doi.org/10.1016/S0169-8095(02)00079-0, 2002.

Herckes, P., ~~H.~~ Chang, H., ~~T.~~ Lee, T., and ~~J. L.~~ Collett, J. L.: Air pollution processing by radiation fogs, Wat. Air Soil Pol., 181(1-4), 65-75, https://doi.org/10.1007/s11270-006-9276-x, 2007.

~~Herckes, P., H. Wortham, P. Mirabel, and M. Millet: Evolution of the fogwater composition in Strasbourg (France) from 1990 to 1999, Atmos. Res., 64(1-4), 53-62, 2002.~~

Hill, K. A., ~~P. B.~~ Shepson, P. B., ~~E. S.~~ Galbavy, E. S., ~~C.~~ Anastasio, C., ~~P. S.~~ Kourtev, P. S., A. Konopka, P. S., and ~~B. H.~~ Stirm, B. H.: Processing of atmospheric nitrogen by clouds above a forest environment, J. Geophs. Res., 112(D11), https://doi.org/10.1029/2006JD008002, 2007.

Hitzenberger, R., ~~A.~~ Berner, A., ~~R.~~ Kromp, R., ~~A.~~ Kasper-Giebl, A., ~~A.~~ Limbeck, A., ~~W.~~ Tscherwenka, W., and ~~H.~~ Puxbaum, H.: Black carbon and other species at a high-elevation European site (Mount Sonnblick, 3106 m, Austria): Concentrations and scavenging efficiencies, J. Geophs. Res., 105(D20), 24637-24645, https://doi.org/10.1029/2000JD900349, 2000.

Hoffmann M. R.: On the kinetics and mechanism of oxidation of aquated sulfur dioxide by ozone., Atmos. Environ., 20, 1145-l 154, https://doi.org/10.1016/0004-6981(86)90147-2, 1986.

Hosono, T., H. Okochi, H., and M. Igawa, M.: Fogwater chemistry at a mountainside in Japan, Bulletin of of thethe Chemical. Society. of Japan, 67(2), 368-374, https://doi.org/10.1246/bcsj.67.368, 1994.

Houghton, H. G.: On the chemical composition of fog and cloud water, J. Meteorol., 12(4), 355-357, https://doi.org/10.1175/1520-0469(1955)012<0355:OTCCOF>2.0.CO;2, 1955.

Huang, Y., H. Guo, H., and F. Liu: The chemical composition of radiative fog-water industrial and non-industrial districts, Acta Geographica Sin.ica, 47(1), 66-73, available at: http://www.geog.com.cn/EN/Y1992/V59/I1/66, 1992.

Husain, L.: A technique for determining in-cloud formation of SO4, Geophys. Res. Lett., Geoph.Res.Let., 16(1), 57-60, https://doi.org/10.1029/GL016i001p00057, 1989.

Husain, L., V. Dutkiewicz, V., M. Hussain, M., H. Khwaja, H., E. Burkhard, E., G. Mehmood, G., G. P. Parekh, G., and E. Canelli, E.: A study of heterogeneous oxidation of SO2 in summer clouds, J. Geophs. Res., 96(D10), 18789-18805, https://doi.org/10.1029/91JD01943, 1991.

Husain, L., O. Rattigan, O., V. Dutkiewicz, V., M. Das, M., C. Judd, C., A. Khan, A., R. Richter, R., R. Balasubramanian, R., K. Swami, K., and C. Walcek, C.: Case studies of the SO2+ H2O2 reaction in clouds, J. Geophs. Res., 105(D8), 9831-9841, https://doi.org/10.1029/1999JD901177, 2000.

Hutchings, J. W., M. S. Robinson, M. S., H. McIlwraith, H., J. T. Kingston, J. T., and P. Herckes, P.: The chemistry of intercepted clouds in Northern Arizona during the North American monsoon season, Wat. Air Soil Pol., 199(1-4), 191-202, https://doi.org/10.1007/s11270-008-9871-0, 2009.

Igawa, M., Y. Tsutsumi, Y., T. Mori, T., and H. Okochi, H.: Fogwater chemistry at a mountainside forest and the estimation of the air pollutant deposition via fog droplets based on the atmospheric quality at the mountain base, Environ. Sci. Technol., Env. Sci. Techn., 32(11), 1566-1572, https://doi.org/10.1007/s11270-008-9871-0, 1998.

Isaac, G., and P. Daum, P.: A winter study of air, cloud and precipitation chemistry in Ontario, Canada, Atmos. Environ., 21(7), 1587-1600, https://doi.org/10.1016/0004-6981(87)90320-9, 1987.

Jacob, D. J., J. W. Munger, J. M. Waldman, and M. R. Hoffmann: The H2SO4 HNO3 NH3 system at high humidities and in fogs: 1. Spatial and temporal patterns in the San Joaquin Valley of California, J. Geoph. Res., 91(D1), 1073 1088, 1986a.Jacob, D. J., J. M. Waldman, J. M., J. W. Munger, J. W., and M. R. Hoffmann, M. R.: A field investigation of physical and chemical mechanisms affecting pollutant concentrations in fog droplets, Tellus B, 36(4), 272-285, https://doi.org/10.3402/tellusb.v36i4.14909, 1984.

Jacob, D. J., J. M. Waldman, J. M., J. W. Munger, J. W., and M. R. Hoffmann, M. R.: Chemical composition of fogwater collected along the California coast, Environ. Sci. Technol., Env. Sci. Techn., 19(8), 730-736, https://doi.org/10.1021/es00138a013, 1985.

Jacob, D. J., Munger, J. W., Waldman, J. M., and Hoffmann, M. R.: The H2SO4-HNO3-NH3 system at high humidities and in fogs: 1. Spatial and temporal patterns in the San Joaquin Valley of California, J. Geophs. Res., 91(D1), 1073-1088, https://doi.org/10.1029/JD091iD01p01073, 1986a.

Jacob, D. J., J. M. Waldman, J. W. Munger, and M. R. Hoffmann: A field investigation of physical and chemical mechanisms affecting pollutant concentrations in fog droplets, Tellus B, 36(4), 272 285, 1984.

Jacob, D. J., J. M. Waldman, J. W. Munger, and M. R. Hoffmann: Chemical composition of fogwater collected along the California coast, Env. Sci. Techn., 19(8), 730-736, 1985.

Jacob, D. J., J. M. Waldman, J. M., J. W. Munger, J. W., and M. R. Hoffmann, M. R.: The H2SO4-HNO3-NH3 system at high humidities and in fogs: 2. Comparison of field data with thermodynamic calculations, J. Geophs. Res., 91(D1), 1089-1096, https://doi.org/10.1029/JD091iD01p01089, 1986b.

Jagels, R., J. Carlisle, J., R. Cunningham, R., S. Serreze, S., and P. Tsai, P.: Impact of acid fog and ozone on coastal red spruce, Wat. Air Soil Pol., 48(1-2), 193-208, https://doi.org/10.1007/BF00282378, 1989.

Jia, S., Wang, X., Zhang, Q., Sarkar, S., Wu, L., Huang, M., and Zhang, J.: Technical note: Comparison and interconversion of pH based on different standard states for aerosol acidity characterization, Atmos. Chem. Phys., 18, 11125–11133, https://doi.org/10.5194/acp-18-11125-2018, 2018.

Jiang, Y., Q. Wang, Q., X. Xu, X., and Z. Wang, Z.: Study on the Fog Weather Process Ionic Species Concentration Variation of The Fog Water in Beijing, paper presented at 5th International Conference on Fog, Fog Collection and Dew, held 25-30 July, 2010, in Münster, Germany, http://www.fogconference.org, id. FOGDEW2010-22, **[Did not find DOI]**, 2010.

Johnson, C. A., L. Sigg, L., and J. Zobrist, J.: Case studies on the chemical composition of fogwater: the influence of local gaseous emissions, Atmos. Environ. (1967), 21(11), 2365-2374, https://doi.org/10.1016/0004-6981(87)90371-4, 1987.

Joos, F., and U. Baltensperger, U.: A field study on chemistry, S (IV) oxidation rates and vertical transport during fog conditions, Atmos. Environ., 25(2), 217-230, https://doi.org/10.1016/0960-1686(91)90292-F, 1991.

Joslin, J., C. McDuffie, C., and P. Brewer, P.: Acidic cloud water and cation loss from red spruce foliage, Wat. Air Soil Pol., 39(3-4), 355-363, https://doi.org/10.1007/BF00279480, 1988.

Kaul, D., T. Gupta, T., S. Tripathi, T., V. Tare, V., and J. Collett Jr, J.: Secondary organic aerosol: a comparison between foggy and nonfoggy days, Environ. Sci. Technol., Env. Sci. Techn., 45(17), 7307-7313, https://doi.org/10.1021/es201081d, 2011.

Keene, W. C., B. W. Mosher, B. W., D. J. Jacob, D. J., J. W. Munger, J. W., R. W. Talbot, R. W., R. S. Artz, R. S., J. R. Maben, J. R., B. C. Daube, B. C., and J. N. Galloway, J. N.: Carboxylic acids in clouds at a high-elevation forested site in central Virginia, J. Geophs. Res., 100(D5), 9345-9357, https://doi.org/10.1029/94JD01247, 1995.

Khemani, L., G. Momin, G., M. S. Naik, M. S., P. P. Rao, P. P., P. Safai, P., and A. Murty, A.: Influence of alkaline particulates on pH of cloud and rain water in India, Atmos. Environ., 21(5), 1137-1145, https://doi.org/10.1016/0004-6981(87)90241-1, 1987.

Khwaja, H. A., S. Brudnoy, S., and L. Husain, L.: Chemical characterization of three summer cloud episodes at Whiteface Mountain, Chemosphere, 31(5), 3357-3381, https://doi.org/10.1016/0045-6535(95)00187-D, 1995.

Kim, D. S., and V. P. Aneja, V. P.: Chemical composition of clouds at Mt. Mitchell, North Carolina, USA, Tellus B, 44(1), 41-53, https://doi.org/10.3402/tellusb.v44i1.15421, 1992.

Kim, M.-G., B.-K. Lee, B.-K., and H. J. Kim, H.-J.: Cloud/fog water chemistry at a high elevation site in South Korea, J. Atmos. Chem., 55(1), 13-29, https://doi.org/10.1007/s10874-005-9004-8, 2006.

Kimball, K. D., R. Jagels, R., G. A. Gordon, G. A., K. C. Weathers, K. C., and J. Carlisle, J.: Differences between New England coastal fog and mountain cloud water chemistry, Wat. Air Soil Pol., 39(3-4), 383-393, https://doi.org/10.1007/BF00279483, 1988.

Klemm, O., and T. Wrzesinsky, T.: Fog deposition fluxes of water and ions to a mountainous site in Central Europe, Tellus B, 59(4), 705-714, https://doi.org/10.1111/j.1600-0889.2007.00287.x, 2007.

Klemm, O., Talbot, R., and Klemm, K.: Sulfur dioxide in coastal New England fog, Atmos. Environ., 26(11), 2063-2075, https://doi.org/10.1016/0960-1686(92)90091-X, 1992.

Formatted: Font: Not Bold, Font color: Auto

Klemm, O., A. Bachmeier, A., R. Talbot, R., and K. Klemm, K.: Fog chemistry at the New England coast: influence of air mass history, Atmos. Environ., 28(6), 1181-1188, https://doi.org/10.1016/1352-2310(94)90295-X, 1994.

Klemm, O., R. Talbot, and K. Klemm: Sulfur dioxide in coastal New England fog, Atmos. Environ., 26(11), 2063-2075, 1992.

Klemm, O., W.-T. Tseng, W.-T., C.-C. Lin, C.-C., K. I. Klemm, K. I., and N. H. G. Lin, N.-H. G.: pH control in fog and rain in East Asia: Temporal advection of clean air masses to Mt. Bamboo, Taiwan, Atmosphere, 6(11), 1785-1800, https://doi.org/10.3390/atmos6111785, 2015.

Klemm, O., and T. Wrzesinsky: Fog deposition fluxes of water and ions to a mountainous site in Central Europe, Tellus B, 59(4), 705-714, 2007.

Kmiec, G., A. Zwozdziak, A., and J. Zwozdziak, J.: Study of cloud and precipitation chemistry at high elevation in the Sudeten mountains, Poland, WIT Trans. Ecol. Envir. on., 21, https://doi.org/10.2495/AIR970871, 1997.

Knote, C., Hodzic, A., Jimenez, J. L., Volkamer, R., Orlando, J. J., Baidar, S., Brioude, J., Fast, J., Gentner, D. R., Goldstein, A. H., Hayes, P. L., Knighton, W. B., Oetjen, H., Setyan, A., Stark, H., Thalman, R., Tyndall, G., Washenfelder, R., Waxman, E., and Zhang, Q.: Simulation of semi-explicit mechanisms of SOA formation from glyoxal in aerosol in a 3-D model, Atmos. Chem. Phys., 14, 6213-6239, https://doi.org/10.5194/acp-14-6213-2014, 2014.

Kolb, D.: The pH concept, J. Chem. Educ., 56, 49, https://doi.org/10.1021/ed056p49, 1979.

Kolb, 1979.-Add

Kotronarou, A., and L. Sigg, L.: Sulfur dioxide oxidation in atmospheric water: role of iron (II) and effect of ligands, Environ. mental Sci. ence & Technol. ogy, 27(13), 2725-2735, https://doi.org/10.1021/es00049a011, 1993.

Kroll, J. H., Cross, E. S., Hunter, J. F., Sidhant, P., TREX XII, TREX XI, Wallace, L. M. M., Croteau, P. L., Jayne, J. T., Worsnop, D. R., Heald, C. L., Murphy, J. G., and Frankel, S. L.: Atmospheric evolution of sulfur emissions from Kilauea: Real-time measurements of oxidation, dilution, and neutralization within a volcanic plume, Environ. Sci. Technolo., 49, 4129-4137, https://doi.org/10.1021/es506119x, 2015.

Lacaux, J., J. Loemba-Ndembi, J., B. Lefeivre, B., B. Cros, B., and R. Delmas, R.: Biogenic emissions and biomass burning influences on the chemistry of the fogwater and stratiform precipitations in the African equatorial forest, Atmos. Environ., 26(4), 541-551, https://doi.org/10.1016/0960-1686(92)90167-J, 1992.

Laj, P., S. Fuzzi, S., M. Facchini, M., J. Lind, J., G. Orsi, G., M. Preiss, M., R. Maser, R., W. Jaeschke, W., E. Seyffer, E., and G. Helas, G.: Cloud processing of soluble gases, Atmos. Environ., 31(16), 2589-2598, https://doi.org/10.1016/S1352-2310(97)00040-X, 1997.

Lakhani, A., R. S. Parmar, R. S., G. S. Satsangi, G. S., and S. Prakash, S.: Chemistry of fogs at Agra, India: Influence of soil particulates and atmospheric gases, Environ. Monit. Assess., 133(1-3), 435-445, https://doi.org/10.1007/s10661-006-9598-6, 2007.

Lammel, G., and G. Metzig, G.: Multiphase chemistry of orographic clouds: observations at subalpine mountain sites, Fresenius', J. Anal. Chem., 340(9), 564-574, https://doi.org/10.1007/BF00322431, 1991.

Lange, C. A., J. Matschullat, J., F. Zimmermann, F., G. Sterzik, G., and O. Wienhaus, O.: Fog frequency and chemical composition of fog water—a relevant contribution to atmospheric deposition in the eastern Erzgebirge, Germany, Atmos. Environ., 37(26), 3731-3739, https://doi.org/10.1016/S1352-2310(03)00350-9, 2003.

Formatted: Font: Not Bold, Font color: Auto

Formatted: Font color: Auto

Formatted: Font color: Dark Red

Formatted: Font: Bold, Font color: Dark Red

Lazrus, A., H. Baynton, H., and J. Lodge Jr., J.: Trace constituents in oceanic cloud water and their origin, Tellus, 22(1), 106-114, https://doi.org/10.1111/j.2153-3490.1970.tb01941.x, 1970.

Lee, Y.-N., and S. E. Schwartz, S. E.: Kinetics of oxidation of aqueous sulfur (IV) by nitrogen dioxide, in: Precipitation Scavenging, Dry Deposition and Resuspension, vol. 1, edited by: H. R. Pruppacher, H. R., Semonin, R. G., and Slinn, W. G. N.et al., pp. 453–470, Elsevier Sci., New York, [Did not find DOI], 1983.

Lei, H.-C., P. A. Tanner, P. A., M.-Y. Huang, M.-Y., Z.-L. Shen, Z.-L., and Y.-X. Wu, Y.-X.: The acidification process under the cloud in southwest China: observation results and simulation, Atmos. Environ., 31(6), 851-861, https://doi.org/10.1016/S1352-2310(96)00247-6, 1997.

Li, J., X. Wang, X., J. Chen, J., C. Zhu, C., W. Li, W., C. Li, C., L. Liu, L., C. Xu, C., L. Wen, L., and L. Xue, L.: Chemical composition and droplet size distribution of cloud at the summit of Mount Tai, China, Atmos. Chem. Phys., 17(16), 9885-9896, https://doi.org/10.5194/acp-17-9885-2017, 2017.

Li, P., X. Li, X., C. Yang, C., X. Wang, X., J. Chen, J., and J. L. Collett Jr., J. L.: Fog water chemistry in Shanghai, Atmos. Environ., 45(24), 4034-4041, https://doi.org/10.1016/j.atmosenv.2011.04.036, 2011.

Li, T., Wang, Z., Wang, Y., Wu, C., Liang, Y., Xia, M., Yu, C., Yun, H., Wang, W., Wang, Y., Guo, J., Herrmann, H., and Wang, T.: Li, T., et al. Chemical characteristics of cloud water and the impacts on aerosol properties at a subtropical mountain site in Hong Kong SAR, Atmos. Chem. Phys. Discuss., 20, 391-407 1-24, https://doi.org/10.5194/acp-20-391-2020https://doi.org/10.5194/acp-2019-481, 20192020.

Li, W., Y. Wang, Y., J. L. Collett Jr., J. L., J. Chen, J., X. Zhang, X., Z. Wang, Z., and W. Wang, W.: Microscopic evaluation of trace metals in cloud droplets in an acid precipitation region, Environ. Sci. Technol., Env. Sci. Techn., 47(9), 4172-4180, https://doi.org/10.1021/es304779t, 2013.

Li, Y., G.-Z. Zhang, G.-Z., M. J. Pu, M.-J., B. Zhu, B., and Z. H. Li, Z.-H.: The chemical composition of fog water in the winter of 2006 of Nanjing., China Environmental Science, 28(5), 395-400, [Did not find DOI], 2008.

Li, Z., and V. P. Aneja, V. P.: Regional analysis of cloud chemistry at high elevations in the eastern United States, Atmos. Environ., 26(11), 2001-2017, https://doi.org/10.1016/0960-1686(92)90085-Y, 1992.

Li, Z.-H., and Z. G. Peng, Z.-G.; Physical and chemical characteristics of the Chongqing winter fog, Acta Meteorol. Sin.,ACTA Meteorologica Sinica, 52(4), 477-483, [Did not find DOI], 1994.

Li, Z.-H., S. N. Dong, S.-N., and Z. G. Peng, Z.-G.: Spatial/Temporal variabilities of chemical constituents fog water sampled in Chongqing, Journal of Nanjing Institute of Meteorology, J. Nanjing Inst. Meteor., 19(1), 63-68, [Did not find DOI], 1996.

Li, Z.-H., and Z.-G. Peng: Physical and chemical characteristics of the Chongqing winter fog, ACTA Meteorologica Sinica, 52(4), 477-483, 1994.

Lin, N.-H., and V. Saxena, V.: In-cloud scavenging and deposition of sulfates and nitrates: Case studies and parameterization, Atmos. Environ., 25(10), 2301-2320, https://doi.org/10.1016/0960-1686(91)90105-G, 1991.

Liu, H.-J., W. Wang, W., J.-H. Gao, J.-H., Y. Pang, Y., M. Wang, M., and D. Tang, D.: Preliminary Study on the ACharacteristics of Acid Fog in Minnan Area, Huanjing Kexue Yanjiu, 9, 30-32, [Did not find DOI], 1996.

Liu, P., W. Leaitch, W., A. Macdonald, A., G. Isaac, G., J. Strapp, J., and H. A. Wiebe, H. A.: Sulphate production in summer cloud over Ontario, Canada, Tellus B, 45(4), 368-389, https://doi.org/10.3402/tellusb.v45i4.15736, 1993.

Liu, M., Song, Y., Zhou, T., Xu, Z., Yan, C., Zheng, M., Wu, Z., Hu, M., Wu, Y., and Zhu, T.: Fine particle pH during severe haze episodes in northern China, Geophys. Res. Lett., 44, 5213–5221, https://doi.org/10.1002/2017GL073210, 2017.

Formatted: Font: Bold, Font color: Dark Red

Liu, X.-H., ~~K.-M.~~Wai, K.-M., Y. Wang, ~~J.~~ Zhou, J., ~~P.-h.~~Li, P.-h., ~~J.~~ Guo, J., ~~P.-j.~~Xu, P.-j., and ~~W.-X.~~Wang, W.-X.: Evaluation of trace elements contamination in cloud/fog water at an elevated mountain site in Northern China, Chemosphere, 88(5), 531-541, https://doi.org/10.1016/j.chemosphere.2012.02.015, 2012.

~~Liu, M., Song, Y., Zhou, T., Xu, Z., Yan, C., Zheng, M., Wu, Z., Hu, M., Wu, Y., Zhu, T.: Fine particle pH during severe haze episodes in northern China, Geophys. Res. Lett., 44, 5213–5221. https://doi.org/10.1002/2017GL073210, 2017.~~

Löflund, M., ~~A.~~ Kasper-Giebl, A., ~~B.~~ Schuster, B., ~~H.~~ Giebl, H., ~~R.~~ Hitzenberger, R., and ~~H.~~ Puxbaum, H.: Formic, acetic, oxalic, malonic and succinic acid concentrations and their contribution to organic carbon in cloud water, Atmos. Environ., 36(9), 1553-1558, https://doi.org/10.1016/S1352-2310(01)00573-8, 2002.

Marais, E. A., Jacob, D. J., Jimenez, J. L., Campuzano-Jost, P., Day, D. A., Hu, W., Krechmer, J., Zhu, L., Kim, P. S., Miller, C. C., Fisher, J. A., Travis, K., Yu, K., Hanisco, T. F., Wolfe, G. M., Arkinson, H. L., Pye, H. O. T., Froyd, K. D., Liao, J., and McNeill, V. F.: Aqueous-phase mechanism for secondary organic aerosol formation from isoprene: application to the southeast United States and co-benefit of SO2 emission controls, Atmos. Chem. Phys., 16, 1603–1618, https://doi.org/10.5194/acp-16-1603-2016, 2016.

Martin, L. R., and Hill, M. W.: The iron catalyzed oxidation of sulfur: reconciliation of the literature rates, Atmos. Environ., 21, 1487-1490, https://doi.org/10.1016/0004-6981(67)90100-X, 1987.

Martin, L. R., Hill, M. W., Tai, A. F., and Good, T. W.: The iron catalyzed oxidation of sulfur (IV) in aqueous solution: differing effects of organics at high and low pH, J. Geophs. Res., 96, 3085-3097, https://doi.org/10.1029/90JD02611, 1991.

Masiol M., Squizzato S., Formenton G., Md Badiuzzaman K., Hopke P.K., Nenes A., Pandis S.N., Tositti L., Benetello F., Visin F., and Pavoni B.: Hybrid multiple-site mass closure and source apportionment of $PM_{2.5}$ and aerosol acidity at major cities in the Po Valley, Sci. Total. Environ., 704, 135287, https://doi.org/10.1016/j.scitotenv.2019.135287, 2020.

McArdle, J.V., and Hoffmann, M.R.: Kinetics and mechanism of the oxidation of aquated sulfur dioxide by hydrogen peroxide at low pH, J. Phys. Chem., 87, 5425-5429, https://doi.org/10.1021/j150644a024, 1983.

Meinrath, G., and Spitzer, P.: Uncertainties in Determination of pH, Microchim. Acta, 135(3-4):155, https://doi.org/10.1007/s006040070, 2000.

Menon, S., ~~V.~~ Saxena, V., and ~~B.~~ Logie, B.: Chemical heterogeneity across cloud droplet size spectra in continental and marine air masses, J. Appl. Metorol., 39(6), 887-903, https://doi.org/10.1175/1520-0450(2000)039<0887:CHACDS>2.0.CO2, 2000.

Michna, P., ~~R. A.~~Werner, R. A., and ~~W.~~ Eugster, W.: Does fog chemistry in Switzerland change with altitude?, Atmos. Res., 151, 31-44, https://doi.org/10.1016/j.atmosres.2014.02.008, 2015.

Miller, D. R., ~~J. E.~~Byrd, J. E., and ~~M. J.~~Perona, M. J.: The source of Pb, Cu, and Zn in fogwater, Wat. Air Soil Pol., 32(3-4), 329-340, https://doi.org/10.1007/BF00225119, 1987.

Miller, E. C., ~~J. A.~~Panek, J. A., ~~A. J.~~Friedland, A. J., ~~J.~~ Kadlecek, J., and ~~V. A.~~Mohnen, V. A.: Atmospheric deposition to a high-elevation forest at Whiteface Mountain, New York, USA, Tellus B, 45(3), 209-227, https://doi.org/10.3402/tellusb.v45i3.15725, 1993.

Millet, M., A. Sanusi, and H. Wortham: Chemical composition of fogwater in an urban area: Strasbourg (France), Environ. Pollut., 94(3), 345-354, https://doi.org/10.1016/S0269-7491(96)00064-4, 1996.

Formatted: Subscript

Millet, M., H. Wortham, H., A. Sanusi, A., and P. Mirabel, P.: Low molecular weight organic acids in fogwater in an urban area: Strasbourg (France), Sci. Total. Environ., STOTEN, 206(1), 57-65, https://doi.org/10.1016/S0048-9697(97)00216-7, 1997.

Minami, Y., and Y. Ishizaka, Y.: Evaluation of chemical composition in fog water near the summit of a high mountain in Japan, Atmos. Environ., 30(19), 3363-3376, https://doi.org/10.1016/1352-2310(96)00029-5, 1996.

Minghua, L. D. C., and S. Demin, S.: Study on air pollution and composition of fog in Shanghai, Shanghai Environmental Science, 3, 005, **[Did not find DOI],** 1999.

Mo, T.-L., S. Z. Xu, S.-Z., and F. Chen, F.: The acidity and chemical composition of fog-water over Zhoushan region, Shanghai Environmental Science, Shanghai Environ. Sci., 8(8), 22-26, **[Did not find DOI],** 1989.

Möller, D.: 15 Jahre Wolkenforschung auf dem Brocken – ein Beitrag zur chemischen, Klimatologie. Rep., available at: https://lau.sachsen-anhalt.de/fileadmin/Bibliothek/Politik_und_Verwaltung/MLU/LAU/Wir_ueber_uns/Veranstaltungen/Archiv/2006/Dateien/Brocken_Magdeburg_Vortrag_08.11.07.pdf, 2007.

Mohnen, V. A., and J. A. Kadlecek, J. A.: Cloud chemistry research at Whiteface Mountain, Tellus B, 41(1), 79-91, https://doi.org/10.3402/tellusb.v41i1.15052, 1989.

Mohnen, V. A., and R. J. Vong, R. J.: A climatology of cloud chemistry for the eastern United States derived from the mountain cloud chemistry project, Environ. Rev., 1(1), 38-54, https://doi.org/10.1139/a93-005, 1993.

Moore, K. F., D. E. Sherman, D. E., J. E. Reilly, J. E., and J. L. Collett, J. L.: Drop size-dependent chemical composition in clouds and fogs. Part I. Observations, Atmos. Environ., 38(10), 1389-1402, https://doi.org/10.1016/j.atmosenv.2003.12.013, 2004.

Mrose, H.: Measurements of pH, and chemical analyses of rain-, snow-, and fog-water, Tellus, 18(2-3), 266-270, https://doi.org/10.3402/tellusa.v18i2-3.9626, 1966.

Muir, P. S.: Fogwater chemistry in a wood-burning community, Western Oregon, J. Air Waste Manage., JAWMA, 41(1), 32-38, https://doi.org/10.1080/10473289.1991.10466822, 1991.

Muir, P. S., K. A. Wade, K. A., B. H. Carter, B. H., T. V. Armentano, T. V., and R. A. Pribush, R. A.: Fog chemistry at an urban midwestern site, Journal of the Air Pollution Control AssociationJ. Air Pol. Contr. Assoc., 36(12), 1359-1361, available at: http://pascal-francis.inist.fr/vibad/index.php?action=getRecordDetail&idt=8211686, 1986.

Munger, J. W.: The Chemical Composition of Fogs and Clouds in Southern California., Atmos. Res., 64, 29–4, available at: https://thesis.library.caltech.edu/629/1/Munger_jw_1989.pdf, 1989.

~~Munger, J. W., J. Collett Jr, B. Daube Jr, and M. R. Hoffmann: Fogwater chemistry at riverside, California, Atmos. Environ. 24(2), 185-205, 1990.~~

Munger, J. W., D. J. Jacob, D. J., J. M. Waldman, J. M., and M. R. Hoffmann, M. R.: Fogwater chemistry in an urban atmosphere, J. Geophs. Res., 88(C9), 5109-5121, https://doi.org/10.1029/JC088iC09p05109, 1983.

Munger, J. W., J. Collett Jr., J., B. Daube Jr., B., and M. R. Hoffmann, M. R.: Fogwater chemistry at rRiverside, California, Atmos. Environ. 24(2), 185-205, https://doi.org/10.1016/0957-1272(90)90025-P, 1990.

Munzert, K.: Chemistry of cloud water and precipitation at an Alpine mountain station, in Acid Deposition at High Elevation Sites, edited, pp. 395-401, Springer, https://doi.org/10.1007/978-94-009-3079-7_21, 1988.

Murphy, J., Gregoire, P. K., Tevlin, A. G., Wentworth, G. R., Ellis, R. A., Markovic, M. Z., and Vandenboer, T.: Observational constraints on particle acidity using measurements and modelling of particles and gases, Faraday Discuss., https://doi.org/10.1039/C7FD00086C, 2017.

Murray, G. L., K. D. Kimball, K. D., L. B. Hill, L. B., J. E. Hislop, J. E., and K. C. Weathers, K. C.: Long-term trends in cloud and rain chemistry on Mount Washington, New Hampshire, Water Air Soil Poll., Water, Air, & Soil Pollution, 224(9), 1653, https://doi.org/10.1007/s11270-013-1653-7, 2013.

Nah, T., Guo, H., Sullivan, A. P., Chen, Y., Tanner, D. J., Nenes, A., Russell, A., Ng, N. L., Huey, L. G., and Weber, R. J.: Characterization of aerosol composition, aerosol acidity, and organic acid partitioning at an agriculturally intensive rural southeastern US site, Atmos. Chem. Phys., 18, 11471–11491, https://doi.org/10.5194/acp-18-11471-2018, 2018.

Nam, J.-C., S. N. Oh, S.-N., J. C. Choi, J.-C., J. Kim, J., and Y. Chun, Y.: Monitoring of acid rain over Korean Peninsula, Wat. Air Soil Pol., 130(1-4), 433-438, https://doi.org/10.1023/A:1013897604712, 2001.

Nath, S., and S. Yadav, S.: A Comparative Study on Fog and Dew Water Chemistry at New Delhi, India, Aerosol Aerosol Air Qual. Res., Air Qual. Res., 18(1), 26-36, https://doi.org/10.4209/aaqr.2017.01.0033, 2018.

Nieberding, F., B. Breuer, B., E. Braeckevelt, E., O. Klemm, O., Q. Song, Q., and Y. Zhang, Y.: Fog Water Chemical Composition on Ailaoshan Mountain, Yunnan Province, SW China, Aerosol Air Qual. Res., 18(1), 37-48, https://doi.org/10.4209/aaqr.2017.01.0060, 2018.

Ogawa, N., R. Kikuchi, R., T. Okamura, T., T. Adzuhata, T., M. Kajikawa, M., and T. Ozeki, T.: Cloud droplet size dependence of the concentrations of various ions in cloud water at a mountain ridge in northern Japan, Atmos. Res., 51, 77-80, https://doi.org/10.1016/S0169-8095(99)00002-2, 1999.

Ogren, J., and H. Rodhe, H.: Measurements of the chemical composition of cloudwater at a clean air site in central Scandinavia, Tellus B, 38(3-4), 190-196, https://doi.org/10.1111/j.1600-0889.1986.tb00186.x, 1986.

Okita, T.: Concentration of sulfate and other inorganic materials in fog and cloud water and in aerosol, Journal of the Meteorological Society of JapanJ. Met. Soc. Jap., 46(2), 120-127, https://doi.org/10.2151/jmsj1965.46.2_120, 1968.

Olivier, J.: Fog-water harvesting along the West Coast of South Africa: A feasibility study, Water SAa, 28(4), 349-360, http://dx.doi.org/10.4314/wsa.v28i4.4908, 2002.

Olivier, J., and C. De Rautenbach, C.: The implementation of fog water collection systems in South Africa, Atmos. Res., 64(1-4), 227-238, https://doi.org/10.1016/S0169-8095(02)00094-7, 2002.

Dal'Osto, M., Airs, R.L., Beale, R., Cree, C., Fitzsimons, M.F., Beddows, D., Harrison, R.M., Ceburnis, D., Dowd, C.O., Rinaldi, M., Paglione, M., Nenes, A., Decesari, S., Simo, R.: Simultaneous Detection of Alkylamines in the Surface Ocean and Atmosphere of the Antarctic Sympagic Environment., ACS Earth Sp. Chem., 3, 854–862. https://doi.org/10.1021/acsearthspacechem.9b00028, 2019.

Parungo, F., C. Nagamoto, C., I. Nolt, I., M. Dias, M. and E. Nickerson, E.: Chemical analysis of cloud water collected over Hawaii, J. Geophs. Res., 87(C11), 8805-8810, https://doi.org/10.1029/JC087iC11p08805, 1982.

Pathak, R. K., Yao, X. H., Lau, A. K. H., and Chan, C. K.: Acidity and concentrations of ionic species of PM2.5 in Hong Kong, Atmos. Environ., 37, 1113–1124, https://doi.org/10.1016/S1352-2310(02)00958-5, 2003.

Pathak, R.K., Wu, W.S., Wang, T.: Summertime PM 2.5 ionic species in four major cities of China : nitrate formation in an ammonia-deficient atmosphere, Atmos. Chem. Phys. 9, 1711–1722, 2009.

Pathak, R. K., Yao, X., and Chan, C. K.: Sampling Artifacts of Acidity and Ionic Species in PM 2.5, Environ. Sci. Technol., Env. Sci. Technol., 38, 254–259, https://doi.org/10.1021/es0342244, 2004.

Pathak, R. K., Wu, W. S., and Wang, T.: Summertime PM 2.5 ionic species in four major cities of China: nitrate formation in an ammonia-deficient atmosphere, Atmos. Chem. Phys., 9, 1711–1722, https://doi.org/10.5194/acp-9-1711-2009, 2009.

Pathak, R.K., Yao, X.H., Lau, A.K.H., Chan, C.K.: Acidity and concentrations of ionic species of PM2.5 in Hong Kong, Atmos. Environ., 37, 1113–1124, 2003.

Plessow, K., K. Acker, K., H. Heinrichs, H., and D. Moller, D.: Time study of trace elements and major ions during two cloud events at the Mt. Brocken, Atmos. Environ., 35(2), 367-378, https://doi.org/10.1016/s1352-2310(00)00134-5, 2001.

Post, D., H. A. Bridgman, H. A., and G. Ayers, G.: Fog and rainwater composition in rural SE Australia, J. Atmos. Chem., 13(1), 83-95, https://doi.org/10.1007/BF00048102, 1991.

Pszenny, A. A. P., Moldanová, J., Keene, W. C., Sander, R., Maben, J. R., Martinez, M., Crutzen, P. J., Perner, D., and Prinn, R. G.: Halogen cycling and aerosol pH in the Hawaiian marine boundary layer, Atmos. Chem. Phys., 4, 147-168, https://doi.org/10.5194/acp-4-147-2004, 2004.

Pye, H. O. T., Zuend, A., Fry, J. L., Isaacman-vanwertz, and G., Capps, S. L.: Coupling of organic and inorganic aerosol systems and the effect on gas – particle partitioning in the southeastern US, Atmos. Chem. Phys., 357–370, https://doi.org/10.5194/acp-18-357-2018, 2018.

Qian, G.-W., Y. Ishizaka, Y., Y. Minami, Y., Y. Kurahashi, Y., B. I. Tjandradewi, B. I., and C. Takenaka, C.: Transformation of individual aerosol particles in acidic fog evolution, J. Meteorol. Soc. Jap., 70(2), 711-722, https://doi.org/10.2151/jmsj1965.70.2_711, 1992.

Radojevic, M., B. J. Tyler, B. J., A. J. Wicks, A. J., M. J. Gay, M. J., and T. W. Choularton, T. W.: Field studies of the SO2 aqueous S(IV) equilibrium in clouds, Atmos. Environ., 24(2), 323-328, https://doi.org/10.1016/0960-1686(90)90112-z, 1990.

Raja, S., R. Raghunathan, X.-Y. Yu, T. Lee, J. Chen, R. R. Kommalapati, K. Murugesan, X. Shen, Y. Qingzhong, and K. T. Valsaraj: Fog chemistry in the Texas–Louisiana gulf coast corridor, Atmos. Environ., 42(9), 2048-2061, 2008.

Raja, S., R. Ravikrishna, R., R. Kommalapati, R., and K. Valsaraj, K.: Monitoring of fogwater chemistry in the gulf coast urban industrial corridor: Baton Rouge (Louisiana), Environ. Monit. Assess., 110(1-3), 99-120, https://doi.org/10.1007/s10661-005-6281-2, 2005.

Raja, S., R. Raghunathan, R., X.-Y. Yu, X.-Y., T. Lee, T., J. Chen, T., R. R. Kommalapati, R. R., K. Murugesan, K., X. Shen, X., Y. Qingzhong, Y., and K. T. Valsaraj, K. T.: Fog chemistry in the Texas–Louisiana gulf coast corridor, Atmos. Environ., 42(9), 2048-2061, https://doi.org/10.1016/j.atmosenv.2007.12.004, 2008.

Rao, X., and J. L. Collett: The drop size-dependence of iron and manganese concentrations in clouds and fogs: Implications for sulfate production, J. Atmos. Chem., 30(2), 273-289, 1998.

Rao, X., and J. L. J. Collett, J. L. J.: Behavior of S (IV) and formaldehyde in a chemically heterogeneous cloud, Environ. Sci. Technol., Env. Sci. Techn., 29(4), 1023-1031, 1023-31, https://doi.org/10.1021/es00004a024, 1995.

Rao, X., and J. L. Collett, J. L.: The drop size-dependence of iron and manganese concentrations in clouds and fogs: Implications for sulfate production, J. Atmos. Chem., 30(2), 273-289, https://doi.org/10.1023/A:1006044614291, 1998.

Rattigan, O., J. Reilly, J., C. Judd, C., K. F. Moore, K. F., M. Das, M., D. E. Sherman, D. E., V. A. Dutkiewicz, V. A., J. L. Collett, J. L., and L. Husain, L.: Sulfur dioxide oxidation in clouds at Whiteface Mountain as a function of drop size, J. Geophs. Res., 106(D15), 17347-17358, https://doi.org/10.1029/2000JD900807, 2001.

Reilly, J. E., O. V. Rattigan, O. V., K. F. Moore, K. F., C. Judd, C., D. E. Sherman, D. E., V. A. Dutkiewicz, V. A., S. M. Kreidenweis, V. A. S. M., L. Husain, L., and J. L. Collett Jr., J. L.: Drop size-dependent S (IV) oxidation in chemically heterogeneous radiation fogs, Atmos. Environ., 35(33), 5717-5728, https://doi.org/10.1016/S1352-2310(01)00373-9, 2001.

Reisinger, L. M., and R. E. Imhoff, R. E.: Analysis of summertime cloud water measurements made in a southern Appalachian spruce forest, Wat. Air Soil Pol., 45(1-2), 1-15, https://doi.org/10.1007/BF00208573, 1989.

Reyes-Rodríguez, G. J., A. Gioda, A., O. L. Mayol-Bracero, O. L., and J. Collett Jr., J.: Organic carbon, total nitrogen, and water-soluble ions in clouds from a tropical montane cloud forest in Puerto Rico, Atmos. Environ., 43(27), 4171-4177, https://doi.org/10.1016/j.atmosenv.2009.05.049, 2009.

~~Richards, L., J. Anderson, D. Blumenthal, J. McDonald, G. Kok, and A. Lazrus: Hydrogen peroxide and sulfur (IV) in Los Angeles cloud water, Atmos. Environ. (1967), 17(4), 911-914, 1983.~~

Richards, L. W.: Airborne chemical measurements in nighttime stratus clouds in the Los Angeles Basin, Atmos. Environ., 29(1), 27-46, https://doi.org/10.1016/1352-2310(94)00218-A, 1995.

Richards, L., J. Anderson, J., D. Blumenthal, D., J. McDonald, J., G. Kok, G., and A. Lazrus, A.: Hydrogen peroxide and sulfur (IV) in Los Angeles cloud water, Atmos. Environ. (1967), 17(4), 911-914, https://doi.org/10.1016/0004-6981(83)90458-4, 1983.

Sagebiel, J. C., and J. N. Seiber, J. N.: Studies on the occurrence and distribution of wood smoke marker compounds in foggy atmospheres, Environ. Toxicol. Chem., 12(5), 813-822, https://doi.org/10.1002/etc.5620120504, 1993.

Salem, T. A., M. Omar, M., and H. A. A. El Gammal, H. A. A.: Evaluation of fog and rain water collected at Delta Barrage, Egypt as a new resource for irrigated agriculture, J. Afr. Earth Sci., 135, 34-40, https://doi.org/10.1016/j.jafrearsci.2017.08.012, 2017.

Sander, R.: Compilation of Henry's law constants (version 4.0) for water as solvent, Atmos. Chem. Phys., 15, 4399-4981, https://doi.org/10.5194/acp-15-4399-2015, 2015.

Sanhueza, E., M. Santana, M., and M. Hermoso, M.: Gas-and aqueous-phase formic and acetic acids at a tropical cloud forest site, Atmos. Environ., 26(8), 1421-1426, https://doi.org/10.1016/0960-1686(92)90127-7, 1992.

Sasakawa, M., and M. Uematsu, M.: Chemical composition of aerosol, sea fog, and rainwater in the marine boundary layer of the northwestern North Pacific and its marginal seas, J. Geophs. Res., 107(D24), https://doi.org/10.1029/2001JD001004, 2002.

Sasakawa, M., and M. Uematsu, M.: Relative contribution of chemical composition to acidification of sea fog (stratus) over the northern North Pacific and its marginal seas, Atmos. Environ., 39(7), 1357-1362, https://doi.org/10.1016/j.atmosenv.2004.11.039, 2005.

Saxena, V., and ~~N. H.~~ Lin, N.-H.: Cloud chemistry measurements and estimates of acidic deposition on an above cloudbase coniferous forest, Atmos. Environ., 24(2), 329-352, https://doi.org/10.1016/0960-1686(90)90113-2, 1990.

Saxena, V., ~~F.~~ Ruggiero, F., and ~~F.~~ Parungo, F.: Airborne measurements of the Antarctic cloud water acidity, Antarct. J. US, 20, 201-203, **[Did not find DOI]**, 1985.

Schemenauer, R. S.: Acidic deposition to forests: The 1985 chemistry of high elevation fog (CHEF) project, Atmos. ~~phere~~ Ocean, 24(4), 303-328, https://doi.org/10.1080/07055900.1986.9649254, 1986.

~~Schemenauer, R. S., C. M. Banic, and N. Urquizo: High elevation fog and precipitation chemistry in southern Quebec, Canada, Atmos. Environ., 29(17), 2235-2252, 1995.~~

Schemenauer, R. S., and ~~P.~~ Cereceda, P.: Monsoon cloudwater chemistry on the Arabian Peninsula, Atmos. Environ., 26(9), 1583-1587, https://doi.org/10.1016/0960-1686(92)90058-S, 1992a.

Schemenauer, R. S., and ~~P.~~ Cereceda, P.: The quality of fog water collected for domestic and agricultural use in Chile, J. Appl. Metorol., 31(3), 275-290, https://doi.org/10.1175/1520-0450(1992)031<0275:TQOFWC>2.0.CO;2, 1992b.

Schemenauer, R. S., ~~C. M.~~ Banic, C. M., and ~~N.~~ Urquizo, N.: High elevation fog and precipitation chemistry in southern Quebec, Canada, Atmos. Environ., 29(17), 2235-2252, https://doi.org/10.1016/1352-2310(95)00153-P, 1995.

Schmitt, G.: The temporal distribution of trace element concentrations in fogwater during individual fog events, in: Atmospheric pollutants in forest areas, edited, ~~pp.~~ 129-141, Springer, https://doi.org/10.1007/978-94-009-4736-8_11, 1986.

Schmitt, G.: Comparison of wet deposition inputs via rain and fog interception at a high elevated forest site, in: Mechanisms and Effects of Pollutant-Transfer into Forests, edited, ~~pp.~~ 213-220, Springer, https://doi.org/10.1007/978-94-009-1023-2_24, 1989.

Schomburg, C. J., ~~D. E.~~ Glotfelty, D. E., and ~~J. N.~~ Seiber, J. N.: Pesticide occurrence and distribution in fog collected near Monterey, California, Environ. Sci. Technol., ~~Env. Sci. Techn.,~~ 25(1), 155-160, https://doi.org/10.1021/es00013a018, 1991.

Schrimpff, E.: Waldsterben infolge hoher Schadstoffkonzentrationen im Nebel, Staub Reinhalt Luft~~Staub-Reinhalt. Luft~~, 43, 240, **[Did not find DOI]**, 1983.

Schunk, C., ~~P.~~ Trautwein, P., ~~H.~~ Hruschka, H., ~~E.~~ Frost, E., ~~L.~~ Dodson, L., ~~A.~~ Derhem, A., ~~J.~~ Bargach, J., and ~~A.~~ Menzel, A.: Testing Water Yield, Efficiency of Different Meshes and Water Quality with a Novel Fog Collector for High Wind Speeds, Aerosol Air Qual. Res., ~~Aerosol Air Qual. Res.,~~ 18(1), 240-253, https://doi.org/10.4209/aaqr.2016.12.0528, https://doi.org/10.4209/aaqr.2016.12.0528, 2018.

Scott, B., and ~~N.~~ Laulainen, N.: On the concentration of sulfate in precipitation, J. Appl. Metorol., 18(2), 138-147, https://doi.org/10.1175/1520-0450(1979)018<0138:OTCOSI>2.0.CO;2, 1979.

Scott, W.: The pH of cloud water and the production of sulfate, Atmos. Environ., 12(4), 917-921, https://doi.org/10.1016/0004-6981(78)90030-6, 1978.

Sedlak, D. L., ~~J.~~ Hoigne, J., ~~M. M.~~ David, M. M., ~~R. N.~~ Colvile, R. N., ~~E.~~ Seyffer, E., ~~K.~~ Acker, K., ~~W.~~ Wiepercht, W., ~~J. A.~~ Lind, J. A., and ~~S.~~ Fuzzi, S.: ~~-~~ The cloudwater chemistry of iron and copper at Great Dun Fell, UK, Atmos. Environ., 31(16), 2515-2526, https://doi.org/10.1016/s1352-2310(96)00080-5, 1997.

Shah, V., Jaegl, L., Thornton, J. A., Lopez-Hilfiker, F. D., Lee, B. H., Schroder, J. C., Campuzano-Jost, P., Jimenez, J. L., and Guo, H., Sullivan, A. P., Weber, R. J., Green, J. R., Fiddler, M. N., Bililign, S., Campos, T. L., Stell, M.,

Weinheimer, A. J., Montzka, D. D., and Brown, S. S.: Chemical feedbacks weaken the wintertime response of particulate sulfate and nitrate to emissions reductions over the eastern United States, Proceedings of the National Academy of Sciences, 115, 32, https://doi.org/10.1073/pnas.1803295115, 8110-8115, 2018.

Shao, J., Chen, Q., Wang, Y., Lu, X., He, P., Sun, Y., Shah, V., Martin, R. V., Philip, S., Song, S., Zhao, Y., Xie, Z., Zhang, L., and Alexander, B.: Heterogeneous sulfate aerosol formation mechanisms during wintertime Chinese haze events: air quality model assessment using observations of sulfate oxygen isotopes in Beijing, Atmos. Chem. Phys., 19, 6107-6123, https://doi.org/10.5194/acp-19-6107-2019, 2019.

Shen, X., T. Lee, T., J. Guo, J., X. Wang, X., P. Li, P., P. Xu, P., Y. Wang, Y., Y. Ren, Y., W. Wang, W., and T. Wang, T.: Aqueous phase sulfate production in clouds in eastern China, Atmos. Environ., 62, 502-511, https://doi.org/10.1016/j.atmosenv.2012.07.079, 2012.

Shen, Z., Y. Wu, Y., M. Huang, M., H. Xiao, H., and H. Lei, H.: Measurement and research on cloudwater over severe acid rain areas of China, Chinese Ssci ence Bbull etin, 41(20), 1726-1729, **[Did not find DOI],** 1996.

Shi, G., Xu, J., Peng, X., Sun, R., Chen, K., Tian, Y., Guan, X., Feng, Y., Yu, H., Nenes, A., and Russell, A. G.: pH of Aerosols in a Polluted Atmosphere: Source Contributions to Highly Acidic Aerosol, Environ. Sci. Technol., Env. Sci. Tech., https://doi.org/10.1021/acs.est.6b05736, 2017.

Shi, X., Nenes, A., Xiao, Z., Song, S., Yu, H., Shi, G., Zhao, Q., Chen, K., Feng, Y., and Russell, A. G.: High-resolution data sets unravel the effects of sources and meteorological conditions on nitrate and its gas–particle Partitioning, Environ. Sci. Technol., 53, 3048-3057, https://doi.org/10.1021/acs.est.8b06524, 2019.

Shi et al., 2019--Add

Siefert, R. L., A. M. Johansen, A. M., M. R. Hoffmann, M. R., and S. O. Pehkonen, S. O.: Measurements of trace metal (Fe, Cu, Mn, Cr) oxidation states in fog and stratus clouds, J. Air Waste Manage., JAWMA, 48(2), 128-143, https://doi.org/10.1080/10473289.1998.10463659, 1998.

Simon, S., O. Klemm, O., T. El-Madany, T., J. Walk, J., K. Amelung, K., P. H. Lin, P.-H., S. C. Chang, S.-C., N. H. Lin, N.-H., G. Engling, G., and S. C. Hsu, S.-C.: Chemical composition of fog water at four sites in Taiwan, Aerosol Air Qual. Res., 16, 618-631, https://doi.org/10.4209/aaqr.2015.03.0154, 2016.

Skybova, M.: Chemical composition of fog/cloud and rain water in the Beskydy Mountains-Czech Republic, Fresen ius Environ. Bull., 15(5), 448-451, available at: https://is.muni.cz/th/avk3s/Horizontalni_depozice.pdf, 2006.

Song, S., Gao, M., Xu, W., Shao, J., Shi, G., Wang, S., and Wang, Y.: Fine-particle pH for Beijing winter haze as inferred from different thermodynamic equilibrium models, Atmos. Chem. Phys., 18, 7423–7438, https://doi.org/10.5194/acp-18-7423-2018, 2018.

Squizzato, S., Masiol, M., Brunelli, A., Pistollato, S., Tarabotti, E., Rampazzo, G., and Pavoni, B.: Factors determining the formation of secondary inorganic aerosol: a case study in the Po Valley (Italy), Atmos. Chem. Phys., 13, 1927–1939, https://doi.org/10.5194/acp-13-1927-2013, 2013.

Straub, D. J.: Radiation fog chemical composition and its temporal trend over an eight year period, Atmos. Environ., 148, 49-61, https://doi.org/10.1016/j.atmosenv.2016.10.031, 2017.

Straub, D. J., T. Lee, T., and J. L. Collett, J. L.: Chemical composition of marine stratocumulus clouds over the eastern Pacific Ocean, J. Geophs. Res., 112(D4), https://doi.org/10.1029/2006JD007439, 2007.

Straub, D. J., J. W. Hutchings, J. W., and P. Herckes, P.: Measurements of fog composition at a rural site, Atmos. Environ., 47, 195-205, https://doi.org/10.1016/j.atmosenv.2011.11.014, 2012.

Formatted: Font: Bold, Font color: Dark Red

~~Straub, D. J., T. Lee, and J. L. Collett: Chemical composition of marine stratocumulus clouds over the eastern Pacific Ocean, J. Geoph. Res., 112(D4), 2007.~~

Sun, M., ~~Y.~~ Wang, Y., ~~T.~~ Wang, T., ~~S.~~ Fan, S., ~~W.~~ Wang, W., ~~P.~~ Li, P., ~~J.~~ Guo, J., and ~~Y.~~ Li, Y.: Cloud and the corresponding precipitation chemistry in south China: Water-soluble components and pollution transport, J. Geophs. Res., 115(D22), https://doi.org/10.1029/2010JD014315, 2010.

Tan, T., Hu, M., Li, M., Guo, Q., Wu, Y., Fang, X., Gu, F., Wang, Y., and Wu, Z.: New insight into PM 2.5 pollution patterns in Beijing based on one-year measurement of chemical compositions, Sci. Total. Environ., ~~STOTEN,~~ 621, 734–743., https://doi.org/10.1016/j.scitotenv.2017.11.208, 2018.

Tang, L.-L., ~~S. J.~~ Niu, S.-J., ~~S. X.~~ Fan, S.-X., ~~X. F.~~ Xu, X.-F., ~~S. H.~~ Jin, S.-H., and ~~J.~~ Xu, J.: Air pollution and mercury characteristic of fog water on fog day in Nanjing suburban, Environ. Chem., 27(1), 105-109, **[Did not find DOI]**, 2008.

Tao, Y., and Murphy, J. G.: The sensitivity of PM2.5 acidity to meteorological parameters and chemical composition changes: 10-year records from six Canadian monitoring sites, Atmos. Chem. Phys., 19, 9309–9320, https://doi.org/10.5194/acp-19-9309-2019, 2019.

~~**Tao et al., 2019--Add**~~

Thalmann, E., ~~R.~~ Burkard, R., ~~T.~~ Wrzesinsky, T., ~~W.~~ Eugster, W., and ~~O.~~ Klemm, O.: Ion fluxes from fog and rain to an agricultural and a forest ecosystem in Europe, Atmos. Res., 64(1-4), 147-158, https://doi.org/10.1016/s0169-8095(02)00087-x, 2002.

Tian, S., Pan, Y., and Wang, Y.: Ion balance and acidity of size-segregated particles during haze episodes in urban Beijing., Atmos. Res., 201, 159–167., https://doi.org/10.1016/j.atmosres.2017.10.016, 2018.

Trautner, F., ~~A.~~ Reischl, A., and ~~O.~~ Hutzinger, O.: Nitrierte Phenole in Nebelwasser, Umweltwissensch Schadstoff-Forsch, ~~Umwelt. Schadstoff Forsch.,~~ 1(3), 10, https://doi.org/10.1007/BF02983902, 1989.

Valle-Díaz, C. J., ~~E.~~ Torres-Delgado, E., ~~S. M.~~ Colón-Santos, S. M., ~~T.~~ Lee, T., ~~J. L.~~ Collett Jr., J. L., ~~W. H.~~ McDowell, W. H., and ~~O. L.~~ Mayol-Bracero, O. L.: Impact of long-range transported African dust on cloud water chemistry at a tropical montane cloud forest in northeastern Puerto Rico, Aerosol Air Qual. Res., 16(3), 653-664, https://doi.org/10.4209/aaqr.2015.05.0320, 2016.

van Pinxteren, D., ~~K. W.~~ Fomba, K. W., ~~S.~~ Mertes, S., ~~K.~~ Müller, K., ~~G.~~ Spindler, G., ~~J.~~ Schneider, J., ~~T.~~ Lee, T., ~~J. L.~~ Collett, J. L., and ~~H.~~ Herrmann, H.: Cloud water composition during HCCT-2010: Scavenging efficiencies, solute concentrations, and droplet size dependence of inorganic ions and dissolved organic carbon, Atmos. Chem. Phys., 16(5), 3185-3205, https://doi.org/10.5194/acp-16-3185-2016, 2016.

Van Valin, C., ~~D.~~ Wellman, D., and ~~L.~~ Stearns, L.: Aerosol and cloudwater properties at whiteface mountain, New York, Wat. Air Soil Pol., 34(4), 369-383, https://doi.org/10.1007/BF00282738, 1987.

Vasconcellos, P. C., ~~F. L.~~ Gonçalves, F. L., ~~S. G.~~ Avila, S. G., ~~V. K.~~ Censon, V. K., and ~~H.~~ Bauer, H.: The Chemical Composition of Winter Fogs at São Paulo Highway Sites, J. Brazil. Chem. Soc.~~Journal of the Brazilian Chemical Society~~, 29(9), 1951-1958, http://dx.doi.org/10.21577/0103-5053.20180072, 2018.

Vasilakos, P., Russell, A., Weber, R., and Nenes, A.: Understanding nitrate formation in a world with less sulfate, Atmos. Chem. Phys., 18, 12765–12775, https://doi.org/10.5194/acp-18-12765-2018, 2018.

Verhoeven, W., ~~R.~~ Herrmann, R., ~~R.~~ Eiden, R., and ~~O.~~ Klemm, O.: A comparison of the chemical composition of fog and rainwater collected in the Fichtelgebirge, Federal Republic of Germany, and from the South Island of New Zealand, Theor. Appl. Climatol., 38(4), 210-221, https://doi.org/10.1007/BF00867414, 1987.

Formatted: Font: 10 pt, Bold, Font color: Dark Red

Formatted: Font: Bold, Font color: Dark Red

Vieira-Filho, M., Pedrotti, J. J., and Fornaro, A.: Water-soluble ions species of size-resolved aerosols : Implications for the atmospheric acidity in São Paulo megacity, Brazil. Atmos. Res. 181, 281–287., https://doi.org/10.1016/j.atmosres.2016.07.006, 2016.

~~Vong, R. J., B. M. Baker, F. J. Brechtel, R. T. Collier, J. M. Harris, A. S. Kowalski, N. C. McDonald, and L. M. Mcinnes: Ionic and trace element composition of cloud water collected on the Olympic Peninsula of Washington State, Atmos. Environ., 31(13), 1991-2001, 1997.~~

Vong, R. J., and P. Guttorp, P.: Co-occurrence of ozone and acidic cloudwater in high-elevation forests, Environ. Sci. Technol., Env. Sci. Techn., 25(7), 1325-1329, **[Did not find DOI]**, 1991.

Vong, R. J., B. M. Baker, B. M., F. J. Brechtel, F. J., R. T. Collier, R. T., J. M. Harris, J. M., A. S. Kowalski, A. S., N. C. McDonald, N. C., and L. M. Mcinnes, L. M.: Ionic and trace element composition of cloud water collected on the Olympic Peninsula of Washington State, Atmos. Environ., 31(13), 1991-2001, https://doi.org/10.1016/S1352-2310(96)00337-8, 1997.

Waldman, J. M., J. W. Munger, J. W., D. J. Jacob, D. J., and M. R. Hoffmann, M. R.: Chemical characterization of stratus cloudwater and its role as a vector for pollutant deposition in a Los Angeles pine forest, Tellus B: Chemical and Physical Meteorology, 37(2), 91-108, https://doi.org/10.3402/tellusb.v37i2.15001, 1985.

Wang, G., Zhang, R., Gomez, M. E., Yang, L., Levy, M., Hu, M., and Lin, Y.: Persistent sulfate formation from London Fog to Chinese haze, Proceedings of the National Academy of Sciences, Proc. Natl. Acad. Sci., 113, 13630–13635., https://doi.org/10.1073/pnas.1616540113, 2016.

Wang, H., Ding, J., Xu, J., Wen, J., Han, J., Wang, K., Shi, G., Feng, Y., Ivey, C. E., Wang, Y., Nenes, A., Zhao, Q., and Russell, A. G.: Aerosols in an arid environment : The role of aerosol water content, particulate acidity, precursors, and relative humidity on secondary inorganic aerosols, Sci. Total. Environ., STOTEN, 646, 564–572., https://doi.org/10.1016/j.scitotenv.2018.07.321, 2019.

Wang, X., J. Chen, J., J. Sun, J., W. Li, W., L. Yang, L., L. Wen, L., W. Wang, W., X. Wang, X., J. L. Collett Jr., J. L., and Y. Shi, Y.: Severe haze episodes and seriously polluted fog water in Ji'nan, China, Sci. Total. Environ., STOTEN, 493, 133-137, https://doi.org/10.1016/j.scitotenv.2014.05.135, 2014.

Wang, Y., J. Guo, J., T. Wang, T., A. Ding, A., J. Gao, J., Y. Zhou, Y., J. L. Collett Jr., J. L., and W. Wang, W.: Influence of regional pollution and sandstorms on the chemical composition of cloud/fog at the summit of Mt. Taishan in northern China, Atmos. Res., 99(3-4), 434-442, https://doi.org/10.1016/j.atmosres.2010.11.010, 2011.

Wang, Y. L., J. W. Zhang, J. W., A. R. Marcotte, A. R., M. Karl, M., C. Dye, C., and P. Herckes, P.: Fog chemistry at three sites in Norway, Atmos. Res., 151, 72-81, https://doi.org/10.1016/j.atmosres.2014.04.016, 2015.

Watanabe, K., Y. Ishizaka, Y., and C. Takenaka, C.: Chemical composition of fog water near the summit of Mt. Norikura in Japan, J. Meterol. Soc. Japn., 77(5), 997-1006, https://doi.org/10.2151/jmsj1965.77.5_997, 1999.

Watanabe, K., Ishizaka, Y., Minami, Y., and Yoshida, K.: Peroxide concentrations in fog water at mountainous sites in Japan, in: Acid Rain 2000, edited, 1559-1564, Springer, https://doi.org/10.1007/978-94-007-0810-5_107, 2001a.

Watanabe, K., Ishizaka, Y., and Takenaka, C.: Chemical characteristics of cloud water over the Japan Sea and the Northwestern Pacific Ocean near the central part of Japan: airborne measurements, Atmos. Environ., 35(4), 645-655, https://doi.org/10.1016/S1352-2310(00)00358-7, 2001b.

Watanabe, K., Y. Takebe, Y., N. Sode, N., Y. Igarashi, Y., H. Takahashi, H., and Y. Dokiya, Y.: Fog and rain water chemistry at Mt. Fuji: A case study during the September 2002 campaign, Atmos. Res., 82(3-4), 652-662, https://doi.org/10.1016/j.atmosres.2006.02.021, 2006.

Watanabe, K., H. Honoki, H., A. Iwai, A., A. Tomatsu, A., K. Noritake, K., N. Miyashita, N., K. Yamada, K., H. Yamada, H., H. Kawamura, H., and K. Aoki, K.: Chemical characteristics of fog water at Mt. Tateyama, near the coast of the Japan Sea in central Japan, Water Air Soil Poll., Water, Air, & Soil Pollution, 211(1-4), 379-393, https://doi.org/10.1007/s11270-009-0307-2, 2010.

Watanabe, K., H. Honoki, H., S. Iwama, S., K. Iwatake, K., S. Mori, S., D. Nishimoto, D., S. Komori, S., Y. Saito, Y., H. Yamada, H., and Y. Uehara, Y.: Chemical composition of fog water at Mt. Tateyama near the coast of the Japan Sea in central Japan, Erdkunde, 233-245, https://doi.org/10.2307/23069696, 2011.

Watanabe, K., Y. Ishizaka, Y. Minami, and K. Yoshida: Peroxide concentrations in fog water at mountainous sites in Japan, in Acid rain 2000, edited, pp. 1559-1564, Springer, 2001a.

Watanabe, K., Y. Ishizaka, and C. Takenaka: Chemical composition of fog water near the summit of Mt. Norikura in Japan, J. Met. Soc. Jap., 77(5), 997-1006, 1999.

Watanabe, K., Y. Ishizaka, and C. Takenaka: Chemical characteristics of cloud water over the Japan Sea and the Northwestern Pacific Ocean near the central part of Japan: airborne measurements, Atmos. Environ., 35(4), 645-655, 2001b.

Watanabe, K., Y. Takebe, N. Sode, Y. Igarashi, H. Takahashi, and Y. Dokiya: Fog and rain water chemistry at Mt. Fuji: A case study during the September 2002 campaign, Atmos. Res., 82(3-4), 652-662, 2006.

Weathers, K. C., and G. E. Likens, G. E.: Clouds in southern Chile: an important source of nitrogen to nitrogen-limited ecosystems?, Environ. Sci. Technol., Env. Sci. Techn., 31(1), 210-213, https://doi.org/10.1021/es9603416, 1996.

Weathers, K. C., G. E. Likens, G. E., F. H. Bormann, F. H., J. S. Eaton, J. S., W. B. Bowden, W. B., J. L. Andersen, J. L., D. A. Cass, D. A., J. N. Galloway, J. N., W. C. Keene, W. C., and K. D. Kimball, K. D.: A regional acidic cloud/fog water event in the eastern United States, Nature, 319(6055), 657, https://doi.org/10.1038/319657a0, 1986.

Weathers, K. C., G. E. Likens, G. E., F. H. Bormann, F. H., S. H. Bicknell, S. H., B. T. Bormann, B. T., B. C. Daube, B. C., J. S. Eaton, J. S., J., N. Galloway, N., and W. C. Keene, W. C.: Cloudwater chemistry from ten sites in North America, Environ. Sci. Technol., Env. Sci. Techn., 22(9), 1018-1026, https://doi.org/10.1021/es00174a004 1988.

Weathers, K. C., G. E. Likens, F. H. Bormann, J. S. Eaton, W. B. Bowden, J. L. Andersen, D. A. Cass, J. N. Galloway, W. C. Keene, and K. D. Kimball: A regional acidic cloud/fog water event in the eastern United States, Nature, 319(6055), 657, 1986.

Weber, R. J., Guo, H., Russell, A. G., and Nenes, A.: High aerosol acidity despite declining atmospheric sulfate concentrations over the past 15 years., Nat. Geosci. 9, 282–285, https://doi.org/10.1038/ngeo2665, 2016.

Wilkinson, J., B. Reynolds, B., C. Neal, C., S. Hill, S., M. Neal, M., and M. Harrow, M.: Major, minor and trace element composition of cloudwater and rainwater at Plynlimon, Hydrol. Earth Syst. Sci., 1(3), 557-569, https://doi.org/10.5194/hess-1-557-1997, 1997.

Winiwarter, W., H. Puxbaum, H., S. Fuzzi, S., M. C. Facchini, M. C., G. Orsi, G., N. Beltz, N., K. Enderle, K., and W. Jaeschke, W.: Organic acid gas and liquid-phase measurements in Po Valley fall-winter conditions in the presence of fog, Tellus B, 40(5), 348-357, https://doi.org/10.1111/j.1600-0889.1988.tb00109.x, 1988.

Wirgot, N., V. Vinatier, V., L. Deguillaume, L., M. Sancelme, M., and A. M. Delort, A. M.: H2O2 modulates the energetic metabolism of the cloud microbiome, Atmos. Chem. Phys., 17(24), 14841-14851, https://doi.org/10.5194/acp-17-14841-2017, 2017.

Wobrock, W., et al.: The Kleiner-Feldberg cloud experiment 1990 - An overview, J. Atmos. Chem., 19(1-2), 3-35, https://doi.org/10.1007/bf00696581, 1994.

Wrzesinsky, T., and O. Klemm, O.: Summertime fog chemistry at a mountainous site in central Europe, Atmos. Environ., 34(9), 1487-1496, https://doi.org/10.1016/s1352-2310(99)00348-9, 2000.

Wu, D., X.-J. Deng, X.-J., Y.-X. Ye, Y.-X., and W.-K. Mao, W.-K.: The study on fog-water chemical composition in Dayaoshan of Naniling Mountain, Acta Meteorol. Sin., ACTA Meteorologica Sinica, 62(4), 476-485, https://doi.org/10.11676/qxxb2004.048, 2004.

Wu, D., F. Li, F., X.-J. Deng, X.-J., X.-Y. Bi, X.-Y., X.-H. Wang, X.-H., and X.-Y. Huang, X.-Y.: Study on the chemical characteristics of polluting fog in Guangzhou area in spring, J. ournal of Trop. ical Meteorol. ogy, 15(1), 68-72, https://doi.org/10.3969/j.issn.1006-8775.2009.01.011, 2009.

Xu, L., Guo, H., Boyd, C.M., Klein, M., Bougiatioti, A., Cerully, K.M., Hite, J.R., Isaacman-vanwertz, G., Kreisberg, N.M., Knote, C., Olson, K., Koss, A., Goldstein, A.H.: Effects of anthropogenic emissions on aerosol formation from isoprene and monoterpenes in the southeastern United States, Proc. Natl. Acad. Sci., 112, 37–42. https://doi.org/10.1073/pnas.1417609112, 2015.

Xu, L., Middlebrook, A. M., Liao, J., de Gouw, J. A., Guo, H. Y., Weber, R. J., Nenes, A., Lopez-Hilfiker, F. D., Lee, B. H., Thornton, J. A., Brock, C. A., Neuman, J. A., Nowak, J. B., Pollack, I. B., Welti, A., Graus, M., Warneke, C., and Ng, N. L.: Enhanced formation of isoprene-derived organic aerosol in sulfur-rich power plant plumes during Southeast Nexus, J. Geophys. Res.-Atmos., 121, 11137-11153, https://doi.org/10.1002/2016jd025156, 2016.

Xu, F., S. J. Niu, S.-J., Y. Zhang, Y., Y. Y. Yue, Y.-Y., L. J. Zhao, L.-J., and S. Q. Cai, S.-Q.: Analyses on chemical characteristic of spring sea fog water on Donghai Island in Zhanjiang, China, China Environmental ScienceChina Env. Sci., 31(3), 353-360, **[Did not find DOI]**, 2011.

Xu, G., D. E. Sherman, D. E., E. Andrews, E., K. Moore, K., D. Straub, D., K. Hoag, K., and J. Collett Jr., J.: The influence of chemical heterogeneity among cloud drop populations on processing of chemical species in winter clouds, Atmos. Res., 51(2), 119-140, https://doi.org/10.1016/S0169-8095(99)00004-6, 1999.

Xu, L., Guo, H., Boyd, C. M., Klein, M., Bougiatioti, A., Cerully, K. M., Hite, J. R., Isaacman-vanwertz, G., Kreisberg, N. M., Knote, C., Olson, K., Koss, A., and Goldstein, A. H.: Effects of anthropogenic emissions on aerosol formation from isoprene and monoterpenes in the southeastern United States, Proceedings of the National Academy of Sciences, Proc. Natl. Acad. Sci., 112, 37–42, https://doi.org/10.1073/pnas.1417609112, 2015.

Xu, L., Middlebrook, A. M., Liao, J., de Gouw, J. A., Guo, H. Y., Weber, R. J., Nenes, A., Lopez-Hilfiker, F. D., Lee, B. H., Thornton, J. A., Brock, C. A., Neuman, J. A., Nowak, J. B., Pollack, I. B., Welti, A., Graus, M., Warneke, C., and Ng, N. L.: Enhanced formation of isoprene-derived organic aerosol in sulfur-rich power plant plumes during Southeast Nexus, J. Geophys. Res.-Atmos., 121, 11137-11153, https://doi.org/10.1002/2016jd025156, 2016.

Xue, H., M. d. L. S. Goncalves, M. d. L. S., M. Reutlinger, M., L. Sigg, L., and W. Stumm, W.: Copper (I) in fogwater: Determination and interactions with sulfite, Environ. mental Sci. Technol., 25(10), 1716-1722, **[Did not find DOI]**, 1991.

Xue, J., Lau, A. K. H., and Zhen, J.: A study of acidity on PM 2.5 in Hong Kong using online ionic chemical composition measurements., Atmos. Environ. 45, 7081–7088, https://doi.org/10.1016/j.atmosenv.2011.09.040, 2011.

Yamaguchi, T., G. Katata, G., I. Noguchi, I., S. Sakai, S., Y. Watanabe, Y., M. Uematsu, M., and H. Furutani, H.: Long-term observation of fog chemistry and estimation of fog water and nitrogen input via fog water deposition at a

mountainous site in Hokkaido, Japan, Atmos. Res., 151, 82-92, https://doi.org/10.1016/j.atmosres.2014.01.023, 2015.

Yang, J., ~~Y.-J.~~ Xie, Y.-J., ~~C.-E.~~ Shi, C.-E., ~~D.-Y.~~ Liu, D.-Y., ~~S.-J.~~ Niu, S.-J., and ~~Z.-H.~~ Li, Z.-H.: Ion composition of fog water and its relation to air pollutants during winter fog events in Nanjing, China, Pure and Applied Geophysics~~Pure Appl. Geoph.~~, 169(5-6), https://doi.org/1037-1052, 10.1007/s00024-011-0342-y, 2012.

Yao, X., Yan, T., Fang, M., and Chan, C. K.: Comparison of thermodynamic predictions for in situ pH in PM 2.5, Atmos. Environ., 40, 2835–2844., https://doi.org/10.1016/j.atmosenv.2006.01.006, 2006.

Yao, X., Ling, T. Y., Fang, M., Ã, and Chan, ~~K.~~ C. K.: Size dependence of in situ pH in submicron atmospheric particles in Hong Kong, Atmos. Environ., 41, 382–393., https://doi.org/10.1016/j.atmosenv.2006.07.037, 2007.

~~Yao, X., Yan, T., Fang, M., Chan, C.K.: Comparison of thermodynamic predictions for in situ pH in PM 2.5, Atmos. Environ., 40, 2835–2844. https://doi.org/10.1016/j.atmosenv.2006.01.006, 2006.~~

Young, A. H., Keene, W. C., Pszenny, A. A. P., Sander, R., Thornton, J. A., Riedel, T. P., and Maben, J. R.: Phase partitioning of soluble trace gases with size-resolved aerosols in near-surface continental air over northern Colorado, USA, during winter, J. Geophys. Res. Atmos., 118, 9414–9427., https://doi.org/10.1002/jgrd.50655, 2013.

Zapletal, M., ~~D.~~ Kunak, D., and ~~P.~~ Chroust, P.: Chemical characterization of rain and fog water in the Cervenohorske sedlo (Hruby Jesenik Mountains, Czech Republic), Water Air and Soil Poll.~~ution~~, 186(1-4), 85-96, https://doi.org/10.1007/s11270-007-9467-0, 2007.

Zellner, R., Herrmann, H., Exner, M., Jacobi, H.-W., Raabe, G. and Reese, A.,: Formation and Reactions of Oxidants in the Aqueous Phase, in P. Warneck (ed), Heterogeneous and Liquid Phase Processes, 146 - 152, Springer, Berlin, 1996.~~Zellner (1994) - Add~~

~~Zellner, R. (edEd.): Global Aspects of Atmospheric Chemistry (Topics in Physical Chemistry, Vol. 6), Steinkopf, Darmstadt (Germany)/Springer, New York, **[Did not find DOI]**, 1999.~~

Zhang, Q., and ~~C.~~ Anastasio, C.: Chemistry of fog waters in ~~California's~~ California's Central Valley—Part 3: concentrations and speciation of organic and inorganic nitrogen, Atmos. Environ., 35(32), 5629-5643, https://doi.org/10.1016/S1352-2310(01)00337-5, 2001.

Zhang, Q., Jimenez, J. L., Worsnop, D. R., and Canagaratna, M.: A Case Study of Urban Particle Acidity and Its Influence on Secondary Organic Aerosol, Environ. Sci. Technol., ~~Env. Sci. Techn.,~~ 41, 3213–3219, https://doi.org/10.1021/es061812j, 2007.

Zhu, X., Prospero, J. M., Millero, F. J., Savoie, D. L., and Brass, G. W.: The solubility of ferric ion in marine mineral aerosol solutions at ambient relative humidities, Mar. Chem., 38, 91–107, https://doi.org/10.1016/0304-4203(92)90069-M, 1992.

Zhu, B., ~~Z.-H.~~ Li, Z.-H., ~~J.-P.~~ Huang, J.-P., ~~J.~~ Yang, J., ~~Y.-S.~~ Huang, Y.-S., and ~~Y.-R.~~ Huang, Y.-R.: Chemical compositions of the fogs in the city and suburban of Xishuang banna, ~~ACTA~~ Acta Scientiae Circumstantiae, 20(3), 316-321, https://doi.org/025322468 (2000)20320316206, 2000.

Zhu, C., ~~J.~~ Chen, J., ~~X.~~ Wang, X., ~~J.~~ Li, J., ~~M.~~ Wei, M., ~~C.~~ Xu, C., ~~X.~~ Xu, X., ~~A.~~ Ding, A., and ~~J. L.~~ Collett Jr., J. L.: Chemical Composition and Bacterial Community in Size-Resolved Cloud Water at the Summit of Mt. Tai, China, Aerosol Air Qual. Res., 18(1), 1-14, https://doi.org/10.4209/aaqr.2016.11.0493, 2018.

Zimmermann, L., and ~~F.~~ Zimmermann, F.: Fog deposition to Norway Spruce stands at high-elevation sites in the Eastern Erzgebirge (Germany), J. Hydrol., 256(3-4), 166-175, https://doi.org/10.1016/s0022-1694(01)00532-7, 2002.

Formatted: Font: Not Bold, Font color: Auto

Formatted: Font: Not Bold, Font color: Auto

Formatted: Font: 10 pt

Zuend, A.: Modelling the thermodynamics of mixed organic-inorganic aerosols to predict water activities and phase separations, PhD thesis, Swiss Federal Institute of Technology in Zurich ~~ETH Zurich~~, https://doi.org/10.3929/ethz-a-005582922, 2007.

Zuo, Y.: Light-induced oxidation of bisulfite-aldehyde adducts in real fog water, Naturwissenschaften, 81(11), 505-507, https://doi.org/10.1007/BF01132683, 1994.